Lighting up Pnictogen-Based Polymers: A Comparison of Phosphorus and Bismuth

by

Sarah M. Parke

A thesis submitted in partial fulfillment of the requirements for the degree of

Doctor of Philosophy

Department of Chemistry
University of Alberta

Abstract

The work described in this thesis outlines the development of fluorescent and phosphorescent emitters based on the Group 15 elements, bismuth and phosphorus.

Work began with the synthesis of a series of bismuth-containing heterocycles, termed bismoles and benzobismoles, via the copper(I) chloride-mediated metallacycle transfer chemistry of zirconacyclopentadienes. TD-DFT computations indicated that participation of the bismuth orbitals in the excitation process is correlated with the observed phosphorescence. This requirement gives rise to a method to predetermine if a system is likely to be phosphorescent, enabling TD-DFT to serve as a guide to direct development of new phosphorescent materials in the future.

Norbornene-functionallized benzobismoles could be polymerized via ring-opening metathesis polymerization to produce weakly red phosphorescent products of high molecular weight. The use of Grubbs' third generation catalyst enabled the formation of a benzobismole-based block copolymer that readily undergoes self-assembly into spherical micelles in THF/hexanes mixtures.

This method of ring-opening metathesis polymerization of could be extended to a highly emissive benzophosphole oxide AIEgen-based monomer to yield fluorescent polymers. While this benzophosphole oxide monomer displayed drastically decreased quantum yield in solution compared to in the solid state, after polymerization the resulting solution state fluorescence quantum yield of the polymer increased to 30 %. Self-assembly of two different benzophosphole oxide block copolymers was achieved and the luminescence of these materials is reported.

Preface

Portions of the work discussed in this thesis were completed in collaboration with other researchers within the Rivard group and Chemistry Department, as well as outside of the University of Alberta.

All X-ray crystallographic studies described in this thesis were performed by Dr. R. McDonald, Dr. M. J. Ferguson, and Dr. Y. Zhou including the mounting of crystals, set-up and operation of the diffractometer, refinement of the structures and preparation of all crystallographic data tables. Elemental analyses and mass spectrometric analyses were performed by the Analytical Instrument Laboratory and Mass Spectrometry Laboratory at the Department of Chemistry, University of Alberta.

The computational studies in this work were made possible by the facilities of the Shared Hierarchical Academic Computing Network (SHARCNET: www.sharcnet.ca), WestGrid (www. westgrid.ca), and Compute/Calcul Canada (www.computecanada.ca). The work in this thesis was supported by the Natural Sciences and Engineering Research Council of Canada, the Canada Foundation for Innovation, and the Faculty of Science at the University of Alberta.

In Chapter 2, lifetime and photoluminescence measurements were conducted by Dr. M. B. A. Narreto in the group of Prof. F. A. Hegmann (University of Alberta). TD-DFT computations were conducted by Dr. E. Hupf in the group of Prof. E. Rivard (University of Alberta) with valuable input from Dr. S. Mebs (Freie Universität Berlin) and the support of Deutsche Forschungsgemeinschaft (DFG). P. Choi and B.

Furlong (summer 2014 undergraduate students in the Rivard group) are also gratefully acknowledged for performing preliminary trial reactions for this work.

In Chapter 3, lifetime, quantum yield, and photoluminescence measurements were conducted by Prof. G. He (Xi'an Jiaotong University) and his student L. Xu under the support of the Natural Science Foundation of China. TEM and SEM measurements were conducted by H. Yu in the group of Prof. J. Veinot (University of Alberta). TD-DFT computations were conducted by Dr. E. Hupf in the group of Prof. E. Rivard (University of Alberta) with the support of DFG. Powder XRD was conducted by K. Nichols in the Department of Earth & Atmospheric Sciences at the University of Alberta. Chiral HPLC measurements were conducted by Dr. E. Fu at the University of Alberta. TGA and DSC measurements were conducted by W. Moffat, J. Jones, and K. Haidukevich at the University of Alberta Analytical Instrument Laboratory. M. P. Boone is thanked for his synthesis of tris(5-(4-phenyl)norbornene)bismuth ($BiAr^{ROMP}_3$) and his great idea to use norbornene-functionalization to impart "ROMPability" to the bismoles.

In Chapter 4, lifetime, quantum yield, and photoluminescence measurements of compound **3** were conducted in part by Dr. E. Hupf in the group of Prof. E. Rivard (University of Alberta). The synthesis and characterization of compound **1** was conducted by G. Matharu as part of her CHEM 401 project, as was the first synthesis of compound **2**.

In Chapter 5, the synthesis of compounds **1**–**4**, and **P1** was initially accomplished by S. Tanaka from the group of Prof. K. Naka (Kyoto Institute of Technology). TEM was conducted by H. Yu in the group of Prof. J. Veinot

(University of Alberta). TGA and DSC measurements were conducted by J. Jones at the University of Alberta Analytical Instrument Laboratory. The TD-DFT computations were conducted under the advisement of Dr. E. Hupf in the group of Prof. E. Rivard (University of Alberta).

According to the policy within our research group, each chapter of this thesis is essentially self-contained, and prepared in the form of a paper that is intended for publication in peer-reviewed journals. A portion of this thesis has been published previously elsewhere, and these publications are listed below.

Chapter 1: (a) Parke, S. M.; Boone, M. P.; Rivard, E. *Chem. Commun*. **2016**, *52*, 9485–9505 and (b) Parke, S. M.; Rivard, E. *Isr. J. Chem*. **2018**, *58*, 915–926.

Chapter 2: Parke, S. M.; Narreto, M. A. B.; Hupf, E.; McDonald, R.; Ferguson, M. J.; Hegmann, F. A.; Rivard, E. *Inorg. Chem*. **2018**, *57*, 7536–7549.

Chapter 3: Parke, S. M.; Hupf, E.; Matharu, G. K.; de Aguiar, I.; Xu, L.; Yu, H.; Boone, M. P.; de Souza, G. L. C.; McDonald, R.; Ferguson, M. J.; He, G.; Brown, A.; Rivard, E. *Angew. Chem. Int. Ed*. **2018**, *57*, 14841–14846.

Dedicated to my family

Acknowledgements

First, I would like to thank my supervisor Prof. Eric Rivard for his continued support these past five years. His enthusiasm and passion for chemistry are astounding. I am grateful for his guidance and encouragement over the years and for all the times he believed in me.

Next, I would like to thank my supervisory and examining committee members, Prof. Joe Gilroy, Prof. Robert Campbell, Prof. Jillian Buriak, Prof. Jon Veinot, and Prof. Mariusz Klobukowski for their support and valuable input to this thesis.

Thank you to all Rivard group members, past and present, but specifically Manu Hupf, Matthew (Cowboy) Roy, Chrissy Braun, Jocelyn Sinclair, Ian Watson, Bruno Luppi, Al Omaña, Sam Baird, Linkun Miao, Mike Boone, Christian Herring-Junghans, Anindya Swarnakar, Alyona Shynkaruk, Patricia Andreiuk, Kate Powers, Mel Lui, Nicole Martinek, Derek Zomerman, Nathan Paisley, and Paul Lummis. I simply can't imagine a better group of people to share a lab with and I feel lucky to have spent my PhD getting to know you all. I want to give a special thank you to Gunwant for her dedication to the bismole project and for being a good friend.

I am grateful to my parents, Jim and Gail, for their continued support and love throughout the years; thank you to Brian and Bob for toughening me up, and Jackson and Ralph for the smiles. Thank you to the extra family members I've gained over the years, Greg, Sue, Megan, Brandon, Rachel, and Brina, for always believing in me too.

The University of Alberta Chemistry Department has amazing technical and support staff that not only make research possible but make studying here a delight. Thank you to Wayne Moffat, Dr. Bob McDonald, Dr. Mike Ferguson, Jason Dibbs, Jennifer Jones, Ryan Lewis, Mark Miskolzie, Jing Zheng, Dr. Randy Whittal, and all the wonderful staff in the machine shop and electronics shop.

Thank you to my rock people, Jody, Seth, Danny, Sean, John, Honey, Tobi, Matthias, Amanda, and François for the enlightening mountain adventures, and for coaxing me out of my comfort zone now and then.

Finally, thank you to my dear Eric. Your love and encouragement over these years has meant the world to me and I can’t imagine having finished this degree without you. Thank you for keeping me sane (relatively) and for always picking me up and dusting me off when I fall down.

Table of Contents

List of Figures

List of Schemes

List of Tables

List of Symbols, Nomenclature, and Abbreviations

{^{n}X}	Decoupled nucleus ^{n}X
$^{1}O_2$	Singlet oxygen
2-MeTHF	2-Methyltetrahydrofuran
Å	Ångström
Ac	Acyl group (–C(O)R)
ACQ	Aggregation-caused quenching
ADF	Amsterdam density functional
AIE	Aggregation-induced emission
AIEgen	AIE luminogen
AIM	Atoms in molecules
AIP	Aggregation-induced phosphorescence
AIPgen	AIP luminogen
APT NMR	Attached proton test NMR
Ar	Aryl
bcp	Bond critical point
BHT	Butylated hydroxytoluene
BPin	Pinacolborane
br	Broad
C_6D_6	Benzene-d_6
cd	Candela
$CDCl_3$	Chloroform-d
°C	Degrees Celsius
ca.	Circa; approximately
c.f.	Confer; compare
CIE	Crystallization induced emission
cm^{-1}	Wavenumbers
Cp	Cyclopentadienyl ligand (η^5-C_5H_5)
CSA	Camphorsulfonic acid

CV	Cyclic voltammetry
d	Doublet
dba	Dibenzylideneacetone
dd	Doublet of doublets
DEPTQ	Distortionless enhancement by polarization transfer including quaternary nuclei
DF	Delayed fluorescence
DFT	Density Functional Theory
DLS	Dynamic light scattering
DMF	N,N-Dimethylformamide
DMSO	Dimethyl sulfoxide
dppf	1,1'-Bis(diphenylphosphino)ferrocene
DSC	Differential scanning calorimetry
dt	Doublet of triplets
E	Variable main group element
E_{0-0}	Zero-point corrected adiabatic energy
E_{adia}	Energy difference between T_1 and S_0
ECP	Effective core potential
EI	Electron ionization
ELI-D	Electron Localizability Indicator
equiv.	Molar equivalents
Em	Emission
Et	Ethyl (C_2H_5)
Et_2O	Diethyl ether
eV	Electron volt
Ex	Excitation
f	Oscillator strength
g	Gram
GPC	Gel permeation chromatography
HOMO	Highest occupied molecular orbital

HPLC	High performance liquid chromatography
HPS	Hexaphenylsilole
HRMS	High resolution mass spectrometry
Hz	Hertz
IEF-PCM	Integral equation formalism polarizable continuum model
^{i}Pr	*iso*-propyl (Me_2CH)
IR	Infrared
ISC	Intersystem crossing
J	NMR coupling constant
K	Kelvin
kDa	Kilodaltons (1,000 g/mol)
LALS	Low angle light scattering
LUMO	Lowest Unoccupied Molecular Orbital
MALDI	Matrix assisted laser desorption/ionization
MCL	Mechanochromic luminescence
Me	Methyl (CH_3)
MeCN	Acetonitrile
Mes	Mesityl (2,4,6-$Me_3C_6H_2$)
mg	Milligram
MHz	Megahertz
mL	Milliliter
mmol	Millimole
mol%	Mole percent
M_n	Number average molecular weight
M_w	Weight average molecular weight
MO	Molecular orbital
mol	Mole
Mp	Melting point
^{n}Bu	*n*-butyl (C_4H_9)
NBO	Natural Bond Orbital

NCI	Noncovalent Interaction
NHC	*N*-Heterocyclic carbene
NICS	Nuclear Independent Chemical Shift
$^{n}J_{AB}$	n-Bond AB coupling constant
nm	Nanometers
^{n}Pr	*n*-propyl group
NMR	Nuclear Magnetic Resonance
ns	Nanoseconds
LED	Light-emitting diode
OFET	Organic field effect transistor
OLED	Organic light-emitting diode
ORTEP	Oak Ridge thermal ellipsoid plot
PDI	Polydispersity index (M_w/M_n)
Ph	Phenyl (C_6F_5)
PL	Photoluminescence
PLED	Polymer light-emitting diode
PMMA	Poly(methyl methacrylate)
ppm	Parts per million
ps	Picoseconds
PXRD	Powder X-ray diffraction
R	Variable functional group
RALS	Right angle light scattering
R_f	Retention factor
RI	Refractive index
ROMP	Ring-opening metathesis polymerization
RSBI	Real space bonding indicators
RTP	Room temperature phosphorescence
s	Singlet
S_n	n^{th} singlet state
^{s}Bu	*sec*-butyl

SEM	Scanning electron microscopy
SOC	Spin-orbit coupling
SPhos	2-Dicyclohexylphosphino-2',6'-dimethoxybiphenyl
STED	Stimulated emission depletion
t	Triplet
TADF	Thermally activated delayed fluorescence
^{t}Bu	*tert*-butyl
Tf	Triflyl
T_n	n^{th} triplet state
TBAF	Tetrabutylammonium fluoride
TD-DFT	Time dependent-density functional theory
T_g	Glass transition temperature
TGA	Thermogravimetric analysis
TEM	Transmission electron microscopy
THF	Tetrahydrofuran
TIPL	Time-independent photoluminescence
T_m	Melt transition temperature
TMEDA	Tetramethylethylenediamine
TMG	*N,N,N′,N′*-Tetramethylguanidine
TPA	Triphenylamine
TRPL	Time-resolved photoluminescence
UFF	Universal force field
UV	Ultraviolet
UV-Vis	Ultraviolet/visible spectroscopy
vol%	Percent by volume
wt%	Percent by weight
XPhos	2-Dicyclohexylphosphino-2′,4′,6′-triisopropylbiphenyl
XRD	X-ray diffraction
ZORA	Zeroth order regular approximation
δ	Partial charge or chemical shift in ppm

ΔE_{S-T}	Singlet and triplet energy gap
η	Eta (number of atoms of a ligand that coordinate)
λ	Wavelength
λ_{ex}	Excitation wavelength
λ_{em}	Emission wavelength
λ_{em_DF}	Delayed fluorescence wavelength
λ_{max}	Wavelength of maximum absorbance
μs	Microseconds
τ	Luminescence lifetime
τ_{DF}	Delayed fluorescence lifetime
τ_F	Fluorescence lifetime
τ_P	Phosphorescence lifetime
Φ	Luminescence quantum yield
Φ_F	Fluorescence quantum yield
Φ_P	Phosphorescence quantum yield

Chapter 1: Introduction

1.1 The Importance of Phosphorescent Materials

Phosphorescent materials are coveted for organic light-emitting diode (OLED) applications due to their potential to attain a theoretical maximum of 100 % electroluminescence efficiency [vs. 25 % from fluorescent materials] due to the ability to harness light emission from triplet excitons (electron-hole pairs).[1] Phosphorescent materials are also desirable in bioimaging because their longer emission lifetimes (μs to s regime) enable time-gated bioimaging in which images free from background (ns lifetime) auto-fluorescence can be acquired.[2]

By taking advantage of effective mixing between singlet and triplet excited states when heavy inorganic elements are present in π-conjugated materials, one can obtain long-lived excitons (up to the millisecond regime), leading to long exciton diffusion lengths within photovoltaically active materials. Such species would be of great value to solar cell development[3] where premature recombination of electron-hole pairs (excitons) leading to energy loss is a major challenge that requires intimate interfacial mixing of donor and acceptor materials at the nanoscale.

From the recent discovery of solid-state phosphorescence in heavy main group element-containing molecules, one could use this property to construct ‘‘host-free’’ OLEDs if the existing challenge of enhancing charge migration through these next generation phosphors can be solved.[4] Furthermore, due to large Stokes shift (difference in energy of the absorbance and emission maxima) inherent to phosphorescent materials, one could use emitting heavy element π-systems to eventually achieve stable near IR emission for bioimaging applications.[5]

1.1.1 Methods to Access Triplet Excited States

In photoinduced phosphorescence, initial excitation from a singlet ground state (S_0) to an excited singlet state (or states) ($S_{n\geq1}$) transpires (process 1 in Figure 1.1) and is followed by spin-forbidden intersystem crossing (ISC) to an excited triplet state (T_n) — process 5 in Figure 1.1. The eventual decay (and possible phosphorescence — process 6 in Figure 1.1) from the triplet T_1 state to a singlet ground state (S_0) is also formally forbidden, that is, there is a spin selection rule dictating that the spin of an electron cannot change during an electronic transition. The long lifetime associated with the forbidden triplet excited state leads to a high susceptibility toward emission quenching via triplet-triplet annihilation and reaction with triplet dioxygen.[6]

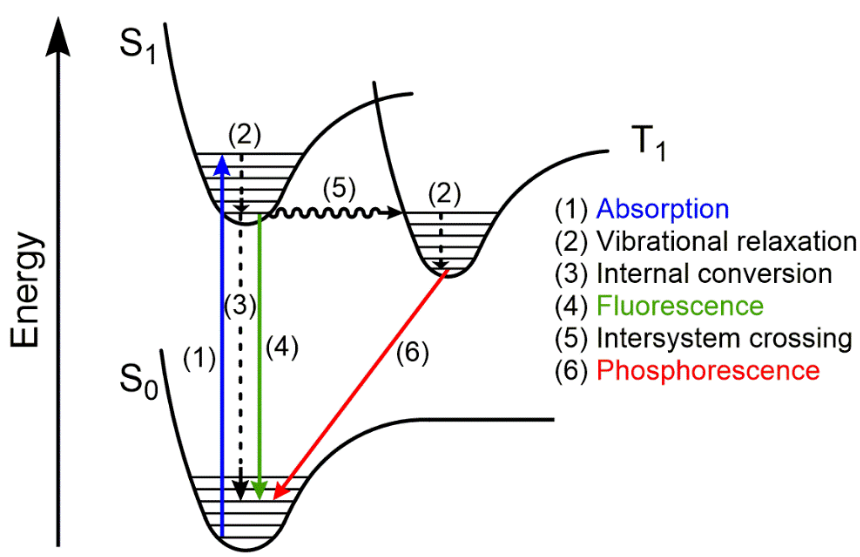

Figure 1.1. Jablonski diagram showing the basic photophysical processes possible upon absorption of a photon by a molecule.

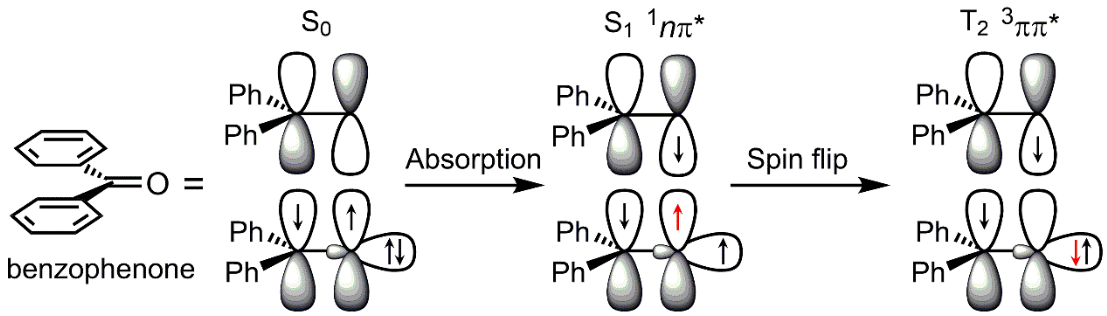

Figure 1.2. An example of intersystem crossing in benzophenone illustrating El-Sayed's rule.

There are several strategies that can be used to achieve efficient intersystem crossing to triplet excited states: 1) El-Sayed's rule states that the rate of intersystem crossing from a singlet to a triplet excited state is increased if the transition occurs between molecular orbitals of different symmetry (*e.g.* $^1\pi\pi^*$ to $^3n\pi^*$ or $^1n\pi^*$ to $^3\pi\pi^*$, see Figure 1.2).[7] This principle has been used to obtain phosphorescence from purely organic compounds such as pyrazines[8] and carbonyl-containing molecules (*e.g.* benzophenone, Figure 1.2).[9] 2) Spin exchange of a radical-ion pair can also lead to population of excited triplet states via a hyperfine coupling-driven intersystem crossing mechanism as is observed in solid isophthalic acid.[10] Herein a singlet radical ion pair is generated by photoexcitation and this singlet pair is converted to a triplet by nuclear spin magnetism-assisted spin conversion; that is, the spin flip is facilitated by the coupling of the nuclear magnetic moments with the magnetic field created by the electrons within the molecule, or the coupling of the nuclear magnetic moments with magnetic field generated by rotations within the molecule.[10] This triplet radical-ion pair then dissociates followed by phosphorescence. 3) The rate of intersystem crossing can be increased by minimizing the energy difference between the lowest singlet excited state and a nearby triplet state (ΔE_{S-T}). ΔE_{S-T} can be decreased by increasing the spatial separation of the HOMO and LUMO through the formation of charge transfer donor-acceptor type species (Figure 1.3). Prominent examples of these donor-acceptor systems include: fluorophore-quencher dyads resulting when carbazole fluorophores and nitrobenzoate[11] (or cyanobenzoate)[12] quenchers are linked through a covalently bound alkyl spacer, or, as for compound **1**, when carbazole donors are attached directly to a benzoate acceptor but with high twist angle between the two moieties (Figure 1.3).[13] Compound **1** adopts a highly twisted conformation (Figure 1.3a) leading to almost complete spatial separation of its HOMO and LUMO (Figure 1.3b). TD-DFT computations have predicted small ΔE_{S1-T2} and ΔE_{S1-T3} energy gaps (less than 0.70 eV), thus **1** is observed to emit by fluorescence as well as longer-lived phosphorescence.[13] 4) The heavy atom effect is the most commonly employed route to obtaining phosphorescent materials. The incorporation of a heavy element facilitates intersystem crossing due to enhanced spin-orbit coupling leading to more effective mixing of excited singlet and triplet states. Most phosphorescent materials that make use of the heavy atom effect rely on the presence of expensive precious metals such as Ir,[14] Pt,[15] Os,[16] and Ru.[16]

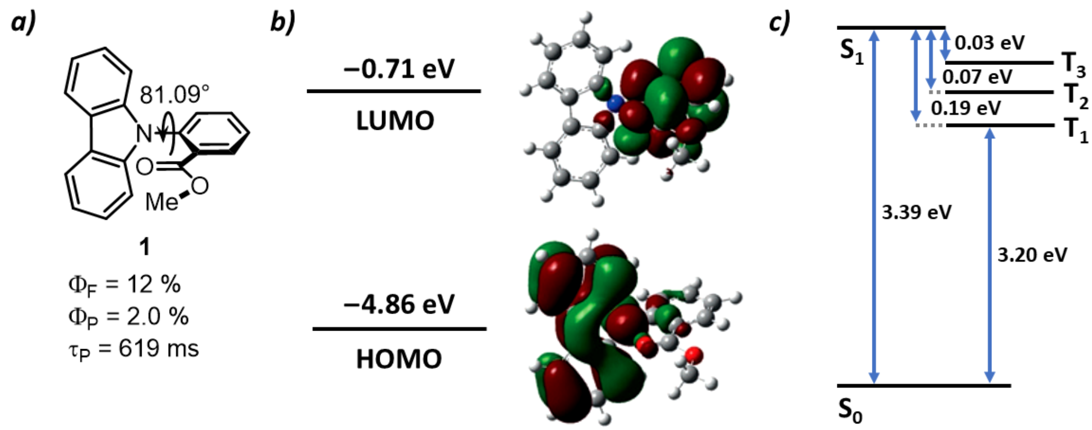

Figure 1.3. a) Structure of emitter **1** (Φ_F = fluorescence quantum yield, Φ_P = phosphorescence quantum yield, τ_P = phosphorescence lifetime); b) DFT computed HOMO and LUMO of **1** showing substantial spatial separation of these orbitals; and c) TD-DFT computed energies of the S_0, S_1, and T_1–T_3 states indicating a small energy difference between S_1 and T_3. Adapted with permission from ref. 13. Copyright (2018) Wiley-VCH.

1.1.2 Challenges that Limit Phosphorescence Quantum Yields

The long lifetime associated with the triplet excited state in phosphorescent materials leads to a high susceptibility toward quenching via non-radiative decay pathways such as triplet-triplet annihilation or quenching of the triplet excited state by molecular oxygen.

Triplet-triplet annihilation occurs when two triplet excited state phosphors interact and combine to create one singlet state annihilator of higher energy and one ground state molecule.[17] The high-energy singlet annihilator can then return to the ground state by emission of a photon (resulting in delayed fluorescence) which is a process known as triplet-triplet annihilation upconversion, or through non-radiative internal conversion during which the excited state energy is lost as heat.[17] A common method to limit triplet-triplet annihilation in the solid state is to design phosphors with sterically bulky peripheral groups, or even building the phosphor into a dendritic framework,[18] to limit the spatial approach of their phosphorescent cores, thereby preventing triplet-triplet annihilation.

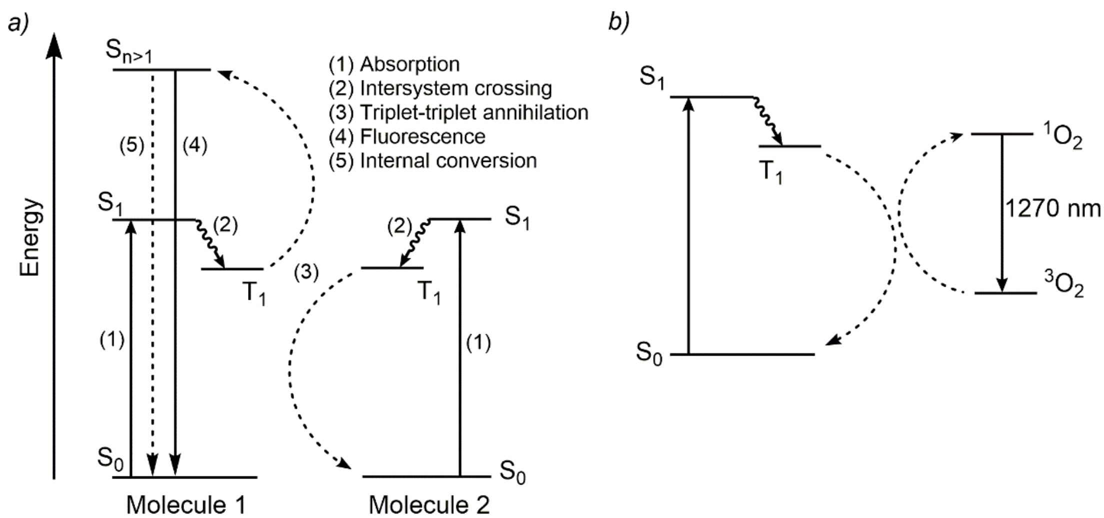

Figure 1.4. Quenching of triplet excited state luminogens by a) triplet-triplet annihilation and b) quenching with molecular oxygen.

In the presence of oxygen, excited triplet state luminogens often undergo diffusion limited collisional quenching with molecular triplet oxygen resulting in the production of excited state singlet oxygen ($^1O_2$) and ground state luminogen.[19] The singlet oxygen is generally short-lived and quickly deactivates via interaction with solvent molecules, emitting its own low energy luminescence (1270 nm), or oxidizes neighbouring molecules.[19]

Phosphorescence quenching by molecular oxygen is often reduced when phosphors are studied in the crystalline state due to the reduced diffusion rate of oxygen through the solid crystal matrix, as observed in thianthrene and carbazolefunctionalize thianthrene, which both display significant phosphorescence in the crystalline state but only fluorescence in aerated solutions or amorphous films (**2** and **3**, Figure 1.5).[20] A similar effect is observed in benzophenone, **4**,[21] and benzophenone-appended carbazoles **5**–**7** (Figure 1.5),[22] in which amorphous films or powders show phosphorescence quenching but phosphorescence emission is enhanced in the crystalline state due to reduced oxygen diffusion through the samples, as well as enhanced rigidity and restricted motion within the molecules.[22]

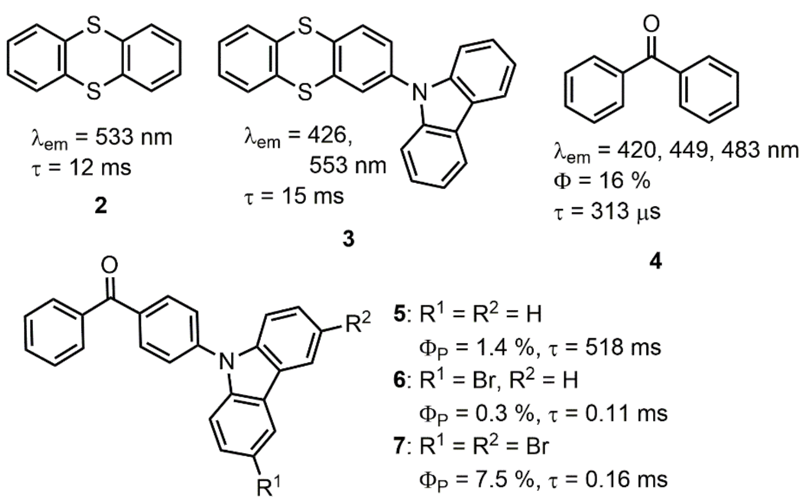

Figure 1.5. Structure of thianthrenes **2** and **3**, benzophenone **4**, and benzophenone-appending carbazoles **5**–**7** (Φ_P = phosphorescence quantum yield, τ = emission lifetime).

A particularly clever way to protect phosphors from oxygen quenching is with cavitands, which are container-like molecules consisting of a cavity that can bind guest molecules providing steric constraint to the trapped guest as well as limiting its contact with molecular oxygen. Cyclodextrans, such as *β*-cyclodextrin, **8** (Figure 1.6) have been employed to enhance the phosphorescence of Pt-based phosphors and prevent oxygen quenching even in solution.[23] Deep-pocket cavitand **9** has been used for the encapsulation of pyrene while providing carboxylate binding sites for Tl^+ cations, this provides protection from oxygen quenching but also makes use of increased spin-orbit coupling (SOC) provided by the heavy Tl^+ cation to enable efficient phosphorescence from the organic pyrene unit, a typical fluorophor.[24]

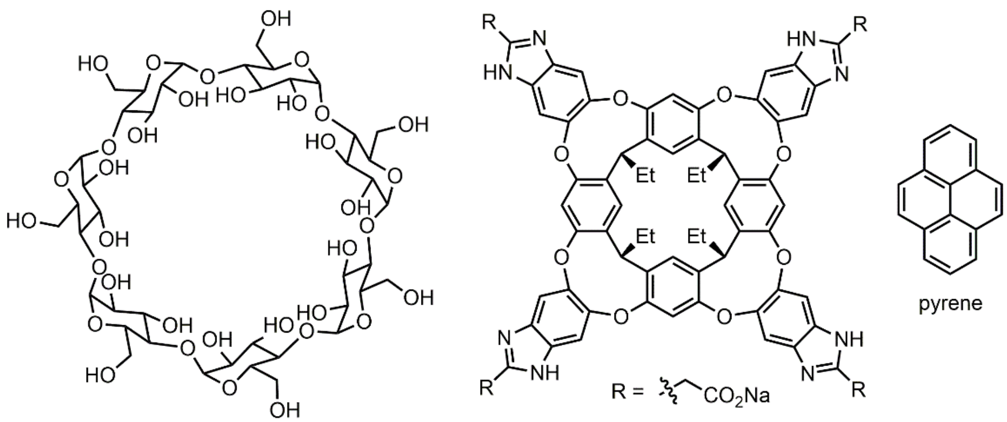

Figure 1.6. *β*-cyclodextran (**8**) and the deep-pocket cavitand **9** which can be used to form binding pockets to protect luminogens from emission quenching by molecular oxygen.

While phosphorescence quenching by molecular oxygen can been considered a hindrance, this phenomenon can also be employed to utilize phosphorescent dyes as oxygen sensors *in vivo* by providing a non-destructive method to detect areas of high and low oxygen concentration in living systems.[25]

1.2 Aggregation Induced Emission

Traditionally, aggregation caused quenching (ACQ) has been a major factor that limits the availability of luminescent materials for OLEDs. Therefore, many emitters must be diluted in a host material to limit self-quenching, which complicates device fabrication as the problem of phase separation of emitter and host must be managed.[26] Moreover if one is seeking to develop luminescent dyes for bioimaging, self-quenching of the luminogens upon localization in a cell can dramatically reduce emission intensity. As a result, the search for new emitters that are resistant to self-quenching has gained tremendous momentum over the last two decades. Interestingly, materials that exhibit luminescence in the solid state but not in solution have been known for more than a century,[27] as Sir George Stokes reported observations on platinocyanides that emit a "brilliant green" in the solid state but in solution "look like mere water".[27a] The term aggregation induced emission (AIE) was first introduced by Ben Zhong Tang and coworkers in 2001 to describe systems that emit much more strongly in the condensed phase versus in solution.[28] Tang's study of 1-methyl-1,2,3,4,5-pentaphenylsilole [$Ph(Me)SiC_4Ph_4$], **10**, which displays strong fluorescence in the solid state but only extremely weak emission in solution, set the stage for a resurgence in activity in this field.[28]

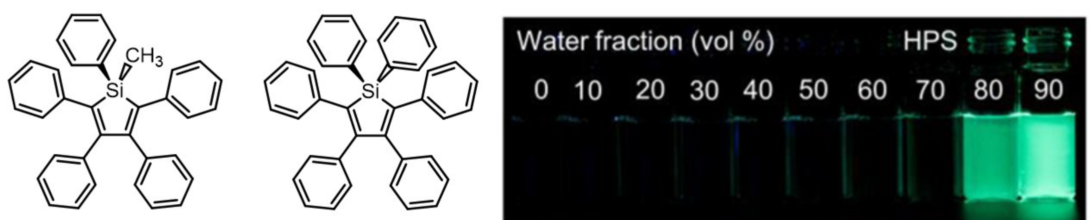

10 11

Figure 1.7. Structure of Ben Zhong Tang's siloles **10** and **11** (left) and fluorescence photographs of solutions or suspensions of hexaphenylsilole (HPS) (**11**; 20 μM) in THF/water mixtures with different fractions of water. Adapted with permission from 31a. Copyright (2015) American Chemical Society.

The most widely accepted explanation for the AIE phenomenon is that upon aggregation of the molecules, intramolecular motions are restricted which concomitantly reduce the rates of non-radiative decay; the reader is directed to review articles by Tang and coworkers which cover many aspects of AIE.[29] Hexaphenylsilole, **11**, has been utilized repeatedly as an example of an AIEgen.[30] Consisting of a silole core appended by six phenyl rings, **11** adopts a propeller-like conformation in which the peripheral phenyl rings adopt large torion angles (30–70°) relative to the central silole plane. The result of this conformation is that the central silole rings of neighbouring molecules cannot undergo close approach, even in the solid state. Thus solid crystals or aggregates of **11** cannot undergo chromophore interactions, such as π-π stacking, which are typically known to contribute to aggregation caused quenching effects in less sterically encumbered planar emitters such as perylene.[31] Additionally, **11** possesses many inter- and intramolecular C–H···π interactions that function to lock the peripheral phenyl rings in place and limit rotations about the exocyclic silole-phenyl bonds in the solid state, an effect which is significant as it is believed that these rotational motions provide the main non-radiative pathway for quenching excited state **11** in solution.

Aggregation induced emission has also been observed in molecule emitters that have no rotatable functional groups, such as dibenzocyclooctatetraene-based emitters **12** and **13**.[32] In solution, **12** and **13** have significant flexibility along their backbones of fused rings as they can interconvert from boat to chair-type conformations (Figure 1.8b). In the crystalline state, compounds **12** and **13** become emissive due to the inability to undergo conformation changes due to the steric restraint imparted by solid-state packing; the lack of planarity along the backbone of the molecules also functions to prevent π-π stacking interactions between the cores of neighbouring molecules.

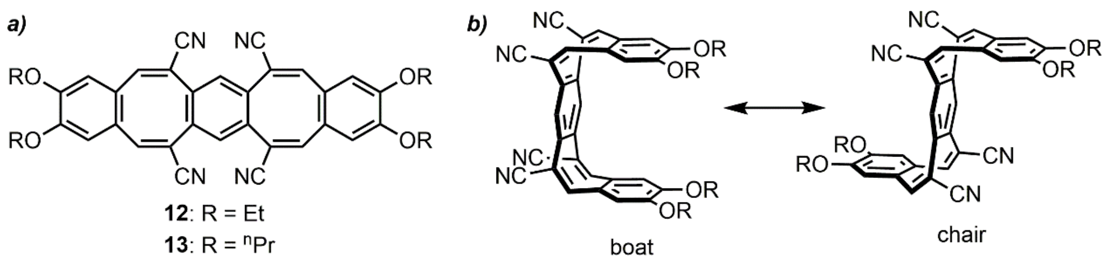

Figure 1.8. a) Structure of dibenzocyclooctatetraene-based emitters **12** and **13** and b) boat versus chair conformations of **12** and **13**.

Additionally, many AIE emitters have been observed to undergo an enhancement in emission intensity upon freezing initially non-emissive solutions into solid glass matrices, or by increasing solution viscosity by the addition of viscosity enhancers like glycerol, lending further support to the hypothesis that intramolecular motions are generally the main route to quenching in solution for these emitters.[33]

Since 2001 there have been an astounding number of molecules and polymers developed that exhibit aggregation induced emission, and the resulting AIEgens have found applications in bioimaging,[34] explosives detection,[35] fingerprint visualization,[36] and in OLEDs.[37]

1.2.1 Aggregation Induced Phosphorescence in the Main Group

While there has been a plethora of aggregation induced emissive fluorophors reported to date,[38] a review of the literature yields far fewer examples of molecules that undergo aggregation induced phosphorescence. There have been great recent reviews on organic AIE phosphors[39] and transition metal-based AIE phosphors[40] to which the reader is referred.

1.2.1.1 Lead-, Bismuth-, and Antimony-Based AIE Phosphors

Early reports by Strasser and Vogler described the phosphorescent behaviour of a series of Pb-, Tl-, and Bi-based β-diketonate complexes **14**–**20** (Figure 1.9).[41,42] The authors noted that the emission intensity of **14** and **15** increased drastically in the solid state or upon encapsulation in a polyester resin matrix when compared to in acetonitrile solution. While the bismuth complex **16** was observed to be emissive in the solid state, it decomposed in solution. The lead(II) congeners **17–20** showed only weak emission in ethanol or 2-methyl tetrahydrofuran (2-MeTHF) at room temperature but this emission was enhanced significantly in a frozen 2-MeTHF glass at 77 K. Upon excitation at 300 nm in the solid state, the Pb(II), Tl(I), and Bi(III) complexes **14**, **15**, and **16** each show emission maxima (λ_{em}) at *ca.* 470 nm. Interestingly, solid samples of **18** and **20** showed both fluorescence (at λ_{em} = 448 and 418 nm, respectively) as well as phosphorescence at *ca.* 500 nm at room temperature. Compound **19** did not exhibit any luminescence in the solid state while **17** displayed a strikingly different solid-state emission spectrum at room temperature, with a broad emission band profile at 525 nm that extends up to 700 nm (attributed to excimer-based emission). While no quantum yields were reported, the authors emphasized that there is a significant enhancement of luminescence in the solid state due to suppression of molecular motion.

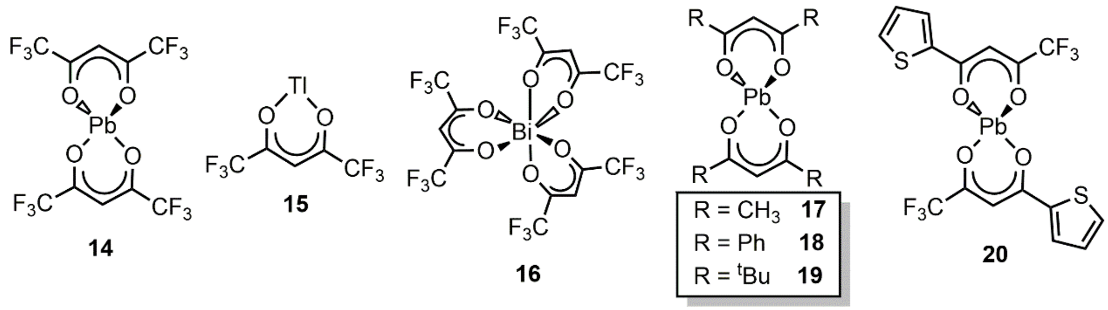

Figure 1.9. Complexes of Pb-, Tl-, and Bi-based *β*-diketonate emitters **14**–**20**.

Bismuth is unique in that it is a heavy enough element to make use of the heavy element effect but also has been found to have low toxicity compared to the heavy elements that surround it on the Periodic Table.[43] Thus achieving phosphorescence by incorporation of this element into molecules is of great interest for various applications, such as in OLEDs and for bioimaging.[44]

Mercier and coworkers reported three different bismuth(III) coordination complexes based on the cationic viologen ligands *N*-methyl-4,4′-bipyridinium (hMV^+) and *N*-methyl-*N*′-oxide-4,4′-bipyridinium (MVO^+): (hMV)[Cl_5Bi(hMV)] (**21**), [Cl_4Bi(MVO)(dmso)]·dmso (**22**), and [Br_4Bi(MVO)(dmso)]·dmso (**23**) (Figure 1.10).[45] Compounds **21–23** yield bright yellow-orange phosphorescence in the solid state (λ_{em} = 545 to 560 nm; quantum yield (Φ) = 5–10 %) in air and the viologen ligands themselves are only weakly fluorescent in the blue region, indicating an active role of the Bi(III) centers in attaining phosphorescence. Of added interest, photoinduced charge transfer processes resulting in photochromism were noticed in (hMV)[Cl_5Bi(hMV)] (**21**).

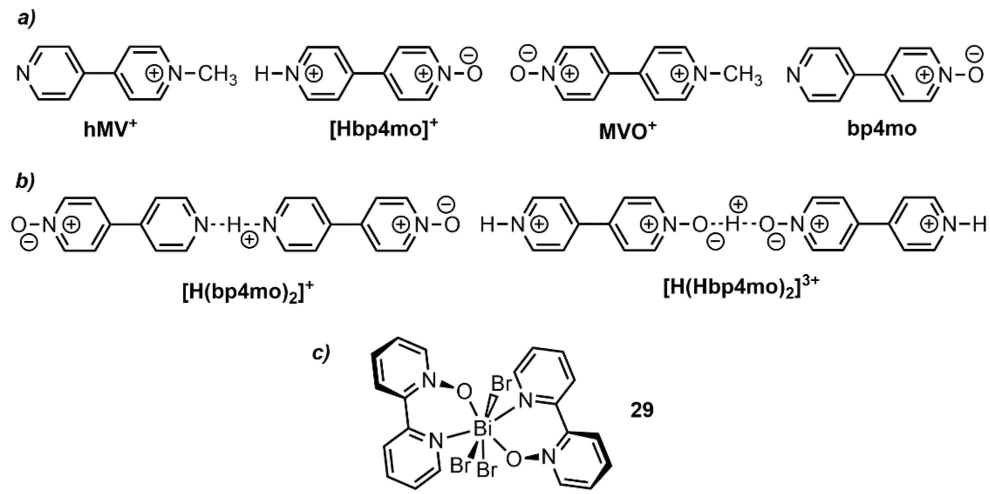

Figure 1.10. a) and b) Cationic violagen ligands utilized for the synthesis of phosphorescent bismuth (III) coordination complexes and, c) the phosphorescent bismuth complex $Br_3Bi(bp2mo)_2$ (**29**).

The Mercier group also prepared the following Bi(III) coordination complexes featuring proton-linked violagen cations $[H(bp4mo)_2]^+$ and $[H(Hbp4mo)_2]^{3+}$ (Figure 1.10b): $[H(bp4mo)_2][BiCl_4]$ (**24**), *ap*-$[(Hbp4mo)_2Bi_2Cl_8]$ (**25**) where the $[H(bp4mo)_2]^+$ cations are bound to the apical sites of the Bi centers, *eq*-$[(Hbp4mo)_2Bi_2Br_8]$ (**26**) where the $[H(bp4mo)_2]^+$ cations are bound to the equatorial sites of the Bi centers, $[Br_4Bi(Hbp4mo)]$ (**27**), and $[H(Hbp4mo)_2][BiCl_6]\cdot$dmso (**28**).[46] While complexes **24** and **28** were non-emissive as solids, complexes that contained bismuth coordinated to the $Hbp4mo^+$ cations through Bi···O interactions were found to exhibit phosphorescence (λ_{em} = 560 nm for **25**, and 530 nm for each **26** and **27**). As for **21**–**23** (*vide supra*), the yellow phosphorescence in compounds **25**–**27** is thought to arise from metal-to-ligand charge transfer processes and **25** was shown to have a quantum yield of 11 %, which was explained by the presence of a packing arrangement in **25** that reduces intermolecular contacts between neighboring organic moieties.[46]

The same group prepared a bismuth(III) tribromide complex of *N*-oxide-2,2′-bipyridine (bp2mo), [$Br_3Bi(bp2mo)_2$] (**29**, Figure 1.10c).[47] Only weak fluorescence was observed for **29** in THF solution (λ_{em} = 442 nm, Φ = 0.01 %, lifetime (τ) = 258 ps), however in the solid state three phosphorescent crystalline polymorphs complexes could be obtained, *α*-**29**, *β*-**29**, and *γ*-**29**. The three polymorphs afford similar absorbance spectra (λ_{max} = 392–395 nm), assigned based on time-dependent density functional theory (TD-DFT) as HOMO ($BiBr_3$ centered) to LUMO (ligand) transitions. Solid state luminescence measurements revealed that polymorph *α*-(**29**) has the most efficient emission (Φ = 17 %, λ_{max} = 525, τ = 4.8 μs), with polymorph *γ*-**29** exhibiting slightly lower efficiency (Φ = 5 %, λ_{max} = 503 nm, τ = 1.0 μs). The moderately phosphorescent *α* and *γ* polymorphs of **29** have stronger intermolecular C–H···O and C–H···π hydrogen bonds in relation to the *β* form, thus leading to a more rigid environment in the former complexes.[47]

Mercier and coworkers also reported two different bismuth coordination polymers that both exhibit aggregation induced phosphorescence (AIP) and mechanochromic luminescence (MCL): ($^{n}Bu_4N$)[$Br_4Bi(bp4mo)$] (**30**) and [$Br_3Bi(bp4mo)$] (**31**) where bp4mo is *N*-oxide-4,4'-bipyridine (Figures 1.11 and 1.12).[48]

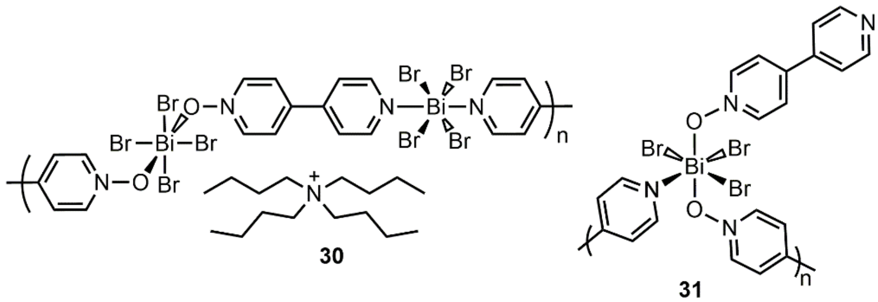

Figure 1.11. Complexes ($^{n}Bu_4N$)[Br_4Bi(bp4mo)] **30** and [Br_3Bi(bp4mo)] **31**.

Compound **30** forms a linear 1D coordination polymer with *N*-oxide-4,4'-bipyridine (bp4mo) ligands bridging each Bi center (Figure 1.12a) with the $^{n}Bu_4N^+$ cations occupying the void spaces resulting in no close Bi–Bi distances. Conversely, in the 1:1 complex [Br_3Bi(bp4mo)] (**31**), a density packed interconnected structure is observed (Figure 1.12b). Both **30** and **31** yield similar absorption profiles in the solid state (λ_{max} = 415 nm and 410 nm, respectively), identified as a charge transfer process from a $BiBr_x$ unit to a bp4mo ligand. In THF, **30** and **31** displayed weak blue fluorescence (Φ = <0.1 %, τ = *ca.* 10 ps), however in the solid state a dramatic increase in phosphorescence quantum yield was found: for **30**, λ_{em} = 550 nm, Φ = 85 %, τ = 18 μs; for **31**, λ_{em} = 510 nm, Φ = 15 %, τ = 1 μs. This finding suggests that the presence of Bi results in efficient intersystem crossing to generate excited triplet states; these long-lived states are quenched in solution by free intramolecular motions that are greatly hindered in the solid phase. The difference in quantum yield between **30** and **31** is likely due to the extra spacing between Bi centers in **30** which could limit triplet-triplet annihilation.[48]

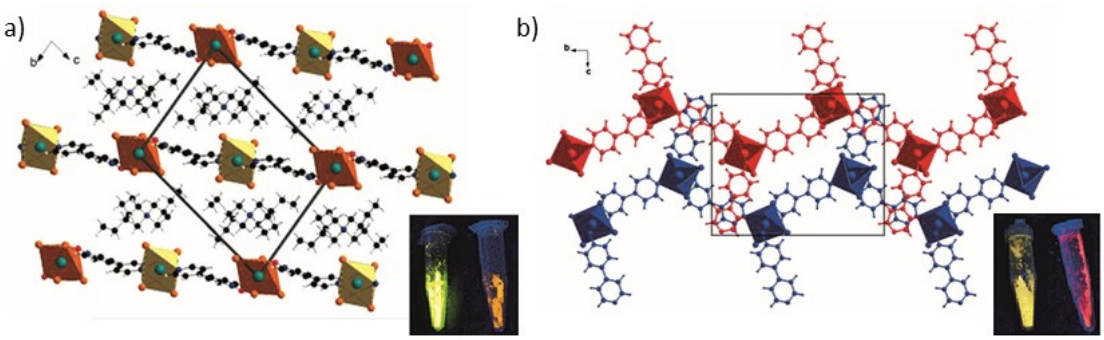

Figure 1.12. Crystal structures of ($^{n}Bu_4N$)[Br_4Br(bp4mo)] **30** (a) and [Br_3Bi(bp4mo)] **31** (b) with insets showing emission before and after grinding under UV light. Adapted with permission from ref. 48. Copyright (2016) Wiley-VCH.

Both compounds **30** and **31** showed pronounced red-shifts in emission upon grinding (Figure 1.12 insets), but this emission change could be reversed by heating the samples above their crystallization temperature of 80 °C or exposing the ground samples to a saturated water atmosphere for a few hours (complete reversal for **30** and partial reversal for **31**).[48] The origin of the mechanochromic luminescence in **30** and **31** was tentatively assigned to a change in the crystal packing by changing the pattern of hydrogen bonding and/or π-π interactions.

Crystallization enhanced phosphorescence was also found within a series of Pb(II) complexes with *N*-oxide-4,4'-bipyridine ligands, PbX_2(bp4mo) (X = Cl or Br, **32** and **33**). The nitrate analogue $Pb(NO_3)_2$(bp4mo) (**34**) afforded a high phosphorescence quantum yield (Φ) of 34 %.[49] The solid state emission in these Pb(II) complexes was quenched upon grinding the crystals, but emission could be recovered upon recrystallization via a heating/cooling cycle.

Huang and coworkers prepared the phosphorescent antimony- and bismuth-based imidazolium salts $[Bmim]_2SbCl_5$ (**35**) and $[Bmim][Cl_4Bi(bipy)]$ (**36**) (bipy = 2,2'-bipyridine) (Figure 1.13).[50,51] Compound **35** forms a supramolecular network in the solid state constructed by hydrogen bonding and anion-π interactions between the $[SbCl_5]^{2-}$ anions and the imidazolium $[Bmim]^+$ cations. The intense phosphorescence of **35** at 583 nm in the solid state (λ_{ex} = 370 nm, Φ = 86 %, τ = 4 μs) was assigned as chlorine-to-antimony charge transfer within the $[SbCl_5]^{2-}$ anion. Two different polymorphs of **36** (*α* and *β*) were crystallized and each showed efficient phosphorescence in the solid state at room temperature (*α*-form: 530 nm, Φ = 26 %; *β*-form: 524 nm, Φ = 37 %) with short phosphorescence lifetimes of 8 and 13 μs, consistent with significant mixing of singlet and triplet excited states due the heavy atom effect. Compounds **35**, *α*-**36**, and *β*-**36** were found to be sensitive to the rigidity of the system as full quenching of emission was noted upon melting.

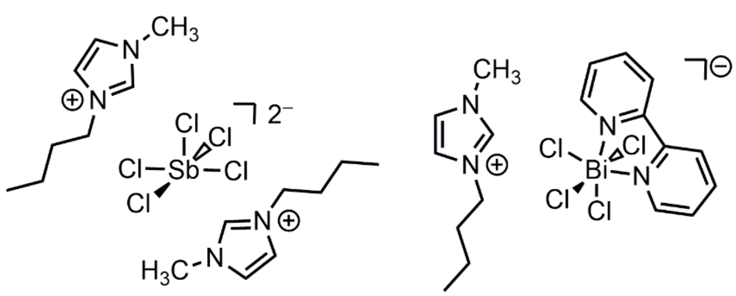

35 **36**

Figure 1.13. Sb- and Bi-based phosphorescent imidazolium (Bmim) salts **35** and **36**.

1.2.1.2 Tellurium-Based AIE Phosphors

The Rivard group began working with tellurophene polymers for the development of new photovoltaic materials.[52] However, it was discovered serendipitously that the bis(pinacolato)tellurophene monomer **37** exhibited aggregation induced phosphorescence in THF/water mixtures (Scheme 1.1 inset). In addition, bright green phosphorescence was noted in the solid state at room temperature in the presence of water and oxygen (535 nm, Φ = 12 %, τ = 166 μs).[53]

The emission in **37** was completely quenched when the Te center was oxidized with Br_2 to form the Te(IV) heterocycle **38** (Scheme 1.1), indicating an active role played by the tellurium(II) center in the phosphorescence of **37**. Coordination of *N*-heterocyclic carbenes (NHC) to the Lewis acidic pinacolboronate (BPin) groups yielded **39** and **40** (Scheme 1.1).[54] Upon coordination of an NHC to both boron centers in **37**, producing **40**, luminescence was shut down entirely. Upon monocoordination, phosphorescence was maintained and the resulting compound, **39**, yielded yellow phosphorescence (λ_{em} = 555 nm, Φ = 1.3 %) from drop-cast films in air.

The effects of film morphology on phosphorescence was studied by measuring the luminescence of films of **37** that had been produced by drop-coating, spin-coating, and thermal evaporation.[55] It was found that samples produced via drop-coating yielded the highest quantum yield (Φ = 12 %) compared to the other methods of films production (Φ = 3.4 % for thermally evaporated film and Φ = 1.7 % for a spin-coated film). The increase in quantum yield correlated with enhanced crystallinity in the films, which presumably reduces oxygen diffusion and quenching in air.[55]

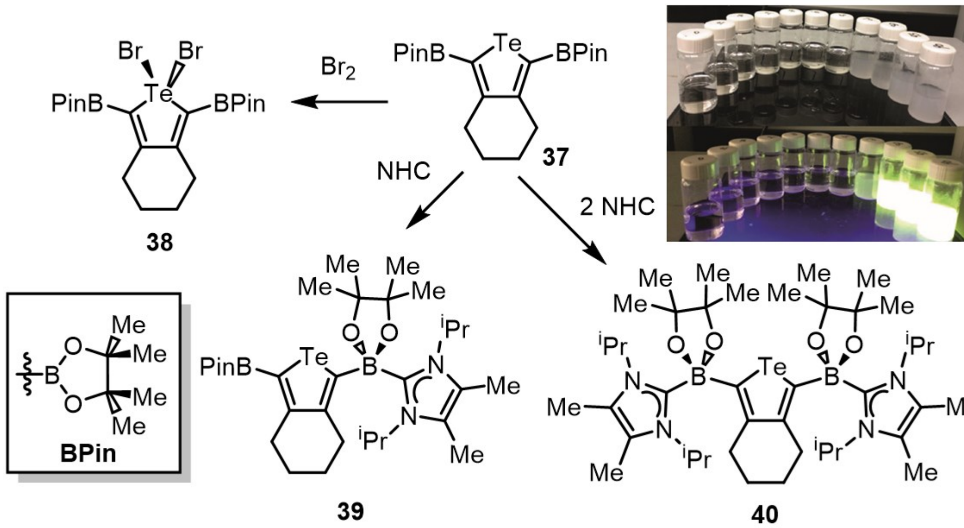

Scheme 1.1. Representative reactivity involving the phosphorescent tellurophene **37**. Inset: aggregation induced phosphorescence of **37** upon addition of water to THF solutions (600 μM **37**, excitation at 365 nm). Adapted with permission from ref. 53. Copyright (2014) Wiley-VCH.

The perborylated tellurophene **41** (Figure 1.14)[53,56] yields the highest solid-state phosphorescence quantum yield for a tellurophene thus far (Φ = 24 %, green emission at 516 nm), and also exhibits both fluorescence (λ_{em} = 420 nm) and phosphorescence in thoroughly degassed solvent (λ_{em} = 570 nm, Φ = 6 % in methylcyclohexane, τ = 10.8 μs).[56] These findings indicate that **41** exhibits emission quenching both by oxygen and intramolecular rotations/vibrations in solution.

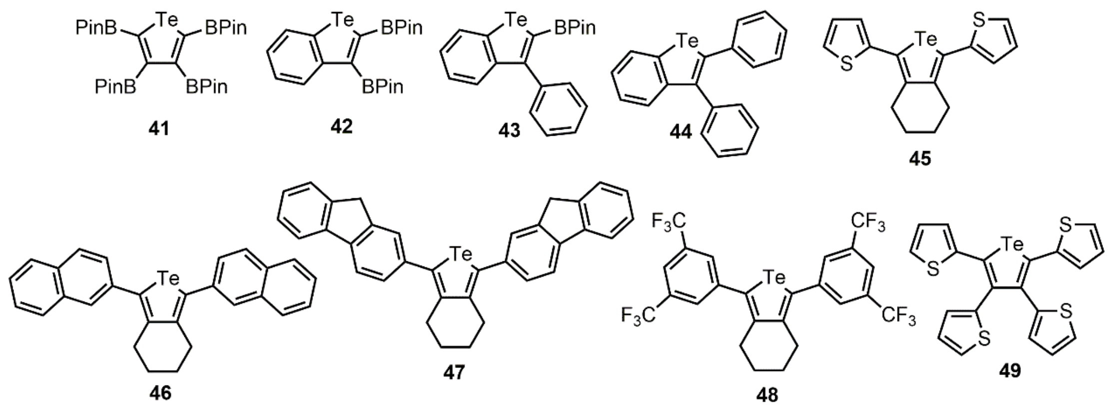

Figure 1.14. a) Initial tellurophenes and benzotellurophenes examined as AIPgens. b) Arylated tellurophenes explored for possible color tuneable phosphorescence in the solid state.

Benzotellurophenes **42**, **43**, and **44** (Figure 1.14) were found to exhibit green phosphorescence in the solid state in air (**42**: λ_{em} = 532 nm, Φ = 1.3 %, τ = 6.1 μs); however, **43** and **44** displayed such weak emission that phosphorescence quantum yields could not be measured.

TD-DFT computations indicate that emission from **37** and **41** requires promotion of an electron from an orbital with lone pair character at the Te atom to an orbital with C–B π-interactions. Moreover, it was found that in many of the emissive tellurophenes, the excited state singlets (S_1 and S_2) were within 0.05 eV of excited triplet states (T_n) thus enabling intersystem crossing to occur. Notably, when the BPin groups were substituted for thiophene (as in **45**) no emission was observed, despite favorable S_n–T_n excited state energy differences (*vide infra*). Despite this evidence that the presence of an uncoordinated BPin group adjacent to the Te was necessary to achieve phosphorescence in tellurophenes, a series of BPin-free phoshoprescent tellurophenes could be synthesized via Suzuki-Miyaura cross-coupling with compound **37**.[56] Accordingly, the naphthalene- (**46**), fluorene- (**47**), and 3,5-bis(trifluoromethyl)phenyl-substituted (**48**) tellurophenes (Figure 1.14) were prepared in moderate yields.[56] While **46** and **47** needed to be cooled to 77 K in order to observe weak phosphorescence (**46**: λ_{em} at 588 nm and 634 nm, and **47**: λ_{em} = 633 nm), the fluoroaryl-capped tellurophene **48** showed bright yellow phosphorescence (λ_{em} = 595 nm, Φ = 9.5 %, τ = 29.3 μs) in the solid state at room temperature (in air). TD-DFT computations were conducted on a range of species (including the non-emissive thienyl-capped tellurophene **49**) and it was noticed that in the tellurophenes that showed phosphorescence, excitation always involved orbital participation from Te. In the case of the non-emissive tetrakis(thienyl)tellurophene **49** (Figure 1.14), minimal orbital participation from Te in the excitation process leads to a reduction of spin-orbit coupling and much less efficient ISC (and a lack of observed phosphorescence); this trend is significant because it gave rise to a similar hypothesis pertaining to bismole molecules reported in Chapters 2 and 3.

Bonifazi and coworkers reported the phosphorescent azabenzotellurophenes **50**, **51**, and **52** (Figure 1.15).[57,58] Emission of **50** and **51** (λ_{em} = 590 and 640 nm, τ = 9.7 μs for **50**, and λ_{em} = 589 and 649 nm, τ = 3.9 μs for **51**) was quenched in the solid state due to the formation of aggregates facilitated by Te···N secondary bonding interactions; however, compound **52**, with R = 2-pyridyl, displayed phosphorescence in the solid state (λ_{em} = 535 nm, τ = 11 μs).

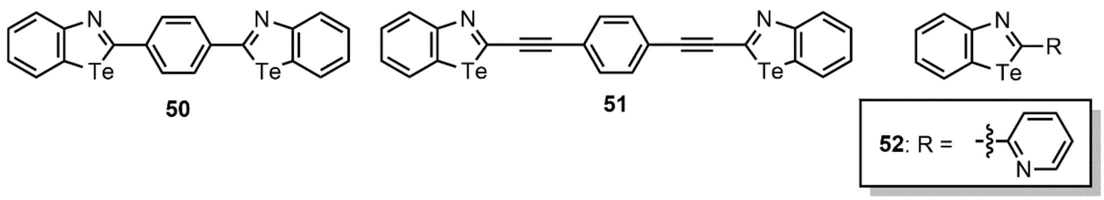

Figure 1.15. Phosphorescent azabenzotellurophenes **50–52**.

1.2.1.3 Boron-, Phosphorus-, and Sulfur-Based AIE Phosphors

While implementation of the heavy element effect remains a reliable method for turning on phosphorescence in π-conjugated materials, there have been recent examples of lighter main group element-based emitters that exhibit aggregation induced phosphorescence.

Phenylboronic acids undergo phosphorescence via a hyperfine coupling-driven intersystem crossing mechanism much like isophthalic acid.[10,59] Crystalline samples of boronic acid derivatives **53–55** (Figure 1.16) were observed to emit ultramarine under illumination with a hand-held UV lamp, however a pale blue emission was then visible for seconds after the UV lamp was turned off.[59] All three molecules were found to exhibit emission via dual delayed fluorescence (DF) and phosphorescence (P) in the solid state (λ_{ex} = 254–287 nm, λ_{em_DF} = 322–331 nm, τ_{DF} = 0.35–0.55 s, τ_{P} = 0.95–1.6 s). The quantum yield of **54** (66 %) was much greater than that of **53** (18 %).

TD-DFT computations of dimers and trimers of **54** revealed that charge transfer transitions from the occupied HOMO–4 orbital of one molecule to the vacant LUMO+1 orbital of a second molecule seem to be facilitated by the boronic acid group of a third molecule which explains why **53**, with only one boronic acid group, has a less intense emission than **54** and **55**. Further evidence for this mechanism arose from the observed decrease in quantum yields of **56**, **57**, and **58** (44 % for **56**, 35 % for **57**, not detectable below a lifetime of 75 ms for **58**) relative to **54** (Φ = 66 %). The authors proposed that the decreased quantum yields of **56**, **57**, and **58** are correlated with increasing steric bulk at the boronic ester which limits close packing interactions required to achieve the abovementioned intermolecular electron transfers in the crystal lattice that are necessary for emission.

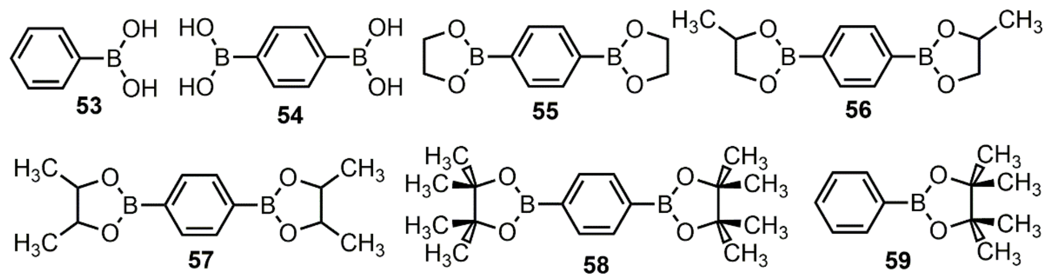

Figure 1.16. Structures of boronic acid derivatives **53–59**.

Interestingly, the arylboronic ester **58** (Figure 1.16) was later discovered to display room temperature phosphorescence.[60] **58** was found to show both blue fluorescence at 305 nm (τ = 8 ns) as well as an extremely long-lived green phosphorescence (460 nm and 500 nm, τ = 1.9 s, Φ = 2 %) in the solid state when excited at 240 nm. Phosphorescence was quenched upon exposure of a ground powder of **58** to oxygen or when **58** was dissolved in ethanol. The solid-state packing structure of **58** was found to lack close intermolecular contacts between the central phenylene rings presumably due to the steric bulk of the BPin groups. The monoborylated arene Ph-BPin (**59**) was found to have similar emission properties as **58** (λ_{em} = 465 nm, λ_{ex} = 245 nm, τ = 1.8 s). TD-DFT calculations were conducted to compare the photophysical properties of **59** to benzene. The nature of the excitation was observed to be π to π* (S_1) while a π to π* transition to give an S_2 state was also allowed for **59** but symmetrically forbidden for benzene. While benzene only shows π and π* orbital contributions to its excited states, compound **59** features substantially different orbital participation in the T_1 state. Specifically, the calculated geometry of the T_1 state in **59** was found to exhibit a significant out-of-plane distortion of the PinB-C_{ipso} moiety and the authors hypothesized that this out-of-plane distortion facilitates the mixing of π and σ* orbitals, leading to increased spin-orbit coupling and enhanced intersystem crossing.

A pair of aromatic thioethers, **60** and **61** (Figure 1.17), were observed to display phosphorescence at 556 nm and 544 nm with lifetimes of 4.95 and 0.87 μs respectively.[61] Degassed dispersions of **60** and **61** did not have increased emission intensity (but did display a slight increase in emission lifetime), suggesting that the aggregates exhibit highly dense packing that limits oxygen diffusion within the particulates. The HOMO-LUMO transitions in **60** and **61** were computed (TD-DFT) to be n(S)→π*(dicyanobenzene) in character, and the authors hypothesize that a fast multiplicity change enabled by the availability of non-bonding electrons allows intersystem crossing as described by El-Sayed's rule.

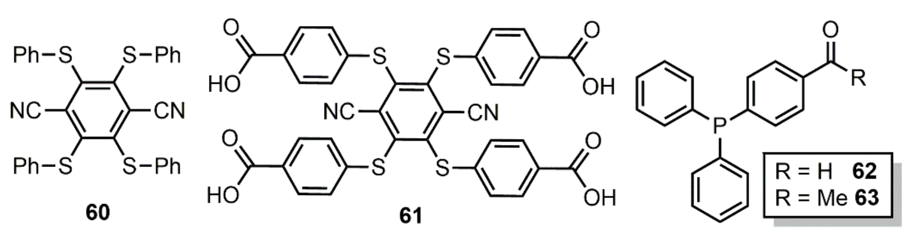

Figure 1.17. Structures of light main group element-based AIP emitters **60–63**.

While phosphorus-containing compounds are no strangers in the world of fluorescence, an interesting report from 2016 highlights the use of phosphorus in the synthesis of phosphorescent emitters.[62] Specifically, the authors report the synthesis and characterization of two different triphenylphosphine derivatives, one with a formyl moiety (**62**) and another with an acetyl moiety (**63**) (Figure 1.17). These carbonyl substituents were chosen specifically to promote intersystem crossing from excited singlet $^1n\pi^*$ to triplet $^3\pi\pi^*$ states (see section 1.1.2). There was no shift in absorption or emission maxima in **62** or **63** upon change of solvent (THF, CH_2Cl_2, and toluene) indicating a lack of charge transfer character. In methylcyclohexane solutions under an N_2 atmosphere, both weak fluorescence (387 and 382 nm for **62** and **63**, respectively) and phosphorescence (544 and 533 nm for **62** and **63**, respectively) transpired, with phosphorescence efficiencies around 1 %. However, efficient orange emission (Φ = 7.1 %, λ_{em} = 555 nm, and τ = 6.9 μs) for **62**, and strong green emission (Φ = 27 %, λ_{em} = 516 nm, τ = 306 μs) for **63** was noted in the solid state. The enhanced phosphorescence in the crystalline state was attributed to the presence of J-aggregates and conformational rigidification.

1.3 Metallacycle Transfer

1.3.1 Synthesis of Zirconacyclopentadienes

The synthesis of the first zirconacyclopentadiene, tetraphenylzirconacyclopentadiene **64**, was reported in 1961 by Braye *et al.* via the reaction of 1,4-dilithiotetraphenylbutadiene with zirconocene dichloride (Cp_2ZrCl_2) to generate **64** as an orange, crystalline product (Scheme 1.2).[63] In 1974, a report by Alt and Rausch[64] described the cyclization reaction occuring when Cp_2ZrMe_2 is photolyzed to produce $Cp_2Zr(II)$ (and methyl radical byproducts) which then undergoes reaction with two equivalents of diphenylacetylene to produce **64** — this latter reaction set the stage for future studies involving low valent "Cp_2Zr" precursors that are capable of cyclization with a range of alkynes.[65]

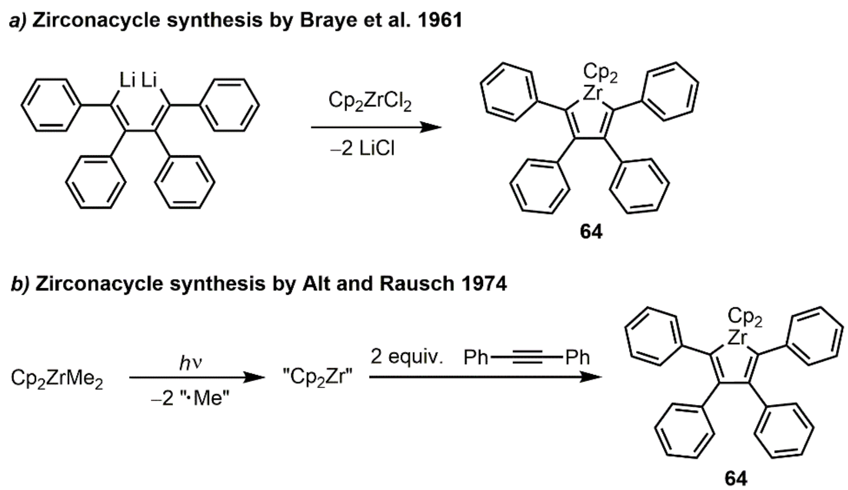

Scheme 1.2. Synthesis of tetraphenylzirconacyclopentadiene/$Cp_2ZrC_4Ph_4$ (**64**) via: a) dilithiumtetraphenylbutadiene with zirconocene dichloride, and b) Cp_2ZrMe_2 photolyzed in the presence of diphenylacetylene.

Two of most common routes to $Cp_2Zr(II)$ species are Negishi's reagent (Cp_2ZrBu_2)[66] and Rosenthal's reagent [$Cp_2Zr(Me_3SiCCSiMe_3)$(pyridine)].[67] Rosenthal's reagent consists of a $Cp_2Zr(II)$ center that is stabilized by pyridine and bis(trimethylsilyl)acetylene ligands that can be displaced to allow for the binding and cyclization of other alkynes upon heating. Negishi's reagent is unstable at room temperature and has been found to decompose via a variety of pathways to form species that act like naked $Cp_2Zr(II)$ as described in Scheme 1.3. Harrod and coworkers reported an in-depth NMR spectroscopic study of this decomposition process and found evidence for the pathway described in Scheme 1.3.[68]

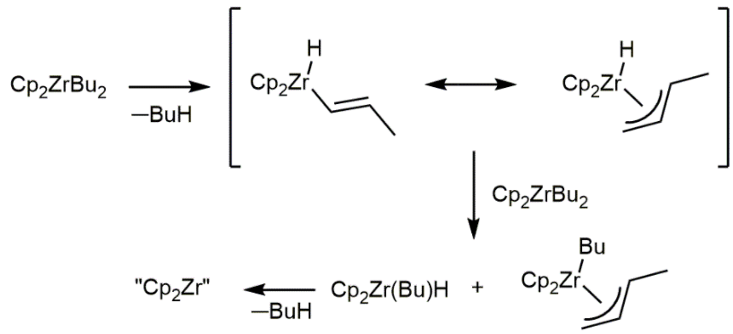

Scheme 1.3. One decomposition pathway to produce "Cp_2Zr" from Negishi's reagent, Cp_2ZrBu_2.

Scheme 1.4a shows the general mechanism for the formation of R-subsituted zirconacyclopentadienes from *in situ* generated $Cp_2Zr(II)$, which is believed to occur in a stepwise fashion.[69] This general cyclization reaction has been found to be tolerant to a variety of R-groups, but the cyclization reaction is sensitive to both the steric and electronic properties of the R-groups.[69] That is, $Cp_2Zr(II)$ can be cyclized with unsymmetric alkynes with control over regioselectivity. Electron-withdrawing substituents have a tendency towards substitution at the β-position of the zirconacycle ring (Scheme 1.4),[69a] and α-directing groups tend to be more sterically hindered;[70] however, when the steric bulk becomes too high, as for mesityl (Mes = 2,4,6-$Me_3C_6H_2$), then β-directing selectivity is observed.[71]

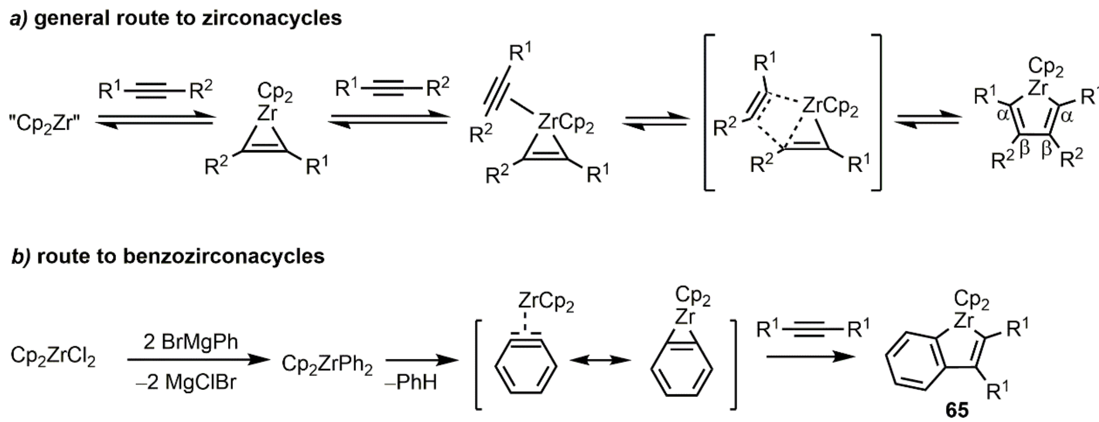

Scheme 1.4. (a) Stepwise mechanism for the formation of zirconacycles from two equivalents of unsymmetrical alkyne. (b) Mechanism for the formation of benzozirconacycles via a benzyne intermediate.

When Cp_2ZrPh_2 is heated, it undergoes an elimination reaction to release benzene and, in the presence of alkynes, forms substituted benzozirconacycles **65** (Scheme 1.4b). Buchwald and coworkers reported a trapping experiment in which the trimethylphosphine adduct of a zirconocene-benzyne $Cp_2Zr(C_6H_4)PMe_3$ was isolated, indicating that the benzozirconacycle formation likely proceeds via a benzyne intermediate.[72]

1.3.2 Metallacycle Transfer and the Fagan-Nugent Reaction

In 1988, Fagan and Nugent reported the first examples of the synthesis of p-block heterocycles via the direct reaction of zirconacyclopentadienes with element halides, as shown in Scheme 1.5.[73] As reported in this original paper and further discussed in a follow-up report,[74] this general transmetallation approach worked efficiently for at least a dozen different p-block element examples but was observed to be slower for the synthesis of stannoles and siloles. For stiboles and bismoles, metallacycle transfer was first performed with $SbCl_3$ and $BiCl_3$ respectively to generate the chloro-heterole before further substitution at the E atom was performed with PhLi (Scheme 1.5).

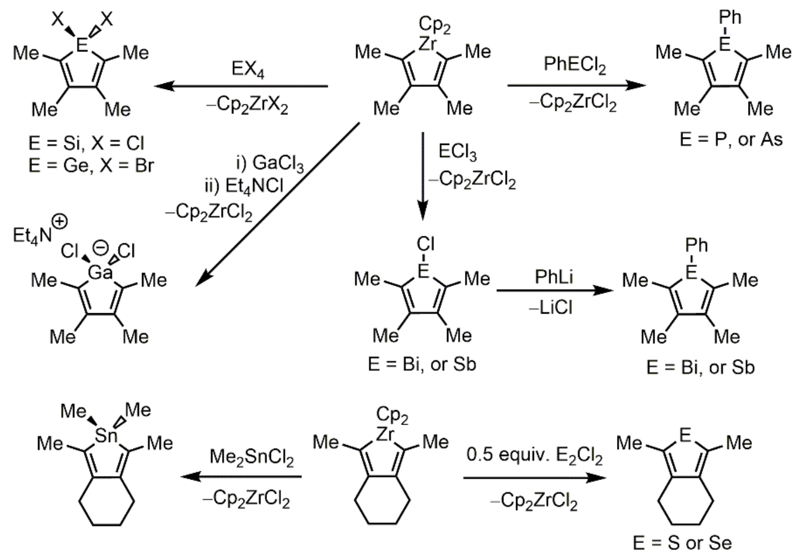

Scheme 1.5. Fagan-Nugent metallacycle transfer.

1.3.3 Zr–E Exchange Facilitated by Copper(I) Chloride

Transmetallation of zirconacyclopentadienes with copper(I) chloride prior to reaction with element halides was reported first by Takahashi and coworkers and led to vast improvements in the yield of stannoles (Sn-based heterocycles).[75] This approach has been widely applied in the synthesis of stannoles[76] and, as described in this thesis, immensely improves the synthesis of bismoles (Bi-based heterocycles).

The nature of the transmetallation products between zirconacyclopentadiene and CuCl was studied by the Xi group.[77] 1,2,3,4-Tetrapropyl-1,4-dilithio-1,3-butadiene and 1,2,3,4-tetraethyl-1,4-dilithio-1,3-butadiene were both found to generate organocopper(I) clusters consisting of diene-stabilized six- or eight-center copper clusters.[78] Similar multi-copper(I) clusters can be isolated upon reacting zirconacyclopentadienes with CuCl, and clusters consisting of up to 10–12 copper(I) centers stabilized by butadiene ligands could be isolated (*e.g.* of 10 Cu cluster complexes **68** and **69** in Scheme 1.6).[77] These clusters were found to undergo similar reactivity to previously reported CuCl-mediated reactions with zirconacycles such as homocoupling of the butadiene backbone to produce **70** (Scheme 1.6).[79]

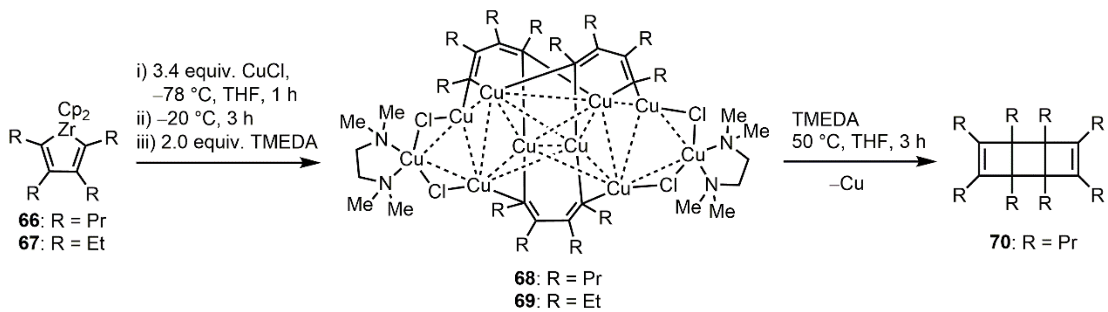

Scheme 1.6. Synthesis of Cu clusters via reaction of zirconacycles **66** and **67** with excess CuCl followed by homocoupling of the butadiene backbone of **68** to produce **70**.

1.4 Group 15 Heterocyclopentadienes

The field of Group 15 element-containing π-conjugated materials is dominated by the lightest members of the series, nitrogen and phosphorus. The number of conjugated materials based upon the isolobal substitution of CH for N (*e.g.* benzene to pyridine and cyclopentadiene to pyrrole) is vast and a discussion of the full impact of these important materials lies outside of the scope of this thesis. As synthetic inorganic chemistry continues to grow as a field, new examples of heterocycles featuring phosphorus, arsenic, antimony and bismuth are surfacing in an increasingly frequent manner.[80]

Heterofluorene analogues were among the first reported P-, As-, Sb-, and Bi-containing heterocycles, and as such they deserve a brief discussion (Figure 1.18). Wittig and Geisler[81] as well as Campbell and Way[82] reported the synthesis of phenylphosphafluorene (**71**) and phenylphosphafluorene oxide (**72**) in the 1950's. Researchers largely shied away from exploring the chemistry of arsenic since the 1960's due to toxicity concerns; however, the first arsenic carbazole analogues (**73**–**75**) and the first arsindoles (**76**–**79**) were reported in 1925 and 1935 respectively.[83] The first stibafluorenes, **80**–**82**, were reported in 1930, by Morgan and Davies[84] and this work was followed by Campbell and Morell in the 1950's.[85] Hellwinkel and Wittig reported the first bismafluorenes (**83** and **84**) in the 1960's.[86]

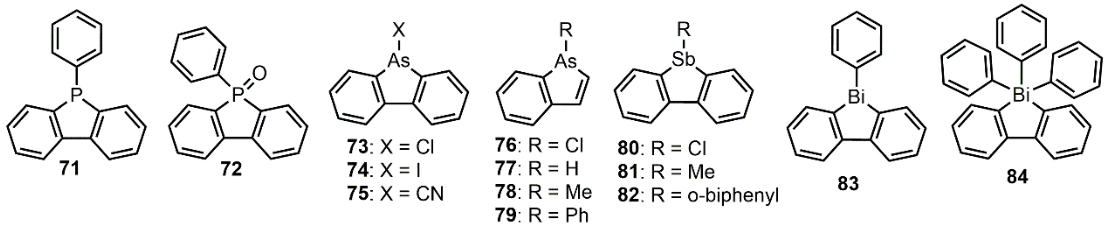

Figure 1.18. Structures of heterofluorenes **71**–**84**, which were among the first reported group 15 heterocycles.

Leavitt *et al*. from The Dow Chemical Company reported a brief note on the synthesis of pentaphenyl- phosphole, arsole, and stibole from dilithiotetraphenylbutadiene and $PhECl_2$ (where E = P, As, or Sb, respectively) in 1959.[87] This general condensation method with dilithiodienes and element dihalides was used as the primary route to generate heterocyclopentadienes prior to the metallacycle transfer route later introduced by Fagan and Nugent. Braye, Hübel, and

Caplier contributed pioneering work in the synthesis of tetraphenylsubstituted heterocycles based on Au, Hg, Hg, B, Tl, Zr, C, Si, Sn, N, P, As, Sb, S, Se and Te.[88]

While pyrrole is planar and aromatic, the aromatic stabilization energy decreases and the geometry about the pnictogen atom becomes more pyramidalized as the nitrogen atom is replaced by heavier pnictogens, due to the increased s-character of the pnictogen atom lone pair. The increased stability of the heteroatom lone pair generally results in the heterocyclopentadiene being less prone to oxidation. Substitution of the heteroatom with heavier pnictogens can result in efficient intersystem crossing to access excited triplet states capable of emission via phosphorescence, an effect that has caught the interest of researchers since the early 1980's when the first luminescence studies on group 15 heterocycles began in earnest with the work of Rodionov and coworkers.[89] The authors noted that as the atomic number of the heteroatom increased, the fluorescence quantum yield decreased and the phosphorescence quantum yield increased, as expected via the heavy element effect. The lifetimes of the phosphorescence also decreased with the heavier element heterocycles presumably due to enhanced spin-orbit coupling facilitated the spin forbidden radiative decay of excited triplet states.[89]

1.4.1 Overview of Phospholes

After the initial syntheses of pentaphenylphosphole by Leavitt and coworkers in 1959,[87] phospholes have attracted much attention. Experimental and theoretical aromaticity studies[90] have concluded that phosphole is only weakly aromatic, that is, it is far less aromatic than pyrrole or thiophene, but slightly more aromatic that cyclopentadiene.[91] Thus, the lone pair at the phosphorus atom is not conjugated with the diene system of the ring and the geometry at the phosphorus center is pyramidalized.

The pyramidalization of phospholes has a drastic effect on the luminescence properties of these species. The localization of the lone pair on the phosphorus atom results in a nucleophilicity at P that allows for coordination to a range of transition metals or facile oxidation of the phosphorus atom to yield phosphole oxides and sulfides, allowing for easy tuning of emission properties without having to synthetically change the phosphole backbone. Additionally, the pyramidalization at the phosphorus atom often suppress close molecular packing in the solid state and can prevent π-π stacking interactions that normally quench emission in aggregated luminogens.[91] As such, phospholes have been of special interest for their aggregation induced emissive properties.[92]

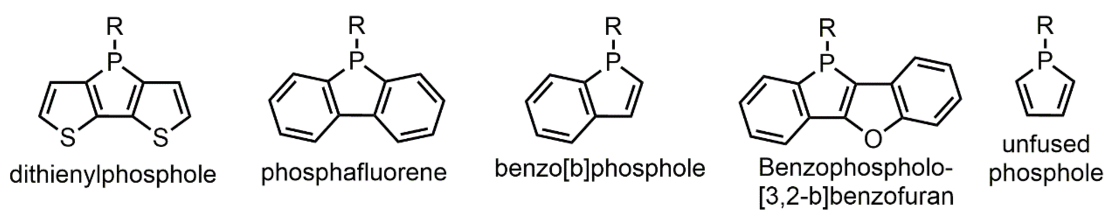

Figure 1.19. General structures of the most common classes of fused and unfused phospholes.

The properties of phospholes are highly dependent upon the parent π-system to which the phosphole ring is fused;[93] therefore, within the vast field of phosphole chemistry, each type of fused phosohole is generally considered to be an independent class of compound with different optical and electronic properties (*e.g.*

dithienylphospholes, phosphafluorenes, benzophospholes, benzophospholefurans, and unfused phospholes, Figure 1.19).[94]

The Baumgartner group pioneered the development of dithienylphospholes as tunable emissive materials[95] capable of being transformed via Suzuki[95d, 95e] and Stille cross-coupling,[95b, 95d] and even polymerized via dehydrogenative homocoupling of Si–H-functionalized dithienylphosphole monomers.[95c] An increased understanding in what controls the band gap of these materials and has led to the development of the dithienylphosphole unit as a valuable building block to make narrow band gap materials for organic photovoltaics.[95e] Phosphafluorenes have found great utility in the field of organic photovoltaics as well as organic field effect transistors (OFETs) and OLEDs. [94] Benzophospholefurans have yielded interest as high quantum yield emitters (Φ > 90 % in many cases) possessing intramolecular charge transfer characteristics from their donor furan to acceptor phosphole moieties. [96]

While there is no shortage of valuable work pertaining to both ring-fused and unfused phospholes, this thesis will focus discussion on the luminescence of benzophospholes, benzophosphole oxides, and their derivatives.

1.4.1.1 Luminescence of Benzophospholes and Benzophosphole Oxides

The first reported synthesis of a benzo[*b*]phosphole was by Rausch and Klemann in 1967.[97] As shown in Scheme 1.7, when diphenylacetylene was reacted with two equivalents of ^{n}BuLi, a dilithiated styrene intermediate formed which could be reacted with $PhPCl_2$ to yield the benzo[*b*]phosphole **65**. Oxidation of **65** with hydrogen peroxide gave the benzophosphole oxide **66**; however, the authors made no mention of any emission.

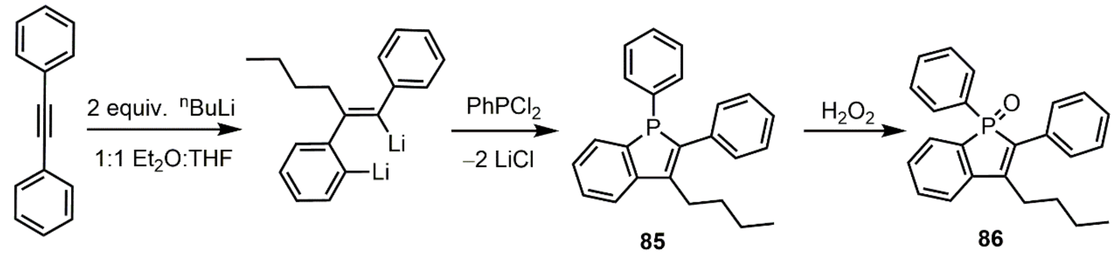

Scheme 1.7. Synthesis of benzophosphole **85** and benzophosphole oxide **86**.

Since the first report of a benzo[*b*]phosphole, several others have optimized the synthesis,[98] yet no reports of benzo[*b*]phosphole emission appeared until 2008.[99, 100] Sanji and Tanaka reported the synthesis of eleven new benzo[*b*]phosphole emitters via a base-mediated intramolecular cyclization of 2-alkynylphenylphosphine oxides, as shown in Scheme 1.8.[100] The benzophosphole oxides **87–90** could be reduced with trichlorosilane and in general, the authors observed that upon reduction the absorption and emission maxima were blue-shifted and the emission intensity decreased. When the phosphole ring was substituted with an electron-donating group, as in **90**, the absorbance and emission maxima were the most red-shifted. As expected, compounds with the most extended π-conjugation, **95–97**, displayed the most red-shifted absorbance and emission maxima.

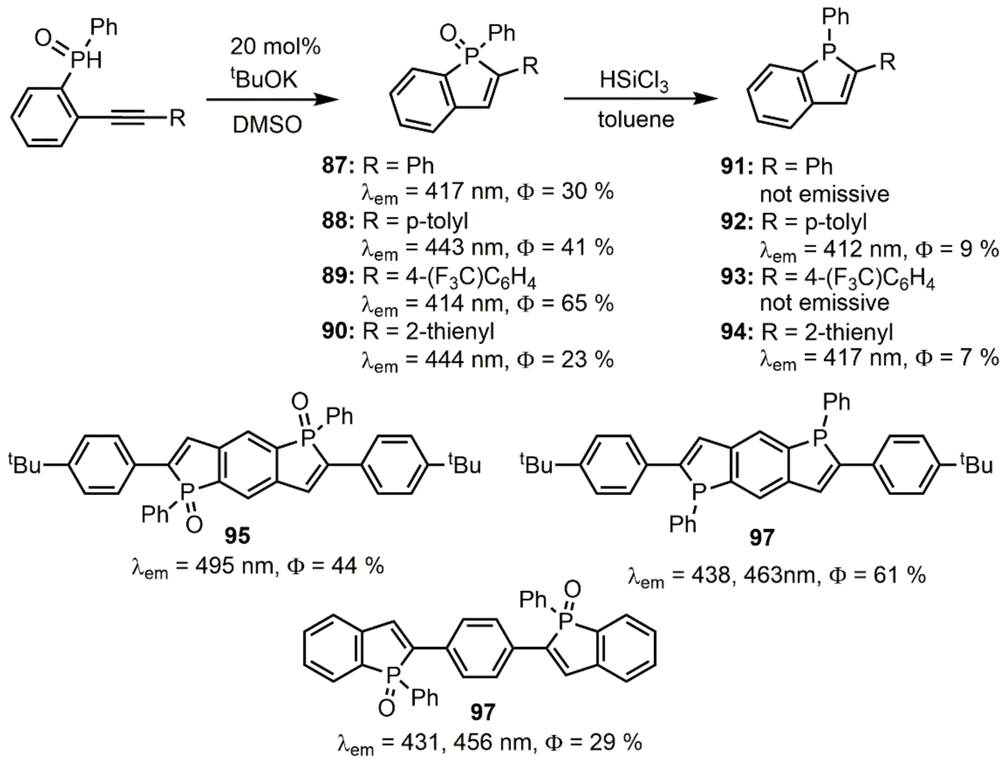

Scheme 1.8. Synthesis and emissive properties of the benzophosphole analogues **87**–**97**.

In 2008, Yamaguchi and coworkers reported the synthesis of a fused bibenzophosphole oxide, **98** in both a *cis* and *trans* form as well as its reduced phosphole analogue, **99**, which could only be isolated as a mixture of *cis* and *trans* isomers (Scheme 1.9).[101] Both isomers of **98** show emission maxima at 480 nm with quantum yields of almost unity (Φ = 98 % in CH_2Cl_2). Compound **99** displayed a decreased quantum yield (Φ = 7 % in CH_2Cl_2) and a blue-shift in emission to 415 nm. Following this original report,[93] the authors studied the luminescence of ring-fused phospholes **100–102** (Scheme 1.9). Compound **100** displayed fluorescence at 443 nm (Φ = 85 % in THF), which is blue-shifted relative to **98**. The authors attributed the lower energy emission in **98** relative to **100** to the energetic stabilization of the LUMO imparted by the electron-withdrawing capacity of the extra phosphoryl group in **98**. Both the *cis* and *trans* isomers of compounds **101** and **102** were isolated and studied separately. Both isomers of **101** and **102** displayed emission maxima at 490 nm, but with the bis(thiophosphole)arene **102** displaying a drastically lower quantum yield (Φ < 1 % in THF for **102** vs. Φ = 50 % in THF for **101**).

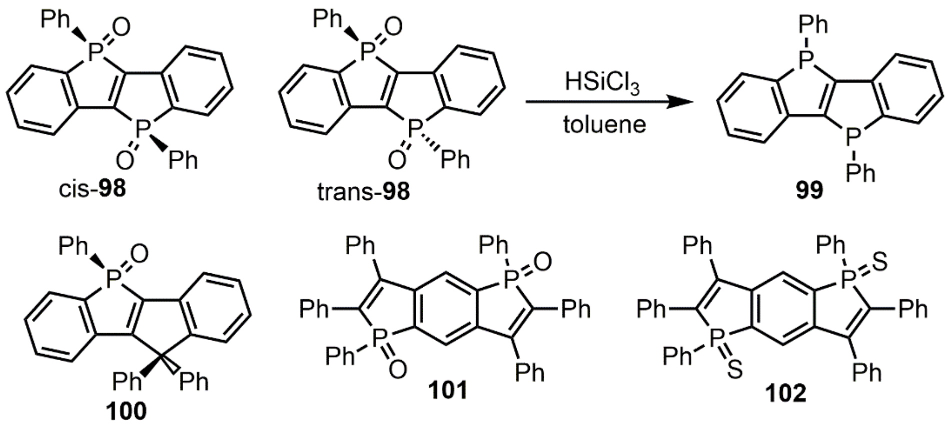

Scheme 1.9. Structures of ring-fused benzophosphole derivatives **98–102**.

In 2015, the Yamaguchi group reported the fluorescent compounds **103**[102] and **104** (Figure 1.20)[103] which demonstrated environment-sensitive luminescence. The triphenylamine (TPA)-appended phosphole oxide **103** displayed a red shift in its emission maximum upon increasing the polarity of the solvent (*e.g.* λ_{em} = 528 nm in toluene vs. λ_{em} = 601 nm in DMSO), indicating a charge transfer-based excitation. Good bioimaging dyes are required to have high photostability and red-shifted absorption/emission to allow for deep tissue imaging and better contrast against the blue-emissive autofluorescence emitting by cells. The suitability of **103** as a bioimaging agent was evaluated by treating adipocytes with **103**. This dye was found to not only have low cytotoxicity, but also surprisingly high photostability, and, due to its emission change in non-polar layers, it could be used to discriminate between hydrophobic lipid droplets and the intercellular fluid within the cells.[102] Building on these findings, a new emissive dye, **104**, was developed, with an aza-crown ether moiety capable of binding sodium ions. In the absence of sodium ions, **104** displayes red fluorescence with a maximum at 656 nm and upon increasing the sodium ion concentration, the emission blue-shifted (up to 620 nm at 200 mM Na^+) enabling a visual response to changes in Na^+ concentration in cells.[103]

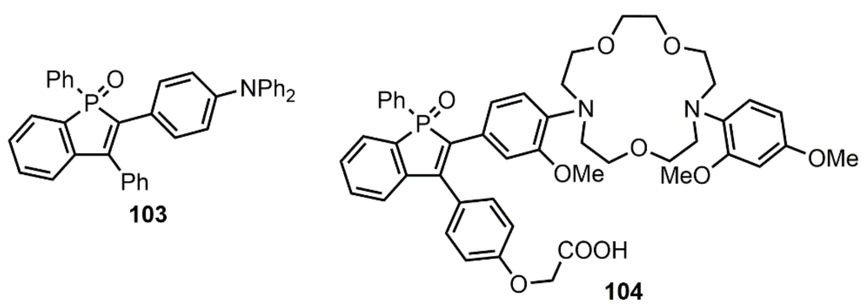

Figure 1.20. Structures of environment-sensitive benzophosphole oxides **103** and **104**.

The abovementioned important work by the Yamaguchi group set the stage for the development of a series of constrained benzophosphole-based red light emitters **105** and **106** (Figure 1.21).[104] While these ring-fused architectures begin to structurally deviate from the parent benzophosphole cores that have been the focus of this discussion, these emitters warrant a brief mention due to their superior photostability, which allows them to be applied as bioimaging agents for stimulated emission depletion (STED) microscopy. The high photostability of these emitters has been attributed to the electron-withdrawing character of the P=O moiety as well as the structurally reinforced framework that arises from the presence of a fully ring-fused ring emissive core.[104]

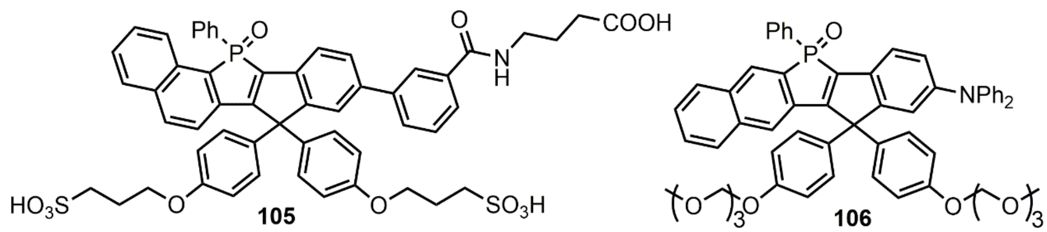

Figure 1.21. Constrained red light emitting benzophosphole oxide emitters **105** and **106**.

Matano and coworkers studied the effects of dimerization on the luminescence of benzophospholes and benzophosphole oxides (compounds **107–111** in Scheme 1.10).[105] The authors also synthesized benzophosphole oxides containing benzo[*b*]thiazole, benzo[*b*]thiophene, or *N*-methylindole groups to give hybrid heteroles **109–111**. Both the *cis* and *trans* isomers of **108** were studied, and while their emission and absorbance maxima were very similar (*cis*-**108** λ_{abs} = 379, λ_{em} = 441 nm and *trans*-**108** λ_{abs} = 380 nm, λ_{em} = 440 nm), their quantum yields and absorption coefficients were vastly different (Φ = 24 %, log ε = 4.25 for *cis*-**108** and Φ = 40 %, log ε = 4.42 for *trans*-**108**). The authors attribute this to an increase in planarity and conjugation as increased conjugation tends to result in a higher oscillator strength of absorption.[92b] **109–111** had red-shifted emission and absorption compared to **108**, but **111** had the largest stokes shift (7000 cm^{-1}) suggesting it goes through significant conformational change in the excited state.

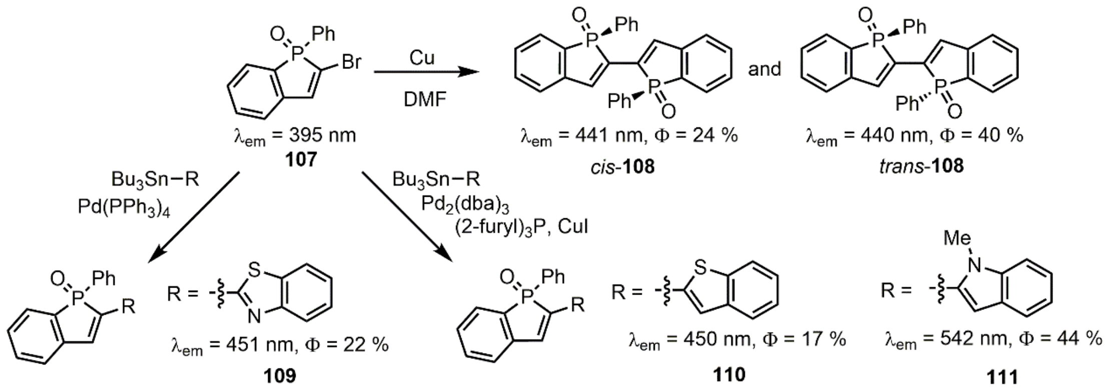

Scheme 1.10. Synthesis of benzophosphole dimer **108** and hybrid heteroles **109–111** from brominated benzophosphole **107**.

Building on their previous study, Matano and coworkers examined the effects of extending π-congugation by starting from the benzophosphole **107** and functionalizing with Heck and Sonogashira coupling to yield **112**–**118** (Scheme 1.11).[106] Benzophospholes with electron donating MeO groups (**112** and **116**) or extended π-conjugation (**115**) displayed the greatest red-shift in their absorption and emission maxima. Interestingly, the incorporation of an electron withdrawing Cl group (**113** and **118**) did not shift the absorption and emission energy relative to the H-substituted analogues (**114** and **117**).

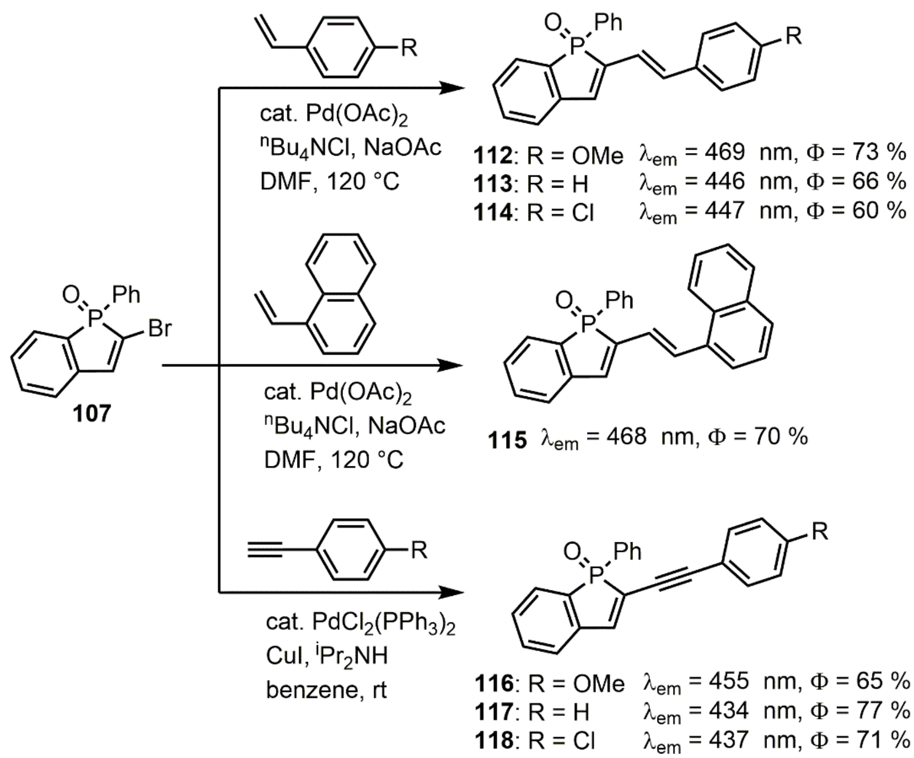

Scheme 1.11. Synthesis of compounds **112**–**118** via Heck and Sonogashira coupling.

Compound **107** could also be functionalized via Suzuki-Miyaura cross-coupling to generate a plethora of arylated benzobismole products **120**–**131** (Scheme 1.12).[107] Additionally, a series of naphthophospholes was synthesized and their luminescence properties compared to their benzo-analogues. Electron-withdrawing substituents were observed to have little effect on the emission and absorption spectra of **120**, **121**, **127**, and **128**, but, as observed previously, electron donating groups such as OMe, NPh_2, or NMe_2 result in bathochromic shifts in emission. As expected, the presence of Ph_2N- and Me_2N-substituents resulted in intramolecular charge transfer from the N-containing donor unit to the phosphole acceptor.

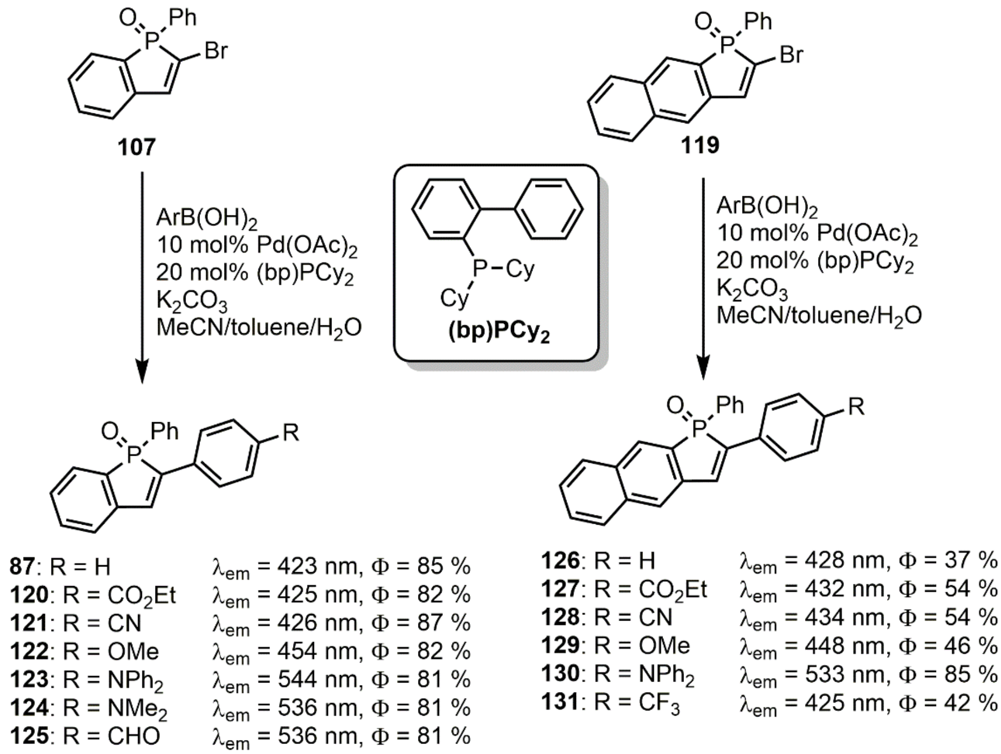

Scheme 1.12. Synthesis of the benzophospholes **87** and **120**–**131** via Suzuki-Miyaura cross-coupling.

Matano and coworkers also prepared a series of alkylated and arylated benzo[*b*]phospholium salts **132**–**137** according to the protocols outlined in Scheme 1.13.[108] While **132**–**137** all displayed fluorescence in solution, the emission intensity of **132**–**134** was found to be the lowest amongst the compound series. Compounds **135**–**137** were found to behave as solvent-separated ion pairs with similar emission properties in both methanol and CH_2Cl_2. Compounds **132**–**134** displayed reduced emission intensity in CH_2Cl_2 compared to methanol due to the formation of contact ion pairs in CH_2Cl_2, where the close-contact of the heavy I^- anion was thought to induce intersystem crossing to deplete the S_1 excited states thereby quenching emission.

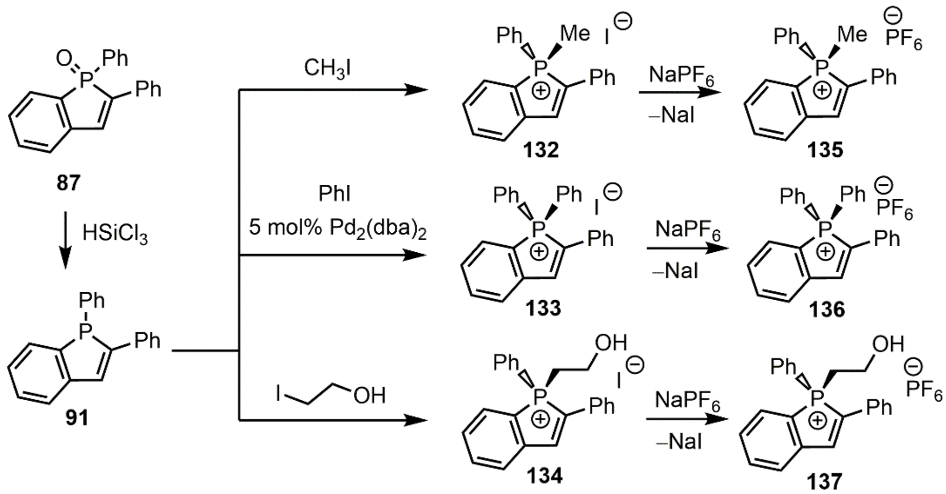

Scheme 1.13. Synthesis of benzo[*b*]phospholium salts **132**–**137**.

Until recently, studies on benzophospholes and their oxide derivatives involved functionalization at the 2- and 3-positions; however, Matano and coworkers described a method to selectively halogenate the 7-position of triphenylbenzophosphole oxide (**138**) to produce **139** (Scheme 1.14).[109] **139** could then be transformed into the compounds **140**–**146** via Suzuki-Miyaura, Stille, or Sonogashira coupling. This allowed for the comparison of the site of substitution with emission properties, such as in 2-pyrrolebenzophosphole **147** and 7-pyrrolebenzophosphole **143** as well as the 2-TPA- (**103**, discussed previously) and 7-TPA-(**140**) substituted compounds. 7-TPA-benzophosphole (**140**) and 7-pyrrole-benzophosphole (**143**) displayed significanty larger Stokes shifts than their 2-substituted analogues, indicating a high degree of conformational change upon excitation to stabilize the excited singlet states. In the case of the TPA-appended phospholes, **103** and **140**, both the 2- and 7-substituted molecules displayed drastic solvatofluorochromism resulting from the significant charge transfer character in their singlet excited states. In the case of pyrrole-substituted phospholes **143** and **147**, only the 7-substituted benzophosphole (**143**) displayed solvatochromism. TD-DFT computations indicated that the S_1 state of **147** is a HOMO to LUMO excitation and both the HOMO and LUMO are spread over the entire π-framework of the molecule.

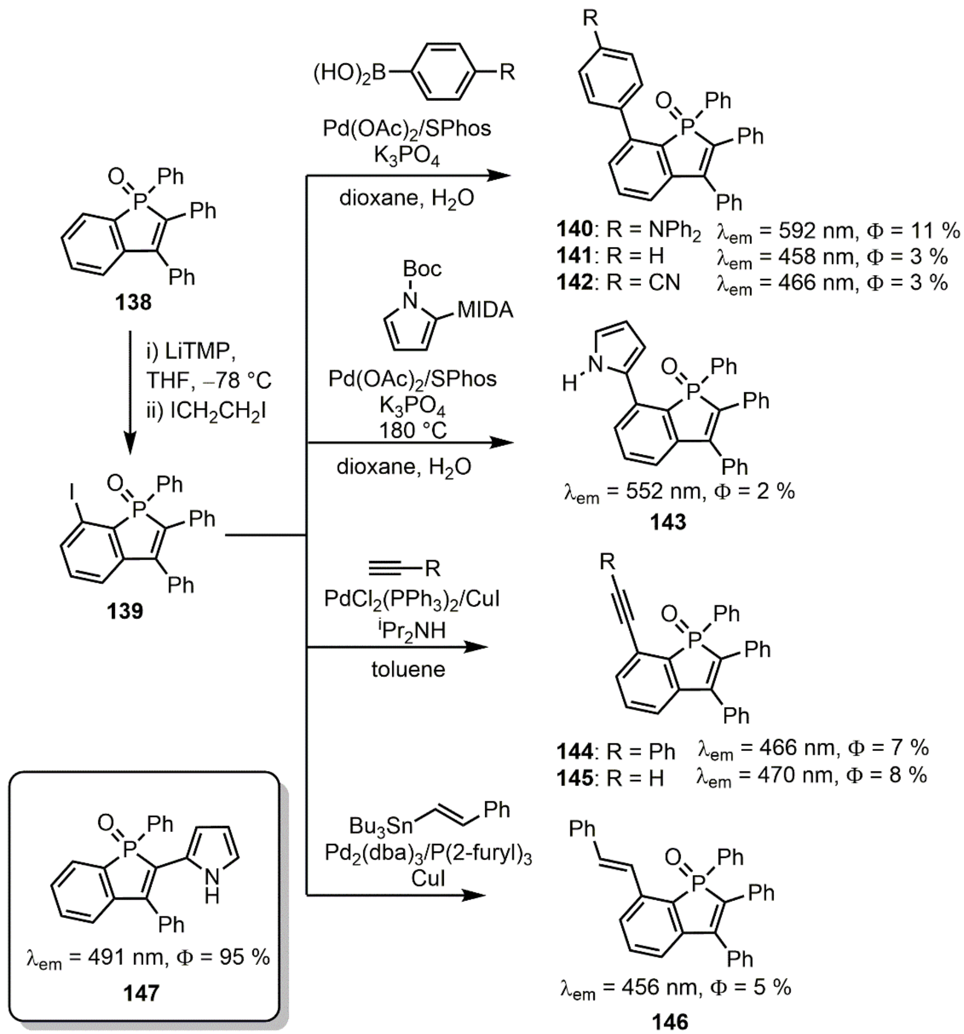

Scheme 1.14. Synthesis of benzophosphole oxides **139**–**146** with functionalization at the 7-position.

Yoshikai and coworkers studied the effects of substitution on the benzophosphole oxide backbone by preparing compounds **148**–**161** (Figure 1.22) and studying their luminescence.[110] As reported in many of the studies already discussed,[100,102,106,107] the presence of electron-donating groups (such as methoxy or amino groups, eg **149**, **151,** and **152**) resulted in red-shifted absorbance and emission maxima relative to the parent molecule **148**, but no shift was observed for electron-withdrawing groups (eg **154** and **155**). Compounds **150**, **156**, and **159** had the highest quantum yields (up to 94 %), and the sulfide species **160** was found to have negligible emission.

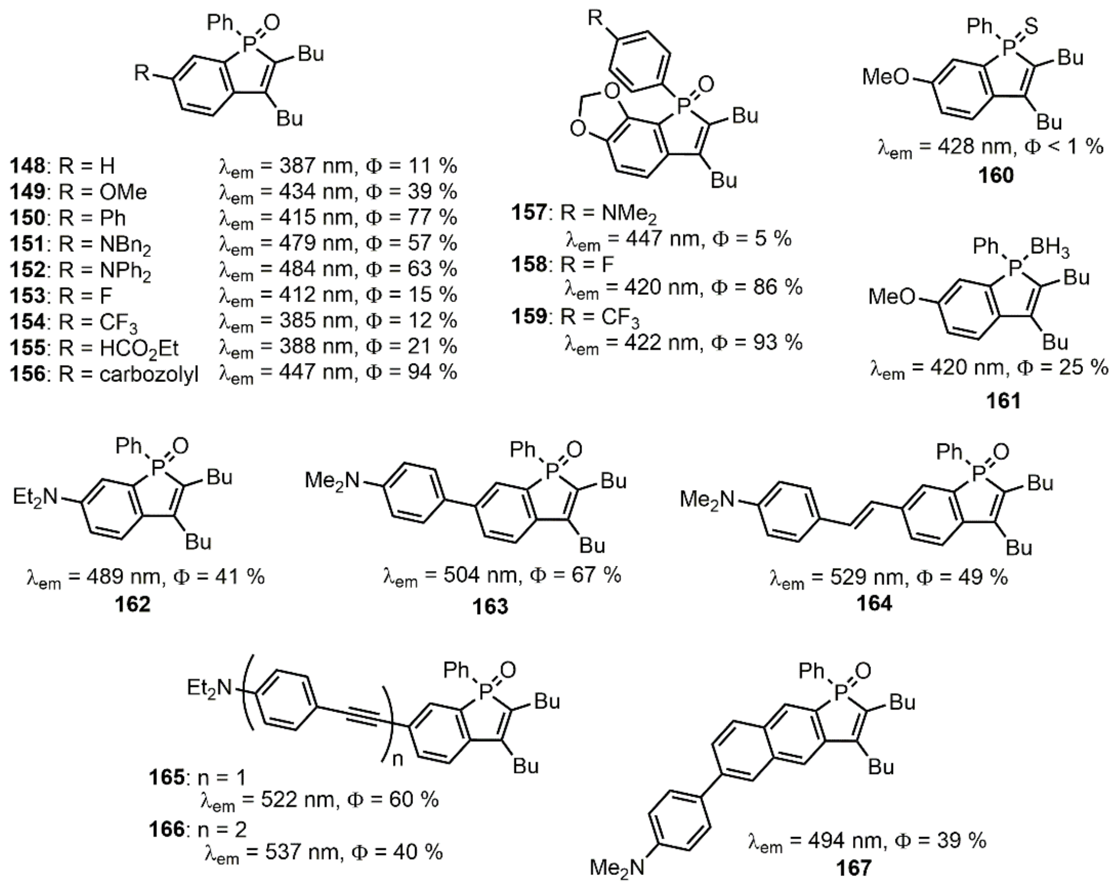

Figure 1.22. Structures of benzophospholes **148**–**167** with susbtitution at the 6-position.

Following up, Yoshikai and coworkers reported a series of donor-acceptor benzo[*b*]phosphole and naphtho[2,3-*b*]phosphole oxides **162–167** (Figure 1.22).[111] Compounds **163–167**, with longer π-spacers between their donor and acceptor units displayed red-shifted emission and larger Stokes shifts.

Morimoto and coworkers reported a series of photochromic benzophospholes **168–170** which undergo reversible photoconversion in acetonitrile and in the solid state (Scheme 1.15).[112] Fluorescence was also observed for **168–170** but with low quantum yields (Φ < 6 %) in acetonitrile for both the open and closed forms, however, the closed ring form, **170b**, was observed to undergo significant aggregation induced emission with an increase in Φ up to 55 % in the solid state.

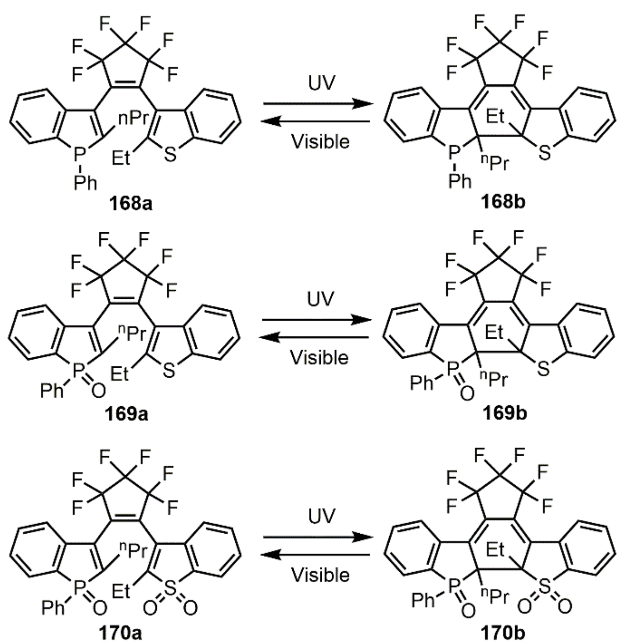

Scheme 1.15. Photochromic benzophospholes **168–170**.

The Tang group examined possible mechanisms of aggregation induced emission in phospholes by directly comparing the properties of pentaphenyl phosphole oxide (**171**) with triphenylbenzophosphole (**172**) and its oxide congener (**138**) (Figure 1.23).[92a] While AIE effects are generally attributed to the restriction of intramolecular rotations, the authors highlight the importance of considering the contributions of intramolecular vibrations in facilitating non-radiative decay. The authors attribute the longer emission lifetime for **138** (6.4 ns) and higher quantum yield (68 % in the solid state, 1 % in THF) relative to **171** (τ = 5.5 s, Φ = 0.3 % and 33 % in THF and the solid state, respectively) to a decreased rate of non-radiative decay for **138**. When the reorganization energy of the first singlet excited states for **171** and **138** are computed and compared, it becomes apparent that the main non-radiative pathway for **171** is not the rotational motion of the peripheral aryl rings but the high frequency stretching motions of the internal phosphole ring. These stretching motions are reduced in **138** due to the rigidity of the core arising from the presence of the fused benzo backbone and the result is a decreased rate of non-radiative decay in **138** and a higher quantum yield.

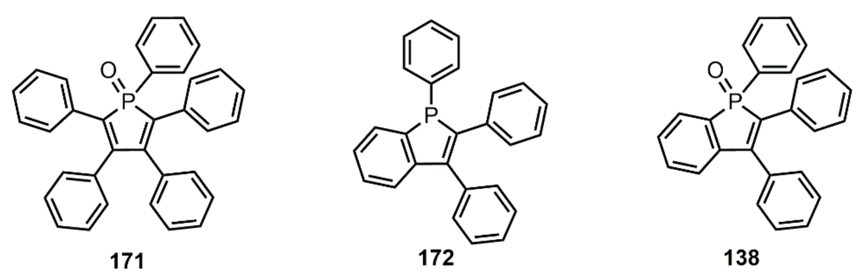

Figure 1.23. Structures of phosphole-based AIEgens **171**, **172**, and **138**.

Building on their prior study, the Tang group explored the effects of functionalization on the luminescence of benzophosphole oxides by synthesizing molecules **173–178** (Figure 1.24).[92b] Interestingly, only some of these new benzophospholes displayed significant aggregation induced emission enhancement like the triphenylbenzophosphole oxide **138**. Extending the conjugation of the aryl rings (as for *para*-biphenyl-substituted benzophosphole **173**) or introduction of electron-donating groups (as for TPA-appended phospholes **177** and **178**) resulted in red-shifted absorption and emission maxima relative to the parent, **138**. *Ortho*- and *meta*-biphenyl phospholes (**175** and **174**) did not yield a red-shift in emission presumably due to the mutual twisting of the aryl rings in the biphenyl units which effectively breaks conjugation. The authors observed that increasing the rigidity imparted by the peripheral aryl groups led to an increase in the quantum yield in solution relative to **138**. Additionally, the donor-acceptor phospholes **177** and **178** emitted via a charge transfer process and exhibited pronounced solvatochromic emission as well as high quantum yields in solution (up to 93 %).

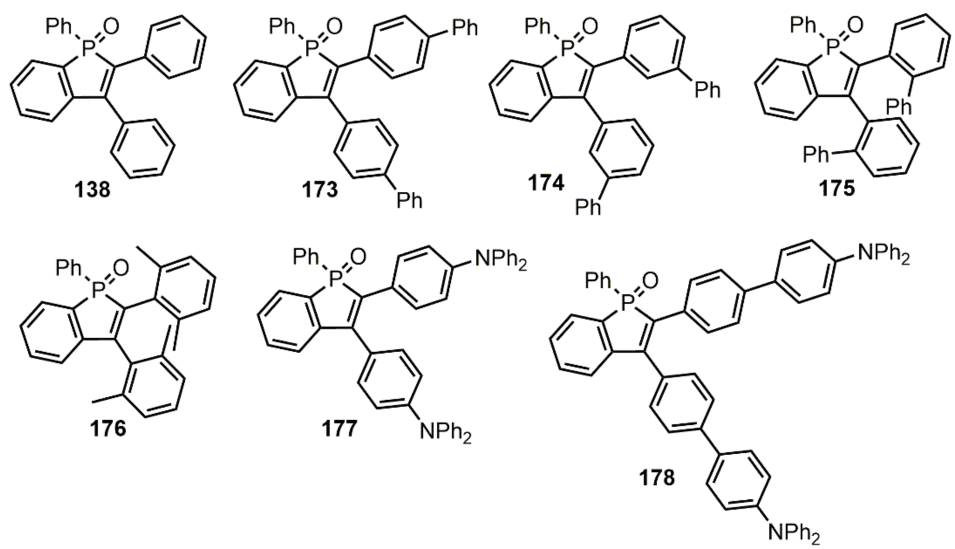

Figure 1.24. Structure of benzophospholes **173**–**178** reported by the Tang group.

Benzophospholes have become an increasingly popular family of emitter due to their ease of tunability, enhanced photostability, and their interesting aggregation induced emission properties. While the study of these molecular emitters has been widely reported, polymer products based on this family have not been explored and the work reported in this thesis will serve to start that journey.

1.4.2 Overview of Arsoles

Like most heterocyclopentadiene derivatives, many of the first arsoles were synthesized via the reaction of dilithiobutadiene reagents with arsenic chlorides.[88] While the metallacycle transfer route reported by Fagan and Nugent in 1988 can be applied to arsenic[73, 74] the use of volatile arsenic reagents (*e.g.* $PhAsCl_2$) is not ideal due to their high toxicity.

In 2015, Naka and coworkers reported the *in situ* generation of $RAsI_2$ from stable $(RAs)_n$ homocycles, which could then be used immediately to generate arsafluorenes (**179** and **180**, Scheme 1.16) without the need for isolation or purification of volatile arsenic halides.[113] This new approach served to mitigate some of the pre-existing concerns pertaining to the dangers related to arsenic heterocycle synthesis and has resulting in a resurgence of interest in the optoelectronic applications of these materials.[114]

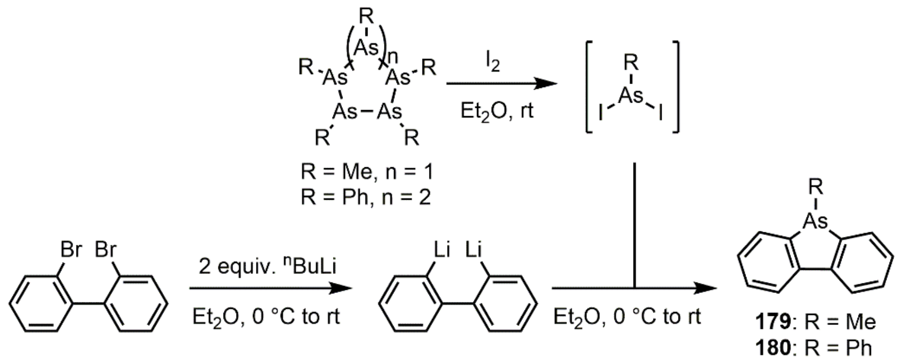

Scheme 1.16. Arsafluorene synthesis via *in situ* iodination of organoarsenic homocycles.

1.4.2.1 Luminescence of Arsoles

Braye *et al*. were the first to notice the fluorescent behaviour of pentaphenylarsole $PhAsC_4Ph_4$ **181**.[88] The fluorescence of pentaphenylarsole was studied in further detail in 1970 in a comparative study between this heterocycle and the analogous pyrrole and phospholes.[115]

While phenylarsafluorene (**180**) exhibited negligible luminescence in solution, solid state fluorescence was observed (λ_{ex} = 324 nm, λ_{em} = 390 nm, Φ = 3 %) at room temperature; and upon cooling a solid sample to 77 K a second emission peak at 515 nm was observed that was attributed to phosphorescence.[113]

By taking advantage of their *in situ* synthesis of $PhAsI_2$, the Naka group prepared a series of fluorescent 2,5-diarylarsoles from titanacyclopentadiene precursors (Scheme 1.17).[116] Optical measurements revealed that the introduction of an arsenic atom in place of phosphorus did not significantly change the emission wavelength in chloroform solution; however a blue-shift of the emission in the solid state by about 20 nm (λ_{em} = 482 nm for **182**, 485 nm for **183**) in comparison to the known phosphole analogue (λ_{em} = 504 nm) was observed. As expected, the arsenic-based heterocycles **182** and **183** are also more stable in the presence of oxygen in comparison to the corresponding phospholes due to an increase in the s-character of the As lone pair in relation to P. Compounds **182** and **183** form stable 1:1 adducts with AuCl which led to an increase in the quantum yield of up to 86 % in chloroform for **187**.

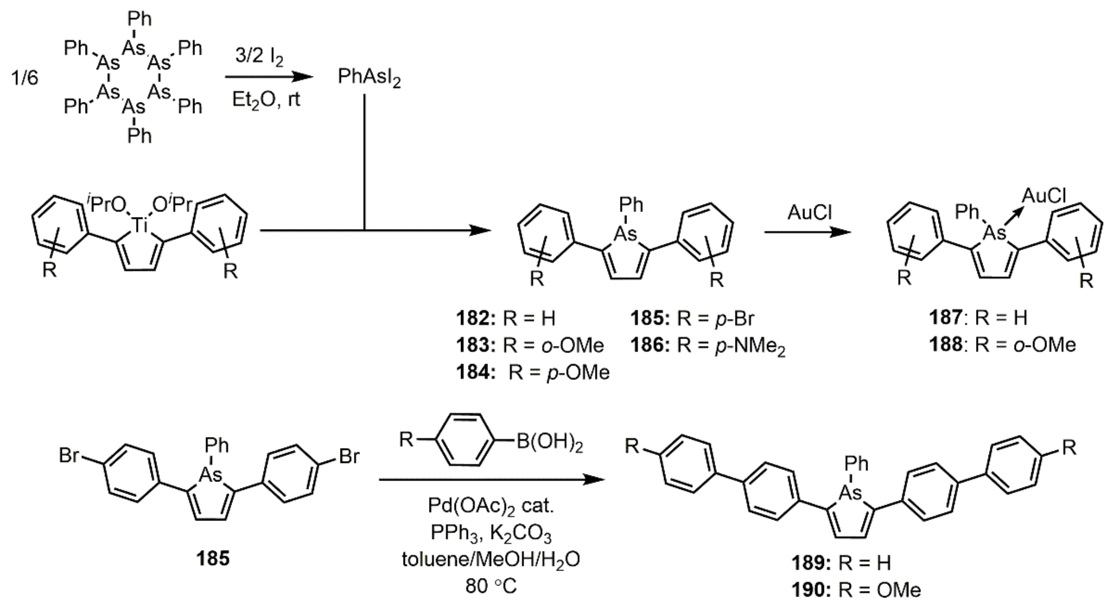

Scheme 1.17. Synthesis of 2,5-diarylarsoles via metallacycle transfer.

The brominated 2,5-diarylarsole **185** could undergo further functionalization via Pd-catalyzed Suzuki–Miyaura cross-coupling (Scheme 1.17) to yield the biphenyl-capped analogues **189** and **190**.[117] This reaction highlights a main advantage of these As-heterocycles in relation to their lighter phosphole congeners, which tend to poison the catalytic activity of the Pd complexes required for cross-coupling. A bathochromic shift in both the absorbance and emission of the arsoles transpires when electron-donating groups are positioned on the phenyl rings (*e.g.* λ_{em} = 548 nm for **186** vs. 458 nm for the parent system **182**), as well as a corresponding increase in the energy of the HOMO (–4.67 eV for **186** vs. –5.59 eV for **182**). Interestingly, it was noticed that the emission colors of these arsenic heterocycles could be modified by mechanical stimuli, such as grinding. A hypsochromic shift by about 10 nm was observed for compounds **182–184**, and **186** upon grinding, but this hypsochromic shift was most pronounced for **185** (*ca.* 50 nm).

Heeney and coworkers reported the synthesis of the first example of a dithienoarsole-containing polymer, **193**, which was obtained via Stille cross-coupling (Scheme 1.18).[118] Using a different approach than Naka and coworkers, $PhAsCl_2$ was first generated *in situ* from phenylarsonic acid $PhAs(O)(OH)_2$ and then reacted with a dodecyl-functionalized dilithiated bithiophene to form **191**. Compound **191** was then brominated to give the air-stable dithienosarsole monomer **192**. (Scheme 1.18) which could be co-polymerized with *trans*-1,2-bis(tributylstannyl)ethene to yield **193** as a dark blue polymer. DFT computations on a trimeric model of **193** indicate a highly planar backbone with very little twisting (less than 11°) between the dithienylarsole units and the adjacent olefinic spacers.

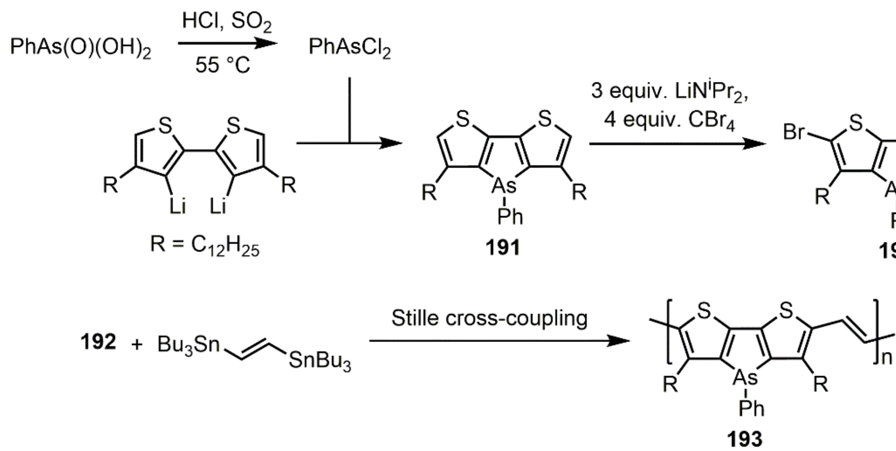

Scheme 1.18. Synthesis of the dithienoarsole polymer **193**.

In a similar study, Naka and coworkers reported the copolymerization of dibromodithenoarsole **195** with a bis(boronic acid)-substituted fluorene via Suzuki-Miyaura cross-coupling to yield the copolymer **196** (Scheme 1.19).[119] Upon polymerization, the fluorescence emission maximum is red-shifted (λ_{ex} = 336 nm, λ_{em} = 407 nm, Φ = 7 % for **195** in $CHCl_3$; λ_{ex} = 375 nm, λ_{em} = *ca.* 545 nm, Φ = 44 % for **196** in $CHCl_3$) indicating effective conjugation along the polymer backbone. Interestingly, while monomeric **195** exhibited an increase in quantum yield in the solid state (Φ = 15 %), polymer **196** was found to have a substantial decrease in quantum yield (~1 %) in the solid state that was attributed to quenching via π-π stacking interactions.[119]

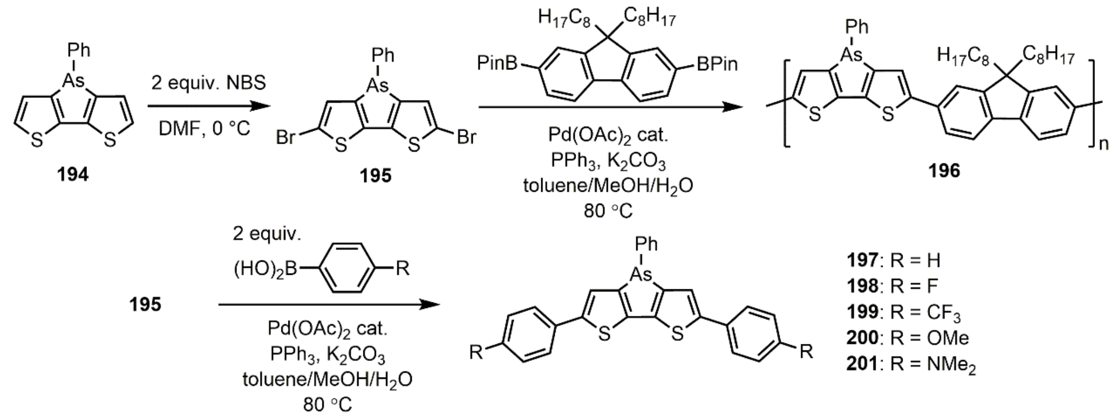

Scheme 1.19. Functionalization of **195** via Suzuki-Miyaura cross-coupling.

Further functionalization of the brominated dithienylarsole **195** was demonstrated via Suzuki-Miyaura cross-coupling with a range of arylboronic acids, as shown in Scheme 1.19.[120] The resulting dimethylamino-substituted arsole **201** displayed the greatest red-shift in its excitation and emission spectra (λ_{em} = 535 nm for **201**; λ_{em} = 474–489 nm for **197**–**200** in CH_2Cl_2). While dithienylarsoles are air stable, oxidation of the As can be achieved upon reaction with hydrogen peroxide, resulting in a red-shift in the emission (oxidized **197**: λ_{em} = 507 nm) relative to the unoxidized parent (**197**: λ_{em} = 474 nm) and an increase in the quantum yield from 23 to 58 %.

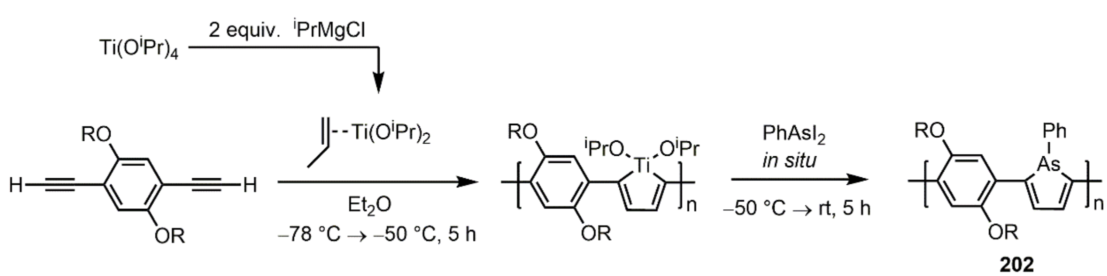

Scheme 1.20. Synthesis of the conjugated arsole copolymer **202**.

Conjugated arsole-containing polymers have also been reported via the post-polymerization modification of a titanacyclopentadiene polymer as shown in Scheme 1.20.[121] Polymer **202** was determined to have HOMO and LUMO energies of –5.43 and –3.24 eV, respectively, as estimated by cyclic voltammetry (CV) and displayed quasi-reversible oxidation and reduction waves. Coordination of gold(I) chloride to the arsole units in **202** was found to narrow the optical bandgap by lowering the LUMO energy level to –3.56 eV (as estimated by CV).

Pentaphenyl arsole $PhAsC_4Ph_4$ **181** and related perarylated arsoles **203** and **204** were synthesized by the reaction of $PhArI_2$ with organocopper complexes (made from opening zirconacycle ring precursors with two equivalents of CuCl, Scheme 1.21).[122] Compounds **181**, **203**, and **204** displayed substantial AIE fluorescence (Φ < 5 % in THF; Φ = 61 %, 35 %, and 28 % for **181**, **203**, and **204**, respectively, in the solid state). The incorporation of electron donating *para*-substituents red-shifted the emission of **203** (λ_{em} = 488 nm) and **204** (λ_{em} = 498 nm) relative to **181** (λ_{em} = 482 nm). TD-DFT computations indicated that electron-donating substitutents in the 2- and 5-positions destabilize the HOMO, resulting in the red-shifted emission.

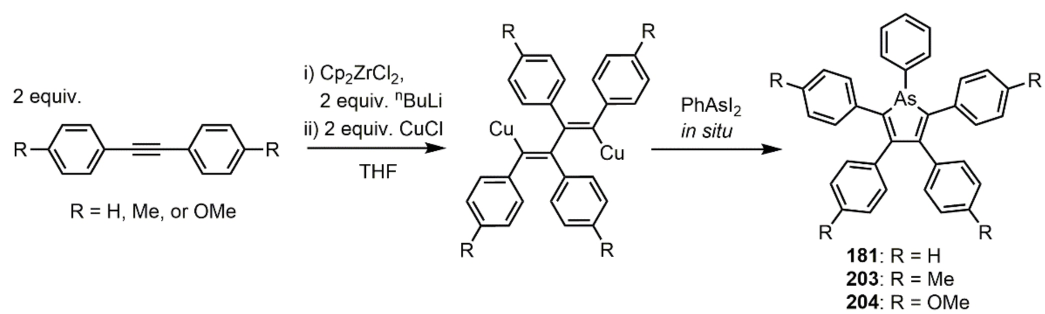

Scheme 1.21. Synthesis of perarylated arsoles **181**, and **203**–**204**.

Heeney and coworkers reported an interesting arsolo-bis(thiazole) derivative **206** in 2017.[123] Compound **206** was observed to have an absorption maximum at 327 nm and an emission maximum at 391 nm (Φ = 4 %) in CH_2Cl_2, which is slightly blue-shifted compared to the analogous dithienylarsole **194** (λ_{em} = 407 nm, Φ = 7 % in $CHCl_3$).

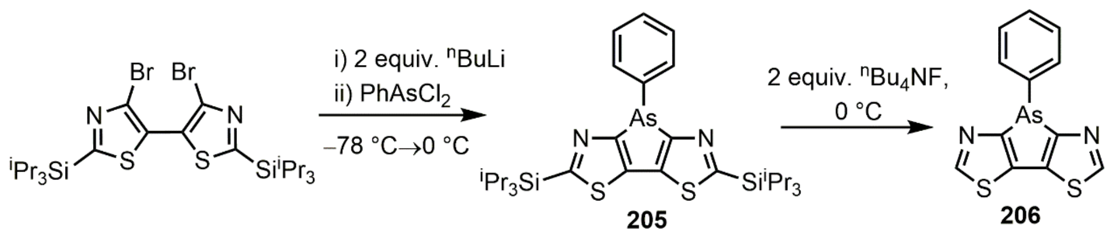

Scheme 1.22. Synthesis of arsolo-bis(thiazole) **206**.

Arsafluorene **207** was synthesized according to the procedure outlined in Scheme 1.23 and used to generate the first example of a polyarsafluorene, **208**.[124] Polymer **208** was observed to have an absorbance maximum at 387 nm, with fluorescence at 458 nm (Φ = 11 %) from spin-coated films.

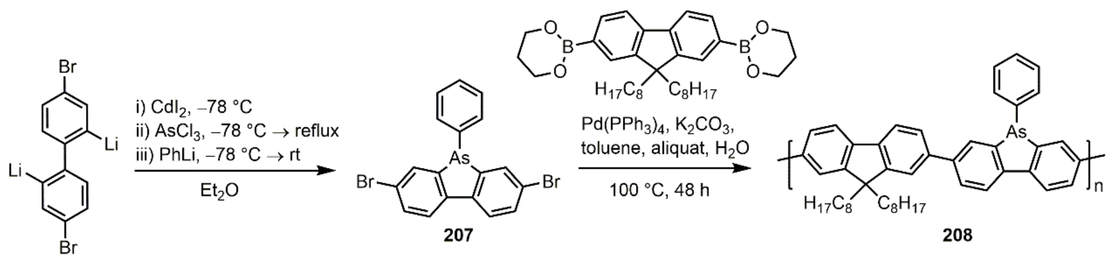

Scheme 1.23. Synthesis of arsafluorene polymer **208** via Suzuki-Miyaura cross-coupling.

1.4.3 Overview of Stiboles

1.4.3.1 Applications of Stiboles

Gabbaï and coworkers have reported the synthesis of stibafluorene and benzostiboles for use in fluoride sensing.[125] The catechol- and tetrachlorocatechol-bound stibafluorenes **209** and **210** as well the alizarin red-bound stibafluorene (**211**) were evaluated for their ability to bind and detect fluoride in solution (Scheme 1.24a). While the catechol-functionalized analogue **209** showed no evidence of F⁻ coordination, **210** and **211** fluoride complexes could be isolated, and **211** showed a color change from yellow to red upon F⁻ binding.

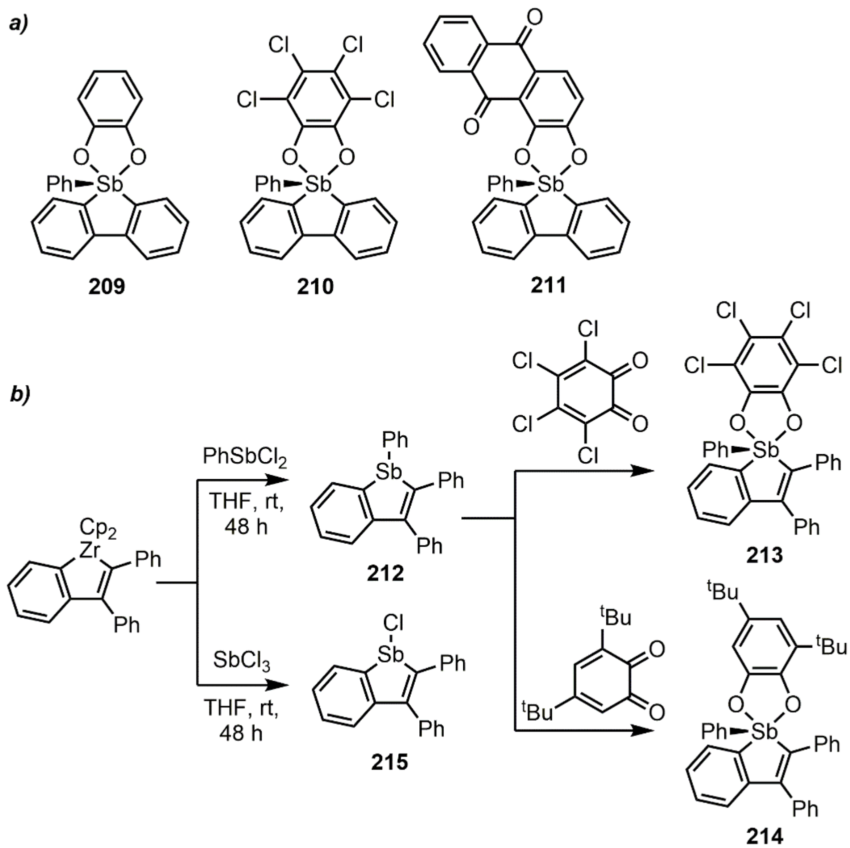

Scheme 1.24. a) Stibafluorene- and b) benzostibole-based fluoride sensors.

Following up on their original work, Gabbaï, Rivard *et al*. reported a study on fluoride detection with the triphenylbenzostiboles **212**–**214** (Scheme 1.24b).[126] Reaction of **213** and **214** with tetrabutylammonium fluoride (TBAF) indicated successful binding of the F^- to the Sb(V) center, as judged by ^{19}F NMR spectroscopy. This reaction was accompanied by an immediate color change from yellow to colorless for both complexes. Compounds **213** could be used in a biphasic CH_2Cl_2/aqueous system coupled with UV-vis spectroscopy to quantify ppm levels of F^- in drinking water. The antimony(III) heterocycle **215** (Scheme 1.24b) was found to undergo a change in color from bright yellow to colorless upon binding not just F^- but also Cl^- and Br^-, indicating that Sb(III) complexes may also show great promise for anion sensing.[127]

1.4.3.2 Luminescence of Stiboles

In 2012, Ohshita and coworkers reported the synthesis and characterization of the first dithienylstiboles (Scheme 1.25a).[128] Three variants were made (**216**–**218**) which demonstrated emission maxima ranging from 420 nm to 443 nm but with recorded quantum yields of only 1–2 % in chloroform. The solid-state emission spectrum for **218** afforded a notable red-shift in emission maxima by about 30 nm, suggesting that packing effects influenced the wavelength of emission. The stiboles were stable to ambient conditions but decomposed upon continuous UV irradiation for one hour. In the case of **218**, small amounts of naphthalene and bis(benzo[*b*]thiophene) were detected after decomposition, suggesting that Sb–C bond scission was leading to loss of antimony metal upon irradiation. The authors also conducted DFT calculations to compare the HOMO and LUMO energies of model dithienometalloles containing S, Sb, or Bi and found that the resulting computed energy levels remained largely invariant to the nature of the heteroatom present.[128]

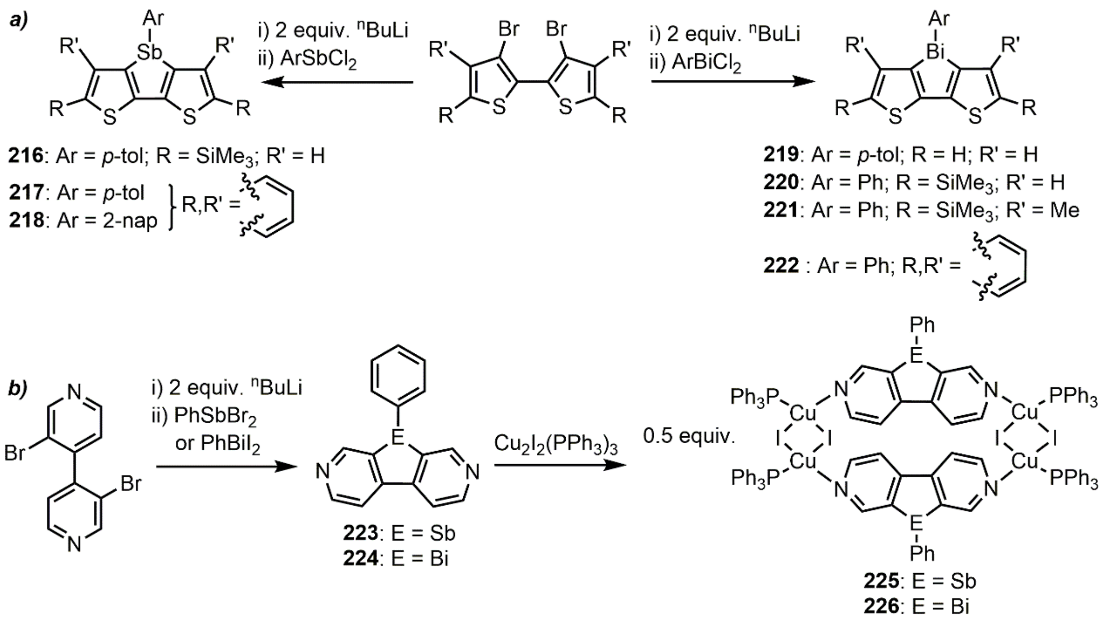

Scheme 1.25. Synthesis of dithienyl- and dipyridino- antimony and bismuth compounds **216–226**.

Ohshita and coworkers recently reported the synthesis of a dipyridinostibole **223** and a dipyridinobismole **224** (Scheme 1.25b).[129] **223** was isolated as an air stable colorless solid. The emission spectrum of **223** in Me-THF at room temperature features a weak emission band at 310 nm that was too low in intensity to determine a quantum yield. When the temperature was lowered to 77 K, an additional emission band at 453 nm was present. Lifetime measurements indicated that the high energy emission band resulted from fluorescence and the lower energy band was due to phosphorescence. The phosphorescence emission band for compound **223** remained present when the molecule was examined in the solid state at 77 K but shifted to 478 nm. Compound **223** was reacted with $Cu_2I_2(PPh_3)_2$ to form the coordination complex **225** which showed a red-shifted emission peak relative to **223** (λ_{em} = 700 nm, Φ < 2 % for **225** in the solid state at 77 K). Stibole **223** was used in conjunction with a poly[(carbazolylthiahexyl)silsesquioxane] host layer to fabricate an OLED which yielded a device with emission at 660 nm, a maximum luminance of 22 cd/m^2 and current efficiency of 0.12 cd/A.[129]

1.4.4 Overview of Bismoles

1.4.4.1 Synthesis and Applications of Bismoles

While the main focus of the following discussion will pertain to the luminescence properties of bismacyclopentadienes, termed bismoles, cyclic organobismuth compounds have been explored for applications in organic synthesis and as such, these topics also warrant brief mention.

A report in 2002 by Takahashi and coworkers describes the synthesis of six-membered heterocycles by reacting zirconacycles with C=O, C=N, and N=N precursors.[130] The authors observed that $BiCl_3$ served as an excellent mediator to the formation of regioselective α-pyrans from zirconacyclopentadienes and diethyl ketomalonate as shown in Scheme 1.26. 2,3,4,5-Tetramethylzirconacyclopentadiene was reacted with $BiCl_3$ and the resulting chlorobismole was monitored for its reactivity with diethyl ketomalonate and found to generate the expected pyran, indicating that the reaction goes through a bismole intermediate.

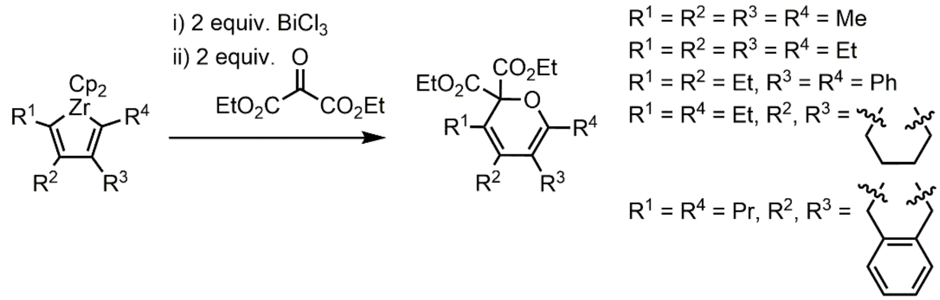

Scheme 1.26. Synthesis of *α*-pyrans from zirconacyclopentadienes via a bismole intermediate.

In 2004, Finet and Fedorov reported the use of the phenylbisma(V)fluorenes **227** and **228** for C-arylation of enol substrates (Scheme 1.27).[131] Bismoles **227** and **228** were found to selectively transfer just the phenyl group to their substrates in the presence of a base (*e.g.* *N*,*N*,*N′*,*N′*-tetramethylguanidine, abbreviated TMG) and no reactivity of the biphenyl backbone was observed.

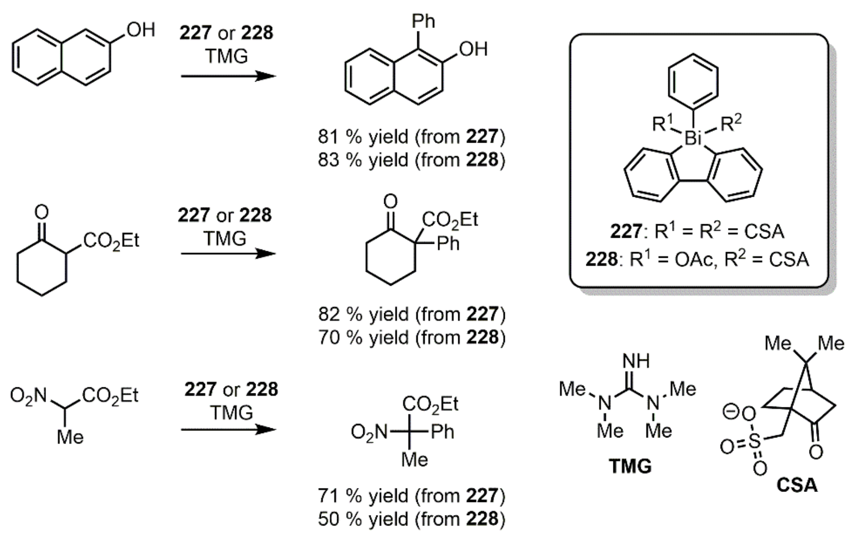

Scheme 1.27. Use of phenylbisma(V)fluorenes as arylation agents.

Pentavalent phenylbisma(V)fluorenes have also been used to effectively oxidatively couple carbonyl compounds to yield synthetically useful 1,4-dicarbonyls

(Scheme 1.28).[132] Dimerization of a variety of lithium enolates derived from ketones and carboxylic esters with **229** was found to be possible with high product yield.

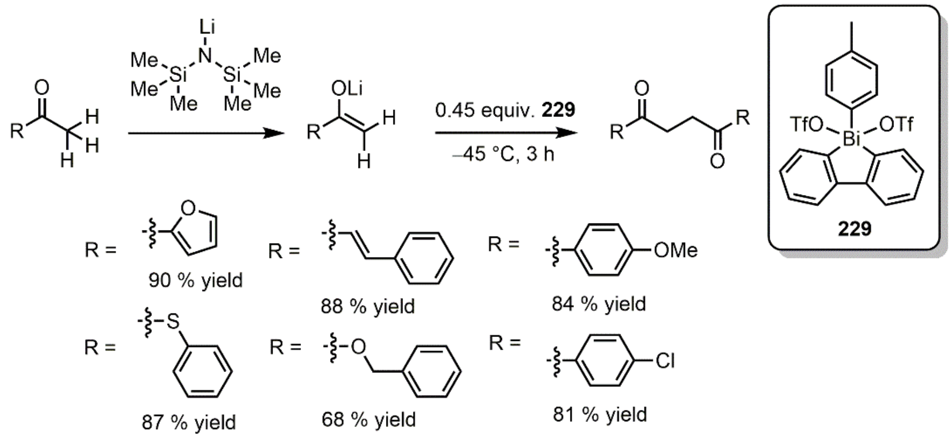

Scheme 1.28. Use of the *o*-tolylbisma(V)fluorene **229** to oxidatively couple carbonyl compounds.

While Fagan and Nugent metallacycle transfer works for bismuth (*vide supra*), in practice, this method is not generally used to prepare substituted bismoles. Though a few studies pertaining to the properties of bismoles have been reported,[133,134,129] the formation of bismole rings was generally accomplished via the reaction of bismuth halides with dilithiodienes. A probable reason for this is that the traditional metallacycle transfer reaction becomes very slow for the heavier main group element halides, as is observed in the production of stannoles and stiboles (*e.g.* Gabbaï's synthesis of triphenylbenzostibole (**212**) and chlorodiphenylbenzostibole (**215**) required 48 hours to complete via metallacycle transfer, see Scheme 1.23b).

As discussed previously (Section 1.3.3) metallacycle transfer to produce stannoles becomes drastically faster when CuCl is used as a transmetallation catalyst, and this thesis will introduce the benefits of applying CuCl towards bismole synthesis as well.

1.4.4.2 Luminescence of Bismoles

In 2006, Chujo and coworkers successfully prepared the polybismole **233**, the first well-defined polymer containing bismuth as an integral (main chain) component (Scheme 1.29).[133] Incorporation of bismuth into a polymer was accomplished in the final step of a series of post-polymerization modification reactions. To begin, the polydiyne **230** was synthesized by Sonogashira coupling; the use of end-capping agents was used to control the resulting molecular weights and impart solubility for subsequent reaction chemistry. Polydiyne **230** was converted to **231** zirconium-mediated cyclization of the alkyne units. The resulting metallopolymer **231** was treated with I_2 to yield polydiiodobutadiene **232**, which was then lithiated and subsequently reacted with $PhBiBr_2$ to form the target bismole-arene polymer **233**. Polymer **233** displayed photoluminescence with λ_{em} = 440 nm (λ_{ex} = 310 nm) in CH_2Cl_2 and a quantum efficiency approaching 13 %. The authors did not comment on whether photoluminescence was possible for **233** in the solid state. The nature of the luminescence of **233** in CH_2Cl_2 remains to be confirmed as no lifetime measurements were taken, however the small Stokes shift noted suggests that the emission is fluorescence.

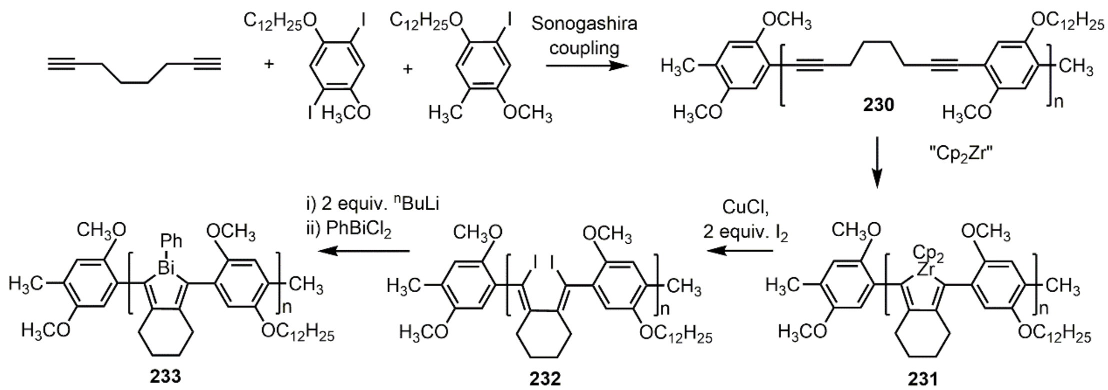

Scheme 1.29. Synthesis of bismole polymer **233**.

Following their pre-established synthetic route for yielding antimony-containing heterocycles, Ohshita and coworkers prepared a series of dithienylbismoles **219**–**222** (Scheme 1.25).[134] The optical data for these ring-fused heterocycles was comparable to known silole analogues[135] with DFT studies revealing minimal participation from Bi to the HOMO states. Compounds **219**–**222** exhibited red photoluminescence in $CHCl_3$ with a sharp band at *ca.* 400 nm accompanied by a broad emission peak from 600–640 nm that was assigned to phosphorescence; in line with this postulate, the long wavelength emission was quenched in the presence of oxygen. In addition, self-quenching of phosphorescence (triplet–triplet annihilation) occurred in the solid state for the relatively planar bismoles **219** and **222**, while some phosphorescence was preserved in the $-SiMe_3$ capped heterocycles **220** and **221** (albeit with Φ values below 0.2 %). In the case of these silylated dithienobismoles, it is likely that close intermolecular contacts are suppressed by the presence of hindered $-SiMe_3$ groups, thus preventing complete triplet–triplet annihilation.

The Ohshita group also reported the synthesis of dipyridinobismole (**224**, Scheme 1.25) which displayed similar emission properties to the analogous dipyridinostibole (**223**).[129] Compound **224** displayed weak fluorescence at 330 nm at room temperature in Me-THF but when cooled to 77 K, **224** showed additional phosphorescence at 454 nm. In the solid state, the phosphorescence with λ_{em} = 484 nm was observed. Like for the stibole analogue, a coordination complex (**226**) could be formed upon reacting **224** with $Cu_2I_2(PPh_3)_3$ and this complex displayed phosphorescence with an emission maximum at 700 nm (Φ < 2 %) at 77 K in the solid state.

As the reports on the luminescent properties of bismoles have thus far been few, this Thesis aims to investigate the underlying mechanisms for luminescence in these emitters, with a focus on selecting for phosphorescence, as well as the synthesis of bismoles using metallacycle transfer, and the development of a synthetic route to access bismole-based polymers. Additionally, the first examples of polybenzophosphole oxides and the effects of polymerization on the emissive propteries of this heterocycle will be discussed.

1.5 References

1. Baldo, M. A.; O'Brien, D. F.; You. Y.; Shoustikov, A.; Sibley, S.; Thompson, M. E.; Forrest, S. R. *Nature* **1998**, *395*, 151–154.
2. (a) Alonso-de Castro, S.; Baggaley, E.; Baraldo, L. M.; Che, C.-M.; Etchenique, R.; Filevich, O.; Ford, P. C.; Habtemariam, A.; Huang, W.; Hung, F.-F.; Li, F.; Liu, S.; Muizzi, D. A.; Ostrowski, A. D.; Pierri, A. E. ; Ruggiero, E.; Salassa, L.;

Weinstein, J. A.; Williams, J. A. G.; Yam, V. W.-W.; Yang, C.; Yeung, M. C.-L.; Zayat, L.; Zhang, K. Y.; Zhao, Q.; Zou, T. *Luminescent and Photoactive Transition Metal Complexes as Biomolecular Probes and Cellular Reagents* (Ed: Lo, K. K.-W.), Springer-Verlag GmbH Heidelberg, 2015. (b) Zhao, Q.; Sun, J. Z. *J. Mater. Chem. C* **2016**, *4*, 10588–10609. (c) Lv, W.; Yang, T.; Yu, Q.; Zhao, Q.; Zhang, K. Y.; Liang, H.; Liu, S.; Li, F.; Huang, W. *Adv. Sci.* **2015**, *2*, 1500107. (d) Zhao, Q.; Huang, C.; Li, F. *Chem. Soc. Rev*. **2011**, *40*, 2508–2524.

3. Tabachnyk, M.; Ehrler, B.; Gélinas, S.; Böhm, M. L.; Walker, B. J.; Musselman, K. P.; Greenham, N. C.; Friend R. H.; Rao, A. *Nat. Mater*. **2014**, *13*, 1033–1038.

4. Rivard, E. *Chem. Lett.* **2015**, *44*, 730–736.

5. You, Y. *Curr. Opin. Chem. Biol*. **2013**, *17*, 699–707.

6. (a) Filatov, M. A.; Baluschev, S.; Landfester, K. *Chem. Soc. Rev*. **2016**, *45*, 4668–4689. (b) Papkovsky, D. B.; Zhdanov, A. V. *Free Radical Biol. Med*. **2016**, *101*, 202–210. (c) Baldo, M. A.; Adachi, C.; Forrest, S. R. *Phys. Rev. B* **2000**, *62*, 10967–10977.

7. Baba, M. *J. Phys. Chem. A* **2011**, *115*, 9514–9519.

8. Gwaiz, A. A.; El-Sayed, M. A. *Chem. Phys. Lett*. **1973**, *19*, 11–15.

9. (a) Yamauchi, S.; Pratt, D. W. *Mol. Phys.* **1979**, *37*, 541–569. (b) Yuan, W. Z.; Shen, X. Y.; Zhao, H.; Lam, J. W. Y.; Tang, L.; Lu, P.; Wang, C.; Liu, Y.; Wang, Z.; Zheng, Q.; Sun, J. Z.; Ma, Y.; Tang, B. Z. *J. Phys. Chem. C* **2010**, *114*, 6090–6099.

10. Kuno, S.; Akeno, H.; Ohtani, H.; Yuasa, H. *Phys. Chem. Chem. Phys.* **2015**, *17*, 15989–15995.

11. Chen, B.; Sun, X.; Evans, R. E.; Zhou, R.; Demas, J. N.; Trindle, C. O.; Zhang, G. *J. Phys. Chem. A* **2015**, *119*, 8854–8859.

12. Wang, T.; Wu, Z.; Sun, W.; Jin, S.; Zhang, X.; Zhou, C.; Jiang, J.; Luo, Y.; Zhang, G. *J. Phys. Chem. A* **2017**, *121*, 7183–7190.

13. Xiong, Y.; Zhao, Z.; Zhao, W.; Ma, H.; Peng, Q.; He, Z.; Zhang, X.; Chen, Y.; He, X.; Lam, J. W. Y.; Tang, B. Z. *Angew. Chem. Int. Ed*. **2018**, *57*, 7997–8001.

14. (a) Ma, D.; Tsuboi, T.; Qiu, Y.; Duan, L. *Adv. Mater*. **2017**, *29*, 1603253. (b) Ma, D.-L.; Lin, S.; Wang, W.; Yang, C.; Leung, C.-H. *Chem. Sci*. **2017**, *8*, 878–889.

15. (a) Fleetham, T.; Li, G.; Li, J. *Adv. Mater*. **2017**, *29*, 1601861. (b) Li, K.; Tong, G. S. M.; Wan, Q.; Cheng, G.; Tong, W.-Y.; Ang, W.-H.; Kwong, W.-L.; Che, C.-M. *Chem. Sci*. **2016**, *7*, 1653–1673.

16. Chi, Y.; Chou, P.-T. *Chem. Soc. Rev*. **2007**, *36*, 1421–1431.

17. Gray, V.; Moth-Poulsen, K.; Albinsson, B.; Abrahamsson, M. *Coord. Chem. Rev*. **2018**, *362*, 54–71.

18. Xu, X.; Yang, X.; Zhao, J.; Zhou, G.; Wong, W.-Y. *Asian J. Org. Chem.* **2015**, *4*, 394–429.

19. Papkovsky, D. B.; Dmitriev R. I. *Chem. Soc. Rev*. **2013**, *42*, 8700–8732.

20. Pander, P.; Swist, A.; Turczyn, R.; Pouget, S.; Djurado, D.; Lazauskas, A.; Pashazadeh, R.; Grazulevicius, J. V.; Motyka, R.; Klimash, A.; Skabara, P. J.; Data, P.; Soloducho, J.; Dias, F. B. *J. Phys. Chem. C* **2018**, *122*, 24958–24966.

21. Yuan, W. Z.; Shen, X. Y.; Zhao, H.; Lam, J. W. Y.; Tang, L.; Lu, P.; Wang, C.; Liu, Y.; Wang, Z.; Zheng, Q.; Sun, J. Z.; Ma, Y.; Tang, B. Z. *J. Phys. Chem. C* **2010**, *114*, 6090–6099.

22. Gong, Y.; Chen, G.; Peng, Q.; Yuan, W. Z.; Xie, Y.; Li, S.; Zhang, Y.; Tang, B. Z. *Adv. Mater.* **2015**, *27*, 6195–6201.

23. Straub, L.; González-Abradelo, D.; Strassert, C. A. *Chem. Commun.* **2017**, *53*, 11806–11809.

24. Easley, C. J.; Mettry, M.; Moses, E. M.; Hooley, R. J.; Bardeen, C. J. *J. Phys. Chem. A* **2018**, *122*, 6578−6584.

25. (a) Xiang, H.; Cheng, J.; Ma, X.; Zhou, X.; Chruma, J. J. *Chem. Soc. Rev*. **2013**, *42*, 6128–6185. (b) Yoshihara, T.; Hirakawa, Y.; Hosaka, M.; Nangaki, M.; Tobita, S. *J. Photochem. Photobiol. C* **2017**, *30*, 71–95. (c) Hussain, F.; Wang, X.; Wang, S. *J. Organomet. Chem.* **2019**, *880*, 300–311.

26. Ding, J.; Wang, B.; Yue, Z.; Yao, B.; Xie, Z.; Cheng, Y.; Wang, L.; Jing, X.; Wang, F. *Angew. Chem. Int. Ed.* **2009**, *48*, 6664–6666.

27. (a) Stokes, G. G. *Philos. Trans. R. Soc. London* **1853**, *143*, 386–396. (b) Levy, L. A. *J. Chem. Soc. Trans.* **1908**, *93*, 1446–1463. (c) Kaufmann, H. *Ber. Dtsch. Chem. Ges.* **1917**, *50*, 1614–1623. (d) Kuhn, A. *Kolloid-Z.* **1942**, *100*, 126–135.

28. Luo, J.; Xie, Z.; Lam, J. W. Y.; Cheng, L.; Chen, H.; Qiu, C.; Kwok, H. S.; Zhan, X.; Liu, Y.; Zhu, D. Tang, B. Z. *Chem. Commun.* **2001**, 1740–1741.

29. (a) Hong, Y.; Lam, J. W. Y.; Tang, B. Z. *Chem. Commun.* **2009**, 4332–4353. (b) Mei, J.; Hong, Y.; Lam, J. W. Y.; Qin, A.; Tang, Y.; Tang, B. Z. *Adv. Mater.* **2014**, *26*, 5429–5479.

30. Tang, B. Z.; Zhan, X.; Yu, G.; Lee, P. P. S.; Liu, Y.; Zhu, D. *J. Mater. Chem.* **2001**, *11*, 2974–2978.

31. (a) Mei, J.; Leung, N. L. C.; Kwok, R. T. K.; Lam, J. W. Y.; Tang, B. Z. *Chem. Rev.* **2015**, *115*, 11718–11940. (b) Hong, Y.; Lam, J. W. Y.; Tang, B. Z. *Chem. Soc. Rev.* **2011**, *40*, 5361–5388.

32. Nishiuchi, T.; Tanaka, K.; Kuwatani, Y.; Sung, J.; Nishinaga, T.; Kim, D.; Iyoda, M. *Chem. Eur. J.* **2013**, *19*, 4110–4116.

33. Chen, J.; Law, C. C. W.; Lam, J. W. Y.; Dong, Y.; Lo, S. M. F.; Williams, I. D.; Zhu, D.; Tang, B. Z. *Chem. Mater*. **2003**, *15*, 1535−1546.

34. (a) Lu, H.; Zheng, Y.; Zhao, X.; Wang, L.; Ma, S.; Han, X.; Xu, B.; Tian, W.; Gao, H. *Angew. Chem. Int. Ed*. **2016**, *55*, 155–159. (b) Shao, A.; Guo, Z.; Zhu, S.; Zhu, S.; Shi, P.; Tian, H.; Zhu, W. *Chem. Sci*. **2014**, *5*, 1383–1389.

35. (a) Wang, J.; Mei, J.; Yuan, W.; Lu, P.; Qin, A.; Sun, J.; Ma, Y.; Tang, B. Z. *J. Mater. Chem.* **2011**, *21*, 4056–4059. (b) Hou, X.-G.; Wu, Y.; Cao, H.-T.; Sun, H.-Z.; Li, H.-B.; Shan, G.-G.; Su, Z.-M. *Chem. Commun.* **2014**, *50*, 6031–6034.

36. (a) Malik, A. H.; Kalita, A.; Iyer, P. K. *ACS Appl. Mater. Interfaces* **2017**, *9*, 37501–37508. (b) Singh, P.; Singh, H.; Sharma, R.; Bhargava, G.; Kumar, S. *J. Mater. Chem. C* **2016**, *4*, 11180–11189.

37. Yang, J.; Huang, J.; Li, Q.; Li, Z. *J. Mater. Chem. C* **2016**, *4*, 2663–2684.

38. (a) Mei, J.; Hong, Y.; Lam, J. W. Y.; Qin, A.; Tang, Y. Tang, B. Z. *Adv. Mat.* **2014**, *26*, 5429–5479. (b) Zhao, Z.; He, B.; Tang, B. Z. *Chem. Sci.* **2015**, *6*, 5347–5365. (c) Wang, M.; Zhang, G.; Zhang, D.; Zhu, D.; Tang, B. Z. *J. Mater. Chem.* **2010**, *20*, 1858–1867. (d) Li, B.; He, T.; Shen, X.; Tang, D.; Yin, S. *Polym. Chem.* **2019**, *10*, 796–818.

39. (a) Baroncini, M.; Bergamini, G.; Ceroni, P. *Chem. Commun.* **2017**, *53*, 2081–2093. (b) Ubba, E.; Tao, Y.; Yang, Z.; Zhao, J.; Wang, L.; Chi, Z. *Chem. Asian. J.* **2018**, *13*, 3106–3121. (c) Zhang, Y.; Mao, H.; Xu, W.; Shi, J.; Cai, Z.; Tong, B.; Dong. Y. *Chem. Eur. J.* **2018**, *24*, 15965–15977.

40. (a) Ravotto, L.; Ceroni, P. *Coord. Chem. Rev.* **2017**, *346*, 62–76. (b) Mauro, M.; Cebrián, C. *Isr. J. Chem.* **2018**, *58*, 901–914.

41. Strasser, A.; Vogler, A. *Inorg. Chem. Commun.* **2004**, *7*, 528–530.

42. Strasser, A.; Vogler, A. *J. Photochem. Photobiol. A* **2004**, *165*, 115–118.

43. (a) Sano, Y.; Satoh, H.; Chiba, M.; Okamoto, M.; Serizawa, K.; Nakashima, H.; Omae, K. *J. Occup. Health* **2005**, *47*, 293–298. (b) Yang, N.; Sun, H. *Coord. Chem. Rev.* **2007**, *251*, 2354–2366.

44. (a) Ohshita, J.; Matsui, S.; Yamamoto, R.; Mizumo, T.; Ooyama, Y.; Harima, Y.; Murafuji, T.; Tao, K.; Kuramochi, Y.; Kaikoh, T.; Higashimura, H. *Organometallics* **2010**, *29*, 3239–3241. (b) Parke, S. M.; Narreto, M. A. B.; Hupf, E.; McDonald, R.; Ferguson, M. J.; Hegmann, F. A.; Rivard, E. *Inorg. Chem*. **2018**, *57*, 7536–7549.

45. Toma, O.; Mercier, N.; Botta, C. *Eur. J. Inorg. Chem.* **2013**, 1113–1117.

46. Toma, O.; Mercier, N.; Allain, M.; Botta, C. *CrystEngComm.* **2013**, *15*, 8565–8571.

47. Toma, O.; Mercier, N.; Allain, M.; Forni, A.; Meinardi, F.; Botta, C. *Dalton Trans.* **2015**, *44*, 14589–14593.

48. Toma, O.; Allain, M.; Meinardi, F.; Forni, A.; Botta, C.; Mercier, N. *Angew. Chem. Int. Ed*. **2016**, *55*, 7998–8002.

49. Toma, O.; Mercier, N.; Allain, M.; Meinardi, F.; Botta, C. *Eur. J. Inorg. Chem*. **2017**, 844–850.

50. Wang, Z.-P.; Wang, J.-Y.; Li, J.-R.; Feng, M.-L.; Zou, G.-D.; Huang, X.-Y. *Chem. Commun*. **2015**, *51*, 3094–3097.

51. Shen, N.; Li, J.; Wu, Z.; Hu, B.; Cheng, C.; Wang, Z.; Gong, L.; Huang, X. *Chem. Eur. J.* **2017**, *23*, 15795–15804.

52. (a) He, G.; Kang, L.; Torres Delgado, W.; Shynkaruk, O.; Ferguson, M. J.; McDonald, R.; Rivard, E. *J. Am. Chem. Soc.* **2013**, *135*, 5360–5363. (b) For a review of this concept, see: Carrera, E. I.; Seferos, D. S. *Macromolecules* **2015**, *48*, 297–308.

53. He, G.; Torres Delgado, W.; Schatz, D. J.; Merten, C.; Mohammadpour, A.; Mayr, L.; Ferguson, M. J.; McDonald, R.; Brown, A.; Shankar, K.; Rivard, E. *Angew. Chem. Int. Ed*. **2014**, *53*, 4587–4591.

54. Braun, C. A.; Zomerman, D.; de Aguiar, I.; Qi, Y.; Torres Delgado, W.; Ferguson, M. J.; McDonald, R.; de Souza, G. L. C.; He, G.; Brown, A.; Rivard, E. *Faraday Discuss*. **2017**, *196*, 255–268.

55. Mohammadpour, A.; Wiltshire, B. D.; Farsinezhad, S.; Zhang, Y.; Askar, A. M.; Kisslinger, R.; Delgado, W. T.; He, G.; Kar, P.; Rivard, E.; Shankar, K. *Org. Electron.* **2016**, *39*, 153–162.

56. Torres Delgado, W.; Braun, C. A.; Boone, M. P.; Shynkaruk, O.; Qi, Y.; McDonald, R.; Ferguson, M. J.; Data, P.; Almeida, S. K. C.; de Aguiar, I.; de Souza, G. L. C.; Brown, A.; He, G.; Rivard, E. *ACS Appl. Mater. Interfaces* **2018**, *10*, 12124–12134.

57. Kremer, A.; Aurisicchio, C.; De Leo, F.; Ventura, B.; Wouters, J.; Armaroli, N.; Barbieri, A.; Bonifazi, D. *Chem. Eur. J.* **2015**, *21*, 15377–15387.

58. Kremer, A.; Fermi, A.; Biot, N.; Wouters, J.; Bonifazi, D. *Chem. Eur. J*. **2016**, *22*, 5665–5675.

59. Kuno, S.; Kanamori, T.; Yijing, Z.; Ohtani, H.; Yuasa, H. *ChemPhotoChem*. **2017**, *1*, 102–106.

60. Shoji, Y.; Ikabata, Y.; Wang, Q.; Nemoto, D.; Sakamoto, A.; Tanaka, N.; Seino, J.; Nakai, H.; Fukushima, T. *J. Am. Chem. Soc.* **2017**, *139*, 2728–2733.

61. (a) Riebe, S.; Vallet, C.; van der Vight, F.; Gonzalez-Abradelo, D.; Wölper, C.; Strassert, C. A.; Jansen, G.; Knauer, S.; Voskuhl, J. *Chem Eur. J*. **2017**, *23*, 13660–13668. For important prior work in this field, see: (b) Bergamini, G.; Fermi, A.; Botta, C.; Giovanella, U.; Di Motta, S.; Negri, F.; Peresutti, R.; Gingras, M.; Ceroni, P. *J. Mater. Chem. C* **2013**, *1*, 2717–2724. (c) Fermi, A.; Bergamini, G.; Peresutti, R.; Marchi, E.; Roy, M.; Ceroni, P.; Gingras, M. *Dyes Pigm*. **2014**, *110*, 113–122.

62. Xue, P.; Wang, P.; Chen, P.; Ding, J.; Lu, R. *RSC Adv.* **2016**, *6*, 51683–51686.

63. Braye, E. H.; Hübel, W.; Caplier, I. *J. Am. Chem. Soc*. **1961**, *83*, 4406–4413.

64. Alt, H.; Rausch, M. D. *J. Am. Chem. Soc.* **1974**, *96*, 5936–5937.

65. (a) Negishi, E.-I.; Takahashi, T. *Acc. Chem. Res.* **1994**, *27*, 124–130. (b) Negishi, E.-I.; Takahashi, T. *Bull. Chem. Soc. Jpn.* **1998**, *71*, 755–769.

66. Negishi, E.; Cederbaum, F. E.; Takahashi, T. *Tetrahedron Lett.* **1986**, *27*, 2829–2832.

67. (a) Rosenthal, U.; Ohff, A.; Baumann, W.; Tillack, A.; Görls, H.; Burlakov, V. V.; Shur, V. B. *Z. Anorg. Allg. Chem.* **1995**, *621*, 77–83. (b) Rosenthal, U.; Ohff, A.; Michkalik, M; Görls, H.; Burlakov, V. V.; Shur, V. B. *Angew. Chem. Int. Ed. Engl.* **1993**, *32*, 1193–1195.

68. Dioumaev, V. K.; Harrod, J. F. *Organometallics*, **1997**, *16*, 1452–1464.

69. (a) Johnson, S. A.; Liu, F.-Q.; Suh, M. C.; Zürcher, S.; Haufe, M.; Mao, S. S. H.; Tilley, T. D. *J. Am. Chem. Soc.* **2003**, *125*, 4199–4211. (b) Gessner, V. H.; Tannaci, J. F.; Miller, A. D.; Tilley, T. D. *Acc. Chem. Res.* **2011**, *44*, 435–446.

70. (a) Hara, R.; Xi, Z.; Kotora, M.; Xi, C.; Takahashi, T. *Org. Lett.* **1996**, *25*, 1003–1004. (b) Miller, A. D.; Johnson, S. A.; Tupper, K. A.; McBee, J. L.; Tilley, T. D. *Organometallics* **2009**, *28*, 1252–1262.

71. Miller, A. D.; Tannaci, J. F.; Johnson, S. A.; Lee, H.; McBee, J. L.; Tilley, T. D. *J. Am. Chem. Soc.* **2009**, *131*, 4917–4927.

72. Buchwald, S. L.; Watson, B. T. *J. Am. Chem. Soc.* **1986**, *108*, 7411–7413.

73. Fagan, P. J.; Nugent, W. A. *J. Am. Chem. Soc*. **1988**, *110*, 2310–2312.

74. Fagan, P. J.; Nugent, W. A.; Calabrese, J. C. *J. Am. Chem. Soc*. **1994**, *116*, 1880–1889.

75. Takahashi, T.; Kotora, M.; Kasai, K.; Suzuki, N. *Organometallics* **1994**, *13*, 4183–4185.

76. (a) Zhang, Z.; Wang, Z.; Haehnel, M.; Eichhorn, A.; Edkins, R. M.; Steffen, A.; Krueger, A.; Lin, Z.; Marder, T. B. *Chem. Commun*. **2016**, *52*, 9707–9710. (b) Houghton, A. Y.; Karttunen, V. A.; Piers, W. E.; Tuononen, H. M. *Chem.*

Commun. **2014**, *50*, 1295–1298. (c) Fan, C.; Piers, W. E.; Parvez, M. *Angew. Chem. Int. Ed.* **2009**, *48*, 2955–2958.

77. Liu, L.; Geng, W.; Yang, Q.; Zhang, W.-X.; Xi, Z. *Organometallics* **2015**, *34*, 4198−4201.
78. Geng, W.; Wei, J.; Zhang, W.-X.; Xi, Z. *J. Am. Chem. Soc*. **2014**, *136*, 610−613.
79. Ubayama, H.; Sun, W.-H.; Takahashi, T.; Xi, Z. *Chem. Commun.* **1998**, *18*, 1931–1932.
80. He, G.; Shynkaruk, O.; Lui M. W.; Rivard, E. *Chem. Rev.* **2014**, *114*, 7815–7880.
81. Wittig, G.; Geissler, G. *Liebigs Ann. Chem.* **1953**, *580*, 44–57.
82. Campbell, I. G. M.; Way, J. K. *Proc. Chem. Soc.* **1959**, 231–232.
83. (a) Aeschlimann, J. A.; Lees, N. D.; McCleland, N. P.; Nicklin, G. N. *J. Chem. Soc. Trans*. **1925**, *127*, 66–69. (b) Das-Gupta, H. N. *J. Indian Chem. Soc.* **1935**, *12*, 627–628. (c) Das-Gupta, H. N. *J. Indian Chem. Soc.* **1937**, *14*, 400–405.
84. Morgan, G. T.; Davies, G. R. *Proc. Royal Soc. A* **1930**, *127*, 1–8.
85. (a) Campbell, I. G. M. *J. Chem. Soc.* **1950**, 3109–3116. (b) Campbell, I. G. M. *J. Chem. Soc.* **1952**, 4448–4453. (c) Campbell, I. G. M.; Morrill, D. J. *J. Chem. Soc.* **1955**, 1662–1670.
86. (a) Wittig, G.; Hellwinkel, D. *Chem. Ber.* **1964**, *97*, 789−793. (b) Hellwinkel, D.; Bach, M. *Liebigs. Ann. Chem.* **1968**, *720*, 198−200.
87. Leavitt, F. C.; Manuel, T. A.; Johnson, F. *J. Am. Chem. Soc.* **1959**, *81*, 3163–3164.
88. Braye, E. H.; Hübel, W.; Caplier, E. *J. Am. Chem. Soc.* **1961**, *83*, 4406–4413.

89. (a) Davydov, S. N.; Rodionov, A. N.; Shigorin, D. N.; Syutkina, O. P.; Krasnova, T. L. *Zh. Fiz. Khim.* **1981**, *55*, 784–787. (b) Davydov, S. N.; Rodionov, A. N.; Shigorin, D. N.; Syutkina, O. P.; Krasnova, T. L. *Zh. Fiz. Khim.* **1980**, *54*, 506–508. (c) Davydov, S. N.; Rodionov, A. N.; Shigorin, D. N.; Syutkina, O. P.; Krasnova, T. L. *Zh. Fiz. Khim.* **1981**, *55*, 784–787.

90. (a) Nyulászi, L.; Hollóczki, O.; Lescop, C.; Hissler, M.; Réau, R. *Org. Biomol. Chem*. **2006**, *4*, 996–998. (b) Szucs, R.; Bouit, P.-A.; Hissler, M.; Nyulaszi, L. *Struct. Chem.* **2015**, *26*, 1351–1357. (c) Schleyer, P. v. R.; Maerker, C.; Dransfeld, A.; Jiao, H.; Hommes, N. J. R. v. E. *J. Am. Chem. Soc*. **1996**, *118*, 6317–6318.

91. Duffy, M. P.; Delaunay, W.; Bouit, P.-A.; Hissler, M. *Chem. Soc. Rev*. **2016**, *45*, 5296–5310.

92. (a) Bu, F.; Wang, E.; Peng, Q.; Hu, R.; Qin, A.; Zhao, Z.; Tang, B. Z. *Chem. Eur. J.* **2015**, *21*, 4440–4449. (b) Zhuang, Z.; Bu, F.; Luo, W.; Peng, H.; Chen, S.; Hu, R.; Qin, A.; Zhao, Z.; Tang, B. Z. *J. Mater. Chem. C* **2017**, *5*, 1836–1842.

93. Fukazawa, A.; Ichihashi, Y.; Kosaka, Y.; Yamaguchi, S. *Chem. Asian J*. **2009**, *4*, 1729–1740.

94. Hibner-Kulicka, P.; Joule, J. A.; Skalik, J.; Bałczewski, P. *RSC Adv*. **2017**, *7*, 9194–9236.

95. (a) Baumgartner, T.; Neuman, T.; Wirges, B. *Angew. Chem. Int. Ed*. **2004**, *43*, 6197–6201. (b) Baumgartner, T.; Bergmans, W.; Kárpáti, T.; Neumann, T.; Nieger, M.; Nyulászi, L. *Chem. Eur. J.* **2005**, *11*, 4687–4699. (c) Baumgartner, T.; Wilk, W. *Org. Lett*. **2006**, *8*, 503–506. (d) Dienes, Y.; Durben, S.; Kárpáti, T.; Neumann, T.; Englert, U.; Nyulászi, L.; Baumgartner, T. *Chem. Eur. J.* **2007**, *13*,

7487–7500. (e) Durben, S.; Nickel, D.; Krüger, R. A.; Sutherland, T. C.; Baumgartner, T. *J. Polym. Sci., Part A: Polym. Chem.* **2008**, *46*, 8179–8190. (f) Romero-Nieto, C.; Durben, S.; Kormos, I. M.; Baumgartner, T. *Adv. Funct. Mater.* **2009**, *19*, 3625–3631. (g) Krüger, R. A.; Gordon, T. J.; Sutherland, T. C.; Baumgartner, T. *J. Polym. Sci., Part A: Polym. Chem.* **2011**, *49*, 1201–1209. (h) Ren, Y.; Baumgartner, T. *Dalton Trans*. **2012**, *41*, 7792–7800.

96. Takahashi, M.; Nakano, K.; Nozaki, K. *J. Org. Chem.* **2015**, *80*, 3790–3797.

97. Rausch, M. D.; Klemann, L. P. *J. Am. Chem. Soc.* **1967**, *89*, 5732–5733.

98. (a) Chan, T. H.; Wong, L. T. L. *Can. J. Chem.* **1971**, *49*, 530–531. (b) Collins, D. J.; Rowley, L. E.; Swan, J. M. *Aust. J. Chem.* **1974**, *27*, 831–839. (c) Holah, D. G. H.; Alan, N. H.; Daniel, K. *J. Heterocycl. Chem.* **1977**, *14*, 705–707. (d) Balthazor, T. M. *J. Org. Chem*. **1980**, *45*, 2519–2522. (e) Nief, F.; Charrier, C.; Mathey, F.; Simalty, M. *Phosphorus Sulfur Silicon Relat. Elem.* **1982**, *13*, 259–267. (f) Quin, L. D.; Rao, N. S.; Topping, R. J.; McPhail, A. T. *J. Am. Chem. Soc*. **1986**, *108*, 4519–4526. (g) Decken, A.; Bottomley, F.; Wilkins, B. E.; Gill, E. D. *Organometallics* **2004**, *23*, 3683–3693. (h) Wu, B.; Yoshikai, N. *Org. Biomol. Chem.* **2016**, *14*, 5402–5416. (i) Chen, Y.-R.; Duan, W.-L. *J. Am. Chem. Soc*. **2013**, *135*, 16754–16757. (j) Liu, L.; Dong, J.; Yan, Y.; Yin, S.-F.; Han, L.-B.; Zhou, Y. *Chem. Commun*. **2019**, *55*, 233–236.

99. Tsuji, H.; Sato, K.; Ilies, L.; Itoh, Y.; Sato, Y.; Nakamura, E. *Org. Lett.* **2008**, *10*, 2263–2265.

100. Sanji, T.; Shiraishi, K.; Kashiwabara, T.; Tanaka, M. *Org. Lett.* **2008**, *10*, 2689–2692.

101. Fukazawa, A.; Hara, M.; Okamoto, T.; Son, E.-C.; Xu, C.; Tamao, K.; Yamaguchi, S. *Org. Lett*. **2008**, *10*, *5*, 913–916.

102. Yamaguchi, E.; Wang, C.; Fukazawa, A.; Taki, M.; Sato, Y.; Sasaki, T.; Ueda, M.; Sasaki, N.; Higashiyama, T.; Yamaguchi, S. *Angew. Chem. Int. Ed*. **2015**, *54*, 4539–4543.

103. Taki, M.; Ogasawara, H.; Osaki, H.; Fukazawa, A.; Sato, Y.; Ogasawara, K.; Higashiyama, T.; Yamaguchi, S. *Chem. Commun.* **2015**, *51*, 11880–11883.

104. Wang, C.; Taki, M.; Sato, Y.; Fukazawa, A.; Higashiyama, T.; Yamaguchi, S. *J. Am. Chem. Soc*. **2017**, *139*, 10374−10381.

105. Hayashi, Y.; Matano, Y.; Suda, K.; Kimura, Y.; Nakao, Y.; Imahori, H. *Chem. Eur. J.* **2012**, *18*, 15972–15983.

106. Matano, Y.; Hayashi, Y.; Suda, K.; Kimura, Y.; Imahori, H. *Org. Lett*. **2013**, *15*, 4458–4461.

107. Matano, Y.; Motegi, Y.; Kawatsu, S.; Kimura, Y. *J. Org. Chem.* **2015**, *80*, 5944−5950.

108. Koyanagi, Y.; Kawaguchi, S.; Fujii, K.; Kimura, Y.; Sasamori, T.; Tokitoh, N.; Matano, Y. *Dalton Trans*. **2017**, *46*, 9517–9527.

109. Wakatsuki, A.; Yukimoto, M.; Minoura, M.; Fujii, K.; Kimura, Y.; Matano, Y. *Dalton Trans*. **2018**, *47*, 7123–7127.

110. Wu, B.; Santra, M.; Yoshikai, N. *Angew. Chem. Int. Ed*. **2014**, *53*, 7543–7546.

111. Yoshikai, N.; Santra, M.; Wu, B. *Organometallics* **2017**, *36*, 2637−2645.

112. Ichikawa, T.; Morimoto, M.; Sotome, H.; Ito, S.; Miyasaka, H.; Irie, M. *Dyes Pigm*. **2016**, *126*, 186–193.

113. Kato, T.; Tanaka, S.; Naka, K. *Chem. Lett*. **2015**, *44*, 1476–1478.

114. Imoto, H.; Naka, K. *Chem. Eur. J*. **2019**, *25*, 1883–1894.

115. Raciszewski, Z.; Braye, E. H. *Photochem. Photobiol.* **1970**, *12*, 429–432.

116. Ishidoshiro, M.; Matsumura, Y.; Imoto, H.; Irie, Y.; Kato, T.; Watase, S.; Matsukawa, K.; Inagi, S.; Tomita, I.; Naka, K. *Org. Lett.* **2015**, *17*, 4854−4857.

117. Ishidoshiro, M.; Imoto, H.; Tanaka, S.; Naka, K. *Dalton Trans*. **2016**, *45*, 8717–8723.

118. Green, J. P.; Han, Y.; Kilmurray, R.; McLachlan, M. A.; Anthopoulos, T. D.; Heeney, M. *Angew. Chem. Int. Ed.* **2016**, *55*, 7148–7151.

119. Kato, T.; Imoto, H.; Tanaka, S.; Ishidoshiro, M.; Naka, K. *Dalton Trans*. **2016**, *45*, 11338–11345.

120. Imoto, H.; Kawashima, I.; Yamazawa, C.; Tanaka, S.; Naka, K. *J. Mater. Chem. C* **2017**, *5*, 6697–6703.

121. Matsumura, Y.; Ishidoshiro, M.; Irie, Y.; Imoto, H.; Naka, K.; Tanaka, K.; Inagi, S.; Tomita, I. *Angew. Chem. Int. Ed*. **2016**, *55*, 15040–15043.

122. Imoto, H.; Urushizaki, A.; Kawashima, I.; Naka, K. *Chem. Eur. J.* **2018**, *24*, 8797–8803.

123. Green, J. P.; Cryer, S. J.; Marafie, J.; White, A. J. P.; Heeney, M. *Organometallics* **2017**, *36*, 2632−2636.

124. Fell, V. H. K.; Mikosch, A.; Steppert, A.-K.; Ogieglo, W.; Senol, E.; Canneson, D.; Bayer, M.; Schoenebeck, F.; Greilich, A.; Kuehne, A. J. C. *Macromolecules* **2017**, *50*, 2338−2343.

125. Hirai, M.; Gabbaï, F. P. *Chem. Sci.* **2014**, *5*, 1886–1893.

126. Christianson, A. M.; Rivard, E.; Gabbaï, F. P. *Organometallics* **2017**, *36*, 2670−2676.

127. Christianson, A. M.; Gabbaï, F. P. *Organometallics* **2017**, *36*, 3013−3015.

128. Ohshita, J.; Fujita, R.; Tanaka, D.; Ooyama, Y.; Kobayashi, N.; Higashimura, H.; Yamamoto, Y. *Chem. Lett*. **2012**, *41*, 1002–1003.

129. Ohshita, J.; Yamaji, K.; Ooyama, Y.; Adachi, Y.; Nakamura, M.; Watase, S. *Organometallics* **2019**, *38*, 1516–1523.

130. Takahashi, T.; Li, Y.; Ito, T.; Xu, F.; Nakajima, K.; Liu, Y. *J. Am. Chem. Soc.* **2002**, *124*, 1144–1145.

131. Finet, J.-P.; Fedorov, A. Y. *Russ. Chem. Bull. Int. Ed.* **2004**, *53*, 1488–1495.

132. Imachi, S.; Mukaiyama, T. *Chem. Lett.* **2007**, *36*, 718–719.

133. Morisaki, Y.; Ohashi, K.; Na, H.-S.; Chujo, Y. *J. Polym. Sci., Part A: Polym. Chem.* **2006**, *44*, 4857−4863.

134. Ohshita, J.; Matsui, S.; Yamamoto, R.; Mizumo, T.; Ooyama, Y.; Harima, Y.; Murafuji, T.; Tao, K.; Kuramochi, Y.; Kaikoh, T.; Higashimura, H. *Organometallics* **2010**, *29*, 3239−3241.

135. Ohshita, J. *Macromol. Chem. Phys*. **2009**, *210*, 1360–1370.

Chapter 2: Understanding the Origin of Phosphorescence in Bismoles: A Synthetic and Computational Study

2.1 Introduction

Main-group element-containing heterocycles represent a valuable and increasingly explored class of π-conjugated material due to their often-luminescent nature and conductive properties.[1] Much of this interest has been spurred by the attractive properties of thiophene- and polythiophene-derivatives and, most notably, conductive poly-3-alkylthiophene.[2] Thiophene-based materials have displayed promising utility in the areas of luminescence,[3] photovoltaics,[4] and field-effect transistors.[5] Chemistry with this building block has thrived in part due to the stability of thiophene products and the easy of functionalization of thiophene, a by-product readily obtained from petroleum distillation, at either the α or the β positions.

The field of pnictogen-containing heterocycles has been dominated by optoelectronically active nitrogen or phosphorus-containing heterocycles, namely, pyrroles[6] and phospholes.[7] Advances in synthetic methods have opened the door for the wider exploration of the heavier group 15 element analogues, as evidenced by recent reports on luminescent arsenic-based heteroles that are less prone to oxidation than their phosphole counterparts.[8] Moreover, the use of antimony heterocycles (stiboles) and their Sb(V) congeners in fluoride ion sensing can be seen as a promising new direction for this field.[9]

The incorporation of heavier p-block elements into π-conjugated materials can also greatly enhance the probability of accessing triplet excited states (and eventual phosphorescence) by increasing the rate of intersystem crossing (ISC) between excited singlet and triplet states, commonly termed as the "heavy element effect".[10] Stable phosphorescent emitters are highly sought in organic light-emitting diodes (OLEDs) due to a possible maximum device efficiency of 100 % versus 25 % for traditional fluorescence-based emitters.[11] Furthermore, phosphorescent compounds that can exhibit long-wavelength red or IR emission are of great value for bioimaging, as there is less interference with undesired background emission.[12] As bismuth compounds are generally considered to have low toxicity[13] and cost, efficient phosphorescent bismuth-based emitters with color tunability would be of significant value to the community. Challenges that have limited progress in this regard are: (1) a lack of a general synthetic procedure to prepare air-stable bismuth-containing heterocycles (especially bismoles) and (2) difficulties in obtaining solid-state phosphorescence in the presence of oxygen due to self-quenching at high concentrations (via triplet−triplet annihilation) and quenching of excited state triplet species by O_2.[14]

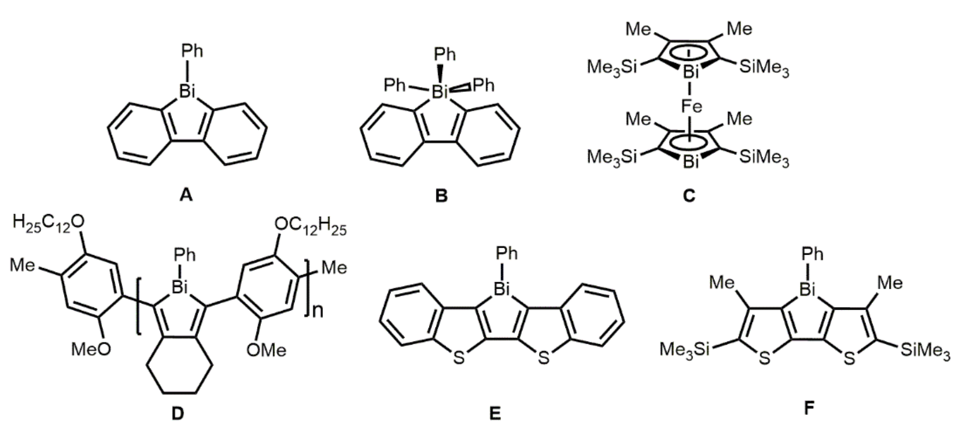

Figure 2.1. Selected bismuth-containing heterocycles exhibiting diverse coordination modes and oxidation states.

Given that this chapter describes the preparation of bismuth-containing five-membered heterocycles (bismoles) and the determination of factors that control their photoluminescence, some key prior studies in this area should be mentioned (Figure 2.1). Approximately 50 years ago Wittig and Hellwinkel published the syntheses of the Bi(III) and Bi(V) bismafluorenes [PhBi(biph)][15] (**A**) and [Ph_3Bi(biph)] (**B**).[16] Later Ashe studied the aromaticity and coordinating properties of formally anionic bismole analogues, including bismaferrocene sandwich complexes (*e.g.* **C**).[17] The first photoluminescent bismuth-containing conjugated polymer (**D**) was reported in 2006 by Chujo and co-workers;[18] although emission lifetime measurements were not reported, the small Stokes shift found in this blue luminescent material was indicative of fluorescence. More recently luminescent dithienylbismoles (*e.g.* **E** and **F**) were prepared by the Ohshita group and show broad photoluminescence (PL) bands at 600−640 nm attributed to weak phosphorescence, as well as concurrent PL at 400 nm due to fluorescence.[19]

While dilithiated butadiene analogues can be used to gain access to Bi heterocycles via condensation reactions with bismuth halides ($RBiCl_2$; R = alkyl or aryl groups; Scheme 2.1, top),[17,19] this current study takes advantage of the mild Fagan-Nugent protocol, whereby zirconium-mediated alkyne cyclization followed by Zr/Bi exchange is used to form bismole rings (Scheme 2.1, bottom).[20] This general procedure has been actively used in our group to gain access to phosphorescent tellurophenes,[21a−e] and herein the first identified examples of phosphorescence from bismoles is reported, a key initial step toward developing these potentially non-toxic emitters for OLED and bioimaging applications.

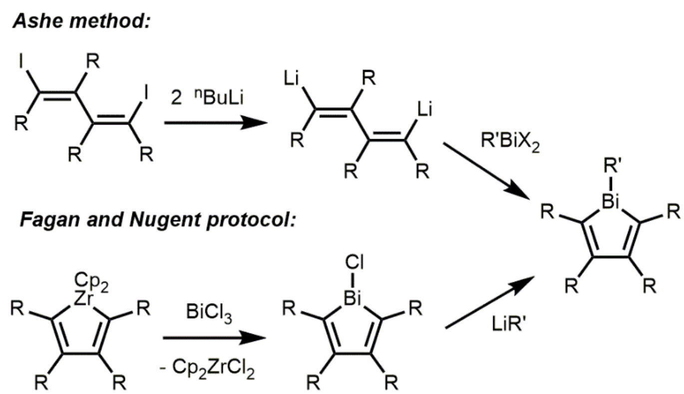

Scheme 2.1. Bismole synthesis via the cyclization of a dilithiated diene (Ashe method) and by metallacycle transfer (Fagan and Nugent protocol).

2.2 Results and Discussion

2.2.1 Synthesis of New Bismoles via Metallacycle Transfer

To gain access to a wider scope of molecular emitters based on the heavy inorganic element, bismuth, metallacycle transfer between the readily available zirconacycle $Cp_2ZrC_4Et_4$[20] and various $ArBiCl_2$ species (Ar = Ph and Mes; Mes = 2,4,6-$Me_3C_6H_2$; Scheme 2.2) was explored. These reactions went to completion under mild conditions to yield the perethylated bismoles $PhBiC_4Et_4$ (**1**) and $MesBiC_4Et_4$ (**2**) in yields of 75 % and 78 %, respectively, as orange and yellow oils, with insoluble Cp_2ZrCl_2 as the common byproduct. Notably, Cp_2ZrCl_2 can be recovered and recycled into the starting zirconacycle $Cp_2ZrC_4Et_4$ via a convenient one-pot procedure.[20] The requisite arylbismuthdihalides $PhBiCl_2$ and $MesBiCl_2$ were prepared *in situ* via the known ligand scrambling reaction between two equivalents of $BiCl_3$ and the respective triarylbismuthines $BiAr_3$ in diethyl ether (Scheme 2.2).[22,23] Compound **1** was observed to undergo decomposition when stored under ambient conditions (64 %

decomposition into unidentifiable insoluble products when stored at room temperature in the presence of air for 24 hours) but remain stable indefinitely in an inert atmosphere. However, compound **2** is stable to water and air, both in solution and in the solid state; this is in sharp contrast to structurally related phospholes,[6] which are readily oxidized in air.

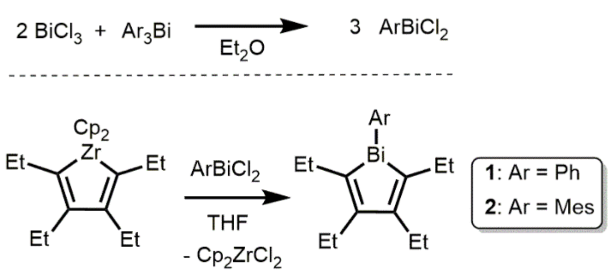

Scheme 2.2. Synthesis of bismoles **1** and **2**.

With the goal of placing reactive pinacolboronate (BPin) groups about the periphery of a bismole (for future ring functionalization via Suzuki-Miyaura cross-coupling),[21e] the known zirconium reagent **B-Cp2Zr-6-B** (Scheme 2.3) was combined with *in situ* derived $MesBiCl_2$. Efficient Zr/Bi exchange only transpired in the presence of 10 mol% CuCl as a catalyst to give the mesityl-functionalized heterocycle **B-MesBi-6-B** (**3**) (Scheme 2.3). The same CuCl-assisted metallacycle transfer protocol was used to generate the 2,5-thiophene-substituted bismole **4** as well as the tetraphenyl-substituted bismoles $PhBiC_4Ph_4$ (**5**) and $MesBiC_4Ph_4$ (**6**) (Scheme 2.3). As desired, compounds **3**–**6** are stable indefinitely in air at room temperature, both in solution and in the solid state.

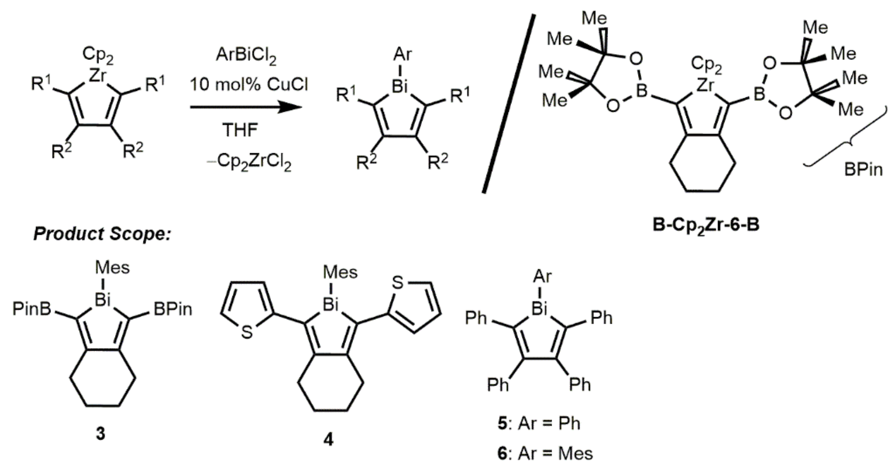

Scheme 2.3. Copper(I) chloride-catalysed metallacycle transfer synthesis of bismoles **3**−**6**.

In addition to the bismoles discussed above, an aryl-substituted bismole containing a proximal $-CH_2NMe_2$ group (**7**, Scheme 2.4) was targeted with the hypothesis that this pendant amine group could be used to modulate luminescence in the final product via a possible hypercoordinate Bi···NMe_2 interaction. Accordingly, the known bismuth dihalide **Ar^{NMe2}BiCl$_2$** (Ar^{NMe2} = 2-$Me_2NCH_2C_6H_4$)[23,24] was combined with the pinacolboronate-capped zirconacycle **B-Cp$_2$Zr-6-B** in the presence of 10 mol% of CuCl as a catalyst. While the formation of the desired arylbismole **7** was confirmed by ^{1}H NMR spectroscopy (*ca*. 90 %, *in situ* yield), there was another minor product formed, which was later identified by X-ray crystallography as the CuCl adduct (**8**) (Scheme 2.4). When a crude mixture containing compounds **7** and **8** (*ca*. 9:1 ratio) was treated with a stoichiometric amount of CuCl, compound **7** was fully converted into the CuCl adduct **8**, which could then be isolated in pure form (59 % yield) by crystallization from toluene at −30 °C. Compound **7** could then be regenerated cleanly by treatment of **8** with a stoichiometric amount of triphenylphosphine to remove the bismole-bound CuCl (Scheme 2.5).

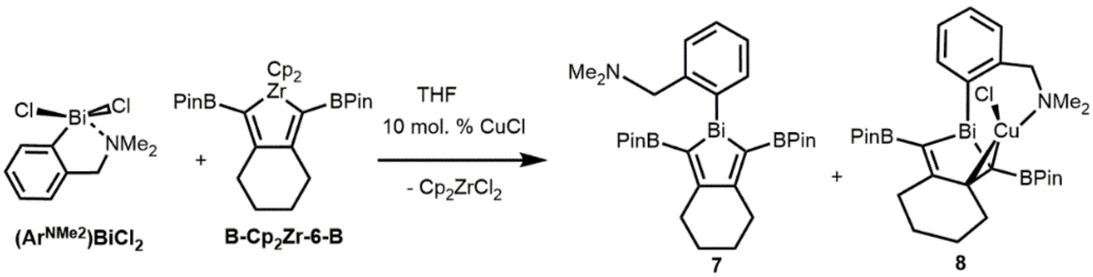

Scheme 2.4. Synthesis of the Ar^{NMe2}-substituted bismoles **7** and **8**.

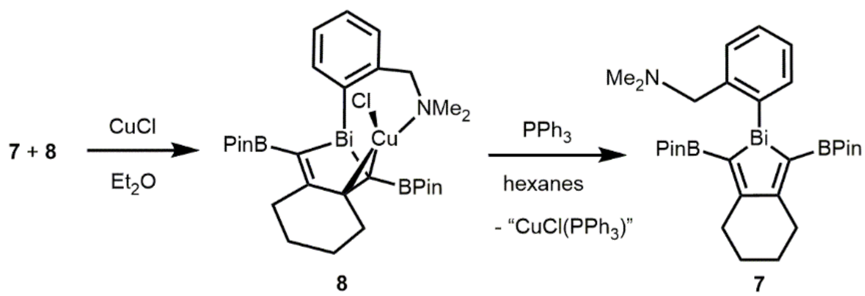

Scheme 2.5. Synthetic route yielding analytically pure **7**.

2.2.2 Structural Characterization of the New Bismoles

The solid-state structures of the new bismoles were investigated to uncover possible intermolecular bismole−bismole interactions and to allow for better interpretation of the luminescence data obtained (*vide infra*). X-ray diffraction experiments were first performed on the aryl-functionalized bismoles **3**−**6**, and the refined structures are presented in Figures 2.2–2.5. When the structure of **3** (Figure 2.2) is compared to its phosphole congener **B-PPh-6-B**,[21a] a substantially pyramidalized geometry can be found about the bismuth center in **3** with a bond angle sum [279.19(17)°] that is much smaller than that found at the phosphorus center in **B-PPh-6-B** [304.53(17)°]; this observation can be explained by an increase in s-orbital character at the bismuth lone pair. In addition, the hindered Mes group in **3** causes the rotation of one BPin group away from being coplanar to the bismole ring by 29.9(4)°, while the other BPin group remains coplanar, as is commonly found in most BPin-functionalized tellurophenes.[21]

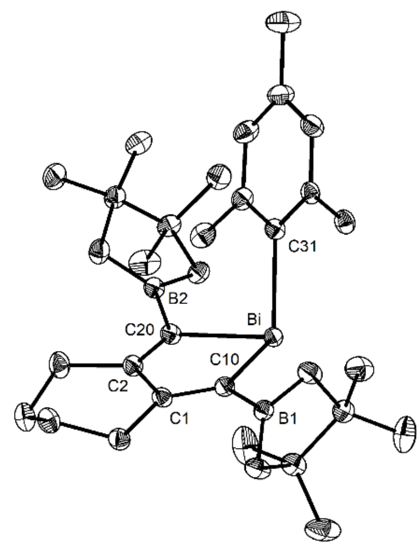

Figure 2.2. Molecular structure of **3** with thermal ellipsoids plotted at a 30 % probability level. All hydrogen atoms were omitted for clarity. Select bond lengths (Å) and angles (deg): Bi−C10 2.243(3), Bi−C20 2.231(3), Bi−C31 2.293(3); C10−Bi−C20 78.48(11), C10−Bi−C31 108.27(11), C20−Bi−C31 92.44(10).

Compound **4** (Figure 2.3) contains a similar overall structural arrangement as **3** with slight canting of the flanking thiophene rings away from being coplanar with the central bismole ring (torsion angles: Bi−C10−C11−C12A = 31.9(4)°, Bi−C20−C21−C22A = 18.9(3)°).

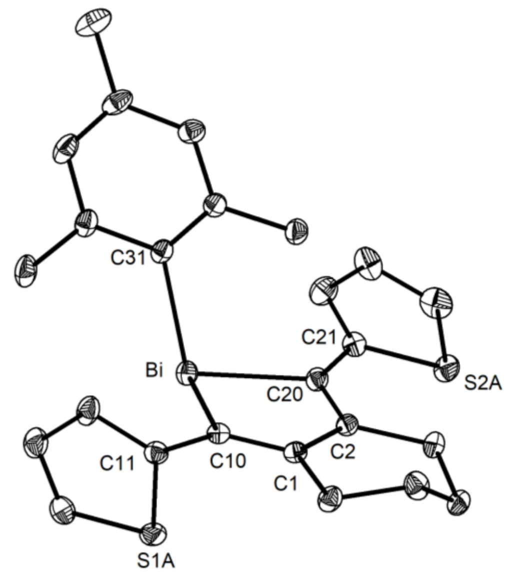

Figure 2.3. Molecular structure of **4** with thermal ellipsoids plotted at a 30 % probability level. All hydrogen atoms were omitted for clarity. Select bond lengths (Å) and angles (deg): Bi−C10 2.236(2), Bi−C20 2.240(2), Bi−C31 2.282(2); C10−Bi−C20 77.93(7), C10−Bi−C31 99.21(7), C20−Bi−C31 104.60(7).

Pentaphenylbismole $PhBiC_4Ph_4$ (**5**) contains a planar BiC_4 (bismole) ring corralled by phenyl groups arranged in a propeller-like fashion (Figure 2.4); a related structural motif is also present in the well-studied silole $Ph(Me)SiC_4Ph_4$, a compound that exhibits pronounced aggregation-induced emission (AIE).[25] The mesityl-functionalized bismole $MesBiC_4Ph_4$ (**6**) (Figure 2.5) adopts a similar overall structure as its phenylated congener **5** but with a slightly wider angle sum at the bismuth [276.6(3)° vs. 264.9(3)° average in **5**] due to the added steric bulk imposed by the mesityl group in **6**. Overall, the intraring C−Bi−C angles remain relatively similar between compounds **3** to **6** (range from 77.93(7) to 79.16(10)°), and the small angle sums at Bi indicate a high amount of s-character in the bismuth lone pair. The combined steric influence of the phenyl substituents in compounds **5** and **6** and the aryl groups at the bismuth (in compounds **3** to **6**) prevent close packing of the bismuth centers in the solid state, leading to intermolecular Bi···Bi distances greater than 4.5 Å. The absence of close intermolecular contacts is often of importance in preserving phosphorescence[21] by limiting luminescence-quenching triplet−triplet annihilation (*vide infra*).

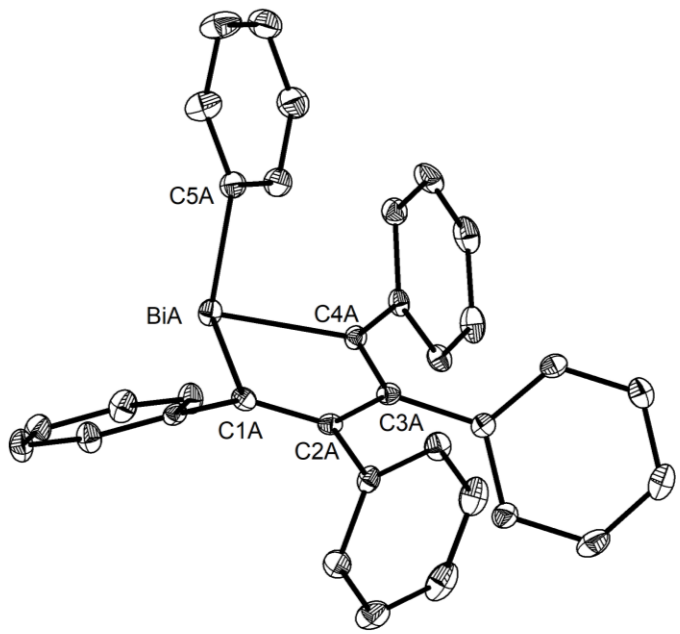

Figure 2.4. Molecular structure of **5** with thermal ellipsoids plotted at a 30% probability level. All hydrogen atoms were omitted for clarity, and only one molecule of the two in the asymmetric unit is shown. Select bond lengths (Å) and angles (deg) with values belonging to a second molecule of **5** shown in square brackets: Bi−C1 2.238(4) [2.248(4)], Bi−C4 2.244(4) [2.224(3)], Bi−C5 2.266(5) [2.265(5)]; C1−Bi−C4 78.06(15) [77.65(16)], C1−Bi−C5 93.49(16) [91.97(16)], C4−Bi−C5 93.96(15) [91.63(15)].

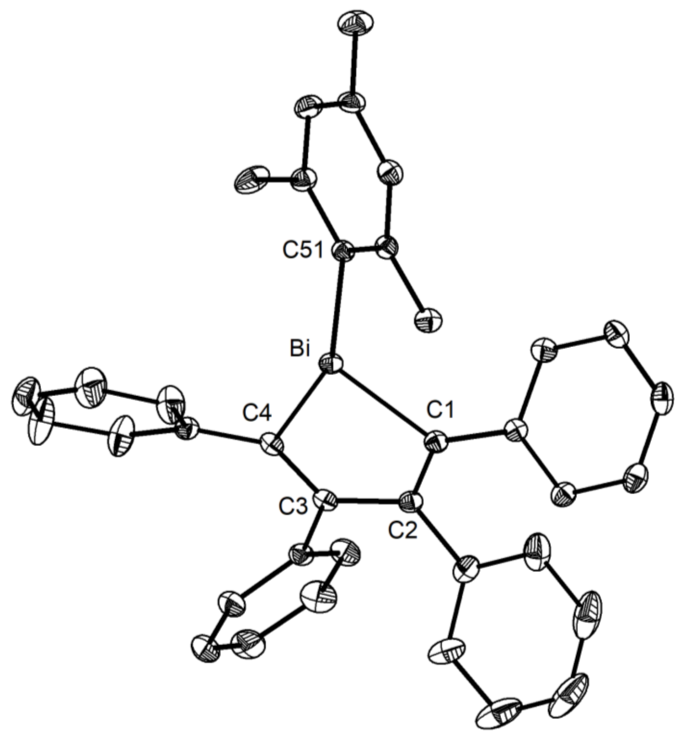

Figure 2.5. Molecular structure of **6** with thermal ellipsoids plotted at a 30 % probability level. All hydrogen atoms were omitted for clarity. Select bond lengths (Å) and angles (deg): Bi−C1 2.244(2), Bi−C4 2.234(2), Bi−C51 2.287(2); C1−Bi−C4 78.04(9), C1−Bi−C51 102.49(8), C4−Bi−C51 96.08(8).

Single crystals of the CuCl−bismole complex **8** were analyzed by single-crystal X-ray diffraction, and the refined molecular structure is shown in Figure 2.6. The most salient structural feature of **8** is the coordination of a CuCl array to one of the C=C π-units within the bismole ring; this interaction reflects the low degree of aromaticity that is inherent to the BiC_4 ring in the precursor **7** (*vide infra*). A distorted trigonal planar geometry exists about the Cu center in **8**, and the proximal C=C π-bond length (C2−C20 = 1.406(4) Å) is, as expected, longer than in the non-complexed C=C π-bond within the bismole ring [C1−C10 distance = 1.350(4) Å]. A

C2−Cu−C20 angle of 40.53(11)° is present in **8**, along with Cu−C2 and Cu−C20 bond distances of 2.060(3) and 1.995(3) Å, respectively, consistent with values in previously reported olefin-Cu complexes.[26]

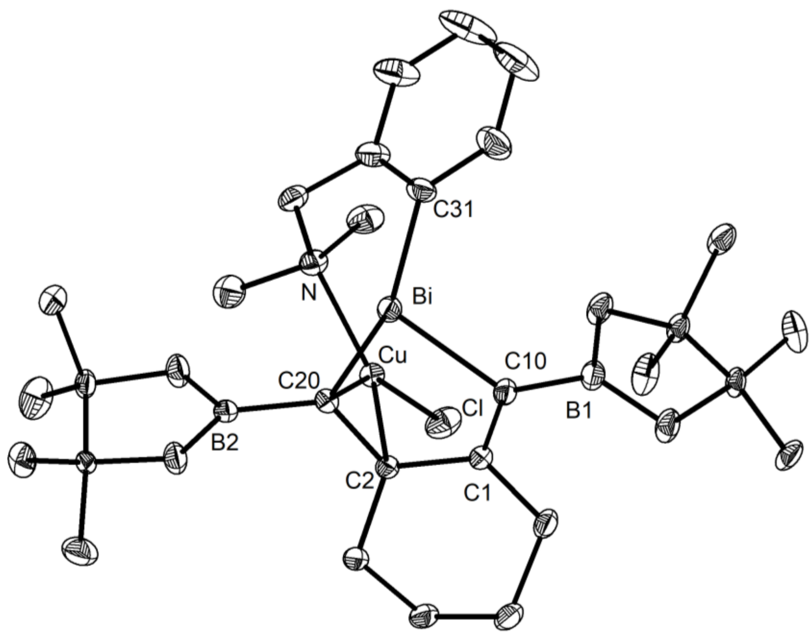

Figure 2.6. Molecular structure of **8** with thermal ellipsoids plotted at a 30% probability level. All hydrogen atoms were omitted for clarity. Select bond lengths (Å) and angles (deg): Bi−C10 2.245(3), Bi−C20 2.255(3), Bi−C31 2.275(3); C10−Bi−C20 79.16(10), C10−Bi−C31 97.64(11), C20−Bi−C31 102.44(11).

There have only been a few reports involving compounds containing structurally authenticated bismuth−copper bonds. For example, Fenske and co-workers[27] prepared the bis(silyl)bismuthide copper(I) complex $(Me_3Si)_2BiCu(PMe_3)_3$ featuring a Bi−Cu bond length of 2.744(1) Å, while Gabbaï and Ke[28] generated a series of $BiCu_3$ coordination complexes with Cu−Bi bond lengths that average to 2.934(2) Å. The Bi···Cu distance of 3.4765(7) Å in **8** is just within the sum of the van der Waals radii (3.47 Å)[29,30] of these elements and suggests that little to no bonding interaction exists.

2.2.3 Real-Space Bonding Indicator and Orbital-Based Analysis for the Cu···Bismole Interaction in 8

To better understand the nature of the Cu−C bonding in the CuCl-complexed bismole **8**, a set of real-space bonding indicators (RSBIs) obtained from density functional theory (DFT) was applied. The topological and integrated bonding and atomic properties were derived from the Atoms-In-Molecules (AIM)[31] and Electron Localizability Indicator (ELI-D)[32] space-partitioning schemes, respectively. Classic covalent interactions such as the C−C σ-bond in ethane are characterized by negative electron density Laplacians at the bond critical point ($\nabla^2\rho(\mathbf{r})_{\mathrm{bcp}}$) and a negative total energy (H) over $\rho(\mathbf{r})_{\mathrm{bcp}}$ ($H/\rho(\mathbf{r})_{\mathrm{bcp}}$) values; in addition, the kinetic energy (G) over $\rho(\mathbf{r})_{\mathrm{bcp}}$ ($G/\rho(\mathbf{r})_{\mathrm{bcp}}$) values are close to zero in such covalent bonds. In contrast, atom−atom contacts that are dominated by electrostatic interactions are characterized by substantially positive $\nabla^2\rho(\mathbf{r})_{\mathrm{bcp}}$ and $G/\rho(\mathbf{r})_{\mathrm{bcp}}$ values as well as an $H/\rho(\mathbf{r})_{\mathrm{bcp}}$ value close to zero. Furthermore, the bonding in **8** was examined by computing Noncovalent Interaction (NCI) indices[33] and via Natural Bond Orbital (NBO)[34] analyses.

The Bi−C bonds in both bismoles **7** and **8** as well as the Cu−N and Cu−Cl contacts in **8** show characteristics of polar covalent bonds, such as positive Laplacians and G/ρ_{bcp} ratios, as well as slightly negative H/ρ_{bcp} ratios. Interestingly, only one Cu−C bond critical point could be found (Figure 2.7a), and this interaction appears to be highly polar in nature with Laplacians and G/ρ_{bcp} ratios of 5.6 e Å^{-5} and 0.96 h e^{-1}, respectively; interestingly, the ellipticity ε of the Cu−C bond critical path (bcp) is very large (1.11) and indicates that the bonding electron density is smeared away from the Cu−C bond path, a sign that the Cu···bismole interaction likely involves two carbon atoms. The lack of "structurally expected" AIM bcps in regions of low electron density and high ε is a known feature of the AIM method, for example, in the description of the metal−ligand interaction in metallocenes.[35]

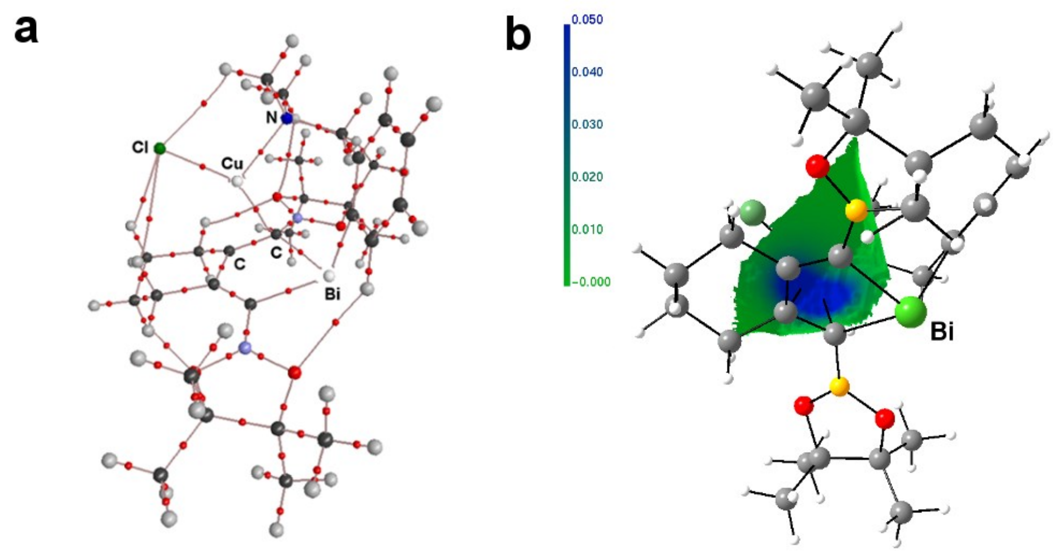

Figure 2.7. (a) AIM bond paths motifs of bismole **8**. (b) Electron density mapped on the AIM Cu atomic basin (given in e bohr^{-3}); the blue region indicates increased electron density positioned toward both C atoms (view from below the C_4Bi unit).

The coordination of the CuCl leads to slightly weaker C=C bonding in **8** as can be seen from smaller ρ_{bcp} values (2.06 e Å^{-3}) and less negative Laplacian (−21.8 e Å^{-5}) and H/ρ_{bcp} values (−1.11 h e^{-1}), assuming participation of both C atoms in the CuCl···bismole interaction. Furthermore, the electron density is smeared toward both C atoms as can be seen by mapping the electron density on the AIM Cu atomic basin (Figure 2.7b). Isosurfaces (localization domain representations) of the ELI-D of bismoles **7** and **8** are given in Figures 2.8 and 2.9, respectively, and show a substantially smaller C=C bonding basin of the coordinated C=C bond in comparison to the uncoordinated C=C bonding basins (Figures 2.8a and 2.9a). The Cu interaction to both C atoms is further substantiated by an NBO analysis, which yields a Wiberg bond index of 0.26 and 0.25 for the two Cu−C interactions. Furthermore, second order perturbation theory analysis reveals the presence of a donor−acceptor interaction between the C=C π bond to an empty d-orbital of the Cu atom [60.01 kcal/mol] and from a Cu d-orbital to the π* orbital of the C=C bond [27.42 kcal/mol]. The Nuclear Independent Chemical Shift (NICS)[36] value for bismole **7** was calculated at the ring critical point of the C_4Bi unit (NICS(0) = −1.8) and indicates only a minimal degree of aromaticity, especially when compared to the lighter pyrroles (*e.g.* C_4H_4NH = −14.0) and also to the parent bismole C_4H_4BiH (−2.7).[37] The rather localized C=C bonds in bismole **7**, in addition to the coordinating N lone pair, account for the ability to form a stable complex with CuCl resulting in bismole **8**.

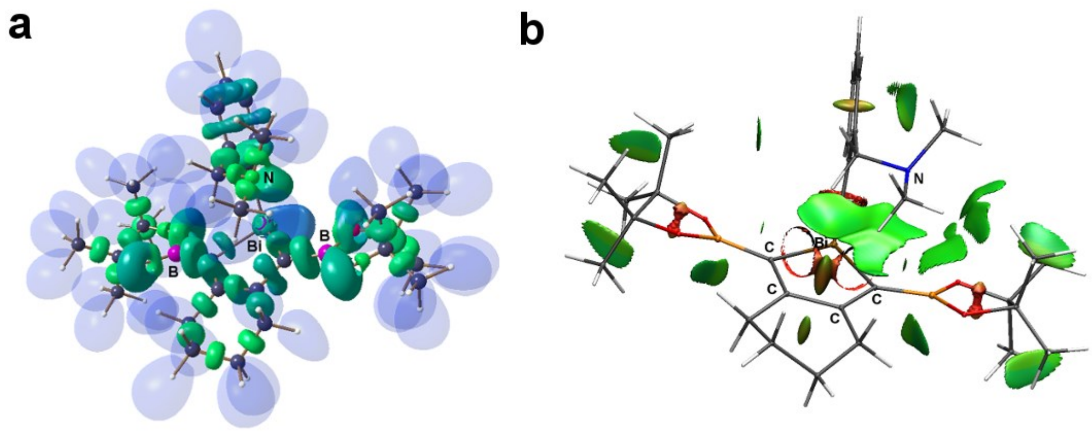

Figure 2.8. (a) Iso-surface representation of the localization domains of the ELI-D (Y = 1.4) of **7**. The basins are color coded from green (small) to blue (large). (b) NCI iso-surfaces ($s(\mathbf{r})$ = 0.5; attractive/repulsive non-covalent bonding aspects given in blue/red).

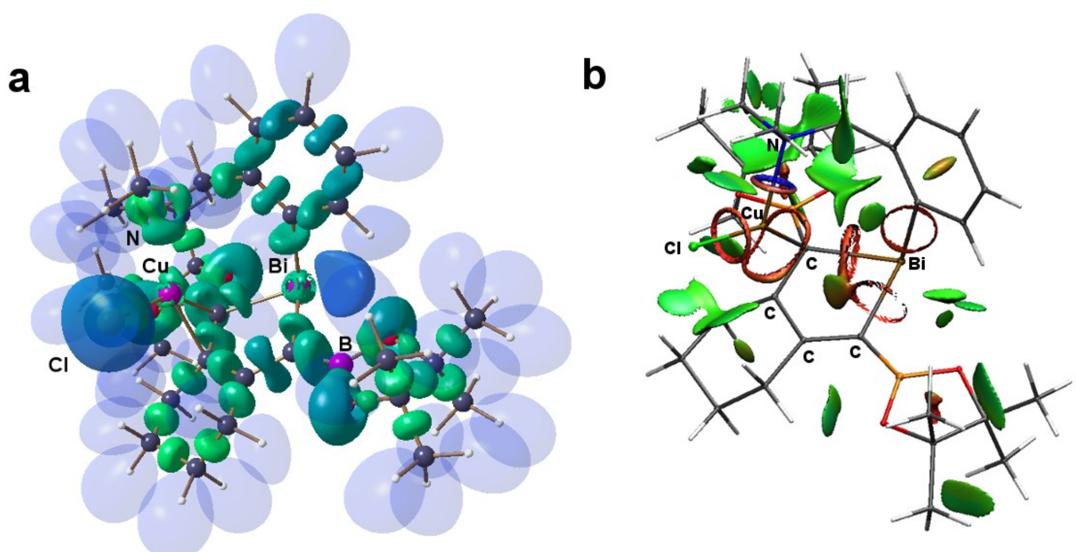

Figure 2.9. (a) Iso-surface representation of the localization domains of the ELI-D (Y = 1.4) of **8**. The basins are color coded from green (small) to blue (large). (b) NCI iso-surfaces (s($\mathbf{r}$) = 0.5; attractive/repulsive non-covalent bonding aspects given in blue/red.

2.2.4 Ultrafast Time-Resolved and Time-Integrated Photoluminescence Measurements

The bismole heterocycles **3**, and **5−8** display UV−vis absorption profiles that extend up to *ca*. 425 nm in tetrahydrofuran (THF), with bismole **4** showing the most red-shifted absorption of the compound series (Figure 2.10). This afforded an opportunity to conduct both ultrafast time-resolved (TRPL) and time-integrated photoluminescence (TIPL) studies using a common excitation source at 400 nm; it was hoped that such ultrafast measurements would allow for examination of the emission behavior of these bismoles at various temperatures under high vacuum and to probe for possible competing emission pathways such as thermally activated delayed fluorescence (TADF).

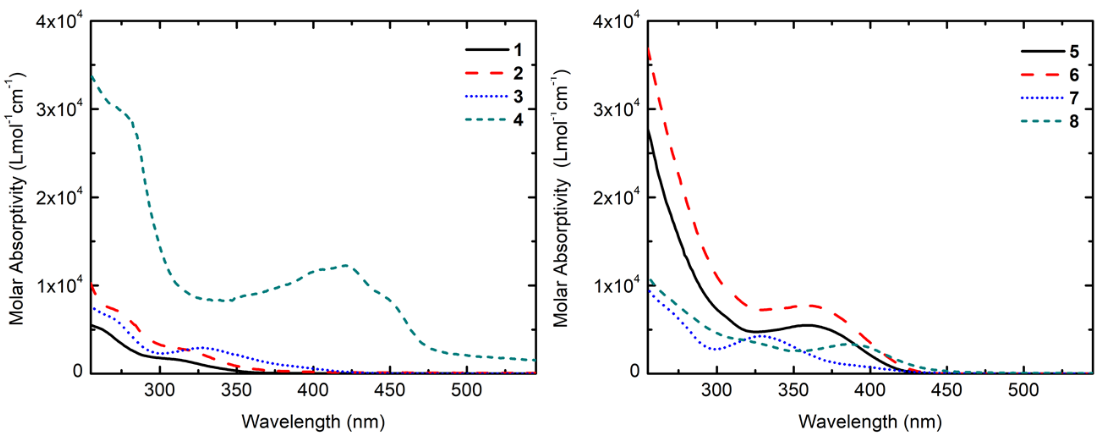

Figure 2.10. UV−Vis absorbance spectra in THF at room temperature for compounds (a) **1−4** and (b) **5−8**.

For these studies, focus was placed on measuring the PL of compounds **4**, **7**, and **8** due to the presence of non-negligible light absorption at 400 nm as well as each bismole being structurally distinct. The samples were drop-cast as films from THF for each photoluminescence (PL) measurement, thus ruling out possible quenching interactions by solvent, and allowing suppression of the molecular rotations that would be possible if the molecules were in solution. Notably, no PL was detected from the ethylated bismoles **1** and **2** due a lack of absorption at 400 nm, and attempts to measure the luminescence of these species upon excitation at a wavelength of *ca*. 290 nm (in the presence or absence of O_2) did not yield any discernible luminescence. One explanation for the lack of visible emission in **1** and **2** is their oily nature, which likely encourages nonradiative decay facilitated by molecular motion.[25] Ultrafast time-resolved and time-integrated photoluminescence studies were not conducted on bismoles **5** and **6** due to a combination of the lack of strong absorption at 400 nm and the lack of emission observable by visual inspection either in solution or in the solid state in the presence or absence of oxygen (see Figure 2.11 for compounds **1**−**8** in 2-MeTHF at 77 K).

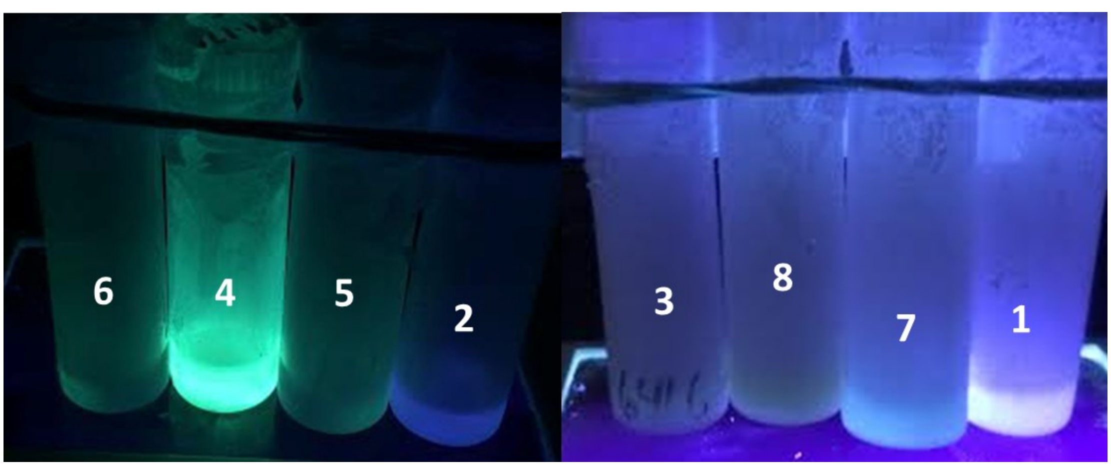

Figure 2.11. Bismoles **1**–**8** in frozen 2-methyltetrahydrofuran (*ca*. 5 mg/mL) at 77 K excited at 365 nm.

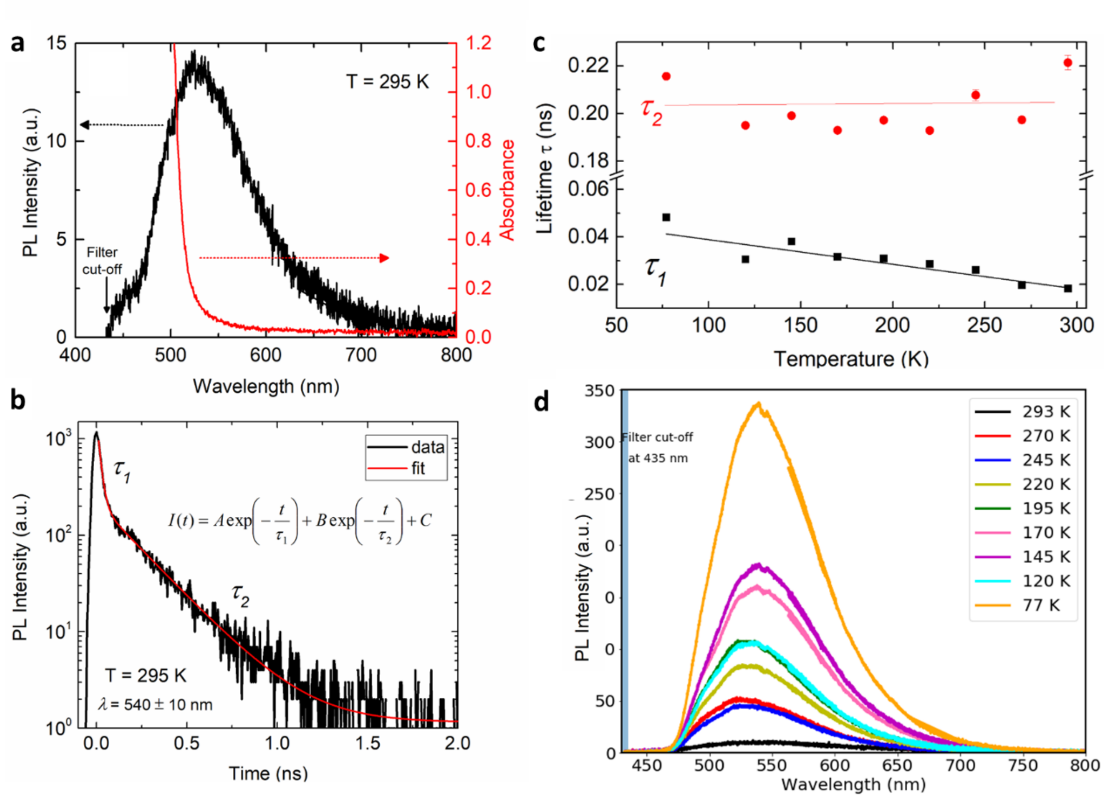

Figure 2.12. (a) TIPL spectra (left y-axis) and absorbance associated with a drop-cast film of **4** (right y-axis) at 295 K. Excitation source is 400 nm, and a long pass filter was used to cutoff wavelengths below 435 nm. (b) TRPL of **4** taken at 540 ± 10 nm at 295 K, which follows a biexponential decay (red line), $I(t)$. (c) Lifetimes τ_1 and τ_2 extracted from the biexponential fits of TRPL at low temperatures. (d) TIPL of **4** at low temperature.

Upon excitation at 400 nm, compound **4** displayed green PL, with weak emission noted at room temperature (Figure 2.12a), which became much more intense upon cooling to 77 K (Figure 2.12d). The dominant emission peak arising at ~530 nm and the resulting small Stokes shift is in line with fluorescence, which was confirmed by nanosecond scale time-resolved photoluminescence (TRPL) measurements, as shown in Figures 2.12b and 2.12c. A 75 % reduction in PL intensity over 28 minutes of irradiation at 400 nm was observed for compound **4**, and despite this slow degradation, TRPL measurements were possible. The TRPL measurements at 540 ± 10 nm follow a biexponential decay, $I(t) = A \exp(-t/\tau_1) + B \exp(-t/\tau_2) + C$, where A and B are the intensities, τ_1 and τ_2 are estimated lifetimes, and C is the offset. The "fast" component at $t < 0.08$ ns could be attributed to the relaxation of excited vibrational modes. These modes are suppressed at low temperature; thus, τ_1 becomes larger, as shown in Figure 2.12c, and fluorescence intensity is enhanced. The "slow" component at $t > 0.1$ ns was assigned as fluorescence from a low-lying singlet transition, which has a consistent lifetime τ_2 at different temperatures. According to TD-DFT calculations (see section 2.2.5), the energy difference between the excited S_1 and the T_2 states is only 0.035 eV (Table 2.1); thus, one might expect intersystem crossing (ISC) to yield phosphorescence (after rapid internal decay from T_2 to an emissive T_1 state). However, the lack of phosphorescence in **4** is likely partly due to the absence of substantial participation of the Bi atom orbital density to these excited states;[21e] thus, spin−orbit coupling (which facilitates ISC) arising from the presence of the heavy element is minimized (*vide infra*).

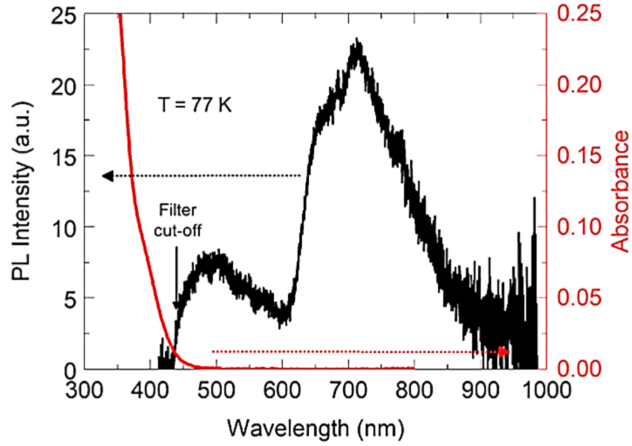

Figure 2.13. TIPL intensity at 77 K (left y-axis) and absorbance (right y-axis) at T = 295 K for **7** (drop-cast film from THF onto quartz plate).

Compound **7** interestingly shows two broad PL peaks upon excitation at 400 nm at 77 K (Figure 2.13). The first peak at *ca*. 485 nm comprises 32 % of the total integrated emission intensity compared to the second low-energy peak at *ca*. 720 nm. The two peaks are indicative of fluorescence and phosphorescence, respectively; however, TRPL could not be measured due to fast photodegradation of the sample in the excitation beam. Note that the weak absorption at 400 nm is responsible for the weak PL, which was only observed at 77 K, where molecular motions are inactivated and phosphorescence then becomes observable.[10e]

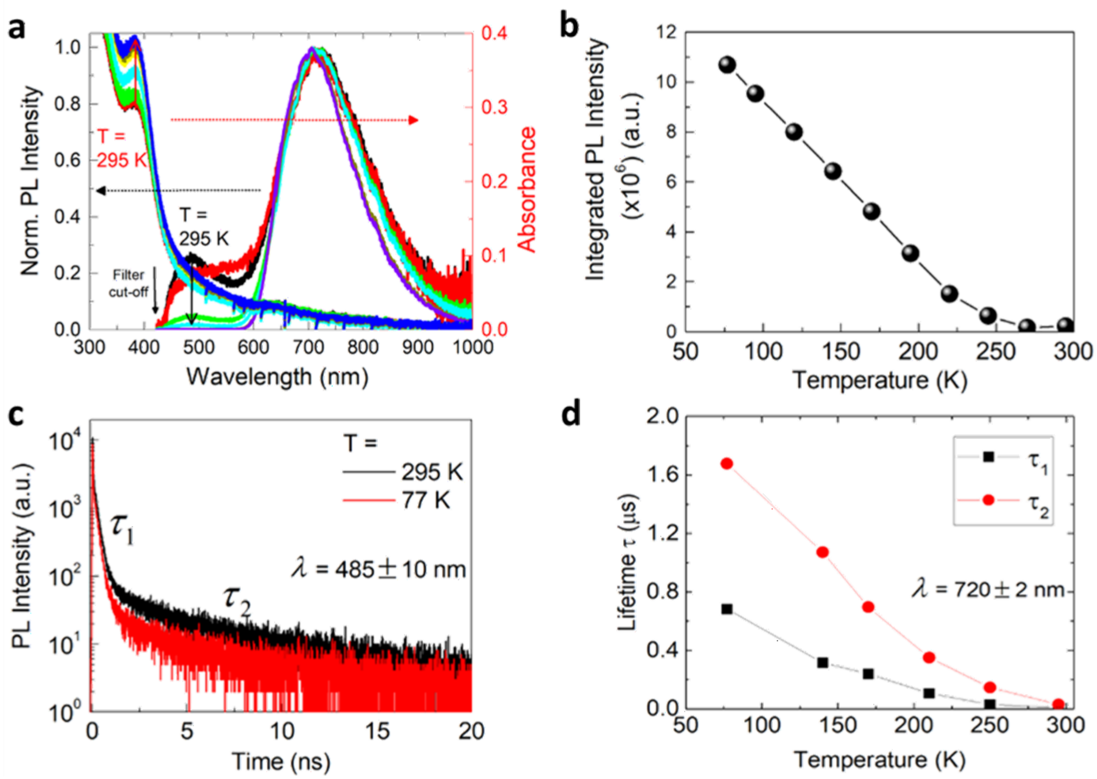

Figure 2.14. (a) Normalized TIPL intensity (left y-axis) and absorbance (right y-axis) at various temperatures of the copper complex **8**. (b) Variation of PL intensity in **8** with an increase in temperature from 77 to 300 K. (c) TRPL in the nanosecond scale for **8** taken at 485 ± 10 nm. (d) Lifetime in the microsecond scale for **8** taken from the TRPL fits to a biexponential decay at 720 ± 2 nm at the indicated temperatures.

The CuCl complex **8** does not yield any luminescence that is visible by eye when excited at 365 nm with a hand-held lamp; however, under the stronger laser (0.2 ± 0.02 mW excitation power) excitation at 400 nm, clear PL is found at room temperature (Figure 2.14); in addition, this compound undergoes much less photodegradation compared to **7**, and this photodegradation becomes almost negligible when **8** is progressively cooled to 77 K (Figure 2.15), thus enabling TRPL to be measured. Relative to the first peak at *ca*. 485 nm, the second red-shifted phosphorescence peak at *ca*. 720 nm accounts for 73 % of the integrated PL intensity of **8** at room temperature. As the temperature is lowered from 200 to 77 K, the overall integrated PL intensity increases with a linear trend (Figure 2.14b), leading to the long wavelength (phosphorescence) emission accounting for 99.75 % of the total PL at 77 K. This observation implies improved ISC efficiency in **8** compared to **7** and **4** and pronounced participation of the Bi atom in the main molecular orbitals involved in the excitation processes; computations support this explanation (*vide infra*). Additionally, as the intensity of the phosphorescence is enhanced, the corresponding emission maximum becomes blue-shifted by 16 nm (0.04 eV) from room temperature to 77 K with slightly narrowing bandwidth, suggestive of the suppression of low-lying vibrational levels from the excited triplet state (as non-radiative pathways).

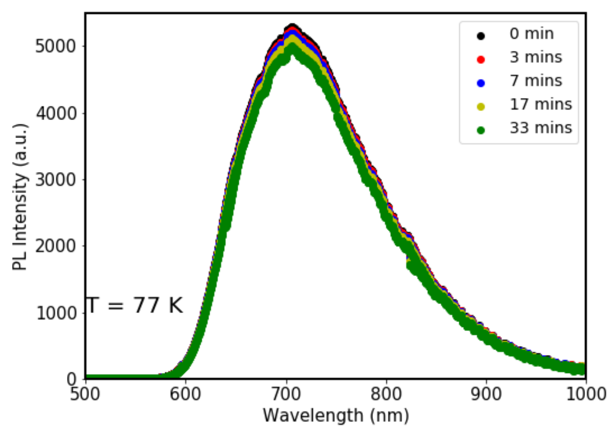

Figure 2.15. TIPL of **8** at 77 K over time.

Analysis of the emission data by time-resolved methods (TRPL) confirmed the presence of dual fluorescence and phosphorescence in **8**, as evidenced by concurrent short-lived (ns time scale) and long-lived (0.1−10 μs) emission, measured at different emission wavelengths, thus ruling out thermally activated delayed fluorescence. Biexponential curves are shown in Figure 2.14c for the short-lifetime emission (ns) with $\tau_1 = 0.226 \pm 0.006$ ns and $\tau_2 = 1.1 \pm 0.3$ ns that do not significantly change at low temperature. It is also noticeable that at $t \leq 0.2$ ns, another fast exponential decay is observed, which may again represent vibrational relaxations being thermally suppressed, enabling rapid ISC and the emergence of the phosphorescence long-lifetime emission profile. For the phosphorescence peak, the increase of intensity is accompanied by a longer TRPL event in the microsecond time scale, and the emission again follows biexponential decay; the temperature dependences of these lifetime values are shown in Figure 2.14d. As the temperature is lowered to 77 K, enhanced phosphorescence is observed accompanied by a longer microsecond lifetime up to ~2 μs. The nature of the biexponential decay could be due to mixed metastable states at *ca*. 720 nm or possibly morphological effects within the cast films.

2.2.5 TD-DFT Computations on the Emissive Bismoles 4, 7, and 8

Time-dependent density functional theory (TD-DFT) computations were performed for the bismoles **4**, **7**, and **8** using the B3LYP functional and the cc-pVTZ(-PP) basis-sets. The calculated Bi−C bond distances of the optimized geometries are systematically *ca*. 0.03 Å longer than the experimentally observed Bi−C distances in **4** and **8**. The largest deviation from the experimental distance is observed for the Cu−N bond in bismole **8**, which is 0.08 Å longer in the optimized gas phase structure. The overestimation of bond distances of polar interactions is a known effect of DFT computations involving the B3LYP functional.[38] However, as all structural trends are fully maintained in the bismoles **4** and **8**, the observed differences are rather insignificant.

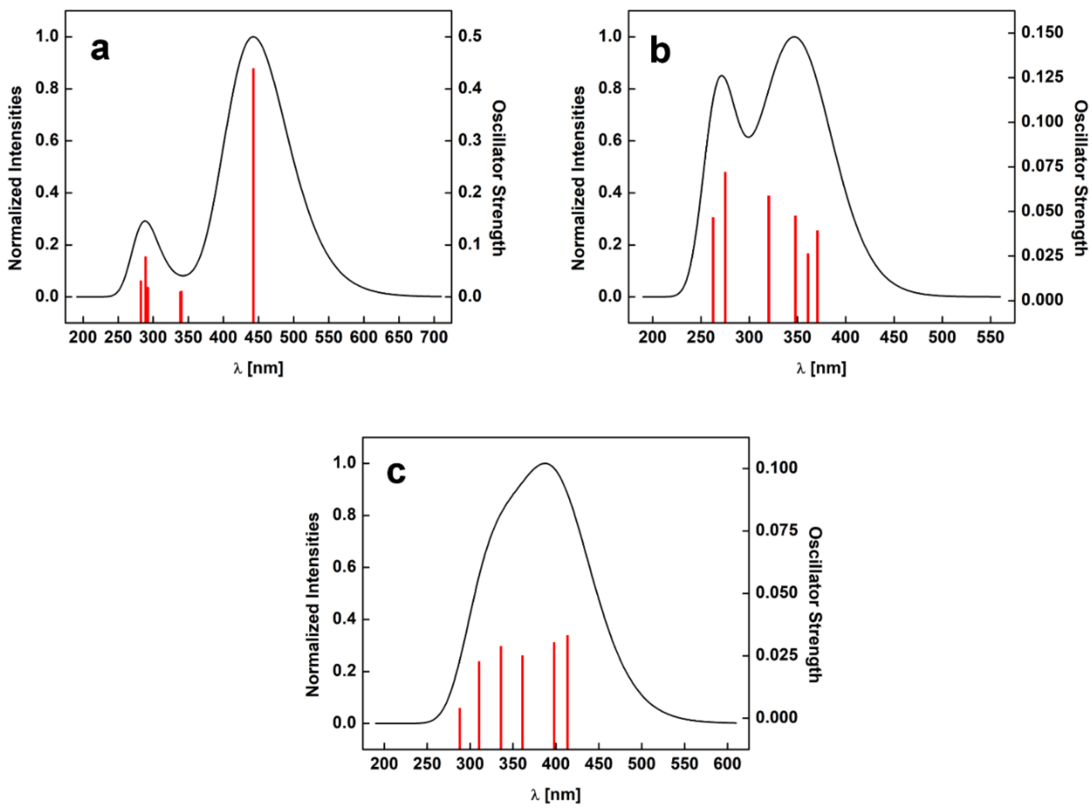

Figure 2.16. Calculated UV-vis spectra of **4** (a), **7** (b) and **8** (c) at the B3LYP/cc-pVTZ(-PP) level of theory including transitions involving the six lowest-lying singlet excited states with the highest oscillator strength (given as red bars).

The predicted absorption maxima for compounds **4**, **7**, and **8** are within 25 nm of the experimentally observed maxima (Figure 2.16). In bismole **4**, the main transition (excitation with the highest oscillator strength) can exclusively be assigned to a HOMO to LUMO transition that is primarily π–π* in character with little contribution from the Bi atom (Figure 2.17a). In contrast, bismoles **7** and **8** show considerable oscillator strength for transitions to low-lying singlet states that can also be attributed to the HOMO−1 to LUMO and the HOMO−2 to LUMO transitions (Figure 2.17b and 2.17c). In bismole **7**, both the HOMO and HOMO−1 to LUMO transitions show the highest oscillator strength (f = 0.0392 and f = 0.0478 respectively) and are mainly π–π* character, whereas the HOMO−2 to LUMO transition (f = 0.0264) shows significant contributions from the Bi atom.

According to TD-DFT studies, bismoles **4**, **7**, and **8** each have low-lying singlet states that are energetically similar (<0.1 eV, Table 2.1 and Figure 2.18) to low-lying triplet excited states. A possible mechanism for the observation of phosphorescence is initial photoexcitation to an S_n state with subsequent intersystem crossing (ISC) to an energetically similar T_n state, followed by relaxation to the lowest T_1 triplet state, then phosphorescence and relaxation to the S_0 ground state. As all investigated methods show the existence of energetically close $S_{1,2,3}$ and T_n states, there is a high probability for ISC to occur. As Bi is an element strongly affected by relativistic effects, enhanced spin−orbit coupling should lead to significant mixing of singlet and triplet states, thus further increasing the probability of ISC.[21e] To determine the degree of mixing, vertical excitation energies including scalar relativistic (ZORA) and spin−orbit relativistic (SO) methods were computed for bismoles **4**, **7**, and **8**. Bismoles **7** and **8** show a low-lying "singlet" state with considerable mixing of singlet and triplet character (**7**: 55.8 % S, 44.0 % T and **8**: 63.4 % S, 36.0 % T; see Tables 2.3 and 2.4). In contrast, mixing of singlet and triplet states for low-lying excited states in bismole **4** is dramatically lower (*e.g.* 91.9 % S, 7.9 % T; Table 2.2). The presence of the CuCl unit also has an effect on the rate of

ISC, as bismole **8** shows more mixing of singlet and triplet character (Table 2.4) when compared to bismole **7** (Table 2.3).

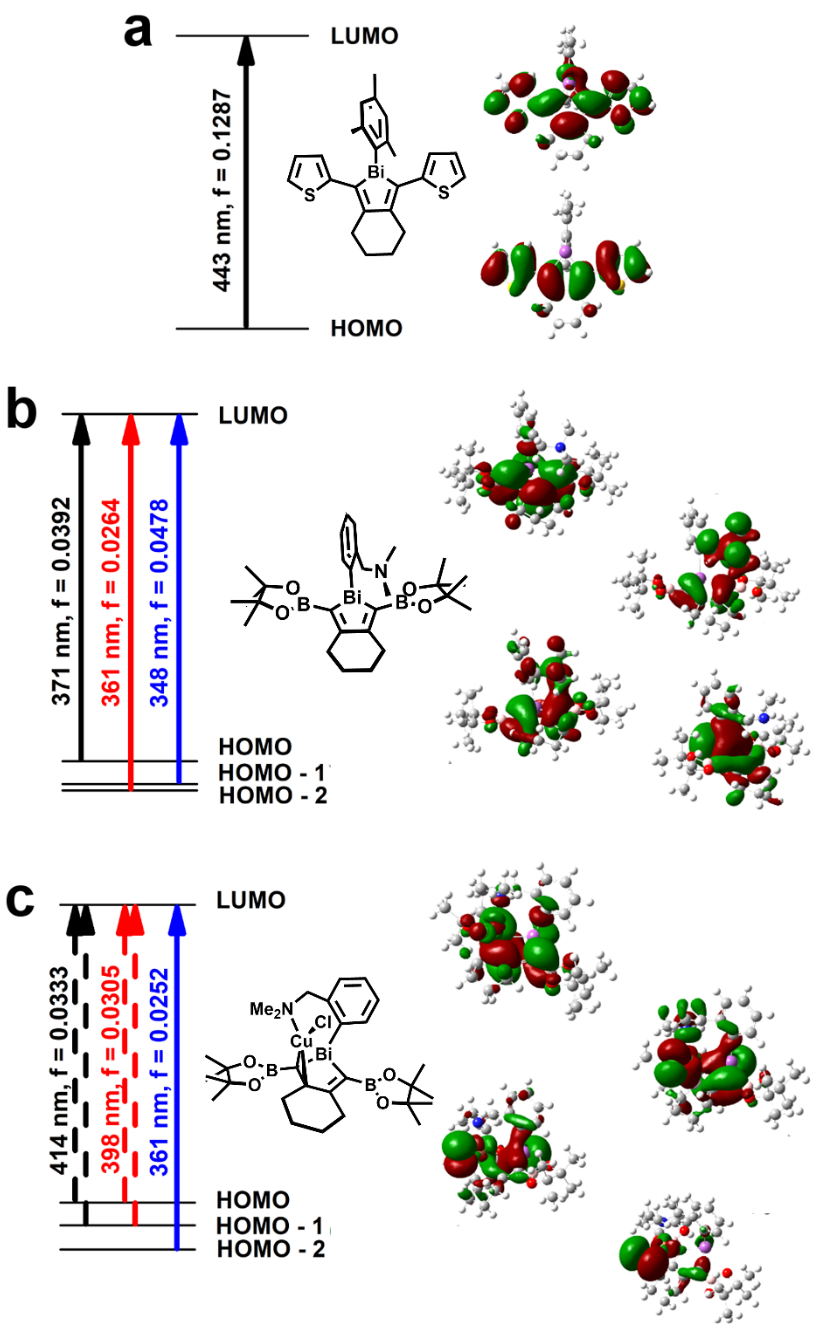

Figure 2.17. TD-DFT computed main transitions for **4** (a), **7** (b), and **8** (c) to low-lying singlet states at the B3LYP/cc-pVTZ(-PP) level of theory and the associated molecular orbitals; isosurface values of +0.02/−0.02 (red/green).

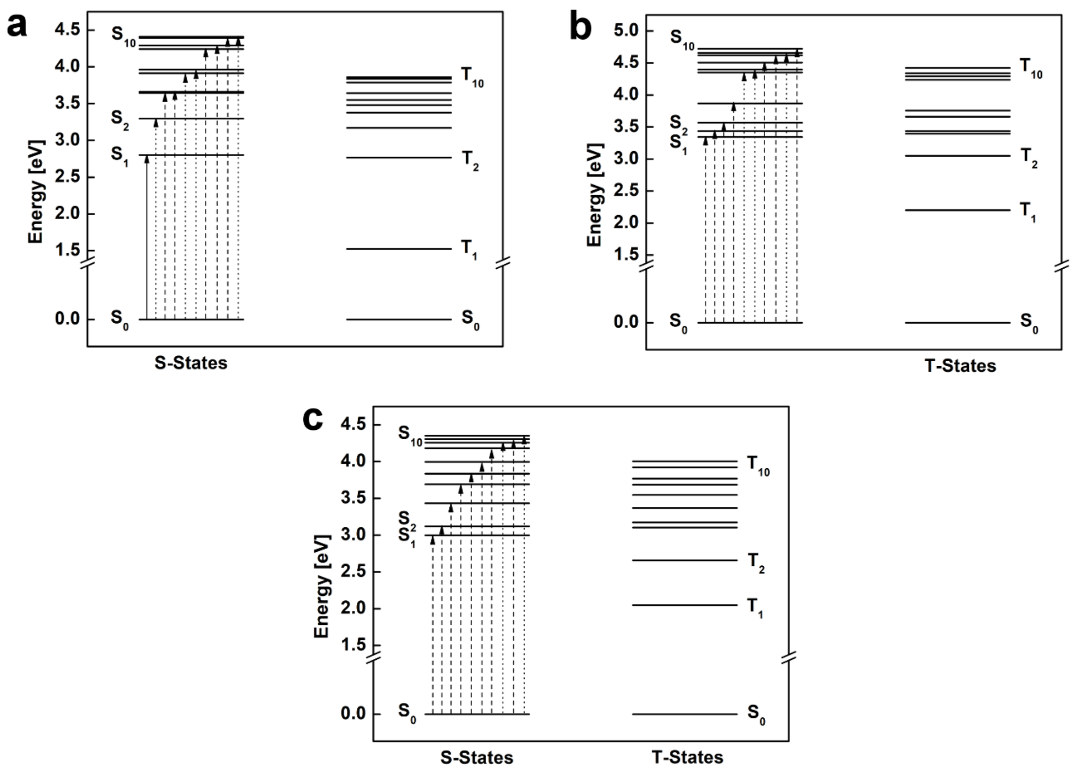

Figure 2.18. Calculated singlet and triplet states of **4** (a), **7** (b) and **8** (c) at the B3LYP/cc-pVTZ(-PP) level of theory. Oscillator strengths are indicated as follows: f ≥ 0.1 (solid); 0.1 > f ≥ 0.01 (dashed); 0.01 > f ≥ 0.001 (dotted).

The phosphorescence energy can be defined as the difference in energy between the S_0 ground state and the T_1 triplet state (E_{adia}) or the zero-point energy corrected difference between these states (E_{0-0}). The phosphorescence energy of **7** (E_{adia} = 1.82 eV, E_{0-0} = 1.76 eV) matches closely with the observed phosphorescence energy of 1.73 eV (720 nm). In contrast, the predicted phosphorescence energy of **8** (E_{adia} = 1.39 eV, E_{0-0} = 1.33 eV) is underestimated by 0.36−0.42 eV in comparison to the experimentally observed 1.75 eV (709 nm). The calculated adiabatic energies of **4** (E_{adia} = 1.27 eV, E_{0-0} = 1.22 eV) predict emission in the near-infrared region (976−

1020 nm) and are in line with the lack of experimentally observed phosphorescence. However, the lack of substantial mixing of excited singlet and triplet states in bismole **4**, because there is minimal orbital participation from Bi in the excitation processes and thus reduced spin−orbit coupling, likely hinders effective ISC to an excited triplet state. In contrast, bismoles **7** and **8** show considerable orbital character from Bi associated with the excited states; thus, spin−orbit coupling becomes more pronounced, and phosphorescence is observed experimentally. While the enhancement of ISC via an external heavy element effect remains a possibility,[35] the lack of observed phosphorescence in **4**, in conjunction with findings from previous studies conducted on tellurophenes in our group,[21e] suggest that participation of the heteroatom in the excitation process seems to be necessary for phosphorescence to occur.

2.3 Conclusions

A series of bismole compounds were synthesized via efficient copper(I) chloride-catalyzed metallacycle transfer, and the luminescence properties of three bismoles, namely, **4**, **7**, and **8**, were studied in detail. Compound **4** was found to exhibit only fluorescence at low temperatures, and this is most likely due to the lack of participation of the bismuth atom in the excitation process leading to minimal singlet and triplet mixing in the lower-energy excited states. Bismoles **7** and **8** were found to exhibit both fluorescence and phosphorescence, and this can be attributed to the increased orbital participation from bismuth in the excitation processes leading to significant mixing of triplet and singlet character in the lower-energy excited states.

2.4 Experimental Section

2.4.1 General Considerations

All reactions were performed using standard Schlenk and glovebox (MBraun) techniques under a nitrogen atmosphere. Solvents were all dried and degassed using a Grubbs-type solvent purification system manufactured by Innovative Technology, Inc., and stored under an atmosphere of nitrogen prior to use. Bismuth(III) chloride was purchased from TCI, and all other chemicals were purchased from Sigma-Aldrich; all commercially obtained chemicals were used as received. Mes_3Bi,[40] $(Ar^{NMe2})BiCl_2$,[24] **(2-thienyl)-Cp_2Zr-6-(2-thienyl)**,[41] **B-Cp_2Zr-6-B**,[41] $Cp_2ZrC_4Et_4$,[42] and $Cp_2ZrC_4Ph_4$[43] were prepared according to literature procedures. ^1H, $^{11}B\{^1H\}$, and $^{13}C\{^1H\}$ NMR spectra were recorded on 400, 500, 600, or 700 MHz Varian Inova instruments and were referenced externally to $SiMe_4$ (^1H, $^{13}C\{^1H\}$), or $F_3B{\cdot}Et_2O$ ($^{11}B\{^1H\}$). Elemental analyses were performed by the Analytical and Instrumentation Laboratory at the University of Alberta. Melting point values were obtained in sealed glass capillaries in nitrogen using a MelTemp melting point apparatus. UV−vis spectroscopic data were obtained using a Cary 400 Scan spectrophotometer.

2.4.2 Synthetic Procedures

Synthesis of $PhBiC_4Et_4$ (1). A suspension of $BiCl_3$ (0.0866 g, 0.275 mmol) in 5 mL of Et_2O was added to a suspension of $BiPh_3$ (0.0596 g, 0.135 mmol) in 5 mL of Et_2O. The reaction mixture was allowed to stir for one hour, after which the formation of a pale-yellow precipitate was observed. The entire reaction mixture was added as a suspension to a solution of $Cp_2ZrC_4Et_4$ (0.157 g, 0.406 mmol) in 5 mL of Et_2O. The reaction mixture was then stirred at room temperature in the absence of light for 21 hours before being evaporated to dryness. The crude mixture was extracted with 15 mL of hexanes and filtered through a 0.5 cm plug of silica. The resulting filtrate was evaporated to dryness *in vacuo* to yield **1** as an orange-red oil (0.136 g, 75 %). ^{1}H NMR (400 MHz, C_6D_6): δ 8.06 (dd, $^{3}J_{HH}$ = 7.8 Hz, $^{4}J_{HH}$ = 1.4 Hz, 2H, Ar*H*), 7.22 (m, 2H, Ar*H*), 7.13 (m, 1H, Ar*H*), 2.70 (dq, $^{2}J_{HH}$ = 15.1 Hz, $^{3}J_{HH}$ = 7.6 Hz, 2H, CH_2CH_3), 2.57 (dq, $^{2}J_{HH}$ = 15.1 Hz, $^{3}J_{HH}$ = 7.6 Hz, 2H, CH_2CH_3), 2.13 (m, 4H, CH_2CH_3), 1.07 (t, $^{3}J_{HH}$ = 7.6 Hz, 6H, CH_2CH_3), 1.00 (t, $^{3}J_{HH}$ = 7.6 Hz, 6H, CH_2CH_3). ^{13}C{^{1}H} NMR (126 MHz, C_6D_6): δ 171.4 (Ar*C*), 163.2 (Ar*C*), 137.7 (Ar*C*), 130.5 (Ar*C*), 127.6 (Ar*C*), 30.1 (CH_2), 26.9 (CH_2), 19.2 (CH_3), 15.1 (CH_3). Anal. Calcd. (%) for $C_{18}H_{25}Bi$: C, 48.00; H, 5.60. Found: C, 49.01; H, 5.93. UV-Vis (THF): 312 nm (shoulder).

Synthesis of $MesBiC_4Et_4$ (2). A suspension of $BiCl_3$ (0.173 g, 0.549 mmol) in 6 mL of Et_2O was added to $BiMes_3$ (0.157 g, 0.277 mmol) in 6 mL of Et_2O and the reaction mixture was allowed to stir at room temperature in the absence of light for 16 hours. The resulting mixture containing $MesBiCl_2$ was transferred as a suspension in Et_2O to a solution of $Cp_2ZrC_4Et_4$ (0.316 g, 0.820 mmol) in 10 mL of Et_2O. The reaction mixture was allowed to stir at room temperature in the absence of light for 27 hours before being evaporated to dryness. The crude product was extracted with 15 mL of hexanes and filtered through a 0.5 cm plug of silica. The volatiles were removed from the filtrate to give **2** as a yellow oil (0.317 g, 78 %). ^{1}H NMR (500 MHz, C_6D_6): δ 6.92 (s, 2H, Ar*H*), 2.75 (dq, $^{2}J_{HH}$ = 15.1 Hz, $^{3}J_{HH}$ = 7.6 Hz, 2H, CH_2CH_3), 2.66 (dq, $^{2}J_{HH}$ = 15.0 Hz, $^{3}J_{HH}$ = 7.5 Hz, 2H, CH_2CH_3), 2.50 (s, 6H, CH_3 in Mes), 2.12–2.23

(m, 4H, CH_2CH_3), 2.10 (s, 3H, CH_3 in Mes), 1.06 (overlapping t, $^3J_{HH}$ = 7.5 Hz, 12H, CH_2CH_3). $^{13}C\{^1H\}$ NMR (126 MHz, C_6D_6): δ 161.3 (ArC), 147.8 (ArC), 137.5 (ArC), 129.1 (ArC), 30.8 (CH_2), 28.1 (CH_3 in Mes), 26.5 (CH_2), 21.1 (CH_3 in Mes), 19.4 (CH_3), 14.5 (CH_3). Anal. Calcd. (%) for $C_{21}H_{31}Bi$: C, 51.22; H, 6.35. Found: C, 50.57; H, 6.69. UV-Vis (THF): 317 nm (shoulder).

Synthesis of B-MesBi-6-B (3). A suspension of $BiCl_3$ (0.169 g, 0.536 mmol) in 5 mL of Et_2O was added to a solution of $BiMes_3$ (0.149 g, 0.264 mmol) in Et_2O; this mixture was stirred at room temperature in the absence of light for 16 hours before being concentrated to 1 mL. The resulting pale yellow suspension was dissolved in 3 mL of THF and the solution added dropwise to a mixture of **B-Cp$_2$Zr-6-B** (0.463 g, 0.798 mmol) and CuCl (0.0027 g, 0.027 mmol) in 12 mL of THF in the absence of light. The reaction mixture was allowed to stir for 2 hours in the dark before being evaporated to dryness. The product was extracted into 13 mL of hexanes and filtered through a 0.5 cm silica plug before being evaporated to dryness. The crude product was recrystallized from Et_2O at –30 °C to give three crystalline fractions which were combined to give pure **3** as a yellow crystalline solid (0.355 g, 65 %). ^1H NMR (400 MHz, C_6D_6): δ 6.93 (s, 2H, ArH), 2.93 (m, 4H, $C{=}CCH_2CH_2$), 2.57 (s, 6H, CH_3 in Mes), 2.09 (s, 3H, CH_3 in Mes), 1.52 (m, 4H, $C{=}CCH_2CH_2$), 1.01 (two closely spaced singlets, 24H, CH_3 in BPin). $^{13}C\{^1H\}$ NMR (126 MHz, C_6D_6): δ 174.6 (BiC=C), 147.4 (*o*-MesC), 136.8 (*p*-MesC), 129.5 (MesCH), 83.1 ($C(CH_3)_2$), 40.6 ($C{=}CCH_2CH_2$), 28.6 (CH_3 in Mes), 24.9 (CH_3 in BPin), 24.8 (CH_3 in BPin), 23.5 ($C{=}CCH_2CH_2$), 21.1 (CH_3 in Mes). $^{11}B\{^1H\}$ NMR (128 MHz, C_6D_6): δ 34.1 (br).

Anal. Calcd. (%) for $C_{29}H_{43}B_2BiO_4$: C, 50.76; H, 6.32. Found: C, 50.84; H, 6.45. UV-Vis (THF): λ_{max} = 327 nm ($\varepsilon = 2.93 \times 10^3$ M^{-1} cm^{-1}). Mp: 155-160 °C (decomp).

Synthesis of (2-thienyl)-BiMes-6-(2-thienyl) (4). A suspension of $BiCl_3$ (0.207 g, 0.656 mmol) in 5 mL of Et_2O was added to a solution of $BiMes_3$ (0.183 g, 0.322 mmol) in 5 mL of Et_2O; this mixture was stirred at room temperature in the absence of light for 16 hours before being concentrated to a volume of *ca.* 1 mL. The resulting pale yellow suspension was dissolved in 5 mL of THF and added dropwise to a mixture of **(2-thienyl)-Cp_2Zr-6-(2-thienyl)** (0.481 g, 0.977 mmol) and CuCl (14.4 mg, 0.145 mmol) in 10 mL of THF and stirred at room temperature in the absence of light for 3 hours, before being filtered through Celite, and the filtrate evaporated to dryness. The crude product was extracted with two 20 mL portions of hexanes; for each extraction, the product was stirred for 3–4 hours in the hexanes and filtered through Celite. The filtrate fractions were combined and concentrated *in vacuo* to a total volume of *ca.* 15–20 mL and stored at –30 °C for 16 hours. The first fraction of precipitate was discarded (as it consisted of Cp_2ZrCl_2 and another unknown Cp-containing by-product) and the mother liquor was concentrated further to *ca.* 5 mL and stored at –30 °C. Subsequent recrystallizations yielded two crystalline fractions which were collected and combined to give **4** as an orange solid (0.184 g, 32 %). Single crystals of suitable quality for X-ray diffraction were obtained by recrystallization of **4** from Et_2O at –30 °C. ^{1}H NMR (400 MHz, C_6D_6): δ 6.88 (s, 2H, Ar*H*), 6.84–6.87 (m, 4H, thienyl-*H*), 6.63 (m, 2H, thienyl-*H*), 2.69–2.79 (m, 2H, CH_2), 2.55–2.65 (m, 2H, CH_2), 2.51 (s, 6H, CH_3 in Mes), 2.02 (s, 3H, CH_3 in Mes), 1.37–1.43 (m, 4H, CH_2). $^{13}C\{^1H\}$ NMR (126 MHz, C_6D_6): δ 157.8 (Ar*C*), 149.6 (thienyl*C*), 147.7 (Ar*C*), 138.2 (Ar*C*), 129.9 (Ar*C*), 128.7 (thienyl*C*), 127.4 (thienyl*C*), 125.6 (thienyl*C*), 36.1 (C=C*C*H_2CH_2), 27.8 (*C*H_3 in Mes), 23.9 (C=CCH_2*C*H_2), 21.2 (*C*H_3 in Mes). Anal. Calcd. (%) for $C_{25}H_{25}BiS_2$: C, 50.16; H, 4.21; S, 10.71. Found: C, 50.67; H, 4.52; S, 10.57. UV-Vis (THF): λ_{max} = 421 nm (ε = 1.21×10^4 M^{-1} cm^{-1}). Mp: 103–105 °C.

Synthesis of $PhBiC_4Ph_4$ (5). A suspension of $BiCl_3$ (0.0488 g, 0.150 mmol) in 5 mL of Et_2O was added to a solution of $BiPh_3$ (0.333 g, 0.0756 mmol) in 5 mL of Et_2O and allowed to stir at room temperature for one hour. This mixture was then concentrated *in vacuo* to *ca*. 1 mL and the pale-yellow suspension was dissolved in 5 mL of THF, and added dropwise to a mixture of $Cp_2ZrC_4Ph_4$ (0.128 g, 0.221 mmol) and CuCl (2.5 mg, 0.025 mmol) in 12 mL of THF. The reaction mixture was allowed to stir at room temperature in the absence of light for 4 hours before being evaporated to dryness. The crude product was extracted into 20 mL of hexanes and filtered through a silica plug (0.5 cm) before the volatiles were removed from the filtrate. The crude product was recrystallized from Et_2O at –30 °C to yield **5** as a yellow powder (0.0473 g, 33 %). Single crystals suitable for X-ray diffraction were obtained by recrystallization of **5** from Et_2O at –30 °C. ^1H NMR (500 MHz, $CDCl_3$): δ 8.29 (m, 2H, *ortho*-H of Bi-Ph), 7.48 (t, $^3J_{HH}$ = 7.5 Hz, 2H, Ar*H*), 7.37 (m, 1H, Ar*H*), 6.91–7.03 (m, 12H, Ar*H*), 6.82–6.87 (m, 8H, Ar*H*). $^{13}C\{^1H\}$ NMR (126 MHz, $CDCl_3$): δ 164.8 (Ar*C*), 145.4 (Ar*C*), 144.9 (Ar*C*), 137.1 (Ar*C*), 131.2 (Ar*C*), 130.3 (Ar*C*), 129.2 (Ar*C*), 128.0 (Ar*C*), 127.9 (Ar*C*), 127.6 (Ar*C*), 126.0 (Ar*C*), 125.7 (Ar*C*).

Anal. Calcd. (%) for $C_{34}H_{25}Bi$: C, 63.55; H, 3.92. Found: C, 63.49; H, 4.30. UV-Vis (THF): λ_{max} = 358 nm ($\varepsilon = 5.47 \times 10^3$ M^{-1} cm^{-1}). Mp: 130–135 °C (decomp).

Synthesis of $MesBiC_4Ph_4$ (6). A suspension of $BiCl_3$ (0.0556 g, 0.176 mmol) in 5 mL of Et_2O was added to a solution of $BiMes_3$ (0.0490 g, 0.0865 mmol) in 5 mL of Et_2O and the mixture was allowed to stir at room temperature in the absence of light for 16 hous before being concentrated *in vacuo* to *ca*. 1 mL. The resulting mixture containing $MesBiCl_2$ was dissolved in 3 mL of THF and added to a mixture of $Cp_2ZrC_4Ph_4$ (0.152 g, 0.263 mmol) and copper(I) chloride (0.0040 g, 0.040 mmol) in 15 mL of THF. The reaction mixture was allowed to stir for 5 hours in the absence of light before being evaporated to dryness. The product was extracted into 20 mL of hexanes and filtered through a 0.5 cm plug of silica. The resulting filtrate was concentrated *in vacuo* to a volume of *ca.* 5 mL and stored at –30 °C for 16 hours after which **6** was obtained as a pale yellow solid (0.104 g, 59 %). Single crystals suitable for X-ray diffraction were obtained by slow recrystallization from Et_2O at –30 °C. ^1H NMR (700 MHz, C_6D_6): δ 7.11 (m, 4H, Ar*H*), 7.02 (d $^3J_{HH}$ = 7.0 Hz, 4H, Ar*H*), 6.94 (s, 2H, Ar*H* in Mes), 6.86–6.89 (m, 8H, Ar*H*), 6.81–6.83 (m, 2H, Ar*H*), 6.71–6.74 (m, 2H, Ar*H*), 2.65 (s, 6H, C*H_3* in Mes), 2.05 (s, 3H, C*H_3* in Mes). $^{13}C\{^1H\}$ NMR (176 MHz, C_6D_6): δ 172.3 (Ar*C*), 163.5 (Ar*C*), 159.6 (Ar*C*), 147.9 (Ar*C*), 145.8 (Ar*C*), 145.6 (Ar*C*), 138.3 (Ar*C*), 130.5 (Ar*C*), 130.3 (Ar*C*), 129.6 (Ar*C*), 126.3 (Ar*C*), 126.1 (Ar*C*), 27.7 (*C*H_3 on Mes), 21.2 (*C*H_3 on Mes). Anal. Calcd. (%) for $C_{37}H_{31}Bi$: C, 64.91; H, 4.56. Found: C, 65.05; H, 4.62. UV-Vis (THF): λ_{max} = 360 nm ($\varepsilon = 7.60 \times 10^3$ M^{-1} cm^{-1}). Mp: 85–95 °C.

Synthesis of 8. Suspended (Ar^{NMe2})$BiCl_2$ (0.216 g, 0.524 mmol) in 5 mL of Et_2O was added to **B-Cp$_2$Zr-6-B** (0.301 g, 0.519 mmol) in 5 mL of Et_2O. A catalytic amount of CuCl (0.0050 g, 0.050 mmol) was added and the mixture was allowed to stir at room temperature in the absence of light for 16 hours. The reaction mixture was filtered through a 1.5 cm plug of Celite, evaporated to dryness, extracted with 20 mL of hexanes, and the extract filtered through another 1.5 cm plug of Celite. The filtrate was then concentrated *in vacuo* to a volume of 12 mL before another filtration through Celite was performed. The filtrate was evaporated to dryness to yield 0.328 g of crude **7**. The crude sample of **7** (*ca*. 0.468 mmol) was dissolved in 10 mL of Et_2O, added to CuCl (0.0462 g, 0.467 mmol), and the mixture stirred at room temperature in the absence of light for 5.5 hours. The reaction mixture was evaporated to dryness, extracted into 15 mL of toluene, and filtered through a 1.5 cm plug of Celite. The filtrate was then concentrated *in vacuo* to a volume of 4 mL and stored at –30 °C for 16 hours (note: if **8** is stored in solution, even at –30 °C, for more than 48 hours the product will begin to decompose into an unidentified insoluble dark green-grey precipitate). Compound **8** was then obtained as a light yellow crystalline solid (0.157 g, 38 %). ^{1}H NMR (500 MHz, C_6D_6): δ 8.51 (d, $^3J_{HH}$ = 7.2 Hz, 1H, Ar*H*), 7.27 (t, $^3J_{HH}$ = 7.2 Hz, 1H, Ar*H*), 6.95–7.03 (m, 2H, Ar*H*), 3.25–3.52 (br, 2H, C=CCH_2CH$_2$), 2.98–3.10 (br, 2H, C=CCH$_2$CH_2), 2.71–3.03 (br, 2H, C=CCH_2CH$_2$), 2.31–2.39 (br, 8H, CH_2N(CH$_3$)$_2$ and N(CH_3)$_2$), 1.42–1.52 (m, 2H, C=CCH$_2$CH_2), 1.07 (s, 12H, CH_3 in BPin), 1.04 (s, 12H, CH_3 in BPin). ^{13}C{^{1}H} NMR (126 MHz, C_6D_6): δ 139.3 (Ar*C*), 129.6 (Ar*C*), 127.1 (Ar*C*), 83.4 (*C*(CH$_3$)$_2$), 70.0 (*C*H$_2$N(CH$_3$)$_2$), 47.6 (CH$_2$N(*C*H$_3$)$_2$), 42.3 (br, C=C*C*H$_2$CH$_2$), 25.1 (*C*H$_3$ in BPin), 24.9 (*C*H$_3$ in BPin), 24.7

(br, C=C$CH_2$$CH_2$). Note: several ArC signals are missing due to the weakness of the signals and instability of **8** in solution which limited the number of scans that could be done. $^{11}B\{^1H\}$ NMR (128 MHz, C_6D_6): δ 32.8. Anal. Calcd. (%) for $C_{29}H_{44}B_2BiClCuNO_4$: C, 43.52; H, 5.54; N, 1.75. Found: C, 44.01; H, 5.82; N, 1.66. UV-Vis (THF): λ_{max} = 386 nm ($\varepsilon = 3.33 \times 10^3$ $M^{-1}cm^{-1}$). Mp: 120 °C (decomp).

Synthesis of 7. Triphenylphosphine (0.0250 g, 0.0953 mmol) in 5 mL of hexanes was added to **8** (0.0757 g, 0.0947 mmol) in 5 mL of hexanes. The reaction mixture was stirred at room temperature for 5 hours before being filtered through a 1.5 cm plug of Celite. The filtrate was evaporated to dryness to give **7** as a spectroscopically pure yellow solid (0.0470 g, 71 %). ^1H NMR (400 MHz, C_6D_6): δ 8.43–8.45 (m, 1H, Ar*H*), 7.35–7.38 (m, 1H, Ar*H*), 7.11–7.14 (m, 2H, Ar*H*), 3.64 (s, 2H, ArCH_2N(CH_3)$_2$), 2.91–2.95 (m, 4H, C=CC$H_2$$CH_2$), 2.24 (s, 6H, N(C$H_3$)$_2$), 1.46–1.59 (m, 4H, C=C$CH_2CH_2$), 1.03 (s, 12H, C$H_3$ in BPin), 1.02 (s, 12H, CH_3 in BPin). $^{13}C\{^1H\}$ NMR (126 MHz, C_6D_6): δ 177.0 (Ar*C*), 145.4 (Ar*C*), 138.8 (Ar*C*), 130.3 (Ar*C*), 130.0 (Ar*C*), 127.3 (Ar*C*), 82.9 (*C*(CH_3)$_2$), 68.7 (*C*H_2N(CH_3)$_2$), 45.3 (CH_2N(*C*H_3)$_2$), 41.6 (C=C*C*$H_2$$CH_2$), 25.0 (*C*$H_3$ in BPin), 24.9 (*C*H_3 in BPin), 23.6 (C=CCH_2*C*H_2). $^{11}B\{^1H\}$ NMR (128 MHz, C_6D_6): δ 34.6. Anal. Calcd. (%) for $C_{29}H_{44}B_2BiNO_4$: C, 49.67; H, 6.32; N, 2.00. Found: C, 48.87; H, 6.25; N, 2.22. UV-Vis (THF): λ_{max} = 329 nm ($\varepsilon = 4.25 \times 10^3$ M^{-1} cm^{-1}). Mp: 105–108 °C (decomp).

2.4.3 Experimental Methods Used to Acquire Time-Integrated Photoluminescence and Time-Resolved Photoluminescence Data

A sample dissolved in toluene or THF (*ca*. 10 mg/mL) was drop-casted onto a 1 mm thick optical grade fused quartz substrate (Starna Scientific Ltd). Samples were then placed in an optical microscopy cryostat (Cryo Industries) with level of vibrations ≤ 15 nm. The chamber was evacuated to a pressure of ~2.2×10^{-7} mbar and then cooled by free-flowing liquid nitrogen with temperatures above 77 K regulated with the aid of a temperature controller (Lakeshore 335). An 800 nm Ti:Sapphire ultrafast laser (Coherent RegA 900) with 65 fs pulse width and 250 kHz repetition rate was used to optically excite the samples at 400 nm via second harmonic signal generation from a barium borate (BBO) crystal. All measurements were carried out at an average of 0.2 ± 0.02 mW excitation power. The time-integrated and time-resolved photoluminescence (TIPL and TRPL, respectively) were collected using a confocal setup with a 435 nm long pass filter (Edmund Optics). The TIPL spectra were measured by a CCD (Princeton Instruments Acton Spectrometer) with a resolution of ± 6.4 nm with a 1000 µm entrance slit. For the nanosecond timescale TRPL, a time-correlated single photon counting (TCSPC) technique was used which consists of a single-photon avalanche photodiode connected to a TCSPC module (PicoHarp 300, Picoquant), providing a time resolution of 54 ± 1 ps. As for the recording of the microsecond lifetime component, a frequency-doubled 800 nm Ti: Sapphire with 1 kHz repetition rate was used for the excitation. A set of parabolic mirrors collected the photoluminescence onto an optical fiber to the Si avalanche photodetector (Thorlabs APD130A, 20 ns time resolution) with a band-pass filter of 705 ± 5 nm.

Emission lifetimes were recorded using a 200 MHz oscilloscope (Tektronix DPO 2024B).

2.4.4 Computational Methodology

Geometry optimizations of the gas phase structure have been performed using density functional theory (DFT) with the B3LYP[44] functional and the cc-pVTZ (for H, B, C, N, O, Cl and S)[45] as well as the cc-pVTZ-PP (for Cu and Bi)[46] basis sets. The initial structures were taken from the experimentally obtained X-ray structures of **4** and **8**. The initial structure of bismole **7** was taken from the optimized geometry of **8** with manual removal of CuCl. The use of the cc-pVTZ and cc-pVTZ-PP basis sets will thereafter be referred to as cc-pVTZ(-PP). The basis sets as well as the effective core potential (ECP) for the Cu and Bi atom have been obtained from the Basis Set Exchange Library.[47] Subsequent frequency analysis confirmed the obtained structures to be a local minimum on the potential energy surface. To calculate the phosphorescence energy, the geometries of the lowest lying triplet states (T_1) of **4**, **7** and **8** were optimized by applying the UB3LYP (spin-unrestricted B3LYP) functional with the same basis sets as specified above. The vertical excitation energies of the first ten singlet and triplet states of **4**, **7** and **8** were predicted by TD-DFT calculations using the B3LYP functional and the cc-pVTZ(-PP) basis sets starting from the respective B3LYP optimized gas phase S_0 geometry. Phosphorescence energies were calculated as the difference of the energies at the UB3LYP optimized T_1 geometry and the B3LYP optimized S_0 geometry. All calculations were been carried out with the Gaussian16 software.[48] The wavefunction files were used for an topological analysis of the electron density according to the Atoms-In-Molecules space-partitioning scheme[31] using AIM2000,[49] whereas DGRID[50] was used to generate and analyze the Electron-Localizability-Indicator (ELI-D) related real-space bonding descriptors[32] applying a grid step size of 0.05 a.u. The NCI grids were computed with NCIplot.[51] Bond paths are displayed with AIM2000,[49] AIM atomic basins, ELI-D and NCI figures are displayed with MolIso[52] and VMD,[53] respectively. The molecular orbitals (MOs) were extracted from the Gaussian16 checkpoint files and were visualized with GaussView 5.0.[54] The final molecular geometries were used to compute the natural bond orbitals (NBOs) using the NBO6 program.[55] Spin-orbit coupling was considered using the TD-DFT framework[56] with the Amsterdam Density Functional (ADF) software.[57] The S_0 ground state optimized geometries of bismoles **4**, **7** and **8** as determined by the Gaussian09 computations were used as input geometries. TD-DFT calculations were determined at the B3LYP/TZ2P level of theory[44,58] using the "core none" option. All calculations with the ADF software include scalar relativistic (ZORA)[59] and spin-orbit relativistic (SO) methods.[53c,60] The NICS(0) values of bismole **7**, C_4H_4BiH and C_4H_4NH were calculated at the AIM ring critical point at the same level of theory stated above using the GIAO[61] formalism as implemented in Gaussian16.

2.4.4.1 Additional Computational Excited State Data for Compounds 4, 7, and 8

Table 2.1. TD-DFT calculated excited states of bismoles **4**, **7** and **8** at the B3LYP/cc-pVTZ(-PP) level of theory.

Excited States	**4** E [eV] and f	Excited States	**7** E [eV] and f	Excited States	**8** E [eV] and f
T_1	1.5246 0.0000	T_1	2.2000 0.0000	T_1	2.0489 0.0000
T_2	2.7663 0.0000	T_2	3.0511 0.0000	T_2	2.6573 0.0000
S_1	2.8012 0.4393	S_1	3.3452 0.0392	S_1	2.9981 0.0333
T_3	3.1691 0.0000	T_3	3.3947 0.0000	T_3	3.1023 0.0000
S_2	3.2943 0.0019	S_2	3.4362 0.0264	S_2	3.1174 0.0305
T_4	3.3781 0.0000	T_4	3.4369 0.0000	T_4	3.1736 0.0000
T_5	3.4801 0.0000	S_3	3.5651 0.0476	T_5	3.3706 0.0000
T_6	3.5492 0.0000	T_5	3.6611 0.0000	S_3	3.4351 0.0252
T_7	3.6433 0.0000	T_6	3.7580 0.0000	T_6	3.5474 0.0000
S_3	3.6460 0.0119	S_4	3.8706 0.0587	T_7	3.6865 0.0000
S_4	3.6615 0.0101	T_7	4.2355 0.0000	S_4	3.6913 0.0289
T_8	3.7862 0.0000	T_8	4.2929 0.0000	T_8	3.7696 0.0000
T_9	3.8358 0.0000	T_9	4.3411 0.0000	S_5	3.8369 0.0179
T_{10}	3.8587 0.0000	S_5	4.3529 0.0051	T_9	3.9205 0.0000
S_5	3.9124 0.0037	S_6	4.3971 0.0040	S_6	3.9946 0.0228
S_6	3.9633 0.0023	T_{10}	4.4212 0.0000	T_{10}	4.0033 0.0000
S_7	4.2412 0.0193	S_7	4.5071 0.0720	S_7	4.1824 0.0149
S_8	4.2895 0.0777	S_8	4.6230 0.0157	S_8	4.2564 0.0084
S_9	4.3926 0.0316	S_9	4.6586 0.0006	S_9	4.3062 0.0278
S_{10}	4.4084 0.0082	S_{10}	4.7220 0.0467	S_{10}	4.3526 0.0041

Table 2.2. TD-DFT calculated excited states of **4** at B3LYP/TZ2P incl. SO coupling.

State	E [eV] and f	S (%)	T (%)	State	E [eV] and f	S (%)	T (%)
0	0.0000 0.5166E-08	99.9	0.0	**21**	3.6868 0.4419E-02	32.4	67.3
1	1.6326 0.1091E-04	0.0	99.9	**22**	3.7048 0.3672E-02	52.5	46.8
2	1.6327 0.6152E-06	0.0	99.9	**23**	3.7194 0.1995E-03	2.5	97.2
3	1.6328 0.3565E-05	0.0	100.0	**24**	3.7279 0.5974E-03	8.3	91.5
4	2.8128 0.4205	91.9	7.9	**25**	3.7609 0.5491E-02	38.8	60.8
5	2.8488 0.3188E-04	0.0	99.8	**26**	3.8003 0.4281E-04	0.3	99.5
6	2.8506 0.9059E-02	2.3	97.6	**27**	3.8019 0.5667E-04	0.4	99.5
7	2.8513 0.2026E-01	4.6	95.2	**28**	3.8062 0.1123E-02	7.6	92.2
8	3.1695 0.1183E-02	1.3	98.6	**29**	3.8607 0.9065E-05	0.0	99.9
9	3.1759 0.3486E-03	0.1	99.7	**30**	3.8608 0.6227E-05	0.0	99.8
10	3.1789 0.6604E-02	2.2	97.6	**31**	3.8626 0.1625E-03	1.5	98.4
11	3.2798 0.2036E-02	94.7	5.1	**32**	3.8813 0.6235E-04	0.4	99.3
12	3.3404 0.9803E-04	0.9	98.9	**33**	3.8815 0.9900E-04	0.6	99.2
13	3.3417 0.5878E-04	0.6	99.1	**34**	3.8825 0.3232E-03	2.4	97.6
14	3.3530 0.1343E-02	12.6	87.1	**35**	3.9045 0.4851E-02	99.2	0.6
15	3.4609 0.3008E-02	23.6	76.3	**36**	3.9485 0.2038E-02	99.4	0.5
16	3.5783 0.4283E-04	0.3	99.4	**37**	4.1586 0.5467E-01	98.1	1.7
17	3.5840 0.3110E-03	3.0	96.6	**38**	4.2917 0.3022E-01	97.8	2.0
18	3.6538 0.1295E-02	11.1	88.7	**39**	4.3902 0.1163E-01	99.8	0.1
19	3.6678 0.9970E-04	1.5	98.3	**40**	4.4059 0.1483E-01	99.7	0.1
20	3.6681 0.3343E-03	5.1	94.7				

Table 2.3. TD-DFT calculated excited states of **7** at B3LYP/TZ2P incl. SO coupling.

State	E [eV] and f	S (%)	T (%)	State	E [eV] and f	S (%)	T (%)
0	0.0000 0.4233E-06	99.3	0.5	21	3.9526 0.2516E-02	8.7	90.9
1	2.3299 0.9397E-05	0.0	99.9	22	4.0161 0.3620E-01	61.7	38.0
2	2.3299 0.5576E-05	0.0	99.99	23	4.2590 0.2875E-03	0.9	98.9
3	2.3301 0.1869E-05	0.0	99.9	24	4.2623 0.4810E-03	1.6	97.9
4	2.9967 0.6880E-04	0.1	99.7	25	4.3089 0.3963E-03	4.6	95.0
5	2.9999 0.3804E-03	0.8	99.1	26	4.3166 0.2188E-03	0.5	99.3
6	3.0191 0.3884E-02	7.8	92.0	27	4.3315 0.1222E-03	0.6	99.2
7	3.2625 0.1506E-01	55.8	44.0	28	4.3326 0.3117E-03	1.5	98.2
8	3.3737 0.3184E-01	96.4	3.4	29	4.3642 0.1525E-02	12.7	87.1
9	3.4094 0.2110E-05	0.0	99.8	30	4.3754 0.8886E-04	0.3	99.6
10	3.4101 0.1080E-03	0.4	99.5	31	4.3782 0.2203E-03	2.8	97.0
11	3.4120 0.5461E-03	1.4	98.4	32	4.3878 0.5227E-02	84.5	15.3
12	3.5078 0.1040E-04	0.0	99.9	33	4.4112 0.2815E-02	94.4	4.9
13	3.5322 0.3513E-02	11.0	88.8	34	4.4643 0.1364E-02	3.7	96.1
14	3.5942 0.4319E-01	81.1	18.8	35	4.4949 0.1736E-02	8.1	91.6
15	3.6117 0.6350E-02	19.8	79.5	36	4.4960 0.4990E-03	1.0	98.8
16	3.7739 0.1964E-01	34.6	65.1	37	4.5935 0.6107E-01	92.0	7.5
17	3.8686 0.3411E-03	0.7	98.9	38	4.6712 0.1193E-01	96.6	3.3
18	3.8720 0.2267E-02	7.8	92.0	39	4.7043 0.7578E-02	93.7	6.0
19	3.9039 0.8275E-02	13.9	85.9	40	4.7627 0.4457E-01	96.2	3.7
20	3.9417 0.1330E-04	0.0	99.8				

Table 2.4. TD-DFT calculated excited states of **8** at B3LYP/TZ2P incl. SO coupling.

State	E [eV] and f	S (%)	T (%)	State	E [eV] and f	S (%)	T (%)
0	0.0000 0.3564E-07	99.6	0.2	21	3.6179 0.9993E-03	3.7	94.9
1	2.1926 0.2671E-04	0.1	99.7	22	3.7008 0.2079E-01	70.1	29.3
2	2.1935 0.6131E-04	0.2	99.6	23	3.7992 0.5079E-02	27.3	71.9
3	2.1945 0.6607E-04	0.2	99.6	24	3.8102 0.1262E-02	6.6	92.8
4	2.6967 0.7481E-04	0.3	99.4	25	3.8191 0.2572E-02	9.6	89.9
5	2.6985 0.1239E-03	0.4	99.3	26	3.8563 0.7659E-03	3.4	96.4
6	2.7010 0.2979E-03	1.2	98.7	27	3.8711 0.1603E-03	0.6	99.1
7	2.9959 0.2718E-01	88.7	11.1	28	3.8749 0.1594E-02	7.5	92.2
8	3.0587 0.1831E-01	63.4	36.0	29	3.8905 0.7897E-02	41.8	57.5
9	3.1269 0.8926E-04	0.3	99.5	30	3.9694 0.5246E-02	22.6	76.7
10	3.1378 0.2926E-02	9.6	90.2	31	3.9760 0.6768E-03	3.0	96.6
11	3.1573 0.6942E-02	24.2	75.2	32	3.9846 0.3278E-02	15.4	84.2
12	3.2413 0.5327E-03	1.8	98.0	33	4.0065 0.8114E-02	36.8	62.1
13	3.2488 0.3067E-03	1.1	98.9	34	4.0974 0.6614E-02	29.5	69.6
14	3.2516 0.6052E-03	2.2	97.7	35	4.1247 0.6341E-03	2.9	96.5
15	3.3788 0.8398E-04	0.0	99.0	36	4.1442 0.5583E-02	23.1	75.9
16	3.3891 0.4056E-02	13.8	84.9	37	4.2498 0.1355E-01	89.3	10.0
17	3.3948 0.6982E-02	24.6	74.7	38	4.2765 0.5924E-02	97.7	2.1
18	3.4452 0.1739E-01	59.2	38.3	39	4.3129 0.2859E-01	98.4	1.4
19	3.5914 0.5150E-02	17.6	81.9	40	4.3565 0.4399E-02	97.1	2.8
20	3.6121 0.1521E-03	0.5	98.7				

2.5 Crystallographic Data

Table 2.5. Crystallographic data for compounds **3**, **4**, and **5**.

Compound	**3**	**4**	**5**
Formula	$C_{29}H_{43}B_2BiO_4$	$C_{28}H_{28}BiS_2$	$C_{34}H_{25}Bi$
Formula weight	686.23	637.60	642.52
Crystal system	Monoclinic	Triclinic	Monoclinic
Space group	$P2_1/c$	$P\bar{1}$	$P2_1$
a (Å)	10.2343(3)	9.1994(4)	11.403(3)
b (Å)	15.8713(5)	10.0707(4)	21.179(5)
c (Å)	18.1272(5)	13.8234(6)	11.908(3)
α (°)	--	80.9431(4)	--
β (°)	95.4938(9)	80.1476(4)	115.595(2)
γ (°)	--	75.9955(4)	--
V (Å^3)	2930.91(15)	1215.22(9)	2593.6(10)
Z	4	2	4
ρ (g/cm^3)	1.555	1.743	1.645
Abs coeff (mm^{-1})	12.04	7.440	6.818
T (K)	173	173	173
$2\theta_{max}$ (°)	145.37	56.75	56.73
Total data	19960	11496	24157
Unique data (R_{int})	5727 (0.0209)	5929(0.0122)	12584(0.0245)
Obs data [I>2(σ(I)]	5605	5604	11786
Params	328	327	632
R_1 [I>2(σ(I)]^a	0.0210	0.0159	0.0192
wR_2 [all data]^a	0.0536	0.0364	0.0349
Max/min $\Delta\rho$ (e$^-$Å^{-3})	1.021/–0.689	0.907/–0.658	0.844/–0.658

$^aR_1 = \Sigma||F_o| - |F_c||/\Sigma|F_o|$; $wR_2 = [\Sigma w(F_o^2 - F_c^2)^2/\Sigma w(F_o^4)]^{1/2}$

Table 2.6. Crystallographic data for compounds **6** and **8**.

Compound	**6**	**8**
Formula	$C_{37}H_{31}Bi$	$C_{31}H_{49}B_2BiClCuNO_{4.5}$
Formula weight	684.60	837.30
Crystal system	Monoclinic	Monoclinic
Space group	$P2_1/c$	$P2_1/n$ (alternate setting of $P2_1/c$)
a (Å)	16.3505(4)	10.9507(3)
b (Å)	10.6036(2)	11.6200(4)
c (Å)	18.0431(4)	27.0561(8)
α (°)	--	--
β (°)	113.3156(6)	94.8831(4)
γ (°)	--	--
V (Å^3)	2872.75(11)	3430.31(18)
Z	4	4
ρ (g/cm^3)	1.583	1.621
Abs coeff (mm^{-1})	12.20	5.857
T (K)	173	173
$2\theta_{max}$ (°)	147.90	56.67
Total data	19998	31526
Unique data (R_{int})	5811(0.0251)	8483(0.0406)
Obs data [I>2($\sigma(I)$]	5764	7009
Params	346	432
R_1 [I>2($\sigma(I)$][a]	0.0198	0.0257
wR_2 [all data][a]	0.0505	0.0609
Max/min $\Delta\rho$ (e$^-$Å^{-3})	0.746/–1.741	1.667/–0.611

[a]$R_1 = \Sigma||F_o| - |F_c||/\Sigma|F_o|$; $wR_2 = [\Sigma w(F_o^2 - F_c^2)^2/\Sigma w(F_o^4)]^{1/2}$

2.6 References

1. Parke, S. P.; Boone, M. P.; Rivard, E. *Chem. Commun.* **2016**, *52*, 9485−9505.

2. (a) Osaka, I.; McCullough, R. D. *Acc. Chem. Res.* **2008**, *41*, 1202–1214. (b) McCullough, R. D. *Adv. Mater*. **1998**, *10*, 93–116. (c) Roncali, J. *Chem. Rev.* **1992**, *92*, 711–738.

3. (a) Berggren, M.; Inganas, O.; Gustafsson, G.; Rasmusson, J.; Andersson, M. R.; Hjertberg, T.; Wennerstrom, O. *Nature* **1994**, *372*, 444–446. (b) Perepichka, I. F.; Perepichka, D. F.; Meng, H. Thiophene-based Materials for Electroluminescent

Applications. In *Electroactive Oligothiophenes and Polythiophenes for Organic Field Effect Transistors*; Perepichka, I. F.; Perepichka, D. F., Ed.; Wiley: Chichester, UK, 2009; 647–672.

4. (a) Zhang, F.; Wu, D.; Xu, Y.; Geng, X. *J. Mater. Chem.* **2011**, *21*, 17590–17600. (b) Chen, J.; Cao, Y. *Acc. Chem. Res*. **2009**, *42*, 1709–1718.
5. (a) Nielsen, C. B.; McCulloch, I. *Prog. Polym. Sci*. **2013**, *38*, 2053–2069. (b) McCulloch, I.; Heeney, M. Thienothiophene Copolymers in Field Effect Transistors. In *Electroactive Oligothiophenes and Polythiophenes for Organic Field Effect Transistors*; Perepichka, I. F.; Perepichka, D. F., Ed.; Wiley: Chichester, UK, 2009; 647–672.
6. (a) Krzeszewski, M.; Gryko, D.; Gryko, D. T. *Acc. Chem. Res.* **2017**, *50*, 2334−2345. (b) Pron, A.; Berrouard, P.; Leclerc, M. *Macromol. Chem. Phys.* **2013**, *214*, 7−16.
7. (a) Baumgartner, T. *Acc. Chem. Res.* **2014**, *47*, 1613−1622. (b) Baumgartner, T.; Réau, R. *Chem. Rev.* **2006**, *106*, 4681−4727.
8. (a) Ishidoshiro, M.; Matsumura, Y.; Imoto, H.; Irie, Y.; Kato, T.; Watase, S.; Matsukawa, K.; Inagi, S.; Tomita, I.; Naka, K. *Org. Lett.* **2015**, *17*, 4854−4857. (b) Matsumura, M.; Muranaka, A.; Kurihara, R.; Kanai, M.; Yoshida, K.; Kakusawa, N.; Hashizume, D.; Uchiyama, M.; Yasuike, S. *Tetrahedron* **2016**, *72*, 8085−8090. (c) Kato, T.; Imoto, H.; Tanaka, S.; Ishidoshiro, M.; Naka, K. *Dalton Trans.* **2016**, *45*, 11338−11345. (d) Ishidoshiro, M.; Imoto, H.; Tanaka, S.; Naka, K. *Dalton Trans.* **2016**, *45*, 8717−8723. (e) Matsumura, Y.; Ishidoshiro, M.; Irie, Y.; Imoto, H.; Naka, K.; Tanaka, K.; Inagi, S.; Tomita, I. *Angew. Chem. Int. Ed*. **2016**, *55*,

15040−15043. (f) Green, J. P.; Han, Y.; Kilmurray, R.; McLachlan, M. A.; Anthopoulos, T. D.; Heeney, M. *Angew. Chem., Int. Ed.* **2016**, *55*, 7148−7151. (g) Green, J. P.; Cryer, S. J.; Marafie, J.; White, A. J. P.; Heeney, M. *Organometallics* **2017**, *36*, 2632−2636. (h) Fell, V. H. K.; Mikosch, A.; Steppert, A.-K.; Ogieglo, W.; Senol, E.; Canneson, D.; Bayer, M.; Schoenebeck, F.; Greilich, A.; Kuehne, A. J. C. *Macromolecules* **2017**, *50*, 2338−2343. (i) Imoto, H.; Sasaki, H.; Tanaka, S.; Yumura, T.; Naka, K. *Organometallics* **2017**, *36*, 2605−2611.

9. (a) Ohshita, J.; Fujita, R.; Tanaka, D.; Ooyama, Y.; Kobayashi, N.; Higashimura, H.; Yamamoto, Y. *Chem. Lett.* **2012**, *41*, 1002–1003. (b) Christianson, A. M.; Rivard, E.; Gabbaï, F. P. *Organometallics* **2017**, *36*, 2670−2676. (c) Christianson, A. M.; Gabbaï, F. P. *Organometallics* **2017**, *36*, 3013−3015.

10. (a) Rivard, E. *Chem. Lett.* **2015**, *44*, 730−736. (b) Jia, W.-L.; Liu, Q.-D.; Wang, R.; Wang, S. *Organometallics* **2003**, *22*, 4070−4078. (c) Vogler, A.; Paukner, A. *Inorg. Chim. Acta* **1989**, *163*, 207−211. (d) Taneda, M.; Maeda, D.; Shimakoshi, H.; Abe, M.; Hisaeda, Y. *Bull. Chem. Soc. Jpn.* **2010**, *83*, 667−671. (e) Matsumoto, T.; Tanaka, K.; Tanaka, K.; Chujo, Y. *Dalton Trans.* **2015**, *44*, 8697−8707. (f) Liu, X.; Zhai, L.; Zhang, W.-W.; Zuo, J.-L.; Yang, Z.-X.; Ren, X.-M. *Dalton Trans.* **2017**, *46*, 7953−7959. (g) Mukherjee, S.; Thilagar, P. *Chem. Commun.* **2015**, *51*, 10988−11003. (h) Ravotto, L.; Ceroni, P. *Coord. Chem. Rev.* **2017**, *346*, 62−76.

11. (a) Tuong Ly, K.; Chen-Cheng, R.-W.; Lin, H.-W.; Shiau, Y.-J.; Liu, S.-H.; Chou, P.-T.; Tsao, C.-S.; Huang, Y.-C.; Chi, Y. *Nat. Photonics* **2017**, *11*, 63−68. (b) Chi, Y.; Chou, P.-T. *Chem. Soc. Rev.* **2010**, *39*, 638−655. (c) Baldo, M. A.;

Lamansky, S.; Burrows, P. E.; Thompson, M. E.; Forrest, S. R. *Appl. Phys. Lett*. **1999**, 75, 4−6.

12. (a) Manjare, S. T.; Kim, Y.; Churchill, D. G. *Acc. Chem. Res.* **2014**, *47*, 2985−2988. (b) Wang, J.; Xue, J.; Yan, Z.; Zhang, S.; Qiao, J.; Zhang, X. *Angew. Chem., Int. Ed.* **2017**, *56*, 14928−14932. (c) Zhao, Q.; Huang, C.; Li, F. *Chem. Soc. Rev.* **2011**, *40*, 2508−2524. (d) Zhao, Q.; Sun, J. Z. *J. Mater. Chem. C* **2016**, *4*, 10588−10609. (e) Guo, Z.; Shao, A.; Zhu, W.-H. *J. Mater. Chem. C* **2016**, *4*, 2640−2646.

13. (a) Sano, Y.; Satoh, H.; Chiba, M.; Okamoto, M.; Serizawa, K.; Nakashima, H.; Omae, K. *J. Occup. Health* **2005**, *47*, 293−298. (b) Yang, N.; Sun, H. *Coord. Chem. Rev.* **2007**, *251*, 2354−2366.

14. (a) Filatov, M. A.; Baluschev, S.; Landfester, K. *Chem. Soc. Rev.* **2016**, *45*, 4668−4689. (b) Papkovsky, D. B.; Zhdanov, A. V. *Free Radical Biol. Med.* **2016**, *101*, 202−210. (c) Baldo, M. A.; Adachi, C.; Forrest, S. R. *Phys. Rev. B* **2000**, *62*, 10967−10977.

15. Wittig, G.; Hellwinkel, D. *Chem. Ber.* **1964**, *97*, 789−793.

16. Hellwinkel, D.; Bach, M. *Liebigs. Ann. Chem.* **1968**, *720*, 198−200.

17. (a) Ashe, A. J., III; Kampf, J. W.; Al-Taweel, S. M. *J. Am. Chem. Soc.* **1992**, *114*, 372−374. (b) Ashe, A. J., III; Kampf, J. W.; Al-Taweel, S. M. *Organometallics* **1992**, *11*, 1491−1496. (c) Ashe, A. J., III; Al-Ahmad, S.; Pilotek, S.; Puranik, D. B.; Elschenbroich, C.; Behrendt, A. *Organometallics* **1995**, *14*, 2689−2698.

18. Morisaki, Y.; Ohashi, K.; Na, H.-S.; Chujo, Y. *J. Polym. Sci., Part A: Polym. Chem.* **2006**, *44*, 4857−4863.

19. Ohshita, J.; Matsui, S.; Yamamoto, R.; Mizumo, T.; Ooyama, Y.; Harima, Y.; Murafuji, T.; Tao, K.; Kuramochi, Y.; Kaikoh, T.; Higashimura, H. *Organometallics* **2010**, *29*, 3239−3241.

20. (a) Fagan, P. J.; Nugent, W. A. *J. Am. Chem. Soc.* **1988**, *110*, 2310−2312. (b) Yan, X.; Xi, C. *Acc. Chem. Res.* **2015**, *48*, 935−946.

21. (a) He, G.; Torres Delgado, W.; Schatz, D. J.; Merten, C.; Mohammadpour, A.; Mayr, L.; Ferguson, M. J.; McDonald, R.; Brown, A.; Shankar, K.; Rivard, E. *Angew. Chem., Int. Ed*. **2014**, *53*, 4587−4591. (b) He, G.; Wiltshire, B. D.; Choi, P.; Savin, A.; Sun, S.; Mohammadpour, A.; Ferguson, M. J.; McDonald, R.; Farsinezhad, S.; Brown, A.; Shankar, K.; Rivard, E. *Chem. Commun.* **2015**, *51*, 5444−5447. (c) Torres Delgado, W.; Shahin, F.; Ferguson, M. J.; McDonald, R.; He, G.; Rivard, E. *Organometallics* **2016**, *35*, 2140−2148. (d) Braun, C. A.; Zomerman, D.; de Aguiar, I.; Qi, Y.; Torres Delgado, W.; Ferguson, M. J.; McDonald, R.; de Souza, G. L. C.; He, G.; Brown, A.; Rivard, E. *Faraday Discuss.* **2017**, *196*, 255−268. (e) Torres Delgado, W.; Braun, C. A.; Boone, M. P.; Shynkaruk, O.; Qi, Y.; McDonald, R.; Ferguson, M. J.; Data, P.; Almeida, S. K. C.; de Aguiar, I.; de Souza, G. L. C.; Brown, A.; He, G.; Rivard, E. *ACS Appl. Mater. Interfaces* **2018**, *10*, 12124–12134. For related important studies on fluorescent tellurium compounds, see: (f) Kryman, M. W.; Schamerhorn, G. A.; Yung, K.; Sathyamoorthy, B.; Sukumaran, D. K.; Ohulchanskyy, T. Y.; Benedict, J. B.; Detty, M. R. *Organometallics* **2013**, *32*, 4321−4333. (g) McCormick, T. M.; Carrera, E. I.; Schon, T. B.; Seferos, D. S. *Chem. Commun.* **2013**, *49*, 11182−11184. (h) Annaka, T.; Nakata, N.; Ishii, A. *Organometallics* **2015**, *34*,

1272−1278. (i) Kremer, A.; Fermi, A.; Biot, N.; Wouters, J.; Bonifazi, D. *Chem. Eur. J.* **2016**, *22*, 5665−5675.

22. Becker, G.; Egner, J.; Meiser, M.; Mundt, O.; Weidlein, J. *Z. Anorg. Allg. Chem.* **1997**, *623*, 941−956.

23. Kindra, D. R.; Peterson, J. K.; Ziller, J. W.; Evans, W. J. *Organometallics* **2015**, *34*, 395−397.

24. Carmalt, C. J.; Cowley, A. H.; Culp, R. D.; Jones, R. A.; Kamepalli, S.; Norman, N. C. *Inorg. Chem.* **1997**, *36*, 2770−2776.

25. (a) Luo, J.; Xie, Z.; Lam, J. W. Y.; Cheng, L.; Chen, H.; Qiu, C.; Kwok, H. S.; Zhan, X.; Liu, Y.; Zhu, D.; Tang, B. Z. *Chem. Commun.* **2001**, 1740−1741. (b) Mei, J.; Leung, N. L. C.; Kwok, R. T. K.; Lam, J. W. Y.; Tang, B. Z. *Chem. Rev.* **2015**, *115*, 11718−11940.

26. Goreshnik, E. A.; Schollmeyer, D.; Myskiv, M. G *Z. Anorg. Allg. Chem.* **2002**, *628*, 2118−2122.

27. Fenske, D.; Rothenberger, A.; Wieber, S. *Z. Anorg. Allg. Chem.* **2003**, *629*, 929−930.

28. Ke, I.-S.; Gabbaï, F. P. *Aust. J. Chem.* **2013**, *66*, 1281−1287.

29. Bondi, A. *J. Phys. Chem.* **1964**, *68*, 441−451.

30. Mantina, M.; Chamberlin, A. C.; Valero, R.; Cramer, C. J.; Truhlar, D. G. *J. Phys. Chem. A* **2009**, *113*, 5806−5812.

31. Bader, R. F. W. *Atoms in Molecules. A Quantum Theory*; Oxford University Press: Oxford, U.K., 1990.

32. (a) Kohout, M. *Int. J. Quantum Chem.* **2004**, *97*, 651−658. (b) Kohout, M.; Wagner, F. R.; Grin, Yu. *Theor. Chem. Acc.* **2008**, *119*, 413−420.

33. Johnson, E. R.; Keinan, S.; Mori-Sánchez, P.; Contreras-García, J.; Cohen, A. J.; Yang, W. *J. Am. Chem. Soc.* **2010**, *132*, 6498−6506.

34. (a) Glendening, E. D.; Landis, C. R.; Weinhold, F. *Comput. Mol. Sci*. **2012**, *2*, 1−42. (b) Weinhold, F. *J. Comput. Chem.* **2012**, *33*, 2363−2379.

35. (a) Flierler, U.; Burzler, M.; Leusser, D.; Henn, J.; Ott, H.; Braunschweig, H.; Stalke, D. *Angew. Chem., Int. Ed.* **2008**, *47*, 4321−4325. (b) Farrugia, L. J.; Evans, C.; Lentz, D.; Roemer, M. *J. Am. Chem. Soc.* **2009**, *131*, 1251−1268. (c) Mebs, S.; Chilleck, M. A.; Grabowsky, S.; Braun, T. *Chem. Eur. J.* **2012**, *18*, 11647−11661.

36. Schleyer, P. v. R.; Jiao, H.; van Eikema Hommes, J. R.; Malkin, V. G.; Malkina, O. L. *J. Am. Chem. Soc.* **1997**, *119*, 12669−12670.

37. Vessally, E. *J. Struct. Chem.* **2008**, *49*, 979−985. For comparison reasons the NICS(0) value for C_4H_4NH given was recalculated at the B3LYP/cc-pVTZ level of theory.

38. (a) Kuta, J.; Patchkovskii, S.; Zgierski, M. Z.; Kozlowski, P. M. *J. Comput. Chem.* **2006**, *27*, 1429−1437. (b) Hocking, R. K.; Deeth, R. J.; Hambley, T. W. *Inorg. Chem.* **2007**, *46*, 8238−8244. (c) Minenkov, J.; Singstad, Å.; Occhipinti, G.; Jensen, V. R. *Dalton Trans.* **2012**, *41*, 5526−5541.

39. (a) Kasha, M. *J. Chem. Phys.* **1952**, *20*, 71−74. (b) McGlynn, S. P.; Sunseri, R.; Christodouleas, N. *J. Chem. Phys.* **1962**, *37*, 1818−1824.

40. Matano, Y.; Kinoshita, M.; Suzuki, H. *Bull. Chem. Soc. Jpn.* **1992**, *65*, 3504−3506.

41. He, G.; Kang, L.; Torres Delgado, W.; Shynkaruk, O.; Ferguson, M. J.; McDonald, R.; Rivard, E. *J. Am. Chem. Soc.* **2013**, *135*, 5360−5363.

42. Freeman, W. P.; Tilley, T. D.; Liable-Sands, L. M.; Rheingold, A. L. *J. Am. Chem. Soc.* **1996**, *118*, 10457−10468.

43. Negishi, E.-I.; Cederbaum, F. E.; Takahashi, T. *Tetrahedron Lett*. **1986**, *27*, 2829−2832.

44. (a) Becke, A. D. *J. Chem. Phys.* **1993**, *98*, 5648−5652. (b) Lee, C.; Yang, W.; Parr, R. G. *Phys. Rev. B* **1988**, *37*, 785−789.

45. (a) Dunning, T. H., Jr. *J. Chem. Phys.* **1989**, *90*, 1007−1023. (b) Woon, D. E.; Dunning, T. H., Jr. *J. Chem. Phys.* **1993**, *98*, 1358−1371.

46. (a) Peterson, K. A.; Puzzarini, C. *Theor. Chem. Acc.* **2005**, *114*, 283−296. (b) Peterson, K. A. *J. Chem. Phys.* **2003**, *119*, 11099−11112.

47. (a) Feller, D. J. *J. Comput. Chem.* **1996**, *17*, 1571−1586. (b) Schuchardt, K. L.; Didier, B. T.; Elsethagen, T.; Sun, L.; Gurumoorthi, V.; Chase, J.; Li, J.; Windus, T. L. *J. Chem. Inf. Model.* **2007**, *47*, 1045−1052.

48. Frisch, M. J.; Trucks, G. W.; Schlegel, H. B.; Scuseria, G. E.; Robb, M. A.; Cheeseman, J. R.; Scalmani, G.; Barone, V.; Petersson, G. A.; Nakatsuji, H.; Li, X.; Caricato, M.; Marenich, A. V.; Bloino, J.; Janesko, B. G.; Gomperts, R.; Mennucci, B.; Hratchian, H. P.; Ortiz, J. V.; Izmaylov, A. F.; Sonnenberg, J. L.; Williams-Young, D.; Ding, F.; Lipparini, F.; Egidi, F.; Goings, J.; Peng, B.; Petrone, A.; Henderson, T.; Ranasinghe, D.; Zakrzewski, V. G.; Gao, J.; Rega, N.; Zheng, G.; Liang, W.; Hada, M.; Ehara, M.; Toyota, K.; Fukuda, R.; Hasegawa, J.; Ishida, M.; Nakajima, T.; Honda, Y.; Kitao, O.; Nakai, H.; Vreven, T.; Throssell,

K.; Montgomery, J. A., Jr.; Peralta, J. E.; Ogliaro, F.; Bearpark, M. J.; Heyd, J. J.; Brothers, E. N.; Kudin, K. N.; Staroverov, V. N.; Keith, T. A.; Kobayashi, R.; Normand, J.; Raghavachari, K.; Rendell, A. P.; Burant, J. C.; Iyengar, S. S.; Tomasi, J.; Cossi, M.; Millam, J. M.; Klene, M.; Adamo, C.; Cammi, R.; Ochterski, J. W.; Martin, R. L.; Morokuma, K.; Farkas, O.; Foresman, J. B.; Fox, D. J. *Gaussian 16*, Revision A.03; Gaussian, Inc.: Wallingford, CT, 2016.

49. Biegler-König, F.; Schönbohm, J.; Bayles, D. *J. Comput. Chem.* **2001**, *22*, 545−559.

50. Kohout, M. *DGRID 4.6*; Springer, 2015.

51. Contreras-García, J.; Johnson, E.; Keinan, S.; Chaudret, R.; Piquemal, J.-P.; Beratan, D.; Yang, W. *J. Chem. Theory Comput.* **2011**, *7*, 625−632.

52. Hübschle, C. B.; Luger, P. *J. Appl. Crystallogr.* **2006**, *39*, 901−904.

53. Humphrey, W.; Dalke, A.; Schulten, K. *J. Mol. Graphics* **1996**, *14*, 33−38.

54. Dennington, R.; Keith, T. A.; Millam, J. M. *GaussView*, Version 5; Semichem Inc.: Shawnee Mission, KS, 2009.

55. Glendening, E. D.; Badenhoop, J. K.; Reed, A. E.; Carpenter, J. E.; Bohmann, J. A.; Morales, C. M.; Landis, C. R.; Weinhold, F. *NBO 6.0*; Theoretical Chemistry Institute, University of Wisconsin: Madison, WI, 2013.

56. (a) van Gisbergen, S. J. A.; Snijders, J. G.; Baerends, E. J. *Comput. Phys. Commun.* **1999**, *118*, 119−138. (b) Rosa, A.; Baerends, E. J.; van Gisbergen, S. J. A.; van Lenthe, E.; Groeneveld, J. A.; Snijders, J. G. *J. Am. Chem. Soc.* **1999**, *121*, 10356−10365. (c) Wang, F.; Ziegler, T. *J. Chem. Phys.* **2005**, *123*,

154102−154113. (d) Wang, F.; Ziegler, T.; van Lenthe, E.; van Gisbergen, S. J. A.; Baerends, E. J. *J. Chem. Phys.* **2005**, *122*, 204103−204114.

57. *ADF2017, SCM, Theoretical Chemistry*; Vrije Universiteit, Amsterdam, The Netherlands, http://www.scm.com (accessed Jan 8, 2018), Baerends, E. J.; Ziegler, T.; Atkins, A. J.; Autschbach, J.; Baseggio, O.; Bashford, D.; Bérces, A.; Bickelhaupt, F. M.; Bo, C.; Boerrigter, P. M.; Cavallo, L.; Daul, C.; Chong, D. P.; Chulhai, D. V.; Deng, L.; Dickson, R. M.; Dieterich, J. M.; Ellis, D. E.; van Faassen, M.; Fan, L.; Fischer, T. H.; Fonseca Guerra, C.; Franchini, M.; Ghysels, A.; Giammona, A.; van Gisbergen, S. J. A.; Goez, A.; Götz, A. W.; Groeneveld, J. A.; Gritsenko, O. V.; Grüning, M.; Gusarov, S.; Harris, F. E.; van den Hoek, P.; Hu, Z.; Jacob, C. R.; Jacobsen, H.; Jensen, L.; Joubert, L.; Kaminski, J. W.; van Kessel, G.; König, C.; Kootstra, F.; Kovalenko, A.; Krykunov, M. V.; van Lenthe, E.; McCormack, D. A.; Michalak, A.; Mitoraj, M.; Morton, S. M.; Neugebauer, J.; Nicu, V. P.; Noodleman, L.; Osinga, V. P.; Patchkovskii, S.; Pavanello, M.; Peeples, C. A.; Philipsen, P. H. T.; Post, D.; Pye, C. C.; Ramanantoanina, H.; Ramos, P.; Ravenek, W.; Rodríguez, J. I.; Ros, P.; Rüger, R.; Schipper, P. R. T.; Schlüns, D.; van Schoot, H.; Schreckenbach, G.; Seldenthuis, J. S.; Seth, M.; Snijders, J. G.; Solà, M.; Stener, M.; Swart, M.; Swerhone, D.; Tognetti, V.; te Velde, G.; Vernooijs, P.; Versluis, L.; Visscher, L.; Visser, O.; Wang, F.; Wesolowski, T. A.; van Wezenbeek, E. M.; Wiesenekker, G.; Wolff, S. K.; Woo, T. K.; Yakovlev, A. L.

58. (a) Campos, C. T.; Jorge, F. E. *Mol. Phys.* **2013**, *111*, 167−173. (b) van Lenthe, E.; Baerends, E. J. *J. Comput. Chem.* **2003**, *24*, 1142−1156.

59. (a) van Lenthe, E.; Baerends, E. J.; Snijders, J. G. *J. Chem. Phys.* **1993**, *99*, 4597−4610. (b) van Lenthe, E.; Baerends, E. J.; Snijders, J. G. *J. Chem. Phys.* **1994**, *101*, 9783−9792. (c) van Lenthe, E.; Ehlers, A. E.; Baerends, E. J. *J. Chem. Phys.* **1999**, *110*, 8943−8953.

60. Visscher, L.; van Lenthe, E. *Chem. Phys. Lett.* **1999**, *306*, 357−365.

61. Cheeseman, J. R.; Trucks, G. W.; Keith, T. A.; Frisch, M. J. *J. Chem. Phys.* **1996**, *104*, 5497−5509.

Chapter 3: Aerobic Solid-State Red Phosphorescence from Benzobismole Monomers and Patternable Self-Assembled Block Copolymers

3.1 Introduction

π-Conjugated materials containing p-block elements have been used as integral components of solar cells, transistors, OLEDs, and, more recently, as luminescent dyes for bioimaging.[1] To date, the vast majority of these materials contain lighter p-block elements (*e.g.* B, Si, S, and P).[2] Encouraging recent synthetic advances have enabled the incorporation of heavier main group elements into cyclic π-frameworks leading to novel properties[1b,3] such as room temperature phosphorescence (RTP).[4] Achieving efficient and stable phosphorescence in the condensed phase is a promising direction in the field of OLEDs,[5] wherein expensive, and potentially toxic, transition metal-containing complexes are generally used to promote the population of emissive excited triplet states via the "heavy element effect".[6] Despite an encouraging early report by Ohshita and coworkers[7] on the detection of dual fluorescence and phosphorescence from dithienylbismoles, heterocyclic bismuth compounds have been scarcely explored as potential emitters of low toxicity,[8] largely due to a lack of suitable synthetic methods for their preparation. Furthermore, phosphorescent polymers are of particular interest for optoelectronic devices due to the simplification of device fabrication via solution processing,[9] while block copolymers allow for the formation of higher-order (including metallized) structures of controllable composition.[10]

It is challenging to prepare red emitting phosphorescent materials that operate in the presence of O_2, a well-known quencher of phosphorescence. Red emission is highly sought for bioimaging applications, wherein interfering background fluorescence (of short wavelength blue and green light) can be readily filtered away from the red emission of the dye.[1c,1d,11] However, in general, one sees a dramatic reduction of quantum yield as longer wavelengths of light are emitted due to an increase in the non-radiative decay rate (Energy Gap Law).[12] To combat oxygen quenching, one can slow down O_2 diffusion by promoting molecular aggregation,[4,13] or by-pass non-radiative processes through establishing photoinduced metal-metal bonding in the solid state.[14] However, a general drawback is the need for tailored intermolecular interactions (such as Br···H bonding)[15] which cannot always be designed *a priori*. In this chapter the modular synthesis of bismuth-containing orange and red phosphorescent molecules and polymers with negligible oxygen quenching in the solid state is reported (Figure 3.1). It is also shown that block copolymers of controllable bismuth content can be made, and that assembly of these copolymers into spherical micelles with bismuth-rich (metallized) cores is possible. The synthetic tools outlined provide a general route to a wide swath of new long-lifetime emitters for possible bioimaging and OLED applications, while the ability to organize bismuth into localized arrays via block copolymer assembly opens the door for the production of Bi nanodot seeds for patterned semi-conductor nanowire growth.[16]

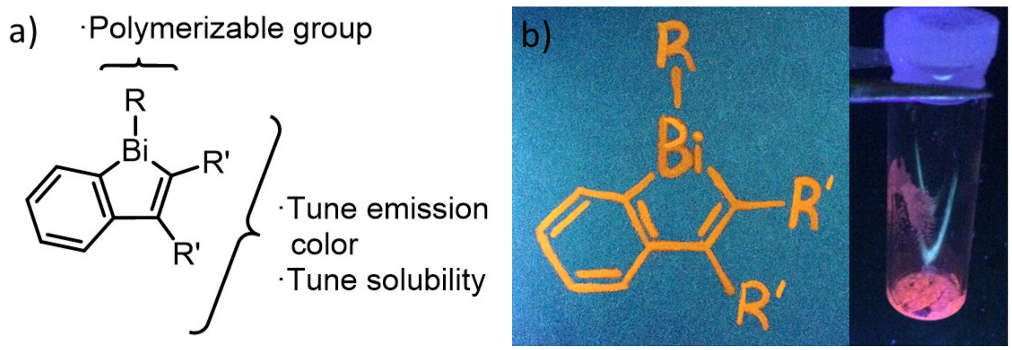

Figure 3.1. (a) Generic benzobismole structure showing the sites of easy modification due to the modular synthetic procedure introduced in this chapter; (b) perfluorinated benzobismole (R = *p*-norbornenephenyl; R′ = C_6F_5) **6** used as an ink to draw on filter paper and crystals of the phenylated benzobismole **3** (R and R′ = Ph; right), both illuminated with 365 nm light in air at room temperature.

3.2 Results and Discussion

3.2.1 Synthesis of Benzobismole Monomers and Parent Molecules

Following a modified Fagan-Nugent protocol,[17] the arylated benzozirconacycles **1** and **2**, were combined with the bismuth(III) dihalides $ArBiCl_2$ (Ar = Ph or Ar^{ROMP}; Scheme 3.1) leading to the formation of the desired benzobismoles **3**–**6** as well as Cp_2ZrCl_2 as a byproduct. The structures of the precursor benzozirconacycles **1** and **2** are presented in Figure 3.2.

The $ArBiCl_2$ reactants were generated *in situ* by the ligand scrambling of triarylbismuthine and 2 equivalents of $BiCl_3$ (Scheme 3.1).[7b] To facilitate Zr/Bi exchange, 10 % CuCl was added, as reported by Takahashi and coworkers to form stannoles, and as used for the synthesis of luminescent bismoles (as was discussed in the previous chapter).[7b,18] Benzobismoles **3**–**6** have been observed to exhibit air and moisture stability when stored at ambient conditions.

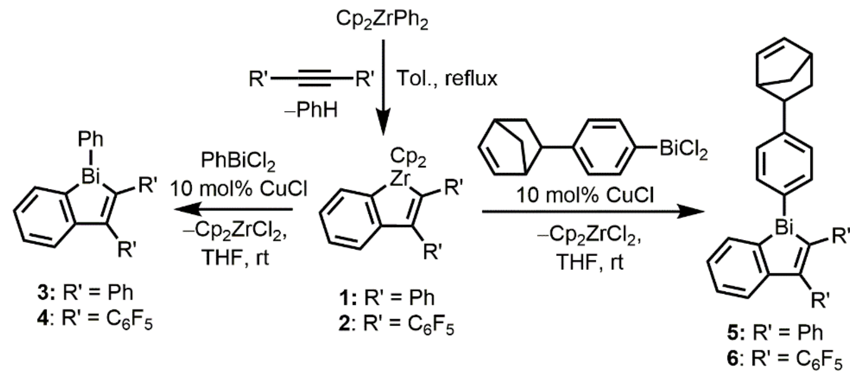

Scheme 3.1. Synthesis of benzobismoles **3**–**6**.

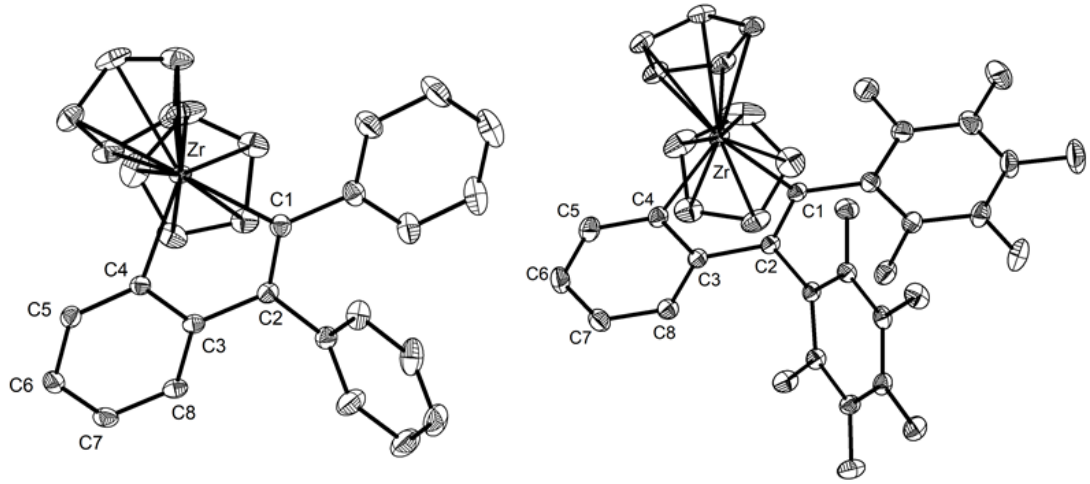

Figure 3.2. Molecular structures of **1** (left) and **2** (right) with ORTEPs at a 30 % probability level. Selected bond lengths (Å) and angles (°): **1**: Zr–C1 2.269(3), Zr–C4 2.260(3), C1–C2 1.358(4), C2–C3 1.489(4), C3–C4 1.419(4); C1–Zr–C4 77.34(10), Zr–C1–C2 113.0(2), Zr–C4–C3 111.49(19). **2**: Zr–C1 2.304(2), Zr–C4 2.266(3), C1–C2 1.352(3), C2–C3 1.492(3), C3–C4 1.421(3); C1–Zr–C4 77.18(9), Zr–C1–C2 111.68(16), Zr–C4–C3 112.33(17). Hydrogen atoms were deleted for clarity.

To provide insight into the molecular structure and solid-state packing arrangement of these benzobismoles, single crystals of **3** and **4** suitable for analysis by X-ray diffraction were obtained by recrystallizing the compounds from CH_2Cl_2

and methanol. The molecular structures of the perphenylated benzobismole **3** and its fluorinated counterpart **4** are depicted in Figure 3.3. In each structure the peripheral aryl rings fan out from the central bismole ring in a propeller-like fashion, reminiscent of the pentaphenyl bismole $PhBiC_4Ph_4$ introduced in the previous chapter,[7b] and prevent close packing of the central bismole rings [closest Bi···Bi contacts > 5.0 Å]. However, each of the canted aryl rings forms close interactions with the rings of neighboring molecules that presumably limit intramolecular rotations in the crystalline state. The sum of the bond angles at the Bi centers [270.3(2)° in **3**; 264.4(2)° in **4**] indicate high s-character within each respective lone pair, and partially explains the air-stability of these compounds.[7b] A racemic sample of **3** could be separated into its constituent isomers by chiral HPLC, while no signs of racemization in 10 % 2-propanol in hexanes was noted for either purified enantiomer (Figure 3.4).

The polymerizable benzobismoles **5** and **6** (Scheme 3.1) each contain two chiral centers and, while chiral HPLC was not performed on these molecules, it can be assumed that pure samples of **5** and **6** are made up of a racemic mixture like compound **3**. Unfortunately, single crystals of either **5** or **6** that were suitable for analysis by X-ray crystallography remained elusive. Interestingly, the $^{13}C\{^1H\}$ NMR spectra for **5** and **6** show inequivalent signals for select carbon nuclei of the *endo*- versus *exo*-norbornyl enantiomers (Figure 3.15 and 3.16).

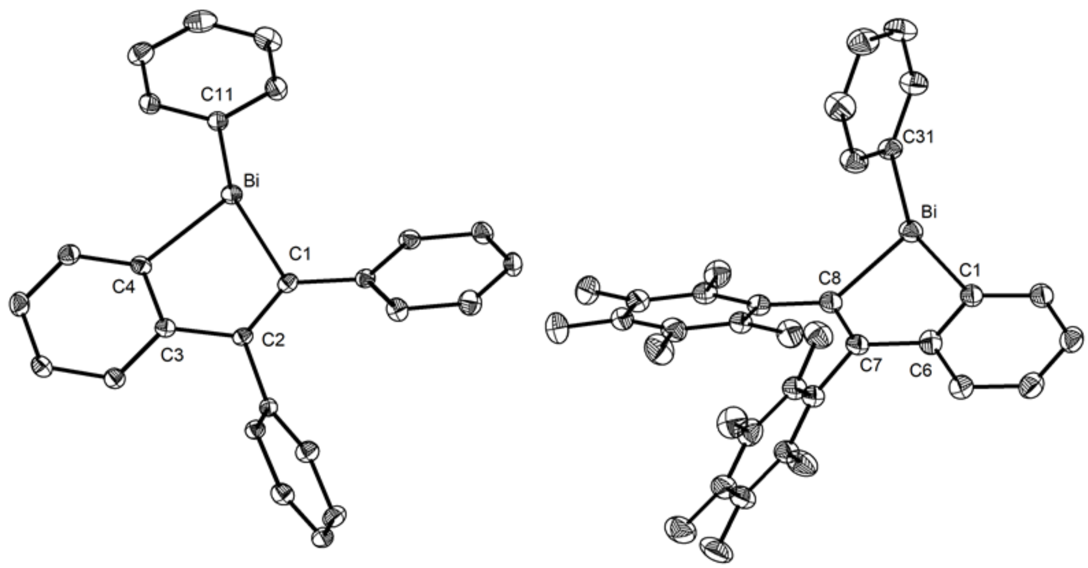

Figure 3.3. Molecular structures of **3** (left) and **4** (right) with ORTEPs at a 30 % probability level. Selected bond lengths (Å) and angles (°): **3**: Bi–C1 2.256(3), Bi–C4 2.221(3), Bi–C11 2.260(4), C2–C3 1.482(5); C1–Bi–C4 78.6(2), C11–Bi–C1 96.8(2), C11–Bi–C4 95.0(2). **4**: Bi–C1 2.238(3), Bi–C8 2.265(3), Bi–C31 2.272(3), C6–C7 1.476(4); C1–Bi–C8 77.7(2), C31–Bi–C1 93.6(2), C31–Bi–C8 93.1(2).

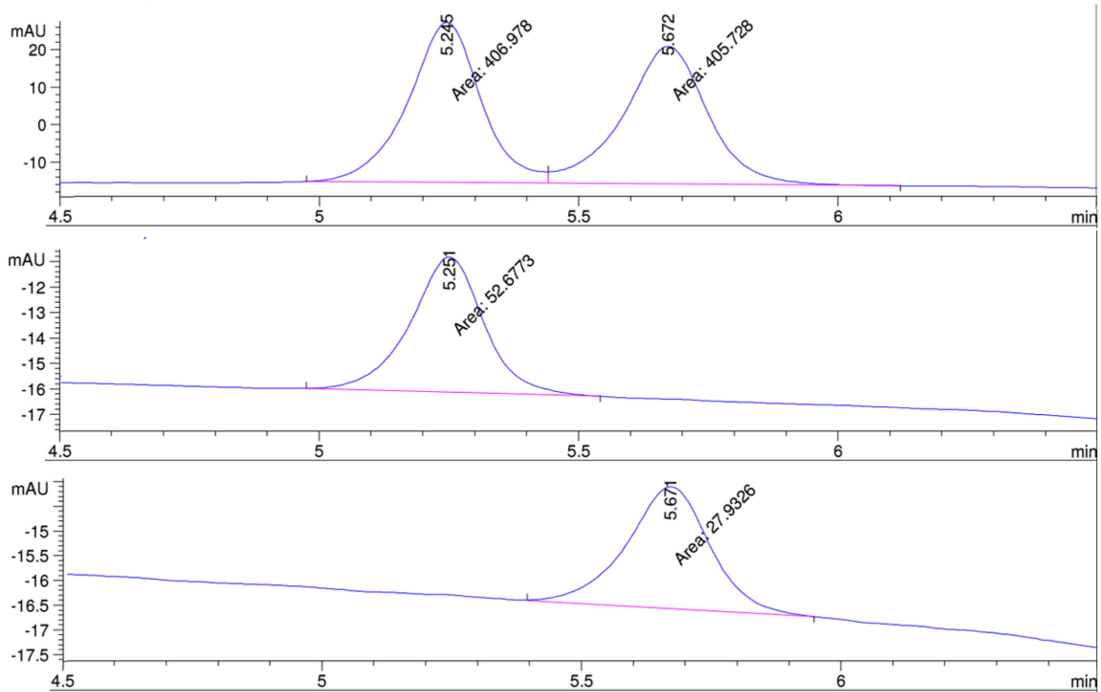

Figure 3.4. Chiral HPLC separation of the two enantiomers of **3** in 0.5 % 2-propanol in hexanes. The samples were injected from a solution of 10 % 2-propanol in hexanes. Trace 1 shows the separation of the racemic mixture into two peaks of equal area. Each fraction was collected manually and re-injected showing just one enantiomer with no racemization in solution (traces 2 and 3).

3.2.2 Photoluminescent Measurements and Crystallization Induced Emission of Benzobismoles 3–6

The perphenylated benzobismole **3** displayed red emission in the crystalline state in air [λ_{ex} = 380 nm, λ_{em} = 610 nm; Figure 3.5a], and the introduction of electron-withdrawing C_6F_5 groups in **4** shifted the emission color to orange-red [λ_{ex} = 336 nm, λ_{em} = 596 nm; Figures 3.1 and 3.5b]. Such large Stokes shifts are generally indicative of phosphorescence. Moreover, in THF/water mixtures (40:60 vol%) these Bi heterocycles show aggregation induced emission (AIE) (Figure 3.6a).[19] Time-dependent luminescence measurements on drop-cast films of **3** and **4** (from hexanes) yielded similar emission lifetimes (τ) in the narrow range of 7.1 to 7.5 μs, in line with phosphorescence.[4]

The installation of the ring-opening metathesis polymerizable norbornene group was shown to have little influence on the luminescence of the benzobismoles, as the solid-state emission properties of **5** and **6** under ambient conditions (λ_{ex} = 377 nm, λ_{em} = 614 nm, τ = 6.6 μs, and λ_{ex} = 354 nm, λ_{em} = 586 nm, τ = 7.1 μs, respectively) closely matched that of their respective parent benzobismoles (Figure 3.5c and 3.5d).

The absolute quantum yields (Φ) of phenylated benzobismoles **3** and **5** in the solid state (prepared by drop-casting from hexanes suspensions) [**3**: 0.8 % and **5**: 0.7 %] were slightly lower than in the respective fluorinated benzobismoles **4** (2.5 %) and **6** (1.6 %). The possible increased quantum yield in **4** and **6** may arise from added restriction in molecular motion imposed by the perfluorinated aryl groups. In accordance with this postulate, the $^{19}F\{^1H\}$ NMR spectra of **4** and **6** indicate that one of the C_6F_5 rings exhibits restricted rotation in solution (see Figures 3.16 and 3.17). As phosphorescence is often quenched by the presence of oxygen, photoluminescence measurements were also taken for solid-state samples in the absence of oxygen; there was no significant increase in quantum yield upon measurement under an argon atmosphere (Figure 3.25). It was hypothesized that the observed resistance to oxygen quenching is due to limited oxygen diffusion through the aggregates.

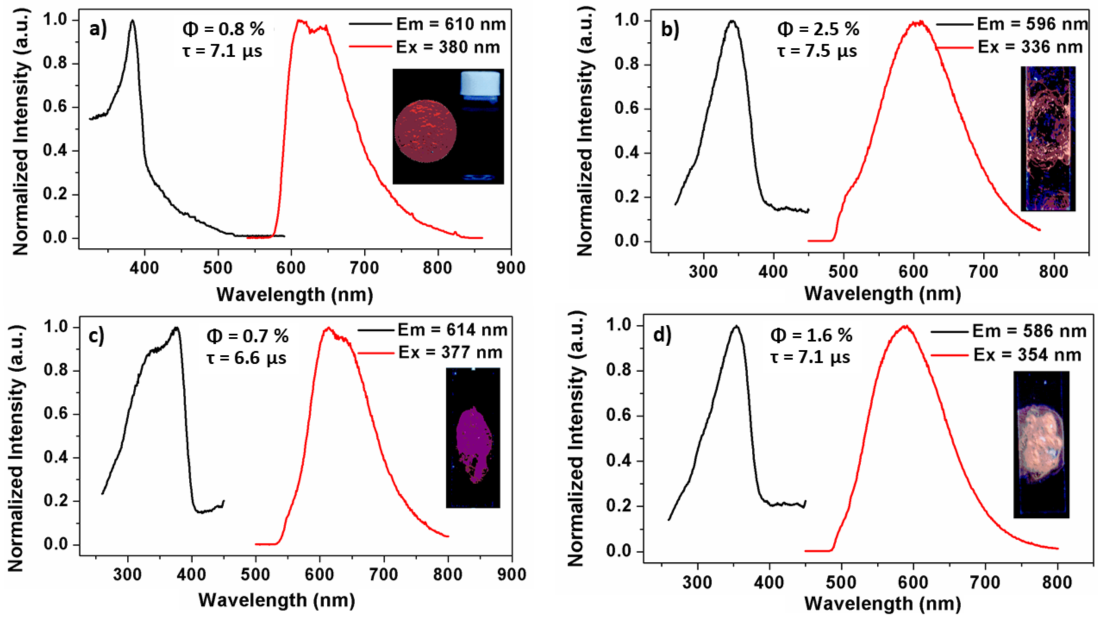

Figure 3.5. Solid state emission and excitation spectra of films of benzobismoles (a) **3**, (b) **4**, (c) **5**, and (d) **6**; all data was recorded in air at room temperature and films were prepared by drop-casting from hexanes.

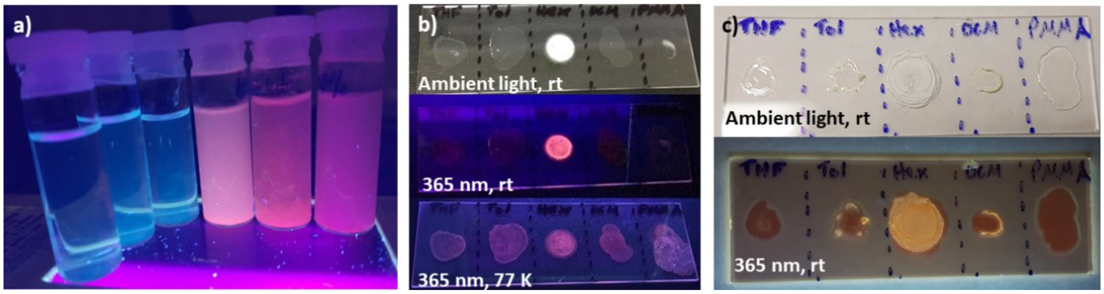

Figure 3.6. (a) Compound **3** at a concentration of 3.0 mM in varying ratios of water/THF (percentage of water in the solvent mixture for each vial is from left to right: 0 %, 20 %, 40 %, 60 %, 80 %, and 90 %). (b) Films of compound **3** drop cast from *ca*. 5 mg/mL THF, toluene, hexanes, CH_2Cl_2, and benzobismole doped PMMA (*ca*. 20 wt% bismole) drop-cast from CH_2Cl_2 at room temperature and 77 K in ambient light and under 365 nm excitation. Films were created by drop-casting three layers of *ca*. 30 µL of solution allowing solvent to evaporate between layers. (c) Films of compound **4** drop-cast from *ca*. 5 mg/mL THF, toluene, hexanes, CH_2Cl_2, and benzobismole-doped PMMA (*ca*. 20 wt% benzobismole) drop-cast from CH_2Cl_2 at room temperature in ambient light and under 365 nm excitation. Films were created by drop casting three layers of *ca*. 30 µL of solution allowing solvent to evaporate between layers.

The phosphorescence of **3** and **4** was highly dependent on the morphology of the solids, an effect that has been previously noted for tellurophenes.[20] When the benzobismoles **3** and **4** were drop-cast from THF, CH_2Cl_2 or toluene, transparent films were formed which did not show discernable emission [Figures 3.6 and 3.7a (inset, right)]. However, the opaque films of **3** and **4**, prepared from fine suspensions in hexanes, yielded significantly brighter phosphorescence [Figures 3.6 and 3.7a (inset; left)]. Accordingly, a drop-cast film of **3** from a hexanes suspension yielded a powder XRD pattern that showed high crystallinity, and matched that predicted from the single-crystal XRD data (Figure 3.7). Alternatively, the non-emissive film made from drop-casting a solution of **3** in CH_2Cl_2 gave a powder pattern indicative of amorphous packing. These data show that **3** and **4** exhibit not only AIE, but more specifically, crystallization induced emission (CIE) in which there is a strong correlation between the crystallinity and the intensity of emission for the materials.[21] However, it should be noted that unlike for other materials that exhibit crystallization induced emission,[13c,22] no mechanochromic luminescence properties were observed; that is, there was no change in luminescence upon grinding or crushing the solid materials. Additionally, there was no change in the luminescence of the amorphous films of **3** and **4** when heat annealing was performed (at either 120 °C or 160 °C).

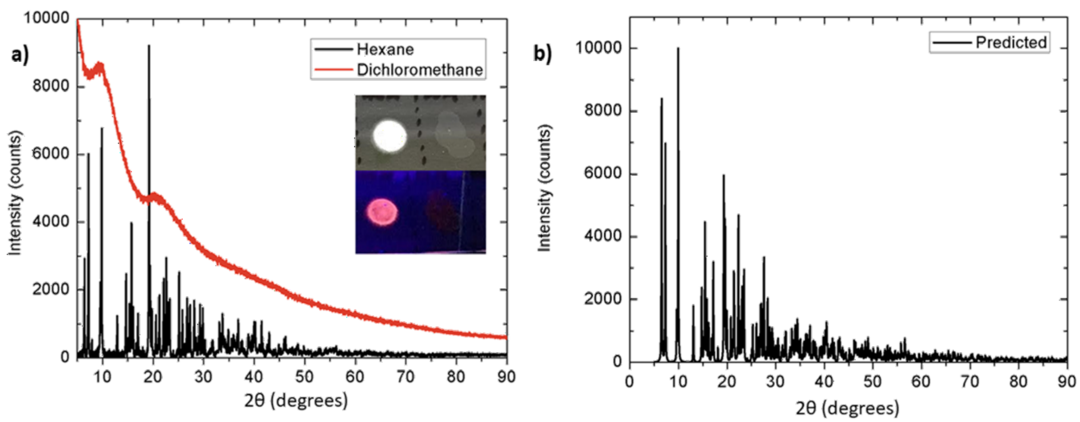

Figure 3.7. (a) Powder XRD patterns of films of **3** drop-cast from CH_2Cl_2 and hexanes; inset: drop-cast films from hexanes (left) and CH_2Cl_2 (right) under ambient light (top) and 365 nm irradiation (bottom) (b) Predicted powder XRD pattern for **3** using Mercury 3.10.1 and the .cif file from the single crystal X-ray diffraction data for **3**.

3.2.3 TD-DFT Computational Study of 3 and 4

Time-dependent density functional theory (TD-DFT) computations were carried out for the Ph- and C_6F_5-substituted benzobismoles **3** and **4** using the B3LYP,[23] (with and without the inclusion of a simulated THF environment) CAM-B3LYP,[24] and M06-2X[25] functionals along with the cc-pVTZ(-PP) basis set with the purpose of evaluating the suibability of each functional for its application towards the benzobismole class. As Bi is strongly affected by relativistic effects, the TZ2P basis set including scalar relativistic (ZORA) and spin-orbit relativistic (SO) effects were applied to account for the likely internal heavy atom effect in benzobismoles **3** and **4**.

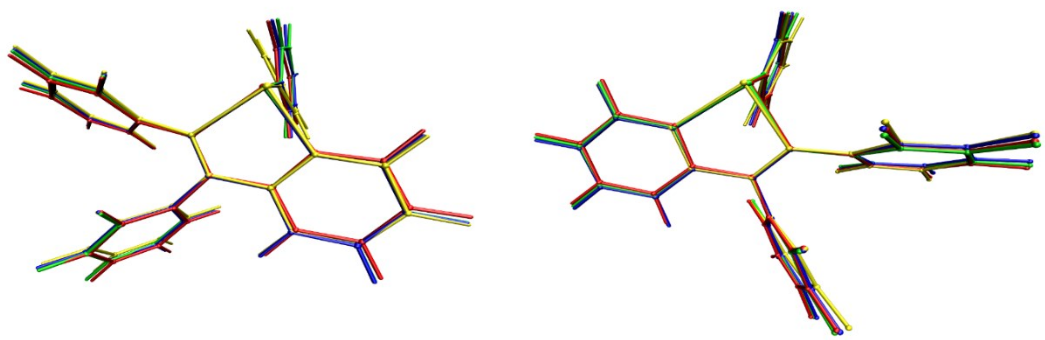

Figure 3.8. Superimposed optimized geometries of benzobismole **3** (left) and **4** (right). The color code is defined as follows: B3LYP/cc-pVTZ(-PP): blue, CAM-B3LYP/cc-pVTZ(-PP): red, B3LYP/cc-pVTZ(-PP) incl. THF: green, B3LYP/TZ2P: yellow.

Geometry optimizations of benzobismoles **3** and **4** at the (CAM-)B3LYP/cc-pVTZ(-PP) and B3LYP/TZ2P level of theory led to very similar geometries, as shown in Figure 3.8, and the B3LYP functional with the inclusion of THF was found to provide the closest agreement of predicted and experimentally obtained UV-vis absorption maxima of benzobismoles **3** and **4** (Figure 3.9). The M06-2X and CAM-B3LYP functionals gave excited singlet states that were systematically shifted to higher energies (*ca*. 0.5–0.6 eV) than those computed by B3LYP. M06-2X was also found to yield triplet excited state energies that were systematically higher when compared to B3LYP (Table 3.2 and 3.3).

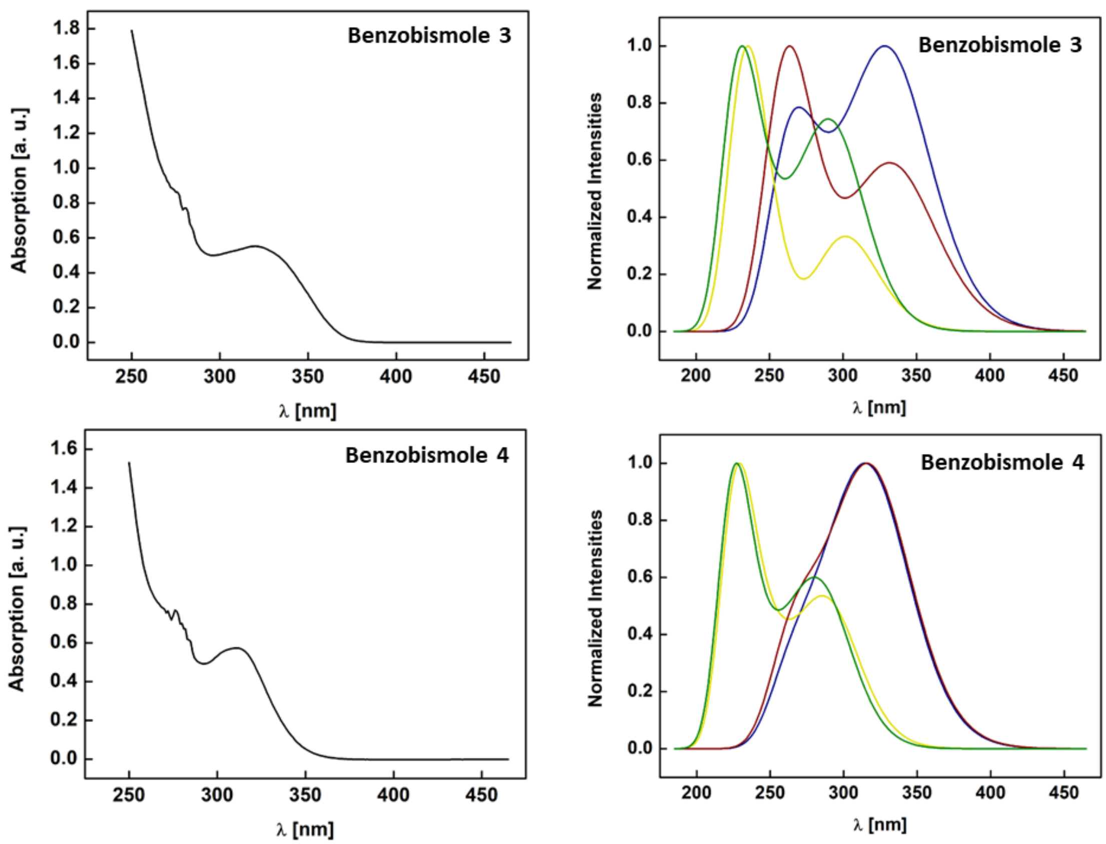

Figure 3.9. Experimental (left) and calculated (right, using the cc-pVTZ(-PP) basis set) UV-vis absorption spectra of benzobismoles **3** and **4** with the inclusion of the six transition states with the highest oscillator strength. The color code is defined as follows: B3LYP: blue, CAM-B3LYP: green, B3LYP incl. THF solvent: red, M06-2X: yellow.

For both benzobismoles **3** and **4**, all three functionals tested (B3LYP, CAM-B3LYP, and M06-2X) predicted the S_0–S_1 transition as having the highest oscillator strength and this transition could be assigned to the HOMO–LUMO transition which is mainly *π*-*π** in nature with the Bi atom contributing to the LUMO. For benzobismole **3** the S_0–S_3 transition was computed to have the next highest oscillator strength (HOMO–1 to LUMO by B3LYP and M06-2X, and HOMO to LUMO+1 for CAM-B3LYP). The HOMO–1 of **3** also has significant electron density around the Bi atom, suggesting that the Bi contributes strongly to the HOMO–1 to LUMO transition as well as the HOMO to LUMO (Figure 3.10).

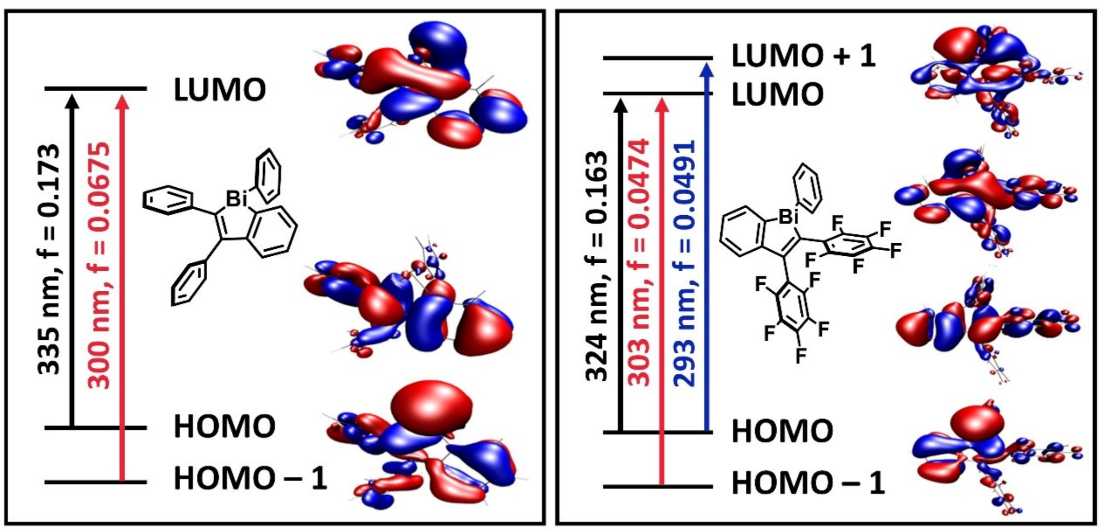

Figure 3.10. TD-DFT [B3LYP/cc-pVTZ(-PP)] computed main transitions including excitation wavelengths and oscillator strengths (f) to low-lying singlet states for **3** (left) and **4** (right) and the associated molecular orbitals; iso-surface values of +0.02/–0.02 (blue/red).

For benzobismole **4** the S_0–S_2 and S_0–S_3 transitions were computed to have the next highest oscillator strengths, after S_0–S_1. The S_0–S_2 transition was computed to be from the HOMO–1 to LUMO, and, as for benzobismole **3**, the HOMO–1 and LUMO for compound **4** show appreciable contribution from the Bi atom (Figure 3.10). These findings support the postulate from Chapter 2 that for bismole systems, contribution from the Bi atom in in the excitation process is necessary to achieve emission by phosphorescence, which is in line with previous studies by the Rivard group with tellurophenes.[26]

All investigated methods show the existence of energetically close low-lying S_n and T_n states, thus the probability for intersystem crossing (ISC) is high. As Bi is strongly affected by relativistic effects, increased spin-orbit (SO) coupling leads to significant mixing of singlet and triplet states, further enhancing the probability of intersystem crossing (ISC). The B3LYP, CAM-B3LYP, and M06-2X functionals (with inclusion of ZORA and SOC relativistic methods) confirm this assumption as the excitation with the highest oscillator strength in compound **3** was determined to involve the transition to an excited state consisting of 34.8–61.3 % singlet and 36.0–65.1 % triplet character depending on the functional (Tables 3.5–3.10). Similar enhanced mixing is observed for compound **4** with singlet and triplet character varying between 47.2–77.5 % and 22.3–52.6 %, respectively (Tables 3.5–3.10).

The phosphorescence energy is defined as the difference in energies between the S_0 ground state and the T_1 triplet state (E_{adia}) or the zero-point energy corrected difference (E_{0-0}). The experimentally observed phosphorescence energy of compound **3**, 2.03 eV, was well predicted by both B3LYP (E_{adia} = 2.05 eV and E_{0-0} = 1.98 eV) and CAM-B3LYP (E_{adia} = 2.13 eV and E_{0-0} = 2.04 eV). Similarly, the observed phosphorescence energy of **4**, 2.08 eV, was closely computed by B3LYP (E_{adia} = 2.12 eV and $E_{0\text{–}0}$ = 2.05 eV) and CAM-B3LYP (E_{adia} = 2.18 eV, $E_{0\text{–}0}$ = 2.09 eV).

(CAM)-B3LYP and M06-2X TD-DFT computations of benzobismoles **3** and **4** describe the involvement of the bismuth center in excitation processes, a requirement which seems to be necessary in order to observe phosphorescence. Furthermore, CAM-B3LYP and B3LYP were both able to predict phosphorescence energies that closely matched the experimentally observed emission. It should be noted that the use of the traditional B3LYP functional provided an adequate description of the low-lying electronic transitions and nature of the excited states and is therefore considered suitable for use in this class of bismoles.

3.2.4 Synthesis and Photoluminescence of ROMP-Based Benzobismole Polymers

Ring-opening metathesis polymerization (ROMP) of the norbornene-substituted benzobismoles **5** and **6** with 1 mol% of Grubbs' 2nd-generation catalyst[27] successfully afforded the air- and moisture-stable homopolymers **P1** and **P2** (Scheme 3.2). The polymerization reactions were found to be rapid with complete monomer conversion in < 6 minutes. Though weaker than for monomers **5** and **6**, polymers **P1** and **P2** display observable red luminescence that is bathochromically-shifted by *ca.* 60 nm from their respective monomers (Figures 3.11 and 3.12). It is hypothesized that an increase in the free volume about the benzobismole units in the polymeric materials allows for increased vibrational and rotational motions (which decrease emission intensity) as well as possible geometric stabilization of singlet and triplet excited states, yielding the bathochromic shift in emission.

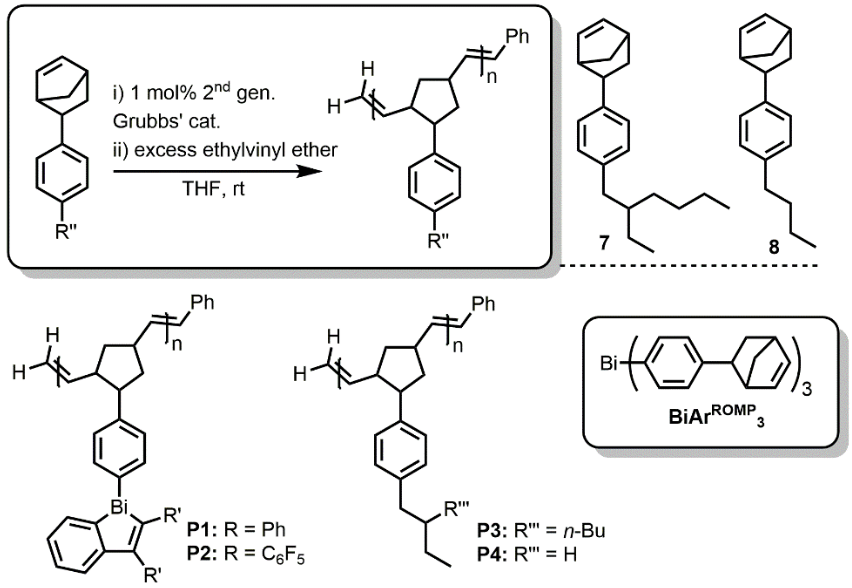

Scheme 3.2. Synthesis of homopolymers **P1**–**P4**, and the cross-linking agent **BiAr^{ROMP}$_3$**.

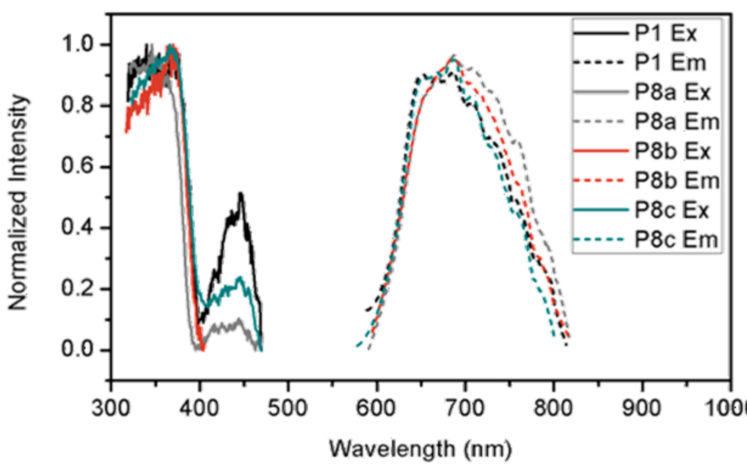

Figure 3.11. Excitation and emission plots of polymer **P1** and **P8** films. The polymer films were made by drop-casting from hexanes and emission was measured in air.

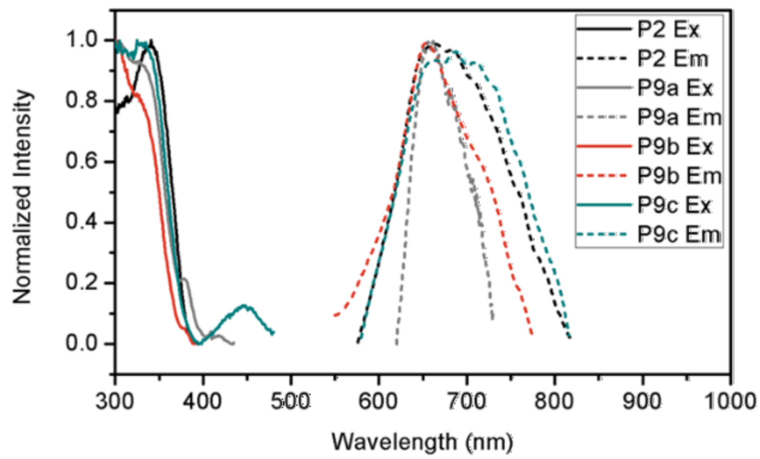

Figure 3.12. Excitation and emission plots of polymer **P2** and **P9** films. The polymer films were made by drop-casting from hexanes and emission was measured in air.

^{1}H and ^{19}F{^{1}H} NMR data for **P1** and **P2** gave expectedly broad resonances (Figures 3.19–3.21), while gel permeation chromatography (GPC) in THF afforded very high molecular weights (M_n = 2.1 MDa and PDI = 1.5 for **P1**; M_n = *ca.* 600 kDa and PDI = 1.6 for **P2**). However, characterization of these polymers was made more difficult by their limited solubility. Powder XRD analysis of **P1** revealed amorphous character as the powder pattern observed showed no significant reflections distinguishable from the glass substrate used for analysis. Heat annealing films of **P1** (up to 120 °C) did not help to increase the crystallinity of the samples according to PXRD (Figure 3.19) and produced no observable change in the luminescence properties of the films. Thermogravimetric analysis (TGA) of **P1** and **P2** indicated thermal stability up to *ca.* 275 °C and differential scanning calorimetry (DSC) indicated no observable T_g or T_m values in the region scanned (–150 °C to 200 °C).

To improve the solubility of the phosphorescent polybenzobismoles, the new alkylated arylnorbornene monomers **7** and **8** (Scheme 3.2) were prepared. The corresponding bismuth-free homopolymers **P3** (M_n = 52 kDa) and **P4** (M_n = 239 kDa) were found to have the desired increased solubility relative to **P1** and **P2** while maintaining thermal stability up to 300 °C (according to TGA). The alkylated copolymer **P5** (M_n = 158 kDa) was synthesized and observed to have a T_g of 30.1 °C. Interestingly, drop-cast films of **P5** displayed a turn-on of blue fluorescence upon heat annealing at 120 °C for 10 minutes (Figure 3.13). The mechanism of this turn-on of emission remains unknown but is assumed to be a result of a heat-induced morphology change; however, PXRD analysis on drop-cast films of **P5** did not show a change in crystallinity upon heating to 120 °C (Figure 3.23). Similar blue fluorescence was observed upon heat annealing films of **P3** and **P4** using the same procedure.

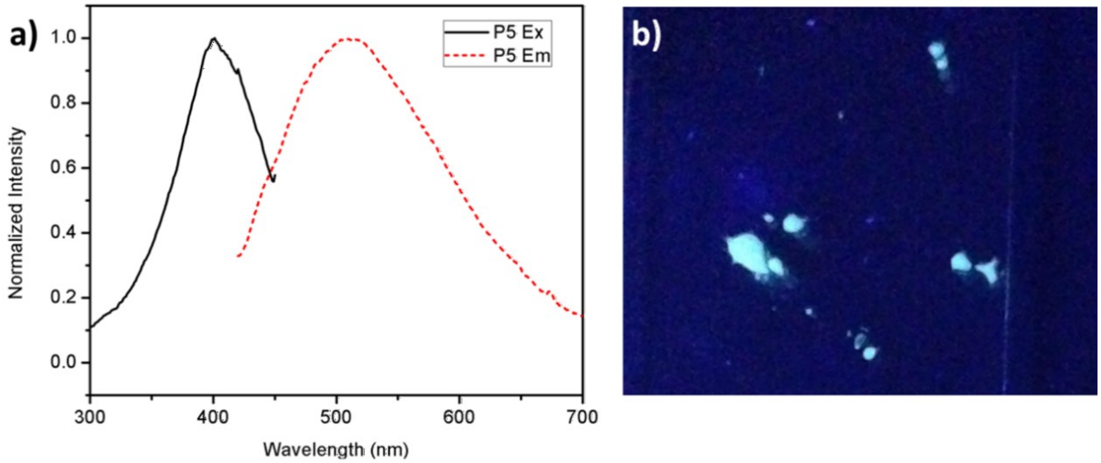

Figure 3.13. (a) Excitation and emission plots of a polymer **P5** film after heat annealing at 120 °C for 10 minutes. (b) Image of **P5** after placing solid pieces of the polymer on a glass slide, heat annealing the sample at 120 °C for 10 minutes and illuminating with 365 nm light.

Random copolymers derived from benzobismole (**5** and **6**) and alkylarene (**7** and **8**) units in differing ratios were also synthesized (**P6–P9,** Scheme 3.3), with a maximum benzobismole content of 38 mol% (as determined by ^{1}H NMR spectroscopy). Each copolymer was soluble in THF and $CHCl_3$ with M_n values all exceeding 150 kDa. TGA analysis indicates thermal stability up to 250 °C (Figures 3.26 and 3.27) for each copolymer. Red luminescence (λ_{em} = 660 nm) was maintained within the mixed benzobismole/alkylarene copolymers (Figures 3.11 and 3.12); however, as in the benzobismole homopolymers **P1** and **P2**, the emission was less intense than for the monomeric benzobismoles **5** and **6**, thus precluding the determination of reliable absolute quantum yields and emission lifetime data.

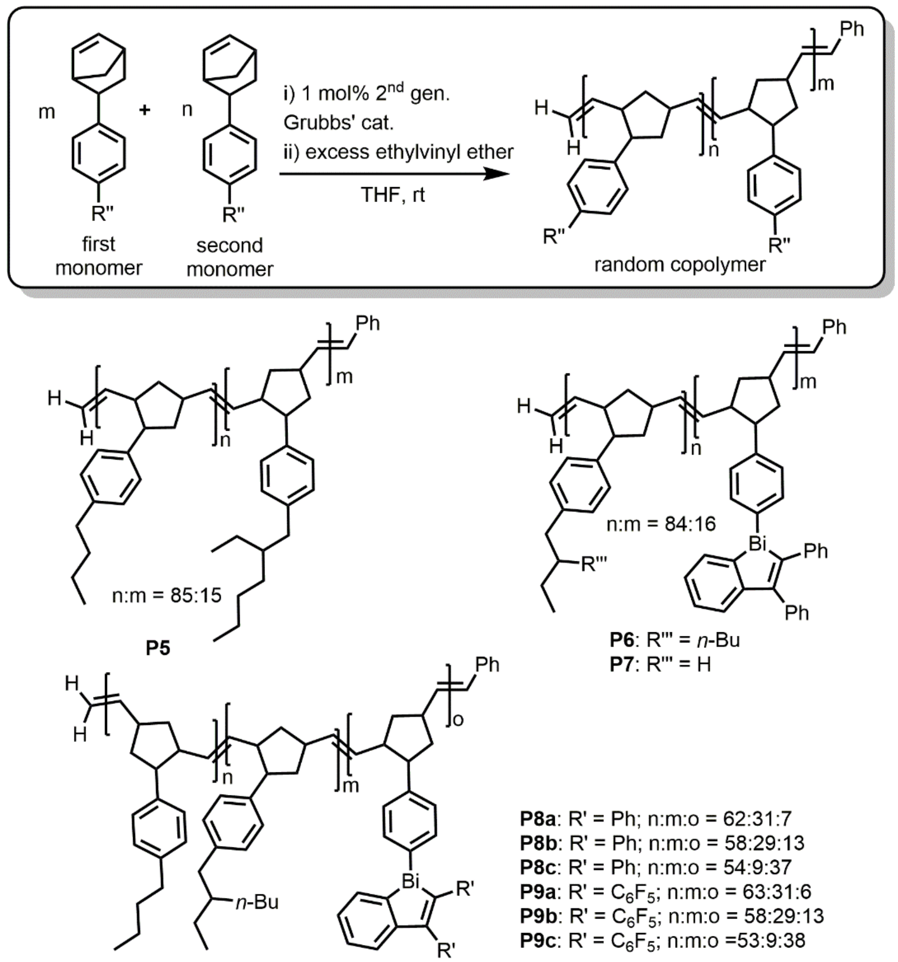

Scheme 3.3. Synthesis of random copolymers **P5**–**P9**.

In order to increase the rigidity of the benzobismole polymer matrix, with the goal of enhancing the phosphorescence intensity, two cross-linked polymers were synthesized. Benzobismole **5** was cross-linked with the trifunctional bismuthine **Bi(Ar$^{\mathbf{ROMP}}$)$_3$** (Scheme 3.4) using 1 mol% Grubbs' 2nd Generation catalyst in THF, with ratios that varied from 25 mol% crosslinker (**P10**) to 80 mol% (**P11**). Both **P10** and **P11** were completely insoluble in common organic solvents, indicating successful cross-linking. Despite the possible decrease in intramolecular motion in

P10 and **P11**, similarly weak red emission was noted as in the non-crosslinked polymers and enhanced emission was observed upon cooling the sample to 77 K. These findings suggest that even within the cross-linked polymer network, the amorphous packing (as indicated by PXRD analysis – Figure 3.24) of the benzobismole side groups allows enough room for internal molecular motions[28] to contribute to increased rates of non-radiative decay.

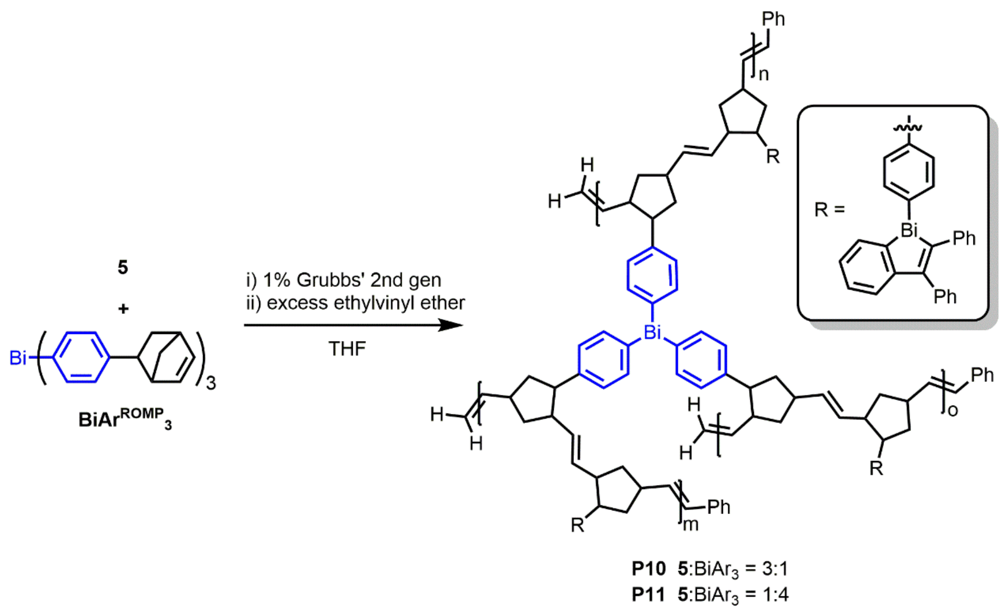

Scheme 3.4. Synthesis of crosslinked polymers **P10** and **P11** using crosslinking agent **BiAr^{ROMP}$_3$**.

3.2.5 Self-Assembly of a Benzobismole-Containing Phosphorescent Block Copolymer

With the goal of obtaining well-defined block copolymers that self-assemble into ordered micelles,[10] living ROMP was instigated using Grubbs' 3rd Generation catalyst. As shown in Scheme 3.5, benzobismole **5** and the arylated norbornene monomer **8** were sequentially copolymerized to yield the THF-soluble block-copolymer **P12**. This block copolymer displayed red emission at λ_{em} = 684 nm (Figure 3.14) in the solid state, while maintaining air and moisture stability and thermal stability up to 250 °C (as indicated by TGA).

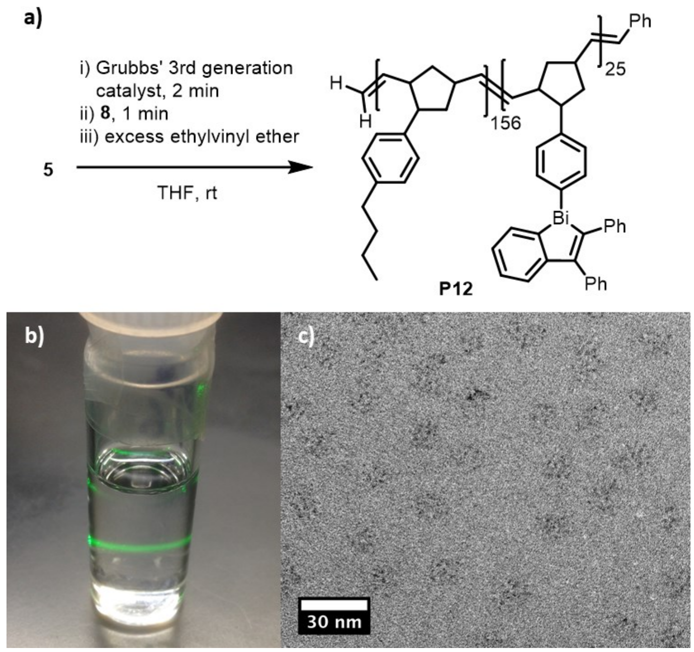

Scheme 3.5. (a) Synthesis of block copolymer **P12**. (b) Tyndall scattering observed upon shining a laser pointer through a 1 mg/mL solution of **P12** in 5 % THF in hexanes. (c) TEM image of **P12** deposited from a 1 mg/mL solution in 5 % THF in hexanes onto a glassy carbon grid.

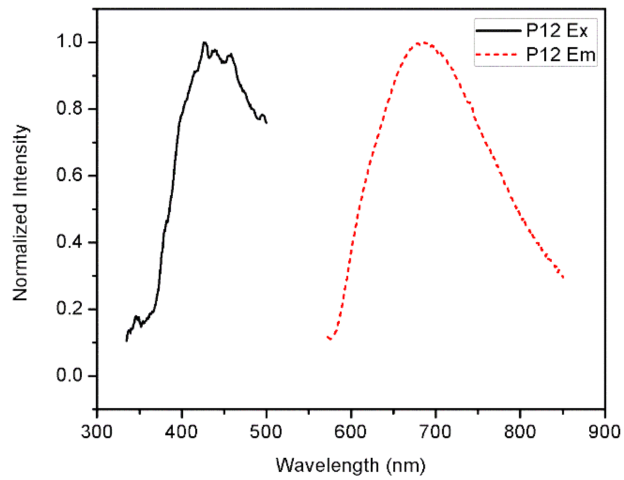

Figure 3.14. Excitation and emission plots of polymer **P12** under ambient conditions in the solid state.

A combination of GPC and ^{1}H NMR analysis indicated a benzobismole/arylalkyl block ratio of *ca*. 1:6 (M_n = 51 kDa) in **P12**. As the alkylarene block has significantly higher solubility in hexanes than the benzobismole segment, a combination of hexanes and THF was used to promote the formation of spherical micelles containing benzobismole blocks cores surrounded by an arylalkyl corona. **P12** was incubated in 5 % THF in hexanes at a concentration of 1 mg/mL at 50 °C for one hour and then allowed to cool to room temperature, after which samples were taken for analysis by TEM and dynamic light scattering (DLS). DLS indicated the presence of a species with an average diameter of 35 nm while TEM shows discrete spherical regions of high contrast Bi in the film state (Scheme 3.5c). Future work will involve pyrolytic conversion of these organized films to possibly yield patterned Bi nanodots[16] or bismuth films with potential anti-bacterial[29] and topological insulating properties.[30]

3.3 Conclusion

In summary, a series of phosphorescent bismuth-containing polymers and block copolymers have been synthesized. A general synthetic strategy to rapidly generate high molecular weight organic and bismuth-containing polymers with red phosphorescence, good solubility, and ordered self-assembly was introduced. Future work in this area will involve the preparation of new main group element (E)-based block copolymers for the controlled self-assembly of strongly emissive structures (by increasing molecular rigidity and via related Zr/E exchange chemistry), along with optimization of the patterning of nanodimensional Bi for semiconductor nanowire growth.[16]

3.4 Experimental Procedure

3.4.1 General Considerations

All reactions were performed using standard Schlenk and glovebox (MBraun) techniques under a nitrogen atmosphere. Solvents were all dried and degassed using a Grubbs-type solvent purification system manufactured by Innovative Technology, Inc., and stored under an atmosphere of nitrogen prior to use. Dimethylformamide was dried over 4 Å molecular sieves for 16 hours prior to distillation under reduced pressure. Bismuth trichloride was purchased from TCI America, iodopentafluorobenzene from Oakwood Chemicals, tetrakis(triphenylphosphine)palladium(0) from Matrix Scientific, and all other chemicals were purchased from Sigma Aldrich and used as received. 5-(4-Bromo-phenyl)norbornene,[31] (pentafluorophenyl)trimethylsilylacetylene,[32] and Cp_2ZrPh_2[33]

were synthesized according to literature procedures. ^{1}H, $^{13}C\{^{1}H\}$, $^{19}F\{^{1}H\}$ NMR spectra were recorded at room temperature using a Varian Inova-400, VNMRS-500, or VNMRS-700 spectrometer and referenced to tetramethylsilane (^{1}H, $^{13}C\{^{1}H\}$) or trichlorofluoromethane ($^{19}F\{^{1}H\}$). Chemical shifts are reported in parts per million (ppm) and coupling constants (J) are given in Hertz (Hz). High resolution mass spectra were obtained on an Agilent Technologies 6220 oaTOF (APPI), Bruker 9.4T Apex-Qe FTICR (MALDI), or Kratos Analytical MS-50G (EI) spectrometer. UV−visible spectroscopic measurements were carried out with a Varian Cary 300 Scan spectrophotometer. Powder XRD analysis was performed on a Rigaku Ultima IV Diffractometer by the Earth and Atmospheric Sciences' X-Ray Diffraction Laboratory at the University of Alberta. Elemental analyses were performed at the Analytical and Instrumentation Laboratory at the University of Alberta. Melting points were measured in sealed glass capillaries under nitrogen using a MelTemp apparatus. GPC was performed at 40 °C using THF as the eluent at a flow rate of 0.5 mL per minute. A Viscotek VE 2001 autosampler, one Viscotek T6000M column, GPC 270 Max dual detector, and Viscotek VE 3580 refractive index detector were used for sample analysis and data collection. Multidetector calibration was done using RI detection in conjunction with low angle light scattering (LALS) and right angle light scattering (RALS) using 99 kDa polystyrene to create the calibration method and 235 kDa polystyrene to verify the calibration. Thermogravimetric analysis was performed under a nitrogen atmosphere on a PerkinElmer Pyris 1 TGA. Differential scanning calorimetry measurements were conducted under a nitrogen atmosphere on a PerkinElmer Pyris 1 DSC. Dynamic light scattering (DLS) was conducted on a Malvern Nanoseries Zetasizer. The steady-state photoluminescence (PL) spectra, emission lifetime (τ) and photoluminescence quantum yields (Φ) were obtained using an Edinburgh FLSP980 fluorescence spectrophotometer equipped with a xenon lamp (Xe900) and an integrating sphere, respectively. The cut-off filters (λ = 575 nm for **3**, λ = 490 nm for **4** and polymers) were used in PL measurements. The films of monomers and polymers which were used for PL measurements were drop-cast from hexanes. The cyclic voltammetry (CV) was measured using a CHI660E B157216 instrument, with a polished gold working electrode, a Pt-net as the counter electrode, and an Ag wire as the reference electrode; ferrocene/ferrocenium (Fc/Fc^+) was used as an internal standard. HAADF-STEM imaging was carried out on an aberration-corrected JEOL JEM-ARM200cF instrument with a cold-field emission gun at 200 kV. The STEM resolution of the microscope is 0.78 Å. The HAADF-STEM images were collected with the JEOL HAADF detector using the following experimental conditions: probe size 6c, condenser lens aperture 30 μm, scan speed 32 μs per pixel, and camera length 8 cm. TEM samples were prepared by depositing a drop of micelle suspensions in THF/hexanes onto a holey carbon coated copper grid (Electron Microscopy Inc.) The grid was kept in a vacuum chamber for at least 24 hours prior to data collection.

3.4.2 Synthetic Procedures

Synthesis of bis(pentafluorophenyl)acetylene. Adapted from reference 32. To a solution of (pentafluorophenyl)trimethylsilylacetylene (405.5 mg, 1.536 mmol) in 2 mL of DMF was added 2 mL of diisopropylamine and degassed water (25 μL, 1.4

mmol). This solution was added to a mixture of tetrakis(triphenylphosphine)palladium (71.8 mg, 0.0622 mmol), copper(I) chloride (152.3 mg, 1.538 mmol), and iodopentafluorobenzene (374.1 mg, 1.273 mmol) in 5 mL of DMF prepared in the absence of light. The reaction mixture was stirred at 80 °C for 16 hours before cooling to room temperature. The reaction mixture was diluted with saturated aqueous ammonium chloride (100 mL), extracted with pentane (100 mL), and then the organic layer washed two more times with saturated aqueous ammonium chloride (100 mL portions). The organic layer was dried with magnesium sulfate and filtered through a plug of silica. The filtrate was concentrated to a volume of *ca.* 5 mL and the product crystallized out at –20 °C to yield a colorless crystalline solid (126 mg, 28 %). ^{19}F NMR (468.6 MHz, $CDCl_3$): δ –134.5 (m, 4F, *o*-F), –149.6 (t, 2F, $^{3}J_{FF}$ = 20.6 Hz, *p*-F), –160.8 (m, 4F, *m*-F). The resulting NMR spectrum matched that previously reported.[32]

Synthesis of 2,3-diphenylbenzozirconocene (1). Adapted from reference 4b. Diphenylacetylene (2.340 g, 13.1 mmol) and Cp_2ZrPh_2 (4.952 g, 13.2 mmol) were combined in 90 mL of toluene and heated at 110 °C for 48 hours. The solvent was removed *in vacuo* and the residue extracted with 25 mL of dry THF and filtered through a 3 cm plug of Celite. The filtrate was evaporated to dryness to yield **1** as an orange solid (5.91 g, 95%). Orange crystals suitable for single-crystal X-ray crystallography were obtained from a concentrated Et_2O solution at –30 °C. ^{1}H NMR (699.8 MHz C_6D_6): δ 7.21–7.22 (m, 2H, *o*-Ph*H*), 7.17–7.19 (m, 1H, benzo*H*), 7.10 (m, 2H, *m*-Ph*H*), 6.94–7.03 (m, 5H, *m*-Ph*H*, *p*-Ph*H* and two benzo*H*), 6.71–6.75 (m, 1H, *p*-Ph*H*), 6.67–6.89 (m, 2H, *o*-Ph*H*), 6.61–6.63 (m, 1H, benzo*H*), 5.97 (s, 10H, Cp-*H*). $^{13}C\{^1H\}$ NMR (176.0 MHz, C_6D_6): δ 194.5 (*C*-Zr), 185.3 (*C*-Zr), 147.7 (Ar*C*), 147.1 (Ar*C*), 146.7 (Ar*C*), 141.8 (*i*-Ph*C*), 136.5 (benzo*C*), 130.9 (*o*-Ph*C*), 128.1 (*m*-Ph*C*), 127.9 (*m*-Ph*C*), 126.8 (*o*-*C*), 126.0 (benzo*C*), 125.9 (*p*-Ph*C*), 125.8 (benzo*C*), 124.2 (benzo*C*), 123.2 (*p*-Ph*C*), 112.9 (Cp*C*).

Synthesis of 2,3-bis(pentafluorophenyl)benzozirconocene (2). Cp_2ZrPh_2 (0.744 g, 1.99 mmol) and bis(pentafluorophenyl)acetylene (0.716 g, 2.00 mmol) and were combined in toluene and stirred at 115 °C for 16 hours. The solvent was removed under vacuum to yield **2** as a pale yellow powder (1.30 g, *ca.* 90 % by ^{1}H NMR spectroscopy). Single crystals (light yellow) suitable for X-ray crystallography were obtained by recrystallization from toluene at –30 °C. ^{1}H NMR shows *ca*. 10 % Cp-containing impurity in **2**, but the sample was used as is and this impurity did not seem to affect further reactions. ^{1}H NMR (699.8 MHz, C_6D_6): δ 7.01–7.05 (m, 2H, benzo*H*), 6.67–6.72 (m, 1H, benzo*H*), 6.52–6.56 (m, 1H, benzo*H*), 5.94 (s, 10H, Cp*H*). $^{13}C\{^1H\}$ NMR (176.0 MHz, C_6D_6): δ 185.9 (Ar*C*), 179.8 (Ar*C*), 144.2 (d, $^1J_{CF}$ = 244 Hz, *o*-C_{C6F5}), 143.4 (Ar*C*), 137.8 (d, $^1J_{CF}$ = 249 Hz, *m*-C_{C6F5}) 137.1 (Ar*C*H), 135.0 (Ar*C*), 126.4 (Ar*C*H), 125.6 (Ar*C*H), 125.2 (Ar*C*H), 121.3 (ipso-C), 115.2 (ipso-C), 113.7 (Cp*C*). $^{13}C\{^{19}F\}$ NMR (176.0 MHz, C_6D_6): δ 185.9 (Ar*C*), 179.8 (Ar*C*), 144.2 (*o*-C_{C6F5}), 143.4 (bs, Ar*C*), 141.3 (*o*-C_{C6F5}), 140.5 (*p*-C_{C6F5}), 138.1 (*p*-C_{C6F5}), 137.8 (*m*-C_{C6F5}), 137.7 (*m*-C_{C6F5}), 135.0 (Ar*C*), 121.4 (*i*-C_{C6F5}), 115.1 (*i*-C_{C6F5}), 113.7 (doublet of triplet of triplets, $^1J_{CH}$ = 173.7 Hz, $^2J_{CH}$ = $^3J_{CH}$ = 6.8 Hz, Cp*C*). $^{19}F\{^1H\}$ NMR (376.7 MHz, C_6D_6): δ –140.4 (m, 2F, *o*-F), –141.6 (m, 2F, *o*-F), –155.0 (t, 1F, $^3J_{FF}$ = 21.3 Hz, *p*-F), –159.7 (t, 1F, $^3J_{FF}$ = 21.6 Hz, *p*-F), –162.1 (td, 2F, $^3J_{FF}$ = 23.6 Hz, $^4J_{FF}$ = 7.6 Hz, *m*-F), –162.7 (td, 2F, $^3J_{FF}$ = 23.8 Hz, $^4J_{FF}$ = 6.4 Hz, *m*-

F). Anal. Calcd. (%) for $C_{30}H_{14}F_{10}Zr$: C, 54.96; H, 2.15. Found: C, 54.72; H, 2.22. Mp: 203–208 °C.

Synthesis of 1,2,3-triphenylbenzobismole (3). A suspension of $BiCl_3$ (0.123 g, 0.389 mmol) in 5 mL of Et_2O was added to a suspension of $BiPh_3$ (0.084 g, 0.191 mmol) in 5 mL of Et_2O, and the mixture was stirred at room temperature for 1 hour, after which time the reaction mixture was concentrated *in vacuo* to *ca.* 0.5 mL. The crude $PhBiCl_2$ mixture was dissolved in 5 mL of THF and added to a mixture of 2,3-diphenylbenzozirconocene (**1**) (0.275 g, 0.580 mmol) and CuCl (6.3 mg, 0.064 mmol) in 12 mL of THF in the dark. The mixture was then stirred at room temperature in the absence of light for 2.5 hours before being evaporated to dryness. The crude reaction mixture was extracted with 60 mL of hexanes and filtered through a 3 cm plug of Celite. The solution was concentrated to a volume of *ca.* 30 mL and filtered through a 0.3 cm plug of silica. The filtrate was further concentrated to 8 mL and stored at –30 °C for 16 hours yielding 0.236 g of crude product. Recrystallization from Et_2O at –30 °C yielded **3** as an off-white powder (0.208 g, 67 %). Crystals suitable for X-ray crystallography could be obtained by layering methanol over a concentrated solution of **3** in dichloromethane at room temperature. ^{1}H NMR (699.8 MHz, C_6H_6): δ 7.97–8.00 (m, 2H, *o*-$H_{Bi\text{-}Ph}$), 7.52–7.54 (m, 1H, benzo*H*), 7.22–7.26 (m, 2H, Ar*H*), 7.11–7.19 (m, 6H, Ar*H*, *m*-$H_{Bi\text{-}Ph}$, and 2 benzo*H*), 7.00–7.06 (m, 5H, *p*-$H_{Bi\text{-}Ph}$, benzo*H*, and Ar*H*), 6.87–6.89 (m, 2H, Ar*H*), 6.84–6.87 (m, 1H, Ar*H*). $^{13}C\{^{1}H\}$ NMR (176.0 MHz, C_6D_6): δ 172.1 (Ar*C*), 167.7 (Ar*C*), 164.0 (Ar*C*), 161.6 (Ar*C*), 154.7 (Ar*C*), 145.3 (Ar*C*), 143.6 (Ar*C*), 137.5 (*o*-$C_{Bi\text{-}Ph}$), 137.0 (benzo*C*H), 131.9 (Ar*C*H), 130.9 (Ar*C*H), 130.5 (Ar*C*H), 130.4 (Ar*C*H), 129.3 (Ar*C*H), 128.8 (Ar*C*H), 127.99 (Ar*C*H), 127.97 (Ar*C*H), 127.6 (Ar*C*H), 127.1 (Ar*C*H), 126.1 (Ar*C*H). Anal. Calcd. (%) for $C_{26}H_{19}Bi$: C, 57.79; H, 3.54. Found: C, 57.84; H, 3.87. UV-Vis (THF): λ_{max} = 320 nm (ε = 5.44 × 10^3 L•$mol^{-1}cm^{-1}$). HRMS (MALDI with DCTB matrix): m/z calcd. for $C_{26}H_{19}Bi$: 540.1291; found: 540.1297 (Δppm = 1.1). Mp: 142–144 °C.

Synthesis of 1-phenyl-2,3-bis(pentafluorophenyl)benzobismole (4). A suspension of $BiCl_3$ (0.146 g, 0.461 mmol) in 4 mL of Et_2O was added to a suspension of $BiPh_3$ (0.101 g, 0.230 mmol) 4 mL of Et_2O and the mixture was stirred at room temperature for 1 hour, after which time it was concentrated *in vacuo* to a volume of *ca.* 0.5 mL. The crude $PhBiCl_2$ mixture was dissolved in 5 mL of THF and added to a mixture of 2,3-bispentafluorophenylbenzozirconocene (**2**) (0.447 g, 0.682 mmol), and CuCl (7.3 mg, 0.074 mmol) in 12 mL of THF in the dark, and stirred at room temperature in the dark for 2.5 hours before being evaporated to dryness. The crude product mixture was extracted with 15 mL of CH_2Cl_2 and filtered two times through Florisil and then the solvent was removed *in vacuo*. The crude product was washed with *ca*. 10 mL of cold (–78 °C) methanol, followed by 10 mL of cold (–78 °C) hexanes to yield **4** (93.0 mg, 19 %) as a white powder. Crystals suitable for X-ray crystallography were grown from a mixture of CH_2Cl_2 and methanol cooled to –30 °C. ^{1}H NMR (699.8 MHz, C_6D_6): δ 7.93 (dd, 2H, $^3J_{HH}$ = 7.8 Hz, $^4J_{HH}$ = 1.1 Hz, *o*-$H_{Bi\text{-}Ph}$), 7.35–7.37 (m, 1H, benzo*H*), 7.17–7.21 (m, 2H, benzo*H*) 7.12–7.14 (m, 2H, *m*-$H_{Bi\text{-}Ph}$), 6.96–7.01 (m, 2H, overlap of benzo*H* and *p*-$H_{Bi\text{-}Ph}$). ^{19}F{^{1}H} NMR (468.6 MHz, C_6D_6): δ –137.9 (d, 1F, $^3J_{FF}$ = 23.4 Hz, *o*-F_{locked_C6F5}), –139.7 (d, 2F, $^3J_{FF}$ = 21.5 Hz, *o*-$F_{unlocked\_C6F5}$), –140.4 (dd, 1F, $^3J_{FF}$ = 24.1 Hz, $^4J_{FF}$ = 4.3 Hz, *o*-F_{locked_C6F5}), –

152.6 (t, 1F, $^{3}J_{FF}$ = 21.6 Hz, p-F$_{locked_C6F5}$), –155.2 (t, 1F, $^{3}J_{FF}$ = 21.7 Hz, p-F$_{unlocked_C6F5}$), –160.4 (td, 1F, $^{3}J_{FF}$ = 22.9 Hz, $^{4}J_{FF}$ = 8.2 Hz, m-F$_{locked_C6F5}$), –161.1 (td, 1F, $^{3}J_{FF}$ = 22.7 Hz, $^{4}J_{FF}$ = 8.6 Hz, m-F$_{locked_C6F5}$), –161.9 (td, 2F, $^{3}J_{FF}$ = 23.6 Hz, $^{3}J_{FF}$ = 6.9 Hz, m-F$_{unlocked_C6F5}$). $^{13}C\{^{1}H\}$ NMR (126.0 MHz, C_6D_6): δ 170.4 (s, Ar*C*), 160.5–160.7 (m, Ar*C*), 157.9 (s, Ar*C*), 157.1–157.4 (m, Ar*C*), 153.8 (s, Ar*C*), 137.6 (s, o-$C_{Bi\text{-}Ph}$), 137.2 (s, benzo*C*H), 131.3 (s, m-$C_{Bi\text{-}Ph}$), 130.2 (s, benzo*C*H), 129.6 (s, benzo*C*H), 128.8 (s, p-$C_{Bi\text{-}Ph}$), 118.9 (m, i-C$_{locked_C6F5}$), 116.9 (m, i-C$_{unlocked_C6F5}$) (note: one benzoCH likely overlaps with residual solvent signal at 128.1 ppm). $^{13}C\{^{19}F\}$ NMR (126.0 MHz, C_6D_6): δ 170.4 (m, Ar*C*), 160.6 (s, Ar*C*), 157.8–158.0 (m, Ar*C*), 157.1–157.4 (m, Ar*C*), 153.8 (d, $^{3}J_{CH}$ = 4.1 Hz, Ar*C*), 144.5 (s, o-C$_{locked_C6F5}$), 143.7 (s, o-C$_{locked_C6F5}$), 142.7 (s, o-C$_{unlocked_C6F5}$), 141.3 (s, p-C$_{locked_C6F5}$), 140.0 (s, p-C$_{unlocked_C6F5}$), 138.2 (s, m-C$_{locked_C6F5}$), 138.1 (s, m-C$_{locked_C6F5}$), 137.7 (s, m-C$_{unlocked_C6F5}$), 131.3 (dd, $^{1}J_{CH}$ = 160.4 Hz, $^{2}J_{CH}$ = 7.2 Hz, m-$C_{Bi\text{-}Ph}$), 128.8 (m, p-$C_{Bi\text{-}Ph}$), 118.9 (s, i-C$_{locked_C6F5}$), 116.9 (s, i-C$_{unlocked_C6F5}$). Anal. Calcd. (%) for $C_{26}H_9F_{10}Bi$: C, 43.35; H, 1.26. Found: C, 43.34; H, 1.39. UV-Vis (THF): λ_{max} = 311 nm (ε = 1.03 × 10^4 L•mol^{-1}cm^{-1}). HRMS (MALDI with DCTB matrix): m/z calculated for $C_{26}H_9F_{10}Bi$: 720.0343; found: 720.0358 (Δppm = 2.0). Mp: 134–140 °C.

Synthesis of tris(5-(4-phenyl)norbornene)bismuth (BiAr$^{ROMP}_3$). 5-(4-Bromo-phenyl)norbornene (5.32 g, 21.4 mmol) in 30 mL of dry THF was added to dried magnesium shavings (0.824 g, 33.9 mmol) in THF (40 mL). The reaction mixture was heated to reflux for 2.5 hours after which the resulting Grignard solution was cooled to 0 °C and added slowly to a solution of $BiCl_3$ (2.24 g, 7.09 mmol) in 30 mL THF at 0 °C. The reaction mixture was gradually warmed up to room temperature and then heated to reflux for 3 hours under nitrogen, after which it was cooled to room temperature and filtered through Celite into *ca*. 50 mL of ice water. The filtrate was extracted with ethyl acetate (4 × 40 mL) and the organic layers were combined, dried over magnesium sulfate, filtered, and the solvent was removed under vacuum. The crude product was purified by recrystallization from chloroform and ethanol at –20 °C to yield **BiAr^{ROMP}$_3$** as yellow crystals (2.96 g, 58 %). ^{1}H NMR (700 MHz, $CDCl_3$): δ 7.68 (d, 6H, $^3J_{HH}$ = 8.1 Hz, Ar*H*), 7.30 (d, 6H, $^3J_{HH}$ = 7.8 Hz, Ar*H*), 6.24–6.26 (m, 3H, vinylic*H*), 6.15–6.17 (m, 3H, vinylic*H*), 2.96 (s, 3H, allylic*H*), 2.90 (s, 3H, allylic*H*), 2.67–2.69 (m, 3H, benzylic*H*), 1.72–1.75 (m, 3H, one H of CH_2), 1.60–1.63 (m, 3H, one H of CH_2) 1.68 (d, 3H, J = 8.5 Hz, one H of CH_2), 1.40–1.44 (m, 3H, one H of CH_2). ^{13}C{^{1}H} NMR (176.0 MHz, $CDCl_3$): δ 151.4 (Bi–*C*), 145.8 (Ar*C*), 137.7 (Ar*C*H), 137.5 (vinylic*C*H), 137.4 (vinylic*C*H), 130.0 (Ar*C*H), 48.3 (allylic*C*H), 45.9 (*C*H_2), 43.9 (benzylic*C*H), 42.4 (allylic*C*H), 33.8 (*C*H_2). Anal. Calcd. (%) for $BiC_{39}H_{39}$: C, 65.36; H, 5.48. Found: C, 64.68; H, 5.39. HRMS (ESI): m/z calculated for $C_{39}H_{39}BiNa^+$: 739.2772; found: 739.2748 (Δppm = 3.2). Mp: 178–188 °C (by DSC).

Synthesis of 1-*para*-norbornenephenyl-2,3-diphenylbenzobismole (5). A suspension of $BiCl_3$ (0.277 g, 0.878 mmol) in 5 mL of Et_2O was added to a suspension of tri(5-(4-phenyl)norbornene)bismuth (0.307 g, 0.428 mmol) in 5 mL of Et_2O and the mixture was allowed to stir at room temperature in the dark for

16 hours, after which it was concentrated *in vacuo* to *ca.* 1 mL. The crude $ArBiCl_2$ mixture was dissolved in 5 mL of THF and added to a mixture of 2,3-diphenylbenzozirconocene **1** (0.616 g, 1.23 mmol) and CuCl (21.6 mg, 0.218 mmol) in 15 mL of THF in the dark and stirred at room temperature for 4 hours before being evaporated to dryness. The crude product mixture was stirred with 20 mL of hexanes for 16 hours, then the supernatant was decanted and filtered through a 0.5 cm pad of silica. The filtrate was concentrated *in vacuo* before cooling to –30 °C to precipitate the crude product in two fractions. These crude fractions were combined (0.480 g), washed with 10 mL of methanol, and collected by vacuum filtration in air to yield pure bismole **5** as an off-white powder (0.406 g, 50 %). ^{1}H NMR (699.8 MHz, C_6D_6): δ 7.95–7.98 (m, 2H, *o*-$H_{Bi\text{-}Ph}$), 7.56–7.59 (m, 1 H, benzo*H*), 7.24–7.29 (m, 3H, Ar*H*), 7.16–7.22 (m, 2H, benzo*H*), 7.02–7.10 (m, 7H, Ar*H*), 6.86–6.92 (m, 2H, Ar*H*), 6.74–6.78 (m, 1H, benzo*H*), 6.04–6.08 (m, 1H, norbornene HC=C*H*), 5.98–6.01 (m, 1H, norbornene HC=C*H*), 2.69 (s, 2H, allylic-C*H*s overlapping), 2.50–2.54 (m, 1H, benzylic-C*H*), 1.48–1.53 (m, 1H, one H of norbornene CH_2), 1.38–1.44 (m, 1H, one H of norbornene CH_2), 1.32–1.39 (m, 2H, norbornene CH_2). ^{13}C{^{1}H} NMR (499.8 MHz, C_6D_6): δ 171.9 (Ar*C*), 167.4 (Ar*C*), 164.0 (Ar*C*), 161.6 (Ar*C*), 151.2 (Ar*C*), 146.0 (Ar*C*), 145.4 (Ar*C*), 143.7 (Ar*C*), 137.6 (Ar*C*H), 137.5 (norbornene HC=*C*H), 137.4 (norbornene HC=*C*H), 137.0 (benzo*C*H), 131.9 (Ar*C*H), 130.5 (Ar*C*Hs, multiple overlapping), 129.4 (Ar*C*H), 128.8 (Ar*C*H), 127.9 (Ar*C*H), 127.5 (Ar*C*H), 127.1 (Ar*C*H), 126.1 (benzo*C*H), 48.5 (allylic-*C*H), 48.4 (allylic-*C*H), 46.1 (norbornene *C*H_2), 44.2 (benzylic-*C*H), 42.6 (allylic*C*H), 33.9 (norbornene *C*H_2), 33.8 (norbornene *C*H_2). Anal. Calcd. (%) for $C_{33}H_{27}Bi$: C, 62.66; H, 4.30. Found: C,

62.40; H, 4.39. UV-Vis (THF): λ_{max} = 320 nm (ε = 8.98 × 10^3 L•$mol^{-1}cm^{-1}$). HRMS (MALDI with DCTB matrix): m/z calculated for $C_{33}H_{27}Bi$: 632.1916; found: 632.1917 (Δppm = 0.2). Mp: 117–121 °C.

Synthesis of 1-*para*-norbornenephenyl-2,3-bis(pentafluorophenyl)benzobismole (6). A suspension of $BiCl_3$ (60.4 mg, 0.192 mmol) in 5 mL of Et_2O was added to a suspension of $BiAr_3$ (67.3 mg, 0.0940 mmol) in 5 mL of Et_2O and the mixture was allowed to stir at room temperature in the dark for 16 hours, after which time the mixture was concentrated *in vacuo* to a volume of *ca.* 0.5 mL. The crude sample of $ArBiCl_2$ was dissolved in 10 mL of THF and added to a mixture of **2** (187 mg, 0.286 mmol), and CuCl (3.0 mg, 0.030 mmol) in 10 mL of THF in the dark. The mixture was stirred at room temperature in the dark for 6 hours before being evaporated to dryness. The crude product was extracted with 15 mL of CH_2Cl_2 and filtered two times through Florisil. The solvent was removed *in vacuo* and the crude solid was washed with 5 mL of methanol and dried *in vacuo* to yield **6** as an off-white powder (102 mg, 44 %). ^{1}H NMR (500 MHz, C_6H_6): δ 7.94 (d, 2H, $^3J_{HH}$ = 8.0 Hz, Ar*H*), 7.39–7.42 (m, 1H, benzo*H*), 7.17–7.25 (m, 2H, benzo*H*), 7.12 (d, 2H, $^3J_{HH}$ = 8.0 Hz, Ar*H*), 6.99–7.02 (m, 1H, benzo*H*), 6.00–6.03 (m, 1H, norbornene HC=C*H*), 5.95–9.97 (m, 1H, norbornene HC=C*H*), 2.61–2.65 (m, 2H, both allylic-C*H*), 2.46 (m, 1H, benzylic-C*H*), 1.33–1.48 (m, 2H, norbornene CH_2), 1.29 (s, 2H, norbornene CH_2). ^{19}F{^{1}H} NMR (376.7 MHz, C_6D_6): δ –137.8 (d, 1F, $^3J_{FF}$ = 20.5 Hz, *o*-F_{locked_C6F5}), –139.6 (d, 2F, $^3J_{FF}$ = 21.8 Hz, *o*-$F_{unlocked\_C6F5}$), –140.4 (d, 1F, $^3J_{FF}$ = 22.6 Hz, *o*-F_{locked_C6F5}), –152.6 (t, 1F, $^3J_{FF}$ = 21.5 Hz, *p*-F_{locked_C6F5}), –155.3 (t, 1F, $^3J_{FF}$ = 21.6 Hz,

p-F$_{unlocked_C6F5}$), –160.3 (td, 1F, $^3J_{FF}$ = 23.0 Hz, $^4J_{FF}$ = 8.2 Hz, m-F$_{locked_C6F5}$), –161.1 (td, 1F, $^3J_{FF}$ = 22.7 Hz, $^4J_{FF}$ = 8.5 Hz, m-F$_{locked_C6F5}$), –161.8 (m, 2F, m-F$_{unlocked_C6F5}$). $^{13}C\{^1H\}$ NMR (126.0 MHz, C_6D_6): δ 170.2 (Ar*C*), 160.4 (Ar*C*), 157.8 (Ar*C*), 153.9 (Ar*C*), 153.8 (Ar*C*), 147.1 (Ar*C*), 144.6 (d, $^1J_{CF}$ = 241.3 Hz, o-C$_{locked_C6F5}$), 143.7 (d, $^1J_{CF}$ = 243.3 Hz, o-C$_{locked_C6F5}$), 142.7 (d, $^1J_{CF}$ = 241.5 Hz, o-C$_{unlocked_C6F5}$), 141.3 (d, $^1J_{CF}$ = 258.1 Hz, p-C$_{locked_C6F5}$), 140.0 (d, $^1J_{CF}$ = 224.3 Hz, p-*C*$_{unloked\_C6F5}$), 137.8 (s, Ar*C*H), 137.7 (dt, $^1J_{CF}$ = 248.0 Hz, $^2J_{CF}$ = 14.2 Hz, m-C$_{unlocked_C6F5}$), 137.4 (vinylic-*C*H), 137.2 (s, benzo*C*H), 130.9 (s, Ar*C*H), 130.2 (s, benzo*C*H), 129.5 (s, benzo*C*H), 128.1 (s, benzo*C*H), 119.0 (t, $^2J_{CF}$ = 17.9 Hz, i-C$_{locked_C6F5}$), 116.9 (t, $^2J_{CF}$ = 20.6 Hz, i-C$_{unlocked_C6F5}$), 48.6 (s, allylic-*C*H), 48.4 (s, allylic *C*H), 46.0 (s, norbornene *C*H$_2$), 44.23 (s, benzylic *C*H), 44.18 (s, benzylic-*C*H), 42.6 (s, allylic-*C*H), 33.8 (s, norbornene *C*H$_2$), 33.7 (s, norbornene *C*H$_2$). $^{13}C\{^{19}F\}$ NMR (126.0 MHz, C_6D_6): δ 170.2 (br, Ar*C*), 160.4 (Ar*C*), 157.8 (t, $^2J_{CH}$ = 7.3 Hz, Ar*C*), 153.7-154.1 (m, Ar*C*), 153.8 (Ar*C*), 147.1 (br, Ar*C*), 144.6 (o-C$_{locked_C6F5}$), 143.7 (o-C$_{locked_C6F5}$), 142.7 (o-C$_{unlocked_C6F5}$), 141.3 (p-C$_{locked_C6F5}$), 140.0 (p-*C*$_{unloked\_C6F5}$), 138.2 (m-C$_{locked_C6F5}$), 138.1 (m-C$_{locked_C6F5}$) 137.8 (dd, $^1J_{CH}$ = 159.9 Hz, $^2J_{CH}$ = 8.2 Hz, Ar*C*H), 137.7 (m-C$_{unlocked_C6F5}$), 137.4 (d, $^1J_{CH}$ = 163.3 Hz, vinylic-*C*H), 130.9 (d, $^1J_{CH}$ = 157.8 Hz, Ar*C*H), 130.2 (d, $^1J_{CH}$ = 148.7 Hz, benzo*C*H), 129.5 (d, $^1J_{CH}$ = 136.0 Hz, benzo*C*H), 128.1 (dd, $^1J_{CH}$ = 159.6 Hz, $^2J_{CH}$ = 7.0 Hz, benzo*C*H), 119.0 (s, i-C$_{locked_C6F5}$), 116.9 (s, i-C$_{unlocked_C6F5}$), 48.6 (d, $^1J_{CH}$ = 150.5 Hz, allylic *C*H), 46.0 (t, $^1J_{CH}$ = 130.6 Hz, norbornene *C*H$_2$), 44.2 (d, $^1J_{CH}$ = 137.1 Hz, benzylic *C*H), 42.6 (d, $^1J_{CH}$ = 157.3 Hz, allylic-*C*H), 33.7 (t, $^1J_{CH}$ = 138.5 Hz, norbornene *C*H$_2$). Anal. Calcd. (%) for $C_{33}H_{17}F_{10}Bi$: C, 48.79; H, 2.11. Found: C, 49.48; H, 2.33. UV-Vis (THF): λ_{max} = 310 nm (ε = 9.47 × 10^3 L•$mol^{-1}cm^{-1}$) HRMS (+APPI): m/z calculated for $C_{33}H_{18}F_{10}Bi$ $(M+H)^+$: 813.1047; found: 813.1044 (Δppm = 0.4). Mp: 163–167 °C.

Synthesis of 5-(4-(2-ethylhexyl)phenyl)norbornene (7). To a solution of 5-(4-bromophenyl)norbornene (0.459 g, 1.85 mmol) in 15 mL THF at –78 °C was added *t*BuLi (2.5 mL, 1.7 M in pentane, 4.2 mmol). The reaction mixture was stirred for 60 minutes at –78 °C and 2-ethylhexylbromide (0.35 mL, 2.0 mmol) was added. The mixture was stirred at –78 °C for 1 hour and then allowed to warm to room temperature and stirred for another hour. The reaction mixture was extracted with 30 mL Et_2O, washed with brine (2 × 30 mL), dried with magnesium sulfate and filtered through silica. The solvent was removed from the filtrate *in vacuo* and the resulting crude oil was heated at 80 °C under reduced pressure (0.5 mbar) for 2 hours, followed by flash column chromatography using petroleum ether on silica (R_f = 0.72) to yield compound **7** as a colorless oil (0.264 g, 51 %). ^{1}H NMR (699.8 MHz, $CDCl_3$): δ 7.17 (d, 2H, $^3J_{HH}$ = 7.9 Hz, Ar*H*), 7.07 (d, 2H, $^3J_{HH}$ = 8.1 Hz, Ar*H*), 6.24–6.26 (m, 1H, vinylic-*H*), 6.15–6.17 (m, 1H, vinylic-*H*), 2.95 (s, 1H, allylic-C*H*), 2.88 (s, 1H, allylic-C*H*), 2.67–2.70 (m, 1H, norbornene benzylic-C*H*), 2.50 (quartet of doublets, 2H, $^2J_{HH}$ = 13.6 Hz and $^3J_{HH}$ = 7.1 Hz, benzylic-CH_2), 1.73–1.75 (m, 1H, one H of norbornene CH_2), 1.57–1.63 (m, 2H, norbornene CH_2), 1.54 (sept, 1H, $^3J_{HH}$ = 6.1 Hz, alkyl C*H*), 1.40–1.42 (m, 1H, one H of norbornene CH_2), 1.23–1.33, (m, 8H, overlapping alkyl CH_2 groups), 0.86–0.88 (overlapping triplets, 6H, overlapping alkyl CH_3). $^{13}C\{^1H\}$ NMR (176.0 MHz, $CDCl_3$): δ 143.3 (Ar*C*), 139.1 (Ar*C*), 137.5 (vinylic-*C*H), 137.4 (vinylic-*C*H), 129.2 (Ar*C*H), 127.4 (Ar*C*H), 48.5 (allylic-*C*H), 45.9 (norbornene *C*H_2), 43.5 (norbornene benzylic-*C*H), 42.4 (allylic-*C*H), 41.2 (alkyl-*C*H), 39.7 (benzylic-*C*H_2), 33.8 (norbornene CH_2), 32.5 (alkyl *C*H_2), 25.5 (alkyl *C*H_2), 23.2 (alkyl *C*H_2), 14.3 (alkyl *C*H_3), 10.9 (alkyl *C*H_3). Anal. Calcd. (%) for $C_{21}H_{30}$: C, 89.29; H, 10.71. Found: C, 89.11; H, 10.79. HRMS (EI): m/z calculated for $C_{21}H_{30}$: 282.2346; found: 282.2347 (Δppm = 0.6).

Synthesis of 5-(4-butylphenyl)norbornene (8). 5-(4-Bromophenyl)-norbornene (0.502 g, 2.02 mmol) and 1-bromobutane (0.22 mL, 2.0 mmol) in 15 mL of THF was stored over 4 Å molecular sieves for 18 hours. This solution was then decanted away from the sieves and cooled to –78 °C prior to the addition of *n*-butyllithium (0.89 mL, 2.5 M in hexanes, 2.2 mmol). After stirring for 60 minutes at –78 °C, the reaction mixture was warmed to room temperature and stirred for another 60 minutes. The crude mixture was extracted with 30 mL of diethyl ether, and the organic layer was washed with brine (2 × 30 mL), dried over magnesium sulfate, filtered through a pad of silica, and the solvent removed *in vacuo* to yield 0.386 g of crude product. Flash column chromatography using petroleum ether on silica (R_f = 0.72) yielded compound **8** as a colorless oil (0.191 g, 42 %). ^{1}H NMR (699.8 MHz, $CDCl_3$): δ 7.19 (d, 2H, $^3J_{HH}$ = 8.4 Hz, Ar*H*), 7.11 (d, 2H, $^3J_{HH}$ = 8.0 Hz, Ar*H*), 6.23–6.27 (m, 1H, vinylic-*H*), 6.14–6.17 (m, 1H, vinylic-*H*), 2.96 (s, 1H, allylic-C*H*), 2.88 (s, 1H, allylic-C*H*), 2.66–2.70 (m, 1H, norbornene benzylic-C*H*), 2.56–2.60 (m, 2H, benzylic-CH_2), 1.71–1.76 (m, 1H, one H of norbornene CH_2), 1.56–1.64 (m, 4H, norbornene CH_2 overlapping with alkyl CH_2), 1.39–1.43 (m, 1H, one H of norbornene CH_2), 1.37 (sextet, 2H, $^3J_{HH}$ = 7.6 Hz, CH_2CH$_3$), 0.93, (t, 3H, $^3J_{HH}$ = 7.6 Hz, CH_3).

$^{13}C\{^1H\}$ NMR (176.0 MHz, $CDCl_3$): δ 143.4 (Ar*C*), 140.2 (Ar*C*), 137.5 (vinylic-*C*H), 137.4 (vinylic-*C*H), 128.4 (Ar*C*H), 127.6 (Ar*C*H), 48.5 (allylic-*C*H), 45.9 (norbornene *C*H_2), 43.5 (benzylic-*C*H), 42.4 (allylic-*C*H), 35.3 (benzylic-*C*H_2), 33.9 (alkyl *C*H_2), 33.7 (norbornene *C*H_2), 22.6 (alkyl *C*H_2), 14.1 (*C*H_3). Anal. Calcd. (%) for $C_{17}H_{22}$: C, 90.20; H, 9.80. Found: C, 90.11; H, 9.89. HRMS (EI): m/z calculated for $C_{17}H_{22}$: 226.1722; found: 226.1723 (Δppm = 0.8).

General polymer synthesis. To a solution of monomer in THF (11 mL to 57 mL depending on reaction scale – *e.g.* 11 mL for 0.77 mmol of monomer (**P1**) and 57 mL for a total of 0.40 mmol monomer (**P5**) to give a final monomer concentration of 7.0 mM in each polymerization) was added a stock solution of second-generation Grubbs' catalyst in THF (catalyst 1 mol% Grubbs' catalyst loading, 80–180 μL of 25 mM catalyst solution added depending on scale of reaction). The reaction mixture was stirred for 60–90 minutes before *ca.* 1 mL of ethyl vinyl ether was added. The reaction mixture was stirred for an additional 30 minutes, concentrated *in vacuo* to a volume of *ca.* 1 mL and then pipetted into 100 mL of vigorously stirring methanol. The product was collected by vacuum filtration and dried. It should be noted for bismole-containing copolymers **P6**–**P9**, the molar ratio of monomers in the reaction feedstock differed slightly than the molar ratio of comonomer incorporation as estimated by ^1H NMR spectroscopy. Table 3.1 below outlines the feedstock molar ratio of comonomers and the incorporated molar ratio of the comonomers. It should also be noted that $^{13}C\{^1H\}$ NMR spectra was unobtainable due to the limited signal to noise observed upon running saturated polymer NMR samples.

Table 3.1. Molar ratio of comonomers in the reaction feedstocks for the synthesis of polymers **P5**–**P9** compared to the molar ratio of comonomer incorporation.

	Molar ratio in feedstock				Molar ratio of incorporation			
	5	**6**	**7**	**8**	**5**	**6**	**7**	**8**
P5	0 %	0%	15 %	85 %	0 %	0 %	15 %	85 %
P6	20 %	0 %	80 %	0 %	16 %	0 %	84 %	0 %
P7	20 %	0 %	0 %	80 %	16 %	0 %	0 %	84 %
P8a	9 %	0 %	30 %	61 %	7 %	0 %	31 %	62 %
P8b	18 %	0 %	27 %	55 %	13 %	0 %	29 %	58 %
P8c	46 %	0 %	8 %	46 %	37 %	0 %	9 %	54 %
P9a	0 %	9 %	30 %	61 %	0 %	6 %	31 %	63 %
P9b	0 %	18 %	27 %	55 %	0 %	13 %	29 %	58 %
P9c	0 %	45 %	8 %	47 %	0 %	38 %	9 %	53 %

* Molar ratio of incorporation determined by ^{1}H NMR spectroscopy.

Homopolymer of 1-*para*-norbornenephenyl-2,3-diphenylbenzobismole (P1): yielded 22 mg (45 %) of a white powder. ^{1}H NMR (700 MHz, $CDCl_3$): δ 7.56–7.93 (3H, Ar*H*), 6.59–7.35 (15H, Ar*H*), 4.85–5.45 (2H, vinylic*H*), 2.14–3.17 (3H, two allylic*H* and one benzylic*H*), 1.53–2.10 (2H, alkyl*H*), 0.86–1.33 (2H, alkly*H*). M_n = 2.1 MDa, M_w = 3.1 MDa, PDI = 1.5, dn/dc = 0.12 mL/g by GPC (in THF).

Homopolymer of 1-*para*-norbornenephenyl-2,3-bipentafluorophenylbenzo-bismole (P2): yielded 48 mg (69 %) of product as an off-white fibrous solid. ^{1}H NMR (700 MHz, $CDCl_3$): δ 7.56–7.94 (br, 3H, Ar*H*), 7.28–7.47 (br, 2H, Ar*H*), 6.64–7.24 (br, 3H, Ar*H*), 4.71–5.40 (br, 2H vinyl*H*), 2.15–3.16 (3H, two allylic*H* and one benzylic*H*), 1.47–2.15 (2H, CH_2), 0.53–1.36 (2H, CH_2). $^{19}F\{^{1}H\}$ NMR (377 MHz, $CDCl_3$): δ –137.5 (br, 1F, *o*-F), –139.1 (br, 2F, *o*-F), –139.6 (br, 1F, *o*-F), –153.2 (br, 1F, *p*-F), –155.9 (br, 1F, *p*-F), –162.5 to –159.9 (m, 4F, *m*-F). M_n = 605 kDa, M_w = 944 kDa, PDI = 1.56, dn/dc = 0.096 mL/g by GPC (in THF).

Homopolymer of 5-(4-(2-ethylhexyl)phenyl)norbornene (P3): yielded 53 mg of product (77 %) as an off-white fibrous solid. ^{1}H NMR (600 MHz, C_6D_6): δ 6.48–7.24 (4H, Ar*H*), 4.84–5.49 (2H, vinyl*H*), 2.23–3.19 (5H, two allylic*H*, three benzylic*H*), 1.68–2.23 (3H, alkyl*H*), 1.45–1.63 (1H, C*H*), 1.0–1.44 (9H, alkyl*H*), 0.71–1.0 (6H, two CH_3 groups). M_n = 52 kDa, M_w = 314 kDa, PDI = 6.0, dn/dc = 0.11 mL/g by GPC (in THF).

Homopolymer of 5-(4-butylphenyl)norbornene (P4): yielded 78 mg (75 %) of a white fibrous product. ^{1}H NMR (700 MHz, C_6D_6): δ 6.66–7.20 (4H, ArH), 4.94–5.52 (2H, vinylicH), 2.33–3.24 (5H, two allylic*H* and three benzylic*H*), 1.68–2.22 (3H, alkyl*H*), 1.49–1.67 (1H, alkyl*H*), 1.02–1.47 (4H, alkyl*H*), 0.77–0.99 (3H, CH_3). M_n = 239 kDa, M_w = 456 kDa, PDI = 1.9, dn/dc = 0.095 mL/g by GPC (in THF).

Copolymer of 5-(4-butylphenyl)norbornene (85 mol%) and 5-(4-(2-ethylhexyl)phenyl)norbornene (15 mol%) (P5): yielded a white fibrous solid (86 mg, 77 %). ^{1}H NMR (700 MHz, C_6D_6): δ 6.66–7.15 (4H, Ar*H*), 4.95–5.49 (2H, vinylic*H*), 2.27–3.24 (5H, two allylic*H* and 3 benzylic*H*), 1.69–2.22 (3H, alkyl*H*), 1.52–1.62 (1H, alkyl*H*), 1.03–1.47 (5H, alkyl*H*), 0.69–0.98 (3.5H, alkyl*H*). M_n = 158 kDa, M_w = 328 kDa, PDI = 2.1, dn/dc = 0.12 mL/g by GPC (in THF).

Copolymer of 5-(4-(2-ethylhexyl)phenyl)norbornene (84 mol%) and 1-*para*-norbornenephenyl-2,3-bis(pentafluorophenyl)benzobismole (16 mol%) (P6): yielded a white fibrous solid (61 mg, 69 %). ^{1}H NMR (700 MHz, $CDCl_3$): δ 7.63–7.90 (0.5H, bismoleAr*H*), 6.64–7.37 (5.6H, Ar*H*), 4.94–5.51 (2H, vinylic*H*), 2.21–3.20 (4.7H, allylic*H* and benzylic*H*), 1.65–2.20 (2.5H, alkyl*H*), 1.46–1.61 (0.8H, alkyl*H*), 1.06–1.45 (7.8H, alkyl*H*), 0.69–0.94 (5.1H, C*H*$_3$). M_n = 355 kDa, M_w = 625 kDa, PDI = 1.8, dn/dc = 0.15 mL/g by GPC (in THF).

Copolymer of 5-(4-butylphenyl)norbornene (84 mol%) and 1-*para*-norbornenephenyl-2,3-bis(pentafluorophenyl)benzobismole (16 mol%) (P7): yielded a white fibrous solid (19 mg, 20 %). ^{1}H NMR (700 MHz, $CDCl_3$): δ 7.63–7.90 (0.5H, bismuthAr*H*), 6.68–7.36 (5.7H, Ar*H*), 4.89–5.49 (2H, vinylic*H*), 2.25–3.24 (4.7H, allylic*H* and benzylic*H*), 1.67–2.17 (2.9H, alkyl*H*), 1.49–1.65 (0.9H, alkyl*H*), 1.03–1.45 (3.5H, alkyl*H*), 0.71–0.99 (2.5H, C*H*$_3$). M_n = 348 kDa, M_w = 621 kDa, PDI = 1.8, dn/dc = 0.13 mL/g by GPC (in THF).

Copolymer P8a: yielded a white powder (61 mg, 69 %). ^{1}H NMR (700 MHz, $CDCl_3$): δ 7.63–7.91 (0.2H, bismoleAr*H*), 6.65–7.37 (4.8H, Ar*H*), 4.88–5.54 (2H, vinylic*H*), 2.24–3.25 (4.9H, allylic*H* and benzylic*H*), 1.68–2.22 (2.8H, alkyl*H*), 1.48–1.66 (1H, alkyl*H* overlapping with H_2O), 1.00–1.47 (5.6H, alkyl*H*), 0.71–0.99 (3.8H, alkyl*H*). M_n = 366 kDa, M_w = 732 kDa, PDI = 2.0, dn/dc = 0.12 mL/g by GPC (in THF).

Copolymer P8b: yielded a white fibrous solid (59 mg, 58 %). ^{1}H NMR (700 MHz, $CDCl_3$): δ 7.65–7.91 (0.4H, bismoleAr*H*), 6.69–7.36 (5.4H, Ar*H*), 4.91–5.51 (2H, vinylic*H*), 2.23–3.23 (4.7H, allylic*H* and benzylic*H*), 1.65–2.21 (2.6H, alkyl*H*), 1.50–1.63 (1H, alkyl*H* overlapping with H_2O), 1.01–1.47 (6.2H, alkyl*H*), 0.72–0.99 (4.3H, alkyl*H*). M_n = 445 kDa, M_w = 786 kDa, PDI = 1.8, dn/dc = 0.13 mL/g by GPC (in THF).

Copolymer P8c: yielded a white fibrous solid (70 mg, 72 %). ^{1}H NMR (700 MHz, $CDCl_3$): δ 7.61–7.94 (1.1H, bismoleAr*H*), 6.63–-7.36 (8.1H, Ar*H*), 4.89–5.52 (2H, vinylic*H*), 2.21–3.21 (4.2H, allylic*H* and benzylic*H*), 1.67–2.19 (2.5H, alkyl*H*), 1.47–1.63 (1.4H, alkyl*H* overlapping with H_2O), 0.99–1.46 (3.8H, alkyl*H*), 0.67–0.99 (2.2H, alkyl*H*). M_n = 1.6 MDa, M_w = 2.2 MDa, PDI = 1.4, dn/dc = 0.08 mL/g by GPC (in THF).

Copolymer P9a: yielded a white fibrous solid (84 mg, 78 %). ^{1}H NMR (700 MHz, $CDCl_3$): δ 7.68–7.96 (0.18H, bismoleAr*H*), 7.33–7.49 (0.12H, bismoleAr*H*), 6.62–7.22 (4H, Ar*H*), 4.91–5.54 (2H, vinylic*H*), 2.24–3.24 (4.9H, allylic*H* and benzylic*H*), 1.67–2.18 (2.9H, alkyl*H*), 1.51–1.65 (1H, alkyl*H*), 1.00–1.47 (5.7H, alkyl*H*), 0.72–0.99 (3.9H, alkyl*H*). ^{19}F{^{1}H} NMR (377 MHz, $CDCl_3$): δ –137.4 (br, 1F, *o*-F), –139.0 (br, 2F, *o*-F), –139.7 (br, 1F, *o*-F), –153.1 (br, 1F, *p*-F), –156.0 (br, 1F, *p*-F), –160.6 (br, 1F, *m*-F), –161.0 (br, 1F, *m*-F), –161.8 (br, 2F, *m*-F). M_n = 249 kDa, M_w = 454 kDa, PDI = 1.8, dn/dc = 0.11 mL/g by GPC (in THF).

Copolymer P9b: yielded a white fibrous solid (82 mg, 78 %). ^{1}H NMR (700 MHz, $CDCl_3$): δ 7.65–7.98 (0.4H, bismoleAr*H*), 7.29–7.44 (0.3, bismoleAr*H*), 6.54–7.23 (3.9H, Ar*H*), 4.88–5.49 (2H, vinylic*H*), 2.21–3.22 (4.8H, allylic*H* and benzylic*H*), 1.66–2.20 (2.6H, alkyl*H*), 1.50–1.65 (0.9H, alkyl*H*), 1.02–1.45 (5.7H, alkyl*H*), 0.70–0.99 (3.9H, alkyl*H*). ^{19}F{^{1}H} NMR (377 MHz, $CDCl_3$): δ –137.3 (br, 1F, *o*-F), –139.0 (br, 2F, *o*-F), –139.6 (br, 1F, *o*-F), –153.1 (br, 1F, *p*-F), –155.9 (br, 1F, *p*-F), –160.6 (br, 1F, *m*-F), –160.9 (br, 1F, *m*-F), –161.8 (br, 2F, *m*-F). M_n = 332 kDa, M_w = 618 kDa, PDI = 1.9, dn/dc = 0.11 mL/g by GPC (in THF).

Copolymer P9c: yielded a white fibrous solid (60 mg, 63 %). ^{1}H NMR (700 MHz, $CDCl_3$): δ = 7.60–8.00 (1.1H, bismoleAr*H*), 7.30–7.51 (0.7H, bismoleAr*H*), 6.61–7.23 (4.0H, Ar*H*), 4.85–6.51 (2H, vinylic*H*), 2.19–3.23 (3.9H, allylic*H* and benzylic*H*), 1.65–2.17 (2.4H, alkyl*H*), 1.50–1.62 (0.9H, alkyl*H*), 0.99–1.45 (3.8H, alkyl*H*), 0.66–0.99 (2.1H, alkyl*H*). $^{19}F\{^{1}H\}$ NMR (377 MHz, $CDCl_3$): δ –137.4 (br, 1F, *o*-F), –139.0 (br, 2F, *o*-F), –139.6 (br, 1F, *o*-F), –153.1 (br, 1F, *p*-F), –155.9 (br, 1F, *p*-F), –160.6 (br, 1F, *m*-F), –161.0 (br, 1F, *m*-F), –161.8 (br, 2F, *m*-F). M_n = 269 kDa, M_w = 416 kDa, PDI = 1.5, dn/dc = 0.081 mL/g by GPC (in THF).

Polymer P10. To a solution of **5** (37.9 mg, 0.0600 mmol) and tri(5-(4-phenyl)norbornene)bismuth (14.6 mg, 0.0204 mmol) in THF (1.1 mL) was added 55 μL of Grubbs' 2nd Generation catalyst in THF (15 mM), the reaction mixture was stirred for 60 minutes before *ca*. 1 mL of ethyl vinyl ether was added. The reaction was stirred for an additional 30 minutes, concentrated *in vacuo* to a volume of *ca*. 1 mL and then pipetted into 30 mL of vigorously stirring methanol prior to collection by vacuum filtration as a fine off-white powder (34 mg, 65 %). A lack of solubility in organic solvents prevented solution NMR characterization. Anal. Calcd. (%) for a 2.94:1 ratio of $C_{33}H_{27}Bi$:$C_{39}H_{39}Bi$: C, 63.35; H, 4.60. Found: C, 61.54; H, 4.61.

Polymer P11. To a solution of **5** (13.0 mg, 0.0206 mmol) and tri(5-(4-phenyl)norbornene)bismuth (58.7 mg, 0.0820 mmol) in THF (1.4 mL) was added 70 μL of Grubbs'2nd Generation catalyst in THF (15 mM), the reaction mixture was stirred for 60 minutes before *ca.* 1 mL of ethyl vinyl ether was added. The reaction was stirred for an additional 30 minutes, concentrated *in vacuo* to a volume of *ca*. 1 mL and then pipetted into 50 mL of vigorously stirring methanol prior to collection by vacuum filtration as a fine off-white powder (49 mg, 68 %). A lack of solubility in organic solvents prevented NMR characterization. Anal. Calcd. (%) for a 1:3.98 ratio of $C_{33}H_{27}Bi$:$C_{39}H_{39}Bi$: C, 64.82; H, 5.24. Found: C, 64.50; H, 5.31.

Polymer P12. To a solution of **5** (39.0 mg, 0.0617 mmol) in THF (0.8 mL) was added 82 μL of Grubbs' 3rd Generation catalyst in THF (45 mM), the reaction mixture was stirred at room temperature for 2 minutes, at which point a 40 μL aliquot for GPC analysis was removed from the mixture and quenched with 0.5 mL ethylvinyl ether. To the remainder of the reaction mixture, **8** (71.0 mg, 0.314 mmol) in THF (0.2 mL) was added and the mixture was stirred for 1 minute. At this point, another 40 μL aliquot for GPC analysis was removed and quenched with 0.5 mL ethylvinyl ether. An additional 0.5 mL of ethylvinyl ether was added to the remainder of the reaction mixture and, after stirring for an additional 15 minutes, this quenched reaction mixture was pipetted into 100 mL of vigorously stirring methanol prior to collection by vacuum filtration as a white fibrous solid (62 mg, 60 %). ^{1}H NMR (700 MHz, $CDCl_3$): δ 7.52–7.93 (0.4H, bismuthAr*H*), 6.55–7.34 (5.8H, Ar*H*), 4.87–5.51 (2H, vinylic*H*), 2.23–3.23 (4.7H, allylic*H* and benzylic*H*), 1.65–2.22 (2.6H, alkyl*H*), 1.47–1.65 (0.9H, alkyl*H*), 1.00–1.47 (3.9H, alkyl*H*), 0.74–1.00 (2.9H, CH_3). M_n = 51 kDa, M_w = 63 kDa, PDI = 1.2, dn/dc = 0.14 mL/g by GPC (in THF).

General Micelle Formation from P12. P12 (between 0.3 mg and 3.0 mg depending on desired final concentration) was dissolved in 150 μL of THF with stirring. 2.85 mL of hexanes was added and the solution was incubated at 50 °C for one hour. The final solvent ratio was 5 % by volume THF in hexanes. The solution was allowed to cool to room temperature before analysis. Samples of final polymer concentration equal to 0.1 mg/mL, 0.3 mg/mL, 0.6 mg/mL, and 1.0 mg/mL were made and studied by dynamic light scattering.

3.5 Select NMR Data

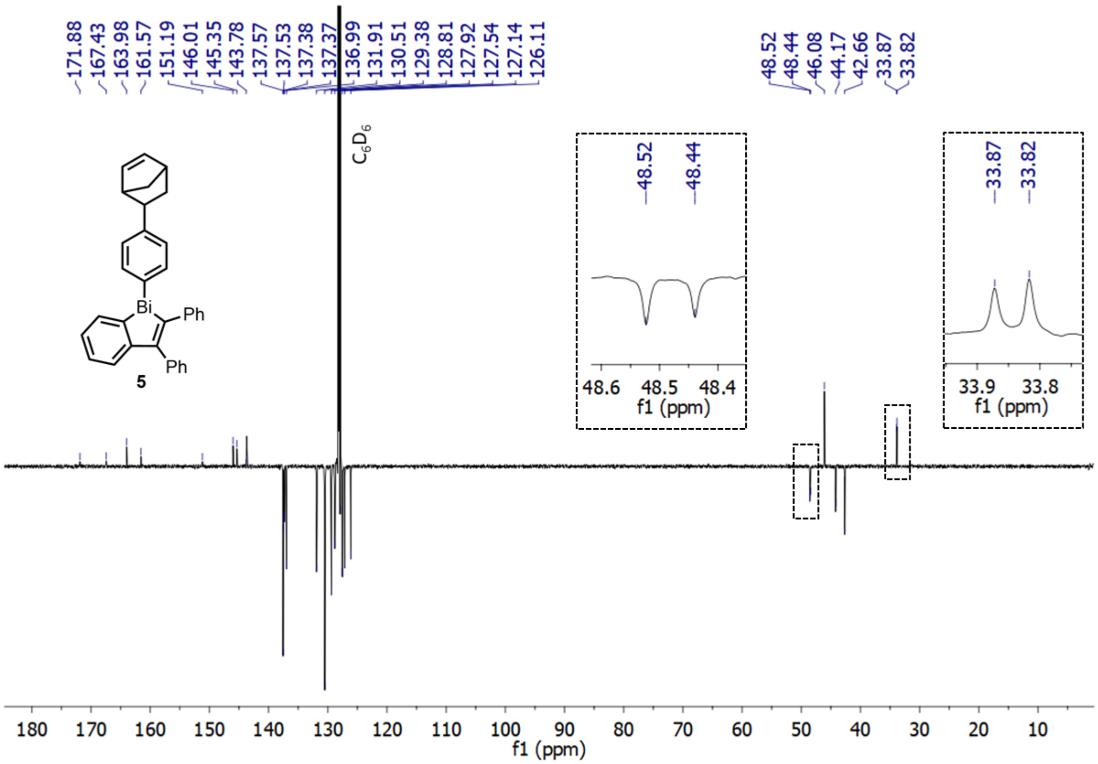

Figure 3.15. ^{13}C DEPTQ 135° NMR spectrum of compound **5** in C_6D_6. Insets show expanded regions displaying inequivalent signals for select carbon nuclei of *endo*- versus *exo*-norbornyl enantiomers.

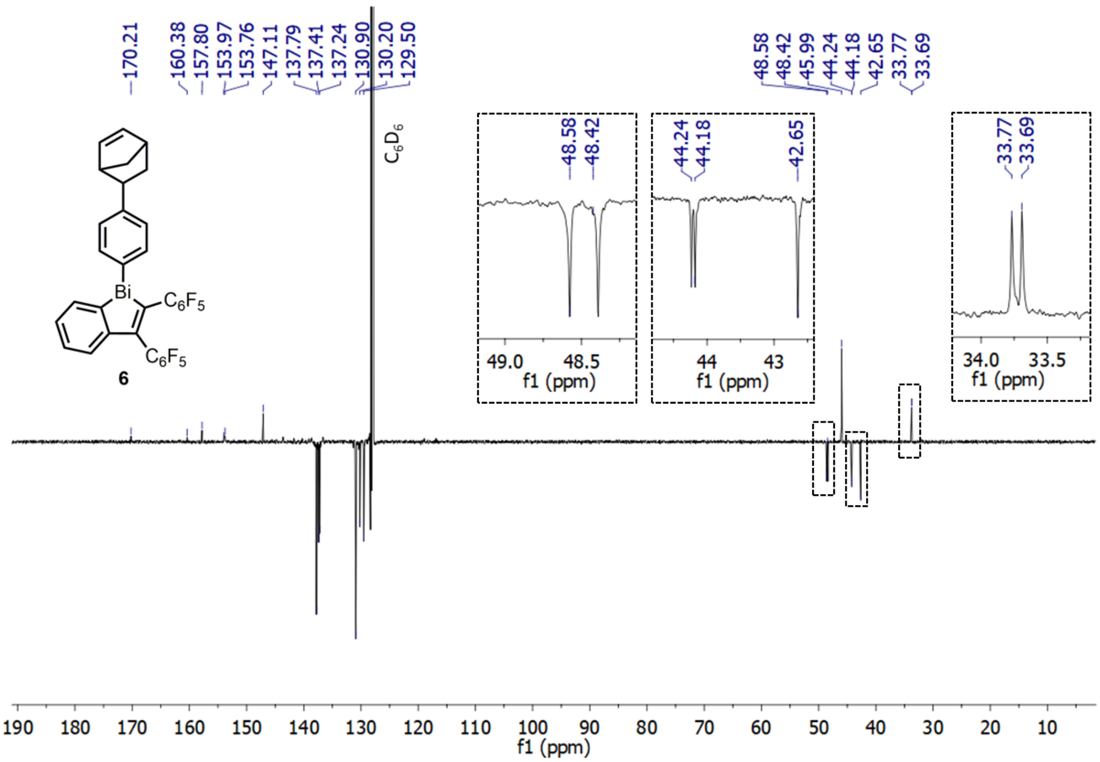

Figure 3.16. ^{13}C DEPTQ 135° NMR spectrum of compound **6** in C_6D_6. Insets show expanded regions displaying inequivalent signals for select carbon nuclei of *endo*- versus *exo*-norbornyl enantiomers.

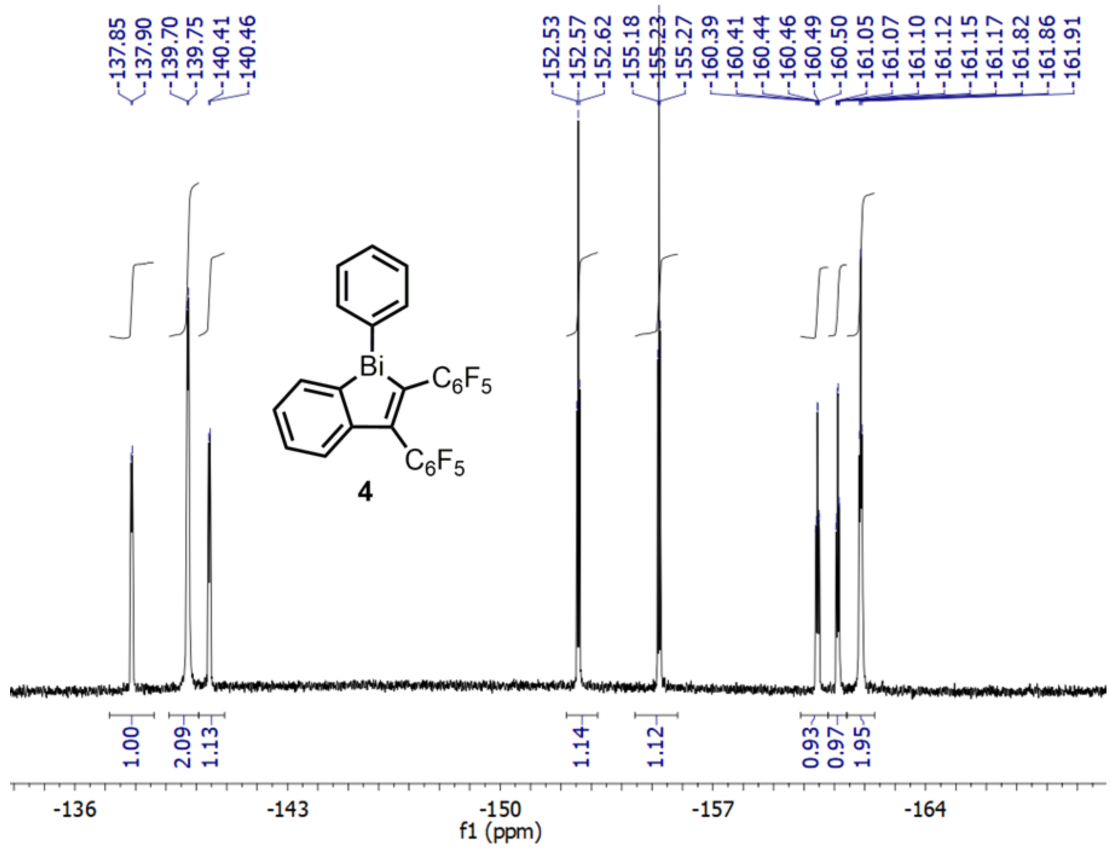

Figure 3.17. $^{19}F\{^{1}H\}$ NMR spectrum of 1-phenyl-2,3-bis(pentafluorophenyl)benzobismole (**4**) in C_6D_6.

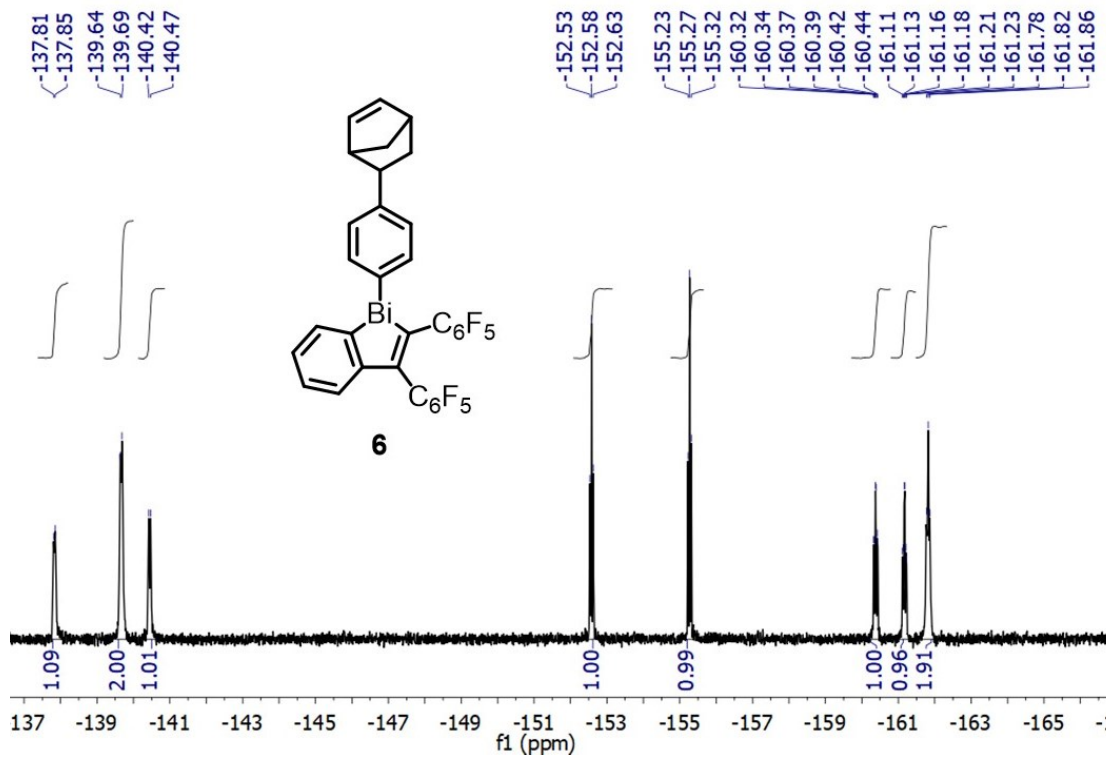

Figure 3.18. $^{19}F\{^{1}H\}$ NMR spectrum of 1-para-norbornenephenyl-2,3-bis(pentafluorophenyl)benzobismole (**6**) in C_6D_6.

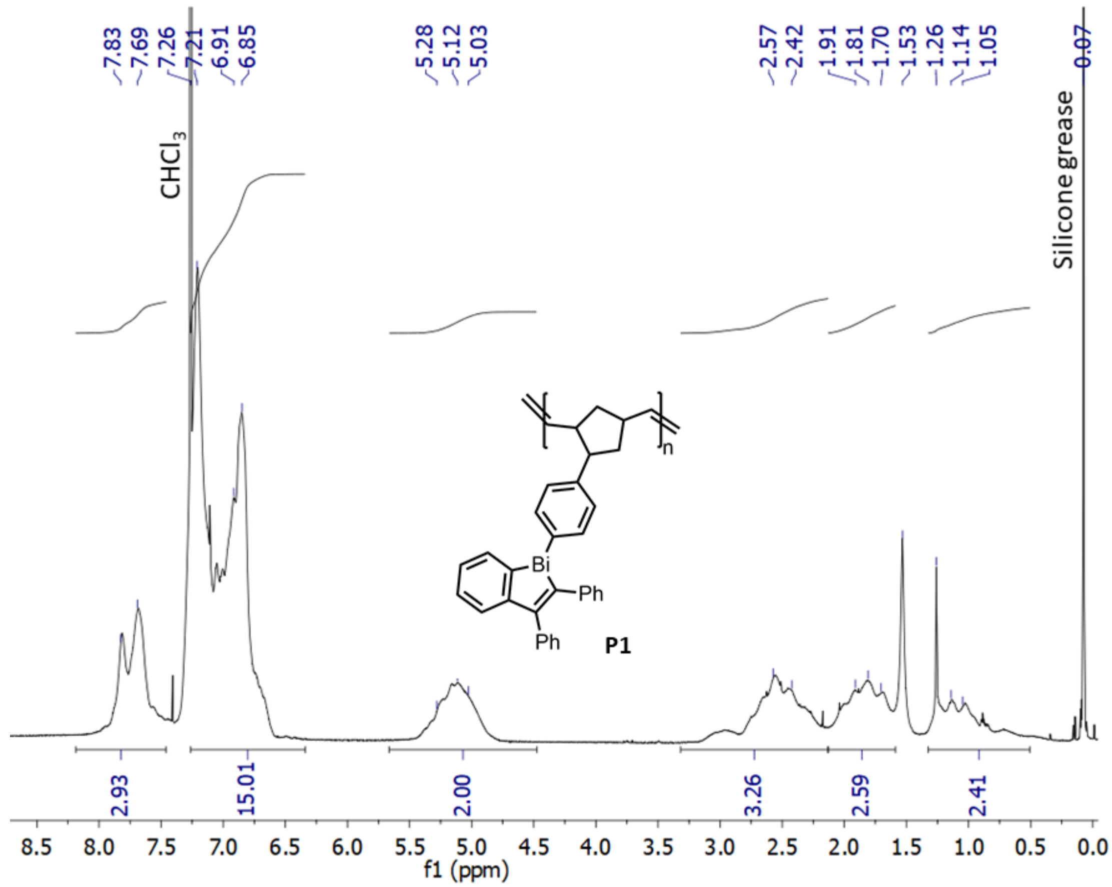

Figure 3.19. ^{1}H NMR spectrum of homopolymer **P1** in $CDCl_3$.

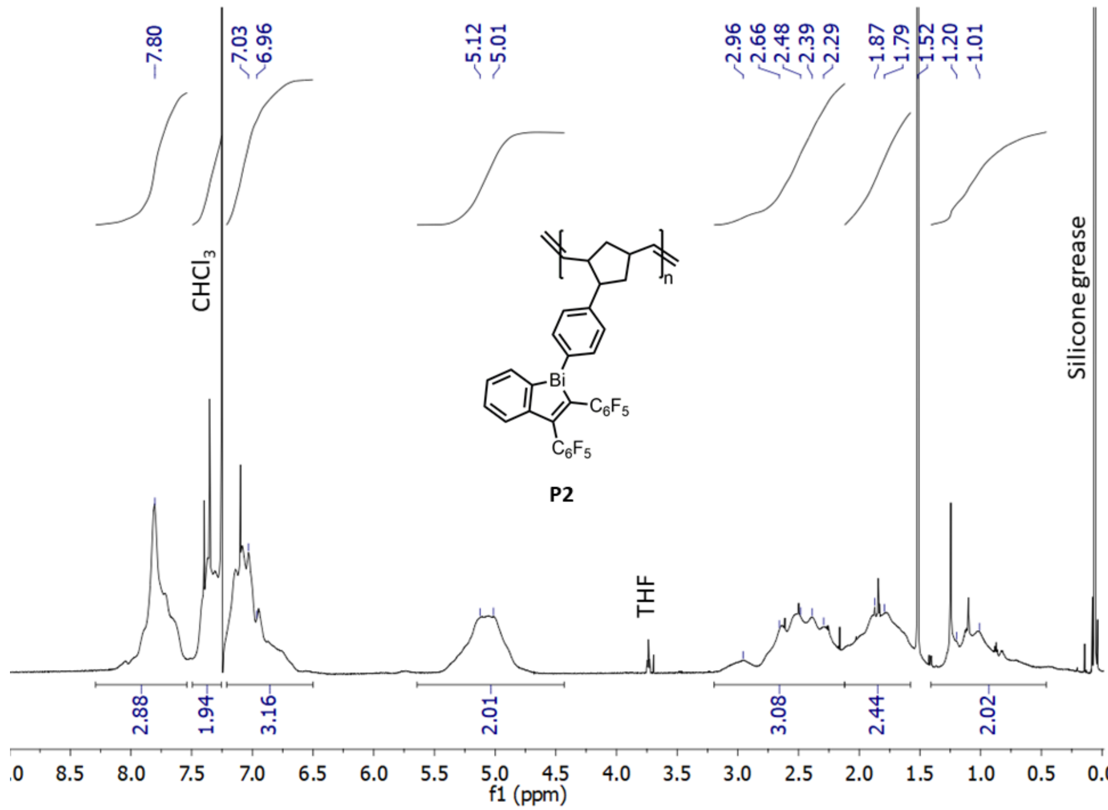

Figure 3.20. ^{1}H NMR spectrum of homopolymer **P2** in $CDCl_3$.

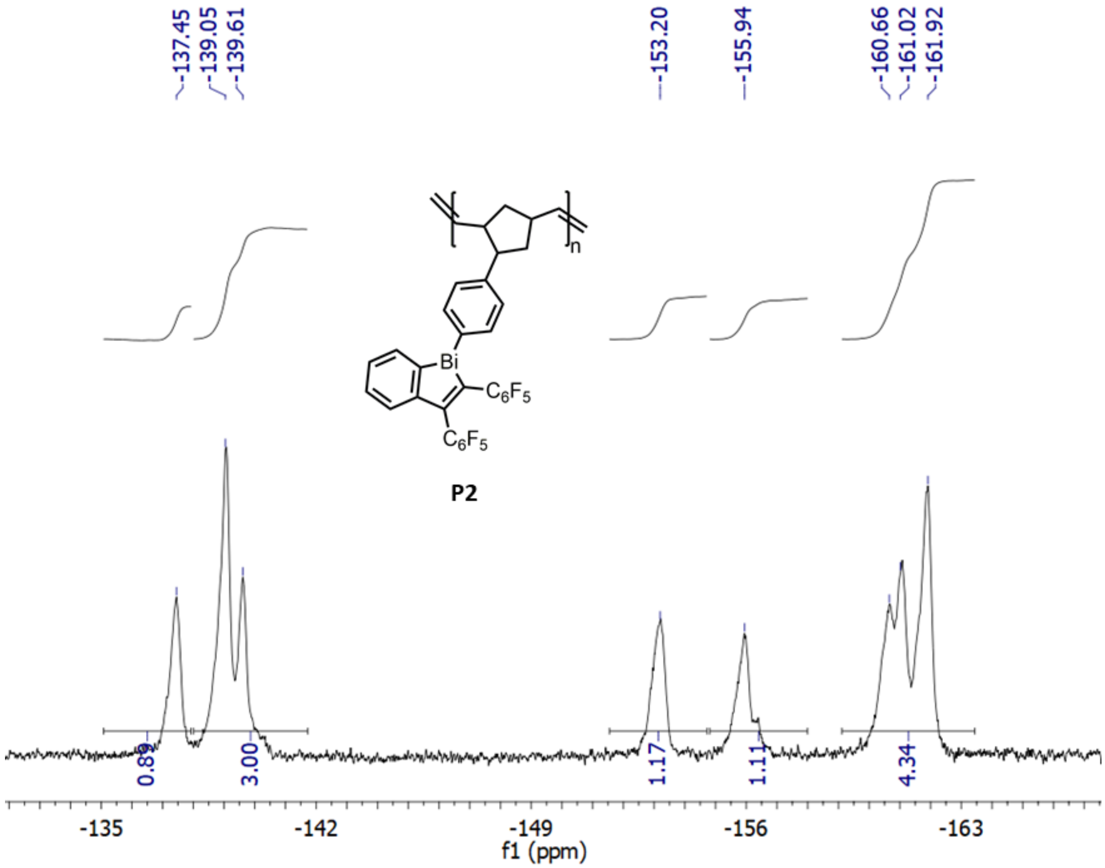

Figure 3.21. $^{19}F\{^{1}H\}$ NMR spectrum of homopolymer **P2** in $CDCl_3$.

3.6 Select PXRD Data

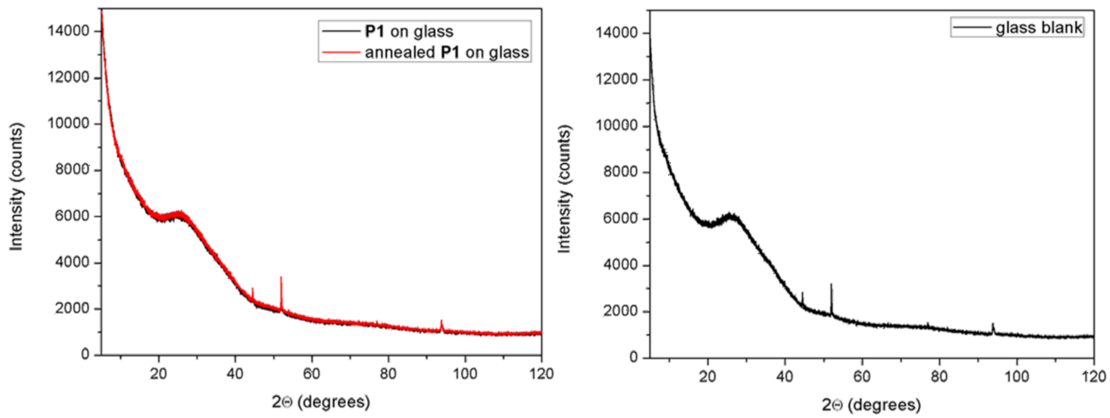

Figure 3.22. Powder XRD pattern for a film of **P1** before and after heat annealing at 120 °C for 45 minutes (left) compared to the PXRD pattern for the glass slide on which **P1** was studied (right).

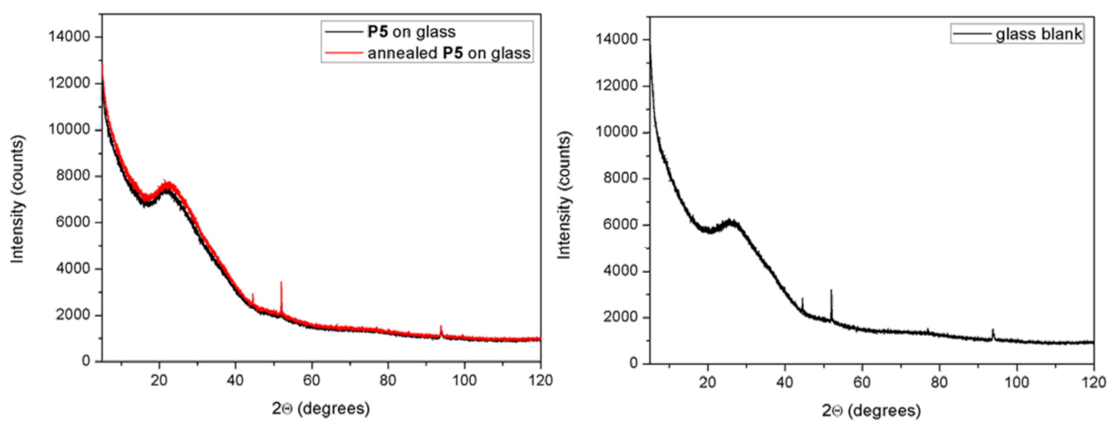

Figure 3.23. Powder XRD pattern for a film of **P5** before and after heat annealing at 120 °C for 45 minutes (left) compared to the PXRD pattern for the glass slide on which **P5** was studied (right).

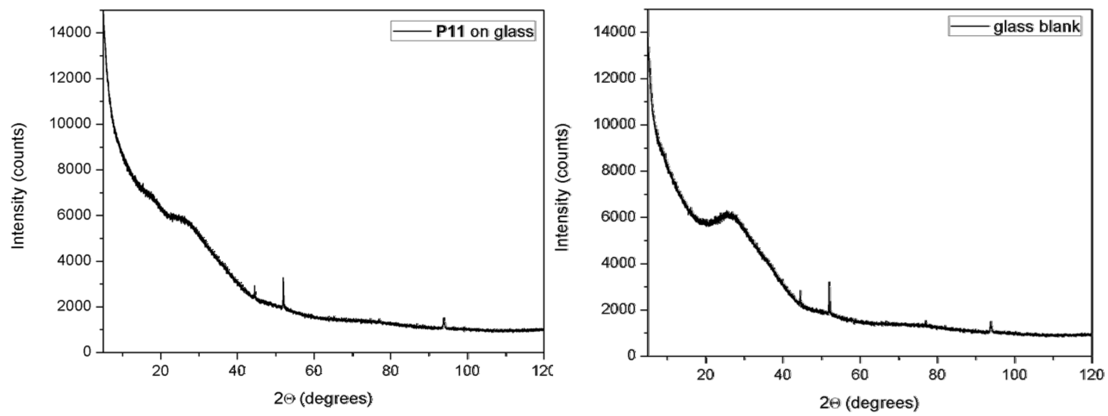

Figure 3.24. Powder XRD pattern for a powder sample of **P11** (left) compared to the PXRD pattern for the glass slide on which **P11** was studied (right).

3.7 Additional PL Data

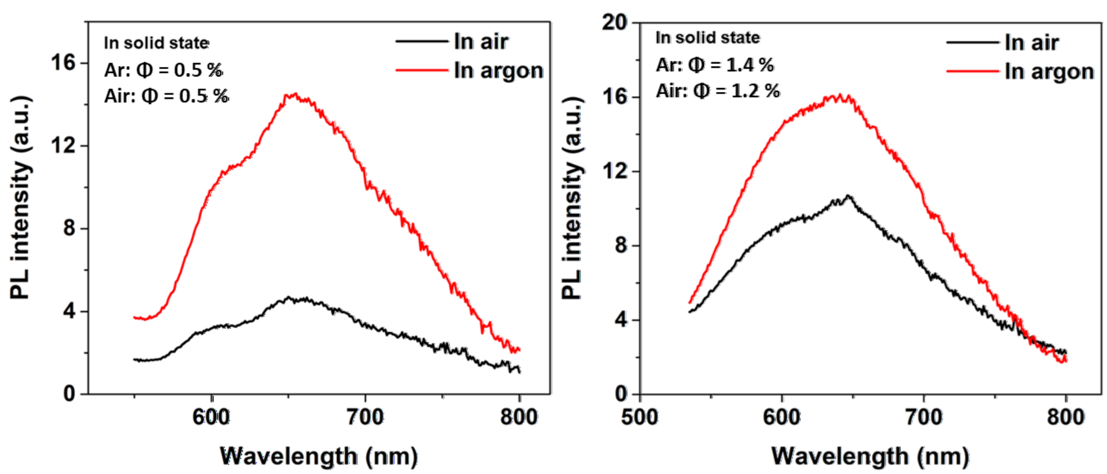

Figure 3.25. Emission plots of **3** (left) and **4** (right) comparing PL under Ar atmosphere compared to in air. Φ values indicate only very slight increases in emission intensity. Samples were measured as powders.

3.8 Select Thermogravimetric Analysis Data

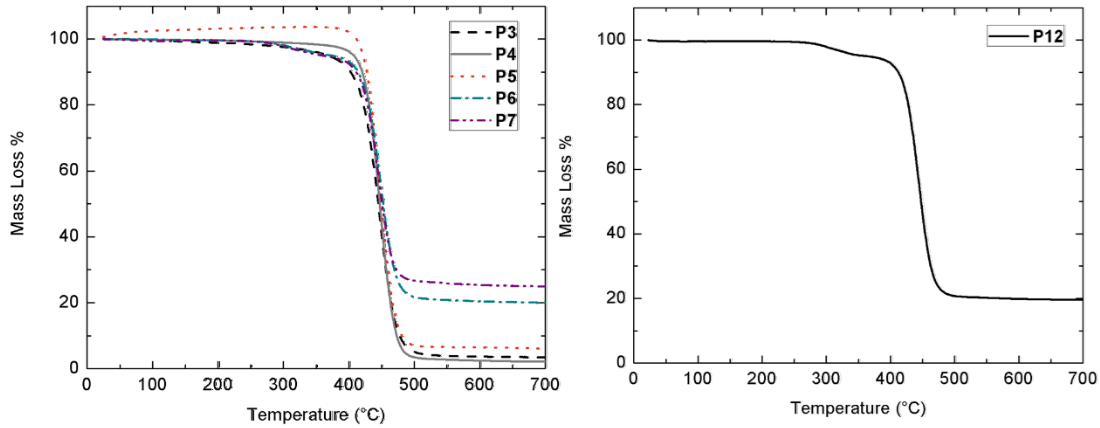

Figure 3.26. TGA plots of polymers **P3**, **P4**, **P5**, **P6**, and **P7** (left) and block copolymer **P12** (right) at a heating rate of 10 °C per minute under an N_2 atmosphere.

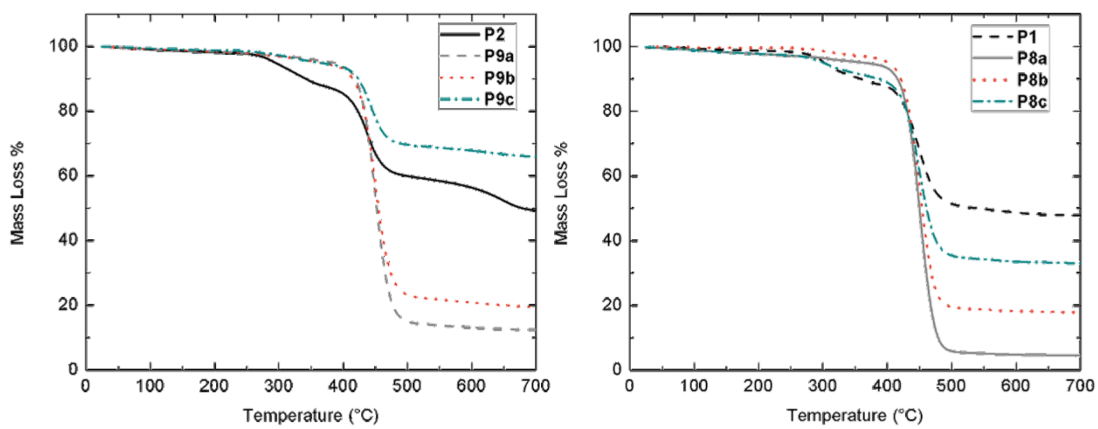

Figure 3.27. TGA plots of polymers **P2** and **P9** (left) and polymers **P1** and **P8** (right) at a heating rate of 10 °C per minute under an N_2 atmosphere.

3.9 Computational Methodology

Geometry optimizations of the gas phase structures were performed using density functional theory (DFT) with the B3LYP,[23] CAM-B3LYP,[24] and M06-2X[25] functionals and cc-pVTZ (for C, H and, if applicable, F)[34] as well as the cc-pVTZ-PP (for Bi)[35] basis sets; the cc-pVTZ-PP basis set uses the corresponding effective core potential (ECP) accounting for 60 electrons. Initial molecular geometries were taken from the experimentally obtained X-ray structures. The use of the cc-pVTZ and cc-pVTZ-PP basis sets will hereafter be referred to as cc-pVTZ(-PP). The basis sets as well as the ECP for the Bi atom have been obtained from the Basis Set Exchange Library.[36] Subsequent frequency analysis confirmed all obtained structures to be local minima on the potential energy surface. To calculate phosphorescence energies, the geometries of the lowest lying triplet states (T_1) of **3** and **4** were optimized by using UB3LYP (spin-unrestricted B3LYP) with the same basis sets as specified above. The dependence of the geometry on solvent effects has been tested by including the polarizable continuum model (IEF-PCM)[37] and universal force field (UFF) atomic radii) with THF as solvent for the geometry optimization at the B3LYP/cc-pVTZ(-PP) level of theory. The vertical excitation energies of the first ten singlet and triplet states of benzobismoles **3** and **4** have been predicted by TD-DFT computations using the (CAM-)B3LYP and M06-2X functionals as well as the cc-pVTZ(-PP) basis sets starting from the B3LYP optimized gas phase S_0 geometry (for B3LYP and M06-2X) and from the CAM-B3LYP optimized S_0 geometry (for CAM-B3LYP), respectively. The influence of THF on the absorption properties has also been predicted by TD-DFT computations at the B3LYP/cc-pVTZ(-PP) level of theory with the geometry optimized in the gas phase. Phosphorescence energies of benzobismoles **3** and **4** have been calculated as the difference of the energies at the U(CAM-)B3LYP optimized T_1 geometry and the (CAM-)B3LYP optimized S_0 geometry, as well as by performing a TD-DFT calculation at the optimized (CAM-)UB3LYP/cc-pVTZ(-PP) T_1 geometries. All computations have been carried out with the Gaussian16 software.[38] With bismuth being an element strongly influenced by relativistic effects, spin-orbit coupling was also considered using the TD-DFT framework[39] with the Amsterdam Density Functional (ADF) software.[40] The S_0 ground state optimized geometry of benzobismoles **3** and **4** were determined at the B3LYP/TZ2P level of theory[23,41] applying the "core small" option. Subsequent TD-DFT calculations to predict excitation energies have been performed at the B3LYP/TZ2P level of theory using the "core none" option. For the CAM-B3LYP functional, the final S_0 geometry derived from the Gaussian16 optimization has been used to save CPU-time. All calculations with the ADF software include scalar relativistic (ZORA)[42] and spin-orbit relativistic (SO) effects.[43] The presented molecular orbitals (MOs) were extracted from the Gaussian16 checkpoint files and are visualized with VMD.[44] The same software was used to present the superimposed structures of the optimized geometries.

3.9.1 Additional Computational Excited State Data for Benzobismoles 3 and 4

Table 3.2. TD-DFT calculated excited states of benzobismole **3** derived from the specified functionals using the cc-pVTZ(-PP) basis set.

B3LYP		B3LYP incl. THF		CAM-B3LYP		M06-2X	
States	E [eV] and f	States	E [eV] and f	States	E [eV] and f	States	E [eV] and f
T_1	2.6014 0.0000	T_1	2.6264 0.0000	T_1	2.6466 0.0000	T_1	3.0006 0.0000
T_2	3.4322 0.0000	T_2	3.4479 0.0000	T_2	3.4538 0.0000	T_2	3.7787 0.0000
T_3	3.6428 0.0000	T_3	3.6651 0.0000	T_3	3.5723 0.0000	T_3	3.9855 0.0000
S_1	3.7043 0.1730	S_1	3.6703 0.3629	T_4	3.5996 0.0000	T_4	4.0027 0.0000
T_4	3.7155 0.0000	T_4	3.7318 0.0000	T_5	3.9266 0.0000	S_1	4.1067 0.1983
T_5	3.8120 0.0000	T_5	3.8181 0.0000	S_1	4.1991 0.1943	T_5	4.1894 0.0000
T_6	3.9262 0.0000	T_6	3.9813 0.0000	T_6	4.2450 0.0000	T_6	4.2616 0.0000
S_2	3.9408 0.0051	S_2	4.0035 0.0250	T_7	4.3651 0.0000	T_7	4.3886 0.0000
T_7	4.0236 0.0000	T_7	4.0416 0.0000	T_8	4.3991 0.0000	S_2	4.4119 0.0454
T_8	4.0880 0.0000	S_3	4.1017 0.1337	T_9	4.4687 0.0000	T_8	4.4673 0.0000
T_9	4.1263 0.0000	T_8	4.1162 0.0000	T_{10}	4.6122 0.0000	T_9	4.5130 0.0000
S_3	4.1301 0.0675	T_9	4.1352 0.0000	S_2	4.6136 0.0511	T_{10}	4.6008 0.0000
T_{10}	4.2144 0.0000	T_{10}	4.2244 0.0000	S_3	4.7106 0.0393	S_3	4.6210 0.0408
S_4	4.4482 0.0015	S_4	4.4367 0.0025	S_4	4.9541 0.0151	S_4	4.8708 0.0165
S_5	4.5384 0.0010	S_5	4.5341 0.0177	S_5	5.1209 0.0320	S_5	4.9924 0.0462
S_6	4.5855 0.0381	S_6	4.5745 0.1080	S_6	5.1352 0.0597	S_6	5.0366 0.0000
S_7	4.6676 0.0597	S_7	4.6447 0.1946	S_7	5.2277 0.0661	S_7	5.1568 0.0406
S_8	4.6870 0.0248	S_8	4.6812 0.0068	S_8	5.3364 0.0060	S_8	5.3108 0.0508
S_9	4.7496 0.0218	S_9	4.7536 0.2098	S_9	5.4144 0.0053	S_9	5.3763 0.1065
S_{10}	4.7949 0.0127	S_{10}	4.8149 0.2080	S_{10}	5.4648 0.2087	S_{10}	5.4234 0.1534

Table 3.3. TD-DFT calculated excited states of benzobismole **4** derived from the specified functionals using the cc-pVTZ(-PP) basis set.

B3LYP		**B3LYP incl. THF**		**CAM-B3LYP**		**M06-2X**	
States	E [eV] and f	States	E [eV] and f	States	E [eV] and f	States	E [eV] and f
T_1	2.6630 0.0000	T_1	2.6922 0.0000	T_1	2.6729 0.0000	T_1	3.0627 0.0000
T_2	3.4642 0.0000	T_2	3.4696 0.0000	T_2	3.4445 0.0000	T_2	3.8004 0.0000
T_3	3.6428 0.0000	T_3	3.6544 0.0000	T_3	3.5497 0.0000	T_3	3.9360 0.0000
T_4	3.7052 0.0000	T_4	3.7184 0.0000	T_4	3.5929 0.0000	T_4	4.0722 0.0000
T_5	3.7704 0.0000	T_5	3.7791 0.0000	T_5	3.9174 0.0000	T_5	4.1075 0.0000
S_1	3.8217 0.1632	S_1	3.8070 0.3152	T_6	4.2378 0.0000	S_1	4.2361 0.1843
T_6	4.0276 0.0000	T_6	4.0350 0.0000	S_1	4.3059 0.1900	T_6	4.2363 0.0000
T_7	4.0801 0.0000	S_2	4.0570 0.1449	T_7	4.3992 0.0000	T_7	4.4494 0.0000
T_8	4.0819 0.0000	T_7	4.1145 0.0000	T_8	4.4440 0.0000	T_8	4.4799 0.0000
S_2	4.0901 0.0474	T_8	4.1505 0.0000	T_9	4.4725 0.0000	S_2	4.5121 0.0649
T_9	4.1269 0.0000	T_9	4.1595 0.0000	T_{10}	4.5213 0.0000	T_9	4.5554 0.0000
T_{10}	4.1596 0.0000	T_{10}	4.1677 0.0000	S_2	4.6734 0.0935	T_{10}	4.5850 0.0000
S_3	4.2349 0.0491	S_3	4.2641 0.0497	S_3	4.9111 0.0213	S_3	4.7664 0.0116
S_4	4.2808 0.055	S_4	4.3076 0.0111	S_4	4.9491 0.0156	S_4	4.8911 0.0466
S_5	4.4390 0.0163	S_5	4.4723 0.0549	S_5	5.0424 0.0305	S_5	4.9442 0.0777
S_6	4.4735 0.0087	S_6	4.5560 0.0223	S_6	5.1098 0.0274	S_6	4.9965 0.0058
S_7	4.5154 0.0069	S_7	4.5704 0.0084	S_7	5.1349 0.0174	S_7	5.1550 0.0152
S_8	4.5674 0.0027	S_8	4.6060 0.0917	S_8	5.2961 0.0080	S_8	5.3402 0.0130
S_9	4.6237 0.0292	S_9	4.6513 0.0088	S_9	5.3752 0.0150	S_9	5.3814 0.0234
S_{10}	4.7302 0.0307	S_{10}	4.7622 0.0697	S_{10}	5.4887 0.3850	S_{10}	5.4472 0.4011

Table 3.4. Nature of main transitions to low lying singlet states of benzobismoles **3** and **4** using the cc-pVTZ(-PP) basis set with a minimum weight of 10 %.

	B3LYP	**B3LYP incl. THF**	**CAM-B3LYP**	**M06-2X**
Transition Bismole 3	Weight [%]	Weight [%]	Weight [%]	Weight [%]
$S_0 – S_1$				
HOMO to LUMO	94.82	97.13	88.42	88.86
$S_0 – S_3$				
HOMO–1 to LUMO	82.55	66.54	17.29	70.95*
HOMO to LUMO+1	10.67	29.33	68.07	11.25*
Transition Bismole 4				
$S_0 – S_1$				
HOMO to LUMO	93.98	96.01	86.50	85.64
$S_0 – S_2$				
HOMO–4 to LUMO				11.76
HOMO–1 to LUMO	69.89	88.01	75.54	61.00
HOMO to LUMO+1	21.44			
$S_0 – S_3$				
HOMO–2 to LUMO		28.57	42.67	50.14
HOMO–1 to LUMO	21.35		14.24**	
HOMO to LUMO+1	64.67	62.19	12.31***	

* For M06-2X the HOMO–1 to LUMO transition is assigned to the S_0-S_2 transition.
** For CAM-B3LYP the 14.24 % is related to HOMO–1 to LUMO+1 transition.
*** For CAM-B3LYP the 12.31 % is related to HOMO–5 to LUMO transition.

Table 3.5. TD-DFT calculated excited states of benzobismole **3** derived from B3LYP/TZ2P (including ZORA and SOC).

States	E [eV] and f	S (%)	T (%)	States	E [eV] and f	S (%)	T (%)
1	0.0000 0.6766E-07	99.5 % GS		**22**	4.0309 0.1227E-01	29.5	69.9
2	2.6624 0.1495E-04	0.1	99.8	**23**	4.0619 0.1612E-03	0.8	98.8
3	2.6628 0.5791E-05	0.0	99.8	**24**	4.0697 0.2211E-03	3.9	95.6
4	2.6636 0.1399E-04	0.0	99.8	**25**	4.0967 0.7887E-02	17.3	76.4
5	3.4848 0.1352E-01	7.5	92.3	**26**	4.1188 0.6080E-02	12.9	85.8
6	3.4947 0.4206E-03	0.2	99.4	**27**	4.1262 0.5318E-03	1.2	95.9
7	3.4989 0.3340E-03	0.7	99.0	**28**	4.1334 0.2521E-03	0.3	98.9
8	3.6577 0.1133	61.3	36.0	**29**	4.1785 0.6190E-03	2.0	97.3
9	3.6962 0.8263E-03	0.4	98.1	**30**	4.1851 0.6251E-03	1.6	98.2
10	3.7105 0.4981E-02	3.0	96.6	**31**	4.2050 0.4248E-02	9.4	89.1
11	3.7125 0.3942E-01	21.3	77.9	**32**	4.2104 0.1865E-02	3.6	95.9
12	3.8140 0.7648E-03	3.6	96.0	**33**	4.2197 0.1836E-02	3.8	95.4
13	3.8175 0.3633E-03	0.6	98.6	**34**	4.2432 0.1045E-01	22.3	77.2
14	3.8195 0.9451E-04	0.5	99.4	**35**	4.4276 0.7480E-02	98.1	1.7
15	3.8596 0.2863E-02	22.2	77.0	**36**	4.4932 0.9612E-03	99.6	0.2
16	3.8793 0.1508E-02	1.6	97.9	**37**	4.6108 0.2616E-01	98.3	1.5
17	3.8818 0.2882E-02	3.8	95.4	**38**	4.6304 0.1246E-01	99.4	0.4
18	3.9099 0.5833E-02	62.3	37.0	**39**	4.6616 0.6952E-02	99.5	0.4
19	3.9549 0.2959E-03	1.9	97.2	**40**	4.6951 0.4017E-01	97.6	2.1
20	3.9581 0.2480E-03	0.0	99.4	**41**	4.7276 0.8340E-01	97.8	2.0
21	3.9689 0.4042E-02	3.4	96.3				

Table 3.6. TD-DFT calculated excited states of benzobismole **3** derived from CAM-B3LYP/TZ2P (including ZORA and SOC).

States	E [eV] and f	S (%)	T (%)	States	E [eV] and f	S (%)	T (%)
1	0.00000 0.1214E-06	99.2 % GS		**22**	4.3715 0.2985E-02	2.1	97.6
2	2.77524 0.2617E-04	0.0	99.9	**23**	4.3906 0.1333E-02	3.0	96.8
3	2.77582 0.5772E-05	0.0	99.9	**24**	4.4095 0.2955E-03	0.4	99.4
4	2.77635 0.6269E-05	0.0	100.0	**25**	4.4360 0.3164E-02	4.2	95.6
5	3.59153 0.8625E-04	0.0	99.8	**26**	4.4689 0.2877E-02	3.6	96.2
6	3.59263 0.6658E-04	0.0	99.7	**27**	4.4878 0.4524E-03	0.8	99.0
7	3.59473 0.2238E-03	0.0	99.7	**28**	4.5177 0.2618E-02	5.8	93.9
8	3.72856 0.3249E-04	0.0	99.8	**29**	4.5306 0.1824E-02	3.0	96.1
9	3.72948 0.1307E-04	0.0	99.8	**30**	4.6259 0.1413E-01	32.4	67.4
10	3.73006 0.1812E-04	0.0	99.8	**31**	4.6333 0.3816E-03	0.8	98.9
11	3.75480 0.1753E-04	0.0	99.8	**32**	4.6393 0.6375E-03	0.9	99.0
12	3.75581 0.1944E-04	0.0	99.8	**33**	4.6638 0.2304E-01	52.9	46.7
13	3.75672 0.1610E-04	0.0	99.8	**34**	4.7272 0.4728E-01	94.3	5.5
14	4.02292 0.1568E-02	1.3	98.2	**35**	4.9678 0.2024E-01	97.9	1.9
15	4.03507 0.2031E-02	1.2	98.5	**36**	5.1291 0.6017E-01	98.2	1.6
16	4.04059 0.1268E-02	0.8	99.0	**37**	5.1619 0.3329E-01	97.2	2.6
17	4.21555 0.1037	52.1	47.4	**38**	5.2437 0.5584E-01	96.8	3.1
18	4.27565 0.2223E-01	11.7	87.5	**39**	5.3364 0.5094E-02	99.9	0.0
19	4.29263 0.1850E-01	10.6	88.5	**40**	5.4104 0.8442E-02	99.7	0.1
20	4.30917 0.4322E-01	22.8	76.8	**41**	5.4691 0.2110	99.7	0.1
21	4.37372 0.3612E-02	2.8	96.9				

Table 3.7. TD-DFT calculated excited states of benzobismole **3** derived from M06-2X/TZ2P (including ZORA and SOC).

States	E [eV] and f	S (%)	T (%)	States	E [eV] and f	S (%)	T (%)
1	0.00000 0.2646E-06	99.1% GS		**22**	4.14365 0.3993E-01	20.1	79.8
2	1.66920 0.7581E-05	0.0	100.0	**23**	4.16994 0.2094E-02	1.6	98.2
3	1.66956 0.4956E-05	0.0	100.0	**24**	4.21159 0.1871E-02	2.3	97.4
4	1.66989 0.2084E-05	0.0	100.0	**25**	4.21818 0.2429E-02	4.5	95.4
5	2.47048 0.1512E-05	0.0	99.8	**26**	4.23882 0.3559E-02	3.1	96.7
6	2.47068 0.4761E-05	0.0	99.8	**27**	4.27788 0.7606E-02	10.1	89.7
7	2.47121 0.1015E-04	0.0	99.8	**28**	4.30257 0.6388E-03	1.2	98.4
8	2.50181 0.8822E-06	0.0	99.8	**29**	4.32284 0.1680E-02	3.2	96.6
9	2.50196 0.5914E-06	0.0	99.8	**30**	4.37480 0.8649E-02	15.2	84.7
10	2.50204 0.5015E-06	0.0	99.8	**31**	4.40613 0.3815E-02	7.1	92.8
11	2.52631 0.1728E-05	0.0	99.8	**32**	4.45808 0.9458E-03	2.8	97.0
12	2.52636 0.6944E-05	0.0	99.9	**33**	4.58179 0.3413E-01	66.3	33.5
13	2.52650 0.3007E-05	0.0	99.8	**34**	4.71540 0.2243E-01	95.0	4.9
14	3.15455 0.1165E-04	0.0	99.8	**35**	4.92220 0.6972E-02	98.3	1.5
15	3.15547 0.5552E-05	0.0	99.8	**36**	5.08757 0.1404E-01	95.6	4.3
16	3.15692 0.2451E-04	0.0	99.8	**37**	5.11678 0.5326E-01	96.4	3.4
17	3.91512 0.3369E-02	2.8	97.1	**38**	5.20134 0.7140E-01	96.9	2.9
18	3.93818 0.1561E-02	1.6	98.0	**39**	5.29533 0.2547E-01	99.9	0.0
19	3.94937 0.1899E-01	10.1	89.6	**40**	5.38223 0.9198E-01	99.6	0.2
20	4.10610 0.5680E-01	30.0	69.9	**41**	5.39450 0.1714	99.4	0.4
21	4.11636 0.6848E-01	34.8	65.1				

Table 3.8. TD-DFT calculated excited states of benzobismole **4** derived from B3LYP/TZ2P (including ZORA and SOC).

States	E [eV] and f	S (%)	T (%)	States	E [eV] and f	S (%)	T (%)
1	0.0000 0.1087E-06	99.6% GS		**22**	4.0423 0.1858E-03	0.4	99.5
2	2.6877 0.4504E-04	0.0	99.8	**23**	4.0425 0.8704E-05	0.0	99.9
3	2.6879 0.6443E-05	0.0	99.8	**24**	4.0647 0.1103E-01	29.9	69.1
4	2.6884 0.1362E-04	0.0	99.9	**25**	4.0858 0.3568E-03	1.1	98.6
5	3.5267 0.1936E-02	1.1	98.7	**26**	4.0896 0.3890E-02	5.0	94.8
6	3.5293 0.4127E-03	0.4	99.2	**27**	4.1013 0.1441E-01	42.4	56.4
7	3.5407 0.3410E-02	3.1	96.6	**28**	4.1400 0.4957E-02	22.1	77.3
8	3.6712 0.2967E-01	17.8	81.5	**29**	4.1693 0.5878E-03	1.0	98.4
9	3.6914 0.7698E-03	0.8	98.6	**30**	4.1806 0.1081E-01	20.6	79.0
10	3.6981 0.1497E-03	0.3	99.3	**31**	4.1960 0.2978E-01	52.6	46.8
11	3.7427 0.1207	70.4	29.2	**32**	4.2021 0.4458E-02	19.3	80.5
12	3.8073 0.8985E-03	0.7	99.1	**33**	4.2219 0.1187E-02	2.7	96.3
13	3.8079 0.6882E-03	0.4	99.4	**34**	4.2539 0.1332E-01	35.5	63.8
14	3.8093 0.1036E-02	0.7	99.0	**35**	4.2655 0.1350E-01	81.8	18.5
15	3.8268 0.2424E-02	2.8	96.9	**36**	4.2838 0.1137E-01	59.2	39.6
16	3.8357 0.3214E-03	0.3	99.5	**37**	4.4036 0.8210E-02	99.2	0.6
17	3.8381 0.6693E-02	4.1	95.7	**38**	4.4655 0.1877E-01	96.0	3.7
18	3.9886 0.8955E-02	25.1	73.2	**39**	4.5509 0.1378E-02	99.7	0.1
19	4.0124 0.1760E-02	2.7	95.9	**40**	4.6484 0.1408E-01	97.9	2.0
20	4.0161 0.2464E-03	0.5	98.4	**41**	4.6917 0.2175E-01	97.7	2.1
21	4.0420 0.2857E-03	0.6	99.2				

Table 3.9. TD-DFT calculated excited states of benzobismole **4** derived from CAM-B3LYP/TZ2P (including ZORA and SOC).

States	E [eV] and f	S (%)	T (%)	States	E [eV] and f	S (%)	T (%)
1	0.00000 0.7287E-07	99.1% GS		**22**	4.45205 0.8170E-02	4.9	94.6
2	2.81036 0.1705E-04	0.0	99.2	**23**	4.46508 0.3528E-02	3.2	96.1
3	2.81096 0.4907E-05	0.0	99.4	**24**	4.53948 0.3740E-02	4.3	95.6
4	2.81129 0.7926E-05	0.0	99.9	**25**	4.54876 0.1583E-03	0.1	99.8
5	3.61475 0.2539E-04	0.0	99.8	**26**	4.54879 0.9208E-05	0.0	99.9
6	3.61531 0.4527E-04	0.0	99.8	**27**	4.54932 0.1609E-03	0.2	99.7
7	3.61857 0.2077E-03	0.2	99.6	**28**	4.56841 0.5855E-02	7.0	92.8
8	3.73705 0.2883E-04	0.1	99.8	**29**	4.58717 0.1479E-02	1.5	98.3
9	3.73823 0.2971E-04	0.0	99.8	**30**	4.62335 0.1608E-02	1.9	97.9
10	3.73881 0.1271E-04	0.0	99.8	**31**	4.62752 0.3722E-03	0.5	99.3
11	3.75495 0.1230E-04	0.0	99.8	**32**	4.63302 0.6379E-03	0.5	99.3
12	3.75554 0.9469E-05	0.0	99.8	**33**	4.75129 0.8367E-01	87.7	12.1
13	3.75613 0.5914E-05	0.0	99.8	**34**	4.98140 0.2338E-01	96.6	3.2
14	4.01565 0.7669E-03	1.0	98.9	**35**	5.00907 0.1566E-01	97.7	2.1
15	4.02868 0.5938E-03	0.6	99.1	**36**	5.09807 0.3775E-01	96.6	3.2
16	4.03245 0.5726E-03	0.5	99.4	**37**	5.16940 0.2406E-01	95.7	4.1
17	4.26637 0.2325E-01	13.0	85.5	**38**	5.21432 0.1402E-01	99.9	0.0
18	4.29372 0.1095E-02	1.0	98.7	**39**	5.37944 0.8848E-02	100	0.0
19	4.31228 0.5289E-02	3.7	96.1	**40**	5.40544 0.1463E-01	99.8	0.0
20	4.37957 0.1491	77.5	22.3	**41**	5.54788 0.3924	99.6	0.2
21	4.43141 0.2767E-02	3.0	96.6				

Table 3.10. TD-DFT calculated excited states of benzobismole **4** derived from M06-2X/TZ2P (including ZORA and SOC).

States	E [eV] and f	S (%)	T (%)	States	E [eV] and f	S (%)	T (%)
1	0.00000 0.1246E-06	99.0% GS		**22**	4.19903 0.2598E-02	4.9	95.0
2	1.65836 0.8720E-05	0.0	100.0	**23**	4.21403 0.8966E-01	47.2	52.6
3	1.65867 0.3128E-05	0.0	100.0	**24**	4.25572 0.4928E-01	28.8	73.0
4	1.65895 0.1848E-05	0.0	99.8	**25**	4.30657 0.1521E-01	9.0	90.7
5	2.45122 0.2989E-05	0.0	99.8	**26**	4.32240 0.8144E-03	0.8	99.0
6	2.45132 0.1967E-05	0.0	99.8	**27**	4.32497 0.1951E-03	0.1	99.8
7	2.45192 0.1352E-04	0.0	99.9	**28**	4.32556 0.5681E-04	0.0	99.9
8	2.48973 0.5369E-06	0.0	99.9	**29**	4.33799 0.1267E-02	2.2	97.4
9	2.48980 0.2892E-06	0.0	99.9	**30**	4.40735 0.4090E-02	5.8	94.0
10	2.48983 0.2936E-06	0.0	99.9	**31**	4.42738 0.7236E-02	10.3	89.6
11	2.52914 0.3125E-05	0.0	99.8	**32**	4.48641 0.2674E-02	2.8	97.0
12	2.52940 0.5169E-05	0.0	99.9	**33**	4.65195 0.5403E-01	80.9	18.9
13	2.52961 0.1643E-05	0.0	99.9	**34**	4.84885 0.1530E-01	93.9	5.9
14	3.13769 0.8442E-05	0.0	99.8	**35**	4.99466 0.2281E-01	96.0	3.8
15	3.13869 0.6972E-05	0.0	99.9	**36**	5.03895 0.2726E-01	95.6	4.3
16	3.14023 0.1850E-04	0.0	99.9	**37**	5.13374 0.3356E-01	93.5	6.3
17	3.93557 0.1256E-02	1.4	98.3	**38**	5.19791 0.1829E-01	99.9	0.0
18	3.95667 0.2448E-03	0.7	99.1	**39**	5.35902 0.1999E-01	99.9	0.0
19	3.97660 0.8849E-02	6.1	93.5	**40**	5.36260 0.7542E-02	99.9	0.0
20	4.16322 0.2673E-01	14.8	85.1	**41**	5.45175 0.3927	99.1	0.7
21	4.18032 0.1478E-02	2.3	97.6				

3.10 X-Ray Crystallographic Data

Crystals of appropriate quality for X-ray diffraction studies were removed from a vial and immediately covered with a thin layer of hydrocarbon oil (Paratone-N). A suitable crystal was then selected, attached to a glass fiber, and quickly placed in a glass vial. All data were collected using a Bruker APEX II CCD detector/D8 diffractometer using Mo/Cu Kα radiation. The data were corrected for absorption through Gaussian integration from indexing of the crystal faces. Structures were solved using the direct methods programs SHELXS-97,[45] and refinements were completed using the program SHELXL-97.[45]

Table 3.11. Crystallographic data for compounds **1–4**.

Compound	**1**	**2**	**3**	**4**
Formula	$C_{30}H_{24}Zr$	$C_{33.5}H_{18}F_{10}Zr$	$C_{26}H_{19}Bi$	$C_{27}H_{11}BiCl_2F_{10}$
Formula weight	475.71	701.70	540.39	805.24
Crystal system	Orthorhombic	Monoclinic	Monoclinic	Monoclinic
Space group	$Pca2_1$	$I2/a$	$P2_1/c$	$P2_1/c$
a (Å)	7.84545(14)	15.7609(3)	12.1357(2)	11.1522(2)
b (Å)	19.2995(4)	15.0677(3)	5.86680(10)	29.2609(6)
c (Å)	14.9618(3)	24.1451(5)	27.1289(5)	8.1580
α (°)	--	--	--	--
β (°)	--	94.3177(8)	91.8645(6)	104.8259(10)
γ (°)	--	--	--	--
V (Å^3)	2265.42(8)	5717.7(2)	1930.49(6)	2573.52(10)
Z	4	8	4	4
ρ (g/cm^3)	1.395	1.630	1.859	2.078
Abs coeff (mm^{-1})	4.063	3.960	17.95	16.19
T (K)	173	173	173	173
$2\theta_{max}$ (°)	147.90	147.95	147.73	147.92
Total data	15024	20121	13052	17880
Unique data (R_{int})	4422(0.0328)	5778(0.0311)	3813(0.0229)	5194(0.0402)
Obs data [I>2(σ(I)]	4380	5531	3780	5001
Params	281	380	244	361
R_1 [I>2(σ(I)]^a	0.0253	0.0367	0.0209	0.0307
wR_2 [all data]^a	0.0642	0.1108	0.0483	0.0837
Max/min $\Delta\rho$ (e$^-$Å^{-3})	0.766/–1.295	1.041/–0.952	1.140/–0.946	2.151/–1.392

$^aR_1 = \Sigma||F_o| - |F_c||/\Sigma|F_o|$; $wR_2 = [\Sigma w(F_o^2 - F_c^2)^2/\Sigma w(F_o^4)]^{1/2}$

3.11 References

1. (a) Grimsdale, A. C.; Chan, K. L.; Martin, R. E.; Jokisz, P. G.; Holmes, A. B. *Chem. Rev.* **2009**, *109*, 897–109. (b) Parke, S. P.; Boone, M. P.; Rivard, E. *Chem. Commun.* **2016**, *52*, 9485−9505. (c) Wang, C.; Taki, M.; Sato, Y.; Fukazawa, A.; Higashiyama, T.; Yamaguchi, S. *J. Am. Chem. Soc*. **2017**, *139*, 10374−10381. (d) Grzybowski, M.; Taki, M.; Senda, K.; Sato, Y.; Ariyoshi, T.; Okada, Y.; Kawakami, R.; Imamura, T.; Yamaguchi, S. *Angew. Chem. Int. Ed*. **2018**, *57*, 10137−10141.

2. (a) Baumgartner, T.; Réau, R. *Chem Rev.* **2006**, *106*, 4681–4727. (b) Cheng, Y.-J.; Yang, S.-H.; Hsu, C.-S. *Chem. Rev*. **2009**, *109*, 5868−5923. (c) Baggett, A. W.; Guo, F.; Li, B.; Liu, S.-Y.; Jäkle, F. *Angew. Chem. Int. Ed*. **2015**, *54*, 11191−11195. (d) Zhang, C.; Zhu, X. *Acc. Chem. Res.* **2017**, *50*, 1342−1350. (e) Stolar, M.; Baumgartner, T. *Chem. Commun.* **2018**, *54*, 3311−3322.

3. (a) Jia, W.-L.; Liu, Q.-D.; Wang, R.; Wang, S. *Organometallics* **2003**, *22*, 4070−4078. (b) He, G.; Kang, L.; Torres Delgado, W.; Shynkaruk, O.; Ferguson, M. J.; McDonald, R.; Rivard, E. *J. Am. Chem. Soc.* **2013**, *135*, 5360−5363. (c) Linshoeft, J.; Baum, E. J.; Hussain, A.; Gates, P. J.; Näther, C.; Staubitz, A. *Angew. Chem. Int. Ed.* **2014**, *53*, 12916−12920. (d) Carrera, E. I.; Seferos, D. S. *Macromolecules* **2015**, *48*, 297−308. (e) Matsumoto, T.; Tanaka, K.; Tanaka, K.; Chujo, Y. *Dalton Trans.* **2015**, *44*, 8697–8707. (f) Ho, P. C.; Szydlowski, P.; Sinclair, J.; Elder, P. J. W.; Kubel, J.; Gendy, C.; Lee, L. M.; Jenkins, H.; Britten, J. F.; Morim, D. R.; Vargas-Baca, I. *Nat. Commun.* **2016**, *7*, 11299. (g) Yang, L.; Gu, W.; Lv, L.; Chen, Y.; Yang, Y.; Ye, P.; Wu, J.; Hong, L.; Peng, A.; Huang, H. *Angew. Chem. Int. Ed*. **2018**, *57*, 1096−1102. (h) Li, G.; Xu, L.; Zhang, W.; Zhou, K.; Ding, Y.; Liu, F.; He, X.; He, G. *Angew. Chem. Int. Ed.* **2018**, *57*, 4897−4901.

4. (a) He, G.; Torres Delgado, W.; Schatz, D. J.; Merten, C.; Mohammadpour, A.; Mayr, L.; Ferguson, M. J.; McDonald, R.; Brown, A.; Shankar, K.; Rivard, E. *Angew. Chem. Int. Ed.* **2014**, *53*, 4587−4591. (b) He, G.; Wiltshire, B. D.; Choi, P.; Savin, A.; Sun, S.; Mohammadpour, A.; Ferguson, M. J.; McDonald, R.; Farinezhad, S.; Brown, A.; Shankar, K.; Rivard, E. *Chem. Commun.* **2015**, *51*, 5444−5447. (c) Kremer, A.; Fermi, A.; Biot. N.; Wouters, J.; Bonifazi, D. *Chem.*

Eur. J. **2016**, *22*, 5665−5675. (d) Xu, L.; Li, G.; Zhang, W.; Zhang, S.; Yin, S.; An, Z.; He, G. *Chem. Commun.* **2018**, *54*, 9226−9229.

5. (a) Baldo, M. A.; Lamansky, S.; Burrows, P. E.; Thompson, M. E.; Forrest, S. R. *Appl. Phys. Lett*. **1999**, *75*, 4–6. (b) Evans, R. C.; Douglas, P.; Winscom, C. J. *Coord. Chem. Rev*. **2006**, *250*, 2093−2126. (c) Chi, Y.; Chang, T.-K.; Ganesan, P.; Rajakumu, P. *Coord. Chem. Rev.* **2017**, *346*, 91−100.

6. (a) Fleetham, T.; Li, G.; Li, J. *Adv. Mater*. **2017**, *29*, 1601861. (b) Powell, B. J. *Coord. Chem. Rev.* **2015**, *295*, 46−79.

7. (a) Ohshita, J.; Matsui, S.; Yamamoto, R.; Mizumo, T.; Ooyama, Y.; Harima, T.; Murafuji, T.; Tao, K.; Kuramochi, Y.; Kaikoh, T.; Higashimura, H. *Organometallics* **2010**, *29*, 3239−3241. For related work, see: (b) Parke, S. M.; Narreto, M. A. B.; Hupf, E.; McDonald, R.; Ferguson, M. J.; Hegmann, F. A.; Rivard, E. *Inorg. Chem.* **2018**, *57*, 7536−7549. (c) Morisaki, Y.; Ohashi, K.; Na, H.-S.; Chujo, Y. *J. Polym. Sci., Part A: Polym. Chem.* **2006**, *44*, 4857−4863. The small Stokes shift involved in the luminescence within the reported bismole copolymer in ref. 7c suggests emission via fluorescence.

8. (a) Sano, Y.; Satoh, H.; Chiba, M.; Okamoto, M.; Serizawa, K.; Nakashima, H.; Omae, K. *J. Occup. Health*, **2005**, *47*, 293−298. (b) Yang, N.; Sun, H. *Coord. Chem. Rev.* **2007**, *251*, 2354−2366.

9. Xu, F.; Kim, H. U.; Kim, J.-H.; Jung, B. J. Grimsdale, A. C.; Hwang, D.-H. *Prog. Polym. Sci.* **2015**, *47*, 92−121.

10. (a) Chai, J.; Wang, D.; Fan, X.; Buriak, J. M. *Nat. Nanotech.* **2007**, *2*, 500−506. (b) Schacher, F. H.; Rupar, P. A.; Manners, I. *Angew. Chem. Int. Ed.* **2012**, *51*,

7898−7921. (c) Qiu, H.; Gao, Y.; Bott, C. E.; Gould, O. E. C.; Harniman, R. L.; Miles, M. J.; Webb, S. E. D.; Winnik, M. A.; Manners, I. *Science* **2016**, *352*, 697−701.

11. (a) You, Y. *Curr. Opinion Chem. Biol.* **2013**, *17*, 699−707. (b) Xiang, H.; Cheng, J.; Ma, X.; Zhou, X.; Chruma, J. J. *Chem. Soc. Rev.* **2013**, *42*, 6128−6185. (c) Ali Fateminia, S. M.; Mao, Z.; Xu, S.; Yang, Z.; Chi, Z.; Liu, B. *Angew. Chem. Int. Ed*. **2017**, *56*, 12160−12164.

12. (a) Robinson, G. W.; Frosch, R. P. *J. Chem. Phys.* **1963**, *38*, 1187−1203. (b) Engleman, R.; Jortner, J. *Mol. Phys.* **1970**, *18*, 145−164.

13. (a) Mukherjee, S.; Thilagar, P. *Chem. Commun*. **2015**, *51*, 10988−11003. (b) Zhao, W.; He, Z.; Lam, J. W. Y.; Peng, Q.; Ma, H.; Shuai, Z.; Bai, G.; Hao, J.; Tang, B. Z. *Chem*. **2016**, *1*, 592−602. (c) Toma, O.; Allain, M.; Meinardi, F.; Forni, A.; Botta, C.; Mercier, N. *Angew. Chem. Int. Ed*. **2016**, *55*, 7998−8002. (d) Chen, Z.; Liu, G.; Pu, S.; Liu, S. H. *Dyes Pigm.* **2017**, *143*, 409−415. (e) Ravotto, L.; Ceroni, P. *Coord. Chem. Rev.* **2017**, *346*, 62−76.

14. Ly, K. T.; Chen-Cheng, R.-W.; Lin, H.-W.; Shiau, Y.-J.; Liu, S.-H.; Chou, P.-T.; Tsao, C.-S. Huang, Y.-C.; Chi, Y. *Nat. Photon.* **2017**, *11*, 63−68.

15. (a) Bolton, O.; Lee, K.; Kim, H. J.; Lin, K. Y.; Kim, J. *Nat. Chem.* **2011**, *3*, 205−210. (b) An, Z.; Zheng, C.; Tao, Y.; Chen, R.; Shi, H.; Chen, T.; Wang, Z.; Li, H.; Deng, R.; Liu, X.; Huang, W. *Nat. Mater.* **2015**, *14*, 685−690.

16. (a) Dong, A.; Tang, R.; Buhro, W. E. *J. Am. Chem. Soc.* **2007**, *129*, 12254−12262. (b) Jheng, S.-L.; Chen, J.-Y.; Tuan, H.-Y. *Mater. Design.* **2018**, *149*, 113−121.

17. Fagan, P. J.; Nugent, W. A. *J. Am. Chem. Soc*. **1988**, *110*, 2310−2312.

18. Ura, Y.; Li, Y.; Xi, Z.; Takahashi, T. *Tetrahedron Lett*. **1998**, *39*, 2787−2790.

19. Mei, J.; Leung, N. L. C.; Kwok, R. T. K.; Lam, J. W. Y.; Tang, B. Z. *Chem. Rev.* **2015**, *115*, 11718−11940.

20. Mohammadpour, A.; Wiltshire, B. D.; Farsinezhad, S.; Zhang, Y.; Askar, A. M.; Kisslinger, R.; Delgado, W. T.; He, G.; Kar, P.; Rivard, E.; Shankar, K. *Org. Electron.* **2016**, *39*, 153−162.

21. (a) Dong, Y.; Lam, J. W. Y.; Li, Z.; Qin, A.; Tong, H.; Dong, Y.; Feng, X.; Tang, B. Z. *J. Inorg. Organomet. Polym. Mater*. **2005**, *12*, 287−291. (b) Dong, Y.; Lam, J. W. Y.; Qin, A.; Sun, J.; Liu, J.; Li, Z.; Sun, J.; Sung, H. H. Y.; Williams, I. D.; Kwok, H. S.; Tang, B. Z. *Chem. Commun*. **2007**, 3255−3257. (c) Dong, Y. Crystallization-induced emission enhancement. In *Aggregation-Induced Emission: Fundamentals*; Qin, A., Tang, B. Z., Eds.; John Wiley & Sons, Ltd: UK, 2014; pp 323−335. (d) Ohtani, S.; Gon, M.; Tanaka, K.; Chujo, Y. *Chem. Eur. J.* **2017**, *23*, 11827−11833. (e) Zheng, C.; Zang, Q.; Nie, H.; Huang, W.; Zhao, Z.; Qin, A.; Hu, R.; Tang, B. Z. *Mater. Chem. Front*. **2018**, *2*, 180−188.

22. (a) Chen, Z.; Zhang, J.; Song, M.; Yin, J.; Yu, G.-A.; Liu, S. H. *Chem. Commun.* **2015**, *51*, 326–329. (b) Gong, Y.; Chen, G.; Peng, Q.; Yuan, W. Z.; Zie, Y.; Li, S.; Zhang, Y.; Tang, B. Z. *Adv. Mater.* **2015**, *27*, 6195–6201.

23. (a) Becke, A. D.; *J. Chem. Phys.* **1993**, *98*, 5648–5652. (b) Lee, C.; Yang, W.; Parr, R. G. *Phys. Rev. B*, **1988**, *37*, 785–789.

24. Yanai, T.; Tew, D.; Handy, N. *Chem. Phys. Lett.* **2004**, *393*, 51–57.

25. Zhao, Y.; Truhlar, D. *Theor. Chem. Acc*. **2008**, *120*, 215–241.

26. Torres Delgado, W.; Braun, C. A.; Boone, M. P.; Shynkaruk, O.; Qi, Y.; McDonald, R.; Ferguson, M. J.; Data, P.; Almeida, S. K. C.; de Aguiar, I.; de Souza, G. L. C.; Brown, A.; He, G.; Rivard, E. *ACS Appl. Mater. Interfaces* **2018**, *10*, 12124−12134.

27. Vougioukalakis, G. C.; Grubbs, R. H. *Chem. Rev.* **2010**, *110*, 1746−1787.

28. Bu, F.; Wang, E.; Peng, Q.; Hu, R.; Qin, A.; Zhao, Z.; Tang, B. Z. *Chem. Eur. J.* **2015**, *21*, 4440−4449.

29. An, J.; Sun, A.; Qiao, Y.; Zhang, P.; Su, M. *J. Mater. Sci.: Mater. Med.* **2015**, *26*, 1−6.

30. (a) Grabov, V. M.; Demidov, E. V.; Ivanova, E. K.; Kablukova, N. S.; Krushelnitckii, A. N.; Senkevich, S. V. *Semiconductors* **2017**, *51*, 831−833. (b) Yang, F. Y.; Liu, K.; Hong, K.; Reich, D. H.; Searson, P. C.; Chien, C. L. *Science* **1999**, *284*, 1335−1337. (c) Takayama, A.; Sato, T.; Souma, S.; Takahashi, T. *J. Vac. Sci. Technol. B* **2012**, *30*, 04E107−1.

31. Harned, A. M.; Song He, H.; Toy, P. H.; Flynn, D. L.; Hanson, P. R. *J. Am. Chem. Soc.* **2005**, *127*, 52–53.

32. Matsuo, D.; Yang, X.; Hamada, A.; Morimoto, K. Kato, T.; Yahiro, M.; Adachi, C.; Orita, A.; Otera, J. *Chem. Lett.* **2010**, *39*, 1300–1302.

33. Jantunen, K. C.; Scott, B. L.; Kiplinger, J. L. *J. Alloy. Compd.* **2007**, *444*, 363–368.

34. Dunning, Jr., T. H. *J. Chem. Phys*. **1989**, *90*, 1007–1023.

35. Peterson, K. A. *J. Chem. Phys*. **2003**, *119*, 11099–11112.

36. (a) Feller, D. *J. Comput. Chem.* **1996**, *17*, 1571–1586. (b) Schuchardt, K. L.; Didier, B. T.; Elsethagen, T.; Sun, L.; Gurumoorthi, V.; Chase, J.; Li, J.; Windus, T. L. *J. Chem. Inf. Model*. **2007**, *47*, 1045–1052.

37. (a) Cances, E.; Mennucci, B.; Tomasi, J. *J. Chem. Phys*. **1997**, *107*, 3032–3041. (b) Cossi, M.; Scalmani, G.; Rega, N.; Barone, V. *J. Chem. Phys*. **2002**, *117*, 43–54.

38. Frisch, M. J.; Trucks, G. W.; Schlegel, H. B.; Scuseria, G. E.; Robb, M. A.; Cheeseman, J. R.; Scalmani, G.; Barone, V.; Petersson, G. A.; Nakatsuji, H.; Li, X.; Caricato, M.; Marenich, A. V.; Bloino, J.; Janesko, B. G.; Gomperts, R.; Mennucci, B.; Hratchian, H. P.; Ortiz, J. V.; Izmaylov, A. F.; Sonnenberg, J. L.; Williams-Young, D.; Ding, F.; Lipparini, F.; Egidi, F.; Goings, J.; Peng, B.; Petrone, A.; Henderson, T.; Ranasinghe, D.; Zakrzewski, V. G.; Gao, J.; Rega, N.; Zheng, G.; Liang, W.; Hada, M.; Ehara, M.; Toyota, K.; Fukuda, R.; Hasegawa, J.; Ishida, M.; Nakajima, T.; Honda, Y.; Kitao, O.; Nakai, H.; Vreven, T.; Throssell, K.; Montgomery, J. A., Jr.; Peralta, J. E.; Ogliaro, F.; Bearpark, M. J.; Heyd, J. J.; Brothers, E. N.; Kudin, K. N.; Staroverov, V. N.; Keith, T. A.; Kobayashi, R.; Normand, J.; Raghavachari, K.; Rendell, A. P.; Burant, J. C.; Iyengar, S. S.; Tomasi, J.; Cossi, M.; Millam, J. M.; Klene, M.; Adamo, C.; Cammi, R.; Ochterski, J. W.; Martin, R. L.; Morokuma, K.; Farkas, O.; Foresman, J. B.; Fox, D. J. *Gaussian 16*, Revision A.03; Gaussian, Inc.: Wallingford, CT, 2016.

39. (a) van Gisbergen, S. J. A.; Snijders, J. G.; Baerends, E. J. *Comp. Phys. Comm*. **1999**, *118*, 119–138. (b) Rosa, A.; Baerends, E. J.; van Gisbergen, S. J. A.; van Lenthe, E.; Groeneveld, J. A.; Snijders, J. G. *J. Am. Chem. Soc.* **1999**, *121*, 10356–

10365. (c) Wang, F.; Ziegler, T. *J. Chem. Phys*. **2005**, *123*, 154102. (d) Wang, F.; Ziegler, T.; van Lenthe, E.; van Gisbergen, S. J. A.; Baerends, E. J. *J. Chem. Phys.* **2005**, *122*, 204103.

40. *ADF2017, SCM, Theoretical Chemistry*; Vrije Universiteit, Amsterdam, The Netherlands, http://www.scm.com. Baerends, E. J.; Ziegler, T.; Atkins, A. J.; Autschbach, J.; Baseggio, O.; Bashford, D.; Bérces, A.; Bickelhaupt, F. M.; Bo, C.; Boerrigter, P. M.; Cavallo, L.; Daul, C.; Chong, D. P.; Chulhai, D. V.; Deng, L.; Dickson, R. M.; Dieterich, J. M.; Ellis, D. E.; van Faassen, M.; Fan, L.; Fischer, T. H.; Fonseca Guerra, C.; Franchini, M.; Ghysels, A.; Giammona, A.; van Gisbergen, S. J. A.; Goez, A.; Götz, A. W.; Groeneveld, J. A.; Gritsenko, O. V.; Grüning, M.; Gusarov, S.; Harris, F. E.; van den Hoek, P.; Hu, Z.; Jacob, C. R.; Jacobsen, H.; Jensen, L.; Joubert, L.; Kaminski, J. W.; van Kessel, G.; König, C.; Kootstra, F.; Kovalenko, A.; Krykunov, M. V.; van Lenthe, E.; McCormack, D. A.; Michalak, A.; Mitoraj, M.; Morton, S. M.; Neugebauer, J.; Nicu, V. P.; Noodleman, L.; Osinga, V. P.; Patchkovskii, S.; Pavanello, M.; Peeples, C. A.; Philipsen, P. H. T.; Post, D.; Pye, C. C.; Ramanantoanina, H.; Ramos, P.; Ravenek, W.; Rodríguez, J. I.; Ros, P.; Rüger, R.; Schipper, P. R. T.; Schlüns, D.; van Schoot, H.; Schreckenbach, G.; Seldenthuis, J. S.; Seth, M.; Snijders, J. G.; Solà, M.; Stener, M.; Swart, M.; Swerhone, D.; Tognetti, V.; te Velde, G.; Vernooijs, P.; Versluis, L.; Visscher, L.; Visser, O.; Wang, F.; Wesolowski, T. A.; van Wezenbeek, E. M.; Wiesenekker, G.; Wolff, S. K.; Woo, T. K.; Yakovlev, A. L.

41. (a) Campos, C. T.; Jorge, F. E. *Mol. Phys*. **2013**, *111*, 167–173. (b) van Lenthe, E.; Baerends, E. J. *J. Comput. Chem.* **2003**, *24*, 1142–1156.

42. (a) van Lenthe, E.; Baerends, E. J.; Snijders, J. G. *J. Chem. Phys*. **1993**, *99*, 4597–4610. (b) van Lenthe, E.; Baerends, E. J.; Snijders, J. G. *J. Chem. Phys*. **1994**, *101*, 9783–9792. (c) van Lenthe, E.; Ehlers, A. E.; Baerends, E. J. *J. Chem. Phys*. **1999**, *110*, 8943–8953.

43. Visscher, L.; van Lenthe, E. *Chem. Phys. Lett*. **1999**, *306*, 357–365.

44. Humphrey, W.; Dalke, A.; Schulten, K. *J. Mol. Graphics* **1996**, *14*, 33–38.

45. Sheldrick, G. M. *Acta Cryst. A* **2008**, *64*, 112–122.

Chapter 4: Towards Enhanced Quantum Efficiency of Benzotellurophene and Benzobismole Phosphors by Restriction of Intramolecular Rotations and Attempted Functionalization via Suzuki-Miyaura Cross-Coupling

4.1 Introduction

Previous work with benzobismoles has indicated that this family of molecules show promise for their phosphorescent properties including difficult to achieve red emission; however, these initial studies suggested that the efficiency of emission is strongly linked to subtle changes in the morphological state of the molecules (see Chapter 3). That is, the phosphorescence quantum yield is strongly dependent upon the crystallinity of the material and the more ordered the packing the higher the quantum yield appears to be. This hypothesis is in line with previously reported theories of aggregation induced emission (AIE) that state AIE stems from reduced molecular motions, chiefly intramolecular rotations (Figure 4.1) and vibrations, in the solid state and this reduced motion results in fewer non-radiative decay pathways from the excited triplet states (leading to higher quantum yields).[1]

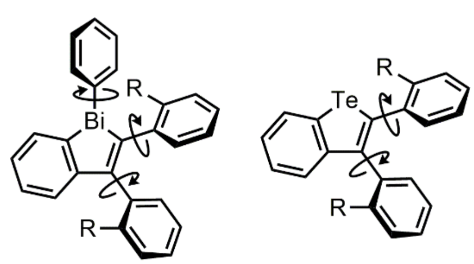

Figure 4.1. Intramolecular rotations in triarylbenzobismoles and diphenylbenzotellurophene thought to contribute to non-radiative decay pathways.

Working from the postulates that: 1) phosphorescence quantum yield is reduced by intramolecular rotations and 2) that the morphology dependence of the emission intensity can be reduced by hindering rotations about the exocyclic heterocycle–aryl bonds, in this Chapter the effects of adding *ortho*-substitution to the exocyclic aryl groups was examined as a reasonable next step in possibly improving phosphorescence quantum yields in Bi- and Te-containing phosphors.

As metallacyle transfer from zirconocene precursors with $ArBiCl_2$ (Ar = aryl group) and a catalytic amount of CuCl was been demonstrated to be a reliable route to generate bismoles,[2] this method was chosen as a route to the *ortho*-tolyl-functionalized heterocycles of interest in this Chapter. Previous work by Tilley and coworkers indicated that cyclization of aryl-acetylenes with low valent Cp_2Zr sources such as Rosenthal's reagent (Scheme 4.1) is limited by the steric hindrance of the aryl substituents on the acetylene.[3] When a mesityl (2,4,6-$Me_3C_6H_2$) group is part of the starting alkyne, cyclization occurs at room temperature with the mesityl group being directed exclusively to the β position on the ring. However, when less sterically bulky *ortho*-tolyl is used, a mixture of isomers is obtained (33 % αβ and 66 % ββ; Scheme 4.1a).[4]

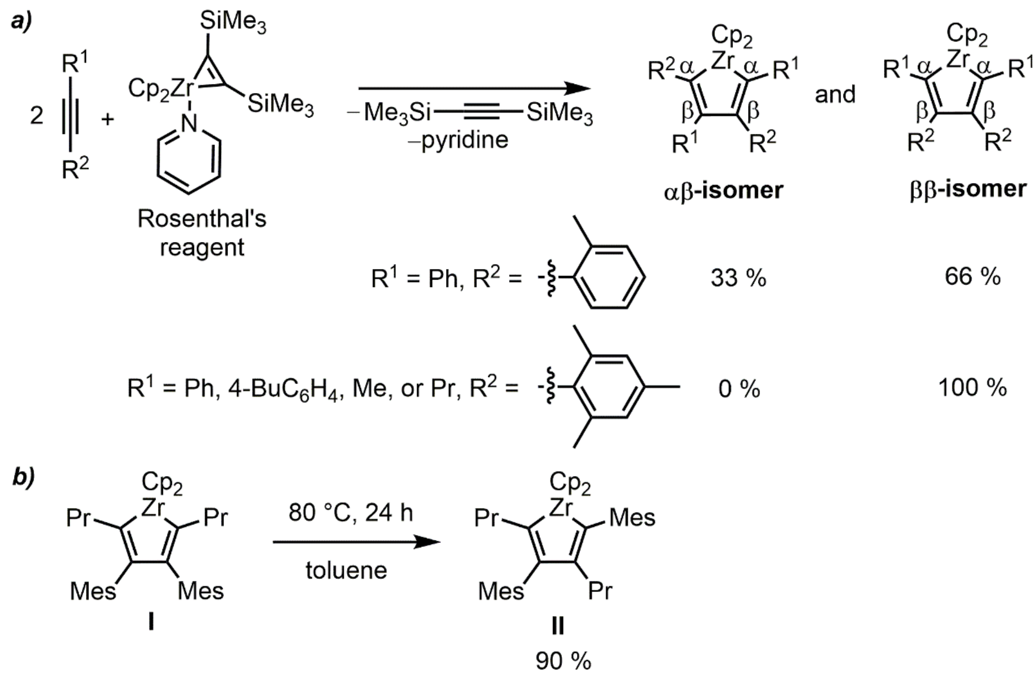

Scheme 4.1. Unsymmetric zirconacyclopentadiene formation studied by Tilley and coworkers.

Interestingly, when $Cp_2Zr[2,5\text{-}Pr_2\text{-}3,4\text{-}Mes_2C_4]$ (**I**, Scheme 4.1b) was heated at 80 °C over the course of one day, conversion to the unsymmetric product, $Cp_2Zr[2,4\text{-}Mes_2\text{-}3,5\text{-}Pr_2C_4]$ (**II**, Scheme 4.1b) was observed.[4] This study indicates that while *ortho*-substitution on arylalkynes has a drastic effect on the synthesis of zirconacyclopentadienes, the cyclization is tolerant to aryl groups having *ortho*-substituents of minimal steric bulk, such as methyl groups. Thus *ortho*-tolyl or mesityl-substituted Bi- and Te- phosphors were targeted.

Thus far, the functionality on the diene backbone of bismole-based emitters has been set during the initial cyclization step, *i.e.* before Zr/Bi metallacycle transfer to insert bismuth into the heterocycle (see Chapters 2 and 3). An alternative method to access a great variety of bismole-based emitters is to introduce functionality after bismole formation by palladium-catalyzed cross-coupling. In an analogous example, the Rivard group previously reported the pinacolboronate (BPin) tellurophene **B-Te-6-B** (Scheme 4.2a) which was demonstrated to undergo efficient Suzuki-Miyaura cross-coupling to yield aryl-functionalized products.[5] Compound **4** (Scheme 4.2b), the mesityl-bismole analogue to **B-Te-6-B**, already discussed in Chapter 2, was evaluated for its suitability as a coupling partner in Suzuki-Miyaura cross-coupling to potentially generate conjugated bismole polymers as shown in Scheme 4.2b.

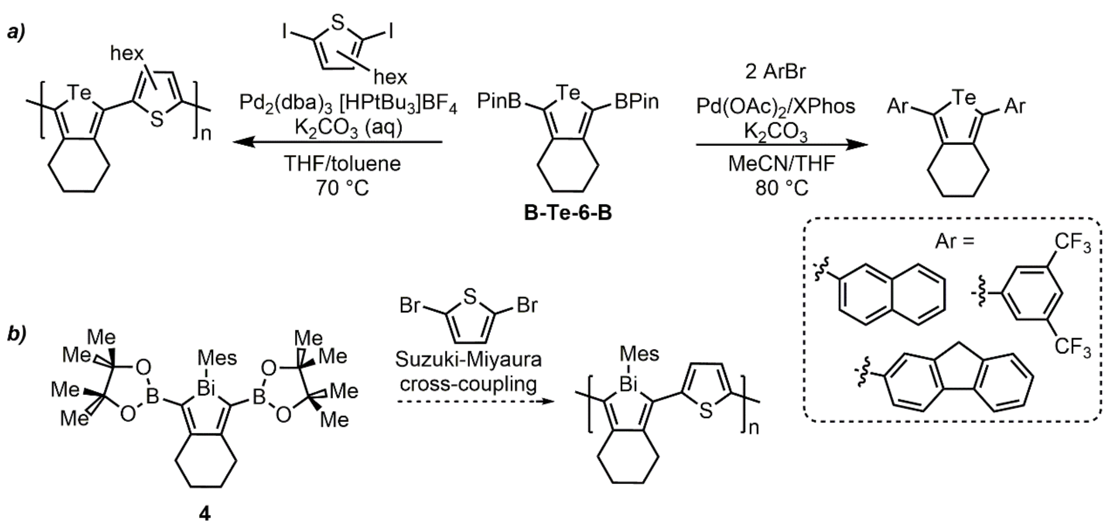

Scheme 4.2. (a) Suzuki-Miyaura cross-coupling of BPin-functionalized tellurophene **B-Te-6-B**, to yield a conjugated polymer with a mixed heterocycle backbone. (b) Synthetic strategy to be applied to bismole **4** to yield conjugated polymers.

4.2 Results and Discussion

4.2.1 Synthesis of *ortho*-Tolyl-Substituted Heterocycles and Structural Analysis

Attempts at cyclization to form 2,3-bis(mesityl)benzozirconocene from bis(mesityl)acetylene and Cp_2ZrPh_2 via Scheme 4.3 was found to yield only unreacted alkyne, suggesting that the mesityl groups are too sterically hindered to allow for cyclization (Scheme 4.3 left). The same reaction with bis(*o*-tolyl)acetylene was found to proceed with a reasonable yield (65 % isolated) to produce zirconocycle **1** (Scheme 4.3 right). Figure 4.2 shows the molecular structure of **1**, as determined by single crystal X-ray diffraction, and the tolyl substitutents are found to be preferentially oriented in an *anti*- conformation in the solid state.

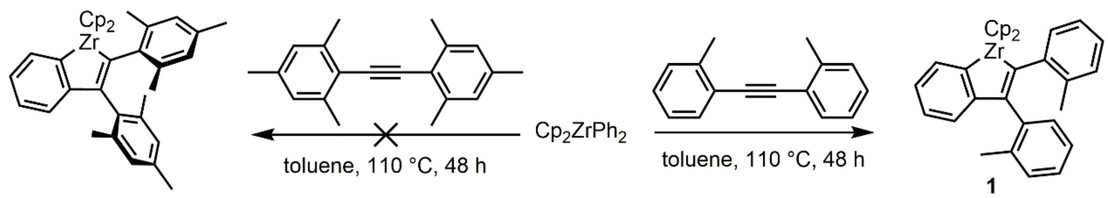

Scheme 4.3. Synthesis of benzozirconacycle **1** from bis(*o*-tolyl)acetylene and Cp_2ZrPh_2, and the attempted synthesis of 2,3-bis(mesityl)benzozirconocene.

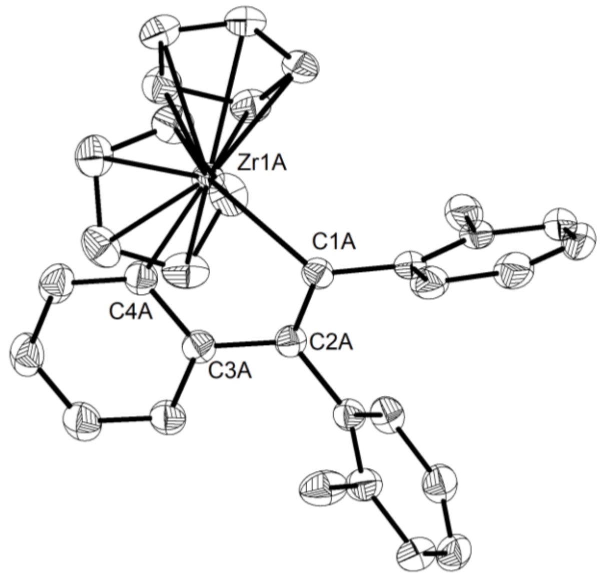

Figure 4.2. Molecular structure of **1** with thermal ellipsoids plotted at a 30 % probability level. All hydrogen atoms were omitted for clarity, and only one molecule of the two in the asymmetric unit is shown. Select bond lengths (Å) and angles (deg) with values belonging to a second molecule of **1** shown in square brackets: Zr1–C1 2.284(4) [2.296(4)], Zr1–C4 2.269(4) [2.249(4)], C1–C2 1.357(5) [1.353(5)], C2–C3 1.487(5) [1.497(5)], C3–C4 1.427(5) [1.426(5)]; C4–Zr1–C1 78.11(13) [77.55(13)], Zr1–C1–C2 111.7(3) [112.6(3)], Zr1–C4–C3 110.5(3) [111.8(3)].

^{1}H NMR spectroscopic analysis of **1** indicated the desired restriction of rotation about the exocyclic heterocycle-aryl C–C bonds as supported by splitting of the Cp signal into two broadened singlets at 6.04 and 5.96 ppm, while similar broadening of the tolyl CH_3 resonances at 2.35 and 2.29 ppm (in toluene-d_8) was noted (Figure 4.3, middle). A variable temperature ^{1}H NMR study of **1** in toluene-d_8 was conducted and Figure 4.3 shows the spectral changes that occured when this sample is cooled to –80 °C or heated to 80 °C. Upon heating to 80 °C, the Cp signals sharpen to two separate signals at 6.08 and 6.01 ppm that each integrate to five hydrogen atoms and the two tolyl CH_3 signals sharpen significantly to afford two singlets at 2.29 and 2.24 ppm that each integrate to three hydrogens. Upon cooling the sample to –80 °C, two separate rotational isomers (presumably the *syn*- and *anti*-isomers) are observed in a ratio of 2:1 as observed by a splitting of the Cp and CH_3 singlets into pairs of doublets (Figure 4.3, top).

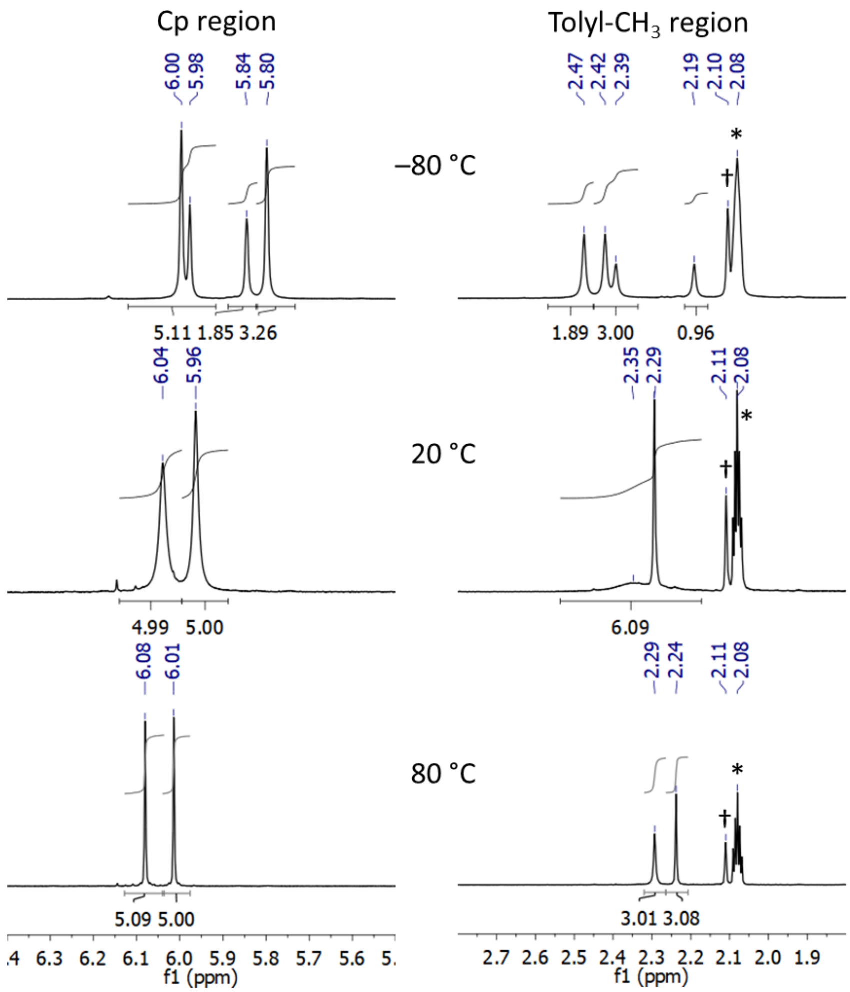

Figure 4.3. Variable temperature ^{1}H NMR of **1** in toluene-d_8 (residual toluene at 2.11, †, and toluene-d_7 2.08 ppm, *, in the above spectra) showing Cp (left) and tolyl methyl (right) regions at –80 °C (top), 20 °C (middle), and 80 °C (bottom). Extra methyl and Cp signals in the –80 °C spectra indicate major and minor rotational isomers (present at a 2:1 ratio).

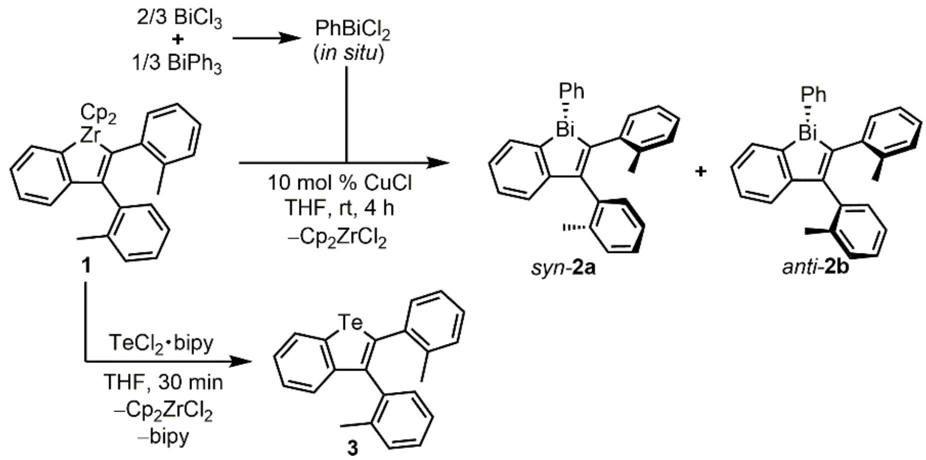

Scheme 4.4. Synthesis of the o-tolyl-substituted benzobismole **2** and benzotellurophene **3**.

Scheme 4.4. depicts the synthesis of benzobismole **2** via copper(I) chloride-mediated metallacycle transfer. Compound **2** could be recrystallized by layering methanol on top of a concentrated solution of **2** in CH_2Cl_2 and allowing slow diffusion of the solvents to promote slow crystal formation at room temperature. Figure 4.4 shows the molecular structure of **2** as determined by single crystal X-ray diffraction. Compound **2** crystallized with two different orientations of the tolyl side groups in a 2:1 ratio: *anti*-**2a** as the major conformation (Figure 4.4) and *syn*-**2b** as the minor conformation.

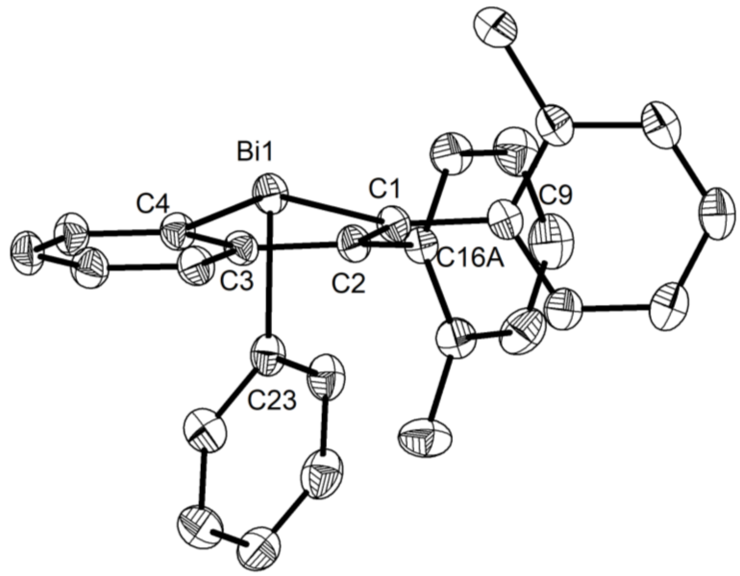

Figure 4.4. Molecular structure of the major isomer of **2** (*anti*) with thermal ellipsoids plotted at a 30 % probability level. All hydrogen atoms were omitted for clarity, and only the major orientation of the disordered tolyl group is displayed. Select bond lengths (Å) and angles (deg): Bi1–C1 2.255(2), Bi–C4 2.231(2), Bi1–C23 2.258(2), C1–C2 1.345(3), C2–C3 1.479(3), C3–C4 1.406(3); C4–Bi1–C1 78.40(8), C4–Bi–C23 94.53(8), C1–Bi1–C23 95.13(8), Bi1–C1–C2 111.28(15), Bi1–C4–C3 111.06(15).

^{1}H NMR spectroscopic analysis of **2** indicated the presence of rotational isomers **2a** and **2b** in solution (both in $CDCl_3$ and toluene-d_8) as concluded by the splitting of the methyl signals for each isomer into two singlets. When variable temperature ^{1}H NMR spectroscopy was performed on benzobismole **2**, the split methyl signals from each isomer did not converge to sharp singlets (as was observed for **1**) indicating that even at 100 °C (in toluene-d_8) **2a** and **2b** do not readily interconvert in solution (see Figure 4.5).

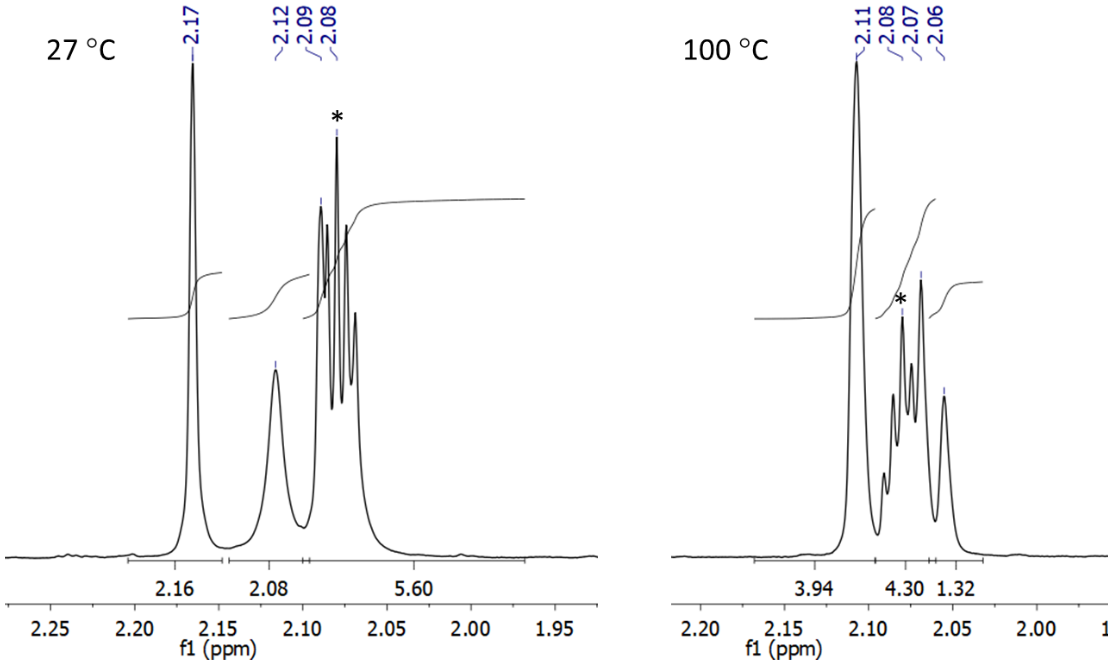

Figure 4.5. Variable temperature ^{1}H NMR spectra of **2** in toluene-d_8 (* toluene-d_7 at 2.08 ppm in the above spectra) the tolyl methyl region at 27 °C (left), and 100 °C (right).

Previous studies from the Rivard group have indicated that the quantum yield of 2,3-diphenylbenzotellurophene was so low that it could not be reliably measured.[6] Thus, in addition to probing the effects of *ortho*-tolyl substitution on the benzobismole class of molecules, the preparation of the bis(o-tolyl)benzotellurophene **3** was also of interest. Therefore, the benzozirconacycle **1** was combined with $TeCl_2$•bipy as per the conditions previously established by the Rivard group (Scheme 4.4 bottom), leading to successful metallacycle transfer to produce **3** in a 39 % isolated yield.

Interestingly, unlike for precursor **1**, and bismole **2**, restricted rotation about the exocyclic heterocycle-tolyl C–C bonds in **3** was not observed in solution at room temperature by ^{1}H NMR spectroscopy. The tolyl CH_3 groups appear at 2.19 and 2.00 ppm (in benzene-d_6 at room temperature) as sharp singlets that each integrate to three hydrogens as expected. Additionally, the molecular structure of **3** was determined by single crystal X-ray crystallography and indicates a *syn* orientation of the tolyl groups in the solid state (Figure 4.6).

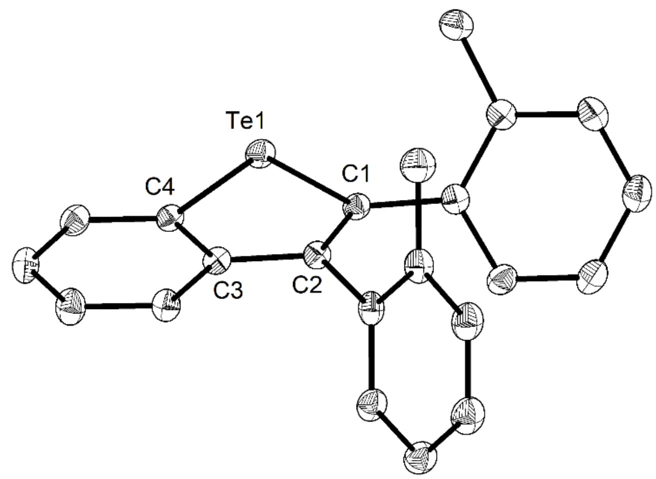

Figure 4.6. Molecular structure of **3** with thermal ellipsoids plotted at a 30 % probability level. All hydrogen atoms were omitted for clarity. Select bond lengths (Å) and angles (deg): Te1–C1 2.097(2), Te1–C4 2.077(2), C1–C2 1.358(3), C2–C3 1.464(3), C3–C4 1.409(3); C1–Te1–C4 81.77(9), Te1–C1–C2 112.36(17), Te1–C4–C3 111.30(17).

Interestingly, examination of the solid-state packing arrangements of both **2** and **3** revealed the presence of closer intermolecular E···E distances than expected. While the closest Bi···Bi separation in 1,2,3-triphenylbenzobismole is 5.8668(2) Å,[2b] benzobismole **2** had a closer Bi···Bi distance of 4.6417(5) Å. The closest Te···Te distance in the benzotellurophene **3** is 3.8377(4) Å, which is within the sum of the van der Waals radii for Te (4.12 Å),[7] and is significantly shorter than the closest Te···Te distance in 2,3-diphenylbenzotellurophene [5.7439(4) Å].[6]

4.2.2 Phosphorescent Properties of 2 and 3

Crystalline benzobismole **2** was found to exhibit weak orange phosphorescence at room temperature (λ_{ex} = 400 nm, λ_{em} = 532 nm, Φ = 1.5 %, τ = 1.9 μs, solid state under N_2). While the measured emission maximum (λ_{em}) was 532 nm, the emission tails out to 700 nm, resulting in the observed orange emission (Figure 4.7 left). Films of **2** drop-cast on quartz plates (from stock solutions of **2** in hexanes, **2** in THF, and 5 wt% **2** in PMMA in THF) were non-emissive.

Like for 2,3-diphenylbenzotellurophene, the phosphorescence intensity of **3** is also very low (λ_{ex} = 392 nm, λ_{em} = 555 nm, Φ = 0.6 %, τ = 3.4 μs, solid state under N_2), but measureable (see Figure 4.7 right), and is red-shifted from the emission observed from 2,3-diphenylbenzotellurophene (λ_{ex} = 337 nm, λ_{em} = 505 nm).[6]

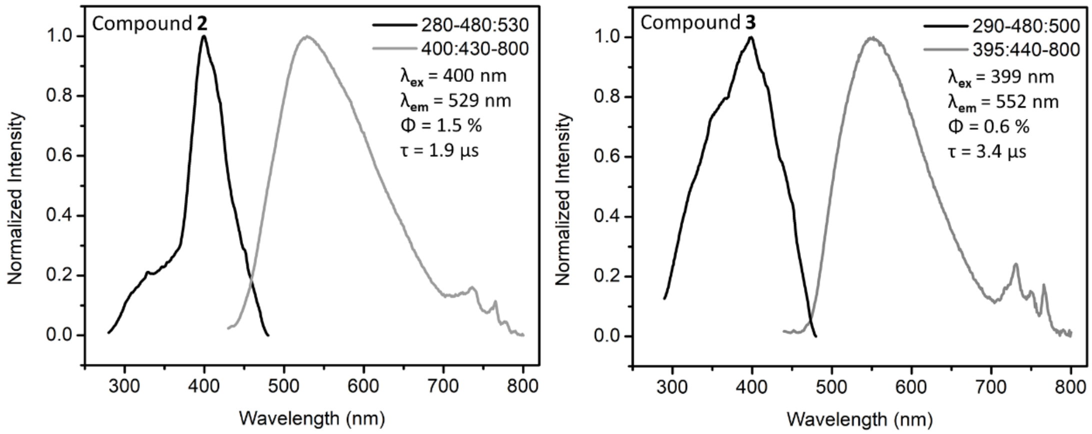

Figure 4.7. Photoluminescence data for benzobismole **2** (left) and benzotellurophene **3** (right) in the solid state under an N_2 atmosphere. Note, the features at $\lambda > 700$ nm are instrument artifacts observed in the baseline of low Φ samples.

The results from this exploration with *ortho*-substitution in benzotellurophenes and benzobismoles indicate that structure rigidification imparted by *ortho*-methyl addition was not enough to enhance quantum yields. While ^{1}H NMR indicated that *ortho*-substitution was an effective method to restrict intramolecular rotations in **2** as intended, *ortho*-methyl-substitution did not provide enough sterical bulk to limit those same intramolecular rotations in benzotellurophene **3**. Examination of the packing structure of **2** and **3** by single crystal X-ray diffraction indicated short Bi···Bi and Te···Te distances suggesting that enhanced solid-state triplet-triplet annihilation may be a potential reason for the low emission intensity. These results highlight the challenges associated with designing efficient phosphorescent AIE materials. The heavy element contribution to the excitation processes within an emitter can be predicted computationally and can be used to determine if emission by phosphorescence is likely, but one must also consider how steric properties of peripheral functional groups will affect the conformational flexibility of the molecule. Arguably most important to the emission intensity of heavy element-based AIE phosphors is the effect of solid-state packing and this effect is extremely difficult to predict in advance.

4.3 Attempted Suzuki-Miyaura Cross-Coupling with BPin-Functionalized Bismole

Seeking to gain access to a wider range of bismoles, the BPin-functionalized bismole **4**[2a] was explored for its potential to undergo Suzuki-Miyaura cross-coupling. If successful, cross-coupling would allow for the synthesis of bismole-based conjugated polymers as well as a plethora of aryl-functionalized bismoles with sterically and electronically tunable environments (*c.f.* Scheme 4.2).

Initial cross-coupling trials involved combining **4** with two equivalents of 2-bromothiophene (**5**) as the coupling partner (Scheme 4.5) because: 1) the successful coupling product, **6**, which was previously discussed in Chapter 2 was known to be air- and moisture-stable; and 2) **6** had already been fully characterized allowing for easy identification by NMR spectroscopy.

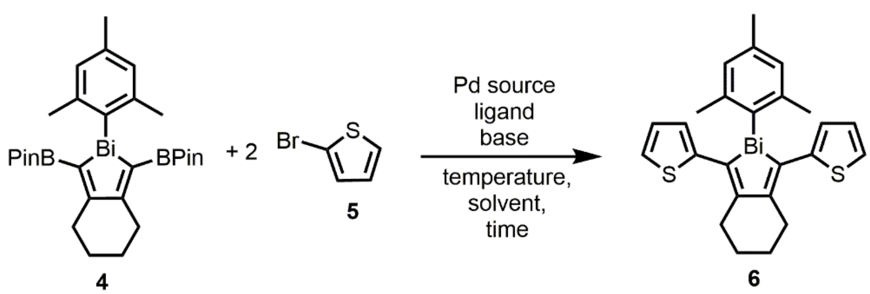

Scheme 4.5. Attempted Suzuki-Miyaura cross-coupling between bismole **4** and 2-bromothiophene (**5**).

Table 4.1 shows the results of these initial cross-coupling trials. Three different palladium sources were evaluated, $Pd(OAc)_2$, $Pd_2(dba)_3$ (dba = dibenzylideneacetone), and $Pd(PPh_3)_4$. The ligand, base, solvent and heating conditions were varied to find a combination that would yield product. While bismole **4** has adequate stability to ambient atmosphere at room temperature, upon heating to 80 °C in toluene under the presence of N_2-sparged water, decomposition into unidentifiable products were observed by NMR spectroscopy. Thus, throughout subsequent Suzuki-Miyaura cross-coupling trials, water- and oxygen-free conditions were maintained. When bismole **4** was heated in the presence of K_3PO_4 (6 equiv.) or CsF (3 equiv.) in THF under microwave heating (120 °C for 40 min), a mix of mesityl-containing byproducts was observed by ^{1}H NMR. Mesitylene (MesH) signals could be identified amongst the mixture of unidentifiable byproducts indicating likely reactivity of the Bi–Mes bond in the basic environment.

Under mild heating conditions (65 °C) and mild bases (*e.g.* entries 1, 2, and 5–7 in Table 4.1) no reaction occurred and unreacted starting material (**4**) could be recovered. When the temperature was increased and the reaction allowed to proceed for a greater length of time (*e.g.* entries 8–11 in Table 4.1), **4** was completely consumed; however, a complicated mixture of unidentifiable products was observed by ^{1}H NMR. These mixtures often contained a mix of mesityl-containing byproducts, as was observed when **4** is heated in THF with only base and no Pd source.

Table 4.1. Attempted Suzuki-Miyaura cross-coupling conditions between bismole **4** and 2-bromothiophene.

Trial	Pd Source	Ligand	Base	Solvent	Heating Conditions	Result
1	$Pd(OAc)_2$	XPhos	K_3PO_4	THF	65 °C/16 h	No reaction
2	$Pd(OAc)_2$	XPhos	K_3PO_4	THF	µwave[a]	No reaction
3	$Pd(OAc)_2$	XPhos	CsF	THF	µwave[a]	Unknown products + **4**
4	$Pd(OAc)_2$	dppf	$CsCO_3$	DMF	100 °C/16 h	Unknown products
5	$Pd(PPh_3)_4$	-----	K_3PO_4	THF	65 °C/16 h	No reaction
6	$Pd_2(dba)_2$	$HP^tBu_3BF_4$	K_3PO_4	THF	65 °C/16 h	No reaction
7	$Pd(OAc)_2$	XPhos	CsF	THF	65 °C/16 h	No reaction
8	$Pd(OAc)_2$	XPhos	CsF	MeCN	µwave[b]	Unknown products
9	$Pd(OAc)_2$	XPhos	K_3PO_4	MeCN	µwave[b]	Unknown products
10	$Pd(OAc)_2$	XPhos	CsF	DMF	µwave[b]	Unknown products
11	$Pd(OAc)_2$	XPhos	K_3PO_4	DMF	µwave[b]	Unknown products

[a] 120 °C, 40 min; [b] 140 °C, 70 min; dppf = 1,1'-bis(diphenylphosphino)ferrocene.

Aryl-transfer chemistry mediated by triarylbismuthines (Ar_3Bi) is known,[8] with many reports of the development of triarylbismuth for use as transmetallating reagents in palladium-catalyzed cross-coupling.[9] For example, Gagnon and coworkers reported detailed studies on the cross-coupling of a variety of triarylbismuth reagents with arylhalides and have noted effective coupling in the presence of pre-catalysts such as $Pd(OAc)_2$, and $Pd(PPh_3)_4$, bases such as K_3PO_4 and $CsCO_3$, and similar solvents and heating conditions employed in Scheme 4.5 and Table 4.1 above.[9a,9b] As product **6** was never observed in any of the cross-coupling trials discussed above, but many Mes-containing products were, it is most likely that the Bi–C bonds are more reactive than the intended B–C bonds to Suzuki-Miyaura conditions.

These findings suggest that palladium-catalyzed cross-coupling methods are likely not possible with Bi-arylated bismoles and that bismole functionalization is best performed prior to insertion of the ArBi moiety into a heterocyclic ring (*i.e.* prior to the CuCl-mediated metallacycle transfer step).

4.4 Conclusions

While restriction of intramolecular rotations in benzobismole **2** could be achieved via installation of peripheral aryl groups with *ortho*-substitution, this did not prove to be a viable route to enhance the efficiency of phosphorescence. Benzotellurophene **3** did not display the expected restricted rotation in solution, but its solid-state packing structure consisted of close Te···Te interactions of less that 3.9 Å, suggesting that the low emission intensity observed could have resulted from substantial triplet-triplet annihilation. These findings serve as a reminder that the largest remaining challenge in designing phosphorescent AIE emitters is predicting how a given molecule will pack in the solid state, as this has a pronounced effect on emission from AIE-based emitters. The reported bismole **4** was studied for its suitability as a substrate for Suzuki-Miyaura cross-coupling and results suggested an inherent lack of stability of the bismole Bi–C bonds towards the reaction conditions necessary to achieve cross-coupling. ^{1}H NMR data was suggestive of **4** acting as a mesityl-transfer reagent under the conditions employed.

4.5 Experimental Section

4.5.1 General Considerations

All reactions were performed using standard Schlenk and glovebox (MBraun) techniques under a nitrogen atmosphere. Solvents were all dried and degassed using a Grubbs-type solvent purification system manufactured by Innovative Technology, Inc., and stored under an atmosphere of nitrogen prior to use. Bismuth trichloride was purchased from TCI America, tetrakis(triphenylphosphine)palladium(0) from Matrix Scientific, and all other chemicals were purchased from Sigma Aldrich and used as received. Bis(*o*-tolyl)acetylene,[10] bis(mesityl)acetylene,[10] Cp_2ZrPh_2,[11] bipy•$TeCl_2$,[12] and **4**[2a] were synthesized according to literature procedures. ^{1}H, $^{11}B\{^{1}H\}$, and $^{13}C\{^{1}H\}$ NMR spectra were recorded on 400, 500, 600, or 700 MHz Varian Inova instruments and were referenced externally to $SiMe_4$ (^{1}H, $^{13}C\{^{1}H\}$), or $F_3B{\cdot}Et_2O$ ($^{11}B\{^{1}H\}$). Chemical shifts are reported in parts per million (ppm) and coupling constants (J) are given in Hertz (Hz). High resolution mass spectra were obtained on an Agilent Technologies 6220 oaTOF (APPI), Bruker 9.4T Apex-Qe FTICR (MALDI), or Kratos Analytical MS-50G (EI) spectrometer. UV−visible spectroscopic measurements were carried out with a Varian Cary 5000 UV/Vis/NIR spectrophotometer. Elemental analyses were performed at the Analytical and Instrumentation Laboratory at the University of Alberta. Melting points were measured in sealed glass capillaries under nitrogen using a MelTemp apparatus. Thermogravimetric analysis was performed under a nitrogen atmosphere on a PerkinElmer Pyris 1 TGA. Differential scanning calorimetry measurements were conducted under a nitrogen atmosphere on a PerkinElmer Pyris 1 DSC. The steady-state photoluminescence (PL) spectra, emission lifetimes (τ), and photoluminescence quantum yields (Φ) were obtained using a PTI QuantaMaster 8075 fluorescence spectrophotometer equipped with a 75W xenon lamp and an integrating sphere. All quantum yields reported herein are absolute. Solid samples were measured in glass capillaries mounted in a custom-made solids holder. Long-pass (λ = 370, 400, or 420 nm) and short-pass cut-off filters (λ = 480 nm) were used in steady-state measurements when necessary.

4.5.2 Synthetic Procedures

Synthesis of 2,3-bis(*o*-tolyl)benzozirconocene (1). Under a nitrogen atmosphere, Cp_2ZrPh_2 (2.320 g, 6.202 mmol) and bis(*o*-tolyl)acetylene (1.263 g, 6.122 mmol) were dissolved in 30 mL of toluene and stirred at 110 °C for 48 hours. The resulting dark red-orange mixture was evaporated to dryness, redissolved in 20 mL of THF, filtered through a 4 cm plug of Celite, and the filtrate was evaporated to dryness to afford a viscous dark red-brown oil. The crude product was dissolved in a minimum volume of toluene (10 mL), topped with a layer of hexanes (10 mL), and the mixture stored at room temperature for 3 days before being cooled to –30 °C for 24 hours. The mother liquor was decanted away from the resulting precipitate, and this solid was washed with 5 mL of cold hexanes (–30 °C) and dried *in vacuo* to afford **1** as a yellow solid (1.995 g, 65 %). Yellow single crystals of **1** suitable for X-ray crystallography were obtained from a concentrated Et_2O solution at –30 °C. ^{1}H NMR (700 MHz, C_6D_6): δ 7.06–6.92 (m, 8H, benzo*H*, Ar*H*), 6.90–6.87 (m, 2H, Ar*H*) 6.72 (t, $^3J_{HH}$ = 7.0 Hz, 1H, benzo*H*), 6.65 (dd, $^3J_{HH}$ = 7.0 Hz, $^4J_{HH}$ = 1.4 Hz, 1H, benzo*H*), 6.05 (s, 5H, CpH), 5.98 (s, 5H, CpH), 2.34 (br s, 6H, ArCH_3). $^{13}C\{^1H\}$ NMR (176 MHz, C_6D_6): δ 184.8 (Zr–C), 146.0 (ArC), 137.0 (ArCH), 135.9 (ArC), 131.5 (ArC), 130.7 (ArCH), 130.0 (ArCH), 128.3 (ArCH), 126.4 (ArCH), 126.0 (ArCH), 125.7 (ArCH), 125.2 (ArCH), 124.8 (ArCH), 124.1 (ArCH), 123.7 (ArCH), 112.9 (Cp), 112.8 (Cp), 21.4 (CH$_3$). Note, the second ArCH$_3$ signal could not be resolved, presumably due to the same broadening effects observed at room temperature in the ^{1}H NMR spectrum, nor could one ArCH peak and four of the quaternary carbon signals. Anal. Calcd. (%) for $C_{32}H_{28}Zr$: C, 76.29; H, 5.60. Found: C, 75.40; H, 5.88. Mp: 190–194 °C.

Synthesis of 1-phenyl-2,3-bis(*o*-tolyl)-benzo[*b*]bismole (2). A suspension of $BiCl_3$ (0.1335 g, 0.4234 mmol) in 5 mL of Et_2O was added to a suspension of $BiPh_3$ (0.0916 g, 0.208 mmol) in 5 mL of Et_2O, and the mixture was stirred at room temperature for 1 hour, after which time the reaction mixture was concentrated to a volume of *ca.* 0.5 mL. The crude $PhBiCl_2$ mixture was fully dissolved by adding 5 mL of THF and the resulting solution of $PhBiCl_2$ was added to a mixture of 2,3-bis(*o*-tolyl)benzozirconocene (**1**) (0.3180 g, 0.6337 mmol) and CuCl (6.3 mg, 0.064 mmol) in 12 mL of THF. The mixture was then stirred at room temperature in the absence of light for 5 hours before being evaporated to dryness. The crude product mixture was stirred with 20 mL of hexanes for 16 hours, then the supernatant was decanted and filtered through a 0.5 cm pad of silica. The filtrate was evaporated to dryness to yield 0.182 g of crude product which was further purified by washing with 10 mL of methanol. Pure **2** was then isolated by vacuum filtration and dried *in vacuo* to yield an off-white powder (0.123 g, 35 %). Crystals suitable for single crystal X-ray crystallography could be obtained by layering methanol on top of a concentrated solution of **2** in dichloromethane at room temperature. ^{1}H NMR (700 MHz, $CDCl_3$): δ 7.90 (dd, $^3J_{HH}$ = 7.9 Hz, $^4J_{HH}$ = 1.2 Hz, 1.35H, Ar*H*), 7.88 (dd, $^3J_{HH}$ = 7.8 Hz, $^4J_{HH}$ = 1.2 Hz, 0.65H, Ar*H*), 7.86 (dd, $^3J_{HH}$ = 7.1 Hz, $^4J_{HH}$ = 1.1 Hz, 0.65H, Ar*H*), 7.83 (dd, $^3J_{HH}$ = 7.0 Hz, $^4J_{HH}$ = 1.1 Hz, 0.35H, Ar*H*), 7.40 (td, $^3J_{HH}$ = 7.3 Hz, $^4J_{HH}$ = 1.3 Hz, 0.65H, Ar*H*), 7.31–7.38 (m, 3.35H, Ar*H*), 7.27–7.31 (m, 1H, Ar*H*), 7.07–7.14 (m, 2.65H, Ar*H*), 7.00–7.03 (m, 1.35H, Ar*H*), 6.96–6.99 (m, 1H, Ar*H*), 6.88 (td, $^3J_{HH}$ = 7.5 Hz, $^4J_{HH}$ = 1.3 Hz, 1H, Ar*H*), 6.82–6.87 (m, 1.35H, Ar*H*), 6.80 (t, $^3J_{HH}$ = 7.5 Hz, 0.65H, Ar*H*), 6.68 (d, $^3J_{HH}$ = 7.6 Hz, 0.35H, Ar*H*), 6.48 (d, $^3J_{HH}$ = 7.6 Hz, 0.65 Hz, Ar*H*), 2.23 (s, 2H, CH_3), 2.15 (s, 2H, CH_3), 2.14 (s, 1H, CH_3), 2.12 (s, 1H, CH_3). Note: both *anti* and *syn* isomers are present in solution and the ^{1}H NMR spectrum was integrated to a total of 23 H atoms and indicated a ratio of 2:1 between the two isomers (with the X-ray crystallographic data suggesting the *anti*-isomer being the larger fraction). ^{13}C{^{1}H} NMR (176 MHz, $CDCl_3$): δ 170.9 (Ar*C*), 166.9 (Ar*C*), 162.8 (Ar*C*), 162.5 (Ar*C*), 161.4 (Ar*C*), 161.3 (Ar*C*), 154.8 (Ar*C*), 144.5 (Ar*C*), 144.2 (Ar*C*), 142.5 (Ar*C*), 142.3 (Ar*C*), 137.6 (Ar*C*H), 137.2 (Ar*C*H), 137.0 (Ar*C*H), 136.8 (Ar*C*H), 136.3 (Ar*C*), 136.0 (Ar*C*), 134.3 (Ar*C*), 134.2 (Ar*C*), 130.9 (Ar*C*H), 130.54 (Ar*C*H), 130.51 (Ar*C*H), 130.4 (Ar*C*H), 130.3 (Ar*C*H), 130.1 (Ar*C*H), 130.0 (Ar*C*H), 129.5 (Ar*C*H), 129.3 (Ar*C*H), 129.2 (Ar*C*H), 128.0 (Ar*C*H), 127.71 (Ar*C*H), 127.69 (Ar*C*H), 127.64 (Ar*C*H), 127.61 (Ar*C*H), 127.5 (Ar*C*H), 127.03 (Ar*C*H), 126.99 (Ar*C*H), 126.6 (Ar*C*H), 125.94 (Ar*C*H), 125.89 (Ar*C*H), 125.7 (Ar*C*H), 125.2 (Ar*C*H), 125.0 (Ar*C*H), 124.8 (Ar*C*H), 21.2 (*C*H_3), 21.0 (*C*H_3), 20.1 (*C*H_3), 20.0 (*C*H_3). Anal. Calcd. (%) for $C_{28}H_{23}Bi$: C, 59.16; H, 4.08. Found: C, 58.87; H, 4.02.

UV-Vis (THF): 263 nm (shoulder), 306 nm (shoulder). HRMS (EI): m/z calcd. for $C_{28}H_{23}Bi$: 568.1603; found: 568.1594 (Δppm = 1.7). Mp: 163–166 °C.

Synthesis of 2,3-bis(*o*-tolyl)-benzo[*b*]tellurophene (3). 2,3-Bis(*o*-tolyl)benzo[*b*]zirconocene (247.3 mg, 0.4928 mmol) and bipy•$TeCl_2$ (185.0 mg, 0.5216 mmol) were dissolved in 10 mL of THF. The resulting mixture was allowed to stir at room temperature for 24 hours and filtered through a plug of Celite. The solvent was removed from the filatrate *in vacuo* and the crude residue was extracted into 20 mL of hexanes and filtered through a plug of silica before the solvent was removed *in vacuo*. The product was further purified by flash chromatography in $CHCl_3$ (R_f = 0.95) to yield **3** (79.0 mg, 39 %) as a white solid. Crystals suitable for single crystal X-ray crystallography could be obtained by layering methanol on top of a concentrated solution of **3** in dichloromethane at room temperature. ^1H NMR (700 MHz, C_6D_6): δ 7.58 (d, $^3J_{HH}$ = 7.8 Hz, 1H, Ar*H*), 7.29–7.31 (m, 1H, Ar*H*), 7.18 (dd, $^3J_{HH}$ = 8.0 Hz, $^4J_{HH}$ = 0.8 Hz, 1H, Ar*H*), 7.05–7.08 (m, 1H, Ar*H*), 7.05 (d, $^3J_{HH}$ = 7.4 Hz, 1H, Ar*H*), 6.93–6.96 (m, 3H, Ar*H*), 6.82–6.91 (m, 4H, Ar*H*), 2.19 (s, 3H, CH_3), 2.00 (s, 3H, CH_3). $^{13}C\{^1H\}$ NMR (176 MHz, C_6D_6): δ 148.6 (Ar*C*), 146.1 (Ar*C*), 139.6 (Ar*C*), 138.6 (Ar*C*), 137.9 (Ar*C*), 137.3 (Ar*C*), 135.8 (Ar*C*), 133.5 (Ar*C*), 132.2 (Ar*C*H), 131.1 (Ar*C*H), 130.42 (Ar*C*H), 130.40 (Ar*C*H), 130.0 (Ar*C*H), 128.9 (Ar*C*H), 128.4 (Ar*C*H), 127.8 (Ar*C*H), 125.8 (Ar*C*H), 125.6 (Ar*C*H), 125.4 (Ar*C*H), 125.1 (Ar*C*H), 21.1 (CH_3), 20.2 (CH_3). Anal. Calcd. (%) for $C_{22}H_{18}Te$: C, 64.45; H, 4.43. Found: C, 64.48; H, 4.44. UV-Vis (THF): λ_{max} = 254 nm (ε = 2.45 × 10^4 $M^{-1}cm^{-1}$), λ_{max} = 324 nm (ε = 7.36 × 10^3 L•$mol^{-1}cm^{-1}$). HRMS (EI): m/z calcd. for $C_{22}H_{18}{}^{130}Te$: 412.0471; found: 412.0464 (Δppm = 1.6). Mp: 127–127 °C.

4.5.3 Attempted Suzuki-Miyaura Cross-Coupling of 4 with Substrate 5

A typical procedure for the reaction of bismole 4 with 2-bromothiophene under microwave heating. In an inert atmosphere, bismole **4** (50 mg, 0.073 mmol), **5** (24 mg, 0.15 mmol), pre-catalyst (type and mol% specified for each trial run – see Table 4.1 and Figures 4.18–4.28), base (type and equivalents specified for each trial run – see Table 4.1 and Figures 4.18–4.28), and ligand (type and mol% specified for each trial run) were transferred to a microwave vial and *ca.* 2 mL of solvent was added. The reaction vessel was sealed under inert conditions and heated in a microwave reactor at either 120 °C for 40 minutes or 140 °C for 70 minutes (as specified in Table 4.1). In the case of THF as the solvent, the reaction mixture was evaporated to dryness and the crude examined by ^{1}H NMR spectroscopy (in C_6D_6 or $CDCl_3$). In the case of DMF and acetonitrile, the reaction mixture was extracted with 10 mL of toluene, evaporated to driness and examined by ^{1}H NMR spectroscopy (in C_6D_6 or $CDCl_3$).

A typical procedure for the reaction of bismole 4 with 2-bromothiophene under standard heating to reflux. In an inert atmosphere, bismole **4** (75 mg, 0.11 mmol), **5** (36 mg, 0.22 mmol), precatalyst (type and mol% specified for each trial run – see Table 4.1 and Figures 4.18–4.28), base (type and equivalents specified for each trial run – see Table 4.1 and Figures 4.18–4.28), and ligand (type and mol% specified for each trial run) were transferred to a Schlenk flask and *ca.* 2 mL of solvent was added. The reaction mixture was heated to reflux under inert atmosphere for 16 hours. In the case of THF as the solvent, the reaction mixture was evaporated to dryness and the crude examined by ^{1}H NMR spectroscopy (in C_6D_6 or $CDCl_3$). In the case of DMF, the reaction mixture was extracted with toluene, evaporated to dryness and examined by ^1H NMR spectroscopy (in C_6D_6 or $CDCl_3$).

4.5.4 UV-Vis Data for 2 and 3

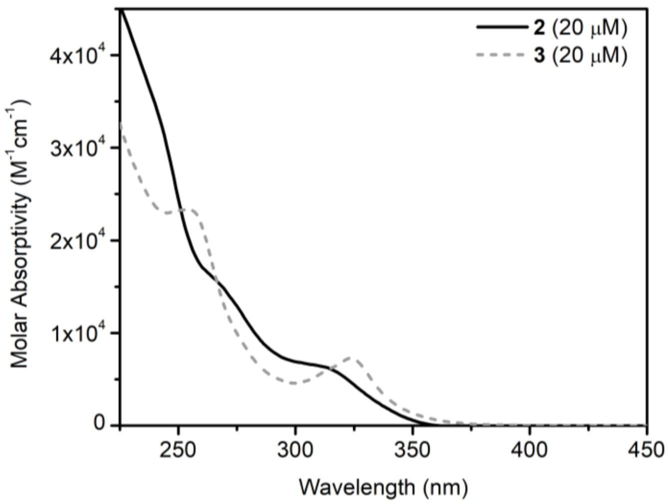

Figure 4.8. UV-vis absorbance spectra of **2** and **3** in THF, each at a concentration of 20 μM.

4.5.5 Additional NMR Data for 1–3

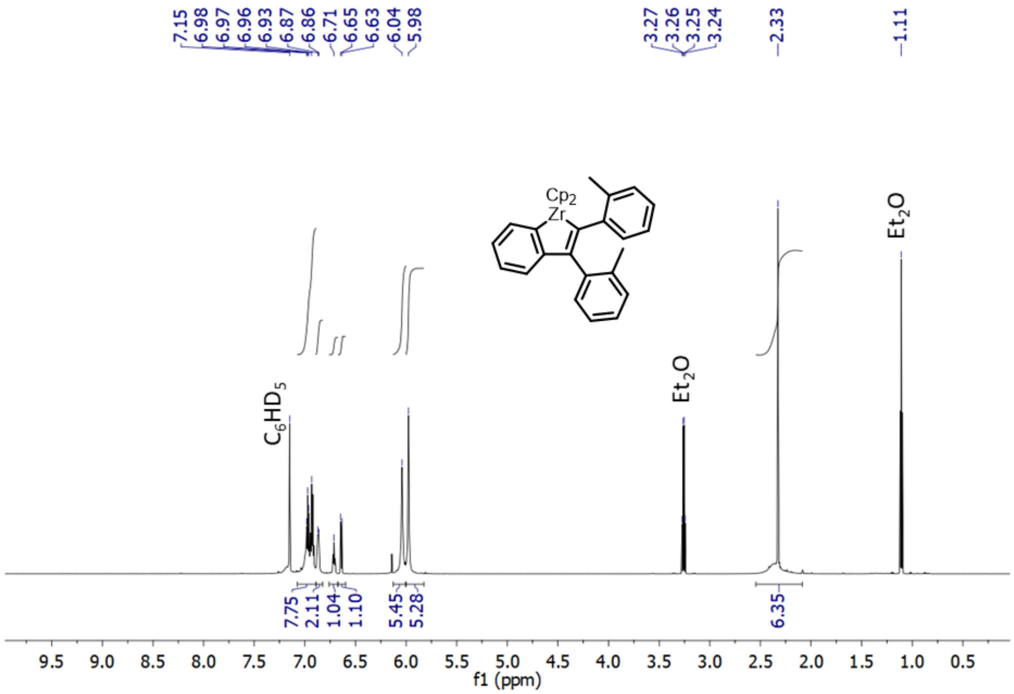

Figure 4.9. ^{1}H NMR spectrum of **1** in C_6D_6.

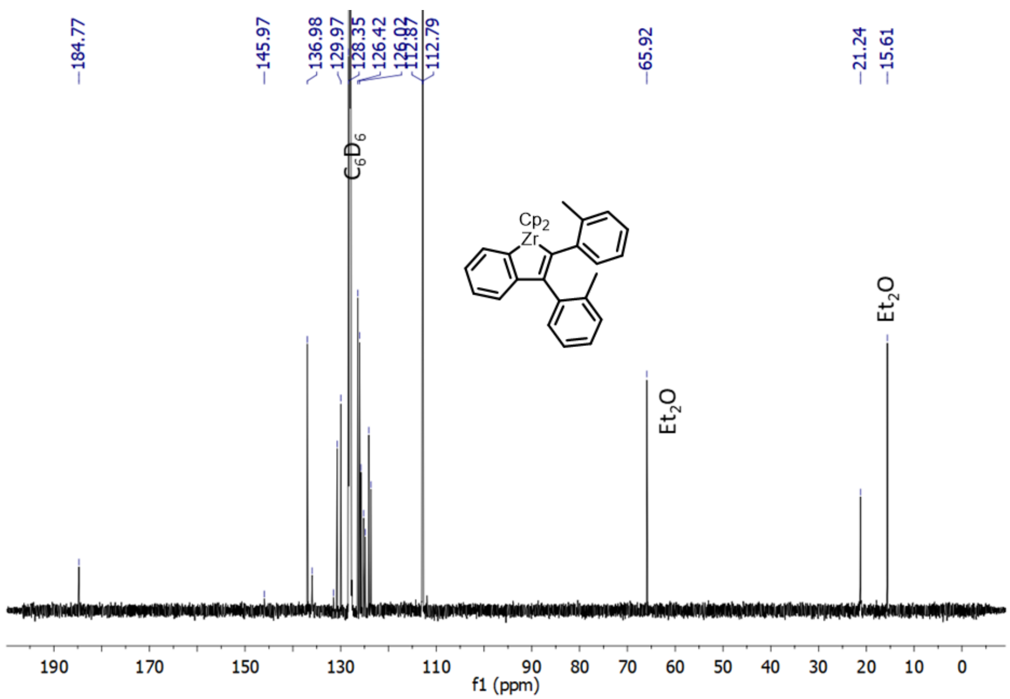

Figure 4.10. $^{13}C\{^{1}H\}$ NMR spectrum of **1** in C_6D_6.

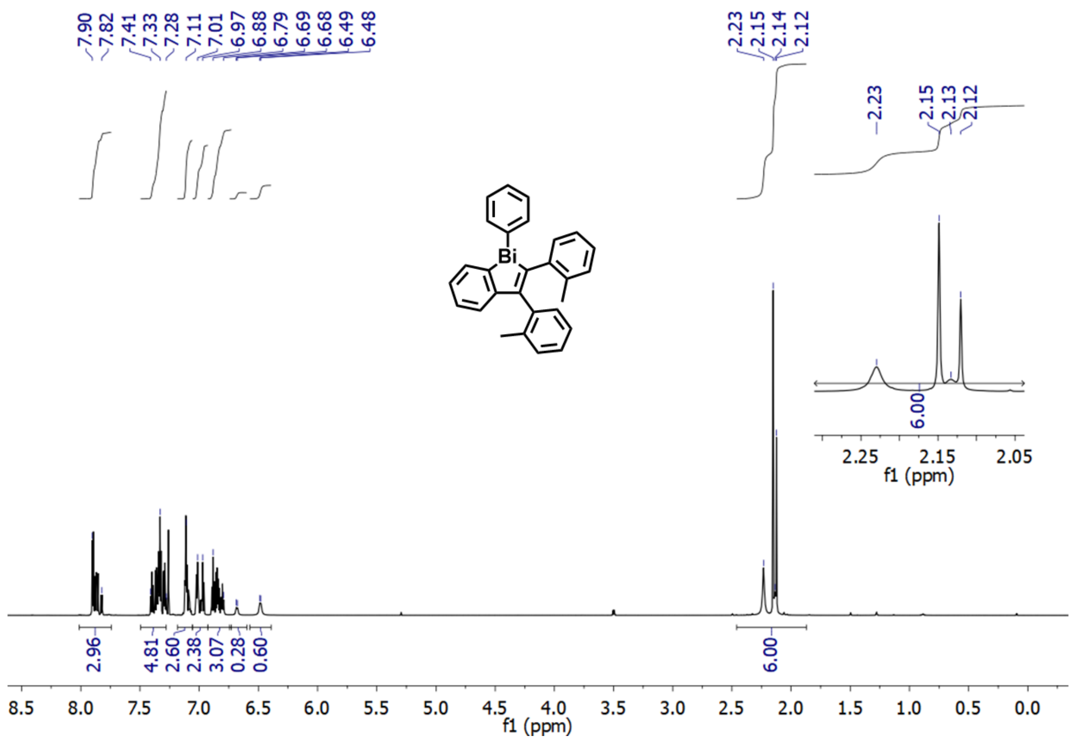

Figure 4.11. ^{1}H NMR spectrum of **2** in $CDCl_3$.

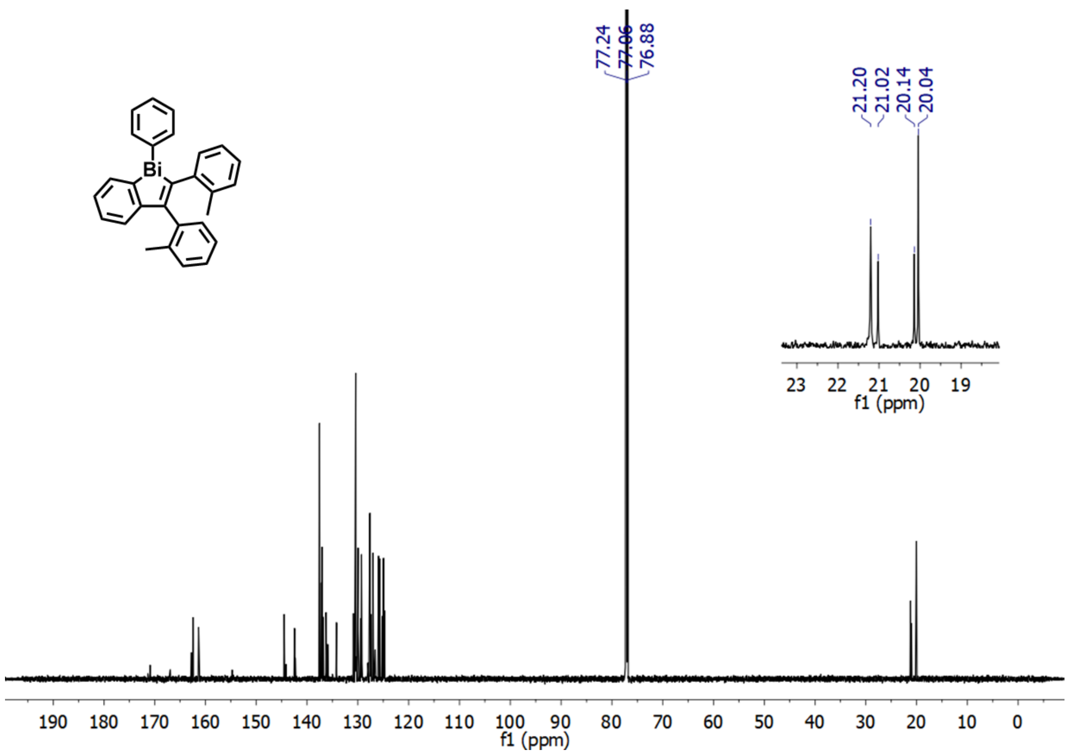

Figure 4.12. $^{13}C\{^1H\}$ NMR spectrum of **2** in $CDCl_3$.

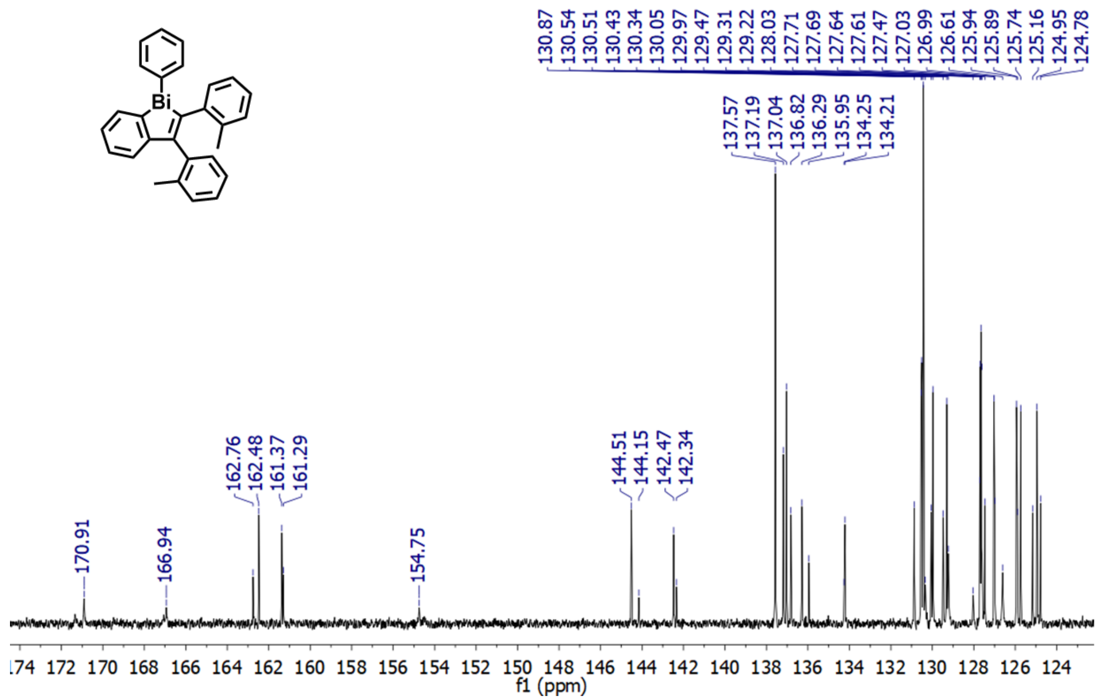

Figure 4.13. Expanded view of the $^{13}C\{^1H\}$ NMR spectrum of **2** in $CDCl_3$.

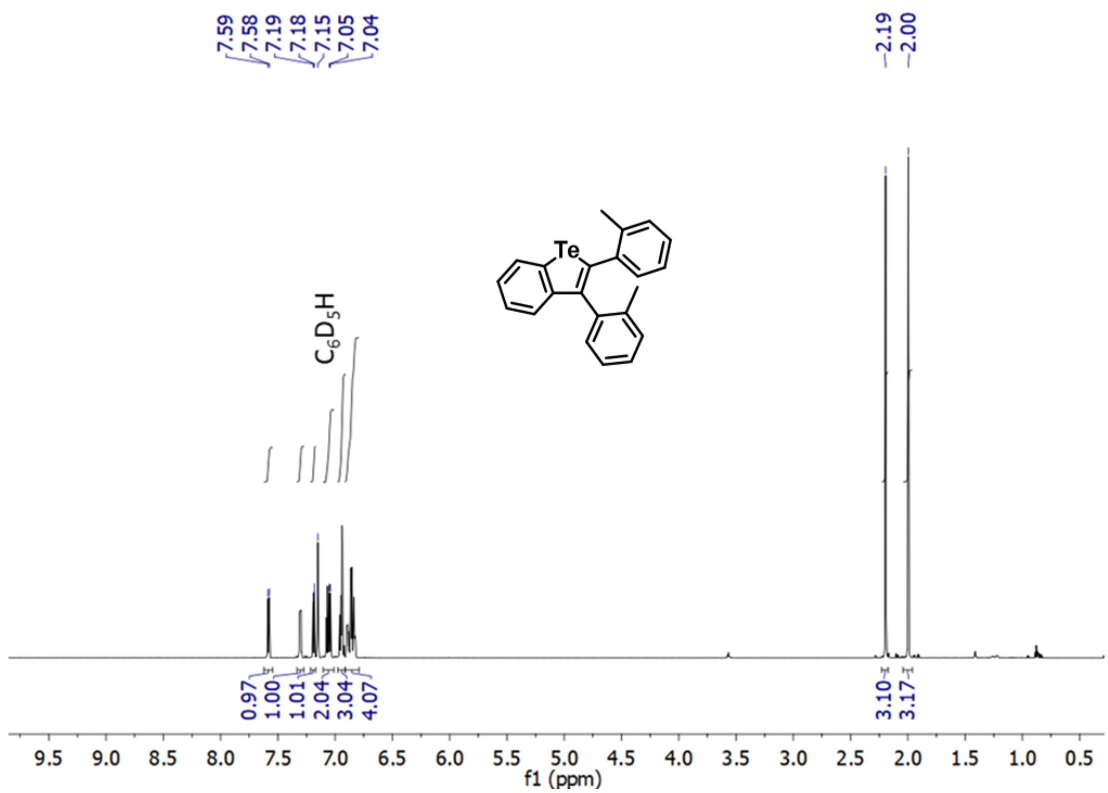

Figure 4.14. ^1H NMR spectrum of **3** in C_6D_6.

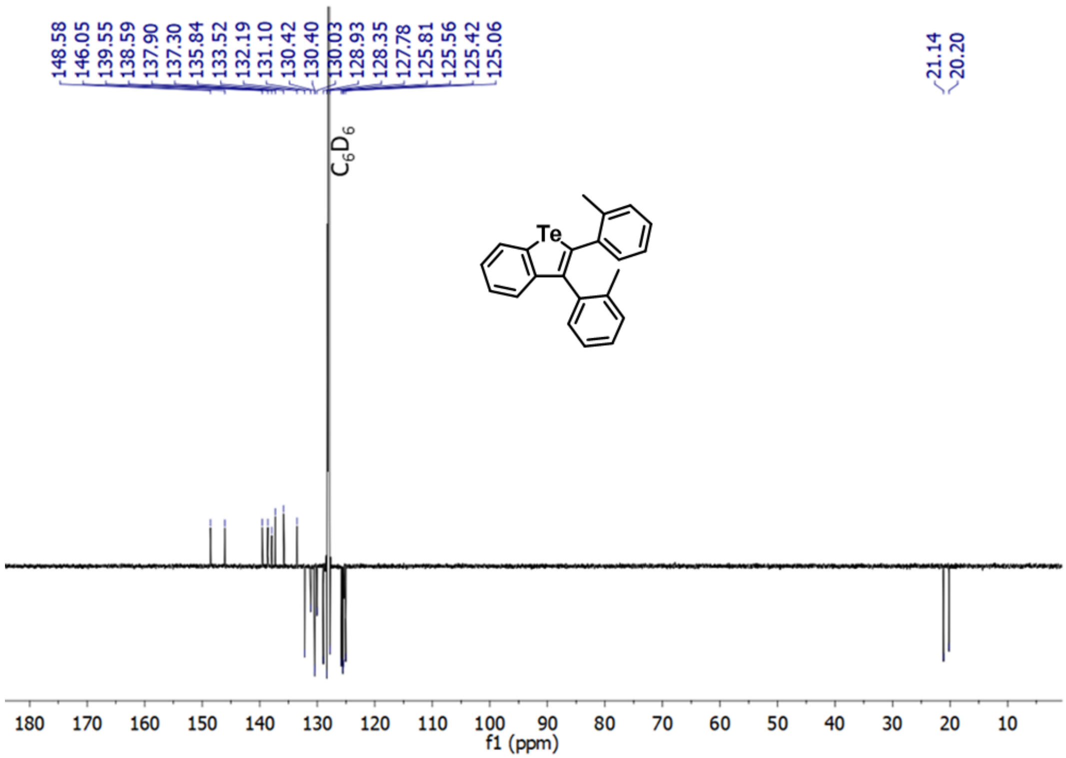

Figure 4.15. ^{13}C APT NMR spectrum of **3** in C_6D_6.

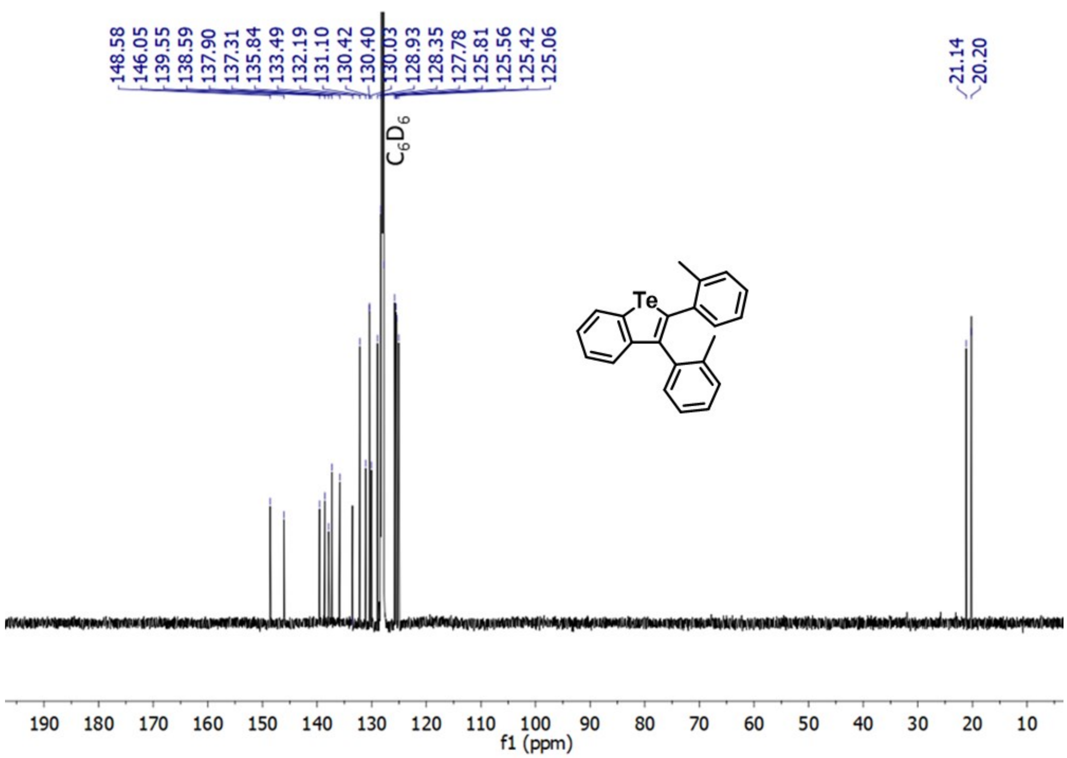

Figure 4.16. $^{13}C\{^{1}H\}$ NMR spectrum of **3** in C_6D_6.

4.5.6 NMR Data for Suzuki-Miyaura Cross-Coupling Trials with Bismole 4

The following ^{1}H NMR data was obtained from a sample of the worked up product mixtures for the indicated reactions of bismole **4** described in the aforementioned Table 4.1. In many cases, attempts at Suzuki-Miyaura cross-coupling between **4** and **5** yielded no reaction and the signals for both reactants are labelled. For the remaining reactions with bismole **4**, the product mixture contained many unidentified products so the ^{1}H NMR spectral data for these reactions are given for the sake of completeness.

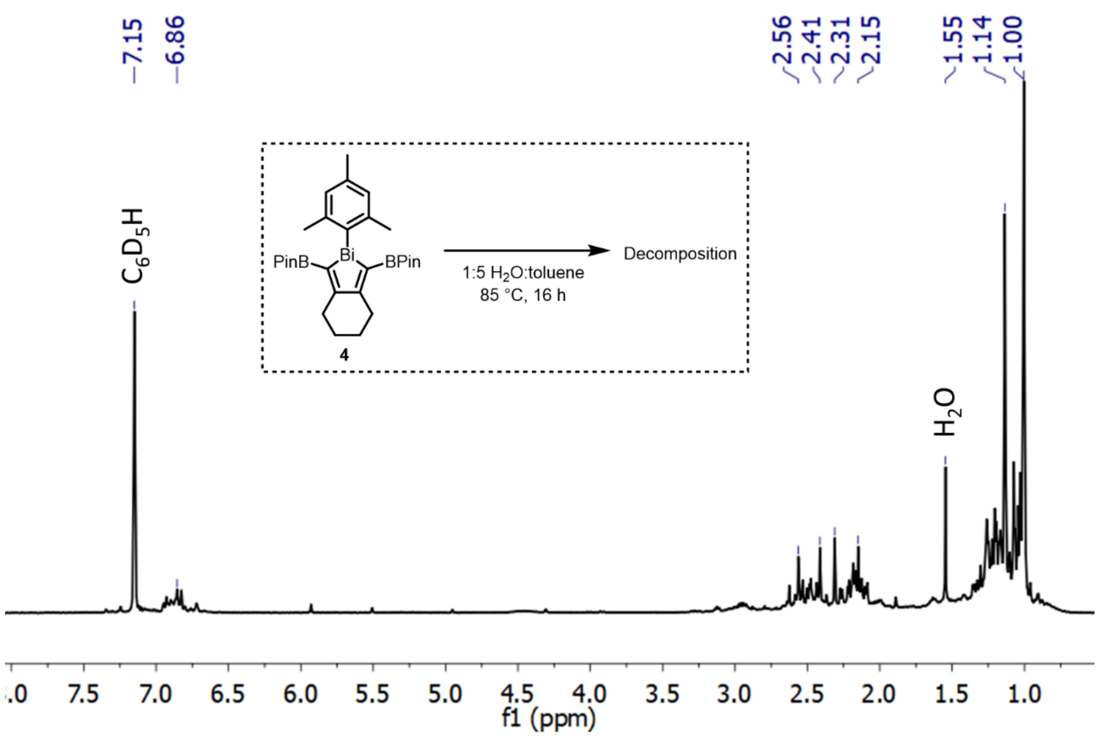

Figure 4.17. ^{1}H NMR spectrum of the results product mixture obtained from reaction of **4** with water in the absence of Pd catalyst or base.

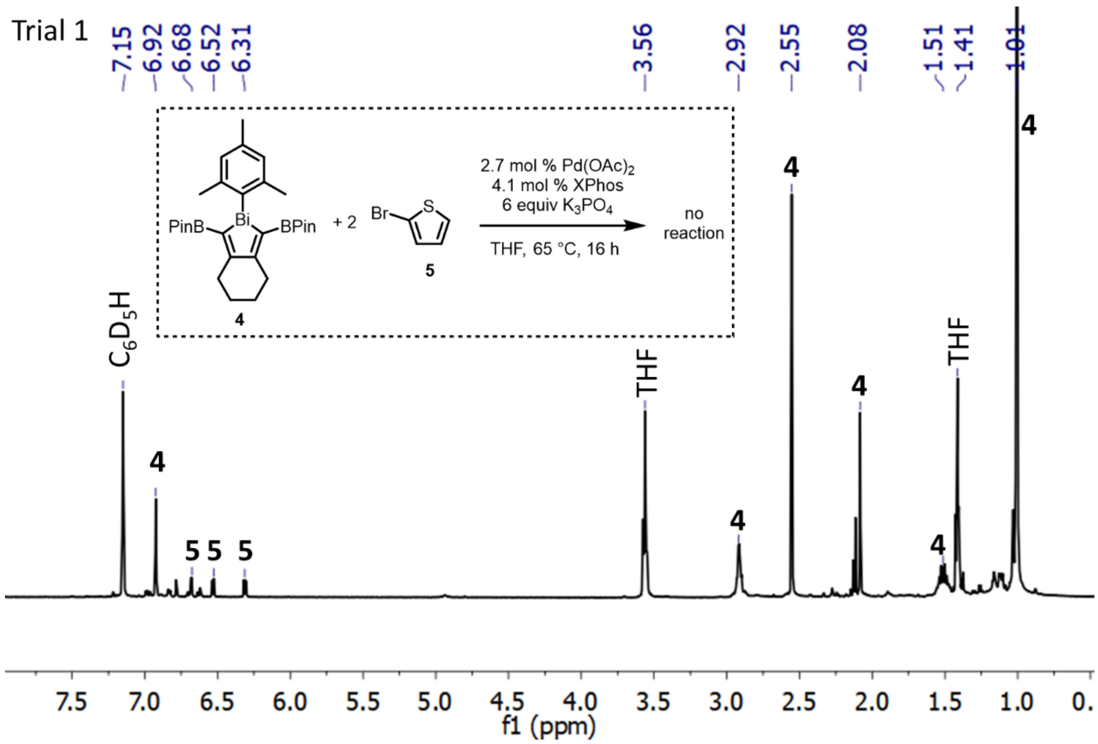

Figure 4.18. ^{1}H NMR spectrum of the mixture obtained from trial run 1 (Table 4.1).

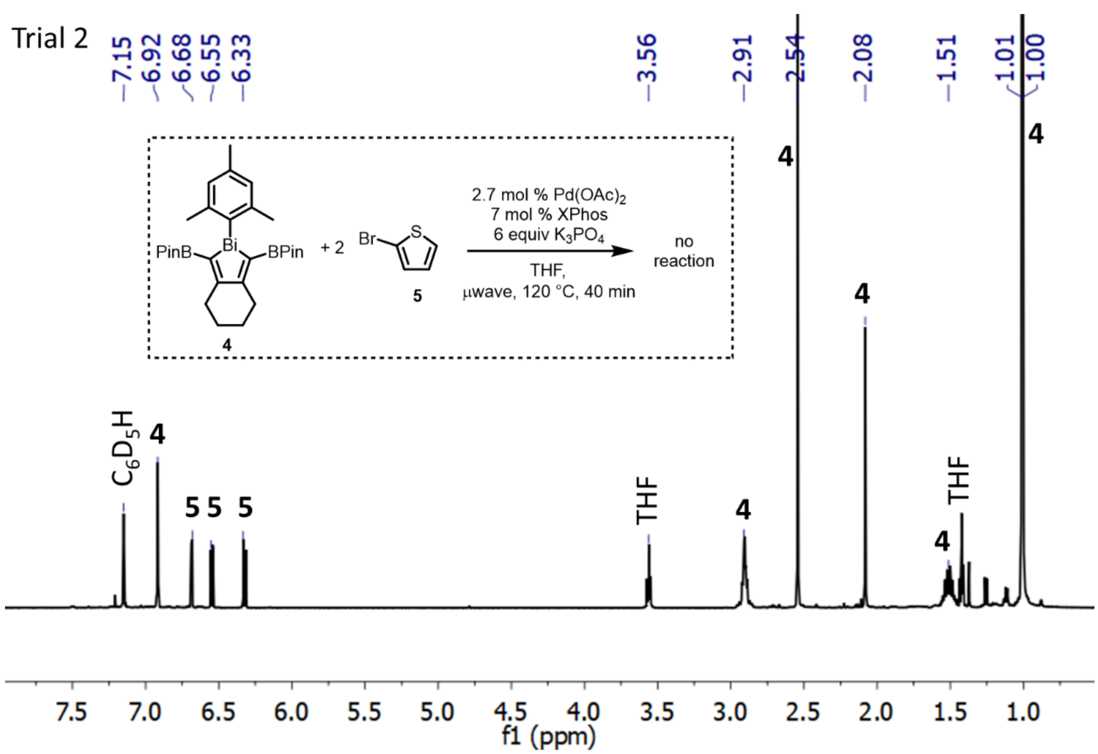

Figure 4.19. ^{1}H NMR spectrum of the mixture obtained from trial run 2 (Table 4.1).

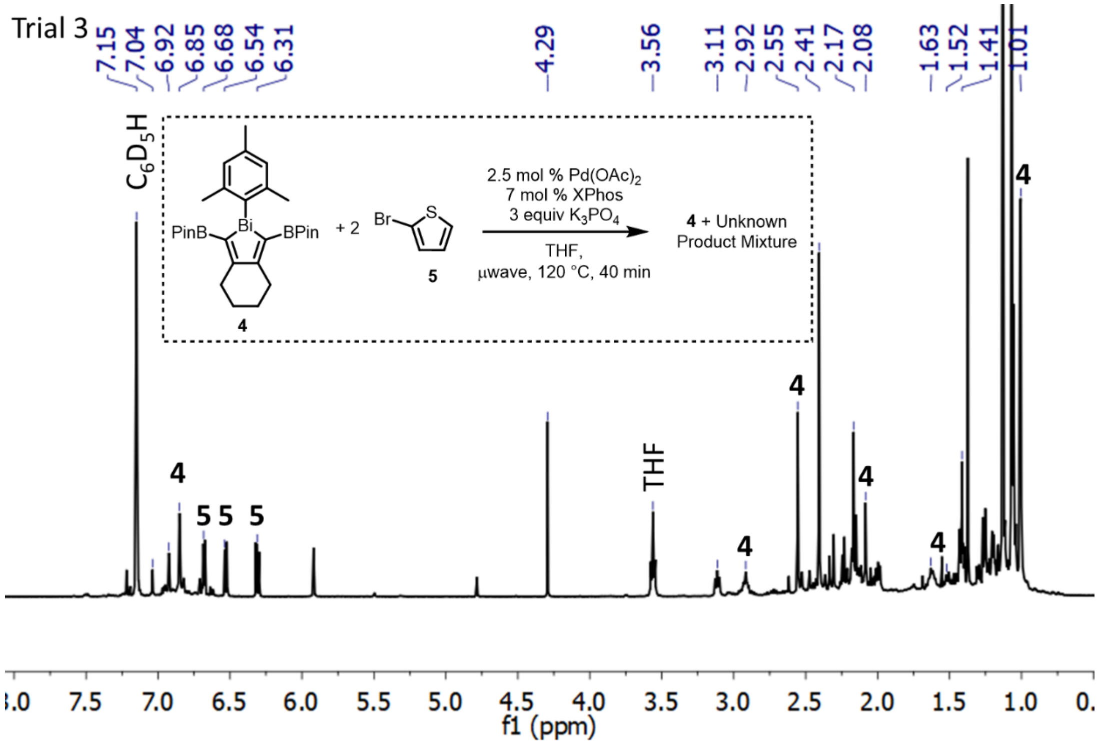

Figure 4.20. ^{1}H NMR spectrum of the mixture obtained from trial run 3 (Table 4.1).

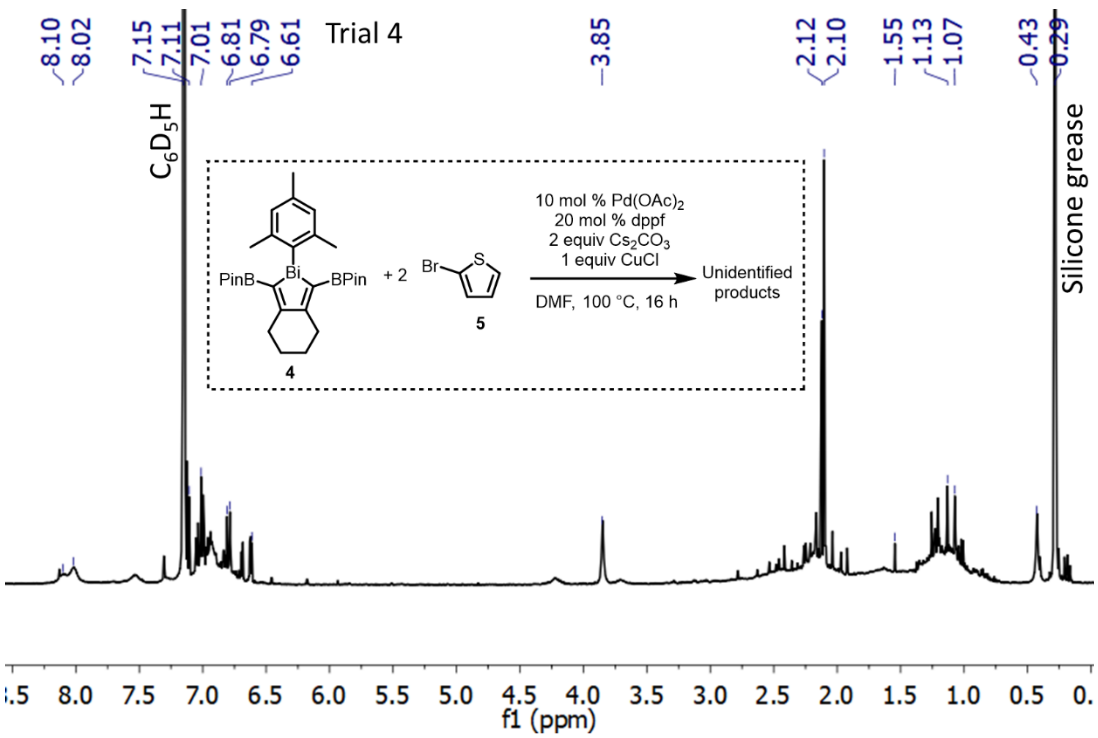

Figure 4.21. ^{1}H NMR spectrum of the mixture obtained from trial run 4 (Table 4.1).

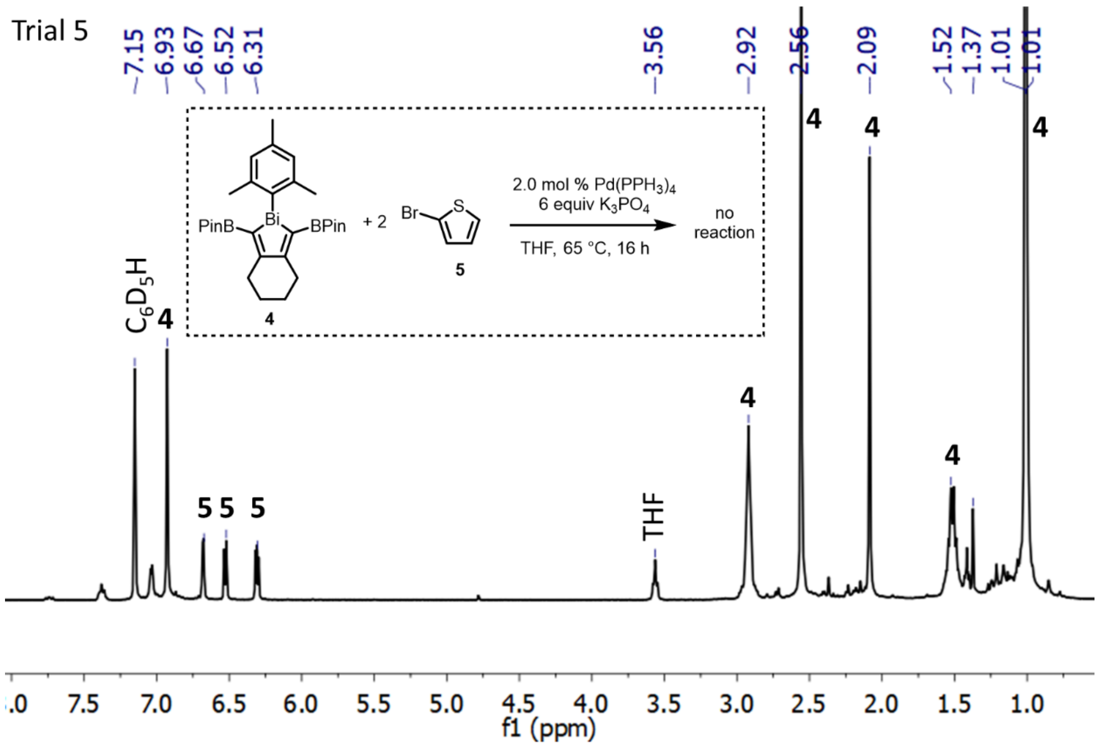

Figure 4.22. ^{1}H NMR spectrum of the mixture obtained from trial run 5 (Table 4.1).

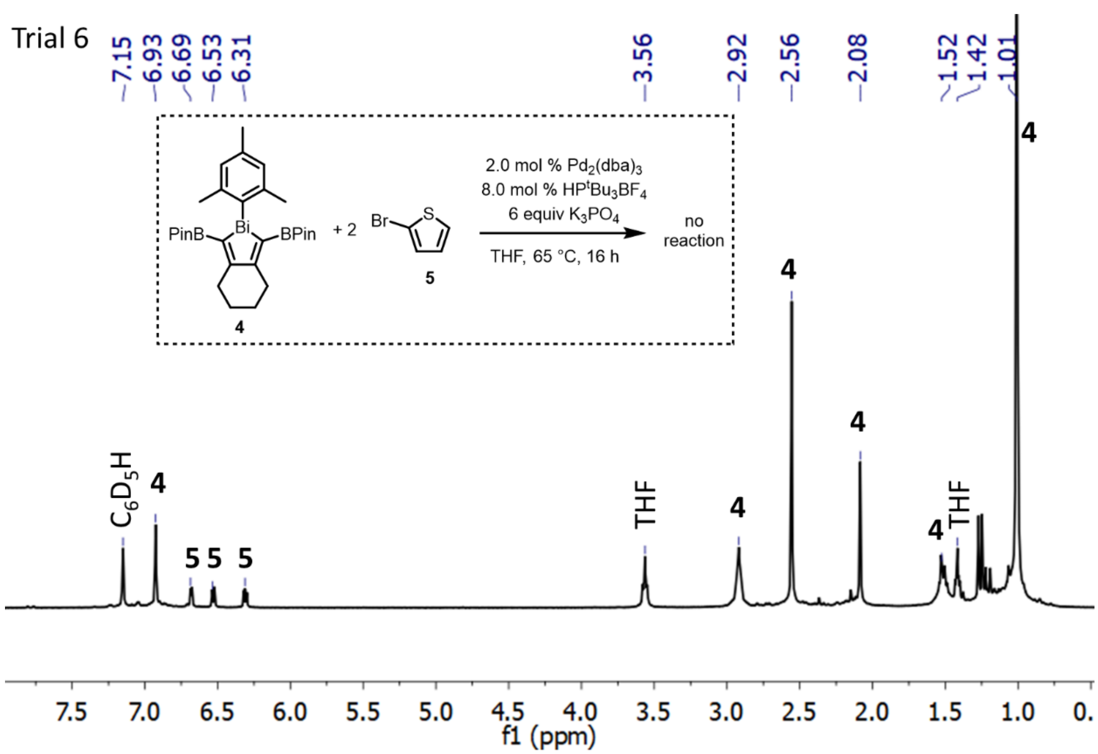

Figure 4.23. ^{1}H NMR spectrum of the mixture obtained from trial run 6 (Table 4.1).

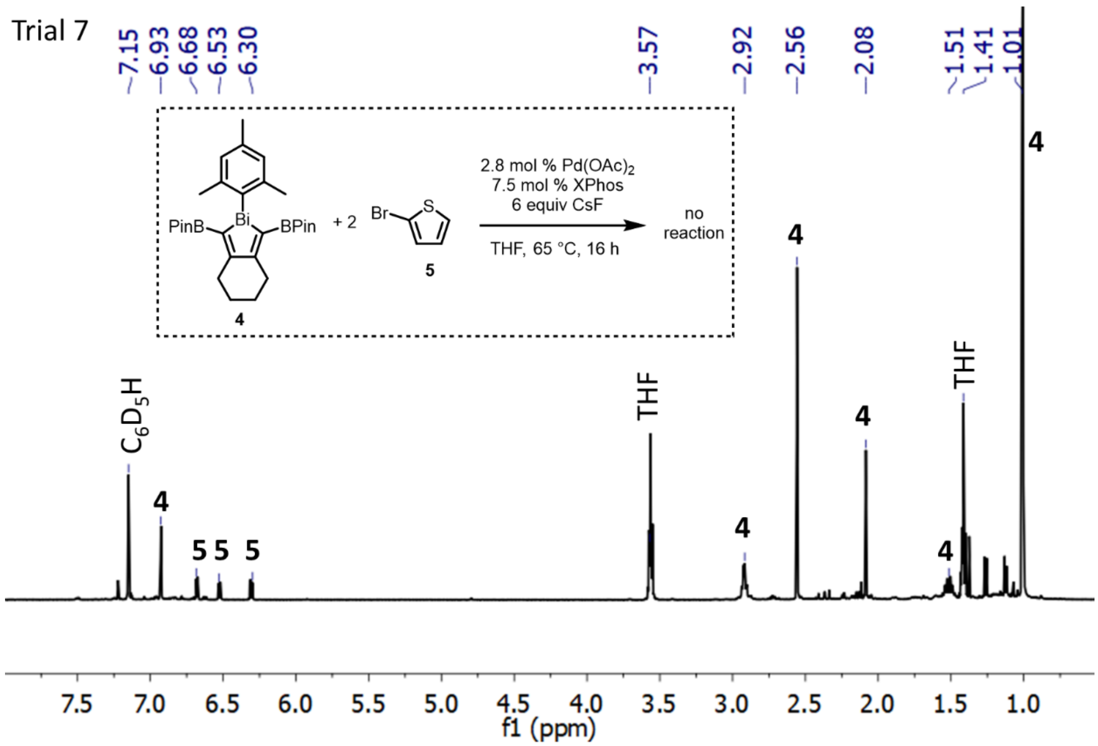

Figure 4.24. ^{1}H NMR spectrum of the mixture obtained from trial run 7 (Table 4.1).

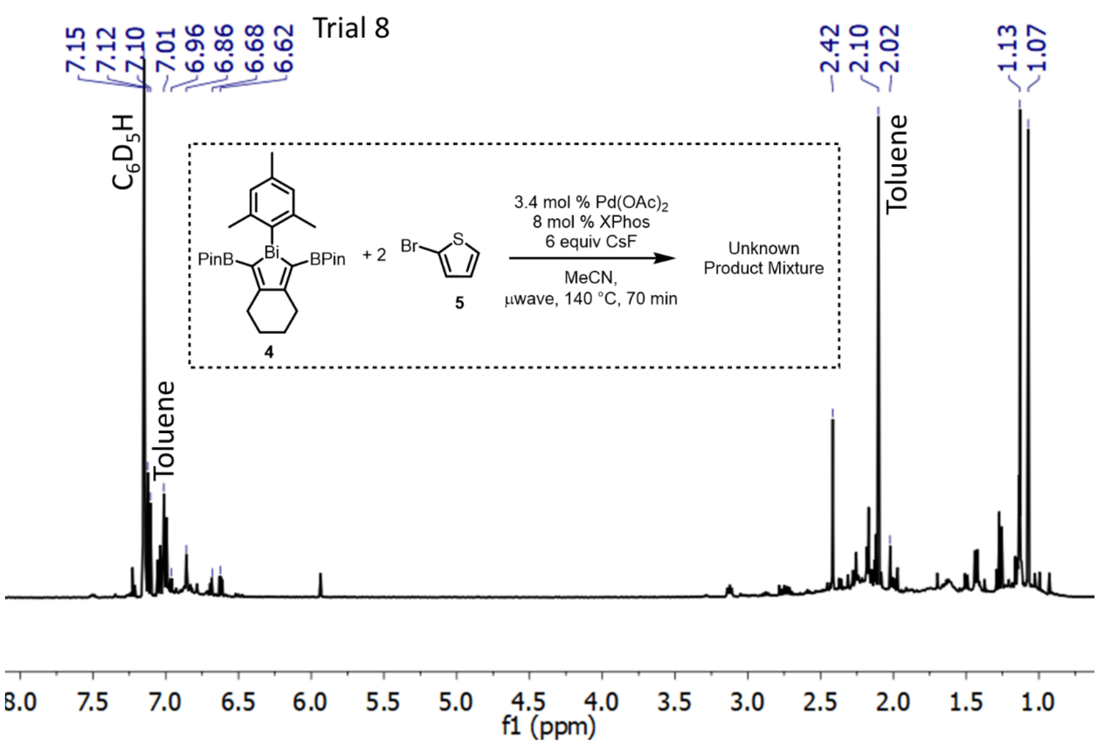

Figure 4.25. ^{1}H NMR spectrum of the mixture obtained from trial run 8 (Table 4.1).

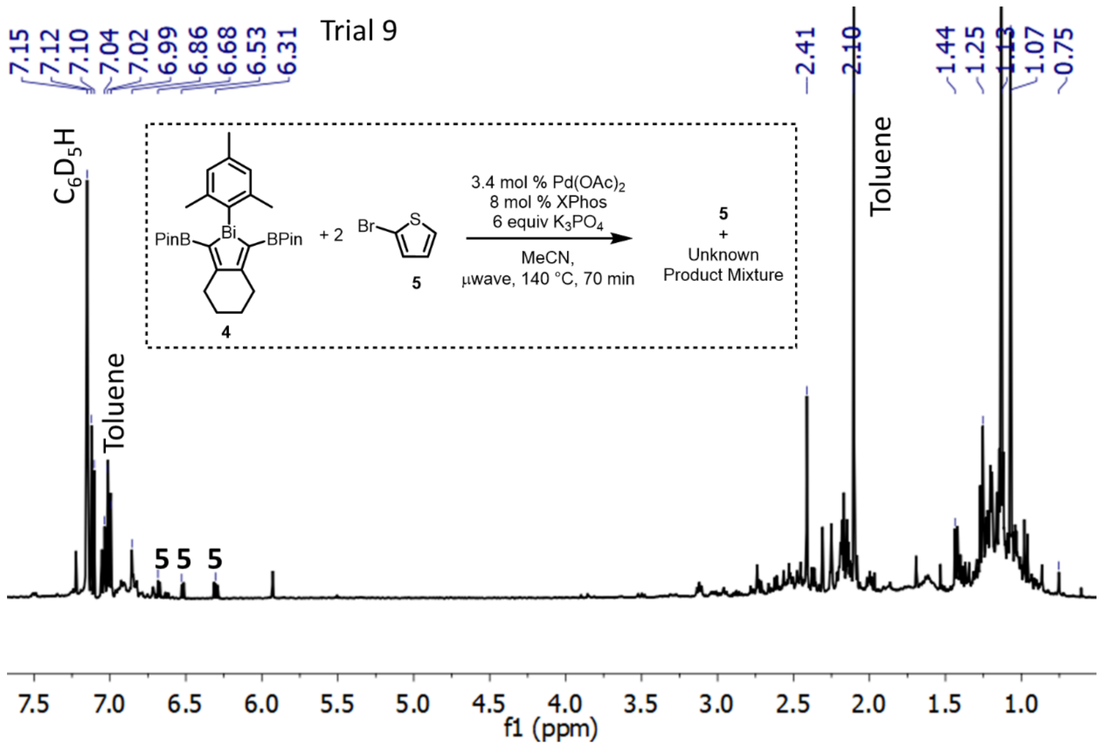

Figure 4.26. ^{1}H NMR spectrum of the mixture obtained from trial run 9 (Table 4.1).

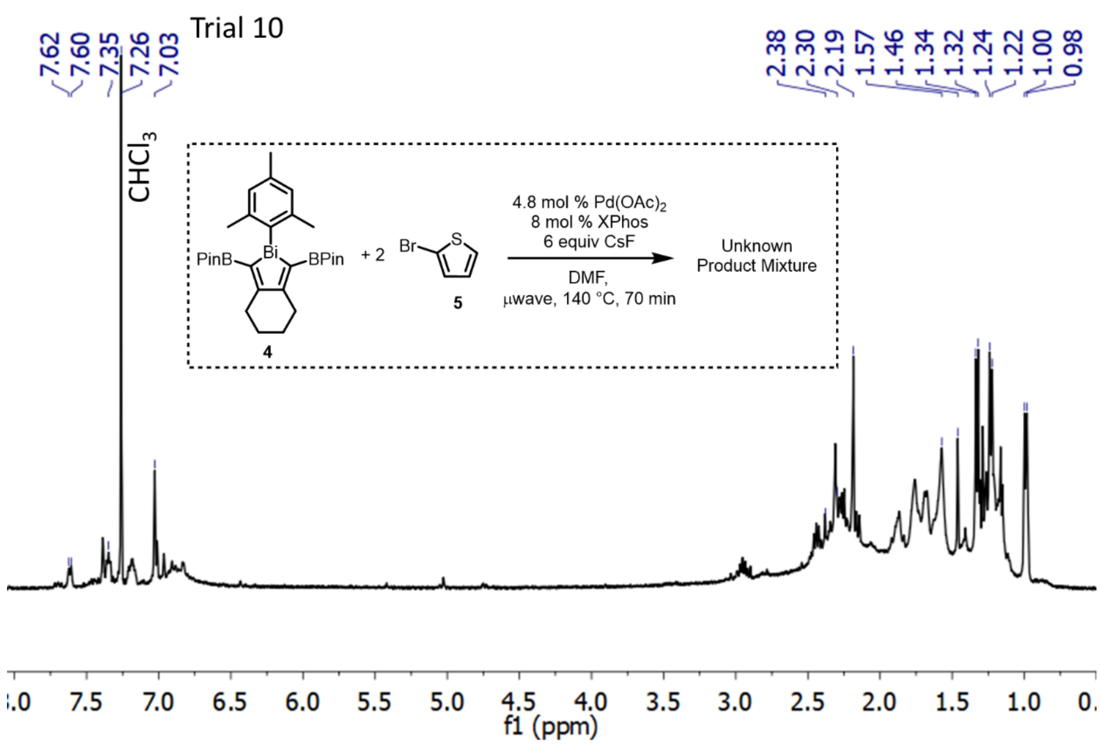

Figure 4.27. ^{1}H NMR spectrum of the mixture obtained from trial run 10 (Table 4.1).

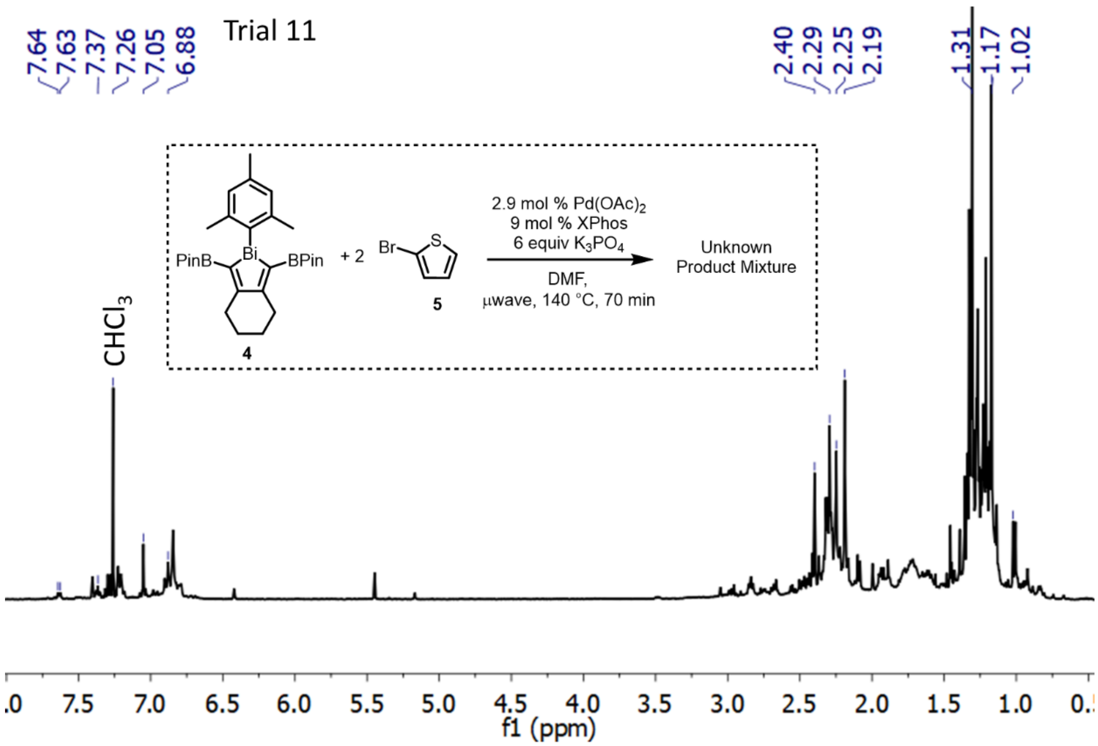

Figure 4.28. ^{1}H NMR spectrum of the mixture obtained from trial run 11 (Table 4.1).

4.5.7 X-Ray Crystallographic Data

Crystals of appropriate quality for X-ray diffraction studies were removed from a vial and immediately covered with a thin layer of hydrocarbon oil (Paratone-N). A suitable crystal was then selected, attached to a glass fiber, and quickly placed on the goniometer. All data were collected using a Bruker APEX II CCD detector/D8 diffractometer using Mo/Cu Kα radiation. The data were corrected for absorption through Gaussian integration from indexing of the crystal faces. Structures were solved using the direct methods programs SHELXS-97,[13] and refinements were completed using the program SHELXL-97.[13]

Table 4.2. Crystallographic data for compounds **1**–**3**.

Compound	**1**	**2**	**3**
Formula	$C_{34}H_{33}O_{0.50}Zr$	$C_{28}H_{23}Bi$	$C_{22}H_{18}Te$
Formula weight	540.82	568.44	409.96
Crystal system	Monoclinic	Monoclinic	Monoclinic
Space group	*C2/c*	$P2_1/c$	$P2_1/c$
a (Å)	29.2593(5)	9.9476(2)	10.6449(2)
b (Å)	16.6976(3)	11.0729(2)	8.5059(2)
c (Å)	25.1161(4)	19.9320(4)	19.4694(4)
α (°)	--	--	--
β (°)	117.3659(10)	91.5700(7)	105.2405(8)
γ (°)	--	--	--
V (Å^3)	10897.5(3)	2194.66(7)	1700.85(6)
Z	16	4	4
ρ (g/cm^3)	1.319	1.720	1.601
Abs coeff (mm^{-1})	3.455	15.82	13.75
T (K)	173	173	173
$2\theta_{max}$ (°)	140.52	148.03	144.68
Total data	34504	15285	11121
Unique data (R_{int})	10364 (0.0521)	4463 (0.0145)	3361 (0.0187)
Obs data [I>2($\sigma(I)$]	8297	4449	3341
Params	644	294	210
R_1 [I>2($\sigma(I)$]^a	0.0477	0.0154	0.0220
wR_2 [all data]^a	0.1399	0.0383	0.0514
Max/min $\Delta\rho$ (e^{-1}Å^{-3})	1.810/–0.757	0.257/–0.778	0.466/–0.431

$^aR_1 = \Sigma||F_o| - |F_c||/\Sigma|F_o|$; $wR_2 = [\Sigma w(F_o^2 - F_c^2)^2/\Sigma w(F_o^4)]^{1/2}$

4.6 References

1. Mei, J.; Leung, N. L. C.; Kwok, R. T. K.; Lam, J. W. Y.; Tang, B. Z. *Chem. Rev.* **2015**, *115*, 11718−11940.

2. (a) Parke, S. M.; Narreto, M. A. B.; Hupf, E.; McDonald, R.; Ferguson, M. J.; Hegmann, F. A.; Rivard, E. *Inorg. Chem*. **2018**, *57*, 7536–7549. (b) Parke, S. M.; Hupf, E.; Matharu, G. K.; de Aguiar, I.; Xu, L.; Yu, H.; Boone, M. P.; de Souza,

G. L. C.; McDonald, R.; Ferguson, M. J.; He, G.; Brown, A.; Rivard, E. *Angew. Chem. Int. Ed*. **2018**, *57*, 14841–14846.

3. Gessner, V. H.; Tannaci, J. F.; Miller, A. D.; Tilley, T. D. *Acc. Chem. Res.* **2011**, *44*, 435–446.

4. Miller, A. D.; Tannaci, J. F.; Johnson, S. A.; Lee, H.; McBee, J. L.; Tilley, T. D. *J. Am. Chem. Soc.* **2009**, *131*, 4917–4927.

5. (a) He, G.; Kang, L.; Torres Delgado, W.; Shynkaruk, O.; Ferguson, M. J.; McDonald, R.; Rivard, E. *J. Am. Chem. Soc.* **2013**, *135*, 5360–5363. (b) Torres Delgado, W.; Braun, C. A.; Boone, M. P.; Shynkaruk, O.; Qi, Y.; McDonald, R.; Ferguson, M. J.; Data, P.; Almeida, S. K. C.; de Aguiar, I.; de Souza, G. L. C.; Brown, A.; He, G.; Rivard, E. *ACS Appl. Mater. Interfaces* **2018**, *10*, 12124–12134.

6. He, G.; Wiltshire, B. D.; Choi, P.; Savin, A.; Sun, S.; Mohammadpour, A.; Ferguson, M. J.; McDonald, R.; Farsinezhad, S.; Brown, A.; Shankar, K.; Rivard, E. *Chem. Commun*. **2015**, *51*, 5444–5447.

7. Mantina, M.; Chamberlin, A. C.; Valero, R.; Cramer, C. J.; Truhlar, D. G. *J. Phys. Chem. A* **2009**, *113*, 5806−5812.

8. (a) Sheppard, G. S. *Synlett* **1999**, *8*, 1207–1210. (b) Gagnon, A.; Dansereau, J.; Le Roch, A. *Synthesis* **2017**, *49*, 1707–1745. (c) Condon, S.; Pichon, C.; Davi, M. *Org. Prep. Proced. Int.* **2014**, *46*, 89–131.

9. (a) Petiot, P.; Gagnon, A. *Eur. J. Org. Chem*. **2013**, 5282–5289. (b) Hébert, M.; Petiot, P.; Benoit, E.; Dansereau, J.; Ahmad, T.; Le Roch, A.; Ottenwaelder, X.; Gagnon, A. *J. Org. Chem*. **2016**, *81*, 5401−5416. (c) Dansereau, J.; Gautreau, S.;

Gagnon, A. *ChemistrySelect* **2017**, *2*, 2593–2599. (d) Zhou, W.-J.; Wang, K.-H.; Wang, J.-X.; Huang, D.-F. *Eur. J. Org. Chem*. **2010**, 416–419. (e) Ohe, T.; Tanaka, T.; Kuroda, M.; Cho, C. S.; Ohe, K.; Uemura, S. *Bull. Chem. Soc. Jpn.* **1999**, *72*, 1851–1855.

10. Yan, H.; Wang, H.; Li, X.; Xin, X.; Wang, C.; Wan, B. *Angew. Chem. Int. Ed*. **2015**, *54*, 10613–10617.

11. Jantunen, K. C.; Scott, B. L.; Kiplinger, J. L. *J. Alloy. Compd.* **2007**, *444*, 363–368.

12. Dutton, J. L.; Farrar, G. J.; Sgro, M. J.; Battista, T. L.; Ragogna, P. J. *Chem. Eur. J.* **2009**, *15*, 10263–10271.

13. Sheldrick, G. M. *Acta Cryst. A* **2008**, *64*, 112–122.

Chapter 5: Self-Assembly of Benzo[*b*]phosphole Oxide-Based Block Copolymers

5.1 Introduction

Phospholes have been widely explored as highly fluorescent materials for organic LEDs,[1] bioimaging agents,[2] and for their ability to coordinate transition metals.[3] While phospholes based on phosphorus (III) centers tend to exhibit high air-sensitivity, oxidation to a phosphorus (V) center through the production of phosphole oxides, phosphole sulfides, or phosphole selenides has been shown to be an effective strategy to impart air-stability while providing a method of tuning optoelectronic properties.[4]

Benzo[*b*]phosphole oxides are of interest due to their high photostability[5] and the prevalence of benzo[*b*]phosphole oxide-based emitters with quantum yields approaching 100 %.[6] Recently, benzophosphole oxides have gained interest for their aggregation induced emission (AIE) properties, wherein greatly enhanced luminescence is observed in the solid (aggregated) states compared to in solution.[7,8] A 2017 report by the group of B. Z. Tang discussed the fluorescent properties of a set of benzo[*b*]phosphole oxides, depicted in Chart 5.1.[8] While **I**, **II**, **VI**, and **VII** all displayed aggregation enhanced emission to varying degrees, **VII** displayed a high solid-state quantum yield (Φ) of 89.4 % and an exceptionally high AIE enhancement ratio ($\Phi_{solid}/\Phi_{solution}$) of 9.6.

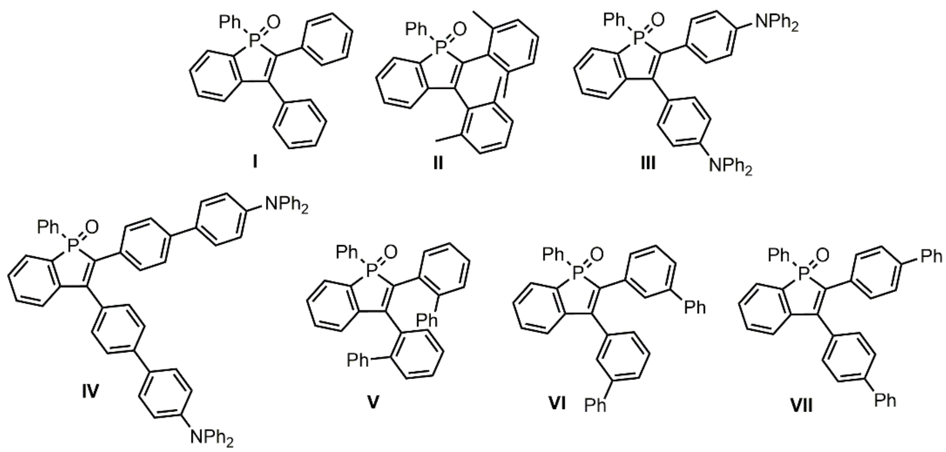

Figure 5.1. Previously reported luminescent benzo[*b*]phosphole oxides serve as a foundation for the study reported herein.

Chapter 3 highlighted an efficient synthetic strategy for the incorporation of luminescent benzobismole units into a soluble block copolymer framework via ring opening metathesis polymerization (ROMP) with Grubbs' 3rd Generation catalyst. The resulting block copolymer was observed to undergo self-assembly in hexanes:THF solutions to yield spherical micelles.[9] Reported herein, this previously reported block copolymer self-assembly approach is extended to yield highly fluorescent benzophosphole analogues. The *para*-biphenyl-substituted benzophosphole (**VII**) core (Figure 5.1) was chosen with the goal of exploiting its high AIE enhancement ratio to visualize micelle formation *in situ*.

5.2 Results and Discussion

5.2.1 Synthesis of Monomers

Zirconacycle **1** was first formed via a cyclization of bis(*para*-biphenyl) acetylene, bpC≡Cbp, and Cp_2ZrPh_2 as shown in Scheme 5.1. Single crystals of the resulting benzozirconacycle **1** that were suitable for X-ray crystallography could be obtained from the slow diffusion of hexanes into a concentrated solution of **1** in toluene; the molecular structure of **1** is shown in Figure 5.2. Following the Fagan and Nugent[10,11] protocol previously used in the Rivard group for the generation of benzotellurophenes[12] and benzobismoles,[9] **1** was reacted with one equivalent of PCl_3 to generate the chlorophosphole **2** in a quantitative yield (Scheme 5.1). The byproduct from metallacycle transfer, zirconocene dichloride, Cp_2ZrCl_2, could not easily be removed from crude **2**, but its amount could be easily quantified by ^1H NMR spectroscopy.

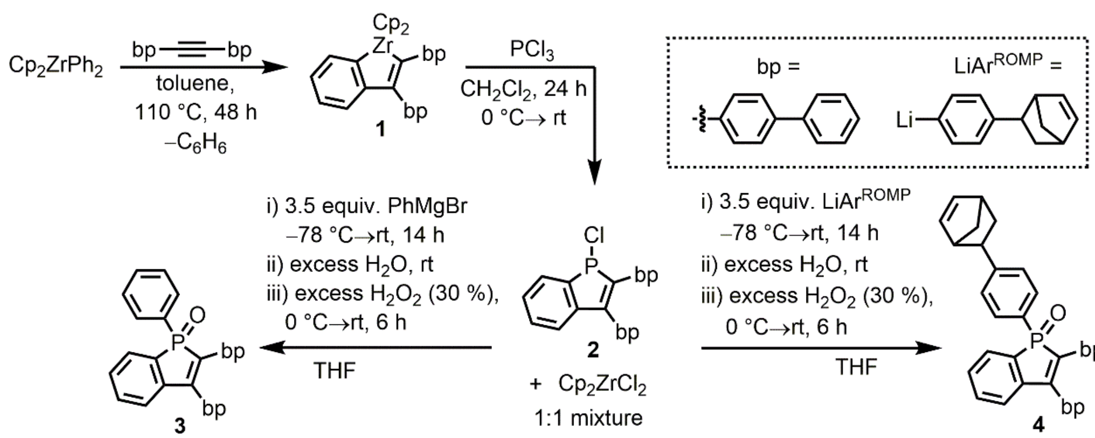

Scheme 5.1. Synthesis of zirconcacycle **1** and subsequent metallacycle transfer to produce phosphole **2**, which could then be converted to the benzophosphole oxides **3** and **4**.

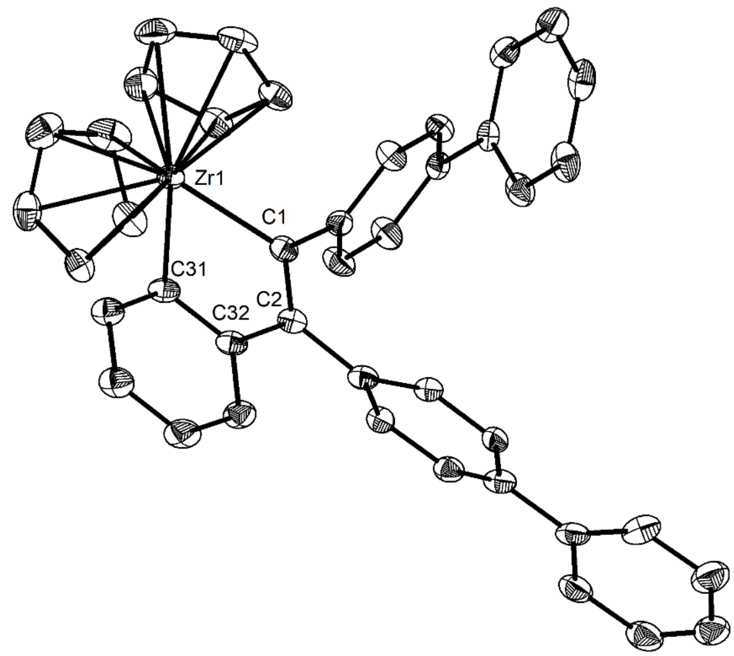

Figure 5.2. Molecular structure of 2,3-bis(*para*-biphenyl)benzozirconocene (**1**) with thermal ellipsoids presented at a 30 % probability level. All hydrogen atoms have been omitted for clarity. Selected bond lengths (Å) and angles (°): Zr1–C1 2.280(3), Zr1–C31 2.270(3), C1–C2 1.359(4), C32–C2 1.494(4), C31–C32 1.415(4); C1–Zr–C31 77.21(10), Zr1–C1–C2 112.91(19), Zr1–C31–C32 111.78(18).

The synthesis of the benzophosphole oxides **3** and **4** were carried out from a *c.a.* 1:1 mixture of **2** and Cp_2ZrCl_2 by using an excess (3.5 equivalents) of PhMgBr or *para*-norbornyl-phenyllithium (denoted as $LiAr^{ROMP}$ in Scheme 5.1), respectively, to account for the expected reactivity of Cp_2ZrCl_2. After the formation of the corresponding P-arylated benzophospholes, oxidation of the phosphorus centers was accomplished using an excess of hydrogen peroxide, as outlined in Scheme 5.1. Any Zr-containing side products could be removed by flash chromatography yielding pure air- and moisture stable, benzophosphole oxides **3** and **4** as yellow solids in 85 % and 71 % yields, respectively.

The molecular structure of the parent benzophosphole oxide, **3**, is shown in Figure 5.3. The planar benzophosphole oxide core is surrounded by peripheral phenyl rings which are twisted out of plane with central ring in a propeller-like fashion, a commonly observed feature for these types of arylated heterocycles. The closest intermolecular P···O separation is 8.5249(13) Å, and this large distance, in conjunction with a lack of close π–π stacking interactions in the solid state, helps explain the high emission quantum yield observed in the solid state (*i.e.* the lack of aggregation-caused quenching, ACQ).

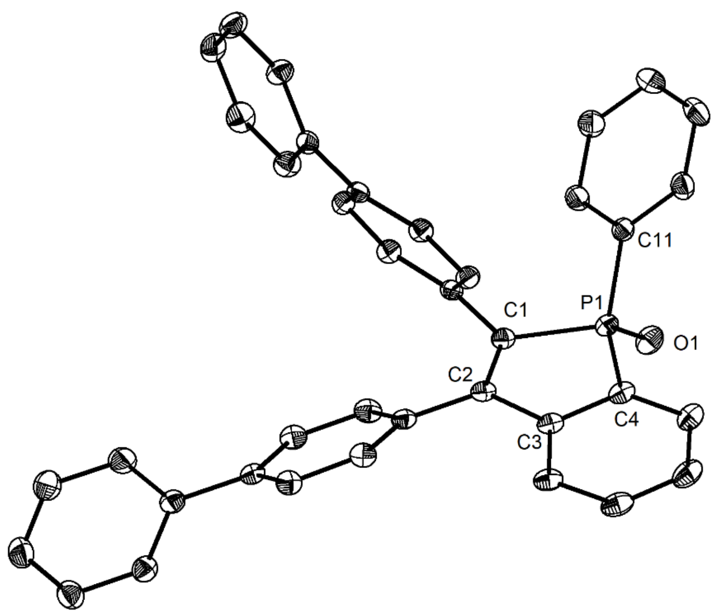

Figure 5.3. Molecular structure of **3** with thermal ellipsoids plotted at a 30 % probability level. All hydrogen atoms were omitted for clarity. Select bond lengths (Å) and angles (deg): P1–C11 1.7979(15), P1–O1 1.4849(11), P1–C1 1.8095(15), P1–C4 1.8002(15), C1–C2 1.357(2), C2–C3 1.493(2), C3–C4 1.401(2); C1–P1–C4 92.50(7), C1–P1–C11 105.43(6), C4–P1–C11 108.85(7), O1–P1–C11 112.30(7), O1–P1–C1 119.13(7), O1–P1–C4 116.57(7), P1–C1–C2 110.52(11), P1–C4–C3 109.31(11).

The ROMP active norbornene-capped pinacolboronate monomer **5** was also synthesized (Scheme 5.2) with the expectation that it may exhibit solid state phosphorescence, as has been observed in similar boronic ester-substituted aryl-based luminogens.[13] Figure 5.4 shows the molecular structure of colorless crystals of **5** as determined via single-crystal X-ray crystallography. The structure of **5** involves some disorder about the norbornyl group; however, the molecular structure indicates the preferential crystallization of the *exo*-isomer. Despite literature precedence for the long-lifetime (> 1 s) phosphorescence of some BPin-substituted aryl compounds,[13] **5** displayed no observable emission in solution or in the solid state, at room temperature or at 77 K in the absence of oxygen (a known quencher of phosphorescence).

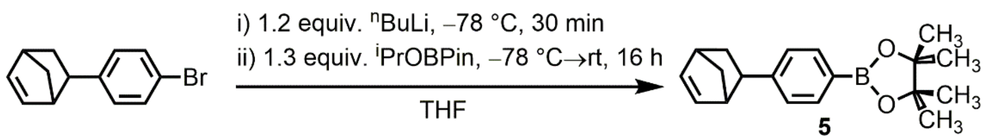

Scheme 5.2. Synthesis of BPin-containing monomer **5**.

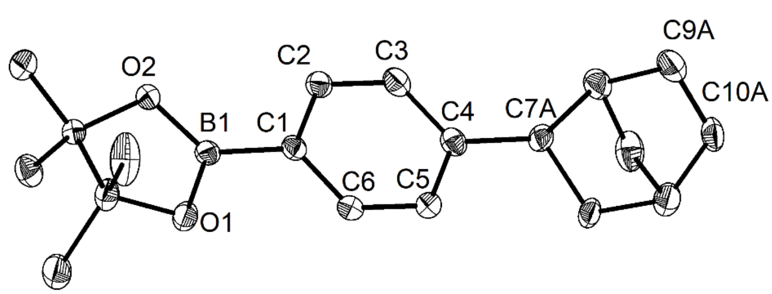

Figure 5.4. Molecular structure of **5** with thermal ellipsoids plotted at a 30 % probability level. Only the major orientation of the disordered norbornenyl group is shown. All hydrogen atoms were omitted for clarity. Select bond lengths (Å) and angles (deg): B1–C1 1.558(3), B1–O1 1.366(2), B1–O2 1.362(2), C4–C7A 1.556(4), C9A–C10A 1.323(7); O1–B1–O2 113.68(16).

5.2.2 Photoluminescence of the Benzophosphole Oxides 3 and 4

Compound **3** has been previously reported to exhibit aggregation induced emission (AIE) with a strong on/off ratio of 9.6, with an absolute quantum yield (Φ) of 89 % as a film (λ_{em} = 492 nm) and Φ = 9.3 % in THF solution (λ_{em} = 486 nm).[8] Photoluminescence (PL) measurements in the present study found **3** to have two excitation maxima when measured in THF: 305 and 361 nm that both lead to emission at 498 nm (Figure 5.5). Comparable to previously reported data, absolute quantum yield measurements on 2.0 μM solutions of **3** in THF yielded Φ = 9.5 % (with λ_{ex} = 360 nm, and Φ = 9.8 % with λ_{em} = 310). To explore whether both excitation peaks were indeed leading to the same emission, the edges of each excitation profile for **3** were probed. Excitation at 260 nm results in a normalized emission spectrum that appears to be identical to the emission spectrum generated upon excitation at 415 nm; thus, both excitation maxima led to emission from the same singlet excited state. In the crystalline state, the emission of **3** exhibits a very slight red-shift (λ_{em} = 510 nm), and the excitation spectrum shows just one broad peak with a maximum at 397 nm (Figure 5.5 left). As previously described, the quantum yield drastically increases to 67 % in the solid state. In films drop-cast from THF, compound **3** displayed emission at 500 nm (Φ = 75 %) with excitation peaks at 347 and 399 nm.

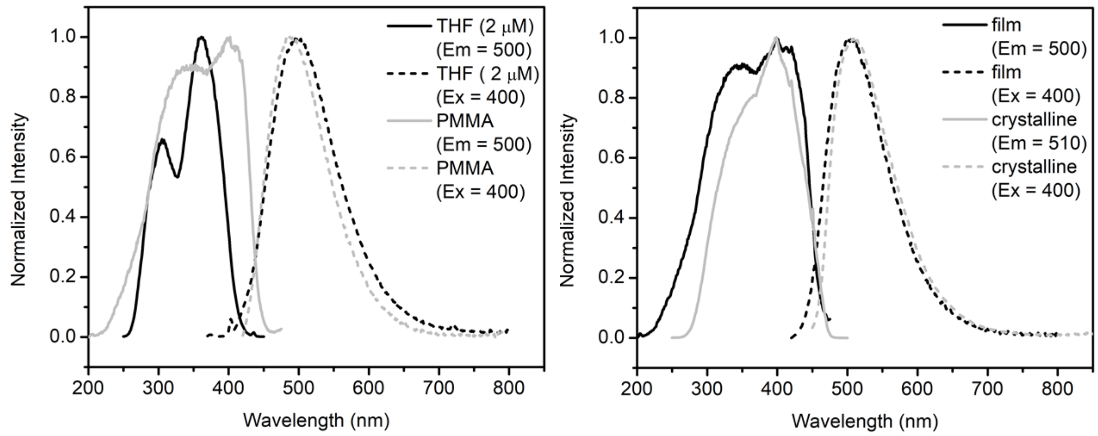

Figure 5.5. Excitation and emission profiles for **3** in solution (2.0 μM in THF) and in PMMA (10 wt% **3**) (left) and excitation and emission profiles for films of **3** (drop-cast from a *ca.* 12 mg/mL solution of **3** in THF) and crystalline **3** (right).

The emissive properties of **4** (bearing a ROMP-active aryl norbornyl group, Scheme 5.1) were comparable to **3** as the norbornyl group did not appear to significantly affect the emission. Emission and excitation spectra for **4** in THF solution (2.0 μM) and in the solid state (crystalline solids and drop-cast from THF solution) can be found in Figure 5.6. Like **3**, **4** shows two excitation peaks in solution (292, and 359 nm) that both lead to the same emission peak (493 nm, Φ = 12 %, τ = 1.9 ns) and an enhancement in emission intensity is observed in the solid state (λ_{em} = 510 nm, Φ = 57 %, τ = 5.7 ns in crystalline samples; λ_{em} = 501 nm, Φ = 63 % in drop-cast films). Both **3** and **4** show visible aggregation in water/THF solutions with a water fraction of 80 % or greater, and this aggregation is accompanied by an increase in PL intensity (see Figure 5.7).

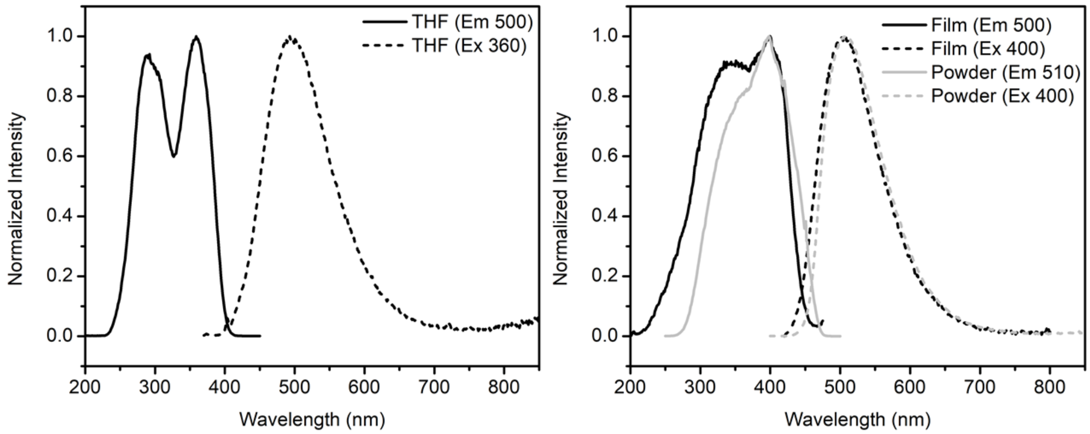

Figure 5.6. Excitation and emission spectra of **4** in THF at a concentration of 2.0 μM (left) and drop-cast films of **4** from a *ca*. 12 mg/mL THF solution onto quartz (right, "Film") and as a crystalline powder (right, "Powder").

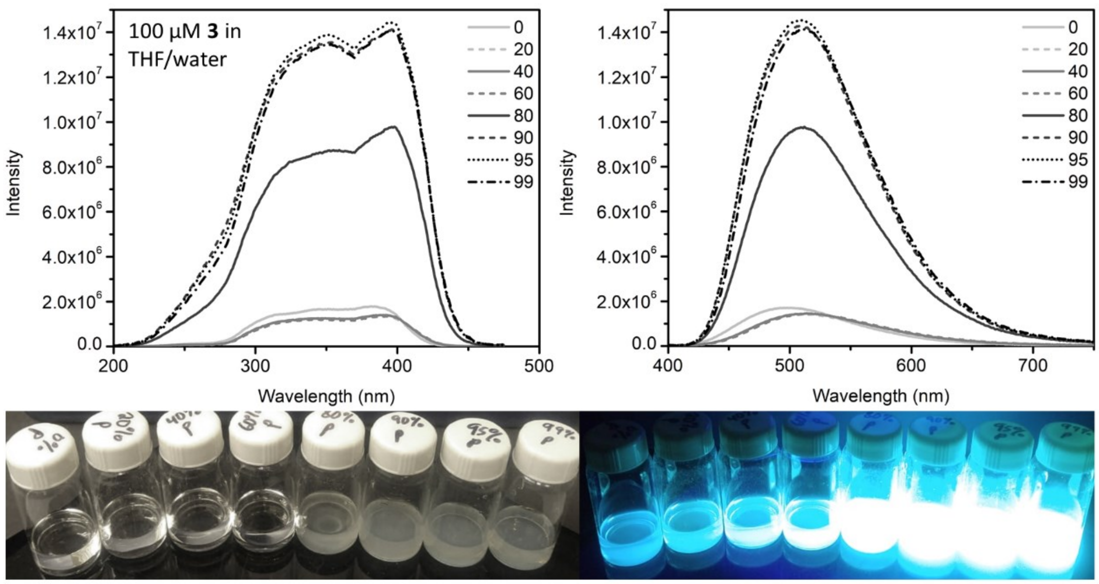

Figure 5.7. Excitation (upper left) and emission plots (upper right) of **3** in 100 μM solutions with varying ratios of water to THF. The legend for the emission and excitation spectra lists the percentage of water in the solvent mixture for each sample. Bottom left: images under ambient light of 100 μM solutions of **3** with percentage of water increasing from left to right. Bottom right: solutions of **3** illuminated under 365 nm light.

5.2.3 TD-DFT Study of Benzophosphole Oxide 3

To gain further insight into the nature of emission in the P-phenylated benzophosphole **3** (and to serve as a structural model for the emissive homopolymers and block-copolymers mentioned above), time-dependent density functional theory (TD-DFT) computations were performed using either the B3LYP[14] or the CAM-B3LYP[15] functionals along with the cc-pVTZ basis-set.[16] The predicted UV-vis absorption spectrum for **3** using the B3LYP functional is comparable to the experimentally observed spectrum with absorbance maxima at 292 nm and 378 nm (slightly red-shifted from 268 nm and 361 nm in the experimental spectrum in THF, see Figure 5.8). The absorption spectrum predicted with the CAM-B3LYP functional is blue-shifted with absorbance maxima at 259 and 326 nm (see Figure 5.9).

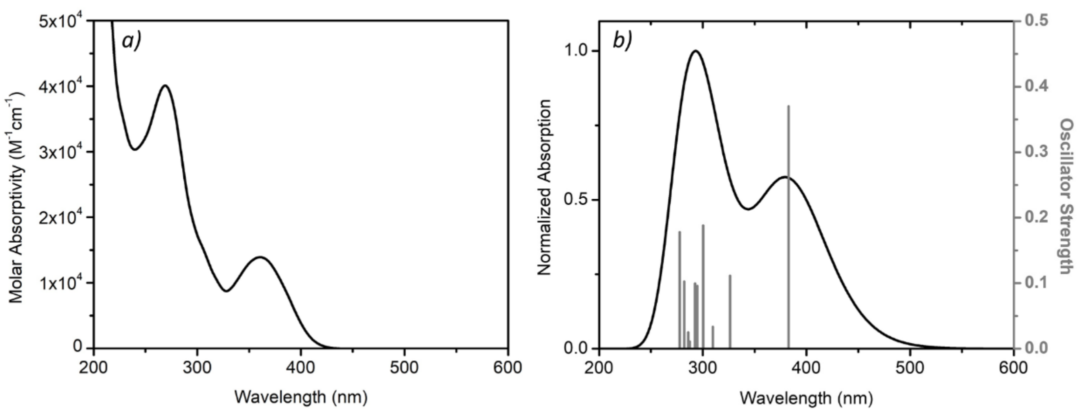

Figure 5.8. Experimentally observed UV-vis spectrum in THF (left) and calculated UV-vis spectra of **3** at the B3LYP/cc-pVTZ level of theory including the first ten singlet excitation states with the oscillator strengths plotted as vertical bars (right).

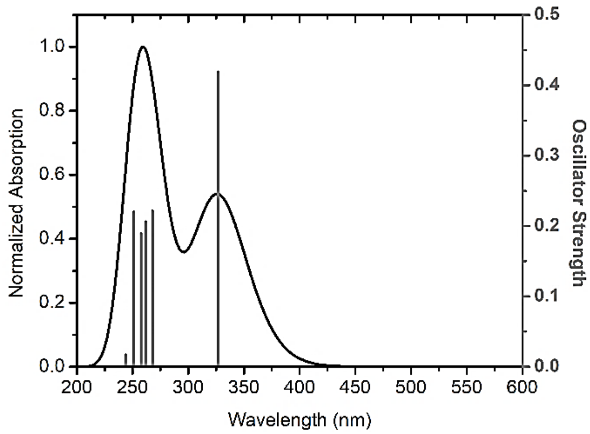

Figure 5.9. Calculated UV-vis spectrum of **3** at the CAM-B3LYP/cc-pVTZ level of theory including the first six singlet excitation states with the oscillator strengths plotted as vertical bars.

The first ten singlet and triplet excited states were calculated using the gas phase ground state geometry with the B3LYP and CAM-B3LYP functionals and these energy values with their respective oscillator strengths are given in Table 5.1. Both functionals predict the most intense transition to be S_0–S_1, which can be assigned to the HOMO to LUMO transition which consists of mainly π (HOMO) and π* (LUMO) with minor contributions of the P-atom only to the LUMO. Further low-lying transitions of notable oscillator strength are predicted to be S_0–S_n (n = 2, 4; B3LYP) and S_0-S_n (n = 2, 3; CAM-B3LYP), which are mainly π-π* in nature with no participation of the P-atom and little participation of the O-atom, (Figure 5.10 and Table 5.2).

Table 5.1. TD-DFT calculated excited states of the parent benzophosphole oxide, **3**, derived from the B3LYP and CAM-B3LYP functionals and the cc-pVTZ basis set.

B3LYP/cc-pVTZ			**CAM-B3LYP/cc-pVTZ**		
Excited State	**Energy (eV)**	**Oscillator Strength**	**Excited State**	**Energy (eV)**	**Oscillator Strength**
T_1	2.2620	0.0000	T_1	2.3440	0.0000
T_2	3.1393	0.0000	T_2	3.1694	0.0000
T_3	3.1988	0.0000	T_3	3.1997	0.0000
S_1	3.2388	0.3697	T_4	3.5775	0.0000
T_4	3.6896	0.0000	T_5	3.6811	0.0000
T_5	3.7076	0.0000	T_6	3.7654	0.0000
T_6	3.7431	0.0000	S_1	3.7965	0.4189
S_2	3.7995	0.1115	T_7	3.9345	0.0000
T_7	3.8289	0.0000	T_8	4.2707	0.0000
T_8	3.9055	0.0000	T_9	4.3761	0.0000
T_9	3.9460	0.0000	T_{10}	4.4175	0.0000
T_{10}	3.9760	0.0000	S_2	4.6292	0.2218
S_3	4.0031	0.0334	S_3	4.7373	0.2063
S_4	4.1273	0.1881	S_4	4.8135	0.1895
S_5	4.2069	0.0959	S_5	4.9374	0.2204
S_6	4.2379	0.0996	S_6	5.0848	0.0171
S_7	4.3151	0.0112	S_7	5.1327	0.3964
S_8	4.3370	0.0248	S_8	5.2084	0.0834
S_9	4.3941	0.1024	S_9	5.2557	0.0001
S_{10}	4.4654	0.1778	S_{10}	5.2880	0.0258

Table 5.2. Nature of main transitions to low lying singlet states of benzophosphole oxide **3** using the B3LYP and CAM-B3LYP functionals and cc-pVTZ basis set with minimum weight of 10 %.

B3LYP/cc-pVTZ

Transition	MOs involved	Weight of MO Involvement (%)
S_0–S_1	HOMO to LUMO	97.8
S_0–S_2	HOMO–1 to LUMO	87.5
S_0–S_3	HOMO–2 to LUMO	81.3
S_0–S_4	HOMO to LUMO+1	64.6
	HOMO to LUMO+2	10.7

CAM-B3LYP/cc-pVTZ

Transition	MOs involved	Weight of MO Involvement (%)
S_0–S_1	HOMO to LUMO	85.6
S_0–S_2	HOMO–1 to LUMO	30.5
	HOMO–2 to LUMO	19.0
	HOMO–9 to LUMO	18.5
S_0–S_3	HOMO–1 to LUMO	17.3
	HOMO to LUMO+2	16.7
	HOMO–2 to LUMO	12.8
S_0–S_4	HOMO to LUMO+1	18.6
	HOMO–2 to LUMO	13.1
	HOMO–3 to LUMO	11.8

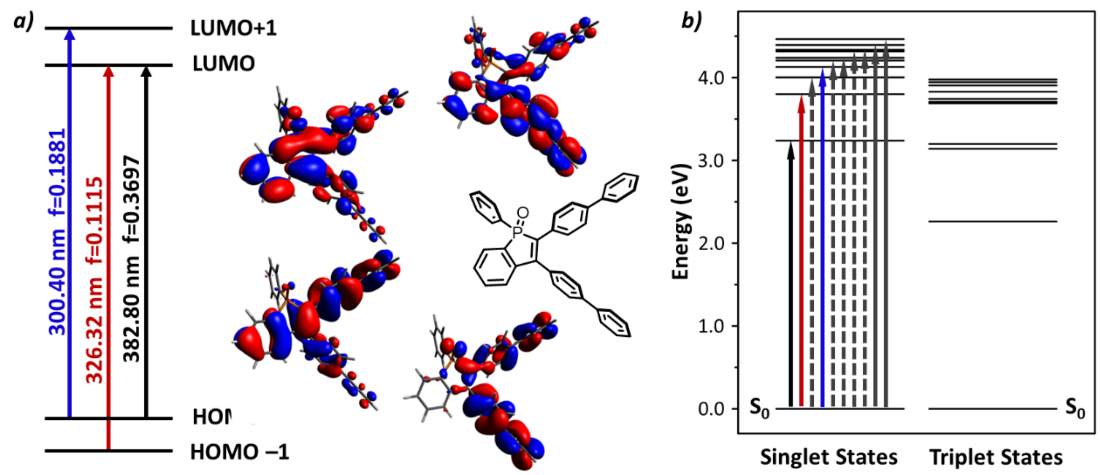

Figure 5.10. a) TD-DFT (B3LYP/cc-pVTZ) computed main transitions including excitation wavelengths and oscillator strengths (f) to low-lying singlet states for **3** and the associated molecular orbitals; iso-surface values of +0.02/–0.02 (blue/red) and b) calculated singlet and triplet states of **3** derived from B3LYP/cc-pVTZ. Oscillator strengths are indicated as follows: $f \geq 0.1$ (solid line); $f < 0.1$ (dashed).

The fluorescence energy can be estimated either by the difference in energies between the S_0 ground state and the S_1 singlet state (E_{adia}) or the zero-point corrected adiabatic energy difference ($E_{0\text{–}0}$). B3LYP and CAM-B3LYP both overestimate the experimentally observed fluorescence energy of 2.48 eV, with B3LYP (E_{adia} = 2.75 eV and $E_{0\text{–}0}$ = 2.70 eV) providing a closer estimate than CAM-B3LYP (E_{adia} = 3.15 eV and $E_{0\text{–}0}$ = 3.10 eV).

5.2.4 Synthesis and Photoluminescence Studies of Benzophosphole Oxide and Arylboronate Homopolymers and Block Copolymers

The benzophosphole oxide (**P1**) and arylboronate homopolymers (**P2**) were first synthesized by combining their respective monomers **4** and **5** with 1 mol% of Grubbs' 3rd Generation catalyst in THF (Scheme 5.3). Both monomers underwent rapid polymerization with full monomer consumption within three minutes. The resulting polymers, **P1** (M_n = 18.4 kDa) and **P2** (M_n = 45.6 kDa) displayed low PDIs of 1.03 and 1.12, respectively, indicating an excellent level of control over the polymerization. Of note, **P1** displayed remarkably high thermal stability; TGA analysis showed significant mass loss only above 400 °C under N_2.

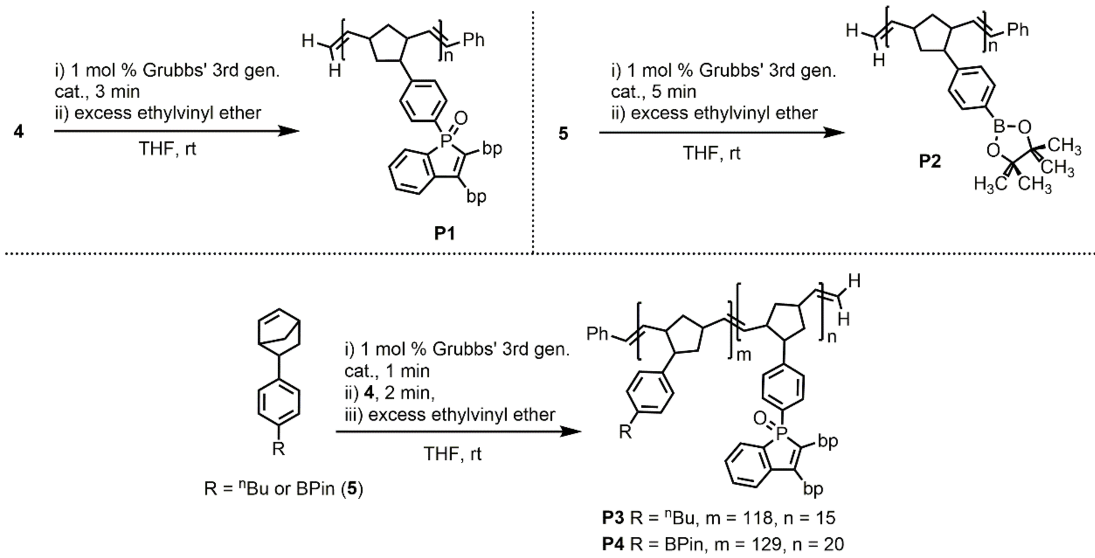

Scheme 5.3. Synthesis of homopolymers **P1** and **P2** and the inorganic-organic block copolymers **P3** and **P4** using 3rd generation Grubbs' catalyst.

The benzophosphole oxide-containing block copolymers **P3** and **P4** were generated from the sequential polymerization of 5-(4-butylphenyl)norbornene or the arylboronate compound **5** with comonomer **4**, respectively according to Scheme 5.3. GPC analysis in combination with ^{1}H NMR spectroscopy allowed for the estimation of the block lengths for **P3** of 15 phosphole units and 118 arylalkyl units per chain (total M_n = 36.2 kDa, PDI = 1.08) and for **P4** 20 phosphole oxide units and 129 BPin units per chain (total M_n = 50.4 kDa, PDI = 1.02). Like for **P1**, **P3** and **P4** display reasonably high thermal stability (stabile to *ca.* 300 °C) by thermogravimetric analysis.

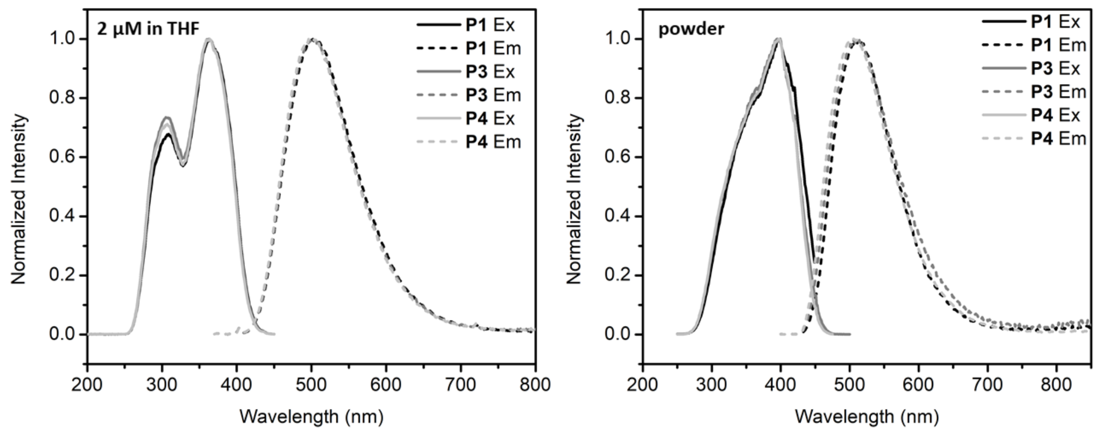

Figure 5.11. Emisison and excitation spectra for **P1**, **P3**, and **P4** in THF (left) at a concentration of 2.0 μM relative to the phosphole unit, and emission and excitation spectra for **P1**, **P3**, and **P4** samples in the solid state (right).

Luminescence measurements on **P1**, **P3** and **P4** were conducted in both THF solution and the solid state in air. As was found for the benzophosphole oxide monomer **4**, phosphole oxide polymers **P1**, **P3** and **P4** each gave two excitation peaks in solution (see Figure 5.11 left and Table 5.3) with a single emission peak centered at *ca.* 500 nm. Unlike for **3** and **4**, which displayed drastically lower quantum yields in solution compared to the solid state (Table 5.3), polymers **P1**, **P3**, and **P4** did not show dramatic decreases in quantum yield in solution relative to the solid state. While **P1** and **P3** show comparable quantum yield values of *ca.* Φ = 30 % in THF solutions as well as in the solid state, **P4** displays a slightly increased quantum yield of 41 % in the solid state (Table 5.3). Thus, incorporation of the benzophosphole oxide unit into a polymer motif was hypothesized to act similarly to aggregation in providing the steric restraint needed to limit intramolecular rotations in the emissive benzophosphole units.

Table 5.3. Summary of photoluminescent data for **3** and **4**, and polymers **P1**, **P3**, and **P4**.

	Solution[a]			Powder		
Compound	λ_{ex}[b]	λ_{em}[c] (Φ)	τ (ns)	λ_{ex}[b]	λ_{em}[c] (Φ)	τ (ns)
3	305, 361	498 (9.5 %)	1.5	397	510 (67 %)	5.9
4	292, 359	493 (12 %)	1.9	398	510 (57 %)	5.7
P1	309, 364	507 (33 %)	4.1	398	512 (32 %)	5.7
P3	305, 363	503 (31 %)	4.1	395	511 (30 %)	5.2
P4	307, 364	501 (33 %)	3.3	398	505 (41 %)	6.4

[a] Measurement taken in THF at a concentration of 2.0 μM relative to each benzophosphole unit. [b] Measured at the emission maximum and reported in nm. [c] Reported in nm, absolute quantum yield (Φ) measured at the lowest energy excitation maximum in the case when two are reported.

When one equivalent of F^- (relative to each BPin unit) in the form of tetrabutylammonium fluoride (TBAF) was added to **P4** in THF, the excitation and emission profile was not altered, but the emission quantum yield was decreased by half (to Φ = 17 % from an initial value of 33 %). The ^{11}B NMR spectrum of **P4** has remained elusive, presumably due to the enhanced broadening of the signal imparted by polymerization. As a result, studying the binding of F^- to **P4** by ^{11}B NMR spectroscopy has not been possible. Instead, the reactivity of monomer **5** in the presence of excess TBAF (*ca.* 10-fold excess) was followed by NMR spectroscopy, and indeed ^{11}B NMR spectroscopy indicated binding of F^- to the BPin as evidenced by a ^{11}B shift from 31.0 ppm in free **5** to 7.2 ppm upon reaction with excess TBAF;

the latter resonance matches those of previously reported complexes featuring fluoride-coordinated BPin groups.[17]

5.2.5 Micelle Formation and Emissive Properties

Micelle formation was anticipated with **P3** and **P4** due to the inherent insolubility of **P1** in hexanes combined with the solubility of **P2** and poly-5-(4-butylphenyl)norbornene in hexanes. As **P3** and **P4** were found to have good solubility in THF, it was expected that a solvent combination of THF and hexanes could be used to drive micelle formation, as was previously observed with a benzobismole block copolymer (see Chapter 3).[9] Initial solvent screening with a polymer concentration of 1.0 mg/mL was performed to determine the optimal THF: hexanes ratio necessary for the micellization of **P3** and **P4**. Dynamic light scattering (DLS) was used to monitor micelle formation and to yield an estimate for the hydrodynamic diameters of micelles of **P3** and **P4**. Table 5.4 outlines the concentrations of micelles studied and the solvent ratios tested. For **P3**, solvent ratios of 10, 20, and 30 % THF in hexanes were found to drive micelle formation, while for **P4**, solvent ratios of 30 and 40 % THF in hexanes were found to yield micelle formation. Attempts at micelle formation of **P4** at lower THF ratios (5, 10, and 20 % THF in hexanes) was found to yield insoluble polymer precipitates. For each block copolymer, a control study with 100 % THF was done to ensure that the large diameters observed by DLS (*i.e.* when micelles were formed) were solvent driven. DLS of fully solvated **P3** and **P4** in pure THF both gave hydrodynamic diameter estimates of 6 nm with no sign of larger micelles in solution indicating that the micelle formation is solvent driven.

Table 5.4. Diameter estimates of spherical micelles of **P3** and **P4**, as determined by dynamic light scattering.

Polymer	Concentration (mg/mL)	solvent ratio THF:hexanes	Avg. Diameter (nm)	Avg. Std. Dev. (nm)
P3	1.0	10 %	37	10
P3	1.0	20 %	41	10
P3	1.0	30 %	47	12
P3	1.0	100 %	6	1
P3	0.1	20 %	32	8
P3	0.3	20 %	38	10
P3	0.5	20 %	38	10
P3	2.0	20 %	42	11
P4	1.0	30 %	29	8
P4	1.0	40 %	27	7
P4	1.0	100 %	6	2
P4	0.1	30 %	1100*	200
P4	0.3	30 %	30	7
P4	0.5	30 %	28	7
P4	2.0	30 %	28	7

* DLS software gave error reports indicating poor quality of fit of data resulting from: 1) the sample being too polydisperse for a proper distribution analysis and cumulant analysis, and 2) the presence of particles too large to be reliably measured by DLS.

To study polymer concentration dependence on micelle formation, micelle solutions of **P3** in 20 % THF in hexanes and **P4** in 30 % THF in hexanes at polymer concentrations of 0.1, 0.3, 0.5, and 2.0 mg/mL were prepared. All four concentrations studied were found to yield micelles of **P3** with average diameters of *ca.* 32–42 nm as determined by DLS (see Table 5.4). Solutions of **P4** at concentrations of 0.3 mg/mL or above in 30 % THF in hexanes were found to yield micelle solutions that were stable for at least 24 hours, but solutions of **P4** at a concentration of 0.1 mg/mL (in 30 or 40 % THF in hexanes) were observed to exhibit significant aggregation leading to precipitation of the polymer after standing at room temperature for 16 hours. TEM imaging of micelles of **P3** (Figure 5.12a) and **P4** (Figure 5.12b) indicated the presence of spherical micelles with a total diameter of 25 ± 4 nm and 20 ± 3 nm, respectively.

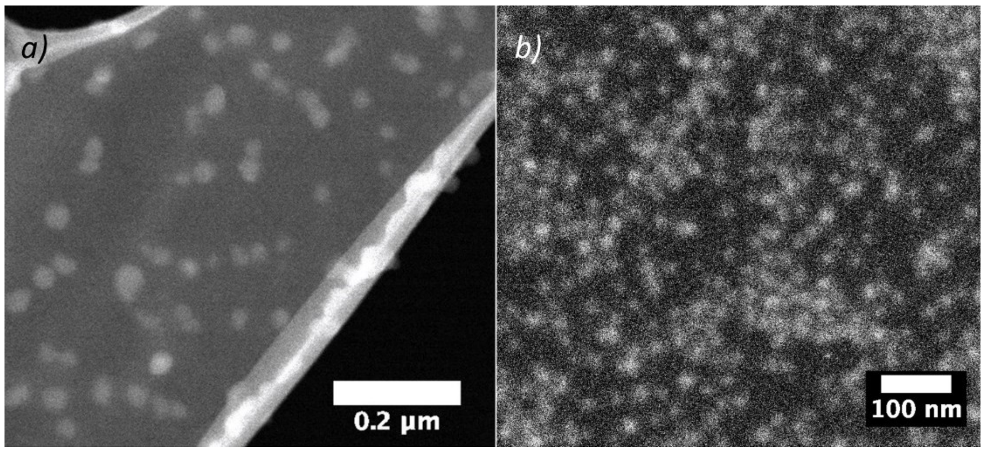

Figure 5.12. Dark field TEM images of micelles of a) **P3** and b) **P4**. TEM samples of **P3** were prepared by depositing a drop of a well-dispered 0.1 mg/mL sample in 20 % THF/hexanes onto a holey carbon supported copper grid, and TEM samples of **P4** micelles were prepared by depositing a drop of a well-dispersed 1.0 mg/mL sample in 30 % THF/hexanes onto an ultra-thin carbon film coated copper grid.

Photoluminescence measurements were conducted on micelle solutions of **P3** as well as of **P4** and the resulting excitation and emission spectra are shown in Figure 5.13. For both **P3** and **P4**, micelle formation was studied at polymer concentrations too high to avoid inner filter effects during PL measurements. Therefore, control PL measurements of **P3** at 0.1 mg/mL (41.5 µM with respect to phosphole) and **P4** at 0.3 mg/mL (119 µM with respect to phosphole) in 100 % THF (Figure 5.14) were conducted to ensure that any emission changes observed during measurement of the micelle solutions were a result of self-assembly effects and not concentration effects.

At 41.5 μM for **P3** and 119 μM for **P4** in 100 % THF, the emission and excitation spectra were comparable to the PL data collected on **P3** and **P4** at 2.0 μM (Figure 5.11 left). As expected, due to inner filter effects, at these higher concentrations (0.1 mg/mL for **P3** and 0.3 mg/mL for **P4**), the quantum yields for **P3** and **P4** were lower than the 2.0 μM measurements (**P3**: Φ = 27 % at 0.1 mg/mL and Φ = 31 % at 2.0 μM in THF and **P4**: Φ = 32 % at 0.3 mg/mL and Φ = 33 % at 2.0 μM in THF). Micelles of **P3** displayed a slightly decreased quantum yield (23 %) relative to the fully solvated (unimeric) **P3** and micelles of **P4** showed only a moderate increase in quantum yield (to 37 %) relative to the fully solvated **P4**. The lack of significant AIE effects upon assembly of the block copolymer micelles of **P3** and **P4** is a consequence of having substantially limited solution-state quenching of the benzophosphole oxide monomer unit by the act of polymerization.

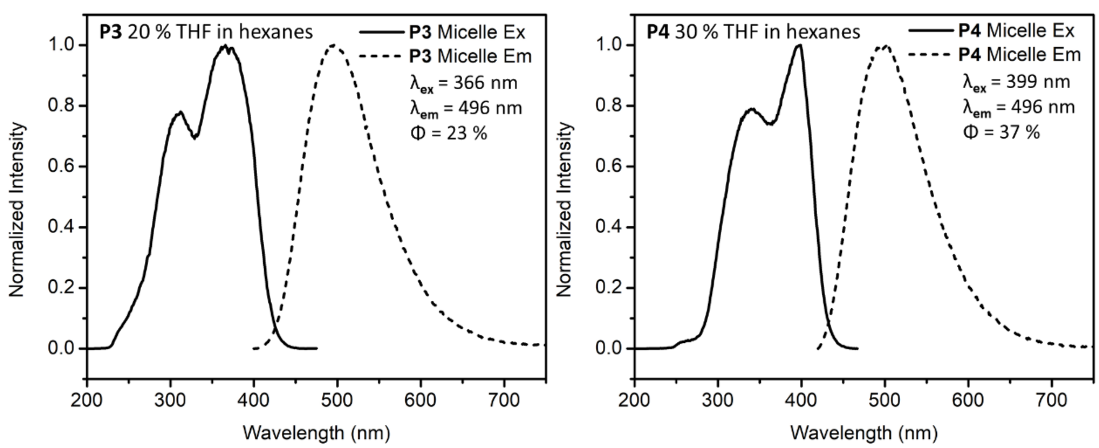

Figure 5.13. Excitation and emission spectra for micelles of **P3** at 0.1 mg/mL (41.5 μM with respect to benzophosphole oxide) in 20 % THF/hexanes (left) and **P4** at 0.3 mg/mL (119 μM with respect to benzophosphole oxide) in 30 % THF/hexanes (right).

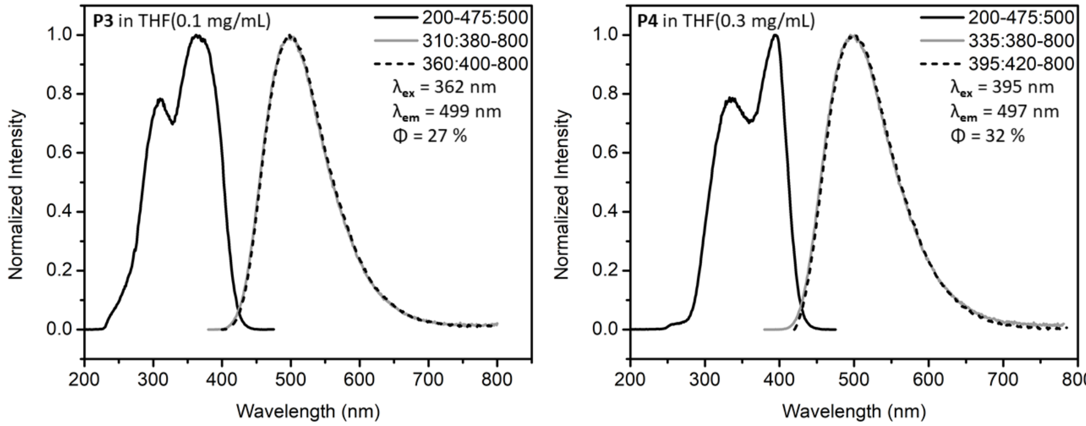

Figure 5.14. Excitation and emission spectra for **P3** at a concentration of 0.1 mg/mL (41.5 µM with respect to benzophosphole oxide) in 100 % THF (left) and **P4** at 0.3 mg/mL (119 µM with respect to benzophosphole oxide) in 100 % THF (right).

Of added note, micelles of **P4** could be disrupted with the addition of F^- in the form of TBAF, and the addition of just 0.25 mole equivalents of F^- (relative to the BPin units) resulted in the precipitation of **P4** from solution to yield luminescent aggregates (λ_{em} = 493 nm, Φ = 25 %) that settled out of solution upon standing (see Figure 5.15). It is proposed that the F^- binds to the BPin groups in the micelle coronas resulting in boronate adducts which are no longer have the necessary solubility in THF/hexanes to drive micelle stabilization. These findings suggest the possibility of utilizing **P4** micelles as a method of fluorometric F^- sensing.

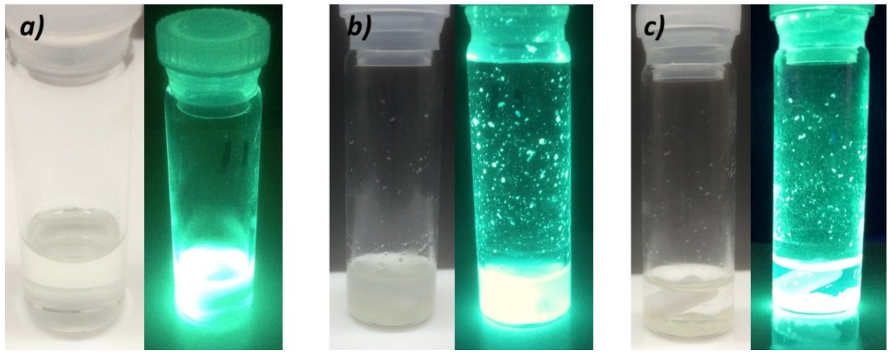

Figure 5.15. a) micelles of **P4** (1.0 mg/mL in 30% THF in hexanes) before addition of TBAF; b) micelles of **P4** immediately after the addition of 0.25 mol% (relative to number of BPin units in **P4**) with stirring; and c) micelles of **P4** after the addition of 0.25 mol% followed by settling for 16 hours. Samples illuminated under ambient light (left) and 365 nm (right).

5.3. Conclusions

Highlty fluorescent benzophosphole oxide-based block copolymers and homopolymers were synthesized via ring-opening metathesis polymerization (ROMP); these block copolymers self-assembled into spherical micelles in THF/hexanes mixtures. This work introduces the first examples of polybenzophosphole oxides and the resulting materials showed substantially higher emission quantum yields in solution compared to their monomeric analogues, likely due to an added restriction of molecular motion in the polymers; thus bright emission is retained in all phases. Addition of substoichiometric quantities of fluoride to a benzophosphole oxide:pinacolboronate spherical micelle in THF/hexanes led to polymer precipitation, which could be visualized under UV light; this process represents a new mode for anion detection, which will be explored in greater detail as part of future work.

5.4 Experimental Section

5.4.1 General Considerations

All reactions were performed using standard Schlenk and glovebox (MBraun) techniques under a nitrogen atmosphere. Solvents were all dried and degassed using a Grubbs-type solvent purification system manufactured by Innovative Technology, Inc., and stored under an atmosphere of nitrogen prior to use. 2-Isopropoxy-4,4,5,5-tetramethyl-1,3,2-dioxaborolane (^{i}PrOBPin) was purchased from Matrix Scientific and all other chemicals were purchased from Sigma-Aldrich and used as received. Cp_2ZrPh_2,[18] bis(*para*-biphenyl)acetylene,[19] 5-(4-Bromophenyl)norbornene,[20] and 5-(4-butylphenyl)norbornene,[9] were synthesized according to literature procedures. ^{1}H, $^{13}C\{^{1}H\}$, and $^{31}P\{^{1}H\}$ NMR spectra were recorded on 400, 500, 600, or 700 MHz Varian Inova instruments and were referenced externally to $SiMe_4$ (^{1}H, $^{13}C\{^{1}H\}$), 85 % H_3PO_4 ($^{31}P\{^{1}H\}$), or $F_3B{\bullet}OEt_2$ ($^{11}B\{^{1}H\}$). Chemical shifts are reported in parts per million (ppm) and coupling constants (*J*) are given in Hertz (Hz). High resolution mass spectra were obtained on Kratos Analytical MS-50G (EI) spectrometer. UV−visible spectroscopic measurements were carried out with a Varian Cary 5000 UV/Vis/NIR spectrophotometer. Elemental analyses were performed at the Analytical and Instrumentation Laboratory at the University of Alberta. Melting points were measured in sealed glass capillaries under nitrogen using a MelTemp apparatus. GPC was performed at 40 °C using THF as the eluent at a flow rate of 0.5 mL per minute. A Viscotek VE 2001 autosampler, three Viscotek I-MBMMW-3078 columns, GPC 270 Max dual detector, and Viscotek VE 3580 refractive index detector (RI) were used for sample analysis and data collection. Multidetector calibration was done using RI detection in conjunction with low-angle light scattering (LALS) and right-angle light scattering (RALS) using 99 kDa polystyrene to create the calibration method and 235 kDa polystyrene to verify the calibration. Thermogravimetric analysis was performed under a nitrogen atmosphere on a PerkinElmer Pyris 1 TGA. Differential scanning calorimetry measurements were conducted under a nitrogen atmosphere on a PerkinElmer Pyris 1 DSC. Dynamic light scattering (DLS) was conducted on a Malvern Nanoseries Zetasizer and the number average was taken as the average particle size reported. The steady-state photoluminescence (PL) spectra, emission lifetime (τ), and photoluminescence quantum yields (Φ) were obtained using a PTI QuantaMaster 8075 fluorescence spectrophotometer equipped with a 75W xenon lamp and an integrating sphere. All quantum yields reported herein are absolute. Lifetime measurements were performed with a 370 nm Horiba NanoLED pulsed excitation source. Solid samples were measured in glass capillaries mounted in a custom-made solids holder, films were drop-cast onto 1 mm thick optical grade fused quartz substrates (Starna Scientific Ltd), and solution samples were measured in butylated hydroxytoluene (BHT)-free THF. Long-pass (λ = 370, 400, or 420 nm) and short-pass cut-off filters (λ = 480 nm) were used in steady-state measurements when necessary. High Angle Annular Dark-Field Scanning Transmission electron microscopy (HAADF-STEM) images were acquired using a JEOL JEM-ARM200CF S/TEM electron microscope at accelerating voltages of 200 kV. Images were collected with the following experimental conditions: probe size 6c, condenser lens aperture 40 μm, and camera length 8 cm, scan speed 30 μs per pixel. Images were processed using Gatan Digital Micrograph software (Version 3.22.1461.0) and

ImageJ (Version 1.51m9). TEM samples of **P3** micelles were prepared by depositing a drop of a well-dispersed 0.1 mg/mL sample in 20 % THF/hexanes onto a holey carbon supported copper grid, (HC-300Cu, Electron Microscopy Inc.). TEM samples of **P4** micelles were prepared by depositing a drop of a well-dispersed 1.0 mg/mL sample in 30 % THF/hexanes onto an ultra-thin carbon film coated copper grid (CF300-Cu-UL, Electron Microscopy Inc.). The grids were kept in a vacuum chamber for at least 24 hours prior to data collection.

5.4.2 Synthetic Procedures

Synthesis of 2,3-bis(*para*-biphenyl)benzozirconocene (1): Under a nitrogen atmosphere, Cp_2ZrPh_2 (152.2 mg, 0.4069 mmol) and bis(*para*-biphenyl)acetylene (131.1 mg, 0.3968 mmol) were dissolved in 20 mL of toluene and stirred at 110 °C for 48 hours. The volatiles were removed *in vacuo*, the crude product was dissolved in 15 mL of THF, the dark red-orange mixture was filtered through Celite, and the volatiles were removed from the filtrate *in vacuo* to give **1** as a yellow solid (249.2 mg, quantitative yield). Yellow single crystals of suitable quality for X-ray crystallography were obtained from the slow diffusion of hexane into a solution of **1** in toluene at room temperature. ^{1}H NMR (700 MHz, C_6D_6): δ 7.46 (d, $^3J_{HH}$ = 8.3 Hz, 2H, Ar*H*), 7.41 (td, $^3J_{HH}$ = 8.4 Hz, $^4J_{HH}$ = 1.2 Hz, 4H, Ar*H*), 7.37 (d, $^3J_{HH}$ = 8.3 Hz, 2H, Ar*H*), 7.34 (d, $^3J_{HH}$ = 8.4 Hz, 2H, Ar*H*), 7.27–7.30 (m, 1H, Ar*H*), 7.13 (m, 4H, Ar*H*), 7.03–7.08 (m, 4H, Ar*H*), 6.80 (d, $^3J_{HH}$ = 8.4 Hz, 2H, Ar*H*), 6.65–6.66 (m, 1H, Ar*H*), 6.02 (s, 10H, Cp*H*). ^{13}C{^{1}H} NMR (176 MHz, C_6D_6): δ 194.0 (Ar*C*), 185.5 (Ar*C*), 147.2 (Ar*C*), 146.7 (Ar*C*), 146.6 (Ar*C*), 141.49 (Ar*C*), 141.47 (Ar*C*), 141.0

(Ar*C*), 138.8 (Ar*C*), 136.6 (Ar*C*H), 136.1 (Ar*C*), 131.4 (Ar*C*H), 129.0 (Ar*C*H), 128.9 (Ar*C*H), 127.4 (Ar*C*H), 127.3 (Ar*C*H), 127.1 (Ar*C*H), 126.97 (Ar*C*H), 126.96 (Ar*C*H), 126.92 (Ar*C*H), 126.8 (Ar*C*H), 126.1 (Ar*C*H), 125.9 (Ar*C*H), 124.3 (Ar*C*H), 113.0 (Cp*C*). Anal. Calcd. for $C_{42}H_{32}Zr$: C, 80.59 %; H, 4.83 %. Found: C, 80.82 %; H, 5.25 %. Mp: 250–258 °C.

Synthesis of 1-chloro-2,3-bis(*p*-biphenyl)benzophosphole (2): PCl_3 (0.16 mL, 1.8 mmol) was added dropwise to a solution of 2,3-bis(*para*-biphenyl)benzozirconocene (0.939 g, 1.50 mmol) in 40 mL of CH_2Cl_2 at 0 °C. This reaction mixture was allowed to slowly warm to room temperature while stirring for a period of 24 hours, after which the volatiles were removed *in vacuo*. This reaction provided a 1:1 mixture of **2** and Cp_2ZrCl_2 in quantitative yield (1.14 g, 1.5 mmol). As separation proved to be difficult, the 1:1 crude mixture was carried forward to the next reaction without further purification. ^{1}H NMR (400 MHz, C_6D_6): δ 7.60–7.65 (m, 1H, ArH), 7.52–7.55 (m, 2H, ArH), 7.39–7.45 (m, 4H, ArH), 7.28–7.37 (m, 5H, ArH), 7.09–7.22 (m, 7H, ArH), 6.98–7.09 (m, 3H, ArH). ^{31}P{^{1}H} NMR (162 MHz, C_6D_6): δ 74.0. Note: ^{1}H NMR spectroscopy indicates minor impurity signals at 8.14 and 4.20 ppm and the presence of *ca*. 41 mol% Cp_2ZrCl_2. However, when the expected reactivity of Cp_2ZrCl_2 with PhMgBr and ArLi reagents was accounted for, the crude product could be reacted in subsequent synthetic steps to produce compound **3** and **4** as described below.

Synthesis of 1-phenyl-2,3-bis(*para*-biphenyl)benzophosphole oxide (3): A 1:1 mixture (0.65 g, 0.85 mmol) of 1-chloro-2,3-bis(*para*-biphenyl)benzophosphole and zirconocene dichloride was dissolved in 10 mL of THF. The solution was cooled to –

78 °C and phenylmagnesium bromide (0.93 mL, 3.0 M solution in Et_2O, 2.8 mmol) was added dropwise. The reaction mixture was stirred for one hour at –78 °C, followed by one hour at 0 °C, and then 12 hours at room temperature before the addition of 20 mL of distilled water. The mixture was cooled to 0 °C and 15 mL of 30 % aqueous H_2O_2 was added. After 6 hours of stirring at room temperature, the crude reaction mixture was extracted with CH_2Cl_2 (3 × 50 mL) and then the organic layers were combined and washed with saturated aqueous $Na_2S_2O_3$ (3 × 20 mL), dried with $MgSO_4$, gravity filtered in air, and the solvent was removed from the filtrate *in vacuo*. The crude product was further purified by flash chromatography using a gradient of 20:1 CH_2Cl_2:ethylacetate to 10:1 CH_2Cl_2:ethylacetate to yield **3** as a bright yellow solid (0.383 g, 85 %). Solid **3** was washed with pentane to remove excess ethyl acetate and dried *in vacuo* with mild heating (*ca.* 50 °C). ^{1}H NMR (700 MHz, $CDCl_3$): δ 7.81–7.85 (m, 2H, Ar*H*), 7.72–7.75 (m, 1H, Ar*H*), 7.71 (d, $^{3}J_{HH}$ = 8.4 Hz, 2H, Ar*H*), 7.67 (dd, $^{3}J_{HH}$ = 8.2 Hz, $^{4}J_{HH}$ = 1.1 Hz, 2H, Ar*H*), 7.44–7.52 (m, 8H, Ar*H*), 7.34–7.45 (m, 10H, Ar*H*), 7.31 (dd, $^{3}J_{HH}$ = 7.7 Hz, $^{4}J_{HH}$ = 2.8 Hz, 1H, Ar*H*), 7.27–7.29 (m, 1H, Ar*H*). $^{13}C\{^{1}H\}$ NMR (176 MHz, $CDCl_3$): δ 149.6 (d, $^{2 \text{ or } 3}J_{CP}$ = 21.6 Hz, Ar*C*), 143.8 (d, $^{2 \text{ or } 3}J_{CP}$ = 26.9 Hz, Ar*C*), 141.5 (Ar*C*), 140.4 (Ar*C*), 140.33 (Ar*C*), 140.28 (Ar*C*), 134.0 (d, $^{1}J_{CP}$ = 95.7 Hz, Ar*C*), 133.3 (d, $^{2 \text{ or } 3}J_{CP}$ =15.1 Hz, Ar*C*), 133.0 (d, $^{4}J_{CP}$ = 1.4 Hz, Ar*C*H), 132.3 (d, $^{4}J_{CP}$ = 2.8 Hz, Ar*C*H), 132.2 (d, $^{1}J_{CP}$ = 105.8 Hz, Ar*C*), 131.8 (d, $^{2 \text{ or } 3}J_{CP}$ = 10.0 Hz, Ar*C*), 131.0 (d, $^{2 \text{ or } 3}J_{CP}$ = 10.6 Hz, Ar*C*H), 130.1 (d, $^{1}J_{CP}$ = 99.7, Ar*C*), 129.6 (Ar*C*H), 129.5 (d, $^{2 \text{ or } 3}J_{CP}$ = 5.8 Hz, Ar*C*H), 129.19 (d, $^{2 \text{ or } 3}J_{CP}$ = 10.5 Hz, Ar*C*H), 129.15 (d, $^{2 \text{ or } 3}J_{CP}$ = 9.5 Hz, Ar*C*H), 128.96 (d, $^{2 \text{ or } 3}J_{CP}$ = 12.3 Hz, Ar*C*H), 128.95 (Ar*C*H), 128.7 (Ar*C*H), 127.8 (Ar*C*H),

127.7 (Ar*C*H), 127.4 (Ar*C*H), 127.1 (Ar*C*H), 127.0 (Ar*C*H), 126.9 (Ar*C*H), 124.1 (d, $^{2\text{ or }3}J_{CP}$ = 10.8 Hz, Ar*C*H). $^{31}P\{^1H\}$ NMR (162 MHz, $CDCl_3$): δ 39.1. Anal. Calcd. for $C_{38}H_{27}PO$: C, 86.02 %; H, 5.13 %. Found: C, 83.98 %; H, 5.12 %. Note: combustion results consistently yielded low carbon values despite the apparent purity of the sample (see ^1H NMR spectrum in Figure 5.30). UV-Vis (THF): λ_{max} = 268 ($\varepsilon = 3.92 \times 10^4$ $M^{-1}cm^{-1}$) and 361 nm ($\varepsilon = 1.35 \times 10^4$ $M^{-1}cm^{-1}$). HRMS (EI): m/z calculated for $C_{38}H_{27}PO$: 530.1799; found: 530.1793 (Δppm = 1.2). Mp: 108–112 °C. PL (solid state): λ_{ex} = 397 nm, λ_{em} = 510 nm, Φ = 67 %, τ = 5.9 ns. PL (2.0 μM in THF): λ_{ex} = 305 and 361 nm; λ_{em} = 498 nm, Φ = 9.8 % (λ_{ex} = 310 nm); and Φ = 9.5 % (λ_{ex} = 360 nm); τ = 1.5 ns.

Synthesis of 1-*para*-norbornenephenyl-2,3-bis(*para*-biphenyl)benzophosphole oxide (4): To a solution of 5-(4-bromophenyl)norbornene (0.575 g, 2.31 mmol) in 12 mL of dry THF at –78 °C was added ^nBuLi (1.0 mL, 2.5 M in hexane, 2.5 mmol). After stirring for one hour at –78 °C, this solution of 4-(norbornyl)phenyllithium was added dropwise to a 1:1 mixture (0.535 g, 0.700 mmol) of 1-chloro-2,3-bis(*para*-biphenyl)benzophosphole (**2**) and Cp_2ZrCl_2 in 10 mL of THF at –78 °C. The reaction mixture was stirred at –78 °C for 30 minutes, followed by one hour at 0 °C, and then 16 hours at room temperature before the addition of 20 mL of distilled water. The mixture was cooled to 0 °C and 15 mL of 30 % aqueous H_2O_2 was added. After 6 hours stirring at room temperature, the crude reaction mixture was extracted with CH_2Cl_2 (3 × 40 mL) and then the organic layers were combined and washed with saturated aqueous $Na_2S_2O_3$ (3 × 15 mL), dried with $MgSO_4$, gravity filtered in air, and the solvent was removed from the filtrate *in vacuo*. The crude product was further purified by flash chromatography using a gradient of 20:1 CH_2Cl_2:ethylacetate to 10:1 CH_2Cl_2:ethylacetate to yield **4** as a bright yellow solid (0.314 g, 72 %). Solid **4** was washed with pentane to remove excess ethyl acetate and dried *in vacuo* with mild heating (*ca.* 50 °C). ^{1}H NMR (400 MHz, $CDCl_3$): δ 7.66–7.75 (m, 7H, Ar*H*), 7.44–7.51 (m, 7H, Ar*H*), 7.35–7.40 (m, 8H, Ar*H*), 7.27–7.35 (m, 4H, Ar*H*), 6.21–6.23 (m, 1H, vinylic*H*), 6.15–6.16 (m, 1H, vinylic*H*), 2.95 (s, 1H, allylic*H*), 2.89 (s, 1H, allylic*H*), 2.67–2.72 (m, 1H, benzylic-C*H*), 1.60–1.71 (m, 2H, norbornene CH_2), 1.51 (d, $^{2}J_{HH}$ = 8.5 Hz, 1H, one H of norbornene CH_2), 1.42 (d, $^{2}J_{HH}$ = 8.5, 1H, one H of norbornene CH_2). ^{13}C{^{1}H} NMR (176 MHz, $CDCl_3$): δ 151.1 (d, $^{4}J_{CP}$ = 2.7 Hz, Ar*C*), 149.4 (d, $^{2\text{ or }3}J_{CP}$ = 21.5 Hz, Ar*C*), 143.7 (d, $^{2\text{ or }3}J_{CP}$ = 26.9 Hz, Ar*C*), 141.4 (Ar*C*), 140.33 (Ar*C*), 140.32 (Ar*C*), 140.29 (Ar*C*), 137.6 (vinylic*C*H), 137.1 (vinylic*C*H), 134.0 (d, $^{1}J_{CP}$ = 95.7 Hz, Ar*C*), 133.4 (d, $^{2\text{ or }3}J_{CP}$ = 15.0 Hz, Ar*C*), 132.9 (Ar*C*H), 132.4 (d, $^{1}J_{CP}$ = 106.2 Hz, Ar*C*), 131.9 (d, $^{2\text{ or }3}J_{CP}$ = 9.7 Hz, Ar*C*), 131.0 (d, $^{2\text{ or }3}J_{CP}$ = 10.9 Hz, Ar*C*H), 129.64 (Ar*C*H), 129.59 (d, $^{4}J_{CP}$ = 5.8 Hz, Ar*C*H), 129.11 (d, $^{2\text{ or }3}J_{CP}$ = 9.4 Hz, Ar*C*H), 129.12 (d, $^{2\text{ or }3}J_{CP}$ = 10.8 Hz, Ar*C*H), 129.0 (Ar*C*H), 128.7 (Ar*C*H), 128.3 (d, $^{2\text{ or }3}J_{CP}$ = 12.6 Hz, Ar*C*H), 127.8 (Ar*C*H), 127.7 (Ar*C*H), 127.4 (Ar*C*H), 127.1 (Ar*C*H), 127.0 (Ar*C*H), 126.9 (Ar*C*H), 126.6 (d, $^{1}J_{CP}$ = 102.4 Hz, Ar*C*), 124.0 (d, $^{2\text{ or }3}J_{CP}$ = 10.8 Hz, Ar*C*H), 47.9 (norbornene-*C*H), 45.9 (norbornene-*C*H_2), 44.0 (norbornene-*C*H), 42.4 (norbornene-*C*H), 33.78 (norbornene-*C*H_2), 33.77 (norbornene-*C*H_2). ^{31}P{^{1}H} NMR (162 MHz, $CDCl_3$): δ 39.5. Anal. Calcd. for $C_{45}H_{35}PO$: C, 86.79 %; H, 5.67 %. Found: C, 83.84 %; H, 5.49 %. Note: combustion results consistently yielded low carbon values despite the apparent purity of the sample (see ^{1}H NMR spectrum in Figure 5.32). UV-Vis (THF): λ_{max} = 269 (ε = 4.05

$\times 10^4$ $M^{-1}cm^{-1}$) and 360 nm ($\varepsilon = 1.31 \times 10^4$ $M^{-1}cm^{-1}$). HRMS (EI): m/z calculated for $C_{45}H_{35}PO$: 622.2426; found: 622.2418 (Δppm = 1.3). Mp: 121–128 °C. PL (solid state): λ_{ex} = 398 nm, λ_{em} = 510 nm, Φ = 57 %, τ = 5.7 ns. PL (2.0 µM in THF): λ_{ex} = 292 and 359 nm; λ_{em} = 493 nm, Φ = 16 % (λ_{ex} = 290 nm); and Φ = 12 % (λ_{ex} = 360 nm); τ = 1.9 ns.

Synthesis of 5: To 5-(4-bromophenyl)norbornene (1.631 g, 6.576 mmol) in 30 mL of THF at –78 °C was added ^{n}BuLi (3.1 mL, 2.5 M in n-hexane, 7.8 mmol) and the reaction mixture was allowed to stir for 30 minutes at –78 °C. 2-Isopropoxy-4,4,5,5-tetramethyl-1,3,2-dioxaborolane (1.7 mL, 8.3 mmol) was added and the reaction mixture was allowed to warm to room temperature and then stirred for 16 hours under N_2. 50 mL of distilled water was then added to reaction mixture and the product was extracted with $CHCl_3$ (3 x 50 mL portions). The organic layers were combined, dried with $MgSO_4$, filtered, and the volatiles removed from the filtrate *in vacuo*. The crude product was purified by recrystallization from hot hexanes (*ca.* 60 °C) to yield 0.702 g (36 %) of **5** as a white crystalline solid. ^{1}H NMR (700 MHz, $CDCl_3$): δ 7.75 (d, $^3J_{HH}$ = 8.0 Hz, 2H, Ar*H*), 7.29 (d, $^3J_{HH}$ = 7.9 Hz, 2H, Ar*H*), 6.23–6.27 (m, 1H, vinylic*H*), 6.15–6.19 (m, 1H, vinylic*H*), 2.97 (s, 1H, allylic*H*), 2.92 (s, 1H, allylic*H*), 2.70–2.76 (m, 1H, benzylic*H*), 1.72–1.78 (m, 1H, one H of norbornene CH_2), 1.60–1.67 (m, 1H, one H of norbornene CH_2), 1.57 (d, $^2J_{HH}$ = 8.5 Hz, 1H, one H of norbornene CH_2), 1.42 (d, $^2J_{HH}$ = 8.7 Hz, 1H, one H of norbornene CH_2), 1.34 (s, 12H, BPinCH_3 groups). ^{13}C{^{1}H} NMR (176 MHz, $CDCl_3$): δ 149.7 (Ar*C*), 137.5 (vinylic*C*), 137.3 (vinylic*C*), 134.9 (Ar*C*H), 127.1 (Ar*C*H), 83.7 (O-*C*), 48.2 (*C*H), 45.8 (*C*H_2), 44.0 (*C*H), 42.4 (*C*H), 33.6 (*C*H_2), 24.9 (*C*H_3). ^{11}B{^{1}H} NMR (128 MHz,

$CDCl_3$): δ 31.0. Anal. Calcd. for $C_{19}H_{25}BO_2$: C, 77.04 %; H, 8.51 %. Found: C, 76.94 %; H, 8.59 %. UV-Vis (THF): λ_{max} = 234 nm (ε = 2.40 × 10^4 $M^{-1}cm^{-1}$). HRMS (EI): m/z calculated for $C_{19}H_{25}O_2{}^{11}B$: 296.1948 found: 296.1944 (Δppm = 1.3). Mp: 93–95 °C.

5.4.3 Polymer Syntheses

Benzophosphole Oxide Homopolymer (P1): To a solution of 1-*para*-norbornenephenyl-2,3-bis(*para*-biphenyl)benzophosphole oxide (57.7 mg, 0.0926 mmol) in THF (0.6 mL) in a 4 mL vial was added 43 µL of Grubbs' 3rd Generation catalyst in THF (21 mM) and the reaction mixture was stirred at room temperature for 3 minutes after which *ca*. 0.5 mL of ethylvinyl ether was added. The reaction mixture was then stirred for an additional 15 minutes and the crude reaction solution concentrated *in vacuo* to a volume of *ca.* 0.5 mL. This solution was then pipetted into 100 mL of vigorously stirring methanol and the resulting light-yellow polymer was collected by vacuum filtration and dried (43 mg, 74 %). ^{1}H NMR (700 MHz, $CDCl_3$): δ 7.48–7.86 (7H, Ar*H*), 6.78–7.48 (19H, Ar*H*), 4.72–5.37 (2H, vinylic*H*), 2.13–3.13 (3H, two allylic*H* and one benzylic*H*), 1.62–2.12 (2H, CH_2), 0.95–1.38 (2H, CH_2). ^{31}P{^{1}H} NMR (202 MHz, $CDCl_3$): δ 39.2. M_n = 18.4 kDa, M_w = 18.8 kDa, PDI = 1.03, dn/dc = 0.083 mL/g by GPC (in THF). UV-vis (THF): λ_{max} = 270 (ε = 4.30 × 10^4 $M^{-1}cm^{-1}$) and 362 nm (ε = 1.44 × 10^4 $M^{-1}cm^{-1}$). PL (solid state): λ_{ex} = 398 nm, λ_{em} = 512 nm, Φ = 32 %, τ = 5.7 ns. PL (2.0 µM in THF): λ_{ex} = 309 and 364 nm, λ_{em} = 507 nm, Φ = 28 % (λ_{ex} = 310 nm); Φ = 33 % (λ_{ex} = 360 nm); τ = 4.1 ns.

BPin Homopolymer (P2): To a solution of **5** (41.8 mg, 0.141 mmol) in THF (1.0 mL) in a 4 mL vial was added 100 μL of Grubbs' 3rd Generation catalyst in THF (14 mM) and the reaction mixture was stirred at room temperature for 5 minutes, after which *ca.* 0.5 mL of ethylvinyl ether was added, and the reaction mixture was stirred for an additional 15 minutes. The crude reaction solution was concentrated *in vacuo* to *ca*. 0.5 mL and was pipetted into 100 mL of vigorously stirring methanol, and the resulting fibrous off-white solid was isolated by filtration and dried (21 mg, 50 %). ^{1}H NMR (700 MHz, $CDCl_3$): δ 7.60–7.78 (2H, Ar*H*), 6.73–7.24 (2H, Ar*H*), 4.92–5.49 (2H, vinylic*H*), 2.28–3.27 (3H, allylic*H* and benzylic*H*), 1.59–2.26 (2H, CH_2), 1.01–1.45 (14H, CH_2 and BPinCH_3). Note: due to low signal intensity, analysis by ^{11}B NMR spectroscopy was not possible. M_n = 45.6 kDa, M_w = 50.9 kDa, PDI = 1.12, dn/dc = 0.11 mL/g by GPC (in THF).

Copolymer of 5-(4-butylphenyl)norbornene (89 mol%) and 1-*para*-norbornenephenyl-2,3-bis(*para*-biphenyl)benzophosphole oxide (11 mol%) (P3): To a solution of 5-(4-butylphenyl)norbornene (32.6 mg, 0.144 mmol) in THF (0.800 mL) in a 4 mL vial was added 63 μL of Grubbs' 3rd Generation catalyst in THF (28 mM). The reaction mixture was stirred at room temperature for 1 minute, at which point a 40 μL aliquot for GPC analysis was removed from the mixture and quenched with 0.5 mL ethylvinyl ether. To the remainder of the reaction mixture, **4** (21.8 mg, 0.0350 mmol) in THF (0.2 mL) was added and the mixture was stirred for 2.5 minutes. At this point, another 40 μL aliquot for GPC analysis was removed and quenched with 0.5 mL of ethylvinyl ether; an additional 1.0 mL of ethylvinyl ether was added to the remainder of the bulk reaction mixture. The quenched reaction mixture was concentrated to under 0.4 mL and pipetted into 100 mL of vigorously stirring methanol; the resulting light yellow fibrous solid was collected by filtration and dried (31 mg, 57 %). ^{1}H NMR (700 MHz, $CDCl_3$): δ 7.48–7.84 (0.61H, phospholeAr*H*), 7.27–7.48 (1.1H, phospholeAr*H*), 6.63–7.23 (4.6H, Ar*H*), 4.84–5.50 (2H, vinylic*H*), 2.23–3.23 (4.7H, allylic*H* and benzylic*H*), 1.67–2.23 (2.6H, alkyl*H*), 1.48–1.65 (1H, alkyl*H*), 0.99–1.46 (3.7H, alkyl*H*), 0.65–0.98 (2.7H, alkyl*H*). ^{31}P{^{1}H} NMR (202 MHz, $CDCl_3$): δ 39.2. M_n = 54.2 kDa, M_w = 58.7 kDa, PDI = 1.08, dn/dc = 0.16 mL/g by GPC (in THF). UV-vis (THF): λ_{max} = 269 nm ($\varepsilon = 4.32 \times 10^4$ $M^{-1}cm^{-1}$), λ_{max} = 362 nm ($\varepsilon = 1.35 \times 10^4$ $M^{-1}cm^{-1}$). PL (solid state): λ_{ex} = 395 nm, λ_{em} = 511 nm, Φ = 30 %, τ = 5.2 ns. PL (2.0 μM; by the benzophosphole oxide unit in THF): λ_{ex} = 363 nm, λ_{ex} = 305 nm, λ_{em} = 503 nm; Φ = 36 % (λ_{ex} = 305 nm); Φ = 31 % (λ_{ex} = 365 nm); τ = 4.1 ns.

BPin Phosphole Block Copolymer (P4): To a solution of BPin monomer **5** (50.0 mg, 0.169 mmol) in THF (1.0 mL) in a 4 mL vial was added 85 μL of Grubbs' 3rd Generation catalyst in THF (26 mM). The reaction mixture was stirred at room temperature for 1 minute, at which point a 50 μL aliquot for GPC analysis was removed from the mixture and quenched with 0.5 mL ethylvinyl ether. To the remainder of the reaction mixture, **4** (26.0 mg, 0.0417 mmol) in THF (0.2 mL) was added and the mixture was stirred for 2 minutes. At this point, another 50 μL aliquot for GPC analysis was removed and quenched with 0.5 mL ethylvinyl ether; an additional 1.0 mL of ethylvinyl ether was added to the remainder of the bulk reaction mixture. The quenched reaction mixture was concentrated *in vacuo* to *ca.* 0.5 mL and pipetted into 100 mL of vigorously stirring methanol. The resulting light-yellow powder was isolated by filtration and dried (52 mg, 68 %). ^{1}H NMR (700 MHz, $CDCl_3$): δ 7.53–7.79 (2.7H, Ar*H*), 7.28–7.49 (1.2H, phospholeAr*H*), 6.70–7.23 (3.0H, Ar*H*), 4.93–5.50 (2H, vinylic*H*), 2.33–3.24 (3.0H, allylic*H* and benzylic*H*), 1.59–2.26 (2.2H, alkyl*H*), 1.29–1.48 (12H, BPinCH_3) 1.01–1.29 (2H, alkyl*H*). ^{31}P{^{1}H} NMR (162 MHz, $CDCl_3$): δ 39.6. Note: due to a low signal intensity, analysis by ^{11}B NMR spectroscopy was not possible. M_n = 50.4 kDa, M_w = 51.6 kDa, PDI = 1.02, dn/dc = 0.15 mL/g by GPC (in THF). UV-vis (THF): λ_{max} = 271 ($\varepsilon = 4.42 \times 10^4$ $M^{-1}cm^{-1}$) and 362 nm ($\varepsilon = 1.36 \times 10^4$ $M^{-1}cm^{-1}$). PL (solid state): λ_{ex} = 398 nm, λ_{em} = 505 nm, Φ = 41 %, τ = 6.4 ns. PL (2.0 μM; by the benzophosphole oxide unit in THF): λ_{ex} = 307 and 364 nm, λ_{em} = 501 nm; Φ = 30 % (λ_{ex} = 305 nm); Φ = 33 % (λ_{ex} = 365 nm); τ = 3.3 ns.

5.4.4 Micelle Formation

Initial solvent screening with a polymer concentration of 1.0 mg/mL was performed to determine the optimal THF:hexanes ratio required to obtain micelle formation. For this initial screening, 1.2–1.5 mL micelle solutions were prepared in each case. First, powder samples of **P3** or **P4** (*ca*. 1.2–4.0 mg depending on the run) were dissolved in BHT-free THF to generate a stock solution. After ensuring complete dissolution of the polymer in the stock solution, the requisite volume of polymer stock solution was measured out, and to it was added additional THF (if necessary, to meet desired final THF ratio), followed by hexanes. The solution was sealed in a vial and incubated in a water bath (50–55 °C) for one hour, then allowed to stand undisturbed at room temperature for 16 hours before further analysis. The presence of micelles was initially detected by the observation of Tyndall scattering, followed by size measurements by DLS. For **P3** at a concentration of 1.0 mg/mL (equivalent to 415 μM with respect to the benzophosphole oxide units), solvent ratios of 10, 20, 30, and 100 % THF in hexanes were studied but only the solvent systems of 10, 20, and 30 % THF in hexanes were found to contain micelles. For **P4** at a concentration of 1.0 mg/mL (equivalent to 397 μM with respect to the benzophosphole oxide units), solvent ratios of 5, 10, 20, 30, 40, and 100 % THF in hexanes were studied but only the solvent systems of 30 and 40 % THF in hexanes were found to contain micelles.

Secondary sample screening was performed to determine optimal polymer concentrations at the predetermined optimal solvent ratio (20 % THF in hexanes for **P3** and 30 % THF in hexanes for **P4**). Using the same general procedure described above for the synthesis of micelles at 1.0 mg/mL, micelle solutions of **P3** in 20 % THF in hexanes at polymer concentrations of 0.1, 0.3, 0.5, and 2.0 mg/mL were prepared. All four concentrations studied were found to yield micelles with average diameters of *ca.* 30–40 nm as determined by DLS. Micelle solutions of **P4** in 30 % THF in hexanes at polymer concentrations of 0.1, 0.3, 0.5, and 2.0 mg/mL were prepared. Interestingly, solutions of **P4** at concentrations of 0.3 mg/mL or above in 30 % THF in hexanes were found to yield micelle solutions that were stable for at least 24 hours, but solutions of **P4** at a concentration of 0.1 mg/mL (in 30 or 40 % THF in hexanes) were repeatedly observed to exhibit significant aggregation and precipitation of the polymer after standing at room temperature for 16 hours.

5.4.4.1 TEM Imaging Statistics of Micelles

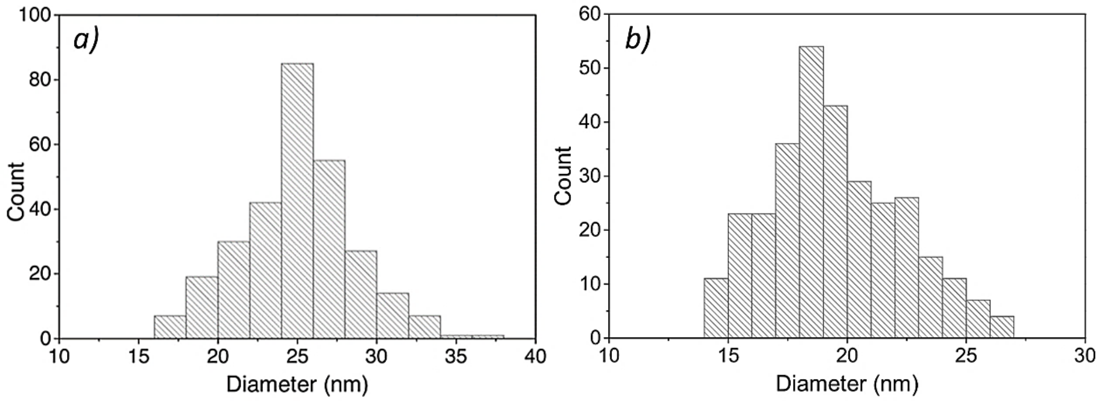

Figure 5.16. Micelle size distribution analysis from TEM images of a) **P3** micelles and b) **P4** micelles.

5.4.5 UV-Vis Absorbance Data

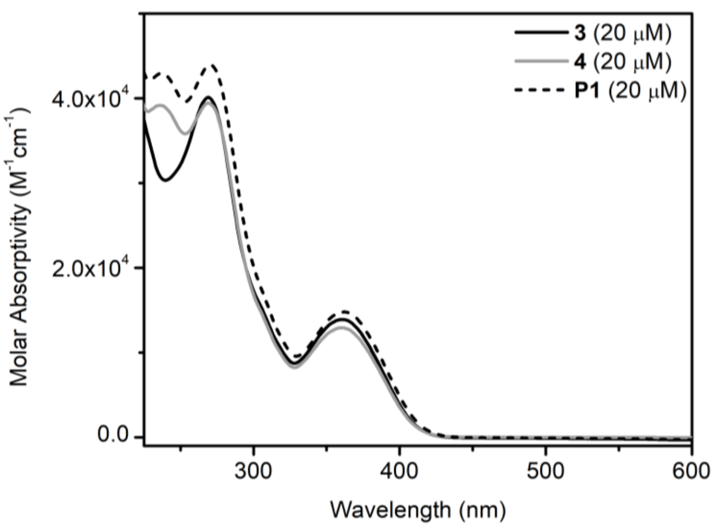

Figure 5.17. UV-vis absorbance spectra for **3**, **4** and homopolymer **P1** at a concentration of 20 μM of benzophosphole oxide units in THF at room temperature.

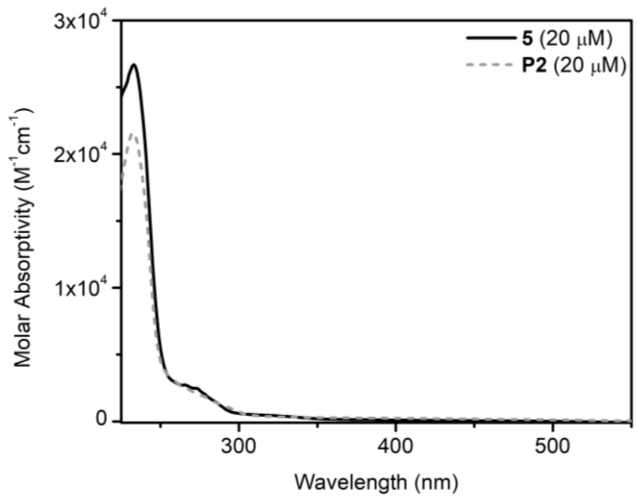

Figure 5.18. UV-vis absorbance spectra for **5** and homopolymer **P2** at a concentration of 20 μM of BPin units in THF at room temperature.

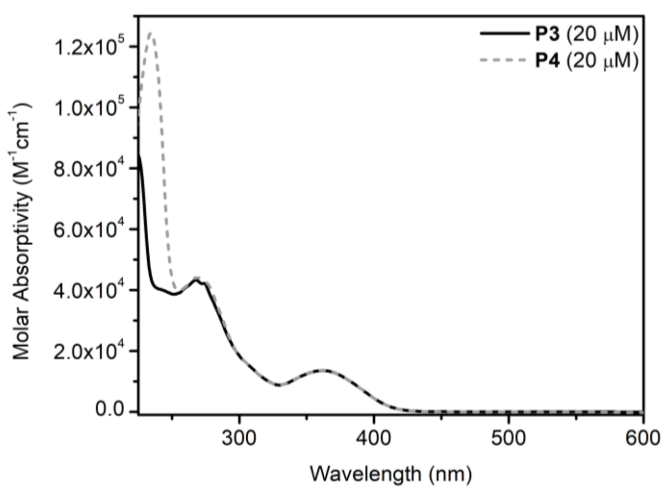

Figure 5.19. UV-vis absorbance spectra for polymers **P3** and **P4** at a concentration of 20 μM of benzophosphole oxide units in THF at room temperature.

5.4.6 Supplemental PL Data

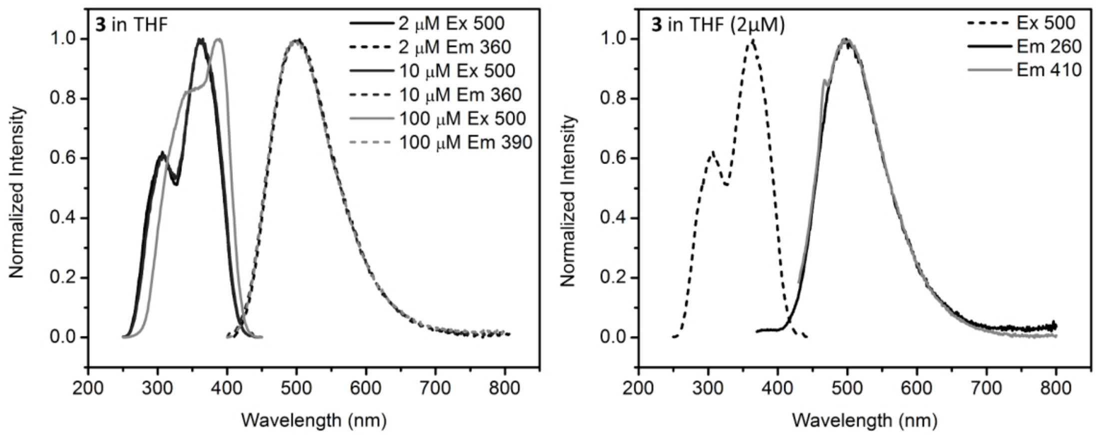

Figure 5.20. Excitation and emission plots of **3** in a THF solution of varying concentration (left) and in a 2.0 μM solution in THF using varying excitation wavelengths (right) under ambient atmosphere.

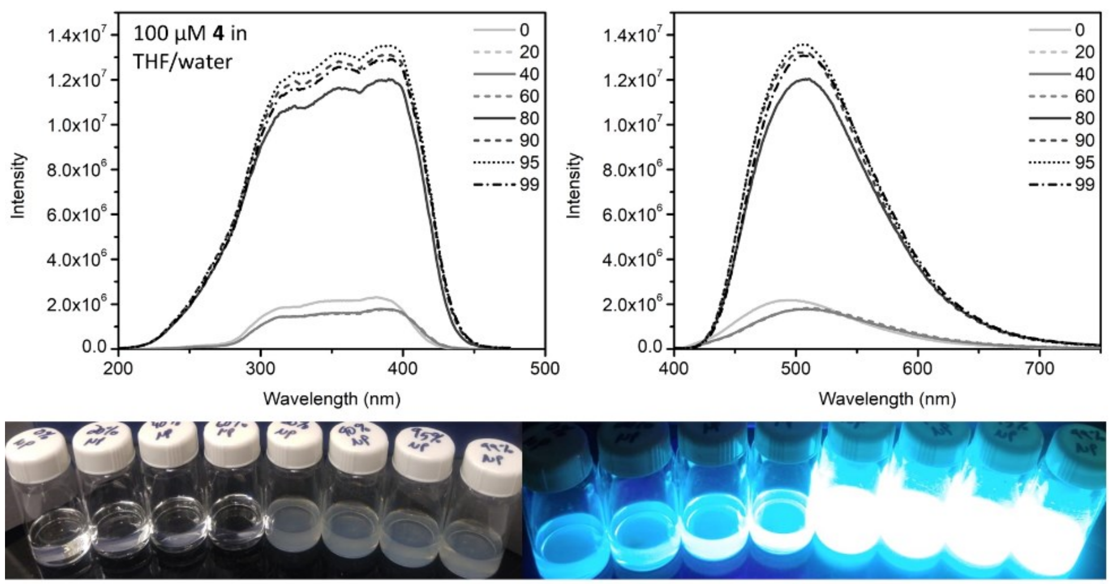

Figure 5.21. Excitation (upper left) and emission plots (upper right) of **4** in 100 μM solutions with varying ratios of water to THF. The legend for the emission and excitation spectra lists the percentage of water in the solvent mixture for each sample. Bottom left: images under ambient light of 100 μM solutions of **4** with percentage of water increasing from left to right. Bottom right: solutions of **4** illuminated under 365 nm light.

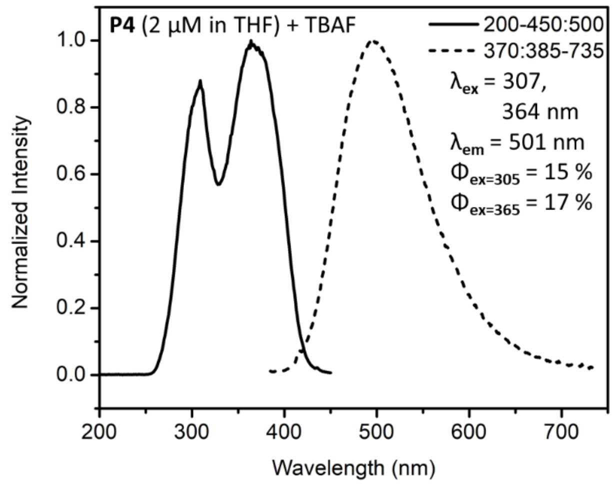

Figure 5.22. Excitation and emission plots of **P4** in a 2.0 µM (with respect to the benzophosphole oxide unit) solution in THF under ambient atmosphere with the addition of 20 mM tetrabutyl ammonium fluoride.

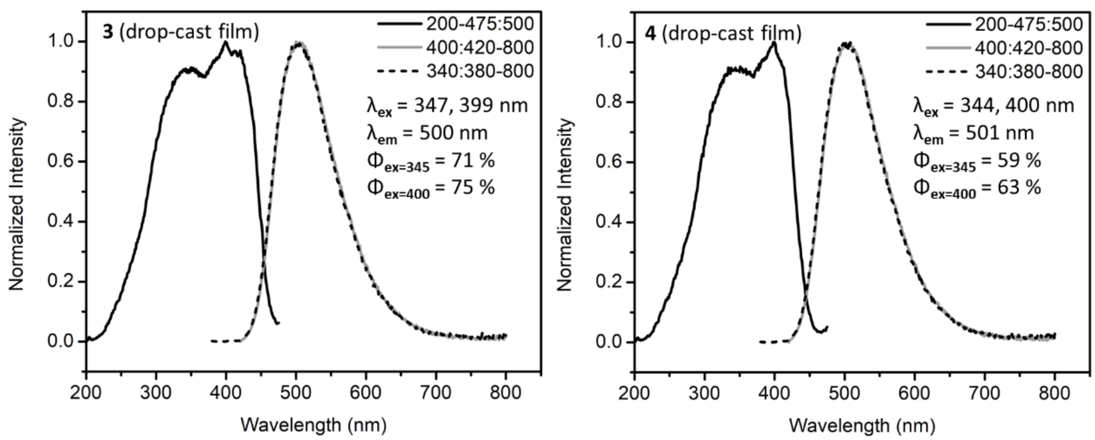

Figure 5.23. Excitation and emission plots of films of **3** (left) and **4** (right) drop-cast from THF onto quartz plates.

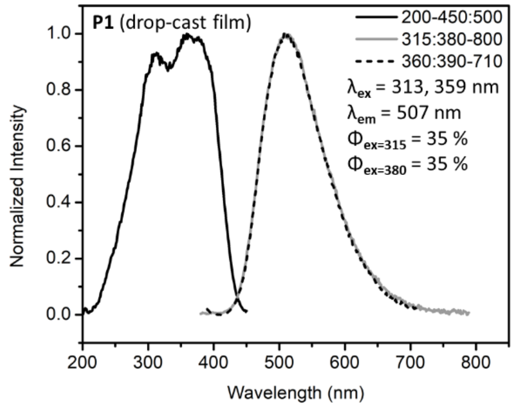

Figure 5.24. Excitation and emission plots of a film of **P1** drop-cast from THF onto quartz.

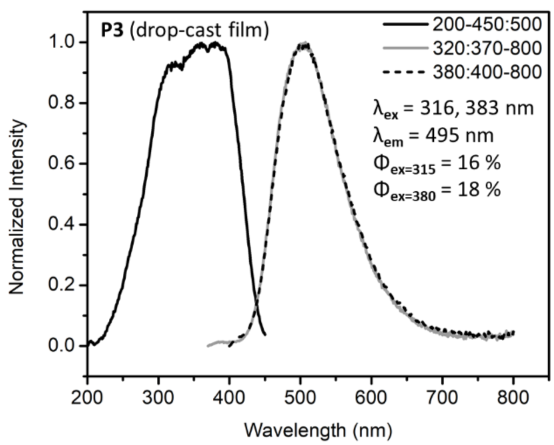

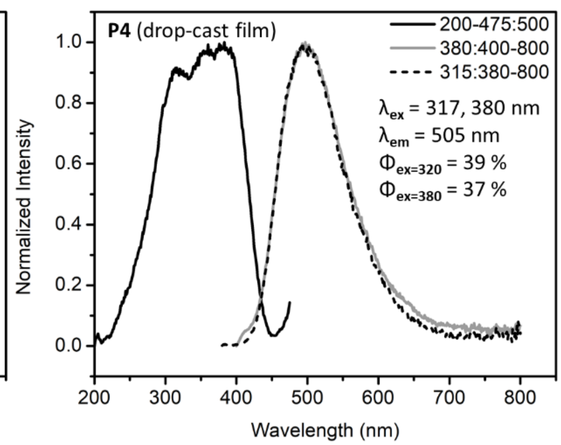

Figure 5.25. Excitation and emission plots of films of **P3** (left) and **P4** (right) drop-cast from THF onto quartz plates.

5.4.7 Thermogravimetric Analysis Data

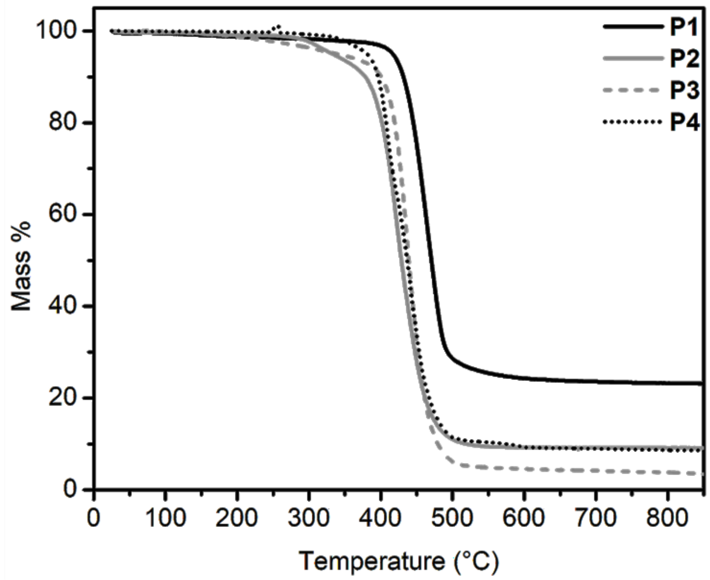

Figure 5.26. TGA plots of polymers **P1–P4** at a heating rate of 10 °C per minute under an N_2 atmosphere.

5.4.8 Selected NMR Data

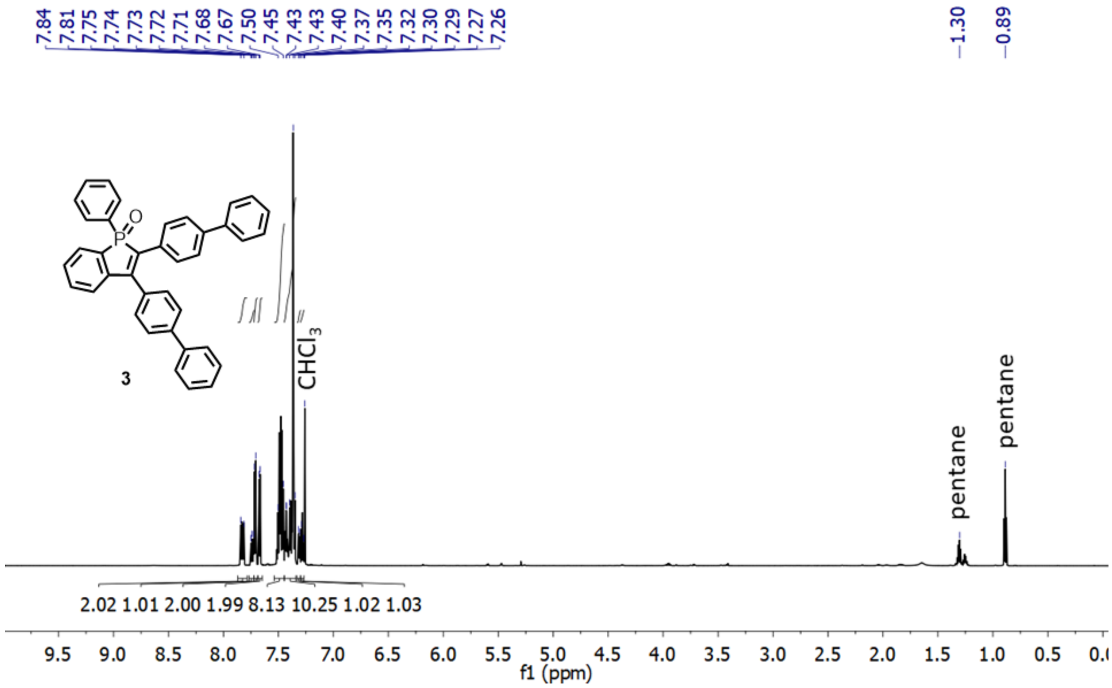

Figure 5.27. ^{1}H NMR spectrum of **3** in $CDCl_3$.

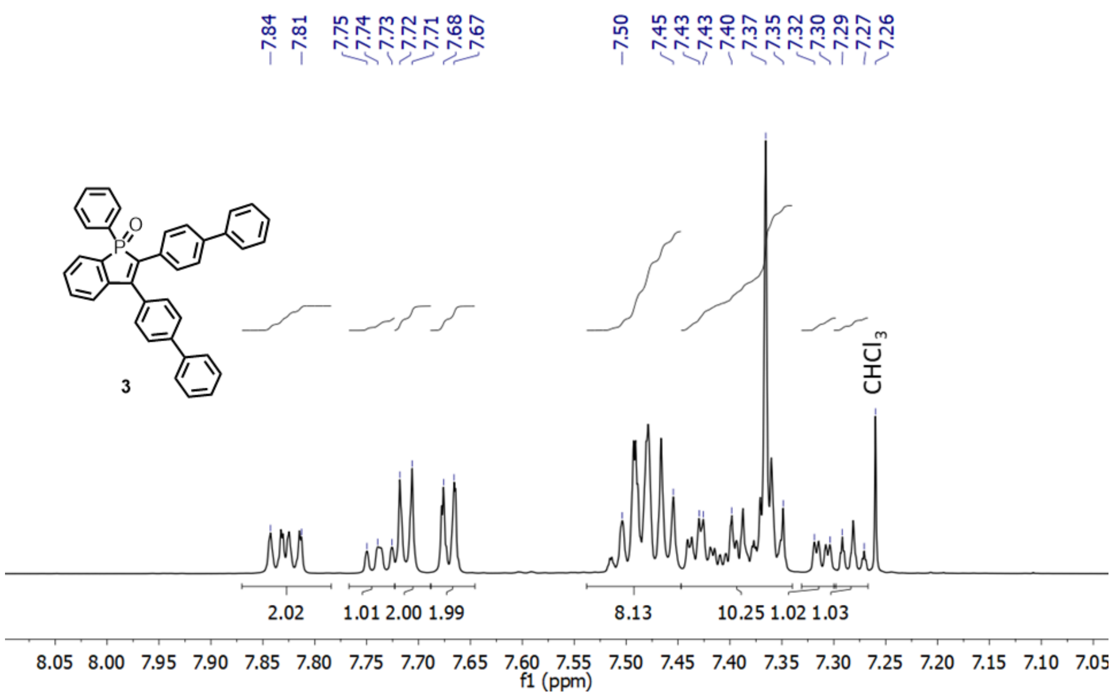

Figure 5.28. Expansion of the ^{1}H NMR spectrum of **3** in $CDCl_3$.

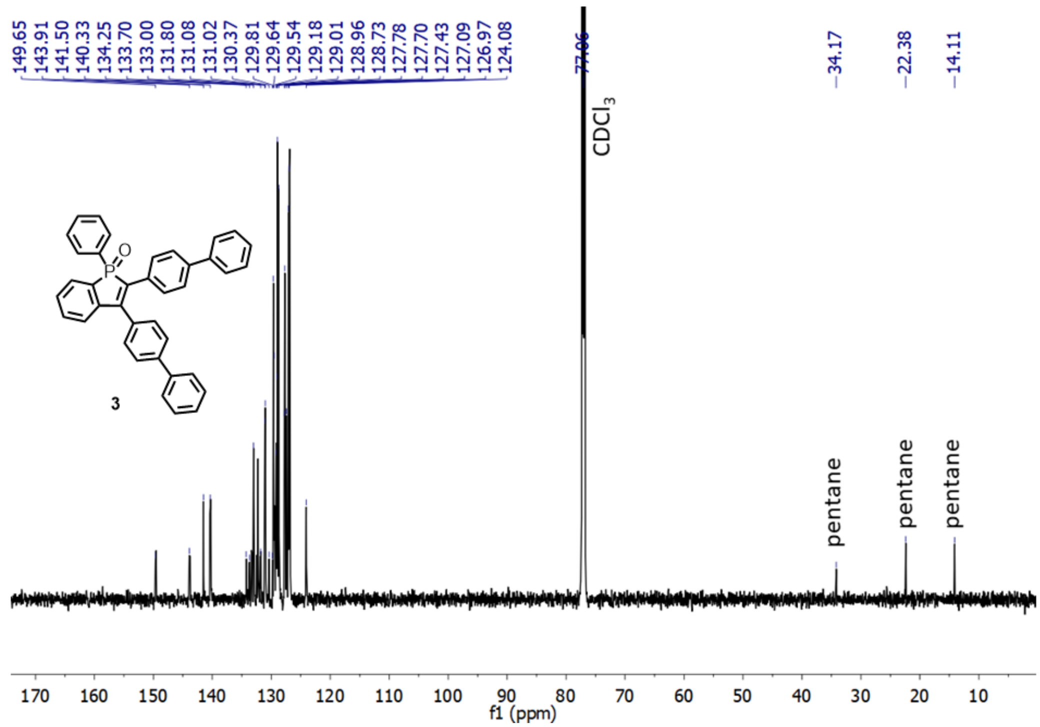

Figure 5.29. $^{13}C\{^{1}H\}$ NMR spectrum of **3** in $CDCl_3$.

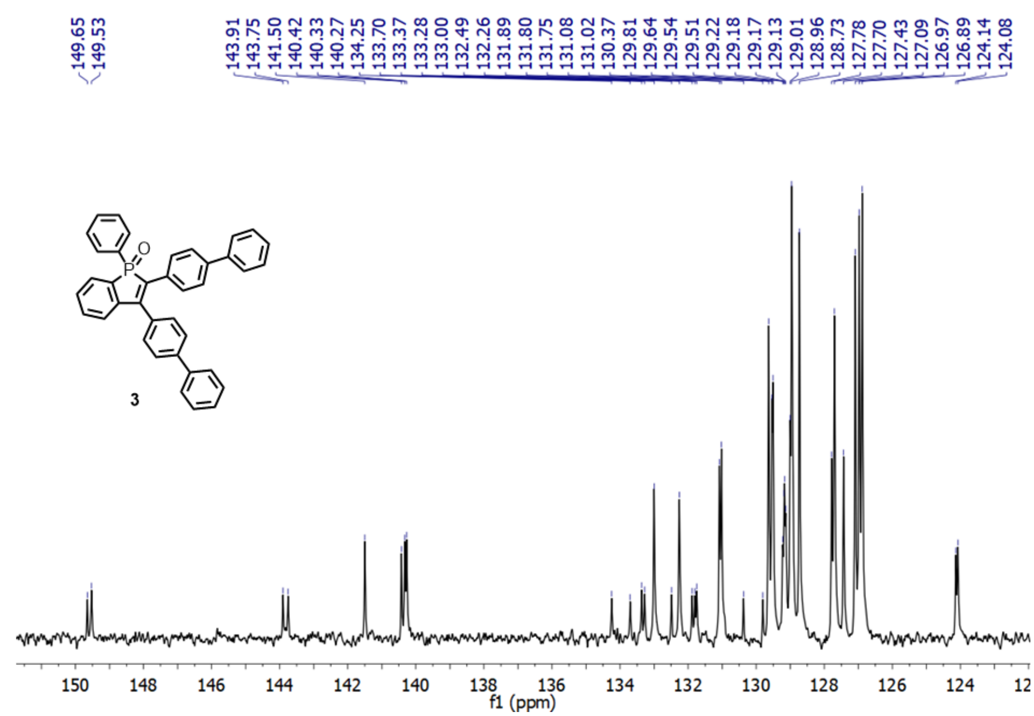

Figure 5.30. Expansion of the $^{13}C\{^{1}H\}$ NMR spectrum of **3** in $CDCl_3$.

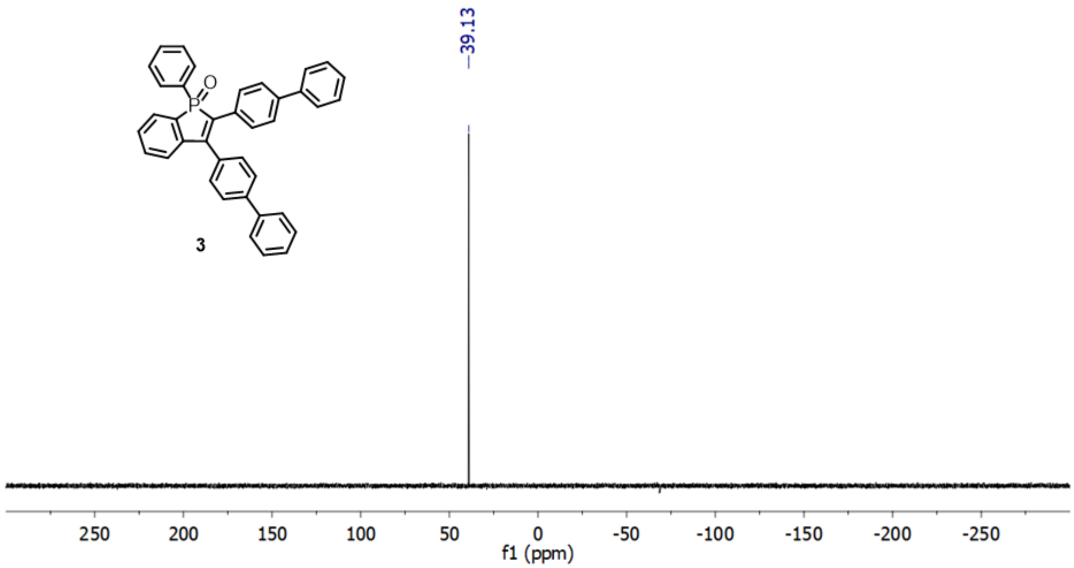

Figure 5.31. $^{31}P\{^{1}H\}$ NMR spectrum of **3** in $CDCl_3$.

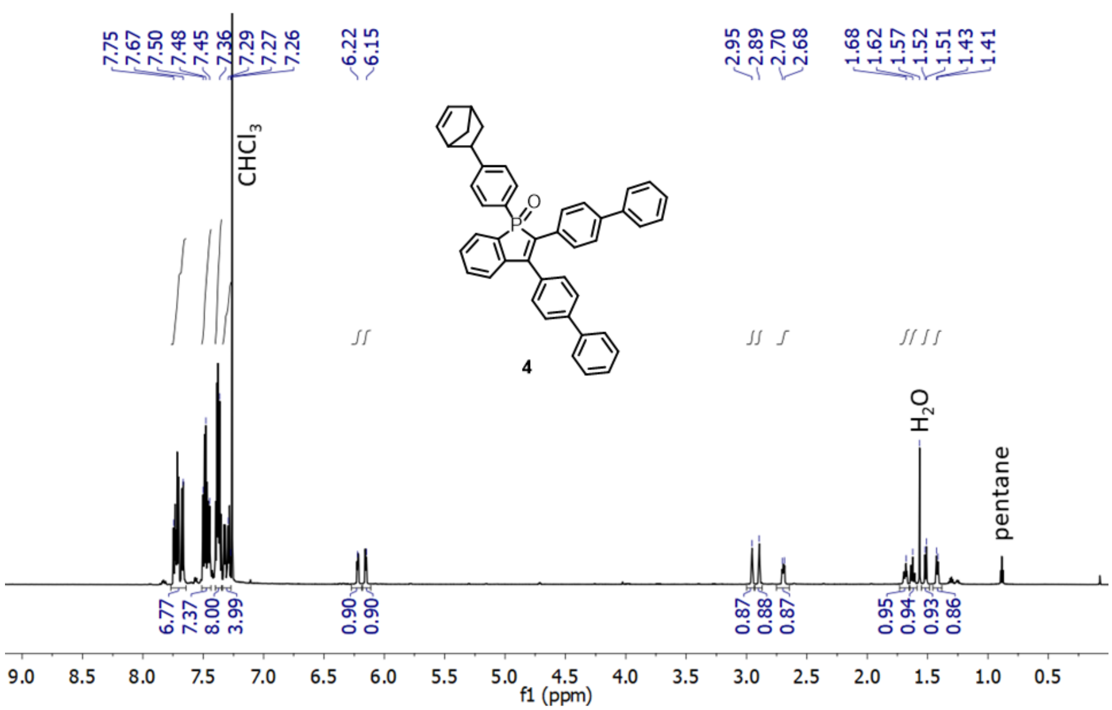

Figure 5.32. ^{1}H NMR spectrum of **4** in $CDCl_3$.

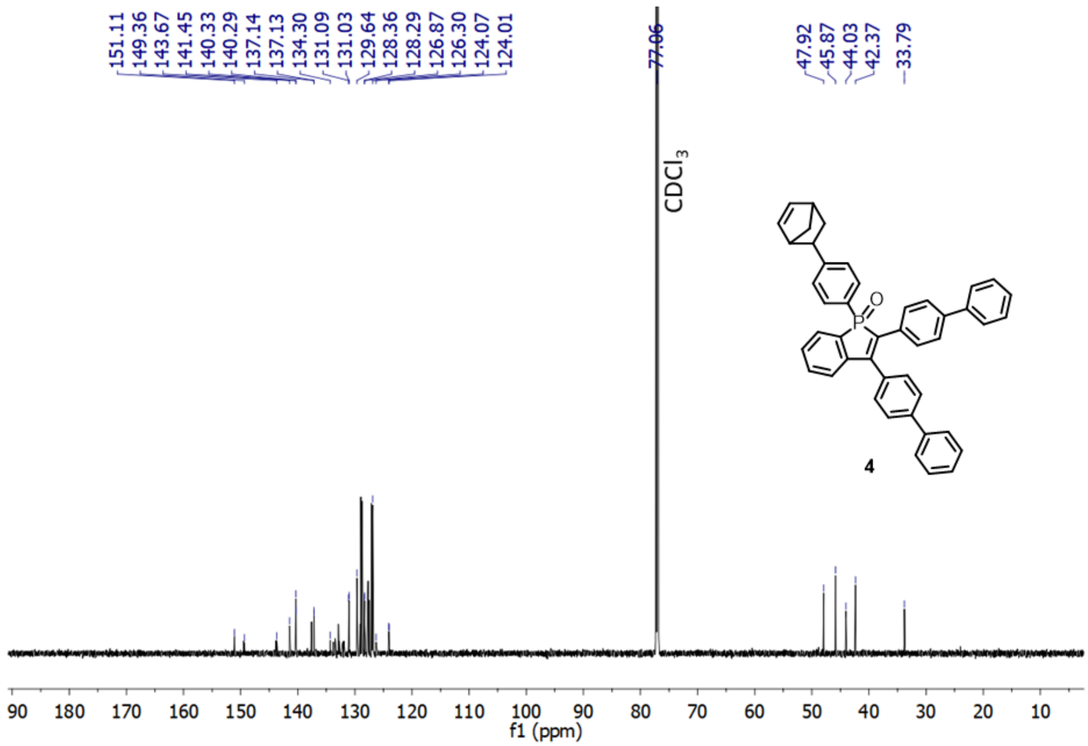

Figure 5.33. $^{13}C\{^1H\}$ NMR spectrum of **4** in $CDCl_3$.

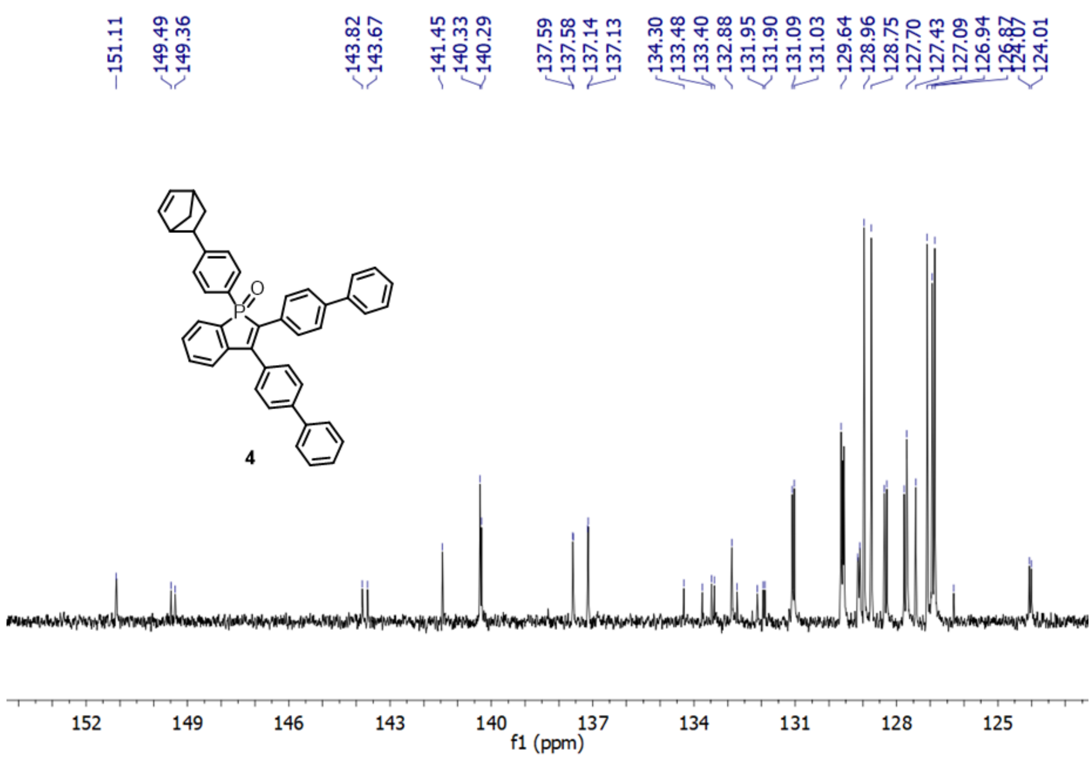

Figure 5.34. Expansion of the $^{13}C\{^1H\}$ NMR spectrum of **4** in $CDCl_3$.

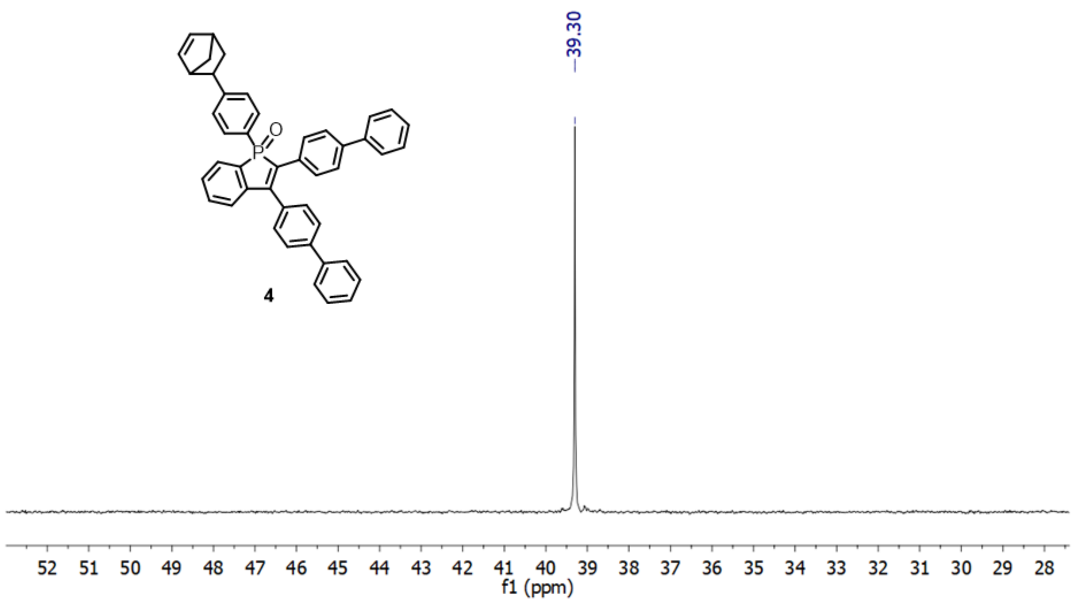

Figure 5.35. $^{31}P\{^{1}H\}$ NMR spectrum of **4** in $CDCl_3$.

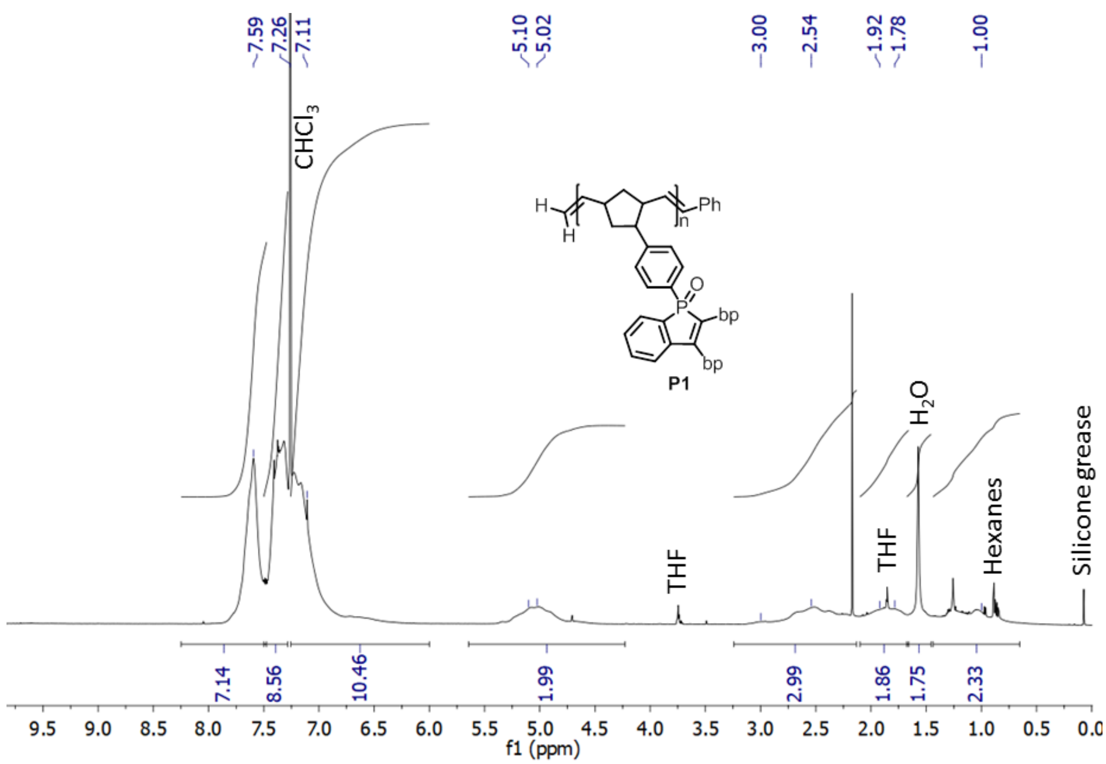

Figure 5.36. ^{1}H NMR spectrum of **P1** in $CDCl_3$.

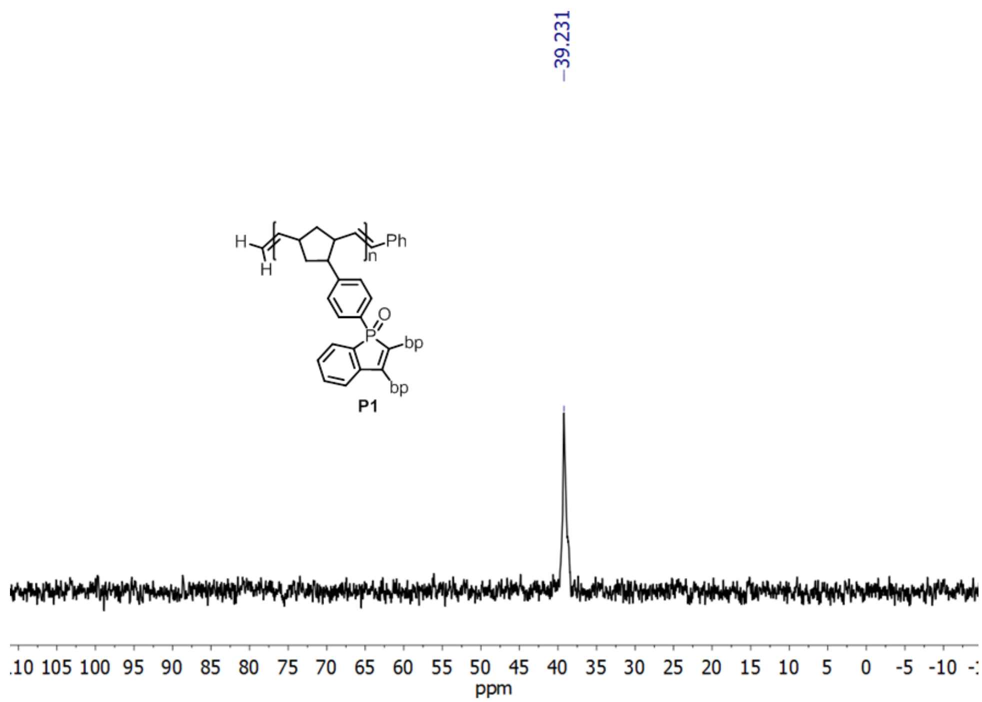

Figure 5.37. $^{31}P\{^{1}H\}$ NMR spectrum of **P1** in $CDCl_3$.

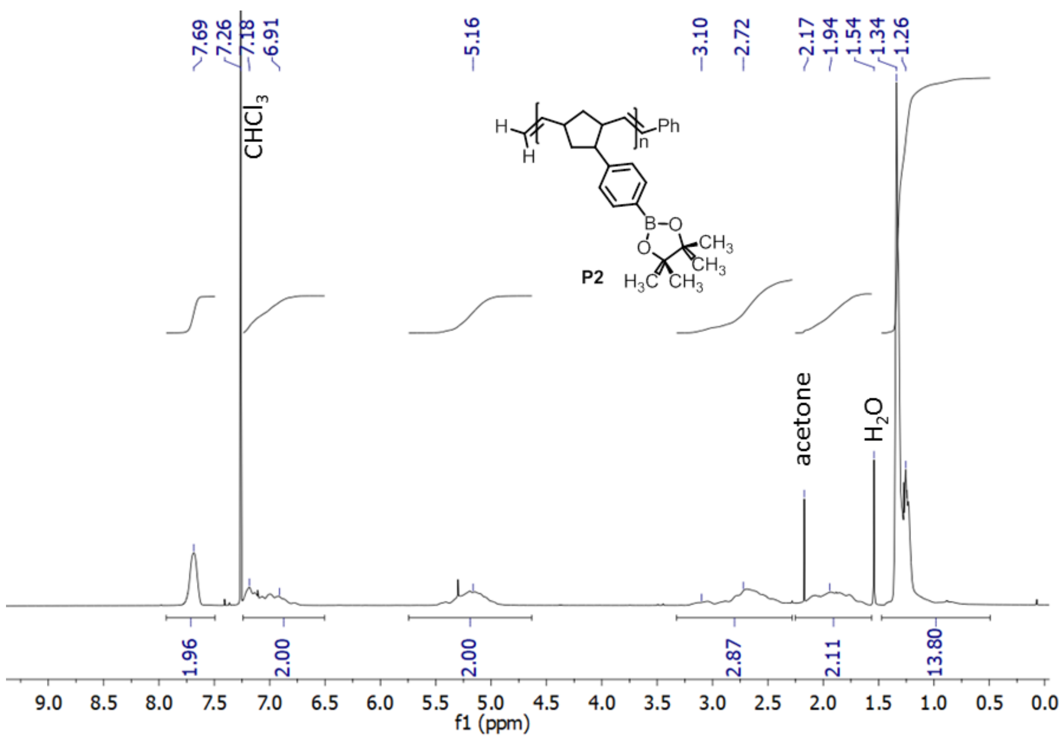

Figure 5.38. ^{1}H NMR spectrum of **P2** in $CDCl_3$.

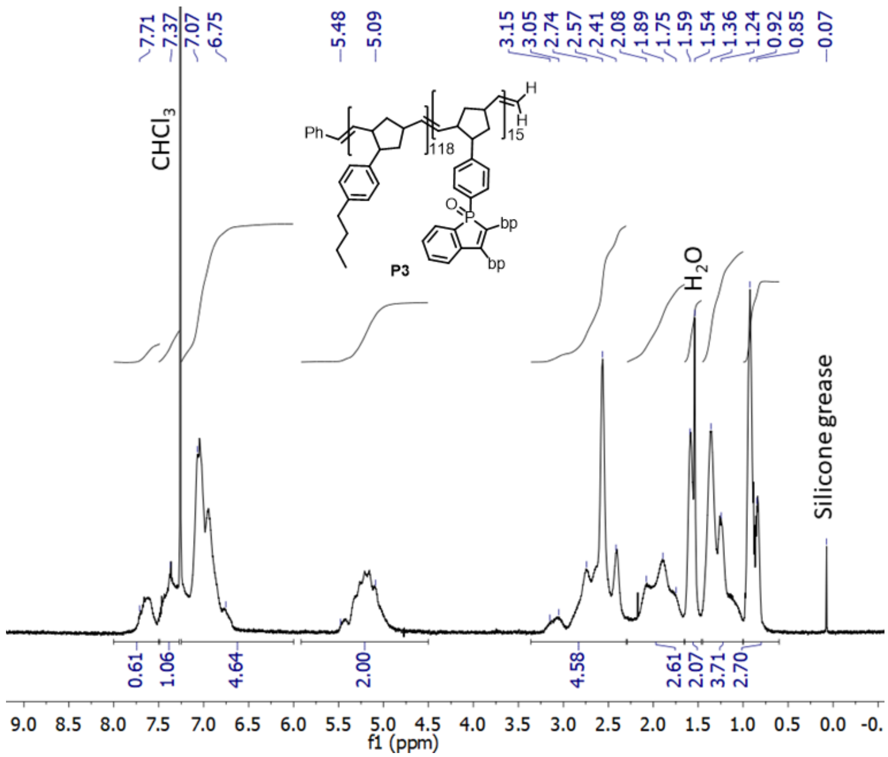

Figure 5.39. [1]H NMR spectrum of **P3** in $CDCl_3$.

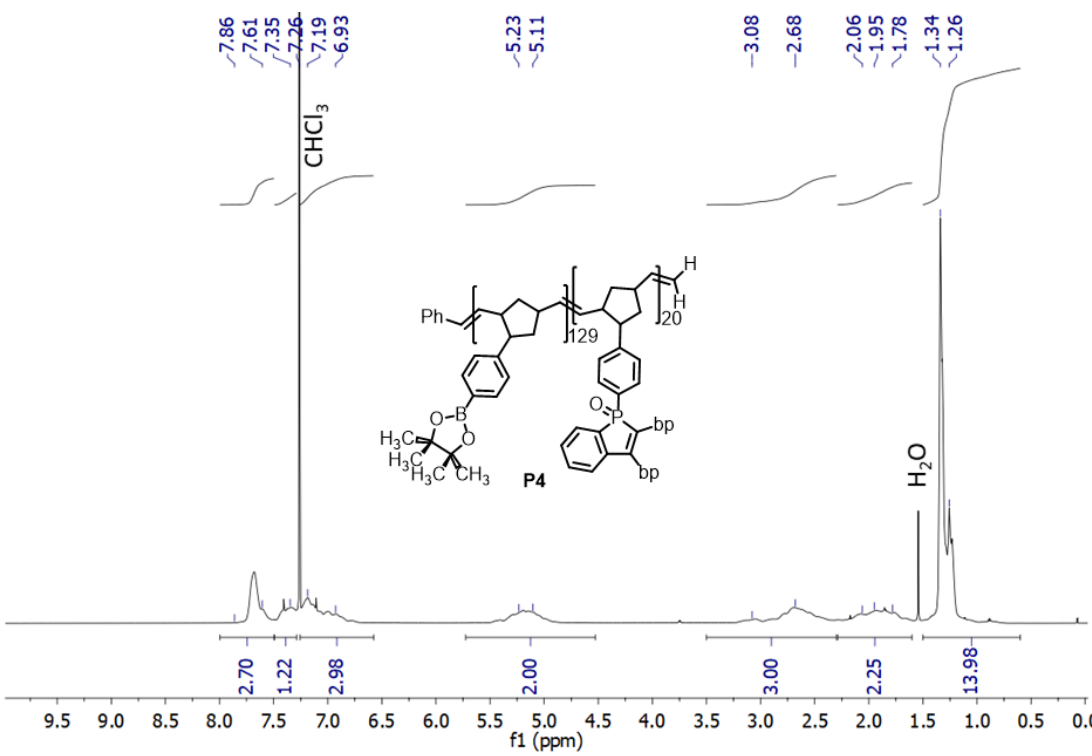

Figure 5.40. [1]H NMR spectrum of **P4** in $CDCl_3$.

5.4.9 Computational Methodology

Geometry optimizations of the gas phase structures were performed using density functional theory (DFT) with B3LYP3,[14] and CAM-B3LYP[15] functionals and the cc-pVTZ[16] basis set. Initial molecular geometries were taken from the experimentally obtained X-ray structures. Subsequent frequency analysis confirmed all obtained structures to be local minima on the potential energy surface. To calculate the fluorescence energy, the geometry of the lowest lying excited singlet state (S_1) was optimized by TD-DFT computations using (CAM-)B3LYP with the same basis sets as specified above. The vertical excitation energies of the first ten singlet and triplet states have been predicted by TD-DFT computations using the (CAM-)B3LYP functionals as well as the cc-pVTZ basis set using the respective (CAM-)B3LYP/cc-pVTZ optimized gas-phase S_0 geometry. Fluorescence energies have then been calculated as the difference of the energies at the (CAM-)B3LYP optimized S_1 geometry and the (CAM-)B3LYP optimized S_0 geometry. All computations were carried out with the Gaussian16 software.[21] The presented molecular orbitals (MOs) were extracted from the Gaussian16 checkpoint files and visualized with Avogadro 1.2.0.[22]

5.4.10 X-Ray Crystallographic Data

Crystals of appropriate quality for X-ray diffraction studies were removed from a vial and immediately covered with a thin layer of hydrocarbon oil (Paratone-N). A suitable crystal was then selected, attached to a glass fiber, and quickly placed in a glass vial. All data were collected using a Bruker APEX II CCD detector/D8 diffractometer using Mo/Cu Kα radiation. The data were corrected for absorption through Gaussian integration from indexing of the crystal faces. Structures were solved using the direct methods programs SHELXS-97,[23] and refinements were completed using the program SHELXL-97.[23]

Table 5.5. Crystallographic data for compounds **1**, **3**, and **5**.

Compound	**1**	**3**	**5**
Formula	$C_{42}H_{22}Zr$	$C_{40}H_{31}Cl_4OP$	$C_{19}H_{25}BO_2$
Formula weight	617.81	700.42	296.20
Crystal system	Monoclinic	Triclinic	Monoclinic
Space group	$P2_1/c$	$P\bar{1}$	$P2_1/n$
a (Å)	7.7223(3)	9.6011(2)	6.5678(7)
b (Å)	19.3512(9)	9.8996(2)	12.5281(13)
c (Å)	20.7657(9)	19.6335(3)	20.649(2)
α (°)	--	84.6658(7)	--
β (°)	96.2200(10)	78.8408(8)	92.3746(17)
γ (°)	--	70.3532(8)	--
V (Å^3)	3084.9(2)	1723.45(6)	1697.6(3)
Z	4	2	4
ρ (g/cm^3)	1.330	1.350	1.159
Abs coeff (mm^{-1})	3.124	3.802	0.072
T (K)	173	173	173
$2\theta_{max}$ (°)	148.38	144.49	58.72
Total data	128892	12009	13410
Unique data (R_{int})	6266(0.0367)	6546(0.0131)	3462(0.0229)
Obs data [I>2(σ(I)]	6194	6010	2926
Params	424	389	257
R_1 [I>2(σ(I)]^a	0.0377	0.0368	0.0527
wR_2 [all data]^a	0.0992	0.1021	0.1375
Max/min $\Delta\rho$ (e$^-$Å^{-3})	0.688/–0.520	0.460/–0.469	0.265/–0.144

$^aR_1 = \Sigma||F_o| - |F_c||/\Sigma|F_o|$; $wR_2 = [\Sigma w(F_o^2 - F_c^2)^2/\Sigma w(F_o^4)]^{1/2}$

5.5. References

1. (a) Fave, C.; Cho, T.-Y.; Hissler, M.; Chen, C.-W.; Luh, T.-Y.; Wu, C.-C.; Réau, R. *J. Am. Chem. Soc.* **2003**, *125*, 9254–9255. (b) Su, H.-C.; Fadhel, O.; Yang, C.-J.; Cho, T.-Y.; Fave, C.; Hissler, M.; Wu, C.-C.; Réau, R. *J. Am. Chem. Soc.* **2006**, *128*, 983–995. (c) Chen, H.; Delaunay, W.; Yu, L.; Joly, D.; Wang, Z.; Li, J.; Wang, Z.; Lescop, C.; Tondelier, D.; Geffroy, B.; Duan, Z.; Hissler, M.; Mathey,

F.; Réau, R. *Angew. Chem. Int. Ed*. **2012**, *51*, 214–217. (d) Baumgartner, T.; Réau, R. *Chem. Rev*. **2006**, *106*, 4681–4724.

2. (a) Taki, M.; Ogasawara, H.; Osaki, H.; Fukazawa, A.; Sato, Y.; Ogasawara, K.; Higashiyama, T.; Yamaguchi, S. *Chem. Commun.* **2015**, *51*, 11880–11883. (b) Fukazawa, A.; Ichihashi, Y.; Kosaka, Y.; Yamaguchi, S. *Chem. Asian J*. **2009**, *4*, 1729–1740.
3. (a) Fourmy, K.; Nguyen, D. H.; Dechy-Cabaret, O.; Gouygou, M. *Catal. Sci. Technol*. **2015**, *5*, 4289–4323. (b) Hibner-Kulicka, P.; Joule, J. A.; Skalik, J.; Bałczewski, P. *RSC Adv*. **2017**, *7*, 9194–9236.
4. (a) Matsumura, M.; Yamada, M.; Muranaka, A.; Kanai, M.; Kakusawa, N.; Hashizume, D.; Uchiyama, M.; Yasuike, S. *Beilstein J. Org. Chem*. **2017**, *13*, 2304–2309. (b) Wu, B.; Santra, M.; Yoshikai, N. *Angew. Chem. Int. Ed*. **2014**, *53*, 7543–7546. (c) Kumaravel, M.; Mague, J. T.; Balakrishna, M. S. *Tetrededron Lett*. **2014**, *55*, 2957–2961.
5. (a) Wang, C.; Fukazawa, A.; Tanabe, Y.; Inai, N.; Yokogawa, D.; Yamaguchi, S. *Chem. Asian J*. **2018**, *13*, 1616–1624. (b) Wang, C.; Taki, M.; Sato, Y.; Fukazawa, A.; Higashiyama, T.; Yamaguchi, S. *J. Am. Chem. Soc.* **2017**, *139*, 10374–10381. (c) Adler, R. A.; Wang, C.; Fukazawa, A.; Yamaguchi, S. *Inorg. Chem.* **2017**, *56*, 8718–8725.
6. See Section 1.4.1.1 for a discussion of the luminescence properties of benzophosphole oxides with examples of fluorescent emitters with quantum yields (Φ) approaching 100 %. For selected references discussing benzophosphole emitters with particularly high Φ, see: (a) Fukazawa, A.; Hara, M.; Okamoto, T.;

Son, E.-C.; Xu, C.; Tamao, K.; Yamaguchi, S. *Org. Lett*. **2008**, *10*, 913–916. (b) Matano, Y.; Motegi, Y.; Kawatsu, S.; Kimura, Y. *J. Org. Chem.* **2015**, *80*, 5944−5950.

7. Bu, F.; Wang, E.; Peng, Q.; Hu, R.; Qin, A.; Zhao, Z.; Tang, B. Z. *Chem. Eur. J.* **2015**, *21*, 4440–4449.
8. Zhuang, Z.; Bu, F.; Luo, W.; Peng, H.; Chen, S.; Hu, R.; Qin, A.; Zhao, Z.; Tang, B. Z. *J. Mater. Chem. C* **2017**, *5*, 1836–1842.
9. Parke, S. M.; Hupf, E.; Matharu, G. K.; de Aguiar, I.; Xu, L.; Yu, H.; Boone, M. P.; de Souza, G. L. C.; McDonald, R.; Ferguson, M. J.; He, G.; Brown, A.; Rivard, E. *Angew. Chem. Int. Ed*. **2018**, *57*, 14841–14846.
10. Fagan, P. J.; Nugent, W. A. *J. Am. Chem. Soc*. **1988**, *110*, 2310–2312.
11. Fagan, P. J.; Nugent, W. A.; Calabrese, J. C. *J. Am. Chem. Soc*. **1994**, *116*, 1880–1889.
12. He, G.; Wiltshire, B. D.; Choi, P.; Savin, A.; Sun, S.; Mohammadpour, A.; Ferguson, M. J.; McDonald, R.; Farsinezhad, S.; Brown, A.; Shankar, K.; Rivard, E. *Chem. Commun.* **2015**, *51*, 5444−5447.
13. (a) Kuno, S.; Kanamori, T.; Yijing, Z.; Ohtani, H.; Yuasa, H. *ChemPhotoChem*. **2017**, *1*, 102–106. (b) Shoji, Y.; Ikabata, Y.; Wang, Q.; Nemoto, D.; Sakamoto, A.; Tanaka, N.; Seino, J.; Nakai, H.; Fukushima, T. *J. Am. Chem. Soc.* **2017**, *139*, 2728–2733.
14. (a) Becke, A. D.; *J. Chem. Phys.* **1993**, *98*, 5648–5652. (b) Lee, C.; Yang, W.; Parr, R. G. *Phys. Rev. B* **1988**, *37*, 785–789.
15. Yanai, T.; Tew, D.; Handy, N. A *Chem. Phys. Lett*. **2004**, *393*, 51–57.

16. (a) Dunning, Jr., T. H. *J. Chem. Phys*. **1989**, *90*, 1007–1023. (b) Woon, D.E.; Dunning, Jr., T. H. *J. Chem. Phys.* **1993**, 98, 1358–1371.

17. Oehlke, A.; Auer, A. A.; Jahre, I.; Walfort, B.; Rüffer, T.; Zoufalá, P.; Lang, H.; Spange, S. *J. Org. Chem*. **2007**, *72*, 4328–4339.

18. Jantunen, K. C.; Scott, B. L.; Kiplinger, J. L. *J. Alloy. Compd.* **2007**, *444*, 363–368.

19. Brown, A. E.; Eichler, B. E. *Tetrahedron Lett.* **2011**, *52*, 1960–1963.

20. Harned, A. M.; Song He, H.; Toy, P. H.; Flynn, D. L.; Hanson, P. R. *J. Am. Chem. Soc.* **2005**, *127*, 52–53.

21. Frisch, M. J.; Trucks, G. W.; Schlegel, H. B.; Scuseria, G. E.; Robb, M. A.; Cheeseman, J. R.; Scalmani, G.; Barone, V.; Petersson, G. A.; Nakatsuji, H.; Li, X.; Caricato, M.; Marenich, A. V.; Bloino, J.; Janesko, B. G.; Gomperts, R.; Mennucci, B.; Hratchian, H. P.; Ortiz, J. V.; Izmaylov, A. F.; Sonnenberg, J. L.; Williams-Young, D.; Ding, F.; Lipparini, F.; Egidi, F.; Goings, J.; Peng, B.; Petrone, A.; Henderson, T.; Ranasinghe, D.; Zakrzewski, V. G.; Gao, J.; Rega, N.; Zheng, G.; Liang, W.; Hada, M.; Ehara, M.; Toyota, K.; Fukuda, R.; Hasegawa, J.; Ishida, M.; Nakajima, T.; Honda, Y.; Kitao, O.; Nakai, H.; Vreven, T.; Throssell, K.; Montgomery, J. A., Jr.; Peralta, J. E.; Ogliaro, F.; Bearpark, M. J.; Heyd, J. J.; Brothers, E. N.; Kudin, K. N.; Staroverov, V. N.; Keith, T. A.; Kobayashi, R.; Normand, J.; Raghavachari, K.; Rendell, A. P.; Burant, J. C.; Iyengar, S. S.; Tomasi, J.; Cossi, M.; Millam, J. M.; Klene, M.; Adamo, C.; Cammi, R.;

Ochterski, J. W.; Martin, R. L.; Morokuma, K.; Farkas, O.; Foresman, J. B.; Fox, D. J. *Gaussian 16*, Revision A.03; Gaussian, Inc.: Wallingford, CT, 2016.

22. (a) Avogadro: An Open-Source Molecular Builder and Visualization Tool—Version 1.2.0. 2016. Available online: http://avogadro.cc/ (accessed on 13 March 2019). (b) Hanweel, M.; Curtis, D.E.; Lonie, D.; Vandermeersch, T.; Zurek, E.; Hutchison, G. *J. Cheminform.* **2012**, *4*, 17.

23. Sheldrick, G. M. *Acta Cryst. A* **2008**, *64*, 112–122.

Chapter 6: Summary and Future Directions

6.1 Summary and Future Work

Chapter 2 involved the synthesis of a series of new bismole compounds via metallacycle transfer catalyzed by copper(I) chloride; this was the first use of copper(I) chloride to facilitate the metallacycle transfer with bismuth. The luminescence of three of these new bismoles, **1–3** (Figure 6.1), was studied in detail. Bismole **1** was observed to only emit via fluorescence, while **2** and **3** were observed to exhibit both fluorescence and phosphorescence, and the emission intensity was enhanced significantly upon cooling the samples. Luminescence studies of **1–3** were paired with TD-DFT computational analysis and compounds **2** and **3** are believed to exhibit phosphorescence due to an increase in orbital participation from bismuth in the excitation processes. This is proposed to lead to significant mixing of triplet and singlet character in the lower-energy excited states allowing for an increase in intersystem crossing. Compound **1** was observed to have reduced mixing of triplet and singlet character in its lower-energy excited states that is most likely due to the limited participation of the bismuth atom in excitation processes. These findings are in line with results previously reported for related tellurophene systems.[1]

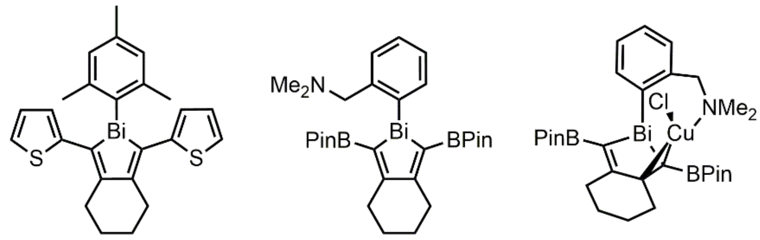

1 2 3

Figure 6.1. Bismoles **1**–**3**, which were discussed in Chapter 2.

While this work has been synthetically interesting, the most important finding from this study has been an increased understanding in the requirements to access phosphorescence from this class of main group element-based emitter. Ideally this study will help to guide the future preparation of luminescent materials containing heavy inorganic elements and reduce the amount of synthetic trial-and-error involved in the development of new luminogens.

Future work could involve a TD-DFT computational study on ring-fused bismole backbones. In contrast to bismoles, the area of phosphole chemistry has been studied in substantially greater detail. As each class of phosphole (*i.e.* dithienyl phospholes, biphenylphospholes, benzophospholes, and unfused phospholes) is considered as a separate family of heterocycle with substantially different electronic, optical, and thermal properties,[2] it is reasonable to extend this assumption to bismole analogues as well. Figure 6.2 shows a range of fused bismoles that could serve as a starting point for this proposed computational study. In particular, π-extended polyacenes like phenanthrene- and pyrene-fused bismoles **9** and **10** are likely to exhibit red-shifted emission that may yield a valuable infrared emitter, which would be of great value for bioimaging applications.[3]

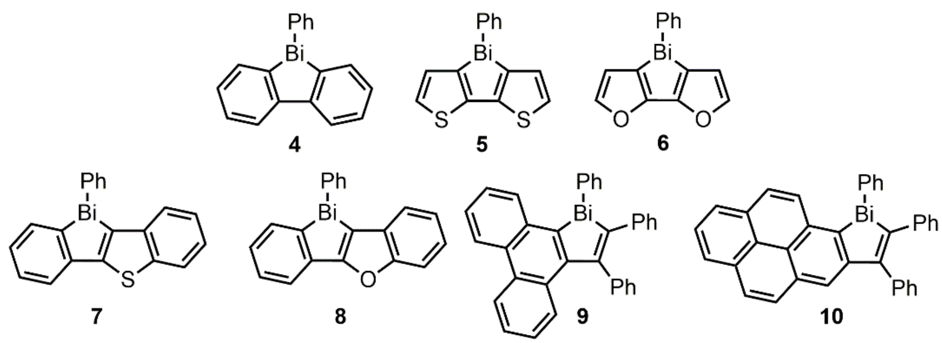

Figure 6.2. Ring-fused bismole parent molecules to serve as a starting point for a TD-DFT study to screen for likely phosphorescent materials.

In Chapter 3, the synthetic strategy outlined in Chapter 2 was applied towards the generation of a series of red phosphorescent benzo[*b*]bismole emitters **11** and **12** and norbornene-functionallized benzo[*b*]bismole-based monomers **13** and **14** (Figure 6.3).

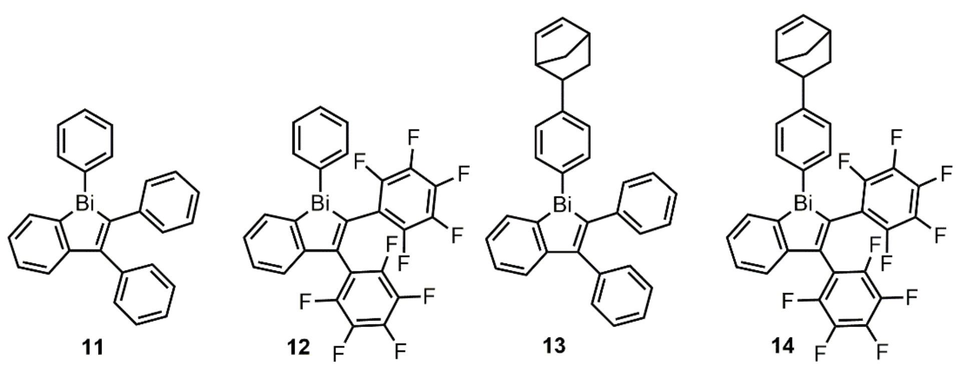

Figure 6.3. Structures of benzobismoles **11**–**14**.

Photoluminescence studies on bismole **11** and **12** indicated that the phosphorescence of these materials is very sensitive to the rigidity of the molecules in their solid-state environments. Compounds **11** and **12** were determined to exhibit crystallization induced emission, in which the quantum yield dropped dramatically when **11** and **12** were packed to give an amorphous solid.

Monomers **13** and **14** were capable of being polymerized by ring-opening metathesis polymerization with Grubbs' 2nd Generation catalyst to yield weakly phosphorescent products of high molecular weight. The solubility of these benzobismole polymers could be enhanced by incorporation of solubilizing alkylated comonomers. The use of Grubbs' 3rd Generation catalyst resulted in a pseudo-living polymerization which enabled the formation of a benzobismole-based block copolymer that readily underwent self-assembly into spherical micelles in THF/hexanes mixtures. Future work could involve studying the effect of polymer block length on micelle shape and size. Optimization of surface adsorption/aggregation of micelles followed by subsequent pyrolysis could allow for the controlled patterning of nanodimensional Bi on substrates, which would be useful as a seed layer for patterned semi-conductor nanowire growth.[4]

Chapter 4 involved the synthesis of benzobismole **15** and benzotellurophene **16**, both of which possessed *ortho*-tolyl groups in the 2- and 3- positions. This substitution pattern was used to test the hypothesis that suppressing intramolecular rotations about the exocyclic heterocycle-aryl bonds could both increase the phosphorescence quantum yields and reduce the morphology dependence of the emission intensity for these benzoheterole systems.

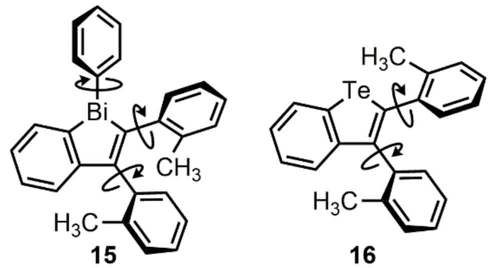

Figure 6.4. Structures of benzoheteroles **15** and **16** with exocyclic bond rotations expected to contribute to non-radiative decay.

^{1}H NMR spectroscopic analysis of **15** indicated the successful hindrance of the rotations about the exocyclic bismole-tolyl C–C bonds as evidenced by the presence of multiple rotational isomers in solution, but this restriction of rotation was not observed in **16**. Phosphorescence quantum yields of **15** and **16** were not enhanced as expected, but the solid-state packing as determined by X-ray crystallography indicated Bi···Bi distances of less than 4.7 Å, and Te···Te distances of less that 3.9 Å, respectively, suggesting that the low emission intensity observed could have resulted from substantial triplet-triplet annihilation (self quenching). These findings serve as a reminder that the largest remaining challenge in designing phosphorescent AIE emitters is predicting how a given molecule will pack in the solid state, as this has a pronounced effect on emission from AIE-based emitters.

Future work could involve implementing a synthetic strategy to force the heteroles to be spaced further apart, in addition to the presence of *ortho*-tolyl substitution. An example of a possible bismole target with a proposed pathway is shown in Scheme 6.1, in which a bismole dimer (**17**) separated by an aryl spacer is proposed.

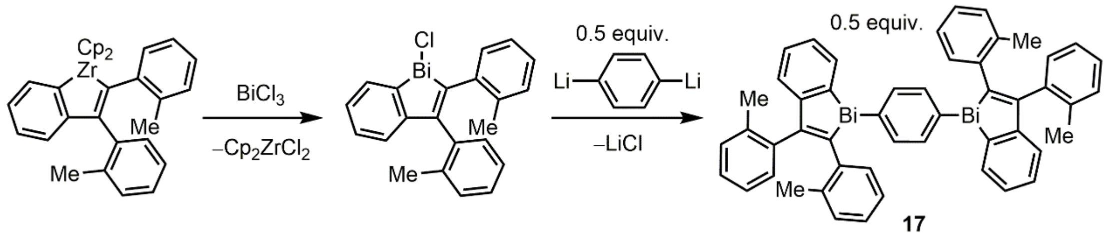

Scheme 6.1. Proposed synthetic route to the benzobismole dimer **17**.

Also in Chapter 4, a pinacolboronate-substituted bismole (**18**) was studied for its suitability as a substrate for Suzuki-Miyaura cross-coupling, however initial results suggested an inherent lack of stability of bismole Bi–C bonds towards the reaction conditions necessary to achieve cross-coupling. The resulting mesityl-containing products suggest the likely due to transmetallation of the Bi–$C_{mesityl}$ bonds of the substrate **18** with the palladium-based catalysts instead of coupling involving the BPin groups.

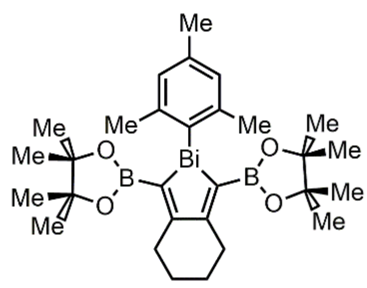

Figure 6.5. Bismole **18**, evaluated for its suitability in functionalization via Suzuki-Miyaura cross-coupling in Chapter 4.

Future studies including more thorough NMR analysis and gas chromatography-mass spectrometry analysis of the crude reaction mixtures from the attempted Suzuki-Miyaura cross-coupling attempts could shed some light on the specific products obtained and aid in describing more specifically the reactivity of **18**.

In Chapter 5, the synthesis of highly fluorescent *para*-biphenyl-substituted benzophospholes via metallacycle transfer was reported. A norbornene-appended benzophosphole, **20**, was found to readily undergo controlled ROMP with Grubbs' 3rd Generation catalyst to produce block copolymers **21** and **22** (Figure 6.6). Copolymers **21** and **22** could be made to undergo self-assembly into spherical micelles in THF/hexanes mixtures as determinted by dynamic light scattering and transmission electron microscopy. These examples represent the first benzophosphole-based polymers and their high quantum yields (30–40 %) and high solubility suggest they may show promise for use in solution processed optoelectronic devices. Most interestingly, polymerization was demonstrated as a method to enhance the emission intensity of a benzophosphole-based AIEgen in solution.

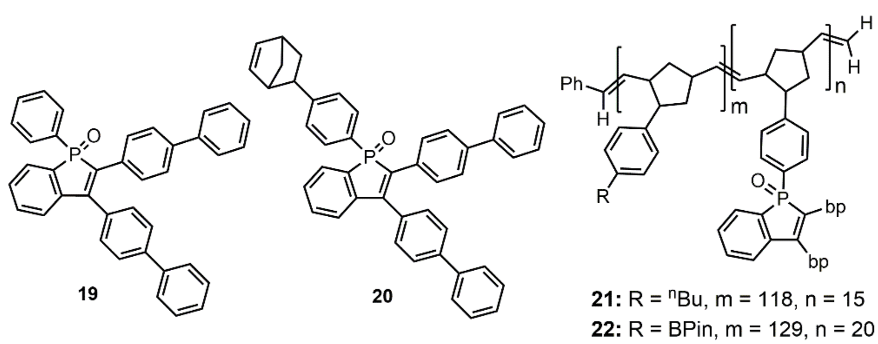

Figure 6.6. Structures of benzophospholes **19** and **20** and block copolymers (**21** and **22**) based on **20** that were reported and discussed in Chapter 5.

A search of the literature uncovers a lack of polymers based on the benzophosphole class of subunit, so additional future work could include the synthesis of benzophosphole polymers with enhanced conjugation along their backbones. Conjugated phosphafluorenes and dithienylphosphole-based materials have been well-explored and have found promising application in organic photovoltaics and organic field effect transistors. Since benzophospholes have been shown to exhibit HOMO–LUMO tunability and remarkable photostability,[5c,6] they too could be excellent materials for similar optoelectronic applications. Scheme 6.2 provides a possible synthetic pathway for the synthesis of conjugated benzophosphole-based polymers. Work in Chapter 5 has described the synthesis of benzophospholes via metallacycle transfer, and work by Matano and coworkers have displayed the feasibility of functionalizing benzophosphole oxides by Suzuki-Miyaura cross-coupling.[5b,7]

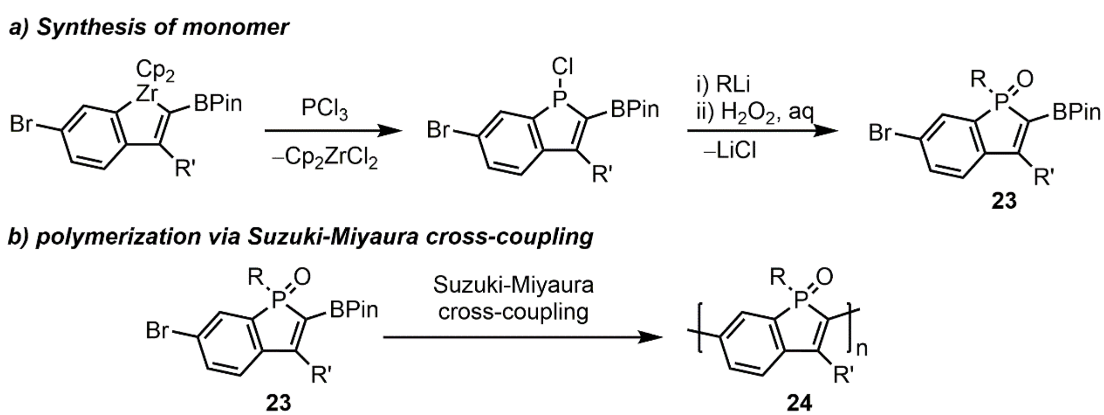

Scheme 6.2. Synthesis of conjugated benzophosphole polymers **24** via metallacycle transfer followed by subsequent Suzuki-Miyaura cross-coupling.

6.2 References

1. Torres Delgado, W.; Braun, C. A.; Boone, M. P.; Shynkaruk, O.; Qi, Y.; McDonald, R.; Ferguson, M. J.; Data, P.; Almeida, S. K. C.; de Aguiar, I.; de Souza, G. L. C.; Brown, A.; He, G.; Rivard, E. *ACS Appl. Mater. Interfaces* **2018**, *10*, 12124−12134.

2. (a) Fukazawa, A.; Ichihashi, Y.; Kosaka, Y.; Yamaguchi, S. *Chem. Asian J*. **2009**, *4*, 1729–1740. (b) Hibner-Kulicka, P.; Joule, J. A.; Skalik, J.; Bałczewski, P. *RSC Adv*. **2017**, *7*, 9194–9236.

3. (a) Ding, F.; Fan, Y.; Sun, Y.; Zhang, F. *Adv. Healthcare Mater*. **2019**, DOI: 10.1002/adhm.201900260 (b) Wu, D.; Chen, L.; Lee, W.; Ko, G.; Yin, J.; Yoon, J. *Coord. Chem. Rev*. **2018**, *354*, 74–97. (c) Zhao, Q.; Sun, J. Z. *J. Mater. Chem. C* **2016**, *4*, 10588–10609.

4. (a) Dong, A.; Tang, R.; Buhro, W. E. *J. Am. Chem. Soc.* **2007**, *129*, 12254−12262. (b) Jheng, S.-L.; Chen, J.-Y.; Tuan, H.-Y. *Mater. Design.* **2018**, *149*, 113−121.

5. (a) Taki, M.; Ogasawara, H.; Osaki, H.; Fukazawa, A.; Sato, Y.; Ogasawara, K.; Higashiyama, T.; Yamaguchi, S. *Chem. Commun.* **2015**, *51*, 11880–11883. (b) Wakatsuki, A.; Yukimoto, M.; Minoura, M.; Fujii, K.; Kimura, Y.; Matano, Y. *Dalton Trans*. **2018**, *47*, 7123–7127. (c) Yamaguchi, E.; Wang, C.; Fukazawa, A.; Taki, M.; Sato, Y.; Sasaki, T.; Uedo, M.; Sasaki, N.; Higashiyama, T.; Yamaguchi, S. *Angew. Chem. Int. Ed*. **2015**, *54*, 4539–4543.

6. (a) Yamaguchi, S.; Fukazawa, A.; Taki, M. *J. Synth. Org. Chem., Jpn.* **2017**, *75*, 1179–1187. (b) Wang, C.; Fukazawa, A.; Taki, M.; Sato, Y.; Higashiyama, T.; Yamaguchi, S. *Angew. Chem. Int. Ed.* **2015**, *54*, 15213 –15217

7. Matano, Y.; Motegi, Y.; Kawatsu, S.; Kimura, Y. *J. Org. Chem.* **2015**, *80*, 5944−5950.

Complete Bibliography

Chapter 1

1. Baldo, M. A.; O'Brien, D. F.; You. Y.; Shoustikov, A.; Sibley, S.; Thompson, M. E.; Forrest, S. R. *Nature* **1998**, *395*, 151–154.

2. (a) Alonso-de Castro, S.; Baggaley, E.; Baraldo, L. M.; Che, C.-M.; Etchenique, R.; Filevich, O.; Ford, P. C.; Habtemariam, A.; Huang, W.; Hung, F.-F.; Li, F.; Liu, S.; Muizzi, D. A.; Ostrowski, A. D.; Pierri, A. E.; Ruggiero, E.; Salassa, L.; Weinstein, J. A.; Williams, J. A. G.; Yam, V. W.-W.; Yang, C.; Yeung, M. C.-L.; Zayat, L.; Zhang, K. Y.; Zhao, Q.; Zou, T. *Luminescent and Photoactive Transition Metal Complexes as Biomolecular Probes and Cellular Reagents* (Ed: Lo, K. K.-W.), Springer-Verlag GmbH Heidelberg, 2015. (b) Zhao, Q.; Sun, J. Z. *J. Mater. Chem. C* **2016**, *4*, 10588–10609. (c) Lv, W.; Yang, T.; Yu, Q.; Zhao, Q.; Zhang, K. Y.; Liang, H.; Liu, S.; Li, F.; Huang, W. *Adv. Sci.* **2015**, *2*, 1500107. (d) Zhao, Q.; Huang, C.; Li, F. *Chem. Soc. Rev*. **2011**, *40*, 2508–2524.

3. Tabachnyk, M.; Ehrler, B.; Gélinas, S.; Böhm, M. L.; Walker, B. J.; Musselman, K. P.; Greenham, N. C.; Friend R. H.; Rao, A. *Nat. Mater*. **2014**, *13*, 1033–1038.

4. Rivard, E. *Chem. Lett.* **2015**, *44*, 730–736.

5. You, Y. *Curr. Opin. Chem. Biol*. **2013**, *17*, 699–707.

6. (a) Filatov, M. A.; Baluschev, S.; Landfester, K. *Chem. Soc. Rev*. **2016**, *45*, 4668–4689. (b) Papkovsky, D. B.; Zhdanov, A. V. *Free Radical Biol. Med*. **2016**, *101*, 202–210. (c) Baldo, M. A.; Adachi, C.; Forrest, S. R. *Phys. Rev. B* **2000**, *62*, 10967–10977.

7. Baba, M. *J. Phys. Chem. A* **2011**, *115*, 9514–9519.

8. Gwaiz, A. A.; El-Sayed, M. A. *Chem. Phys. Lett*. **1973**, *19*, 11–15.

9. (a) Yamauchi, S.; Pratt, D. W. *Mol. Phys.* **1979**, *37*, 541–569. (b) Yuan, W. Z.; Shen, X. Y.; Zhao, H.; Lam, J. W. Y.; Tang, L.; Lu, P.; Wang, C.; Liu, Y.; Wang, Z.; Zheng, Q.; Sun, J. Z.; Ma, Y.; Tang, B. Z. *J. Phys. Chem. C* **2010**, *114*, 6090–6099.

10. Kuno, S.; Akeno, H.; Ohtani, H.; Yuasa, H. *Phys. Chem. Chem. Phys.* **2015**, *17*, 15989–15995.

11. Chen, B.; Sun, X.; Evans, R. E.; Zhou, R.; Demas, J. N.; Trindle, C. O.; Zhang, G. *J. Phys. Chem. A* **2015**, *119*, 8854–8859.

12. Wang, T.; Wu, Z.; Sun, W.; Jin, S.; Zhang, X.; Zhou, C.; Jiang, J.; Luo, Y.; Zhang, G. *J. Phys. Chem. A* **2017**, *121*, 7183–7190.

13. Xiong, Y.; Zhao, Z.; Zhao, W.; Ma, H.; Peng, Q.; He, Z.; Zhang, X.; Chen, Y.; He, X.; Lam, J. W. Y.; Tang, B. Z. *Angew. Chem. Int. Ed*. **2018**, *57*, 7997–8001.

14. (a) Ma, D.; Tsuboi, T.; Qiu, Y.; Duan, L. *Adv. Mater*. **2017**, *29*, 1603253. (b) Ma, D.-L.; Lin, S.; Wang, W.; Yang, C.; Leung, C.-H. *Chem. Sci*. **2017**, *8*, 878–889.

15. (a) Fleetham, T.; Li, G.; Li, J. *Adv. Mater*. **2017**, *29*, 1601861. (b) Li, K.; Tong, G. S. M.; Wan, Q.; Cheng, G.; Tong, W.-Y.; Ang, W.-H.; Kwong, W.-L.; Che, C.-M. *Chem. Sci*. **2016**, *7*, 1653–1673.

16. Chi, Y.; Chou, P.-T. *Chem. Soc. Rev*. **2007**, *36*, 1421–1431.

17. Gray, V.; Moth-Poulsen, K.; Albinsson, B.; Abrahamsson, M. *Coord. Chem. Rev*. **2018**, *362*, 54–71.

18. Xu, X.; Yang, X.; Zhao, J.; Zhou, G.; Wong, W.-Y. *Asian J. Org. Chem.* **2015**, *4*, 394–429.

19. Papkovsky, D. B.; Dmitriev R. I. *Chem. Soc. Rev*. **2013**, *42*, 8700–8732.

20. Pander, P.; Swist, A.; Turczyn, R.; Pouget, S.; Djurado, D.; Lazauskas, A.; Pashazadeh, R.; Grazulevicius, J. V.; Motyka, R.; Klimash, A.; Skabara, P. J.; Data, P.; Soloducho, J.; Dias, F. B. *J. Phys. Chem. C* **2018**, *122*, 24958–24966.

21. Yuan, W. Z.; Shen, X. Y.; Zhao, H.; Lam, J. W. Y.; Tang, L.; Lu, P.; Wang, C.; Liu, Y.; Wang, Z.; Zheng, Q.; Sun, J. Z.; Ma, Y.; Tang, B. Z. *J. Phys. Chem. C* **2010**, *114*, 6090–6099.

22. Gong, Y.; Chen, G.; Peng, Q.; Yuan, W. Z.; Xie, Y.; Li, S.; Zhang, Y.; Tang, B. Z. *Adv. Mater.* **2015**, *27*, 6195–6201.

23. Straub, L.; González-Abradelo, D.; Strassert, C. A. *Chem. Commun.* **2017**, *53*, 11806–11809.

24. Easley, C. J.; Mettry, M.; Moses, E. M.; Hooley, R. J.; Bardeen, C. J. *J. Phys. Chem. A* **2018**, *122*, 6578−6584.

25. (a) Xiang, H.; Cheng, J.; Ma, X.; Zhou, X.; Chruma, J. J. *Chem. Soc. Rev*. **2013**, *42*, 6128–6185. (b) Yoshihara, T.; Hirakawa, Y.; Hosaka, M.; Nangaki, M.; Tobita, S. *J. Photochem. Photobiol. C* **2017**, *30*, 71–95. (c) Hussain, F.; Wang, X.; Wang, S. *J. Organomet. Chem.* **2019**, *880*, 300–311.

26. Ding, J.; Wang, B.; Yue, Z.; Yao, B.; Xie, Z.; Cheng, Y.; Wang, L.; Jing, X.; Wang, F. *Angew. Chem. Int. Ed.* **2009**, *48*, 6664–6666.

27. (a) Stokes, G. G. *Philos. Trans. R. Soc. London* **1853**, *143*, 386–396. (b) Levy, L. A. *J. Chem. Soc. Trans.* **1908**, *93*, 1446–1463. (c) Kaufmann, H. *Ber. Dtsch. Chem. Ges.* **1917**, *50*, 1614–1623. (d) Kuhn, A. *Kolloid-Z.* **1942**, *100*, 126–135.

28. Luo, J.; Xie, Z.; Lam, J. W. Y.; Cheng, L.; Chen, H.; Qiu, C.; Kwok, H. S.; Zhan, X.; Liu, Y.; Zhu, D. Tang, B. Z. *Chem. Commun.* **2001**, 1740–1741.

29. (a) Hong, Y.; Lam, J. W. Y.; Tang, B. Z. *Chem. Commun.* **2009**, 4332–4353. (b) Mei, J.; Hong, Y.; Lam, J. W. Y.; Qin, A.; Tang, Y.; Tang, B. Z. *Adv. Mater.* **2014**, *26*, 5429–5479.

30. Tang, B. Z.; Zhan, X.; Yu, G.; Lee, P. P. S.; Liu, Y.; Zhu, D. *J. Mater. Chem.* **2001**, *11*, 2974–2978.

31. (a) Mei, J.; Leung, N. L. C.; Kwok, R. T. K.; Lam, J. W. Y.; Tang, B. Z. *Chem. Rev.* **2015**, *115*, 11718–11940. (b) Hong, Y.; Lam, J. W. Y.; Tang, B. Z. *Chem. Soc. Rev.* **2011**, *40*, 5361–5388.

32. Nishiuchi, T.; Tanaka, K.; Kuwatani, Y.; Sung, J.; Nishinaga, T.; Kim, D.; Iyoda, M. *Chem. Eur. J.* **2013**, *19*, 4110–4116.

33. Chen, J.; Law, C. C. W.; Lam, J. W. Y.; Dong, Y.; Lo, S. M. F.; Williams, I. D.; Zhu, D.; Tang, B. Z. *Chem. Mater*. **2003**, *15*, 1535−1546.

34. (a) Lu, H.; Zheng, Y.; Zhao, X.; Wang, L.; Ma, S.; Han, X.; Xu, B.; Tian, W.; Gao, H. *Angew. Chem. Int. Ed*. **2016**, *55*, 155–159. (b) Shao, A.; Guo, Z.; Zhu, S.; Zhu, S.; Shi, P.; Tian, H.; Zhu, W. *Chem. Sci*. **2014**, *5*, 1383–1389.

35. (a) Wang, J.; Mei, J.; Yuan, W.; Lu, P.; Qin, A.; Sun, J.; Ma, Y.; Tang, B. Z. *J. Mater. Chem.* **2011**, *21*, 4056–4059. (b) Hou, X.-G.; Wu, Y.; Cao, H.-T.; Sun, H.-Z.; Li, H.-B.; Shan, G.-G.; Su, Z.-M. *Chem. Commun.* **2014**, *50*, 6031–6034.

36. (a) Malik, A. H.; Kalita, A.; Iyer, P. K. *ACS Appl. Mater. Interfaces* **2017**, *9*, 37501–37508. (b) Singh, P.; Singh, H.; Sharma, R.; Bhargava, G.; Kumar, S. *J. Mater. Chem. C* **2016**, *4*, 11180–11189.

37. Yang, J.; Huang, J.; Li, Q.; Li, Z. *J. Mater. Chem. C* **2016**, *4*, 2663–2684.

38. (a) Mei, J.; Hong, Y.; Lam, J. W. Y.; Qin, A.; Tang, Y. Tang, B. Z. *Adv. Mat.* **2014**, *26*, 5429–5479. (b) Zhao, Z.; He, B.; Tang, B. Z. *Chem. Sci.* **2015**, *6*, 5347–5365. (c) Wang, M.; Zhang, G.; Zhang, D.; Zhu, D.; Tang, B. Z. *J. Mater. Chem.* **2010**, *20*, 1858–1867. (d) Li, B.; He, T.; Shen, X.; Tang, D.; Yin, S. *Polym. Chem.* **2019**, *10*, 796–818.

39. (a) Baroncini, M.; Bergamini, G.; Ceroni, P. *Chem. Commun.* **2017**, *53*, 2081–2093. (b) Ubba, E.; Tao, Y.; Yang, Z.; Zhao, J.; Wang, L.; Chi, Z. *Chem. Asian. J.* **2018**, *13*, 3106–3121. (c) Zhang, Y.; Mao, H.; Xu, W.; Shi, J.; Cai, Z.; Tong, B.; Dong. Y. *Chem. Eur. J.* **2018**, *24*, 15965–15977.

40. (a) Ravotto, L.; Ceroni, P. *Coord. Chem. Rev.* **2017**, *346*, 62–76. (b) Mauro, M.; Cebrián, C. *Isr. J. Chem.* **2018**, *58*, 901–914.

41. Strasser, A.; Vogler, A. *Inorg. Chem. Commun.* **2004**, *7*, 528–530.

42. Strasser, A.; Vogler, A. *J. Photochem. Photobiol. A* **2004**, *165*, 115–118.

43. (a) Sano, Y.; Satoh, H.; Chiba, M.; Okamoto, M.; Serizawa, K.; Nakashima, H.; Omae, K. *J. Occup. Health* **2005**, *47*, 293–298. (b) Yang, N.; Sun, H. *Coord. Chem. Rev.* **2007**, *251*, 2354–2366.

44. (a) Ohshita, J.; Matsui, S.; Yamamoto, R.; Mizumo, T.; Ooyama, Y.; Harima, Y.; Murafuji, T.; Tao, K.; Kuramochi, Y.; Kaikoh, T.; Higashimura, H. *Organometallics* **2010**, *29*, 3239–3241. (b) Parke, S. M.; Narreto, M. A. B.; Hupf,

E.; McDonald, R.; Ferguson, M. J.; Hegmann, F. A.; Rivard, E. *Inorg. Chem*. **2018**, *57*, 7536–7549.

45. Toma, O.; Mercier, N.; Botta, C. *Eur. J. Inorg. Chem.* **2013**, 1113–1117.

46. Toma, O.; Mercier, N.; Allain, M.; Botta, C. *CrystEngComm.* **2013**, *15*, 8565–8571.

47. Toma, O.; Mercier, N.; Allain, M.; Forni, A.; Meinardi, F.; Botta, C. *Dalton Trans.* **2015**, *44*, 14589–14593.

48. Toma, O.; Allain, M.; Meinardi, F.; Forni, A.; Botta, C.; Mercier, N. *Angew. Chem. Int. Ed*. **2016**, *55*, 7998–8002.

49. Toma, O.; Mercier, N.; Allain, M.; Meinardi, F.; Botta, C. *Eur. J. Inorg. Chem*. **2017**, 844–850.

50. Wang, Z.-P.; Wang, J.-Y.; Li, J.-R.; Feng, M.-L.; Zou, G.-D.; Huang, X.-Y. *Chem. Commun*. **2015**, *51*, 3094–3097.

51. Shen, N.; Li, J.; Wu, Z.; Hu, B.; Cheng, C.; Wang, Z.; Gong, L.; Huang, X. *Chem. Eur. J.* **2017**, *23*, 15795–15804.

52. (a) He, G.; Kang, L.; Torres Delgado, W.; Shynkaruk, O.; Ferguson, M. J.; McDonald, R.; Rivard, E. *J. Am. Chem. Soc.* **2013**, *135*, 5360–5363. (b) For a review of this concept, see: Carrera, E. I.; Seferos, D. S. *Macromolecules* **2015**, *48*, 297–308.

53. He, G.; Torres Delgado, W.; Schatz, D. J.; Merten, C.; Mohammadpour, A.; Mayr, L.; Ferguson, M. J.; McDonald, R.; Brown, A.; Shankar, K.; Rivard, E. *Angew. Chem. Int. Ed*. **2014**, *53*, 4587–4591.

54. Braun, C. A.; Zomerman, D.; de Aguiar, I.; Qi, Y.; Torres Delgado, W.; Ferguson, M. J.; McDonald, R.; de Souza, G. L. C.; He, G.; Brown, A.; Rivard, E. *Faraday Discuss*. **2017**, *196*, 255–268.

55. Mohammadpour, A.; Wiltshire, B. D.; Farsinezhad, S.; Zhang, Y.; Askar, A. M.; Kisslinger, R.; Delgado, W. T.; He, G.; Kar, P.; Rivard, E.; Shankar, K. *Org. Electron.* **2016**, *39*, 153–162.

56. Torres Delgado, W.; Braun, C. A.; Boone, M. P.; Shynkaruk, O.; Qi, Y.; McDonald, R.; Ferguson, M. J.; Data, P.; Almeida, S. K. C.; de Aguiar, I.; de Souza, G. L. C.; Brown, A.; He, G.; Rivard, E. *ACS Appl. Mater. Interfaces* **2018**, *10*, 12124–12134.

57. Kremer, A.; Aurisicchio, C.; De Leo, F.; Ventura, B.; Wouters, J.; Armaroli, N.; Barbieri, A.; Bonifazi, D. *Chem. Eur. J.* **2015**, *21*, 15377–15387.

58. Kremer, A.; Fermi, A.; Biot, N.; Wouters, J.; Bonifazi, D. *Chem. Eur. J*. **2016**, *22*, 5665–5675.

59. Kuno, S.; Kanamori, T.; Yijing, Z.; Ohtani, H.; Yuasa, H. *ChemPhotoChem*. **2017**, *1*, 102–106.

60. Shoji, Y.; Ikabata, Y.; Wang, Q.; Nemoto, D.; Sakamoto, A.; Tanaka, N.; Seino, J.; Nakai, H.; Fukushima, T. *J. Am. Chem. Soc.* **2017**, *139*, 2728–2733.

61. (a) Riebe, S.; Vallet, C.; van der Vight, F.; Gonzalez-Abradelo, D.; Wölper, C.; Strassert, C. A.; Jansen, G.; Knauer, S.; Voskuhl, J. *Chem Eur. J.* **2017**, *23*, 13660–13668. For important prior work in this field, see: (b) Bergamini, G.; Fermi, A.; Botta, C.; Giovanella, U.; Di Motta, S.; Negri, F.; Peresutti, R.; Gingras, M.; Ceroni, P. *J. Mater. Chem. C* **2013**, *1*, 2717–2724. (c) Fermi, A.;

Bergamini, G.; Peresutti, R.; Marchi, E.; Roy, M.; Ceroni, P.; Gingras, M. *Dyes Pigm.* **2014**, *110*, 113–122.

62. Xue, P.; Wang, P.; Chen, P.; Ding, J.; Lu, R. *RSC Adv.* **2016**, *6*, 51683–51686.

63. Braye, E. H.; Hübel, W.; Caplier, I. *J. Am. Chem. Soc*. **1961**, *83*, 4406–4413.

64. Alt, H.; Rausch, M. D. *J. Am. Chem. Soc.* **1974**, *96*, 5936–5937.

65. (a) Negishi, E.-I.; Takahashi, T. *Acc. Chem. Res.* **1994**, *27*, 124–130. (b) Negishi, E.-I.; Takahashi, T. *Bull. Chem. Soc. Jpn.* **1998**, *71*, 755–769.

66. Negishi, E.; Cederbaum, F. E.; Takahashi, T. *Tetrahedron Lett.* **1986**, *27*, 2829–2832.

67. (a) Rosenthal, U.; Ohff, A.; Baumann, W.; Tillack, A.; Görls, H.; Burlakov, V. V.; Shur, V. B. *Z. Anorg. Allg. Chem.* **1995**, *621*, 77–83. (b) Rosenthal, U.; Ohff, A.; Michkalik, M; Görls, H.; Burlakov, V. V.; Shur, V. B. *Angew. Chem. Int. Ed. Engl.* **1993**, *32*, 1193–1195.

68. Dioumaev, V. K.; Harrod, J. F. *Organometallics*, **1997**, *16*, 1452–1464.

69. (a) Johnson, S. A.; Liu, F.-Q.; Suh, M. C.; Zürcher, S.; Haufe, M.; Mao, S. S. H.; Tilley, T. D. *J. Am. Chem. Soc.* **2003**, *125*, 4199–4211. (b) Gessner, V. H.; Tannaci, J. F.; Miller, A. D.; Tilley, T. D. *Acc. Chem. Res.* **2011**, *44*, 435–446.

70. (a) Hara, R.; Xi, Z.; Kotora, M.; Xi, C.; Takahashi, T. *Org. Lett.* **1996**, *25*, 1003–1004. (b) Miller, A. D.; Johnson, S. A.; Tupper, K. A.; McBee, J. L.; Tilley, T. D. *Organometallics* **2009**, *28*, 1252–1262.

71. Miller, A. D.; Tannaci, J. F.; Johnson, S. A.; Lee, H.; McBee, J. L.; Tilley, T. D. *J. Am. Chem. Soc.* **2009**, *131*, 4917–4927.

72. Buchwald, S. L.; Watson, B. T. *J. Am. Chem. Soc.* **1986**, *108*, 7411–7413.

73. Fagan, P. J.; Nugent, W. A. *J. Am. Chem. Soc*. **1988**, *110*, 2310–2312.

74. Fagan, P. J.; Nugent, W. A.; Calabrese, J. C. *J. Am. Chem. Soc*. **1994**, *116*, 1880–1889.

75. Takahashi, T.; Kotora, M.; Kasai, K.; Suzuki, N. *Organometallics* **1994**, *13*, 4183–4185.

76. (a) Zhang, Z.; Wang, Z.; Haehnel, M.; Eichhorn, A.; Edkins, R. M.; Steffen, A.; Krueger, A.; Lin, Z.; Marder, T. B. *Chem. Commun*. **2016**, *52*, 9707–9710. (b) Houghton, A. Y.; Karttunen, V. A.; Piers, W. E.; Tuononen, H. M. *Chem. Commun*. **2014**, *50*, 1295–1298. (c) Fan, C.; Piers, W. E.; Parvez, M. *Angew. Chem. Int. Ed.* **2009**, *48*, 2955–2958.

77. Liu, L.; Geng, W.; Yang, Q.; Zhang, W.-X.; Xi, Z. *Organometallics* **2015**, *34*, 4198−4201.

78. Geng, W.; Wei, J.; Zhang, W.-X.; Xi, Z. *J. Am. Chem. Soc*. **2014**, *136*, 610−613.

79. Ubayama, H.; Sun, W.-H.; Takahashi, T.; Xi, Z. *Chem. Commun.* **1998**, *18*, 1931–1932.

80. He, G.; Shynkaruk, O.; Lui M. W.; Rivard, E. *Chem. Rev.* **2014**, *114*, 7815–7880.

81. Wittig, G.; Geissler, G. *Liebigs Ann. Chem.* **1953**, *580*, 44–57.

82. Campbell, I. G. M.; Way, J. K. *Proc. Chem. Soc.* **1959**, 231–232.

83. (a) Aeschlimann, J. A.; Lees, N. D.; McCleland, N. P.; Nicklin, G. N. *J. Chem. Soc. Trans*. **1925**, *127*, 66–69. (b) Das-Gupta, H. N. *J. Indian Chem. Soc.* **1935**, *12*, 627–628. (c) Das-Gupta, H. N. *J. Indian Chem. Soc.* **1937**, *14*, 400–405.

84. Morgan, G. T.; Davies, G. R. *Proc. Royal Soc. A* **1930**, *127*, 1–8.

85. (a) Campbell, I. G. M. *J. Chem. Soc.* **1950**, 3109–3116. (b) Campbell, I. G. M. *J. Chem. Soc.* **1952**, 4448–4453. (c) Campbell, I. G. M. Morrill, D. J. *J. Chem. Soc.* **1955**, 1662–1670.

86. (a) Wittig, G.; Hellwinkel, D. *Chem. Ber.* **1964**, *97*, 789−793. (b) Hellwinkel, D.; Bach, M. *Liebigs. Ann. Chem.* **1968**, *720*, 198−200.

87. Leavitt, F. C.; Manuel, T. A.; Johnson, F. *J. Am. Chem. Soc.* **1959**, *81*, 3163–3164.

88. Braye, E. H.; Hübel, W.; Caplier, E. *J. Am. Chem. Soc.* **1961**, *83*, 4406–4413.

89. (a) Davydov, S. N.; Rodionov, A. N.; Shigorin, D. N.; Syutkina, O. P.; Krasnova, T. L. *Zh. Fiz. Khim.* **1981**, *55*, 784–787. (b) Davydov, S. N.; Rodionov, A. N.; Shigorin, D. N.; Syutkina, O. P.; Krasnova, T. L. *Zh. Fiz. Khim.* **1980**, *54*, 506–508. (c) Davydov, S. N.; Rodionov, A. N.; Shigorin, D. N.; Syutkina, O. P.; Krasnova, T. L. *Zh. Fiz. Khim.* **1981**, *55*, 784–787.

90. (a) Nyulászi, L.; Hollóczki, O.; Lescop, C.; Hissler, M.; Réau, R. *Org. Biomol. Chem*. **2006**, *4*, 996–998. (b) Szucs, R.; Bouit, P.-A.; Hissler, M.; Nyulaszi, L. *Struct. Chem.* **2015**, *26*, 1351–1357. (c) Schleyer, P. v. R.; Maerker, C.; Dransfeld, A.; Jiao, H.; Hommes, N. J. R. v. E. *J. Am. Chem. Soc*. **1996**, *118*, 6317–6318.

91. Duffy, M. P.; Delaunay, W.; Bouit, P.-A.; Hissler, M. *Chem. Soc. Rev*. **2016**, *45*, 5296–5310.

92. (a) Bu, F.; Wang, E.; Peng, Q.; Hu, R.; Qin, A.; Zhao, Z.; Tang, B. Z. *Chem. Eur. J.* **2015**, *21*, 4440–4449. (b) Zhuang, Z.; Bu, F.; Luo, W.; Peng, H.; Chen, S.; Hu, R.; Qin, A.; Zhao, Z.; Tang, B. Z. *J. Mater. Chem. C* **2017**, *5*, 1836–1842.

93. Fukazawa, A.; Ichihashi, Y.; Kosaka, Y.; Yamaguchi, S. *Chem. Asian J*. **2009**, *4*, 1729–1740.

94. Hibner-Kulicka, P.; Joule, J. A.; Skalik, J.; Bałczewski, P. *RSC Adv*. **2017**, *7*, 9194–9236.

95. (a) Baumgartner, T.; Neuman, T.; Wirges, B. *Angew. Chem. Int. Ed*. **2004**, *43*, 6197–6201. (b) Baumgartner, T.; Bergmans, W.; Kárpáti, T.; Neumann, T.; Nieger, M.; Nyulászi, L. *Chem. Eur. J.* **2005**, *11*, 4687–4699. (c) Baumgartner, T.; Wilk, W. *Org. Lett*. **2006**, *8*, 503–506. (d) Dienes, Y.; Durben, S.; Kárpáti, T.; Neumann, T.; Englert, U.; Nyulászi, L.; Baumgartner, T. *Chem. Eur. J.* **2007**, *13*, 7487–7500. (e) Durben, S.; Nickel, D.; Krüger, R. A.; Sutherland, T. C.; Baumgartner, T. *J. Polym. Sci., Part A: Polym. Chem.* **2008**, *46*, 8179–8190. (f) Romero-Nieto, C.; Durben, S.; Kormos, I. M.; Baumgartner, T. *Adv. Funct. Mater.* **2009**, *19*, 3625–3631. (g) Krüger, R. A.; Gordon, T. J.; Sutherland, T. C.; Baumgartner, T. *J. Polym. Sci., Part A: Polym. Chem.* **2011**, *49*, 1201–1209. (h) Ren, Y.; Baumgartner, T. *Dalton Trans*. **2012**, *41*, 7792–7800.

96. Takahashi, M.; Nakano, K.; Nozaki, K. *J. Org. Chem.* **2015**, *80*, 3790–3797.

97. Rausch, M. D.; Klemann, L. P. *J. Am. Chem. Soc.* **1967**, *89*, 5732–5733.

98. (a) Chan, T. H.; Wong, L. T. L. *Can. J. Chem.* **1971**, *49*, 530–531. (b) Collins, D. J.; Rowley, L. E.; Swan, J. M. *Aust. J. Chem.* **1974**, *27*, 831–839. (c) Holah, D. G. H.; Alan, N. H.; Daniel, K. *J. Heterocycl. Chem.* **1977**, *14*, 705–707. (d) Balthazor, T. M. *J. Org. Chem*. **1980**, *45*, 2519–2522. (e) Nief, F.; Charrier, C.; Mathey, F.; Simalty, M. *Phosphorus Sulfur Silicon Relat. Elem.* **1982**, *13*, 259–267. (f) Quin, L. D.; Rao, N. S.; Topping, R. J.; McPhail, A. T. *J. Am. Chem. Soc*. **1986**, *108*,

4519–4526. (g) Decken, A.; Bottomley, F.; Wilkins, B. E.; Gill, E. D. *Organometallics* **2004**, *23*, 3683–3693. (h) Wu, B.; Yoshikai, N. *Org. Biomol. Chem.* **2016**, *14*, 5402–5416. (i) Chen, Y.-R.; Duan, W.-L. *J. Am. Chem. Soc*. **2013**, *135*, 16754–16757. (j) Liu, L.; Dong, J.; Yan, Y.; Yin, S.-F.; Han, L.-B.; Zhou, Y. *Chem. Commun*. **2019**, *55*, 233–236.

99. Tsuji, H.; Sato, K.; Ilies, L.; Itoh, Y.; Sato, Y.; Nakamura, E. *Org. Lett.* **2008**, *10*, 2263–2265.

100. Sanji, T.; Shiraishi, K.; Kashiwabara, T.; Tanaka, M. *Org. Lett.* **2008**, *10*, 2689–2692.

101. Fukazawa, A.; Hara, M.; Okamoto, T.; Son, E.-C.; Xu, C.; Tamao, K.; Yamaguchi, S. *Org. Lett*. **2008**, *10*, *5*, 913–916.

102. Yamaguchi, E.; Wang, C.; Fukazawa, A.; Taki, M.; Sato, Y.; Sasaki, T.; Ueda, M.; Sasaki, N.; Higashiyama, T.; Yamaguchi, S. *Angew. Chem. Int. Ed*. **2015**, *54*, 4539–4543.

103. Taki, M.; Ogasawara, H.; Osaki, H.; Fukazawa, A.; Sato, Y.; Ogasawara, K.; Higashiyama, T.; Yamaguchi, S. *Chem. Commun.* **2015**, *51*, 11880–11883.

104. Wang, C.; Taki, M.; Sato, Y.; Fukazawa, A.; Higashiyama, T.; Yamaguchi, S. *J. Am. Chem. Soc*. **2017**, *139*, 10374−10381.

105. Hayashi, Y.; Matano, Y.; Suda, K.; Kimura, Y.; Nakao, Y.; Imahori, H. *Chem. Eur. J.* **2012**, *18*, 15972–15983.

106. Matano, Y.; Hayashi, Y.; Suda, K.; Kimura, Y.; Imahori, H. *Org. Lett*. **2013**, *15*, 4458–4461.

107. Matano, Y.; Motegi, Y.; Kawatsu, S.; Kimura, Y. *J. Org. Chem.* **2015**, *80*, 5944−5950.

108. Koyanagi, Y.; Kawaguchi, S.; Fujii, K.; Kimura, Y.; Sasamori, T.; Tokitoh, N.; Matano, Y. *Dalton Trans*. **2017**, *46*, 9517–9527.

109. Wakatsuki, A.; Yukimoto, M.; Minoura, M.; Fujii, K.; Kimura, Y.; Matano, Y. *Dalton Trans*. **2018**, *47*, 7123–7127.

110. Wu, B.; Santra, M.; Yoshikai, N. *Angew. Chem. Int. Ed*. **2014**, *53*, 7543–7546.

111. Yoshikai, N.; Santra, M.; Wu, B. *Organometallics* **2017**, *36*, 2637−2645.

112. Ichikawa, T.; Morimoto, M.; Sotome, H.; Ito, S.; Miyasaka, H.; Irie, M. *Dyes Pigm*. **2016**, *126*, 186–193.

113. Kato, T.; Tanaka, S.; Naka, K. *Chem. Lett*. **2015**, *44*, 1476–1478.

114. Imoto, H.; Naka, K. *Chem. Eur. J.* **2019**, *25*, 1883–1894.

115. Raciszewski, Z.; Braye, E. H. *Photochem. Photobiol.* **1970**, *12*, 429–432.

116. Ishidoshiro, M.; Matsumura, Y.; Imoto, H.; Irie, Y.; Kato, T.; Watase, S.; Matsukawa, K.; Inagi, S.; Tomita, I.; Naka, K. *Org. Lett.* **2015**, *17*, 4854−4857.

117. Ishidoshiro, M.; Imoto, H.; Tanaka, S.; Naka, K. *Dalton Trans*. **2016**, *45*, 8717–8723.

118. Green, J. P.; Han, Y.; Kilmurray, R.; McLachlan, M. A.; Anthopoulos, T. D.; Heeney, M. *Angew. Chem. Int. Ed.* **2016**, *55*, 7148–7151.

119. Kato, T.; Imoto, H.; Tanaka, S.; Ishidoshiro, M.; Naka, K. *Dalton Trans*. **2016**, *45*, 11338–11345.

120. Imoto, H.; Kawashima, I.; Yamazawa, C.; Tanaka, S.; Naka, K. *J. Mater. Chem. C* **2017**, *5*, 6697–6703.

121. Matsumura, Y.; Ishidoshiro, M.; Irie, Y.; Imoto, H.; Naka, K.; Tanaka, K.; Inagi, S.; Tomita, I. *Angew. Chem. Int. Ed*. **2016**, *55*, 15040–15043.

122. Imoto, H.; Urushizaki, A.; Kawashima, I.; Naka, K. *Chem. Eur. J.* **2018**, *24*, 8797–8803.

123. Green, J. P.; Cryer, S. J.; Marafie, J.; White, A. J. P.; Heeney, M. *Organometallics* **2017**, *36*, 2632−2636.

124. Fell, V. H. K.; Mikosch, A.; Steppert, A.-K.; Ogieglo, W.; Senol, E.; Canneson, D.; Bayer, M.; Schoenebeck, F.; Greilich, A.; Kuehne, A. J. C. *Macromolecules* **2017**, *50*, 2338−2343.

125. Hirai, M.; Gabbaï, F. P. *Chem. Sci.* **2014**, *5*, 1886–1893.

126. Christianson, A. M.; Rivard, E.; Gabbaï, F. P. *Organometallics* **2017**, *36*, 2670−2676.

127. Christianson, A. M.; Gabbaï, F. P. *Organometallics* **2017**, *36*, 3013−3015.

128. Ohshita, J.; Fujita, R.; Tanaka, D.; Ooyama, Y.; Kobayashi, N.; Higashimura, H.; Yamamoto, Y. *Chem. Lett*. **2012**, *41*, 1002–1003.

129. Ohshita, J.; Yamaji, K.; Ooyama, Y.; Adachi, Y.; Nakamura, M.; Watase, S. *Organometallics* **2019**, *38*, 1516–1523.

130. Takahashi, T.; Li, Y.; Ito, T.; Xu, F.; Nakajima, K.; Liu, Y. *J. Am. Chem. Soc.* **2002**, *124*, 1144–1145.

131. Finet, J.-P.; Fedorov, A. Y. *Russ. Chem. Bull. Int. Ed.* **2004**, *53*, 1488–1495.

132. Imachi, S.; Mukaiyama, T. *Chem. Lett.* **2007**, *36*, 718–719.

133. Morisaki, Y.; Ohashi, K.; Na, H.-S.; Chujo, Y. *J. Polym. Sci., Part A: Polym. Chem.* **2006**, *44*, 4857−4863.

134. Ohshita, J.; Matsui, S.; Yamamoto, R.; Mizumo, T.; Ooyama, Y.; Harima, Y.; Murafuji, T.; Tao, K.; Kuramochi, Y.; Kaikoh, T.; Higashimura, H. *Organometallics* **2010**, *29*, 3239−3241.

135. Ohshita, J. *Macromol. Chem. Phys*. **2009**, *210*, 1360–1370.

Chapter 2

1. Parke, S. P.; Boone, M. P.; Rivard, E. *Chem. Commun.* **2016**, *52*, 9485−9505.

2. (a) Osaka, I.; McCullough, R. D. *Acc. Chem. Res.* **2008**, *41*, 1202–1214. (b) McCullough, R. D. *Adv. Mater*. **1998**, *10*, 93–116. (c) Roncali, J. *Chem. Rev*. **1992**, *92*, 711–738.

3. (a) Berggren, M.; Inganas, O.; Gustafsson, G.; Rasmusson, J.; Andersson, M. R.; Hjertberg, T.; Wennerstrom, O. *Nature* **1994**, *372*, 444–446. (b) Perepichka, I. F.; Perepichka, D. F.; Meng, H. Thiophene-based Materials for Electroluminescent Applications. In *Electroactive Oligothiophenes and Polythiophenes for Organic Field Effect Transistors*; Perepichka, I. F.; Perepichka, D. F., Ed.; Wiley: Chichester, UK, 2009; 647–672.

4. (a) Zhang, F.; Wu, D.; Xu, Y.; Geng, X. *J. Mater. Chem.* **2011**, *21*, 17590–17600. (b) Chen, J.; Cao, Y. *Acc. Chem. Res*. **2009**, *42*, 1709–1718.

5. (a) Nielsen, C. B.; McCulloch, I. *Prog. Polym. Sci*. **2013**, *38*, 2053–2069. (b) McCulloch, I.; Heeney, M. Thienothiophene Copolymers in Field Effect Transistors. In *Electroactive Oligothiophenes and Polythiophenes for Organic Field Effect Transistors*; Perepichka, I. F.; Perepichka, D. F., Ed.; Wiley: Chichester, UK, 2009; 647–672.

6. (a) Krzeszewski, M.; Gryko, D.; Gryko, D. T. *Acc. Chem. Res.* **2017**, *50*, 2334−2345. (b) Pron, A.; Berrouard, P.; Leclerc, M. *Macromol. Chem. Phys.* **2013**, *214*, 7−16.

7. (a) Baumgartner, T. *Acc. Chem. Res.* **2014**, *47*, 1613−1622. (b) Baumgartner, T.; Réau, R. *Chem. Rev.* **2006**, *106*, 4681−4727.

8. (a) Ishidoshiro, M.; Matsumura, Y.; Imoto, H.; Irie, Y.; Kato, T.; Watase, S.; Matsukawa, K.; Inagi, S.; Tomita, I.; Naka, K. *Org. Lett.* **2015**, *17*, 4854−4857. (b) Matsumura, M.; Muranaka, A.; Kurihara, R.; Kanai, M.; Yoshida, K.; Kakusawa, N.; Hashizume, D.; Uchiyama, M.; Yasuike, S. *Tetrahedron* **2016**, *72*, 8085−8090. (c) Kato, T.; Imoto, H.; Tanaka, S.; Ishidoshiro, M.; Naka, K. *Dalton Trans.* **2016**, *45*, 11338−11345. (d) Ishidoshiro, M.; Imoto, H.; Tanaka, S.; Naka, K. *Dalton Trans.* **2016**, *45*, 8717−8723. (e) Matsumura, Y.; Ishidoshiro, M.; Irie, Y.; Imoto, H.; Naka, K.; Tanaka, K.; Inagi, S.; Tomita, I. *Angew. Chem. Int. Ed*. **2016**, *55*, 15040−15043. (f) Green, J. P.; Han, Y.; Kilmurray, R.; McLachlan, M. A.; Anthopoulos, T. D.; Heeney, M. *Angew. Chem., Int. Ed.* **2016**, *55*, 7148−7151. (g) Green, J. P.; Cryer, S. J.; Marafie, J.; White, A. J. P.; Heeney, M. *Organometallics* **2017**, *36*, 2632−2636. (h) Fell, V. H. K.; Mikosch, A.; Steppert, A.-K.; Ogieglo, W.; Senol, E.; Canneson, D.; Bayer, M.; Schoenebeck, F.; Greilich, A.; Kuehne, A. J. C. *Macromolecules* **2017**, *50*, 2338−2343. (i) Imoto, H.; Sasaki, H.; Tanaka, S.; Yumura, T.; Naka, K. *Organometallics* **2017**, *36*, 2605−2611.

9. (a) Ohshita, J.; Fujita, R.; Tanaka, D.; Ooyama, Y.; Kobayashi, N.; Higashimura, H.; Yamamoto, Y. *Chem. Lett.* **2012**, *41*, 1002–1003. (b) Christianson, A. M.;

Rivard, E.; Gabbaï, F. P. *Organometallics* **2017**, *36*, 2670−2676. (c) Christianson, A. M.; Gabbaï, F. P. *Organometallics* **2017**, *36*, 3013−3015.

10. (a) Rivard, E. *Chem. Lett.* **2015**, *44*, 730−736. (b) Jia, W.-L.; Liu, Q.-D.; Wang, R.; Wang, S. *Organometallics* **2003**, *22*, 4070−4078. (c) Vogler, A.; Paukner, A. *Inorg. Chim. Acta* **1989**, *163*, 207−211. (d) Taneda, M.; Maeda, D.; Shimakoshi, H.; Abe, M.; Hisaeda, Y. *Bull. Chem. Soc. Jpn.* **2010**, *83*, 667−671. (e) Matsumoto, T.; Tanaka, K.; Tanaka, K.; Chujo, Y. *Dalton Trans.* **2015**, *44*, 8697−8707. (f) Liu, X.; Zhai, L.; Zhang, W.-W.; Zuo, J.-L.; Yang, Z.-X.; Ren, X.-M. *Dalton Trans.* **2017**, *46*, 7953−7959. (g) Mukherjee, S.; Thilagar, P. *Chem. Commun.* **2015**, *51*, 10988−11003. (h) Ravotto, L.; Ceroni, P. *Coord. Chem. Rev.* **2017**, *346*, 62−76.
11. (a) Tuong Ly, K.; Chen-Cheng, R.-W.; Lin, H.-W.; Shiau, Y.-J.; Liu, S.-H.; Chou, P.-T.; Tsao, C.-S.; Huang, Y.-C.; Chi, Y. *Nat. Photonics* **2017**, *11*, 63−68. (b) Chi, Y.; Chou, P.-T. *Chem. Soc. Rev.* **2010**, *39*, 638−655. (c) Baldo, M. A.; Lamansky, S.; Burrows, P. E.; Thompson, M. E.; Forrest, S. R. *Appl. Phys. Lett*. **1999**, 75, 4−6.
12. (a) Manjare, S. T.; Kim, Y.; Churchill, D. G. *Acc. Chem. Res.* **2014**, *47*, 2985−2988. (b) Wang, J.; Xue, J.; Yan, Z.; Zhang, S.; Qiao, J.; Zhang, X. *Angew. Chem., Int. Ed.* **2017**, *56*, 14928−14932. (c) Zhao, Q.; Huang, C.; Li, F. *Chem. Soc. Rev.* **2011**, *40*, 2508−2524. (d) Zhao, Q.; Sun, J. Z. *J. Mater. Chem. C* **2016**, *4*, 10588−10609. (e) Guo, Z.; Shao, A.; Zhu, W.-H. *J. Mater. Chem. C* **2016**, *4*, 2640−2646.

13. (a) Sano, Y.; Satoh, H.; Chiba, M.; Okamoto, M.; Serizawa, K.; Nakashima, H.; Omae, K. *J. Occup. Health* **2005**, *47*, 293−298. (b) Yang, N.; Sun, H. *Coord. Chem. Rev.* **2007**, *251*, 2354−2366.

14. (a) Filatov, M. A.; Baluschev, S.; Landfester, K. *Chem. Soc. Rev.* **2016**, *45*, 4668−4689. (b) Papkovsky, D. B.; Zhdanov, A. V. *Free Radical Biol. Med.* **2016**, *101*, 202−210. (c) Baldo, M. A.; Adachi, C.; Forrest, S. R. *Phys. Rev. B* **2000**, *62*, 10967−10977.

15. Wittig, G.; Hellwinkel, D. *Chem. Ber.* **1964**, *97*, 789−793.

16. Hellwinkel, D.; Bach, M. *Liebigs. Ann. Chem.* **1968**, *720*, 198−200.

17. (a) Ashe, A. J., III; Kampf, J. W.; Al-Taweel, S. M. *J. Am. Chem. Soc.* **1992**, *114*, 372−374. (b) Ashe, A. J., III; Kampf, J. W.; Al-Taweel, S. M. *Organometallics* **1992**, *11*, 1491−1496. (c) Ashe, A. J., III; Al-Ahmad, S.; Pilotek, S.; Puranik, D. B.; Elschenbroich, C.; Behrendt, A. *Organometallics* **1995**, *14*, 2689−2698.

18. Morisaki, Y.; Ohashi, K.; Na, H.-S.; Chujo, Y. *J. Polym. Sci., Part A: Polym. Chem.* **2006**, *44*, 4857−4863.

19. Ohshita, J.; Matsui, S.; Yamamoto, R.; Mizumo, T.; Ooyama, Y.; Harima, Y.; Murafuji, T.; Tao, K.; Kuramochi, Y.; Kaikoh, T.; Higashimura, H. *Organometallics* **2010**, *29*, 3239−3241.

20. (a) Fagan, P. J.; Nugent, W. A. *J. Am. Chem. Soc.* **1988**, *110*, 2310−2312. (b) Yan, X.; Xi, C. *Acc. Chem. Res.* **2015**, *48*, 935−946.

21. (a) He, G.; Torres Delgado, W.; Schatz, D. J.; Merten, C.; Mohammadpour, A.; Mayr, L.; Ferguson, M. J.; McDonald, R.; Brown, A.; Shankar, K.; Rivard, E. *Angew. Chem., Int. Ed*. **2014**, *53*, 4587−4591. (b) He, G.; Wiltshire, B. D.; Choi,

P.; Savin, A.; Sun, S.; Mohammadpour, A.; Ferguson, M. J.; McDonald, R.; Farsinezhad, S.; Brown, A.; Shankar, K.; Rivard, E. *Chem. Commun.* **2015**, *51*, 5444−5447. (c) Torres Delgado, W.; Shahin, F.; Ferguson, M. J.; McDonald, R.; He, G.; Rivard, E. *Organometallics* **2016**, *35*, 2140−2148. (d) Braun, C. A.; Zomerman, D.; de Aguiar, I.; Qi, Y.; Torres Delgado, W.; Ferguson, M. J.; McDonald, R.; de Souza, G. L. C.; He, G.; Brown, A.; Rivard, E. *Faraday Discuss.* **2017**, *196*, 255−268. (e) Torres Delgado, W.; Braun, C. A.; Boone, M. P.; Shynkaruk, O.; Qi, Y.; McDonald, R.; Ferguson, M. J.; Data, P.; Almeida, S. K. C.; de Aguiar, I.; de Souza, G. L. C.; Brown, A.; He, G.; Rivard, E. *ACS Appl. Mater. Interfaces* **2018**, *10*, 12124–12134. For related important studies on fluorescent tellurium compounds, see: (f) Kryman, M. W.; Schamerhorn, G. A.; Yung, K.; Sathyamoorthy, B.; Sukumaran, D. K.; Ohulchanskyy, T. Y.; Benedict, J. B.; Detty, M. R. *Organometallics* **2013**, *32*, 4321−4333. (g) McCormick, T. M.; Carrera, E. I.; Schon, T. B.; Seferos, D. S. *Chem. Commun.* **2013**, *49*, 11182−11184. (h) Annaka, T.; Nakata, N.; Ishii, A. *Organometallics* **2015**, *34*, 1272−1278. (i) Kremer, A.; Fermi, A.; Biot, N.; Wouters, J.; Bonifazi, D. *Chem. Eur. J.* **2016**, *22*, 5665−5675.

22. Becker, G.; Egner, J.; Meiser, M.; Mundt, O.; Weidlein, J. *Z. Anorg. Allg. Chem.* **1997**, *623*, 941−956.

23. Kindra, D. R.; Peterson, J. K.; Ziller, J. W.; Evans, W. J. *Organometallics* **2015**, *34*, 395−397.

24. Carmalt, C. J.; Cowley, A. H.; Culp, R. D.; Jones, R. A.; Kamepalli, S.; Norman, N. C. *Inorg. Chem.* **1997**, *36*, 2770−2776.

25. (a) Luo, J.; Xie, Z.; Lam, J. W. Y.; Cheng, L.; Chen, H.; Qiu, C.; Kwok, H. S.; Zhan, X.; Liu, Y.; Zhu, D.; Tang, B. Z. *Chem. Commun.* **2001**, 1740−1741. (b) Mei, J.; Leung, N. L. C.; Kwok, R. T. K.; Lam, J. W. Y.; Tang, B. Z. *Chem. Rev.* **2015**, *115*, 11718−11940.

26. Goreshnik, E. A.; Schollmeyer, D.; Myskiv, M. G *Z. Anorg. Allg. Chem.* **2002**, *628*, 2118−2122.

27. Fenske, D.; Rothenberger, A.; Wieber, S. *Z. Anorg. Allg. Chem.* **2003**, *629*, 929−930.

28. Ke, I.-S.; Gabbaï, F. P. *Aust. J. Chem.* **2013**, *66*, 1281−1287.

29. Bondi, A. *J. Phys. Chem.* **1964**, *68*, 441−451.

30. Mantina, M.; Chamberlin, A. C.; Valero, R.; Cramer, C. J.; Truhlar, D. G. *J. Phys. Chem. A* **2009**, *113*, 5806−5812.

31. Bader, R. F. W. *Atoms in Molecules. A Quantum Theory*; Oxford University Press: Oxford, U.K., 1990.

32. (a) Kohout, M. *Int. J. Quantum Chem.* **2004**, *97*, 651−658. (b) Kohout, M.; Wagner, F. R.; Grin, Yu. *Theor. Chem. Acc.* **2008**, *119*, 413−420.

33. Johnson, E. R.; Keinan, S.; Mori-Sánchez, P.; Contreras-García, J.; Cohen, A. J.; Yang, W. *J. Am. Chem. Soc.* **2010**, *132*, 6498−6506.

34. (a) Glendening, E. D.; Landis, C. R.; Weinhold, F. *Comput. Mol. Sci*. **2012**, *2*, 1−42. (b) Weinhold, F. *J. Comput. Chem.* **2012**, *33*, 2363−2379.

35. (a) Flierler, U.; Burzler, M.; Leusser, D.; Henn, J.; Ott, H.; Braunschweig, H.; Stalke, D. *Angew. Chem., Int. Ed.* **2008**, *47*, 4321−4325. (b) Farrugia, L. J.; Evans,

C.; Lentz, D.; Roemer, M. *J. Am. Chem. Soc.* **2009**, *131*, 1251−1268. (c) Mebs, S.; Chilleck, M. A.; Grabowsky, S.; Braun, T. *Chem. Eur. J.* **2012**, *18*, 11647−11661.

36. Schleyer, P. v. R.; Jiao, H.; van Eikema Hommes, J. R.; Malkin, V. G.; Malkina, O. L. *J. Am. Chem. Soc.* **1997**, *119*, 12669−12670.

37. Vessally, E. *J. Struct. Chem.* **2008**, *49*, 979−985. For comparison reasons the NICS(0) value for C_4H_4NH given was recalculated at the B3LYP/cc-pVTZ level of theory.

38. (a) Kuta, J.; Patchkovskii, S.; Zgierski, M. Z.; Kozlowski, P. M. *J. Comput. Chem.* **2006**, *27*, 1429−1437. (b) Hocking, R. K.; Deeth, R. J.; Hambley, T. W. *Inorg. Chem.* **2007**, *46*, 8238−8244. (c) Minenkov, J.; Singstad, Å.; Occhipinti, G.; Jensen, V. R. *Dalton Trans.* **2012**, *41*, 5526−5541.

39. (a) Kasha, M. *J. Chem. Phys.* **1952**, *20*, 71−74. (b) McGlynn, S. P.; Sunseri, R.; Christodouleas, N. *J. Chem. Phys.* **1962**, *37*, 1818−1824.

40. Matano, Y.; Kinoshita, M.; Suzuki, H. *Bull. Chem. Soc. Jpn.* **1992**, *65*, 3504−3506.

41. He, G.; Kang, L.; Torres Delgado, W.; Shynkaruk, O.; Ferguson, M. J.; McDonald, R.; Rivard, E. *J. Am. Chem. Soc.* **2013**, *135*, 5360−5363.

42. Freeman, W. P.; Tilley, T. D.; Liable-Sands, L. M.; Rheingold, A. L. *J. Am. Chem. Soc.* **1996**, *118*, 10457−10468.

43. Negishi, E.-I.; Cederbaum, F. E.; Takahashi, T. *Tetrahedron Lett*. **1986**, *27*, 2829−2832.

44. (a) Becke, A. D. *J. Chem. Phys.* **1993**, *98*, 5648−5652. (b) Lee, C.; Yang, W.; Parr, R. G. *Phys. Rev. B* **1988**, *37*, 785−789.

45. (a) Dunning, T. H., Jr. *J. Chem. Phys.* **1989**, *90*, 1007−1023. (b) Woon, D. E.; Dunning, T. H., Jr. *J. Chem. Phys.* **1993**, *98*, 1358−1371.

46. (a) Peterson, K. A.; Puzzarini, C. *Theor. Chem. Acc.* **2005**, *114*, 283−296. (b) Peterson, K. A. *J. Chem. Phys.* **2003**, *119*, 11099−11112.

47. (a) Feller, D. J. *J. Comput. Chem.* **1996**, *17*, 1571−1586. (b) Schuchardt, K. L.; Didier, B. T.; Elsethagen, T.; Sun, L.; Gurumoorthi, V.; Chase, J.; Li, J.; Windus, T. L. *J. Chem. Inf. Model.* **2007**, *47*, 1045−1052.

48. Frisch, M. J.; Trucks, G. W.; Schlegel, H. B.; Scuseria, G. E.; Robb, M. A.; Cheeseman, J. R.; Scalmani, G.; Barone, V.; Petersson, G. A.; Nakatsuji, H.; Li, X.; Caricato, M.; Marenich, A. V.; Bloino, J.; Janesko, B. G.; Gomperts, R.; Mennucci, B.; Hratchian, H. P.; Ortiz, J. V.; Izmaylov, A. F.; Sonnenberg, J. L.; Williams-Young, D.; Ding, F.; Lipparini, F.; Egidi, F.; Goings, J.; Peng, B.; Petrone, A.; Henderson, T.; Ranasinghe, D.; Zakrzewski, V. G.; Gao, J.; Rega, N.; Zheng, G.; Liang, W.; Hada, M.; Ehara, M.; Toyota, K.; Fukuda, R.; Hasegawa, J.; Ishida, M.; Nakajima, T.; Honda, Y.; Kitao, O.; Nakai, H.; Vreven, T.; Throssell, K.; Montgomery, J. A., Jr.; Peralta, J. E.; Ogliaro, F.; Bearpark, M. J.; Heyd, J. J.; Brothers, E. N.; Kudin, K. N.; Staroverov, V. N.; Keith, T. A.; Kobayashi, R.; Normand, J.; Raghavachari, K.; Rendell, A. P.; Burant, J. C.; Iyengar, S. S.; Tomasi, J.; Cossi, M.; Millam, J. M.; Klene, M.; Adamo, C.; Cammi, R.; Ochterski, J. W.; Martin, R. L.; Morokuma, K.; Farkas, O.; Foresman, J. B.; Fox, D. J. *Gaussian 16*, Revision A.03; Gaussian, Inc.: Wallingford, CT, 2016.

49. Biegler-König, F.; Schönbohm, J.; Bayles, D. *J. Comput. Chem.* **2001**, *22*, 545−559.

50. Kohout, M. *DGRID 4.6*; Springer, 2015.

51. Contreras-García, J.; Johnson, E.; Keinan, S.; Chaudret, R.; Piquemal, J.-P.; Beratan, D.; Yang, W. *J. Chem. Theory Comput.* **2011**, *7*, 625−632.

52. Hübschle, C. B.; Luger, P. *J. Appl. Crystallogr.* **2006**, *39*, 901−904.

53. Humphrey, W.; Dalke, A.; Schulten, K. *J. Mol. Graphics* **1996**, *14*, 33−38.

54. Dennington, R.; Keith, T. A.; Millam, J. M. *GaussView*, Version 5; Semichem Inc.: Shawnee Mission, KS, 2009.

55. Glendening, E. D.; Badenhoop, J. K.; Reed, A. E.; Carpenter, J. E.; Bohmann, J. A.; Morales, C. M.; Landis, C. R.; Weinhold, F. *NBO 6.0*; Theoretical Chemistry Institute, University of Wisconsin: Madison, WI, 2013.

56. (a) van Gisbergen, S. J. A.; Snijders, J. G.; Baerends, E. J. *Comput. Phys. Commun.* **1999**, *118*, 119−138. (b) Rosa, A.; Baerends, E. J.; van Gisbergen, S. J. A.; van Lenthe, E.; Groeneveld, J. A.; Snijders, J. G. *J. Am. Chem. Soc.* **1999**, *121*, 10356−10365. (c) Wang, F.; Ziegler, T. *J. Chem. Phys.* **2005**, *123*, 154102−154113. (d) Wang, F.; Ziegler, T.; van Lenthe, E.; van Gisbergen, S. J. A.; Baerends, E. J. *J. Chem. Phys.* **2005**, *122*, 204103−204114.

57. *ADF2017, SCM, Theoretical Chemistry*; Vrije Universiteit, Amsterdam, The Netherlands, http://www.scm.com (accessed Jan 8, 2018), Baerends, E. J.; Ziegler, T.; Atkins, A. J.; Autschbach, J.; Baseggio, O.; Bashford, D.; Bérces, A.; Bickelhaupt, F. M.; Bo, C.; Boerrigter, P. M.; Cavallo, L.; Daul, C.; Chong, D. P.; Chulhai, D. V.; Deng, L.; Dickson, R. M.; Dieterich, J. M.; Ellis, D. E.; van Faassen, M.; Fan, L.; Fischer, T. H.; Fonseca Guerra, C.; Franchini, M.; Ghysels, A.; Giammona, A.; van Gisbergen, S. J. A.; Goez, A.; Götz, A. W.; Groeneveld, J.

A.; Gritsenko, O. V.; Grüning, M.; Gusarov, S.; Harris, F. E.; van den Hoek, P.; Hu, Z.; Jacob, C. R.; Jacobsen, H.; Jensen, L.; Joubert, L.; Kaminski, J. W.; van Kessel, G.; König, C.; Kootstra, F.; Kovalenko, A.; Krykunov, M. V.; van Lenthe, E.; McCormack, D. A.; Michalak, A.; Mitoraj, M.; Morton, S. M.; Neugebauer, J.; Nicu, V. P.; Noodleman, L.; Osinga, V. P.; Patchkovskii, S.; Pavanello, M.; Peeples, C. A.; Philipsen, P. H. T.; Post, D.; Pye, C. C.; Ramanantoanina, H.; Ramos, P.; Ravenek, W.; Rodríguez, J. I.; Ros, P.; Rüger, R.; Schipper, P. R. T.; Schlüns, D.; van Schoot, H.; Schreckenbach, G.; Seldenthuis, J. S.; Seth, M.; Snijders, J. G.; Solà, M.; Stener, M.; Swart, M.; Swerhone, D.; Tognetti, V.; te Velde, G.; Vernooijs, P.; Versluis, L.; Visscher, L.; Visser, O.; Wang, F.; Wesolowski, T. A.; van Wezenbeek, E. M.; Wiesenekker, G.; Wolff, S. K.; Woo, T. K.; Yakovlev, A. L.

58. (a) Campos, C. T.; Jorge, F. E. *Mol. Phys.* **2013**, *111*, 167−173. (b) van Lenthe, E.; Baerends, E. J. *J. Comput. Chem.* **2003**, *24*, 1142−1156.

59. (a) van Lenthe, E.; Baerends, E. J.; Snijders, J. G. *J. Chem. Phys.* **1993**, *99*, 4597−4610. (b) van Lenthe, E.; Baerends, E. J.; Snijders, J. G. *J. Chem. Phys.* **1994**, *101*, 9783−9792. (c) van Lenthe, E.; Ehlers, A. E.; Baerends, E. J. *J. Chem. Phys.* **1999**, *110*, 8943−8953.

60. Visscher, L.; van Lenthe, E. *Chem. Phys. Lett.* **1999**, *306*, 357−365.

61. Cheeseman, J. R.; Trucks, G. W.; Keith, T. A.; Frisch, M. J. *J. Chem. Phys.* **1996**, *104*, 5497−5509.

Chapter 3

1. (a) Grimsdale, A. C.; Chan, K. L.; Martin, R. E.; Jokisz, P. G.; Holmes, A. B. *Chem. Rev.* **2009**, *109*, 897–109. (b) Parke, S. P.; Boone, M. P.; Rivard, E. *Chem. Commun.* **2016**, *52*, 9485−9505. (c) Wang, C.; Taki, M.; Sato, Y.; Fukazawa, A.; Higashiyama, T.; Yamaguchi, S. *J. Am. Chem. Soc*. **2017**, *139*, 10374−10381. (d) Grzybowski, M.; Taki, M.; Senda, K.; Sato, Y.; Ariyoshi, T.; Okada, Y.; Kawakami, R.; Imamura, T.; Yamaguchi, S. *Angew. Chem. Int. Ed*. **2018**, *57*, 10137−10141.
2. (a) Baumgartner, T.; Réau, R. *Chem Rev.* **2006**, *106*, 4681–4727. (b) Cheng, Y.-J.; Yang, S.-H.; Hsu, C.-S. *Chem. Rev*. **2009**, *109*, 5868−5923. (c) Baggett, A. W.; Guo, F.; Li, B.; Liu, S.-Y.; Jäkle, F. *Angew. Chem. Int. Ed*. **2015**, *54*, 11191−11195. (d) Zhang, C.; Zhu, X. *Acc. Chem. Res.* **2017**, *50*, 1342−1350. (e) Stolar, M.; Baumgartner, T. *Chem. Commun.* **2018**, *54*, 3311−3322.
3. (a) Jia, W.-L.; Liu, Q.-D.; Wang, R.; Wang, S. *Organometallics* **2003**, *22*, 4070−4078. (b) He, G.; Kang, L.; Torres Delgado, W.; Shynkaruk, O.; Ferguson, M. J.; McDonald, R.; Rivard, E. *J. Am. Chem. Soc.* **2013**, *135*, 5360−5363. (c) Linshoeft, J.; Baum, E. J.; Hussain, A.; Gates, P. J.; Näther, C.; Staubitz, A. *Angew. Chem. Int. Ed.* **2014**, *53*, 12916−12920. (d) Carrera, E. I.; Seferos, D. S. *Macromolecules* **2015**, *48*, 297−308. (e) Matsumoto, T.; Tanaka, K.; Tanaka, K.; Chujo, Y. *Dalton Trans.* **2015**, *44*, 8697–8707. (f) Ho, P. C.; Szydlowski, P.; Sinclair, J.; Elder, P. J. W.; Kubel, J.; Gendy, C.; Lee, L. M.; Jenkins, H.; Britten, J. F.; Morim, D. R.; Vargas-Baca, I. *Nat. Commun.* **2016**, *7*, 11299. (g) Yang, L.; Gu, W.; Lv, L.; Chen, Y.; Yang, Y.; Ye, P.; Wu, J.; Hong, L.; Peng, A.; Huang, H.

Angew. Chem. Int. Ed. **2018**, *57*, 1096−1102. (h) Li, G.; Xu, L.; Zhang, W.; Zhou, K.; Ding, Y.; Liu, F.; He, X.; He, G. *Angew. Chem. Int. Ed.* **2018**, *57*, 4897−4901.

4. (a) He, G.; Torres Delgado, W.; Schatz, D. J.; Merten, C.; Mohammadpour, A.; Mayr, L.; Ferguson, M. J.; McDonald, R.; Brown, A.; Shankar, K.; Rivard, E. *Angew. Chem. Int. Ed.* **2014**, *53*, 4587−4591. (b) He, G.; Wiltshire, B. D.; Choi, P.; Savin, A.; Sun, S.; Mohammadpour, A.; Ferguson, M. J.; McDonald, R.; Farinezhad, S.; Brown, A.; Shankar, K.; Rivard, E. *Chem. Commun.* **2015**, *51*, 5444−5447. (c) Kremer, A.; Fermi, A.; Biot. N.; Wouters, J.; Bonifazi, D. *Chem. Eur. J*. **2016**, *22*, 5665−5675. (d) Xu, L.; Li, G.; Zhang, W.; Zhang, S.; Yin, S.; An, Z.; He, G. *Chem. Commun.* **2018**, *54*, 9226−9229.

5. (a) Baldo, M. A.; Lamansky, S.; Burrows, P. E.; Thompson, M. E.; Forrest, S. R. *Appl. Phys. Lett*. **1999**, *75*, 4–6. (b) Evans, R. C.; Douglas, P.; Winscom, C. J. *Coord. Chem. Rev*. **2006**, *250*, 2093−2126. (c) Chi, Y.; Chang, T.-K.; Ganesan, P.; Rajakumu, P. *Coord. Chem. Rev.* **2017**, *346*, 91−100.

6. (a) Fleetham, T.; Li, G.; Li, J. *Adv. Mater*. **2017**, *29*, 1601861. (b) Powell, B. J. *Coord. Chem. Rev.* **2015**, *295*, 46−79.

7. (a) Ohshita, J.; Matsui, S.; Yamamoto, R.; Mizumo, T.; Ooyama, Y.; Harima, T.; Murafuji, T.; Tao, K.; Kuramochi, Y.; Kaikoh, T.; Higashimura, H. *Organometallics* **2010**, *29*, 3239−3241. For related work, see: (b) Parke, S. M.; Narreto, M. A. B.; Hupf, E.; McDonald, R.; Ferguson, M. J.; Hegmann, F. A.; Rivard, E. *Inorg. Chem.* **2018**, *57*, 7536−7549. (c) Morisaki, Y.; Ohashi, K.; Na, H.-S.; Chujo, Y. *J. Polym. Sci., Part A: Polym. Chem.* **2006**, *44*, 4857−4863. The

small Stokes shift involved in the luminescence within the reported bismole copolymer in ref. 7c suggests emission via fluorescence.

8. (a) Sano, Y.; Satoh, H.; Chiba, M.; Okamoto, M.; Serizawa, K.; Nakashima, H.; Omae, K. *J. Occup. Health*, **2005**, *47*, 293−298. (b) Yang, N.; Sun, H. *Coord. Chem. Rev.* **2007**, *251*, 2354−2366.

9. Xu, F.; Kim, H. U.; Kim, J.-H.; Jung, B. J. Grimsdale, A. C.; Hwang, D.-H. *Prog. Polym. Sci.* **2015**, *47*, 92−121.

10. (a) Chai, J.; Wang, D.; Fan, X.; Buriak, J. M. *Nat. Nanotech.* **2007**, *2*, 500−506. (b) Schacher, F. H.; Rupar, P. A.; Manners, I. *Angew. Chem. Int. Ed.* **2012**, *51*, 7898−7921. (c) Qiu, H.; Gao, Y.; Bott, C. E.; Gould, O. E. C.; Harniman, R. L.; Miles, M. J.; Webb, S. E. D.; Winnik, M. A.; Manners, I. *Science* **2016**, *352*, 697−701.

11. (a) You, Y. *Curr. Opinion Chem. Biol.* **2013**, *17*, 699−707. (b) Xiang, H.; Cheng, J.; Ma, X.; Zhou, X.; Chruma, J. J. *Chem. Soc. Rev.* **2013**, *42*, 6128−6185. (c) Ali Fateminia, S. M.; Mao, Z.; Xu, S.; Yang, Z.; Chi, Z.; Liu, B. *Angew. Chem. Int. Ed*. **2017**, *56*, 12160−12164.

12. (a) Robinson, G. W.; Frosch, R. P. *J. Chem. Phys.* **1963**, *38*, 1187−1203. (b) Engleman, R.; Jortner, J. *Mol. Phys.* **1970**, *18*, 145−164.

13. (a) Mukherjee, S.; Thilagar, P. *Chem. Commun*. **2015**, *51*, 10988−11003. (b) Zhao, W.; He, Z.; Lam, J. W. Y.; Peng, Q.; Ma, H.; Shuai, Z.; Bai, G.; Hao, J.; Tang, B. Z. *Chem*. **2016**, *1*, 592−602. (c) Toma, O.; Allain, M.; Meinardi, F.; Forni, A.; Botta, C.; Mercier, N. *Angew. Chem. Int. Ed*. **2016**, *55*, 7998−8002. (d)

Chen, Z.; Liu, G.; Pu, S.; Liu, S. H. *Dyes Pigm.* **2017**, *143*, 409−415. (e) Ravotto, L.; Ceroni, P. *Coord. Chem. Rev.* **2017**, *346*, 62−76.

14. Ly, K. T.; Chen-Cheng, R.-W.; Lin, H.-W.; Shiau, Y.-J.; Liu, S.-H.; Chou, P.-T.; Tsao, C.-S. Huang, Y.-C.; Chi, Y. *Nat. Photon.* **2017**, *11*, 63−68.

15. (a) Bolton, O.; Lee, K.; Kim, H. J.; Lin, K. Y.; Kim, J. *Nat. Chem.* **2011**, *3*, 205−210. (b) An, Z.; Zheng, C.; Tao, Y.; Chen, R.; Shi, H.; Chen, T.; Wang, Z.; Li, H.; Deng, R.; Liu, X.; Huang, W. *Nat. Mater.* **2015**, *14*, 685−690.

16. (a) Dong, A.; Tang, R.; Buhro, W. E. *J. Am. Chem. Soc.* **2007**, *129*, 12254−12262. (b) Jheng, S.-L.; Chen, J.-Y.; Tuan, H.-Y. *Mater. Design.* **2018**, *149*, 113−121.

17. Fagan, P. J.; Nugent, W. A. *J. Am. Chem. Soc*. **1988**, *110*, 2310−2312.

18. Ura, Y.; Li, Y.; Xi, Z.; Takahashi, T. *Tetrahedron Lett*. **1998**, *39*, 2787−2790.

19. Mei, J.; Leung, N. L. C.; Kwok, R. T. K.; Lam, J. W. Y.; Tang, B. Z. *Chem. Rev.* **2015**, *115*, 11718−11940.

20. Mohammadpour, A.; Wiltshire, B. D.; Farsinezhad, S.; Zhang, Y.; Askar, A. M.; Kisslinger, R.; Delgado, W. T.; He, G.; Kar, P.; Rivard, E.; Shankar, K. *Org. Electron.* **2016**, *39*, 153−162.

21. (a) Dong, Y.; Lam, J. W. Y.; Li, Z.; Qin, A.; Tong, H.; Dong, Y.; Feng, X.; Tang, B. Z. *J. Inorg. Organomet. Polym. Mater*. **2005**, *12*, 287−291. (b) Dong, Y.; Lam, J. W. Y.; Qin, A.; Sun, J.; Liu, J.; Li, Z.; Sun, J.; Sung, H. H. Y.; Williams, I. D.; Kwok, H. S.; Tang, B. Z. *Chem. Commun*. **2007**, 3255−3257. (c) Dong, Y. Crystallization-induced emission enhancement. In *Aggregation-Induced Emission: Fundamentals*; Qin, A., Tang, B. Z., Eds.; John Wiley & Sons, Ltd: UK, 2014; pp

323−335. (d) Ohtani, S.; Gon, M.; Tanaka, K.; Chujo, Y. *Chem. Eur. J.* **2017**, *23*, 11827−11833. (e) Zheng, C.; Zang, Q.; Nie, H.; Huang, W.; Zhao, Z.; Qin, A.; Hu, R.; Tang, B. Z. *Mater. Chem. Front*. **2018**, *2*, 180−188.

22. (a) Chen, Z.; Zhang, J.; Song, M.; Yin, J.; Yu, G.-A.; Liu, S. H. *Chem. Commun.* **2015**, *51*, 326–329. (b) Gong, Y.; Chen, G.; Peng, Q.; Yuan, W. Z.; Zie, Y.; Li, S.; Zhang, Y.; Tang, B. Z. *Adv. Mater.* **2015**, *27*, 6195–6201.

23. (a) Becke, A. D.; *J. Chem. Phys.* **1993**, *98*, 5648–5652. (b) Lee, C.; Yang, W.; Parr, R. G. *Phys. Rev. B*, **1988**, *37*, 785–789.

24. Yanai, T.; Tew, D.; Handy, N. *Chem. Phys. Lett.* **2004**, *393*, 51–57.

25. Zhao, Y.; Truhlar, D. *Theor. Chem. Acc*. **2008**, *120*, 215–241.

26. Torres Delgado, W.; Braun, C. A.; Boone, M. P.; Shynkaruk, O.; Qi, Y.; McDonald, R.; Ferguson, M. J.; Data, P.; Almeida, S. K. C.; de Aguiar, I.; de Souza, G. L. C.; Brown, A.; He, G.; Rivard, E. *ACS Appl. Mater. Interfaces* **2018**, *10*, 12124−12134.

27. Vougioukalakis, G. C.; Grubbs, R. H. *Chem. Rev.* **2010**, *110*, 1746−1787.

28. Bu, F.; Wang, E.; Peng, Q.; Hu, R.; Qin, A.; Zhao, Z.; Tang, B. Z. *Chem. Eur. J.* **2015**, *21*, 4440−4449.

29. An, J.; Sun, A.; Qiao, Y.; Zhang, P.; Su, M. *J. Mater. Sci.: Mater. Med.* **2015**, *26*, 1−6.

30. (a) Grabov, V. M.; Demidov, E. V.; Ivanova, E. K.; Kablukova, N. S.; Krushelnitckii, A. N.; Senkevich, S. V. *Semiconductors* **2017**, *51*, 831−833. (b) Yang, F. Y.; Liu, K.; Hong, K.; Reich, D. H.; Searson, P. C.; Chien, C. L. *Science*

1999, *284*, 1335−1337. (c) Takayama, A.; Sato, T.; Souma, S.; Takahashi, T. *J. Vac. Sci. Technol. B* **2012**, *30*, 04E107−1.

31. Harned, A. M.; Song He, H.; Toy, P. H.; Flynn, D. L.; Hanson, P. R. *J. Am. Chem. Soc.* **2005**, *127*, 52–53.

32. Matsuo, D.; Yang, X.; Hamada, A.; Morimoto, K. Kato, T.; Yahiro, M.; Adachi, C.; Orita, A.; Otera, J. *Chem. Lett.* **2010**, *39*, 1300–1302.

33. Jantunen, K. C.; Scott, B. L.; Kiplinger, J. L. *J. Alloy. Compd.* **2007**, *444*, 363–368.

34. Dunning, Jr., T. H. *J. Chem. Phys*. **1989**, *90*, 1007–1023.

35. Peterson, K. A. *J. Chem. Phys*. **2003**, *119*, 11099–11112.

36. (a) Feller, D. *J. Comput. Chem.* **1996**, *17*, 1571–1586. (b) Schuchardt, K. L.; Didier, B. T.; Elsethagen, T.; Sun, L.; Gurumoorthi, V.; Chase, J.; Li, J.; Windus, T. L. *J. Chem. Inf. Model*. **2007**, *47*, 1045–1052.

37. (a) Cances, E.; Mennucci, B.; Tomasi, J. *J. Chem. Phys*. **1997**, *107*, 3032–3041. (b) Cossi, M.; Scalmani, G.; Rega, N.; Barone, V. *J. Chem. Phys*. **2002**, *117*, 43–54.

38. Frisch, M. J.; Trucks, G. W.; Schlegel, H. B.; Scuseria, G. E.; Robb, M. A.; Cheeseman, J. R.; Scalmani, G.; Barone, V.; Petersson, G. A.; Nakatsuji, H.; Li, X.; Caricato, M.; Marenich, A. V.; Bloino, J.; Janesko, B. G.; Gomperts, R.; Mennucci, B.; Hratchian, H. P.; Ortiz, J. V.; Izmaylov, A. F.; Sonnenberg, J. L.; Williams-Young, D.; Ding, F.; Lipparini, F.; Egidi, F.; Goings, J.; Peng, B.; Petrone, A.; Henderson, T.; Ranasinghe, D.; Zakrzewski, V. G.; Gao, J.; Rega, N.; Zheng, G.; Liang, W.; Hada, M.; Ehara, M.; Toyota, K.; Fukuda, R.; Hasegawa, J.;

Ishida, M.; Nakajima, T.; Honda, Y.; Kitao, O.; Nakai, H.; Vreven, T.; Throssell, K.; Montgomery, J. A., Jr.; Peralta, J. E.; Ogliaro, F.; Bearpark, M. J.; Heyd, J. J.; Brothers, E. N.; Kudin, K. N.; Staroverov, V. N.; Keith, T. A.; Kobayashi, R.; Normand, J.; Raghavachari, K.; Rendell, A. P.; Burant, J. C.; Iyengar, S. S.; Tomasi, J.; Cossi, M.; Millam, J. M.; Klene, M.; Adamo, C.; Cammi, R.; Ochterski, J. W.; Martin, R. L.; Morokuma, K.; Farkas, O.; Foresman, J. B.; Fox, D. J. *Gaussian 16*, Revision A.03; Gaussian, Inc.: Wallingford, CT, 2016.

39. (a) van Gisbergen, S. J. A.; Snijders, J. G.; Baerends, E. J. *Comp. Phys. Comm*. **1999**, *118*, 119–138. (b) Rosa, A.; Baerends, E. J.; van Gisbergen, S. J. A.; van Lenthe, E.; Groeneveld, J. A.; Snijders, J. G. *J. Am. Chem. Soc.* **1999**, *121*, 10356–10365. (c) Wang, F.; Ziegler, T. *J. Chem. Phys*. **2005**, *123*, 154102. (d) Wang, F.; Ziegler, T.; van Lenthe, E.; van Gisbergen, S. J. A.; Baerends, E. J. *J. Chem. Phys.* **2005**, *122*, 204103.

40. *ADF2017, SCM, Theoretical Chemistry*; Vrije Universiteit, Amsterdam, The Netherlands, http://www.scm.com. Baerends, E. J.; Ziegler, T.; Atkins, A. J.; Autschbach, J.; Baseggio, O.; Bashford, D.; Bérces, A.; Bickelhaupt, F. M.; Bo, C.; Boerrigter, P. M.; Cavallo, L.; Daul, C.; Chong, D. P.; Chulhai, D. V.; Deng, L.; Dickson, R. M.; Dieterich, J. M.; Ellis, D. E.; van Faassen, M.; Fan, L.; Fischer, T. H.; Fonseca Guerra, C.; Franchini, M.; Ghysels, A.; Giammona, A.; van Gisbergen, S. J. A.; Goez, A.; Götz, A. W.; Groeneveld, J. A.; Gritsenko, O. V.; Grüning, M.; Gusarov, S.; Harris, F. E.; van den Hoek, P.; Hu, Z.; Jacob, C. R.; Jacobsen, H.; Jensen, L.; Joubert, L.; Kaminski, J. W.; van Kessel, G.; König, C.; Kootstra, F.; Kovalenko, A.; Krykunov, M. V.; van Lenthe, E.; McCormack,

D. A.; Michalak, A.; Mitoraj, M.; Morton, S. M.; Neugebauer, J.; Nicu, V. P.; Noodleman, L.; Osinga, V. P.; Patchkovskii, S.; Pavanello, M.; Peeples, C. A.; Philipsen, P. H. T.; Post, D.; Pye, C. C.; Ramanantoanina, H.; Ramos, P.; Ravenek, W.; Rodríguez, J. I.; Ros, P.; Rüger, R.; Schipper, P. R. T.; Schlüns, D.; van Schoot, H.; Schreckenbach, G.; Seldenthuis, J. S.; Seth, M.; Snijders, J. G.; Solà, M.; Stener, M.; Swart, M.; Swerhone, D.; Tognetti, V.; te Velde, G.; Vernooijs, P.; Versluis, L.; Visscher, L.; Visser, O.; Wang, F.; Wesolowski, T. A.; van Wezenbeek, E. M.; Wiesenekker, G.; Wolff, S. K.; Woo, T. K.; Yakovlev, A. L.

41. (a) Campos, C. T.; Jorge, F. E. *Mol. Phys*. **2013**, *111*, 167–173. (b) van Lenthe, E.; Baerends, E. J. *J. Comput. Chem.* **2003**, *24*, 1142–1156.

42. (a) van Lenthe, E.; Baerends, E. J.; Snijders, J. G. *J. Chem. Phys*. **1993**, *99*, 4597–4610. (b) van Lenthe, E.; Baerends, E. J.; Snijders, J. G. *J. Chem. Phys*. **1994**, *101*, 9783–9792. (c) van Lenthe, E.; Ehlers, A. E.; Baerends, E. J. *J. Chem. Phys*. **1999**, *110*, 8943–8953.

43. Visscher, L.; van Lenthe, E. *Chem. Phys. Lett*. **1999**, *306*, 357–365.

44. Humphrey, W.; Dalke, A.; Schulten, K. *J. Mol. Graphics* **1996**, *14*, 33–38.

45. Sheldrick, G. M. *Acta Cryst. A* **2008**, *64*, 112–122.

Chapter 4

1. Mei, J.; Leung, N. L. C.; Kwok, R. T. K.; Lam, J. W. Y.; Tang, B. Z. *Chem. Rev.* **2015**, *115*, 11718−11940.

2. (a) Parke, S. M.; Narreto, M. A. B.; Hupf, E.; McDonald, R.; Ferguson, M. J.; Hegmann, F. A.; Rivard, E. *Inorg. Chem*. **2018**, *57*, 7536–7549. (b) Parke, S. M.;

Hupf, E.; Matharu, G. K.; de Aguiar, I.; Xu, L.; Yu, H.; Boone, M. P.; de Souza, G. L. C.; McDonald, R.; Ferguson, M. J.; He, G.; Brown, A.; Rivard, E. *Angew. Chem. Int. Ed*. **2018**, *57*, 14841–14846.

3. Gessner, V. H.; Tannaci, J. F.; Miller, A. D.; Tilley, T. D. *Acc. Chem. Res.* **2011**, *44*, 435–446.

4. Miller, A. D.; Tannaci, J. F.; Johnson, S. A.; Lee, H.; McBee, J. L.; Tilley, T. D. *J. Am. Chem. Soc.* **2009**, *131*, 4917–4927.

5. (a) He, G.; Kang, L.; Torres Delgado, W.; Shynkaruk, O.; Ferguson, M. J.; McDonald, R.; Rivard, E. *J. Am. Chem. Soc.* **2013**, *135*, 5360–5363. (b) Torres Delgado, W.; Braun, C. A.; Boone, M. P.; Shynkaruk, O.; Qi, Y.; McDonald, R.; Ferguson, M. J.; Data, P.; Almeida, S. K. C.; de Aguiar, I.; de Souza, G. L. C.; Brown, A.; He, G.; Rivard, E. *ACS Appl. Mater. Interfaces* **2018**, *10*, 12124–12134.

6. He, G.; Wiltshire, B. D.; Choi, P.; Savin, A.; Sun, S.; Mohammadpour, A.; Ferguson, M. J.; McDonald, R.; Farsinezhad, S.; Brown, A.; Shankar, K.; Rivard, E. *Chem. Commun*. **2015**, *51*, 5444–5447.

7. Mantina, M.; Chamberlin, A. C.; Valero, R.; Cramer, C. J.; Truhlar, D. G. *J. Phys. Chem. A* **2009**, *113*, 5806−5812.

8. (a) Sheppard, G. S. *Synlett* **1999**, *8*, 1207–1210. (b) Gagnon, A.; Dansereau, J.; Le Roch, A. *Synthesis* **2017**, *49*, 1707–1745. (c) Condon, S.; Pichon, C.; Davi, M. *Org. Prep. Proced. Int.* **2014**, *46*, 89–131.

9. (a) Petiot, P.; Gagnon, A. *Eur. J. Org. Chem*. **2013**, 5282–5289. (b) Hébert, M.; Petiot, P.; Benoit, E.; Dansereau, J.; Ahmad, T.; Le Roch, A.; Ottenwaelder, X.;

Gagnon, A. *J. Org. Chem*. **2016**, *81*, 5401−5416. (c) Dansereau, J.; Gautreau, S.; Gagnon, A. *ChemistrySelect* **2017**, *2*, 2593–2599. (d) Zhou, W.-J.; Wang, K.-H.; Wang, J.-X.; Huang, D.-F. *Eur. J. Org. Chem*. **2010**, 416–419. (e) Ohe, T.; Tanaka, T.; Kuroda, M.; Cho, C. S.; Ohe, K.; Uemura, S. *Bull. Chem. Soc. Jpn.* **1999**, *72*, 1851–1855.

10. Yan, H.; Wang, H.; Li, X.; Xin, X.; Wang, C.; Wan, B. *Angew. Chem. Int. Ed*. **2015**, *54*, 10613–10617.
11. Jantunen, K. C.; Scott, B. L.; Kiplinger, J. L. *J. Alloy. Compd.* **2007**, *444*, 363–368.
12. Dutton, J. L.; Farrar, G. J.; Sgro, M. J.; Battista, T. L.; Ragogna, P. J. *Chem. Eur. J.* **2009**, *15*, 10263–10271.
13. Sheldrick, G. M. *Acta Cryst. A* **2008**, *64*, 112–122.

Chapter 5

1. (a) Fave, C.; Cho, T.-Y.; Hissler, M.; Chen, C.-W.; Luh, T.-Y.; Wu, C.-C.; Réau, R. *J. Am. Chem. Soc.* **2003**, *125*, 9254–9255. (b) Su, H.-C.; Fadhel, O.; Yang, C.-J.; Cho, T.-Y.; Fave, C.; Hissler, M.; Wu, C.-C.; Réau, R. *J. Am. Chem. Soc.* **2006**, *128*, 983–995. (c) Chen, H.; Delaunay, W.; Yu, L.; Joly, D.; Wang, Z.; Li, J.; Wang, Z.; Lescop, C.; Tondelier, D.; Geffroy, B.; Duan, Z.; Hissler, M.; Mathey, F.; Réau, R. *Angew. Chem. Int. Ed*. **2012**, *51*, 214–217. (d) Baumgartner, T.; Réau, R. *Chem. Rev*. **2006**, *106*, 4681–4724.
2. (a) Taki, M.; Ogasawara, H.; Osaki, H.; Fukazawa, A.; Sato, Y.; Ogasawara, K.; Higashiyama, T.; Yamaguchi, S. *Chem. Commun.* **2015**, *51*, 11880–11883. (b)

Fukazawa, A.; Ichihashi, Y.; Kosaka, Y.; Yamaguchi, S. *Chem. Asian J*. **2009**, *4*, 1729–1740.

3. (a) Fourmy, K.; Nguyen, D. H.; Dechy-Cabaret, O.; Gouygou, M. *Catal. Sci. Technol*. **2015**, *5*, 4289–4323. (b) Hibner-Kulicka, P.; Joule, J. A.; Skalik, J.; Bałczewski, P. *RSC Adv*. **2017**, *7*, 9194–9236.
4. (a) Matsumura, M.; Yamada, M.; Muranaka, A.; Kanai, M.; Kakusawa, N.; Hashizume, D.; Uchiyama, M.; Yasuike, S. *Beilstein J. Org. Chem*. **2017**, *13*, 2304–2309. (b) Wu, B.; Santra, M.; Yoshikai, N. *Angew. Chem. Int. Ed*. **2014**, *53*, 7543–7546. (c) Kumaravel, M.; Mague, J. T.; Balakrishna, M. S. *Tetrededron Lett*. **2014**, *55*, 2957–2961.
5. (a) Wang, C.; Fukazawa, A.; Tanabe, Y.; Inai, N.; Yokogawa, D.; Yamaguchi, S. *Chem. Asian J*. **2018**, *13*, 1616–1624. (b) Wang, C.; Taki, M.; Sato, Y.; Fukazawa, A.; Higashiyama, T.; Yamaguchi, S. *J. Am. Chem. Soc.* **2017**, *139*, 10374–10381. (c) Adler, R. A.; Wang, C.; Fukazawa, A.; Yamaguchi, S. *Inorg. Chem.* **2017**, *56*, 8718–8725.
6. See Section 1.4.1.1 for a discussion of the luminescence properties of benzophosphole oxides with examples of fluorescent emitters with quantum yields (Φ) approaching 100 %. For selected references discussing benzophosphole emitters with particularly high Φ, see: (a) Fukazawa, A.; Hara, M.; Okamoto, T.; Son, E.-C.; Xu, C.; Tamao, K.; Yamaguchi, S. *Org. Lett*. **2008**, *10*, 913–916. (b) Matano, Y.; Motegi, Y.; Kawatsu, S.; Kimura, Y. *J. Org. Chem.* **2015**, *80*, 5944−5950.

7. Bu, F.; Wang, E.; Peng, Q.; Hu, R.; Qin, A.; Zhao, Z.; Tang, B. Z. *Chem. Eur. J.* **2015**, *21*, 4440–4449.

8. Zhuang, Z.; Bu, F.; Luo, W.; Peng, H.; Chen, S.; Hu, R.; Qin, A.; Zhao, Z.; Tang, B. Z. *J. Mater. Chem. C* **2017**, *5*, 1836–1842.

9. Parke, S. M.; Hupf, E.; Matharu, G. K.; de Aguiar, I.; Xu, L.; Yu, H.; Boone, M. P.; de Souza, G. L. C.; McDonald, R.; Ferguson, M. J.; He, G.; Brown, A.; Rivard, E. *Angew. Chem. Int. Ed*. **2018**, *57*, 14841–14846.

10. Fagan, P. J.; Nugent, W. A. *J. Am. Chem. Soc*. **1988**, *110*, 2310–2312.

11. Fagan, P. J.; Nugent, W. A.; Calabrese, J. C. *J. Am. Chem. Soc*. **1994**, *116*, 1880–1889.

12. He, G.; Wiltshire, B. D.; Choi, P.; Savin, A.; Sun, S.; Mohammadpour, A.; Ferguson, M. J.; McDonald, R.; Farsinezhad, S.; Brown, A.; Shankar, K.; Rivard, E. *Chem. Commun.* **2015**, *51*, 5444−5447.

13. (a) Kuno, S.; Kanamori, T.; Yijing, Z.; Ohtani, H.; Yuasa, H. *ChemPhotoChem*. **2017**, *1*, 102–106. (b) Shoji, Y.; Ikabata, Y.; Wang, Q.; Nemoto, D.; Sakamoto, A.; Tanaka, N.; Seino, J.; Nakai, H.; Fukushima, T. *J. Am. Chem. Soc.* **2017**, *139*, 2728–2733.

14. Adamo, C.; Jacquemin, D. *Chem. Soc. Rev*. **2013**, *42*, 845–856.

15. Oehlke, A.; Auer, A. A.; Jahre, I.; Walfort, B.; Rüffer, T.; Zoufalá, P.; Lang, H.; Spange, S. *J. Org. Chem*. **2007**, *72*, 4328–4339.

16. Jantunen, K. C.; Scott, B. L.; Kiplinger, J. L. *J. Alloy. Compd.* **2007**, *444*, 363–368.

17. Brown, A. E.; Eichler, B. E. *Tetrahedron Lett.* **2011**, *52*, 1960–1963.

18. Harned, A. M.; Song He, H.; Toy, P. H.; Flynn, D. L.; Hanson, P. R. *J. Am. Chem. Soc.* **2005**, *127*, 52–53.

19. Becke, A. D.; *J. Chem. Phys.* **1993**, *98*, 5648–5652. (b) Lee, C.; Yang, W.; Parr, R. G. *Phys. Rev. B* **1988**, *37*, 785–789.

20. (a) Dunning, Jr., T. H. *J. Chem. Phys*. **1989**, *90*, 1007–1023. (b) Woon, D.E.; Dunning, Jr., T. H. *J. Chem. Phys.* **1993**, 98, 1358–1371.

21. Frisch, M. J.; Trucks, G. W.; Schlegel, H. B.; Scuseria, G. E.; Robb, M. A.; Cheeseman, J. R.; Scalmani, G.; Barone, V.; Petersson, G. A.; Nakatsuji, H.; Li, X.; Caricato, M.; Marenich, A. V.; Bloino, J.; Janesko, B. G.; Gomperts, R.; Mennucci, B.; Hratchian, H. P.; Ortiz, J. V.; Izmaylov, A. F.; Sonnenberg, J. L.; Williams-Young, D.; Ding, F.; Lipparini, F.; Egidi, F.; Goings, J.; Peng, B.; Petrone, A.; Henderson, T.; Ranasinghe, D.; Zakrzewski, V. G.; Gao, J.; Rega, N.; Zheng, G.; Liang, W.; Hada, M.; Ehara, M.; Toyota, K.; Fukuda, R.; Hasegawa, J.; Ishida, M.; Nakajima, T.; Honda, Y.; Kitao, O.; Nakai, H.; Vreven, T.; Throssell, K.; Montgomery, J. A., Jr.; Peralta, J. E.; Ogliaro, F.; Bearpark, M. J.; Heyd, J. J.; Brothers, E. N.; Kudin, K. N.; Staroverov, V. N.; Keith, T. A.; Kobayashi, R.; Normand, J.; Raghavachari, K.; Rendell, A. P.; Burant, J. C.; Iyengar, S. S.; Tomasi, J.; Cossi, M.; Millam, J. M.; Klene, M.; Adamo, C.; Cammi, R.; Ochterski, J. W.; Martin, R. L.; Morokuma, K.; Farkas, O.; Foresman, J. B.; Fox, D. J. *Gaussian 16*, Revision A.03; Gaussian, Inc.: Wallingford, CT, 2016.

22. (a) Avogadro: An Open-Source Molecular Builder and Visualization Tool—Version 1.2.0. 2016. Available online: http://avogadro.cc/ (accessed on 13 March

2019). (b) Hanweel, M.; Curtis, D.E.; Lonie, D.; Vandermeersch, T.; Zurek, E.; Hutchison, G. *J. Cheminform.* **2012**, *4*, 17.

23. Sheldrick, G. M. *Acta Cryst. A* **2008**, *64*, 112–122.

Chapter 6

1. Torres Delgado, W.; Braun, C. A.; Boone, M. P.; Shynkaruk, O.; Qi, Y.; McDonald, R.; Ferguson, M. J.; Data, P.; Almeida, S. K. C.; de Aguiar, I.; de Souza, G. L. C.; Brown, A.; He, G.; Rivard, E. *ACS Appl. Mater. Interfaces* **2018**, *10*, 12124−12134.

2. (a) Fukazawa, A.; Ichihashi, Y.; Kosaka, Y.; Yamaguchi, S. *Chem. Asian J.* **2009**, *4*, 1729–1740. (b) Hibner-Kulicka, P.; Joule, J. A.; Skalik, J.; Bałczewski, P. *RSC Adv*. **2017**, *7*, 9194–9236.

3. (a) Ding, F.; Fan, Y.; Sun, Y.; Zhang, F. *Adv. Healthcare Mater*. **2019**, DOI: 10.1002/adhm.201900260. (b) Wu, D.; Chen, L.; Lee, W.; Ko, G.; Yin, J.; Yoon, J. *Coord. Chem. Rev*. **2018**, *354*, 74–97. (c) Zhao, Q.; Sun, J. Z. *J. Mater. Chem. C* **2016**, *4*, 10588–10609.

4. (a) Dong, A.; Tang, R.; Buhro, W. E. *J. Am. Chem. Soc.* **2007**, *129*, 12254−12262. (b) Jheng, S.-L.; Chen, J.-Y.; Tuan, H.-Y. *Mater. Design.* **2018**, *149*, 113−121.

5. Adamo, C.; Jacquemin, D. *Chem. Soc. Rev.* **2013**, *42*, 845–856.

6. (a) Taki, M.; Ogasawara, H.; Osaki, H.; Fukazawa, A.; Sato, Y.; Ogasawara, K.; Higashiyama, T.; Yamaguchi, S. *Chem. Commun.* **2015**, *51*, 11880–11883. (b) Wakatsuki, A.; Yukimoto, M.; Minoura, M.; Fujii, K.; Kimura, Y.; Matano, Y. *Dalton Trans*. **2018**, *47*, 7123–7127. (c) Yamaguchi, E.; Wang, C.; Fukazawa, A.;

Taki, M.; Sato, Y.; Sasaki, T.; Uedo, M.; Sasaki, N.; Higashiyama, T.; Yamaguchi, S. *Angew. Chem. Int. Ed*. **2015**, *54*, 4539–4543.

7. (a) Yamaguchi, S.; Fukazawa, A.; Taki, M. *J. Synth. Org. Chem., Jpn.* **2017**, *75*, 1179–1187. (b) Wang, C.; Fukazawa, A.; Taki, M.; Sato, Y.; Higashiyama, T.; Yamaguchi, S. *Angew. Chem. Int. Ed.* **2015**, *54*, 15213 –15217

8. Matano, Y.; Motegi, Y.; Kawatsu, S.; Kimura, Y. *J. Org. Chem.* **2015**, *80*, 5944−5950.